DYNAMIC GEOTECHNICAL TESTING

ASTM STP 654

AMERICAN SOCIETY FOR TESTING AND MATERIALS

DYNAMIC GEOTECHNICAL TESTING

A symposium
sponsored by ASTM
Committee D-18 on Soil
and Rock for Engineering
Purposes
AMERICAN SOCIETY FOR
TESTING AND MATERIALS
Denver, Colo., 28 June 1977

ASTM SPECIAL TECHNICAL PUBLICATION 654
M. L. Silver, University of Illinois
Drew Tiedemann, Bureau of Reclamation
symposium cochairmen

04-654000-38

AMERICAN SOCIETY FOR TESTING AND MATERIALS
1916 Race Street, Philadelphia, Pa. 19103

Library of Congress Catalog Card Number: 78-55316

NOTE

The Society is not responsible, as a body,
for the statements and opinions
advanced in this publication.

Printed in Baltimore, Md.
September 1978

Second Printing, Ann Arbor, Mich.
September 1982

Foreword

The papers in this publication were presented at a symposium held in Denver, Colo., 28 June 1977. The symposium was sponsored by the American Society for Testing and Materials' Committee D-18 on Soil and Rock for Engineering Purposes. M. L. Silver, University of Illinois, and Drew Tiedemann, U.S. Bureau of Reclamation, presided as symposium cochairmen.

Related ASTM Publications

Performance Monitoring for Geotechnical Construction, STP 584 (1975), 04-584000-38

Soil Specimen Preparation for Laboratory Testing, STP 599 (1976), 04-599000-38

Dispersive Clays, Related Piping and Erosion in Geotechnical Projects, STP 623 (1977), 04-623000-38

A Note of Appreciation to Reviewers

This publication is made possible by the authors and, also, the unheralded efforts of the reviewers. This body of technical experts whose dedication, sacrifice of time and effort, and collective wisdom in reviewing the papers must be acknowledged. The quality level of ASTM publications is a direct function of their respected opinions. On behalf of ASTM we acknowledge with appreciation their contribution.

ASTM Committee on Publications

Editorial Staff

Contents

Introduction

Rapid and important changes in dynamic testing in Geotechnical Engineering over the last decade suggested to ASTM the need to bring together experts for an evaluation of the present state of practice in laboratory and field testing to determine dynamic soil and rock behavior. The result was a "Symposium on Dynamic Soil and Rock Testing in the Field and the Laboratory for Seismic Studies" held 28 June in Denver, Colorado, during the 81st Annual Meeting of the American Society for Testing and Materials. The Symposium was sponsored by ASTM Committee D-18 on Soil and Rock for Engineering Purposes.

The Symposium consisted of two one-half day sessions: The first session on dynamic field testing of soil and rock and the second session on dynamic laboratory testing. Both sessions featured invited talks by experts who described practical methods for using existing test methods to obtain better information about the dynamic behavior of geotechnical materials. In addition, the invited speakers described how new testing techniques could be used to provide additional information on dynamic soil and rock behavior. These invited speakers were not asked to review all the literature on dynamic testing and to present a dry discussion on what people have done in the past. The authors were, on the other hand, asked (1) to critically review what is being done in dynamic testing, (2) to suggest ways of improving existing techniques, and (3) to suggest new techniques for solving current problems that compromise our understanding of the dynamic behavior of soil and rock. The first group of papers presented in this volume shows that the invited authors did an admirable job of meeting this challenge.

In addition to the invited oral presentations, technical papers on either laboratory or field dynamic testing subjects were submitted to the Symposium for publication only. These papers provided a basis for some of the conclusions presented for the oral presentations by the invited speakers and form the basis for a better understanding of the dynamic behavior of geotechnical materials.

A brief description of the oral presentations on Dynamic Field Testing of Soil and Rock is given by S. D. Wilson in his paper on *in situ* determination of dynamic soil properties summarizing our knowledge of field techniques for determining the engineering properties of large soil masses in the field. His remarks form the basis for an improved understanding of the advantages and disadvantages of different field testing methods and an understanding of problems in the interpretation of field test results.

The important problem of *in situ* density determination and its effect on dynamic soil behavior was covered well by W. F. Marcuson who summarized years of experience of the Corps of Engineers in developing ways to determine the *in situ* density of cohesionless soils.

To conclude the session on field determination of dynamic properties, J. H. Schmertmann presented an important paper describing the use of penetration testing as a possible measure of dynamic soil behavior. In this paper he suggested new ways to interpret standard penetration test results which should lead to more rational use of the penetration test in field dynamic studies and to better interpretation of SPT test results.

A lively panel discussion chaired by Drew Tiedemann invoked some lively questions from the audience on what is the relative accuracy and importance of field testing and what should be done to improve our ability to measure dynamic properties of soil and rock.

The afternoon session on dynamic laboratory testing of soil and rock was keynoted by Julio Valera in his oral presentation describing how better coordination between the design engineer and the laboratory can lead to an improved understanding of dynamic soil and rock behavior. In this talk, Dr. Valera pointed out the importance of close cooperation between the engineer and the designer from the very beginning of any testing program requiring the determination of dynamic properties in the laboratory.

The important question of specimen preparation and its influence on dynamic soil behavior was discussed by Richard Ladd, who pointed out how cohesionless soils cannot be directly modeled in the laboratory without attention being given to the selection of specimen preparation technique. This fact, known for a long time for cohesive soils, is now drawing the attention of a number of researchers and Mr. Ladd's presentation helps to describe the importance of this variable in predicting field behavior from laboratory test results.

Three speakers were invited to discuss the three most common methods of laboratory determination of the dynamic properties of soil and rock: (1) Cyclic Triaxial Strength Testing, (2) Cyclic Triaxial Properties Testing, and (3) Resonant Column Testing.

Cyclic triaxial strength testing was discussed by F. C. Townsend, who pointed out how testing details can influence laboratory determined cyclic triaxial strength values used to measure the liquefaction behavior of soils. He pointed out how small testing details can influence strength results. Cyclic triaxial properties testing was described by M. L. Silver who described how test equipment features can affect test results as well as how different analysis procedures can be used to interpret test results in more meaningful ways. Resonant column testing was described by V. P. Drnevich who clearly and accurately described limitations of the test and described methods of determining when the rigidity of the specimen and the rigidity of the testing apparatus are adequate enough to give accurate measures of soil properties under dynamic conditions.

An animated and controversial panel discussion on "Nontraditional Testing Methods to Determine Dynamic Soil Behavior" chaired by Dr. Silver completed the afternoon session. Members of the panel made clear their ideas on how laboratory test results should be interpreted to evaluate field performance of soil and rock. Particular attention was directed to the need for improved measurement of *in situ* soil densities and the need for better sampling procedures for cohesionless soils.

An overview of the entire Symposium shows that the goal of providing practitioners with entailed suggestions on how to perform and use the results of field and laboratory dynamic tests was achieved. The invited papers summarizing our knowledge of the uses and abuses of laboratory and field test procedures, as well as the detailed papers describing particular test procedures found in this volume are excellent references for the engineer wanting more information on how to achieve better measurement of the dynamic properties of soil and rock for improved design and analysis of all types of Civil Engineering structures.

The cochairmen of this Symposium would like to thank the ASTM staff and members of Committee D-18 for their support and help in organizing and publishing the results of the Symposium.

M. L. Silver

University of Illinois, Chicago, Ill.; symposium cochairman.

Drew Tiedemann

Bureau of Reclamation, Denver, Colo.; symposium cochairman.

R. J. Hoar[1] *and K. H. Stokoe II*[1]

Generation and Measurement of Shear Waves *In Situ*

REFERENCE: Hoar, R. J. and Stokoe, K. H., II, "**Generation and Measurement of Shear Waves *In Situ*,**" *Dynamic Geotechnical Testing, ASTM STP 654,* American Society for Testing and Materials, 1978, pp. 3-29.

ABSTRACT: Field procedures used to measure *in situ* shear wave velocity by crosshole and downhole seismic methods are presented along with typical travel time records. Identification of the initial shear wave arrival is enhanced by use of a reversible torsional source in the crosshole method and a reversible embedded source in the downhole method. Correct triggering of recording equipment is critical in these measurements. Characteristics of three triggering systems—a velocity transducer, a resistance-capacitance (RC) circuit, and an electrical step trigger—are presented. Incorrect triggering can cause errors greater than 50 percent in field measurement of shear wave velocity. Other variables such as borehole casing, borehole disturbance, and source and sensor configuration also affect velocity measurement. The effects of many of the variables can be minimized by basing wave velocity computations on interval travel times of the initial arrival. It is recommended that any ASTM standards for crosshole and downhole seismic methods include field check procedures for correct timing and triggering of recording equipment and field measurement of borehole verticality.

KEY WORDS: crosshole method, downhole method, dynamics, field tests, geophysical prospecting, seismic investigations, seismic waves, shear modulus, shear wave velocity, torsional source, triggering, soils

Accurate *in situ* shear wave velocity data are essential in evaluating the dynamic response of soil or structures supported on soil during earthquake loading, ocean-wave loading, machine loading, or other types of dynamic loading. Geophysical methods such as crosshole, downhole, surface refraction, and steady-state vibration are commonly used for onshore investigation of *in situ* shear wave velocity [*1-7*].[2] *In situ* shear wave velocities are used to determine *in situ* moduli by the relation

[1] Research assistant and assistant professor, respectively, Department of Civil Engineering, University of Texas, Austin, Tex. 78712.

[2] The italic numbers in brackets refer to the list of references appended to this paper.

$$G = \frac{\gamma_T}{g} v_S^2 \tag{1}$$

where

G = shear modulus,
γ_T = total unit weight of soil,
g = acceleration due to gravity, and
v_S = shear wave velocity.

Geophysical measurement of v_S, and hence G, normally evaluates these properties at shearing strains below 0.001 percent (although a crosshole technique has been developed which involves higher shearing strains [*8–10*]). Moduli determined in this manner are commonly referred to as low-amplitude moduli and are many times denoted as G_{max}. These moduli represent initial tangent moduli used in nonlinear stress-strain relations for static and dynamic analyses. Moduli at higher shearing strain amplitudes are normally determined in the laboratory or are estimated from empirical relationships.

During the past few years, there has been considerable controversy over the worth of *in situ* shear wave velocity measurement. This controversy has resulted from very significant variations in values of v_S reported by different investigators for measurements made over the same travel paths at the same sites. Some reasons for such scatter could be: (1) improper generation and sensing of shear waves, (2) poor quality control, and (3) use of poorly trained and poorly supervised personnel. However, even if these deficiencies are corrected, variables still remain in the measurement techniques which can affect the results and which are not properly controlled or fully understood.

Variables such as (1) type and configuration of the source, (2) sensor configuration, and (3) type, diameter, and spacing of the boreholes can affect measured values of v_S [*3,6,11*]. The main reason for the apparent unconcern for these variables is that they were insignificant when geophysical methods were originally used to measure compression wave velocities over distances of several hundred feet or more. However, for engineering investigation of shear wave velocities, measurements are now made over distances of tens of feet and these variables can significantly affect the results.

The objectives of this paper are (1) to outline field procedures for crosshole and downhole seismic survey methods which can be successfully used to make accurate *in situ* shear wave velocity measurement for engineering purposes; (2) to stress the importance of proper quality control, especially correct timing and triggering of recording equipment and measurement of borehole verticality; and (3) to outline some of the factors which affect *in situ* measurement of v_S. Field measurements, although viewed as very important by the engineering profession, seem many times to be relegated to a second-echelon status. In fact, if properly performed, *in situ* shear wave velocity measurements are one of the most accurate measurements of "undisturbed" soil properties which can be performed today.

Crosshole Seismic Survey Method

The crosshole seismic survey method is well suited for determining the variation of *in situ* shear wave velocity with depth. By this method, the *time* for body waves to travel between several points at the same depth within a soil mass is measured. Body waves may be either compression waves, *P*-waves, or shear waves, *S*- waves, with compression waves having a higher wave velocity than shear waves for the same soil conditions. Wave velocities are calculated from corresponding travel times once the distance of travel has been determined.

In engineering work, emphasis is placed on measurement of shear wave travel time and hence determination of v_S. The key components in such a measurement system are (1) a source which is rich in shear wave generation and weak in compression wave generation and which is directional, repeatable, and reversible; (2) receivers with the proper frequency response which are oriented in the direction of *S*-wave particle motion; (3) a recording system with the proper frequency response with which accurate time measurements can be made and a permanent record produced; and (4) a triggering system which correctly triggers the recorder.

One measurement system which fulfills these requirements employs the standard penetration test (SPT) as the source, velocity transducers with natural frequencies between 4 and 20 Hz as receivers, a storage oscilloscope with camera as the recording system, and a velocity transducer or electrical triggering system. This system, which is regularly used in the field, is described herein.

Field Procedure

The procedure used in the field is to drill and case three (or more) boreholes to the desired depth several days prior to the start of testing. Drilling mud is often used to reduce borehole disturbance from stress relief and squeezing [*10*]. Each borehole is logged during drilling to determine, at a minimum, soil types and layering with particular attention paid to the thickness and inclination of layering. Borehole diameters are as small as feasible to minimize factors which can affect the measurements such as disturbance, screening, and wave interaction effects. Typically, borehole diameters range from 10.2 to 15.2 cm (4 to 6 in.).

The boreholes are cased with either aluminum or plastic casing. Casing with an inner diameter of about 7.6 cm (3 in.) is used because it is compatible with geophysical equipment as well as with equipment used to measure borehole verticality. Each casing is grouted in place with cement grout in an attempt to insure intimate contact and good coupling with the surrounding soil. Backfilling with sand around the casing does not seem to work as well [*11*], especially for deep holes. (The effects of many of the borehole variables on *in situ* measurement of v_S are not completely understood.)

Figure 1*a* shows the relative location of these boreholes in which receivers are placed when the test is performed. Borehole spacing on the order of 3 to 4.6 m (10 to 15 ft) is used. This close spacing is used to increase the probability of measurement of a direct wave in each layer, to reduce the probability of measurement of refracted waves, and to optimize development of a unique velocity profile. If borehole spacing on the order of 15 to 30 m (50 to 100 ft) or more is used, development of a unique profile from the measurements is much less likely and requires much more judgment on the part of the investigator.

Close borehole spacing is also used so that the same phase of each wave is propagated to each detection point [*3*]. This spacing may, however, be altered somewhat during drilling as dictated by layering detected at the site.

Three or more boreholes are used so that possible refracted waves can be evaluated [*3,6,11*]. In addition, the boreholes are located in a linear array as shown in Fig. 1*a* to minimize anisotropic effects which might occur in a data set and which would further complicate data reduction and increase scatter in the measurements.

In this manner, receiver boreholes are drilled and cased several days before the seismic crew arrives at the site. This greatly reduces standby time of the drilling and seismic crews.

Crosshole Shooting in the Field

To perform the seismic test, a drill rig is positioned at the location of the source borehole shown in Fig. 1*a*. The drill rig is used to advance a fourth borehole. If site conditions permit, an uncased borehole (which is most economical) is used. After the borehole is advanced to the depth at which measurements are to be performed, SPT equipment is inserted in the borehole. Vertical velocity transducers (usually part of a three-dimensional transducer package) are wedged in two (or more) of the receiver boreholes at the same depth. Good mechanical coupling between the receivers and borehole walls is required.

The seismic test is then performed with the standard penetration test as the source. This is done by attaching a vertical velocity transducer to the drill rod several feet above ground level. Each time the 63.5-kg (140 lb) hammer is dropped, it excites the transducer attached to the drill rod, which in turn produces a signal that triggers the storage oscilloscope. At the same time, the drop of the hammer sends a compression wave down

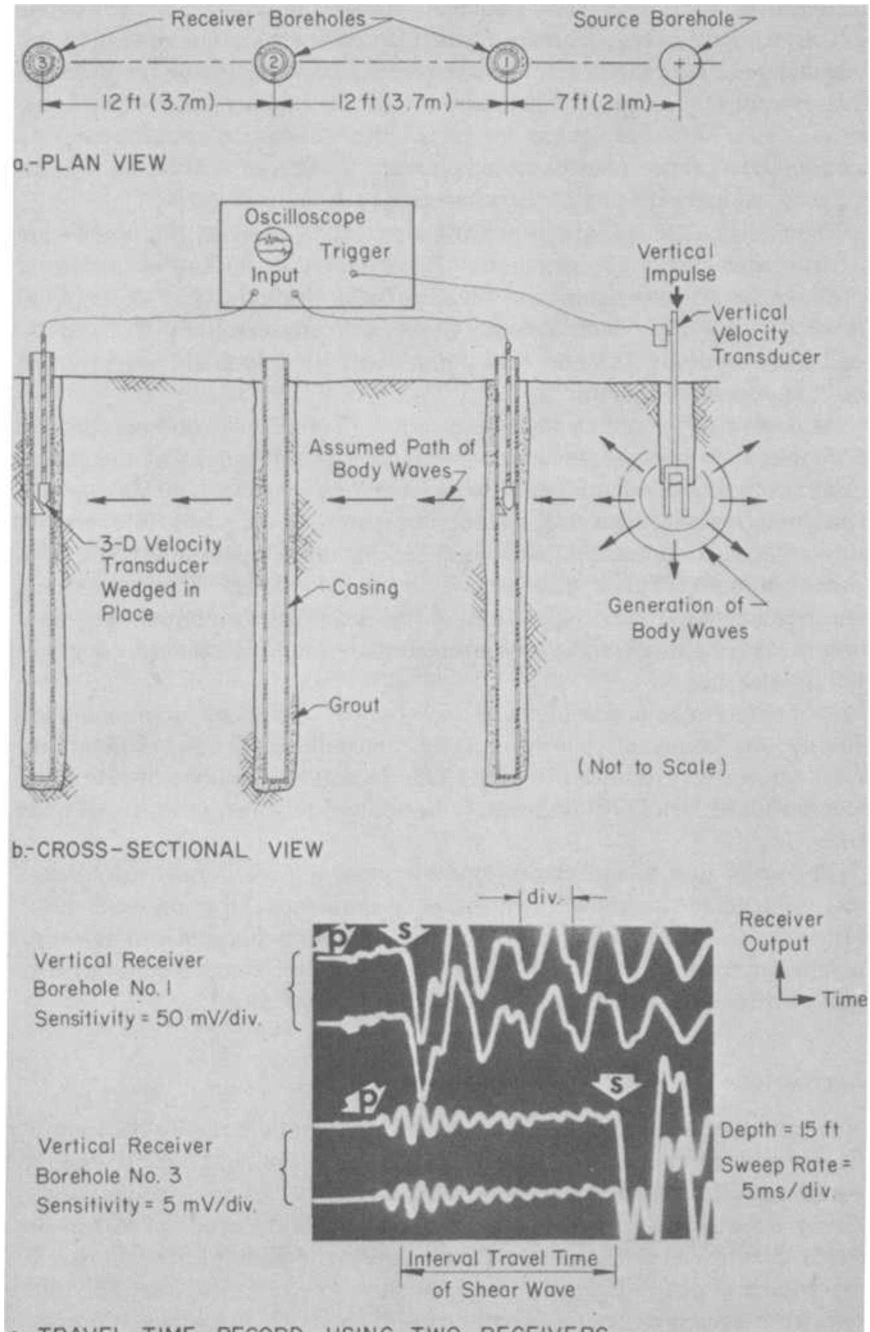

FIG. 1—*Crosshole seismic survey method.*

the drill rod. This compression wave is coupled into the soil at the bottom of the rod. Body waves generated in the soil and their arrivals at the velocity transducers in the cased boreholes are recorded on the storage oscilloscope. This procedure of dropping the hammer and recording the arrivals is done several times with the equipment in the initial position to determine an average arrival time and also to demonstrate the reproducibility of the test. A cross-sectional view of this arrangement is shown in Fig. *1b*.

When using the standard penetration test as the source, the split spoon is first seated about 30 cm (about 12 in.) into the soil at the bottom of the borehole. Measurements are then made by dropping the 63.5-kg (140 lb) weight only a few centimeters. In fact, at this point, the SPT hammer can be removed and a hand-held hammer with an electrical trigger can be used to generate the impulse.

After travel time measurements are made between the source and these boreholes, the velocity transducers are removed and wedged at the source depth in other boreholes. The seismic test is then repeated. In this manner, travel time measurements are made between the source and all combinations of horizontal travel paths between the three cased boreholes. The source borehole is then advanced to the next depth at which travel time measurements are to be made, and the travel-time-measurement procedure is repeated. In this manner, measurements are made at selected depths to the final depth.

If the site is composed of many layers with significant inclination, the complete test sequence may have to be repeated with a new source borehole. (A reversed profile is run *[12]*.) This second-source borehole would be located about 2.1 m (7 ft) to the left of Borehole 3 for the procedure depicted in Fig. 1.

The verticality of each cased borehole must be determined. Verticality measurements are combined with center-to-center spacings of the boreholes at the ground surface to determine distances between boreholes at all cross-hole measurement depths. With these horizontal distances, lengths of travel paths of direct and refracted waves can then be evaluated.

Interpretation of Travel Time Records

Output recorded on the storage oscilloscope from vertical velocity transducers wedged in two cased boreholes is shown in Fig. *1c*. The photograph consists of two sets of traces (two traces in each set) across the oscilloscope viewing screen which resulted from two 5-cm (2 in.) drops of the 63.5-kg (140 lb) hammer. The upper set of two traces is the output from the velocity transducer wedged in borehole No. 1 for the two hammer drops. The location of the trace on the oscilloscope viewing screen was changed between hammer drops. The lower set of two traces is the output from the vertical velocity transducer wedged in Borehole 3 for the same two hammer drops.

The location of this trace was also changed between hammer drops. As can be seen in the photograph, the traces in each set are almost identical.

For the purpose of identifying P-wave and S-wave arrivals in these records, consider the next to the bottom trace in Fig. 1c. This trace is composed of three basic parts. The first part, which is on the left side of the trace, is the initial smooth portion of the trace. This results from the fact that the hammer drop has started the trace moving across the face of the oscilloscope but no energy has yet arrived at the transducer wedged in the cased borehole. The second part encompasses the time between the first arrival, denoted by the P, and the second arrival, denoted by the S. This part is made up of waves of lower amplitude and higher frequency (typically 200 to 2000 Hz, with frequencies in the upper portion of this range normally found in measurements below the water table) when compared with the remainder of the trace. This portion of the trace is considered to represent energy transmitted by the P-wave. The third part of the trace is made up of waves of higher amplitude and lower frequency (typically 50 to 300 Hz) and is due, at least initially, to the arrival of the shear wave. The shear wave arrival is identified as the beginning of the first high-energy excursion [*4*] and is denoted by the S in the photograph.

Shear wave and compression wave travel times measured in this manner are interval travel times between cased boreholes and are not travel times between the source and a cased borehole. An interval travel time determination using the initial S-wave arrival is illustrated in Fig. 1c. Following this procedure, interval travel times of the initial arrivals of P- and S-waves are determined between all cased boreholes at all measurement depths.

One advantage of using interval travel times rather than travel times between the source and receiver is that effects of triggering, casing, and borehole disturbance are minimized and many times eliminated. A second advantage is that for borehole spacings recommended herein the verticality of the source borehole does not have to be determined in those cases where the source borehole can be assumed to be out-of-plumb by less than 0.6 m (2 ft) at any depth. Finally, with this procedure it is possible to detect measurement of refracted waves under most conditions. The one condition when refracted wave velocity can be erroneously interpreted as direct wave velocity is when measurements are made near a strong velocity contrast. However, this error can be determined upon evaluation of the complete velocity profile combined with relative measurement locations, and appropriate corrections can be made.

It should be noted that interval P- and S-wave velocities are sometimes determined using reference points other than the initial arrivals. For instance, the first trough, first crossover point, or first peak of each wave after the initial arrival may be used as the reference point. It is assumed in this procedure that the wave signature after the initial arrival is the same at each receiver location. At times these reference points will give slightly longer interval travel times than those determined using initial arrivals This is especially true as the length of the travel path increases and for reference points selected well past the initial arrival. Hence, lower wave velocities may be determined with reference points other than the initial arrival.

The interval travel time of the initial *S*-wave arrival determined from the record (a Polaroid picture) shown in Fig. 1*c* was 20.6 ms. The length of the direct travel path in this case was 5.95 m (19.5 ft). Therefore, v_S equaled 289 m/s (947 ft/s). The interval travel time of the initial *P*-wave arrival determined from a second record with an expanded sweep rate (to improve the resolution) was 3.8 ms. For the same path length, the compression wave velocity was 1567 m/s (5137 ft/s). The soil was saturated in this case, and the *P*-wave velocity was really the *P*-wave velocity in water. Also, evaluation of the complete velocity profile showed good agreement among all interval velocities at this depth and no strong velocity contrast nearby. Hence, these velocities represent direct wave velocities at this depth.

Recording Equipment

As seen in Fig. 1*c*, travel time measurements are in the millisecond range and wave frequencies are in the range of hundreds of hertz. The recording device must properly time and respond in these ranges. An oscilloscope is an excellent recording device in these time and frequency ranges. However, it should be calibrated in the field for proper timing (and triggering), as discussed later. Time delays with triggering can also be used, as discussed later, which effectively expand the width of the oscilloscope viewing screen many times.

Filtering of the signal should be minimized because filtering can significantly distort the signal and erroneously alter arrival times.

Although only two receivers are displayed in Fig. 1*c*, four or more receivers can be viewed at one time with an oscilloscope. In addition, photographic records used with oscilloscope recording represent good permanent records.

Other oscilloscopes are available such as digital and enhancement types which may at times significantly improve the records.

Source and Receivers

It can be seen from the record in Fig. 1*c* that the SPT represents a source which is rich in shear wave generation and weak in compression wave generation for horizontal wave propagation. Other research [*13*] has noted that much energy goes into shear energy in SPT. In addition, this source is repeatable and reversible [*11*], although it was not reversed in any of these records.

The record in Fig. 1*c* is also enhanced by properly orienting the receiver.

The SPT generates a horizontally propagating *SV*-wave [*4*]. (Driving a Shelby tube also works well.) Therefore, shear wave monitoring is most appropriate with a vertical receiver under these conditions. In this regard, a horizontal receiver sensing in the direction parallel to the wave path is best for compression wave monitoring.

Crosshole Test with Torsional Source

Recently, a new mechanical source which creates a torsional impulse in the bottom of the source borehole has been developed for use in the crosshole test. A torsional impulsive source has many benefits. By its nature, it is very rich in shear wave generation while generating very little *P*-wave energy. In addition, it is easily handled, is repeatable, and is reversible. Because it is reversible, the polarity of the initial shear wave arrival can be reversed on successive reversed impulses, which enhances positive identification of the initial shear wave arrival [*14*].

With the torsional source, an impulse (twist) is applied above ground and is transmitted down a rod to a base embedded in the soil. Three different bases—a tube, a vane, and a plate—have been studied. These bases along with proper receiver orientation for the crosshole test are shown in Figs. 2*a*, 2*b*, and 2*c* for tube, vane, and plate sources, respectively. A torsional source produces horizontally polarized shear waves (*SH*-waves), and,

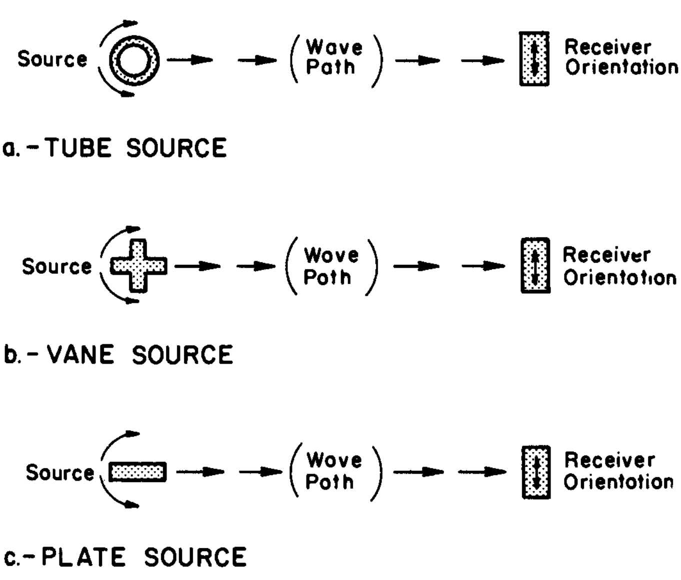

FIG. 2—*Plan view of crosshole shooting with torsional sources.*

therefore, the receiver orientation is horizontal and transverse to the direct-wave path.

Travel time records generated by tube, vane, and plate torsional sources are shown in Figs. *3a*, *3b*, and *3c*, respectively. For each source, receiver signals from both clockwise and counterclockwise torsional impulses are shown on the same record. The initial compression and shear wave arrivals are denoted in Fig. 3 by *P* and *S*, respectively.

The travel time records in Fig. 3 show that the polarity of the initial shear wave arrival is reversed on successive clockwise and counterclockwise torsional impulses for all torsional sources. For the tube source, some compression wave energy is produced, but the polarity of the initial compression wave arrival is not reversed on successive clockwise and counterclockwise torsional impulses. Due to the small amplitude of the compression wave for both the vane and plate sources, it is not readily apparent when the compression wave arrives or if it reverses on successive clockwise and counterclockwise torsional impulses for the receivers displayed.

Direct-wave path lengths for the travel time records shown in Fig. 3 were slightly different for each source. The length was greatest for the tube source and least for the plate source. For this reason, identification of the initial arrival of both the compression and shear wave is different for each source. Calculated shear and compression wave velocities based on these results were each within 5 percent and averaged 165 and 253 m/s (540 and 830 ft/s), respectively.

Oscilloscope sensitivities for the travel time records shown in Fig. 3 were 5 mV/Div. for the tube source and 2 mV/Div. for the vane and plate sources. Comparison of the three different travel time records in Fig. 3 shows that the amplitude of the initial shear wave is greatest for the tube source. Not only was the travel path longer for the tube source, but the oscilloscope sensitivity was less than that used for the vane and plate sources. For these reasons, the tube source is considered superior. However, small signals generated by all these torsional sources with the available torsional impulse would necessitate the use of a signal enhancement oscilloscope or some other type of signal-stacking unit to make travel time measurements over travel paths greater than about 3 m (10 ft) or in a noisy environment.

Wave Velocities

Values of v_S measured in soil typically range from 120 to 430 m/s (about 400 to 1400 ft/s). These values may be measured either above or below the water table. Values of the compression wave velocity, v_P, in soil depend upon the degree of saturation. For dry soil, values typically range from 210 to 760 m/s (about 700 to 2500 ft/s). A similar range for v_P is found for soils with a degree of saturation of 98 percent or less. For saturated soils,

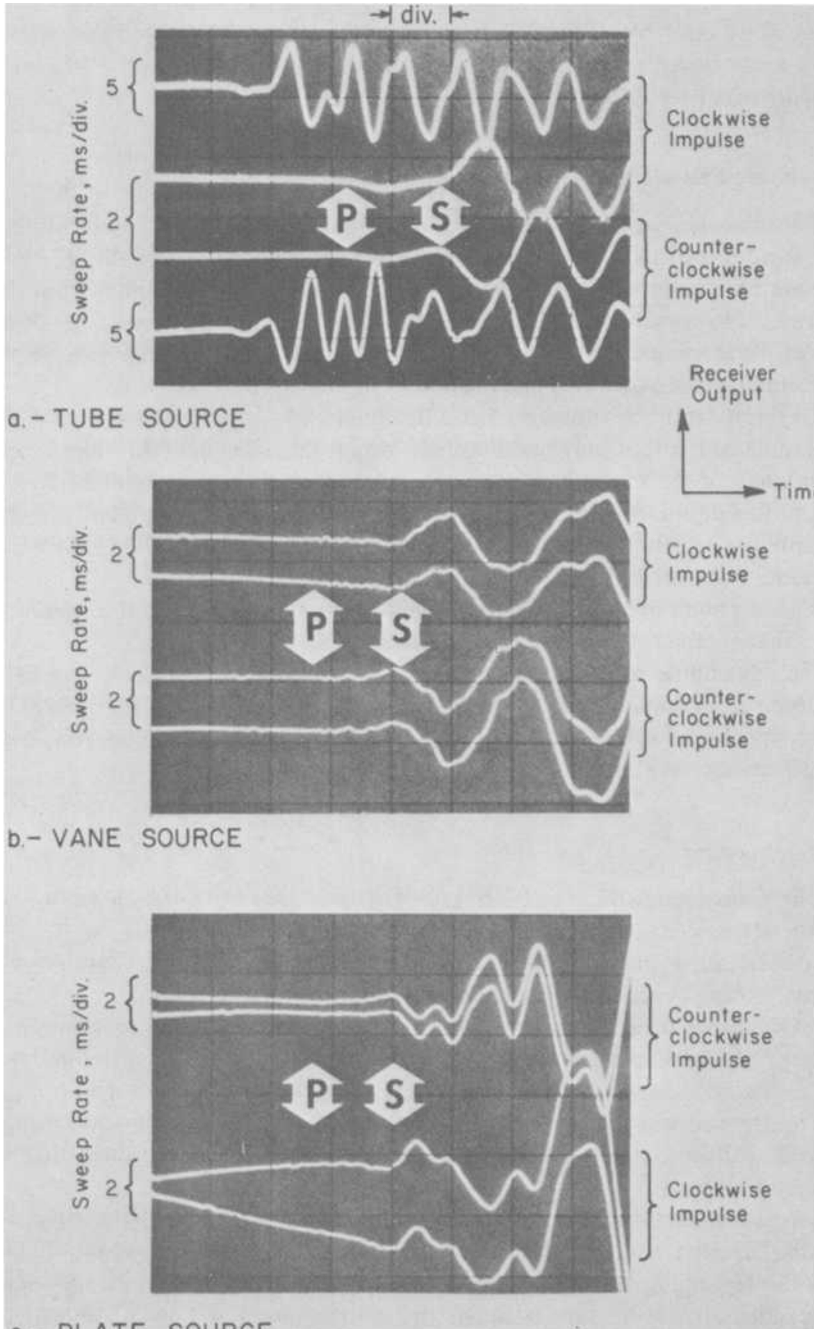

FIG. 3—*Travel-time records for crosshole shooting with torsionally induced shear waves.*

values of v_P are typically 1525 m/s (5000 ft/s). For submerged fills, these soils seem never to be completely saturated [3] and v_p may be 915 m/s (3000 ft/s) or less [15,16].

Downhole Seismic Survey Method

The downhole seismic survey method is also well suited for determining the variation of *in situ* shear wave velocity with depth. With this method the *time* for body waves to travel between the surface and points within the soil mass is measured. Body waves must be either compression or shear waves. Wave velocities are calculated from the corresponding travel time once the distance of travel has been determined.

One important advantage of the downhole test in comparison with the crosshole test is that only one borehole is required. On the other hand, one advantage of the crosshole test is that the wave travel path is almost constant with depth, whereas the wave travel path increases with depth in the downhole test. Both tests have, however, the advantage that lower-velocity material overlain by higher-velocity material may be detected.

The key components in the downhole test are the same as in the crosshole test, that is, the source, receivers, recorder, and trigger.

One downhole measurement system which is regularly used in the field is described herein. Many of the variables and much of the reasoning already discussed in the crosshole test also apply to the downhole test, and this discussion will not be repeated.

Field Procedure

The procedure used in the field is to drill and case one borehole (or more) to the desired depth several days prior to the start of testing. As in the crosshole test, either aluminum or plastic casing with an inner diameter of about 7.6 cm (3 in.) is used, and the casing is grouted in place.

At the same time, a concrete block is cast in place. The block is about a 0.6-m (2 ft) cube and is embedded about 0.6 m (2 ft) into the ground. The block should be located about 6 m (20 ft) from the casing as shown in Fig. 4*a*. (If the source is too close to the borehole, easily identifiable shear wave arrivals will not be seen.) This concrete block is used as the source in the downhole tests.

Two short sections of angle iron are placed in the block at the time of casting. Each section extends about 0.3 m (1 ft) out of the concrete block at a 45 deg angle with the vertical. The sections of angle iron are oriented perpendicular to the line between the source and borehole as shown in Fig. 4*a*.

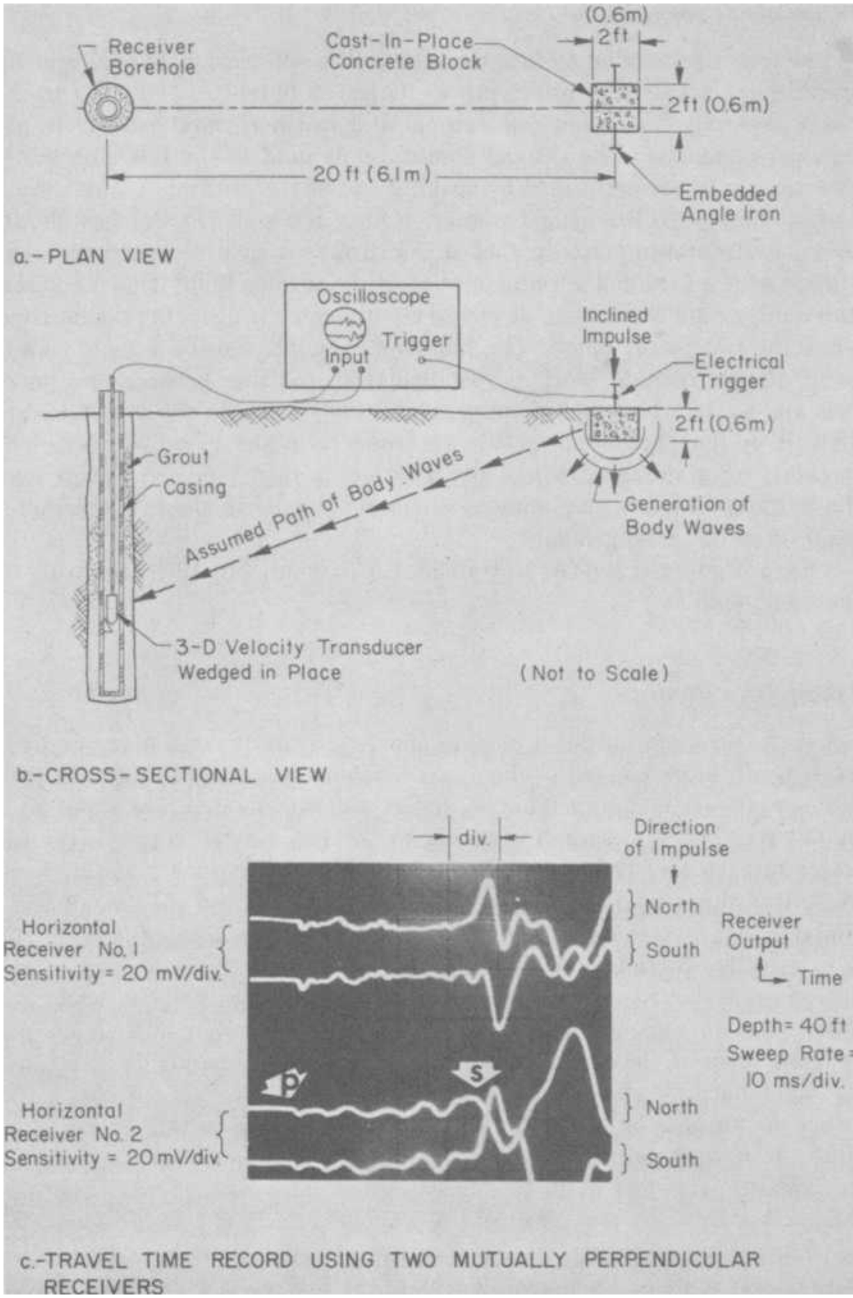

FIG. 4—*Downhole seismic survey method.*

Downhole Shooting in the Field

The test is performed by first wedging a three-dimensional (3-D) velocity transducer package at some depth in the cased borehole. (The 3-D transducer assembly consists of one vertical and two horizontal velocity transducers in one case. The vertical transducer is used in the crosshole test.) The seismic test is performed by striking one of the protruding angle irons with a 4.5-kg (10 lb) sledgehammer. (Other research [*17-21*] has shown that a horizontal impulse applied at the surface is rich in shear wave generation as is a torsional impulse applied at the surface [*22*].) The angle iron and hammer are wired to an electrical circuit which triggers the oscilloscope when the two pieces touch. The hammer blow also causes a slight movement of the concrete block perpendicular to the line between the borehole and source. This movement generates body waves in the soil and their arrivals at the horizontal velocity transducers in the cased borehole are recorded on a storage oscilloscope. The test is then repeated except that the block is struck in the opposite direction. Figure 4*b* shows a schematic diagram of this arrangement.

This procedure is repeated at about 1.5 to 3 m (5 to 10 ft) intervals to the final depth.

Travel Time Record

Results recorded on the storage oscilloscope from the two horizontal velocity transducers wedged in the cased borehole are shown in Fig. 4*c*. This photograph was taken for the transducers wedged at a depth of about 12.2 m (40 ft). The photograph is made up of two sets of traces with two traces in each set. The upper set of two traces is from one horizontal velocity transducer while the lower set of two traces is from the second horizontal velocity transducer. (The transducers were sensing motion in perpendicular directions.) The upper trace in each set represents wave energy generated by striking the concrete block in one direction while the lower trace in each set represents wave energy generated by striking the concrete block in the opposite direction. The vertical location of each trace on the oscilloscope viewing screen was changed between hammer blows.

For the purpose of identifying *P*- and *S*-wave arrivals in this record, consider the bottom set of two traces in Fig. 4*c*. Each trace is composed of three basic parts just as in the records from the crosshole test. The difference between the crosshole and downhole records is evident when the two bottom traces in Fig. 2*c* are compared. Notice that the compression wave energy remains coincident in each of the two traces for hammer blows in opposite directions. Shear wave energy is, however, polarized under these conditions, which results in the initial shear wave arrival reversing in the two traces for hammer blows in opposite directions. The initial shear wave arrival is identified as the beginning of this reversal in energy and is denoted by the S in the figure.

In this manner, S-wave and P-wave travel times are determined at various depths in the borehole. Correct triggering is very important in this procedure because results at each depth are recorded separately. It is possible, however, to use two or more sets of 3-D transducers at known vertical spacings and record these results at once. In this case, true interval velocities are measured and triggering is less important. However, triggering for opposite hammer blows in one data set still should be identical.

In these tests, orientation of the horizontal transducers with respect to the source was not controlled because the transducers were raised and lowered by means of a flexible cable system. This system was used because of its easy operation. If a rigid system was used to place the transducers, then one of the horizontal transducers could have been oriented parallel to the hammer blow, and the S-wave arrival in Fig. 4*c* would have been even more pronounced.

Triggering Systems

Triggering of recording equipment in crosshole and downhole seismic tests seems to be one of the most overlooked parts of these tests in engineering investigations. Triggering is, however, critical to proper time measurements (unless measuring interval velocities with simultaneous monitoring of several detection points). The characteristics of the triggering system in use and how it interacts with the recording device must be thoroughly understood by the user. It should never be assumed that triggering of the recording equipment occurs at the exact instant the impulse is applied.

Typical triggers in use with mechanical sources today are velocity transducers and electrical circuits. The function of these triggers is to produce a voltage change when activated as a result of applying an impulse at the source. This voltage change then starts the timing device some finite amount of time after the impulse. It is not so important that a delay occurs, but it is very important that the length of this time delay be known.

As already shown, a storage oscilloscope is a convenient timing device. A typical storage oscilloscope is pictured in Fig. 5*a*, with the main components, viewing screen, storage controls, signal amplifiers, and time base unit indicated. Since the quantity being measured is time, the most important component is the time base unit. The time base unit of the oscilloscope is pictured in Fig. 5*b*. For triggering purposes the important controls on the time base unit are the level, coupling, and slope selectors, numbered 3, 6, and 7, respectively, in Fig. 5*b*. In this discussion these three selectors are collectively termed "oscilloscope trigger settings" or just "trigger settings." The level and slope selectors determine the voltage level (approximate range +5 to −5 V) and slope (positive or negative), respectively, of the

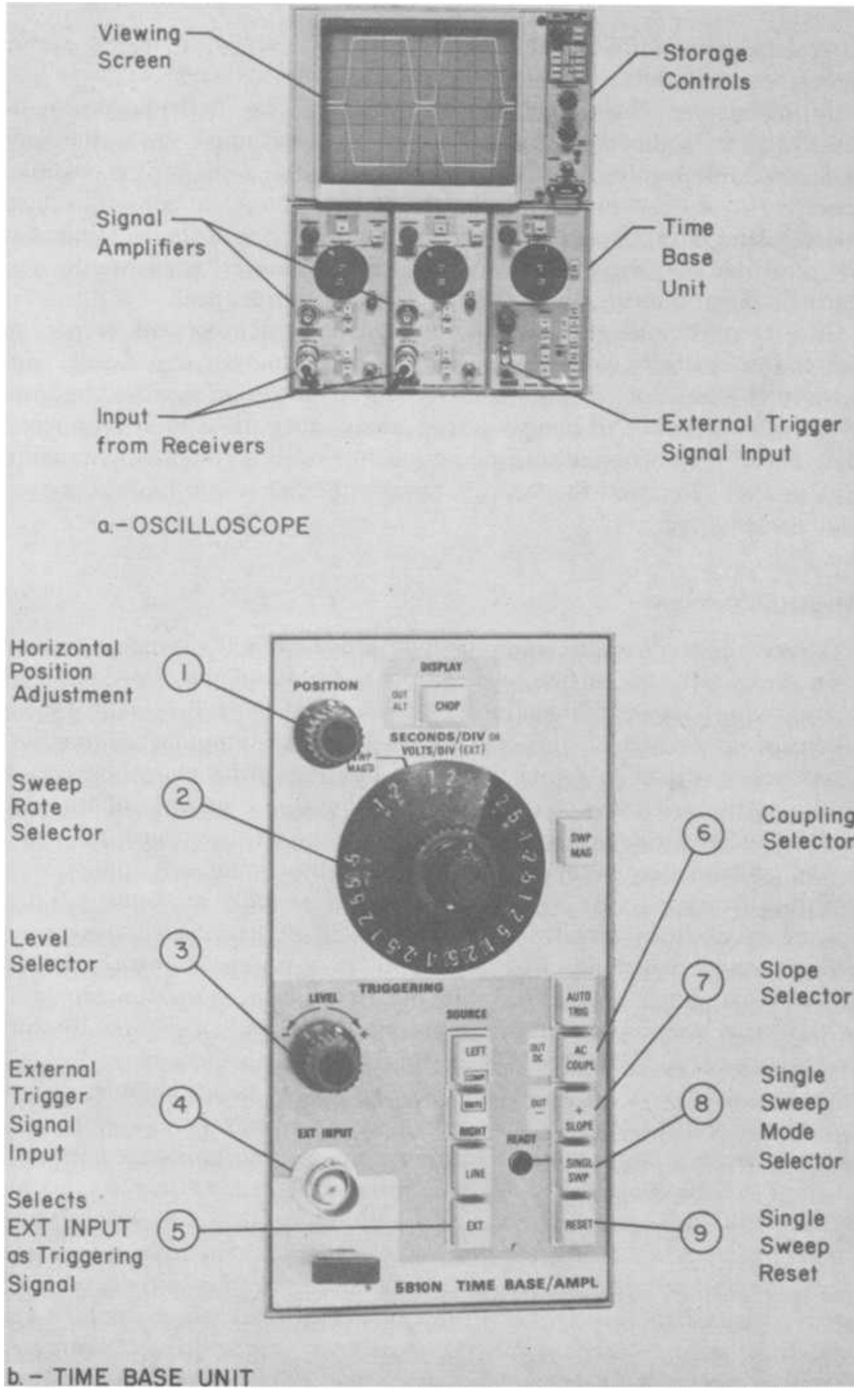

FIG. 5—*Travel-time measuring system.*

triggering signal on which a sweep of the trace across the viewing screen will be initiated. The coupling selector determines whether the trigger signal will be either a-c or d-c coupled. In the a-c coupling mode, any d-c component of the triggering signal is blocked and the mean signal (in the external trigger mode) is taken as the zero level.

Errors in timing occur when, as a result of selected values of level, coupling, and slope, triggering of the oscilloscope occurs some unknown time after the impulse is applied to the source. For discussion herein, correct triggering is defined as less than a 10-μs delay between the time of the impulse and the start of oscilloscope sweep. For *in situ* measurement of v_S with travel paths between 3 and 9 m (10 to 30 ft) and wave velocities less than 430 m/s (1400 ft/s), this definition is valid since the delay time would be less than 0.2 percent of the total measured travel time (neglecting travel time in the rod). However, for *in situ* investigations in rock over travel paths of similar lengths, the delay time associated with correct triggering would have to be much smaller to have a comparable percentage error.

Velocity Transducer Trigger

When a velocity transducer is used as a trigger in the crosshole test, it is typically mounted on the impulse rod somewhere near the application of the impulse as shown in Fig. 1*b*. The applied impulse generates a wave in the impulse rod which excites the velocity transducer. As a result, the transducer produces a signal which triggers the oscilloscope. The time when this signal actually activates the oscilloscope sweep depends on the form of the signal and on the oscilloscope trigger settings.

Delays in triggering with velocity transducer signals using different level and slope settings for a downward impulse are shown in Fig. 6. The velocity transducer in these tests was mounted about 2.5 cm (1 in.) horizontally from the point of application of the impulse. The top trace in Figs. 6*a* and 6*b* is the velocity transducer signal for correct triggering using an electrical circuit trigger. The bottom set of traces in each figure (three traces in each set) is composed of velocity transducer signals from similar impulses except that the transducer signals in these cases were also used to trigger the oscilloscope sweep. The oscilloscope sweep was triggered at different points on the transducer signal waveform because different level settings were used with the time base unit.

Numbers in Figs. 6*a* and 6*b* on the correctly triggered signals show the points at which the oscilloscope sweep was triggered when the transducer signals were used. For a positive slope setting, triggering was delayed approximately 0.8, 0.7, and 0.6 ms for level settings of about +5, ±0, and −5 V, respectively, as shown in Fig. 6*a*. For a negative slope setting, triggering was delayed approximately 0.9, 0.2, and 0.4 ms for level settings of about +5, −0, and −5 V, respectively, as shown in Fig. 6*b*. Delays in

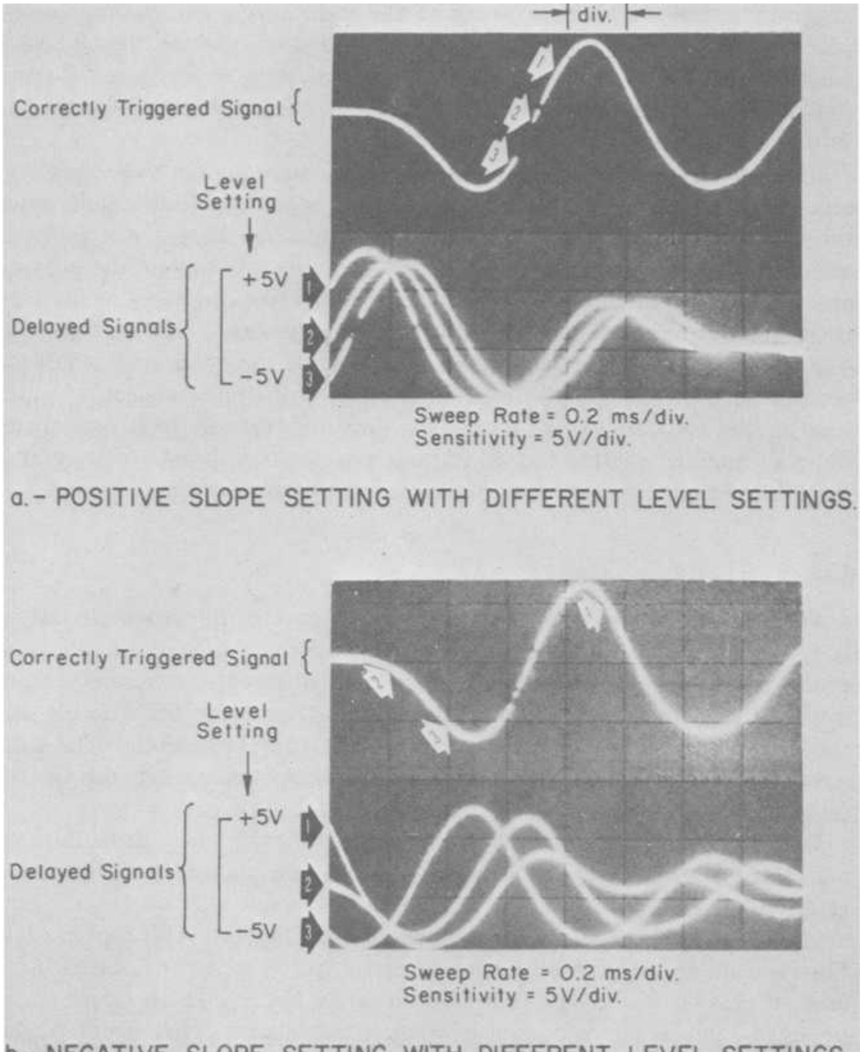

FIG. 6—*Delayed triggering resulting from different time base settings using velocity transducer trigger.*

triggering were essentially the same for either a-c or d-c coupling. These results as well as others with a velocity transducer trigger for different trigger settings are given in Table 1.

With a velocity transducer trigger, the amplitude and frequency of the signal also affect the delay time. The amplitude and frequency of a velocity transducer signal depend, however, on many variables such as (1) impulse characteristics; (2) striking materials; (3) length, diameter, and

TABLE 1—*Delays in triggering oscilloscope.*

Type of Trigger	Impulse Direction	Oscilloscope Trigger Settings: Coupling	Slope	Level, V	Approximate Time Delay, ms	Comments
Velocity transducer ($f_n \simeq 8$ Hz)	down	minor effect	+	+5	0.8	time delay dependent upon amplitude and frequency of velocity transducer signal
				±0	0.7	
				−5	0.6	
			−	+5	0.9	transducer signal dependent upon amplitude and frequency of excitation
				+0	1.1	
				−0	0.2	
				−5	0.4	some delay between time of impulse and initial transducer signal. Delay is amplitude and frequency dependent (In this work, delay ≃ 0.1 ms)
	up		+	+5	0.4	
				+0	0.2	
				−0	1.1	
				−5	0.9	
			−	+5	0.6	pretriggering can be a problem with low level settings and high background noise
				±0	0.7	
				−5	0.8	
RC circuit (shown in Fig. 8*a*)	independent	dc[a]	+	+7	17.0	approximately 10-μs variation depending upon positive voltage level for proper settings
				+0	1.0	
				−0	0.01	
				−7	NT[b]	
			−[a]	0 to 5[a]	<0.01	more than one capacitor discharge can cause inconsistent and unpredictable delays for incorrect settings
				−0	<0.01	
				−5	NT	
		ac	+	+5	NT	delays dependent upon capacitive time constant, RC, for incorrect settings
				±0	11.0	
				−5	1.5	
			−	+5	NT	
				±0	70.0	
				−5	<0.05	
Electrical step trigger (shown in Fig. 9*b*)	independent	dc	+[a]	0 to 5[a]	<0.01	for a-c coupling, delays similar to those for RC circuit
				−0	NT	
				−5	NT	
			−	+5	1.1RC	delays dependent upon capacitive time constant, RC, for incorrect settings
				+0	1.1RC	
				−0	NT	
				−5	NT	

[a]Proper settings for correct triggering.
[b]NT = no triggering.

material of the impulse rod; (4) material on which the impulse rod is resting; (5) distance between impulse application and transducer; (6) rod-transducer coupling; (7) type and size of transducer package, and (8) response characteristics of the transducer. Thus, delays in triggering with a velocity transducer trigger depend on the test configuration. It is expected that these errors could easily double or halve from those given in Table 1 depending on the test configuration. Since the test configuration changes with depth, a variation in delayed triggering might also occur at a single site. It is very important that this triggering system be calibrated in the field.

If triggering was assumed instantaneous, then too short a travel time and too high a velocity are determined when using velocity transducer triggers for source-to-receiver measurements. This error may, however, be small, and it decreases as the actual travel time increases.

One other field problem which can occur with velocity transducer triggers is pretriggering, that is, triggering before the impulse occurs. This can occur in noisy environments, with low level settings, or with a combination of both conditions. When pretriggering occurs, too long a travel time is measured and hence too low a velocity is determined.

RC Trigger

An electrical trigger is thought to be one of the best types of triggers, and a resistance-capacitance (RC) circuit is one of the simplest of these. An RC circuit diagram with the appropriate connections to activate an oscilloscope is shown in Fig. 7*a*. Signals produced by this circuit are shown in Fig. 7*b*. The RC-circuit signal was used to activate the oscilloscope trace which simultaneously displayed the trigger signal. Four different traces are shown which represent the same trigger signal, but as shown in the Fig. 7*b*, the oscilloscope was activated at different times because different trigger settings were used.

The bottom trace in Fig. 7*b* represents correct triggering. The upper three traces were triggered on a positive slope. Numbers on the bottom trace show the points at which the upper three traces were triggered. Delayed triggering of approximately 16, 8, and 3 ms occurred for traces numbered 1, 2, and 3, respectively. These delays differed because different trigger level settings were used. These level settings were about 7, 5, and 2 V for the traces numbered 1, 2, and 3, respectively. The trigger signals for all four traces shown in Fig. 7*b* were d-c coupled.

For this RC circuit, delayed triggering errors from about 1 to 17 ms can occur for d-c coupling and positive slope setting. If the trigger signal is a-c coupled, delayed triggering errors as large as 70 ms can occur with a negative slope setting. For any similar RC circuit, actual delayed triggering errors will depend on the capacitive time constant, which is the product

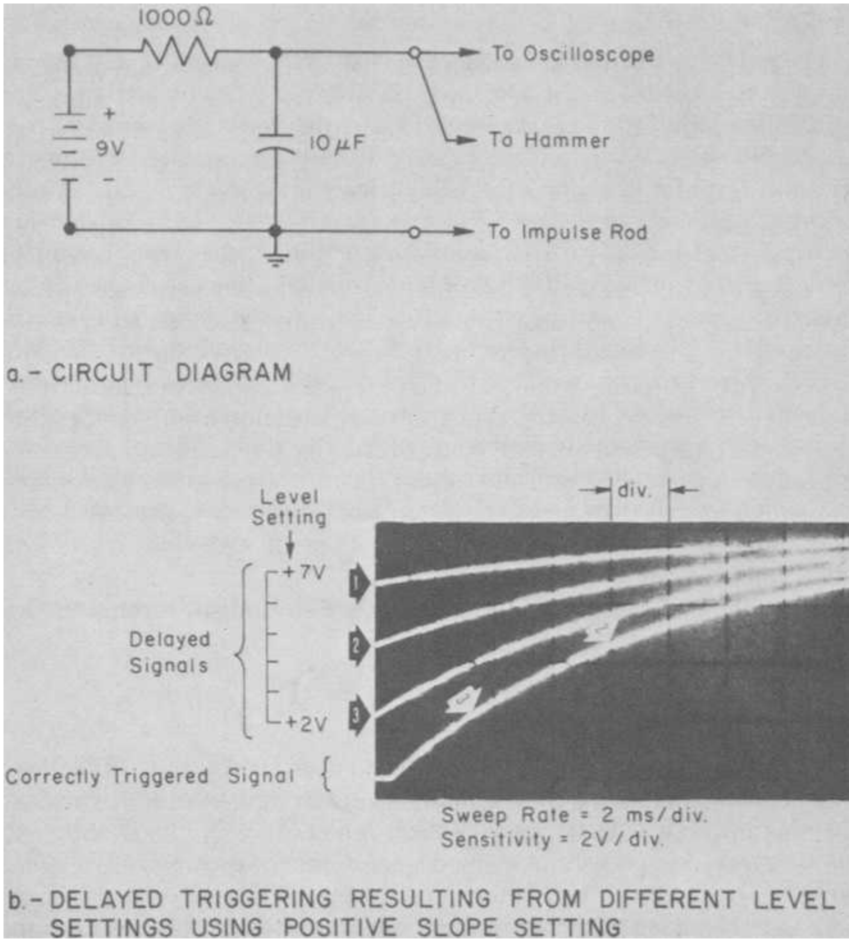

FIG. 7—*RC trigger.*

of the resistance and capacitance in the circuit. The larger the capacitive time constant, the larger would be the delayed triggering errors for both a-c and d-c coupling.

For a negative slope setting with positive level settings and d-c coupling, correct triggering occurs. In this case the trigger behaves as most users assume. These results as well as others are given in Table 1.

Also, the process of applying an impulse to a rod can cause the capacitor in the RC circuit to discharge more than once for any one impulse, resulting in a "noisy" trigger signal. This can cause inconsistent and unpredictable errors for the same trigger setting when a positive slope setting is used.

Step Trigger

The previous discussion has shown that the effectiveness of any triggering system is dependent on how the oscilloscope is set to be activated, and also on the form of the trigger signal. Thus, the signal from an ideal trigger should activate the oscilloscope only if the trigger settings are correct. The d-c signal for one form of an ideal trigger is shown in Fig. 8*a* and the circuit diagram for this "step" trigger is shown in Fig. 8*b*. The rise time for this signal is about 0.1 μs, and, once activated, the signal cannot be retriggered and will remain constant for a period of time determined by the external resistor, R, and capacitor, C. Since an oscilloscope can be activated only by a changing trigger signal, for d-c coupling with this step trigger, correct triggering will occur when the signal is increasing, incorrect triggering will occur when the signal is decreasing, or no triggering will occur. If the time period over which the trigger signal remains at a constant voltage is long compared with the travel time for the generated wave train (say about 1 s), incorrect triggering is obvious because the generated body waves will have past the detection point before the oscilloscope is triggered and hence will not be recorded.

Table 1 shows the response of this trigger, which is highly recommended for field use.

Planned Trigger Delays

Delays in triggering can have a beneficial effect if the value of the time delay is known with sufficient accuracy. A travel-time record for crosshole shooting illustrating this beneficial effect is shown in Fig. 9. The top and middle traces are correctly triggered signals with sweep rates of 5 and 2 ms/Div., respectively. The bottom trace also has a sweep rate of 2 ms/Div., but triggering of the oscilloscope sweep was delayed 10 ms after the impulse was applied. Thus, the middle and bottom traces are the same signal, except the oscilloscope sweep for the bottom trace was delayed 10 ms.

Travel times for initial arrival of both compression and shear waves can be determined only to the nearest 0.5 ms from the top trace. If the sweep rate is changed to increase the sensitivity with which travel time measurements can be made, the middle trace results. Travel times from this trace can be determined to the nearest 0.2 ms, but only the initial compression wave arrival is visible. If the oscilloscope sweep for the middle trace is delayed 10 ms, the bottom trace results. On the bottom trace, both the compression and shear wave arrivals can be determined to the nearest 0.2 ms.

Thus, proper use of delayed triggering can increase the precision and

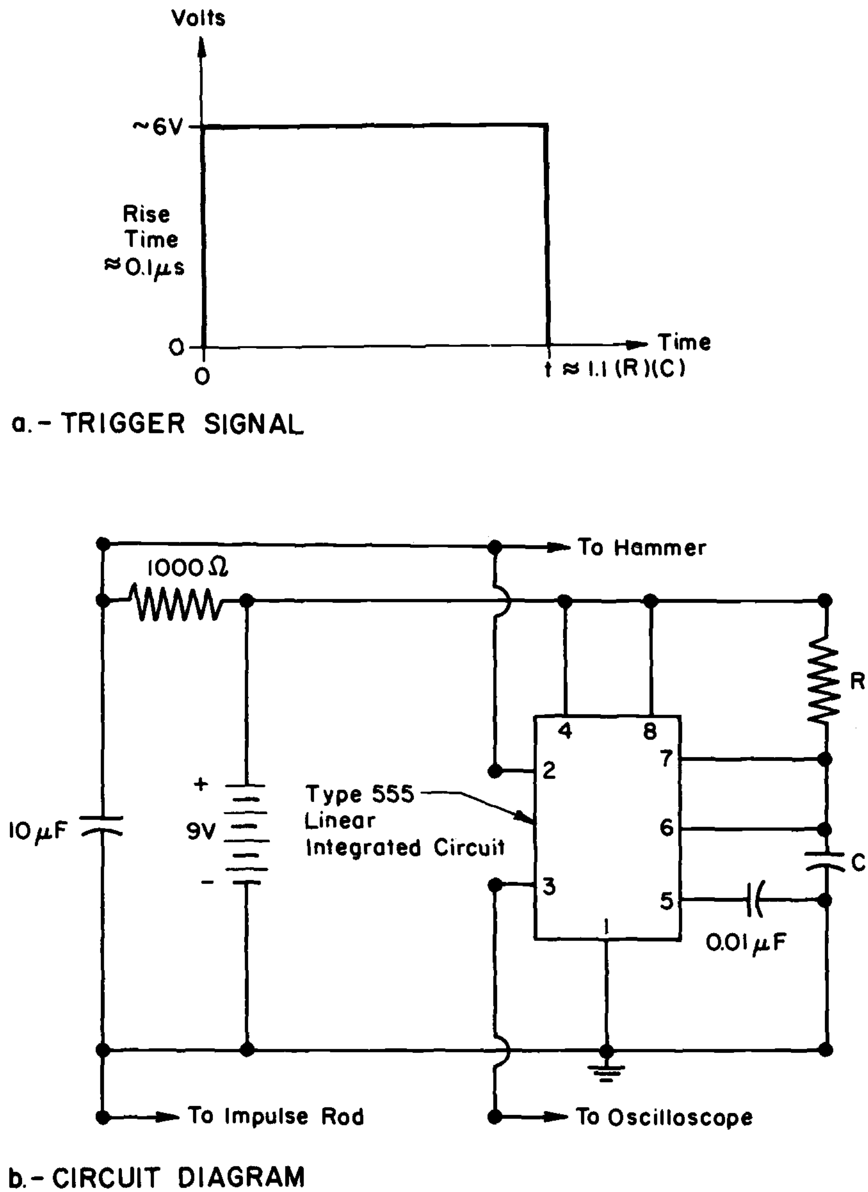

FIG. 8—*Electrical step trigger.*

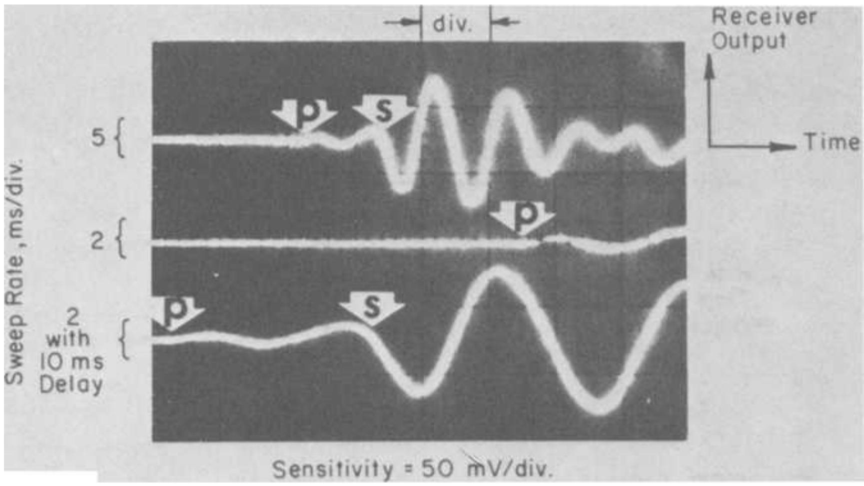

FIG. 9—*Travel-time records for crosshole shooting with delayed triggering.*

resolution with which travel times can be measured. This, in effect, allows the oscilloscope viewing screen to appear much wider than it actually is. This is especially important when the distance from source to receivers is large compared with the distance between receivers as in the downhole test. In addition, when interval travel times are to be measured, triggering of each trace can be delayed independently to further increase timing accuracy.

Field Calibration

In the crosshole and downhole seismic tests, field calibration of the equipment should be performed, at a minimum, at the start and end of each investigation (or each day). Timing and triggering of the recording equipment should be checked. Figure 10 illustrates a typical check. In the upper portion of the record is a square wave calibration signal with which the sweep rate is checked. In the lower portion of the record are three traces with which triggering is checked.

To check triggering, a compression wave is propagated over a known length of impulse rod, and the output of the receiver at the bottom of the rod is displayed. The rod travel time is then determined and compared with the predicted time. Three traces in Fig. 10 show how the measured travel time will depend to some extent on the transducer and transducer package used to make the measurement.

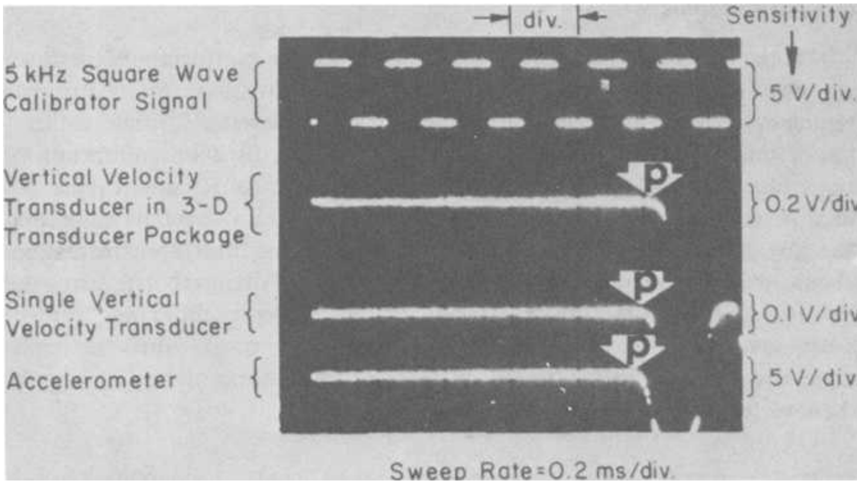

FIG. 10—*Calibration record to check triggering and timing of oscilloscope in the field.*

Conclusions

Crosshole and downhole seismic survey methods can be successfully used to make accurate *in situ* shear wave velocity measurements for engineering purposes. Field procedures for each method which work well are outlined herein.

In the crosshole seismic test, the standard penetration test generates easily identifiable *SV*-waves. A new mechanical torsional source for use in the crosshole seismic test which generates *SH*-waves is also presented. With the torsional source, the initial arrival of the shear wave can be reversed for easy identification. In the downhole seismic test, a reversible embedded source is used which is rich in shear wave generation.

Correct triggering of recording equipment is critical in these measurements. The characteristics of three triggers, a velocity transducer, an RC circuit, and an electrical step trigger, are discussed. The electrical step trigger is the most reliable in terms of correct triggering and is highly recommended for use in the field.

Delayed triggering of a known time interval can improve resolution in measuring *P*- and *S*-wave travel times, especially in the downhole seismic test.

Field check procedures for correct timing and triggering of recording equipment should be performed. Field measurement of borehole verticality is necessary in the crosshole seismic test.

Recommendations

It is recommended that ASTM procedures for performing crosshole and downhole seismic survey tests incorporate provisions for (1) proper frequency response of recording equipment and receivers, (2) field calibration of timing and voltage of recording equipment, (3) field calibration of triggering, (4) field measurement of borehole verticality, and (5) use of three or more boreholes in the crosshole test. It is also strongly suggested that any ASTM procedures consider recommending that (1) a reversible seismic mechanical source be used in the tests, (2) delayed triggering be used if long travel times are measured with an analog oscilloscope, and (3) direct-wave velocities based on source-to-receiver travel times be compared with wave velocities based on interval travel times of initial arrivals whenever possible.

Acknowledgments

The authors would like to thank V. R. McLamore and T. D. Hennon of Fugro, Inc. for suggesting the downhole source, J. R. Hall, Jr., and Y. Cho of D'Appolonia Consulting Engineers, Inc., for suggesting the electrical step trigger, G. Castro of Geotechnical Engineers, Inc. for permission to publish some of the crosshole and downhole records shown herein, and R. F. Ballard, Jr., of the U.S. Army Engineer Waterways Experiment Station for many helpful and constructive comments. Funding from the Bureau of Engineering Research at The University of Texas at Austin, the Fugro Technical Development Program, and the U.S. Army Engineer Waterways Experiment Station Contract No. DACW39-77-M-1554 is greatly appreciated.

References

[*1*] Fry, Z. B., "A Procedure for Determining Elastic Moduli of Soils by Field Vibratory Techniques," Miscellaneous Paper No. 4-577, U.S. Army Engineer Waterways Experiment Station, Corps of Engineers, Vicksburg, Miss., June 1963.

[*2*] Duke, C. M. in *Proceedings,* Fourth World Conference on Earthquake Engineering, Santiago, Chile, 1969, pp. 39-54.

[*3*] Murphy, V. J. in *Proceedings,* International Conference on Microzonation for Safer Construction, Research and Application, Vol. 2, Seattle, Washington, 1972, pp. 131-159.

[*4*] Stokoe, K. H., II, and Woods, R. D., *Journal of the Soil Mechanics and Foundations Division,* American Society of Civil Engineers, Vol. 98, No. SM5, May 1972, pp. 443-460.

[*5*] Mooney, H. M., *Journal of the Geotechnical Engineering Division,* American Society of Civil Engineers, Vol. 100, No. GT8, Aug. 1974, pp. 905-923.

[*6*] Ballard, R. F., Jr., and McLean, F. G. in *Proceedings,* Conference on *In Situ* Measurement of Soil Properties, American Society of Civil Engineers, Vol. 1, Raleigh, N.C., June 1975, pp. 121-150.

[*7*] Ballard, R. F., Jr., *Journal of the Geotechnical Engineering Division,* American Society of Civil Engineers, Vol. 102, No. GT12, Dec. 1976, pp. 1261-1273.

[8] Miller, R. P., Troncoso, J. H., and Brown, F. R., Jr. in *Proceedings*, Conference on *In Situ* Measurement of Soil Properties, American Society of Civil Engineers, Vol. 1, Raleigh, N.C., June 1975, pp. 319-335.
[9] Troncoso, J. H., Brown, F. R., Jr., and Miller, R. P. in *Proceedings*, Sixth World Conference on Earthquake Engineering, Vol. 6, New Delhi, India, Jan. 1977, pp. 165-170.
[10] Shannon and Wilson, Inc., and Agbabian Associates, "*In Situ* Impulse Test: An Experimental and Analytical Evaluation of Data Interpretation Procedures," Report No. NUREG-0028, Nuclear Regulatory Commission, Sept. 1976.
[11] Stokoe, K. H., II, and Abdel-razzak, K. G. in *Proceedings*, Conference on *In Situ* Measurement of Soil Properties, American Society of Civil Engineers, Vol. 1, Raleigh, N.C., June 1975, pp. 422-449.
[12] Grant, F. S. and West, G. F., *Interpretation Theory in Applied Geophysics*, McGraw-Hill, New York, 1965.
[13] Hartman, J. P. and Schmertmann, J. H. in *Proceedings*, Conference on *In Situ* Measurement of Soil Properties, American Society of Civil Engineering, Vol. 1, Raleigh, N.C., June 1975, pp. 190-207.
[14] Schwarz, S. C. and Musser, J. M. in *Proceedings*, International Conference on Microzonation for Safer Construction, Research and Application, Vol. 2, Seattle, Wash., 1972, pp. 593-608.
[15] Richart, F. E., Jr., Hall, J. R., Jr., and Woods, R. D., *Vibration of Soils and Foundations*, Prentice-Hall, Inc., Englewood Cliffs, New Jersey, 1970.
[16] Gibson, F. W., *Journal of the Acoustical Society of America*, Vol. 48, Nov. 1970, pp. 1195-1197.
[17] Jolly, R. M., *Geophysics*, Vol. 21, No. 4, Oct. 1956, pp. 705-938.
[18] White, J. E., Heaps, S. N., and Lawrence, P. L., *Geophysics*, Vol. 21, No. 3, July 1956, pp. 715-723.
[19] Shima, Etsuzo, Yanagisawa, M., and Allam, A., *Bulletin of the Earthquake Research Institute*, Vol. 46, 1968, pp. 517-528.
[20] Shima, Etsuzo, and Ohta, Yutaka, *Bulletin of the Earthquake Research Institute*, Vol. 45, 1967, pp. 19-31.
[21] Beeston, H. E. and McEvilly, T. V., *Earthquake Engineering and Structural Dynamics*, Vol. 5, 1977, pp. 181-190.
[22] Applegate, J. K., "A Torsional Seismic Source," presented in partial fulfillment of the requirements for the degree of Doctor of Philosophy, to the Colorado School of Mines, Golden, Colo., 1974.

V. R. McLamore,[1] *D. G. Anderson,*[1] *and C. Espana*[1]

Crosshole Testing Using Explosive and Mechanical Energy Sources

REFERENCE: McLamore, V. R., Anderson, D. G., and Espana, C., "**Crosshole Testing Using Explosive and Mechanical Energy Sources,**" *Dynamic Geotechnical Testing, ASTM STP 654,* American Society for Testing and Materials, 1978, pp. 30–55.

ABSTRACT: Five crosshole-type seismic surveys, each employing the two commonly used seismic wave generation sources (explosive and mechanical), are studied to evaluate the reliability of each source technique to produce comparable seismic velocities. The study documents field procedures and equipment and discusses seismic wave identification and velocity analysis techniques. Comparison of the resulting velocities (compressional and shear) produced by the two different sources indicates that quite similar results can be obtained when proper field and interpretation procedures are used. General field considerations to be included in a crosshole survey using either source mechanism are discussed as a guide to producing high-quality seismic velocity results. These include the number of borings and their spacing and arrangement, test depth intervals, verticality measurements, hole coupling, orientation of sensors, and measurement of the instant of energy generation.

KEY WORDS: clays, crosshole tests, dynamics, explosives, geophysics, limestone, mechanical, sands, seismic velocities, seismic waves, soils

Crosshole seismic testing is now generally recognized as one of the few reliable methods for obtaining information about seismic velocities, and hence dynamic moduli, of *in situ* soils. Moduli determined on the basis of crosshole tests are used directly during design of machine foundations [*1*][2] and in conjunction with laboratory values of moduli during earthquake and blast response analyses of major structures [*2–5*]. Moduli determined from crosshole test programs have also been used as a basis for predicting settlement of soils [*6*].

Procedures for conducting crosshole tests have been discussed by a number of individuals [*7–14*]. In general the method involves generating seismic waves at a particular depth in one boring (energy hole) and recording the

[1] Senior geophysicist, project engineer, and manager of engineering, respectively, Fugro, Inc., Long Beach, Calif. 90807.

[2] The italic numbers in brackets refer to the list of references appended to this paper.

arrivals of seismic waves at the same depth in one or more other borings (receiving hole). A variety of different mechanisms can be used to generate the seismic wave. In general, they can be grouped into two categories: (1) explosive sources, which include blasting agents, air guns, gas guns, sparkers, and similar devices; and (2) mechanical sources, which include a hammer striking a pipe that extends from the surface to the bottom of a boring [*9*], downhole devices involving mechanical hammers [*14*] or vibrators [*13*], and falling weights that drop onto the bottom of borings [*15,16*].

Within the engineering profession, there are some controversies regarding the reliability of each type of source to produce meaningful results. It is generally agreed that explosive sources produce well-defined compression wave (*P*-wave) arrivals, but the arrival of the slower traveling shear waves (*S*-waves) are less obvious. Hence, there is some question as to the ability of the explosive method to produce accurate *S*-wave velocities. Although mechanical sources produce clearly definable *S*-wave arrivals with more consistency than the explosive source, *P*-wave arrivals are not as distinct and can be subject to question. There is also some concern that the frequency content from the two sources may be significantly different, thereby influencing velocity determinations because of emergent arrivals of low-frequency energy or dispersion within the materials.

Over the past several years the authors have been involved in a number of crosshole tests in which both explosive (blasting agent) and mechanical (hammer-drill rod) procedures were used to initiate seismic waves. In order to clarify the reliability of the two methods, five of these surveys from four sites were selected to compare values of *P*- and *S*-wave velocities determined by each source method. The study considers factors of interest to practicing geotechnical engineers and geophysicists. These factors include the ability to identify wave arrivals, the analysis of travel-time data, and conditions and techniques which affect the quality of wave arrivals. The study provides support to the suitability of both techniques for obtaining comparable velocity data.

Site Characteristics

Four sites were involved in this comparative study. At three sites, data from a single crosshole survey were evaluated. At the fourth, data from two surveys were evaluated. Each site was the proposed location of a nuclear power station. It was necessary, therefore, to assure that *P*- and *S*-wave velocities were accurate. This consideration justified the expense of performing surveys with each type of source mechanism and the use of multiple receiving holes to increase the statistical reliability of the velocities. It also required that the verticality of each boring be determined.

Soil profiles for the four sites differed considerably. One of the sites was composed primarily of dense sands and gravels; two were layered sands and clays, and the fourth consisted of cemeted sands overlying clayey sands and weathered marine limestone.

Field Procedures and Data Interpretation

General procedures utilized when performing the crosshole studies and evaluating *P*-wave and *S*-wave records are described in the following.

Array Configuration

Linear arrays, or versions of linear arrays, were used for all but the mechanical source survey at Site E, as shown in Fig. 1. Spacing of receiver holes for each unit varied from less than 6 m (20 ft) to more than 15 m (49 ft); thus refracted waves could be detected while average seismic velocities for the sites were being established. Borings within the crosshole surveys extended from 60 to 150 m (200 to 490 ft) below the ground surface, although the comparative study was performed only for the upper 30 to 60 m (100 to 200 ft). Borings for the receiving geophones and explosive source were drilled and cased prior to conducting the crosshole tests. Casings were grouted with a cement mixture in Surveys A, B, C, and D, but were sand packed in Survey E. Either thick-walled plastic (PVC) pipe or steel pipe was used for casing. The steel casing was used for source holes during explosive tests because it could withstand numerous shots per depth interval without being destroyed. Plastic casing was typically used for receiving holes because of its lower cost. Each boring was surveyed for verticality using magnetic or gyro-type well survey systems. Table 1 summarizes observed drifts and directions in each boring as well as type of casing.

Explosive Crosshole Tests

Explosive crosshole tests were conducted using seismic blasting caps and small explosive charges such as Water Work Boosters and Detaprimers, both trade names of E. I. Dupont Co. Caps were lowered to the depth of interest and detonated with a battery-actuated, condenser-discharge blaster system. Seismic caps are only about 25 by 5 mm (1 by 0.2 in.) in size and weigh less than about 100 g (3.5 oz); hence, a weighted steel holder was used to provide sufficient weight to be sure the cap reached the desired depth in the boring.

The size of charge used during a test depended on the test depth and the water table location. At most sites, a single seismic cap was sufficient to produce *P*- and *S*-wave energy over distances of 30 m (100 ft) or more at depths below the water table. Above the water table and especially in the upper 10 m (33 ft) or so, *P*-wave energy attenuated more rapidly; there-

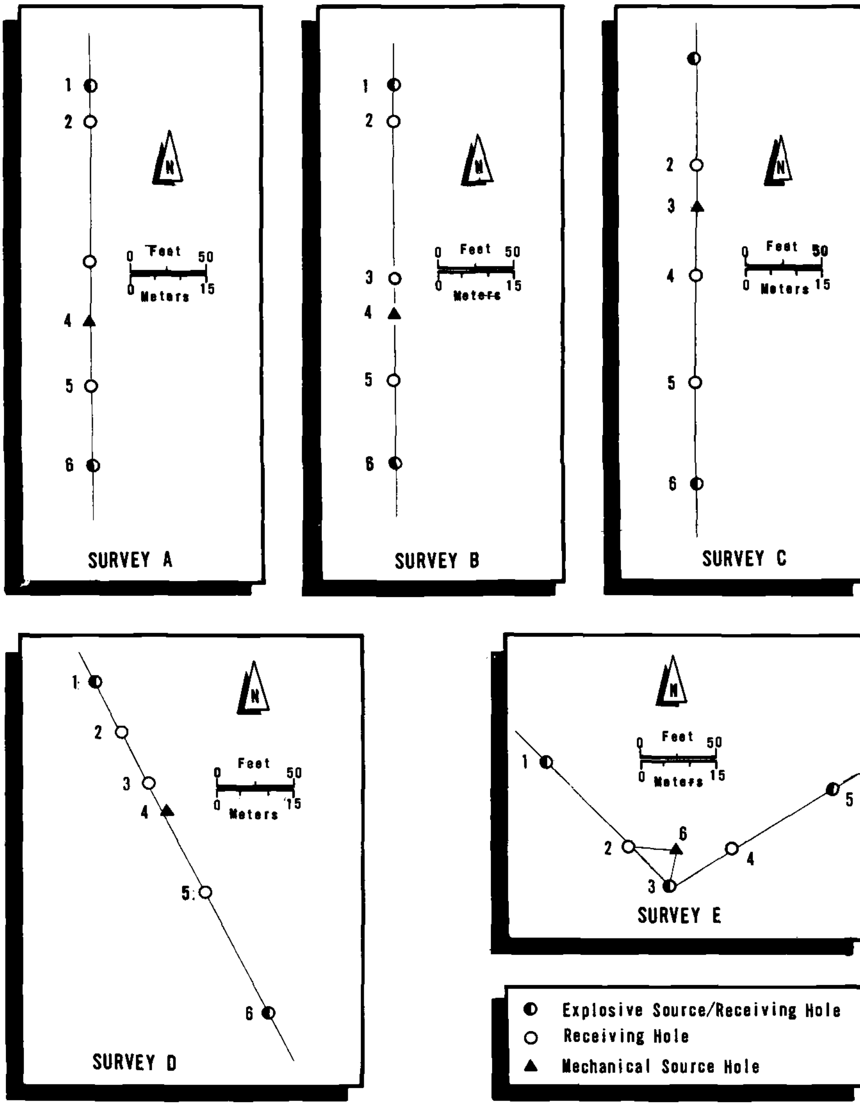

FIG. 1—*Plan views of crosshole arrays.*

fore, *P*-wave recordings often required much larger charges. Such larger-sized charges frequently generated high levels of air waves and reverberations that interfered with *S*-wave measurements. Thus, it was often necessary to shoot separate, different-sized shots to obtain both *P*- and *S*-wave recordings above the water table.

TABLE 1—*Verticality and casing data.*

Survey	Boring Number	Hole Type	Casing	Deviation: Bottom of Comparative Study: Depth ft[a]	Deviation: Bottom of Comparative Study: Drift, ft, direction	Deviation: Bottom of Hole: Depth, ft	Deviation: Bottom of Hole: Drift, ft, direction
A	1	R,[b] SE[c]	S[d]	200	3.8 SW	500	28.6 NW
	2	R	PVC[e]	200	0.4 NW	483	4.0 SW
	3	R	PVC	200	3.5 W	480	12.0 W
	4	SM[f]	S	200	1.5 W	200	1.5 W
	5	R	PVC	200	3.6 NW	250	5.5 NW
	6	R, SE	S	200	1.4 S	493	8.3 E
B	1	R, SE	S	180	0.8 W	500	10.4 W
	2	R	PVC	180	2.8 NE	500	5.9 SE
	3	R	S	180	1.4 W	500	27.7 NW
	4	SM	PVC	174	1.6 NW	174	1.6 NW
	5	R	PVC	180	4.8 SW	500	30.8 SW
	6	R, SE	S	180	3.6 W	480	16.3 SW

C	1	R, SE	S	160	0.7 S	350	1.6 E
	2	R	PVC	160	0.2 NW	357	3.1 NW
	3	SM	S	150	2.7 SW	150	2.7 SW
	4	R	PVC	160	2.1 NW	339	20.1 SW
	5	R	PVC	160	5.5 SW	350	7.2 SW
	6	R, SE	S	160	1.9 W	340	7.6 SW
D	1	R, SE	S	100	0.6 E	300	2.0 E
	2	R	PVC	100	0.4 N	300	3.6 NE
	3	R	PVC	100	1.7 SW	429	18.3 SW
	4	SM	S	90	1.3 SE	90	1.3 SE
	5	R	PVC	100	2.0 SE	300	12.8 SE
	6	R, SE	S	100	1.1 SE	280	2.7 SSE
E	1	R, SE	S	130	2.4 N	210	—
	2	R	PVC	200	3.0 S	229	3.0 SW
	3	R, SE	S	200	7.6 NW	210	7.7 NW
	4	R	PVC	200	10.8 NW	219	11.3 NW
	5	R, SE	S	132	2.8 NW	210	3.0 NW
	6	SM	S	148	4.2 N	205	4.2 N

[a] 1 ft = 0.305 m.
[b] R = receiving.
[c] SE = source-explosive.
[d] S = steel.
[e] PVC = polyvinyl chloride.
[f] SM = source-mechanical.

Mechanical Crosshole Tests

Mechanical crosshole tests utilized the hammer-drill rod (Stokoe-Woods) procedure. In this method a boring was advanced to the depth of interest by rotary-wash drilling methods and the drill bit or sampler was left at the bottom of the hole. Horizontally propagating, vertically polarized *S*-waves were then induced by striking the drill bit vertically with a 4-kg (8.8 lb) hammer. The instant of hammer contact with the drill rod was used to initiate the timing process. The contact completed an electrical circuit which included a galvanometer in the recorder and a battery. For most of the surveys, a geophone (velocity-sensitive transducer) was emplaced at the bottom of the drill rod to record the instant that energy arrived. This instant was used as the starting point for measuring wave travel times.

Recording Equipment

Three-component packages containing Mark Products geophones were used to detect wave arrivals at receiving holes. One of the geophones in the package was oriented vertically and the other two horizontally in mutually perpendicular directions. These geophones have a natural frequency of 4.5 Hz, and their response is relatively flat from approximately eight to several hundred Hertz. Each three-component geophone package was pushed firmly against the casing wall at the test depth by a flat spring.

An SIE recording oscillograph was usually used to record the signals from the geophones. However, for the mechanical tests in Survey E, a Tektronix storage oscilloscope and Polaroid camera were used. When both *P*- and *S*-wave arrivals were desired, data from each depth were obtained at two or more instrument gain settings to enhance the distinction of *P*- and *S*-wave arrivals. Higher gain settings were generally required for *P*-wave detection.

Wave Identification

Traces from each test were evaluated to determine *P*- and *S*-wave arrivals. The *P*-wave arrival typically was marked by the first sharp offset of the recorded traces, as shown in Figs. 2 and 3. These records were obtained below the water table using an explosive source. This type of record was not always the case. Figures 4 and 5 show records obtained above the water table from explosive sources and Figs. 6 through 9 show records for the mechanical source. Compared with Figs. 2 and 3, the onset of *P*-waves in Figs. 4–9 was less evident due to either noise on the traces, lower signal amplitude, or lower frequency.

The *S*-wave arrival for the explosive source was identified by the increase in signal amplitude and an apparent decrease in frequency content as shown in Figs. 2–5. Because of *P*-wave interference, the exact onset of the *S*-wave

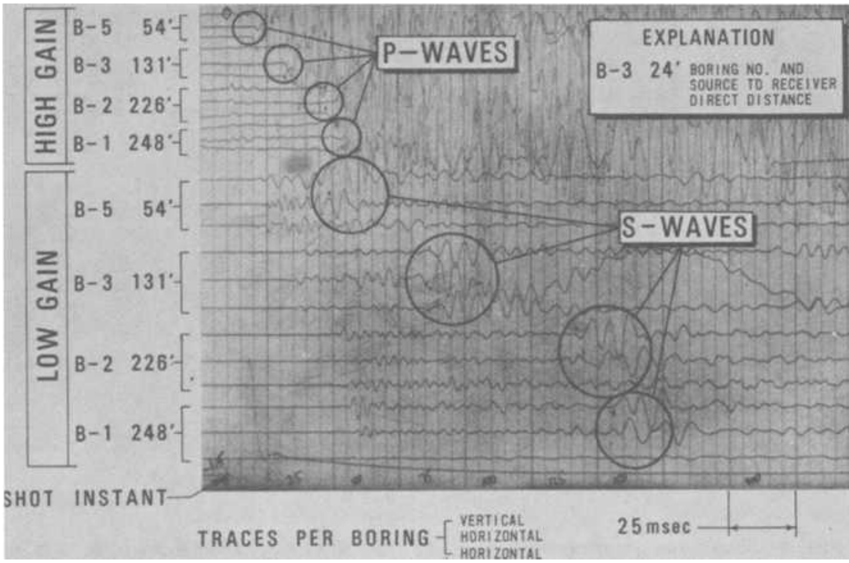

FIG. 2—*Seismogram from explosive source (2 caps). Survey A, below water table (1 ft = 0.305 m).*

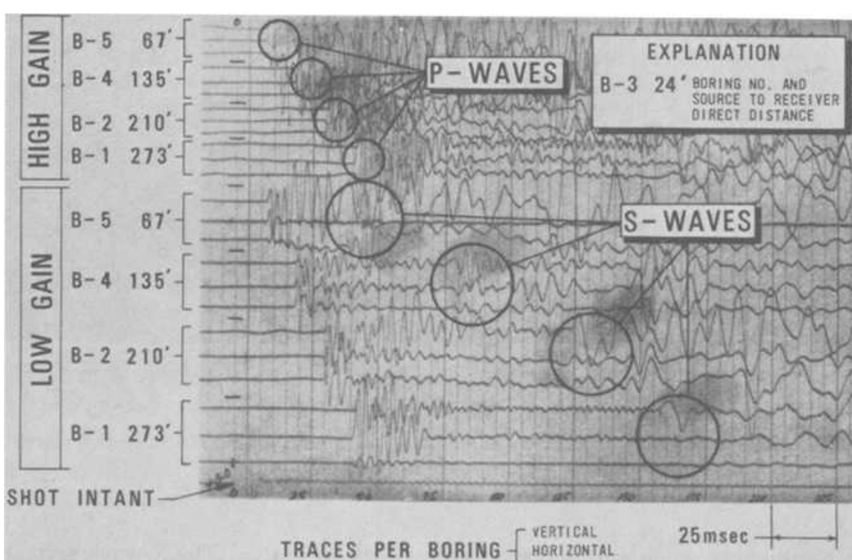

FIG. 3—*Seismogram from explosive source (1 cap). Survey C, below water table (1 ft = 0.305 m).*

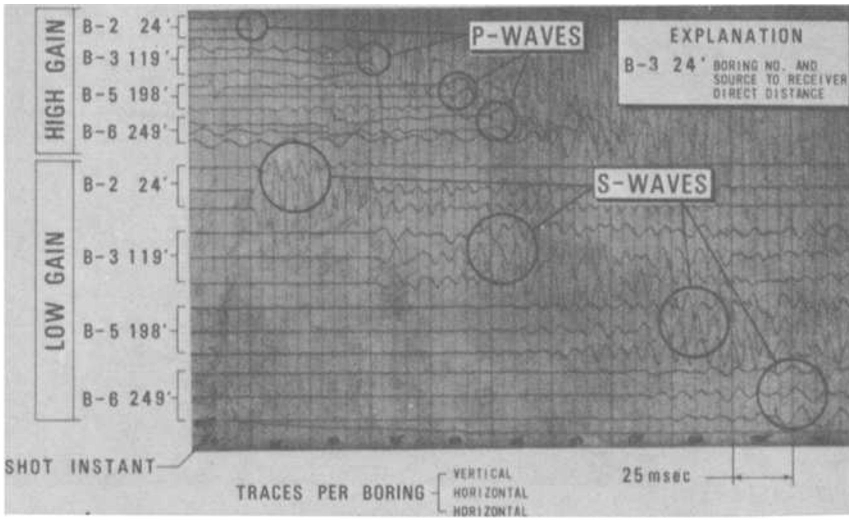

FIG. 4—*Seismogram from explosive source (1 cap). Survey A, above water table (1 ft = 0.305 m).*

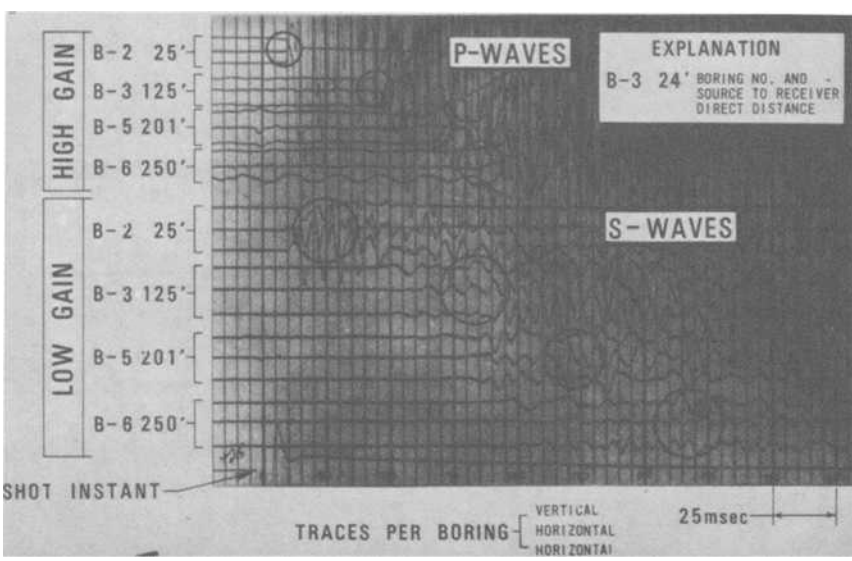

FIG. 5—*Seismogram from explosive source (1 deta prime). Survey B, above water table (1 ft = 0.305 m).*

was subject to some ambiguity on many of these traces. The *S*-wave arrival for the mechanical source (Figs. 6-9) was identified by noticeable change in amplitude after the *P*-wave arrival. Ambiguity still existed at times regarding the actual onset of the *S*-wave due to the low-frequency content of

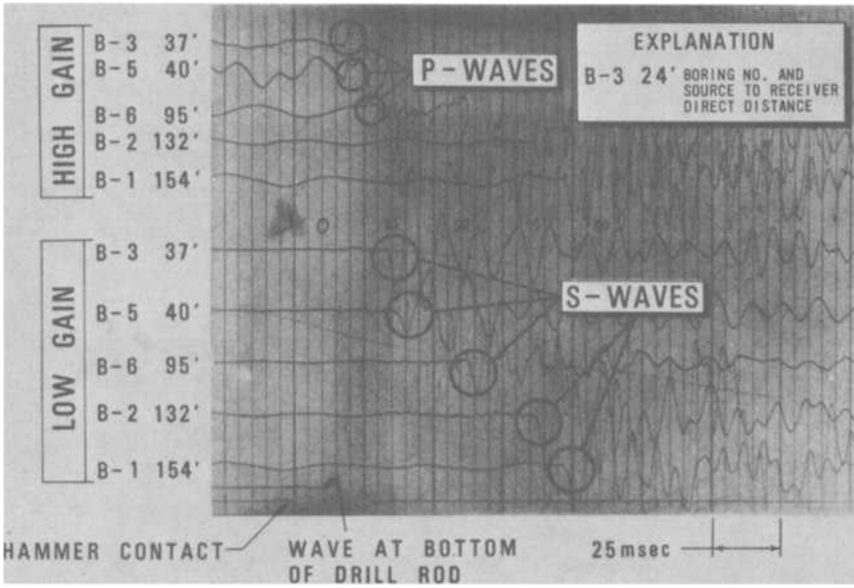

FIG. 6—*Seismogram from mechanical energy source. Survey A, below water table (1 ft = 0.305 m).*

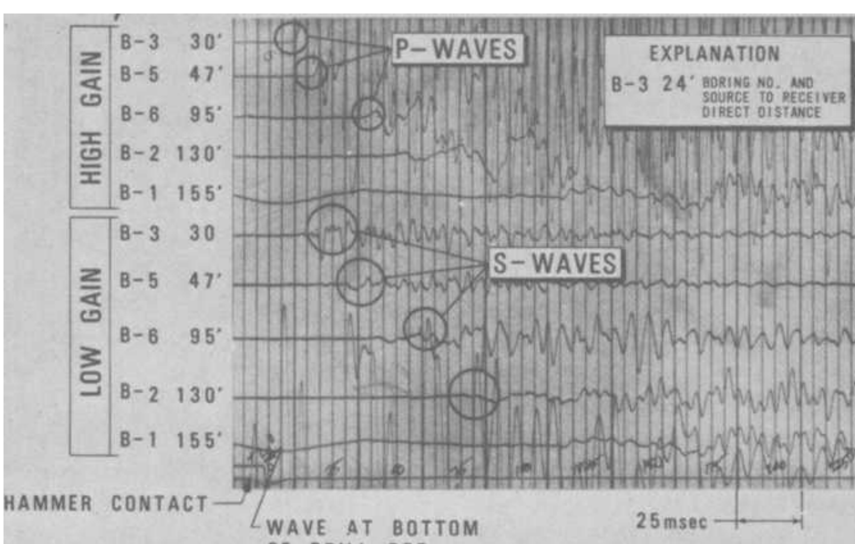

FIG. 7—*Seismogram from mechanical energy source. Survey B, above water table (1 ft = 0.305 m).*

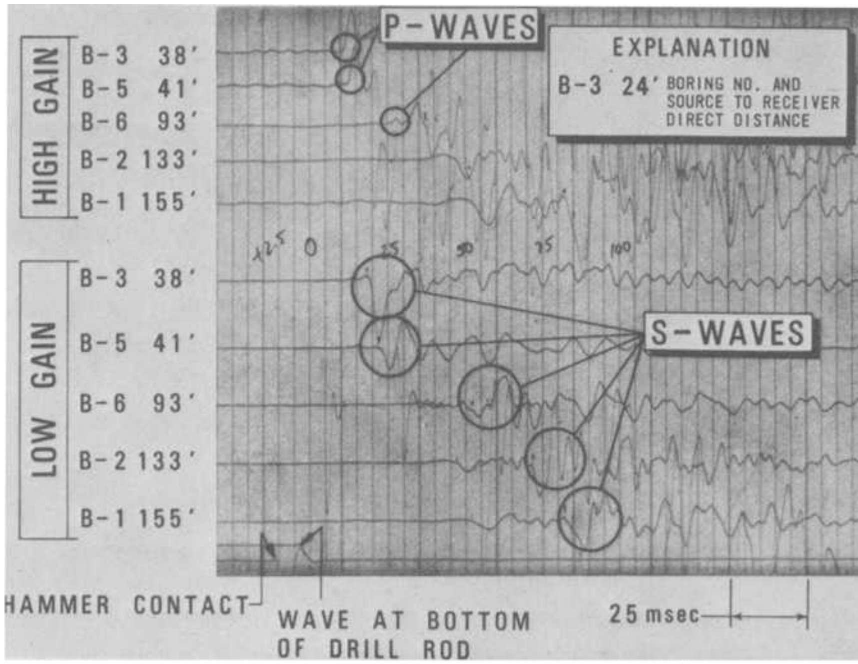

FIG. 8—*Seismogram from mechanical energy source. Survey A. above water table (1 ft = 0.305 m).*

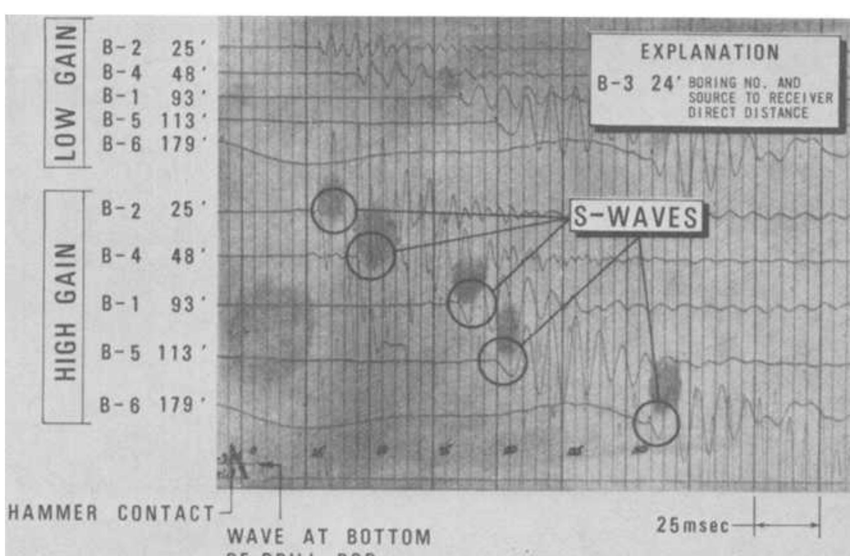

FIG. 9—*Seismogram from mechanical energy source. Survey C, above water table (1 ft = 0.305 m).*

the waves and some P-wave interference effects. In these cases, errors in arrival times of about a millisecond or so could have been made depending on the actual point selected.

Velocity Analysis

Most of the velocity analyses were based on the "interval velocity" concept. In this method it is assumed that the seismic waves traveled along a straight line, and, by monitoring wave progress at different points along the line, each observation point could be considered a new origin and the time to reach the point could be ignored. The velocity could then be based on the time taken for a wave to travel across the line to a succeeding observation point rather than from the time between a source and a receiver.

The data from each test level were plotted on time-versus-distance graphs such as that shown in Fig. 10. When a single line could readily be drawn through all points, as was the case in Fig. 10, a best-fit line was calculated through the data points by least-squares regression. The velocity for the waves was determined by the inverse slope of the best-fit line. Since this process did not require the origin time, this was in a sense a form of "interval velocity" analysis. For each test depth, data from mechanical and explosive borings were plotted from the same origin so that systematic differences between the sources could be identified. If a best-fit line passed through the origin, as in Fig. 10, it was concluded that: (1) no significant error had been made in determining the instant of energy generation; (2) the initial onset of wave arrivals had been correctly identified; and (3) data were not significantly affected by refraction.

In cases where the onset of the waves could not be clearly established, a prominent portion of the wave form, such as the first peak or trough, was timed. Although time-distance graphs using these times were similar to Fig. 10, the best-fit line crossed the ordinate above the origin. In this case the distance above the origin gave a measure of the time between actual onsets of the waves and prominent portions that were timed.

Cases of refraction were identified when a single straight line could not readily be passed through all data points as shown in Fig. 11. In this illustration, it was interpreted that data beyond a distance of 15 m (49 ft) had resulted from waves that had refracted along a higher-velocity layer. The only direct, or unrefracted, data available were from the nearest geophones to each source boring, and no "interval times" were available for the direct waves.

Comparison of Velocity Data

Comparisons of P- and S-wave velocities obtained from the two energy sources are presented in Figs. 12 through 16. Velocities from the mechanical

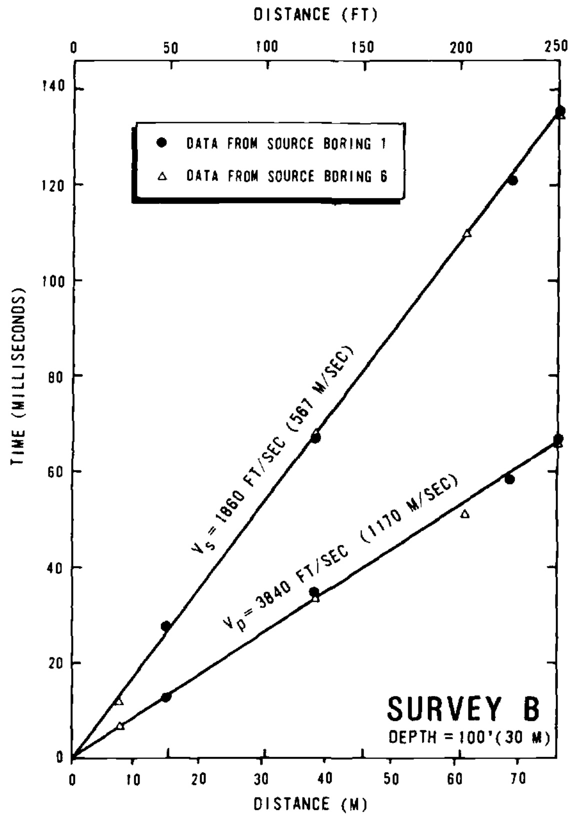

FIG. 10—*Graph of time-distance data where no refraction occurred.*

source are plotted as triangles in these figures; circles denote velocities from explosive sources. For most of the plotted velocity values, vertical bars are drawn to show the width of the 95 percent confidence interval. These bounds are established by performing least-square fits through travel-time data. Bars were omitted when less than four data points were available at a given depth interval, except for the mechanical results from Survey E, where only two values were available. The two triangles at each level in Fig. 16 represent the two measured values.

Evaluation of Velocity Comparisons

The comparative study presented in Figs. 12-16 involved five separate surveys in which over 1700 P- and S-wave measurements were made in the upper 60 m (200 ft) of four distinctly different soil profiles. It was evident

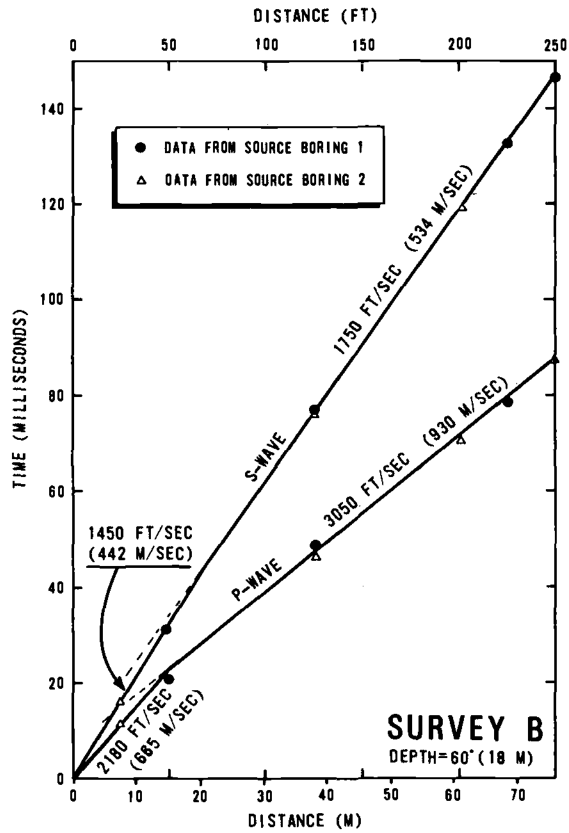

FIG. 11—*Graph of time-distance data where refraction occurred (1 ft = 0.305 m).*

from the data comparisons that velocities obtained by using both source mechanisms were more or less the same; nevertheless, certain differences were noted from case to case, as discussed in the following.

Average Velocities and Data Scatter

Velocity comparisons indicated that average *S*-wave velocities obtained from the mechanical and explosive source mechanisms agreed very well. In general the difference between the two values was less than 5 percent, and this is within the statistical accuracy of the tests. The poorest *S*-wave comparison occurred for Survey E, where identification of *S*-wave arrivals from the explosive source was particularly ambiguous. This was due to many secondary arrivals resulting from reflections and refractions introduced by heterogeneities in the material. At this site, *S*-wave data from the mechanical

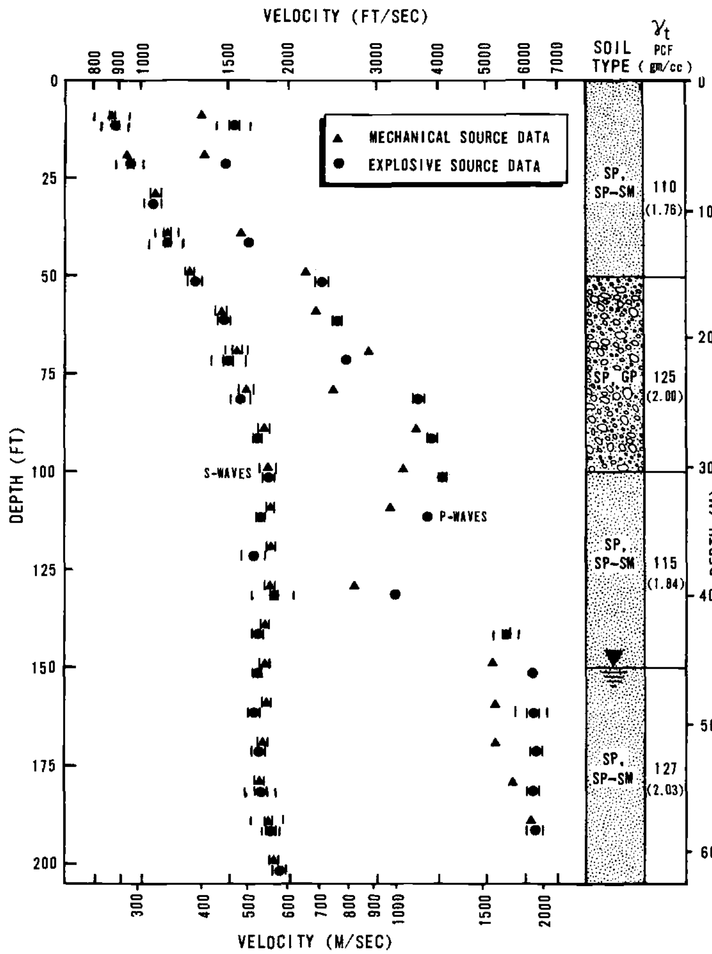

FIG. 12—*Seismic velocities obtained from Survey A (1 ft = 0.305 m).*

source were obtained in only two receiving borings, and therefore the statistical reliability of the data was low. Scatter of *S*-wave data for the surveys varied from case to case, but generally the explosive method defined larger bounds than the mechanical. For all but Survey E, the 95 percent confidence level in data was within ±6 percent of the best-fit velocities and in most cases was within 3 percent. For Survey E the bounds approached 30 percent in some cases. The large bounds in Survey E were attributed primarily to the difficulties associated with identifying *S*-waves, as noted previously. Because casings were sand-packed in this survey, however, coupling may not have been as good and thus more data scatter occurred.

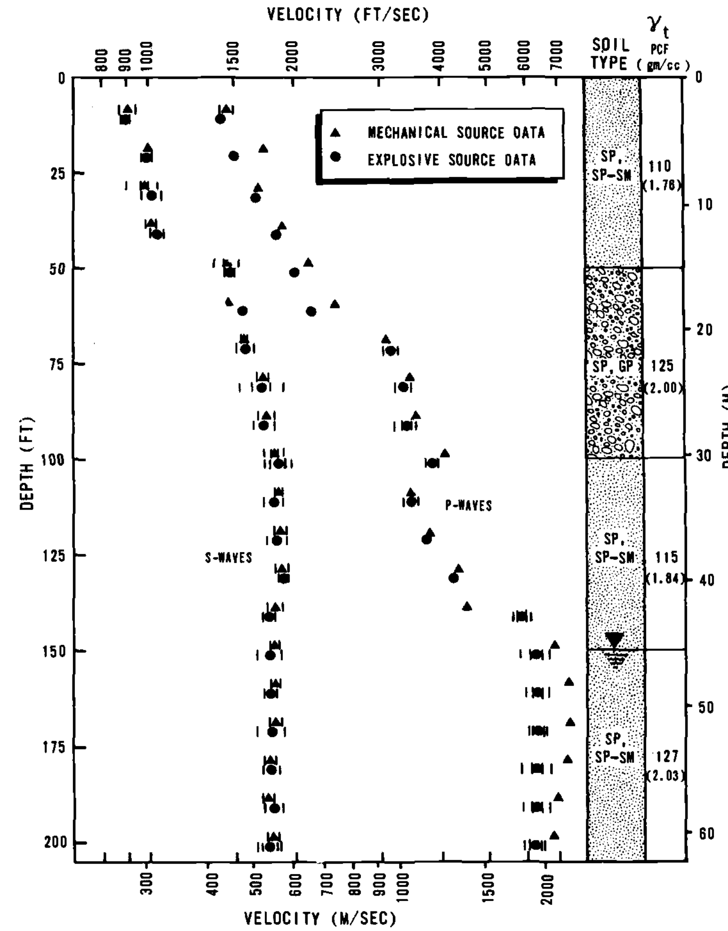

FIG. 13—*Seismic velocities obtained from Survey B (1 ft = 0.305 m).*

P-wave velocities determined by the two methods generally differed by more than the *S*-wave velocities. This is particularly true for Survey A (Fig. 12), where average *P*-wave velocities from the mechanical source were 15 to 20 percent lower than those from the explosive source. For this case the shapes of the two *P*-wave velocity profiles were very similar. It is thought that the differences between the two resulted because the *P*-wave signal from the mechanical source attenuated to such a degree that initial arrivals were not detected. At Survey B (essentially the same site as Survey A), the comparison between *P*-wave velocity values was much better. In both surveys the mechanical *P*-wave velocities were based on only one or two

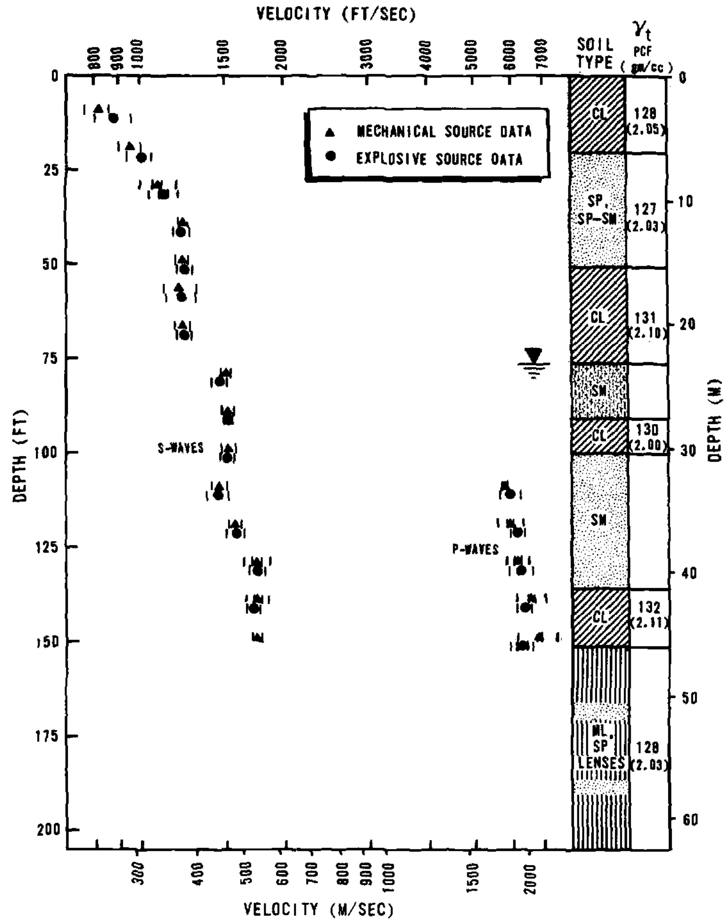

FIG. 14—*Seismic velocities obtained from Survey C (1 ft = 0.305 m).*

traces. The difference between Surveys A and B may have been caused by the shorter distance between the mechanical source hole and the closest receiving hole at Site B. This could have produced a sufficiently better signal-to-noise ratio which permitted a more accurate identification of the wave arrival. *P*-wave velocity comparisons were not made at Survey C because of the lack of usable *P*-wave data from the mechanical source.

The close comparison of the *S*-wave velocities and poorer comparison of the *P*-wave velocities from the mechanical and explosive source mechanisms must be attributed in part to the intent of the surveys. Mechanical methods were used to obtain more definitive *S*-wave velocities above the water table, where the explosive records frequently have a low signal-to-noise ratio. No

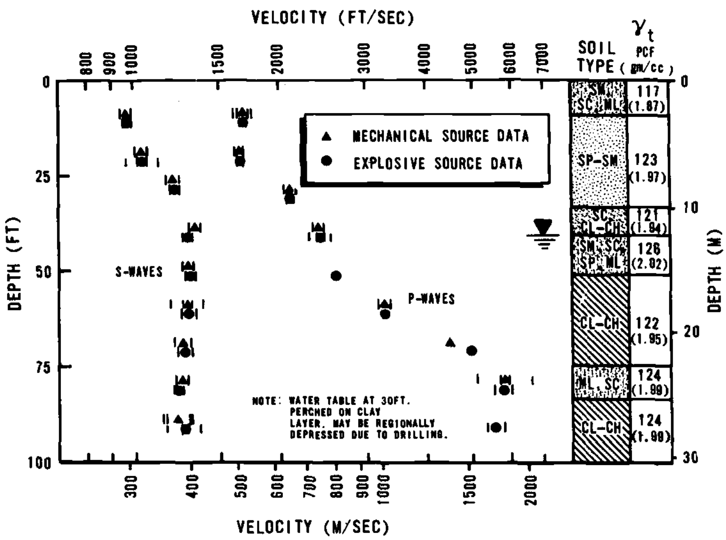

FIG. 15—*Seismic velocities obtained from Survey D (1 ft = 0.305 m).*

special field effort was made to obtain *P*-waves during the mechanical source measurements; hence, greater differences in the *P*-wave comparisons would have been expected.

Signal Characteristics

The characteristics of the seismic waves from the explosive and mechanical sources were observed to differ in two respects. First, the explosive source produced a high signal-to-noise ratio (SNR) for the *P*-wave but a relatively low SNR for the *S*-wave. For this discussion, SNR is defined as the amplitude of the first peak (or trough) following the wave arrival relative to the amplitude of any signal which existed slightly prior to the arrival of that signal. The SNR for the explosive source generally exceeded 10 for the *P*-wave but was about 1.0 to 2.0 for the *S*-wave. The mechanical sources gave the reverse response. The SNR for the *P*-wave was less than 1.0 for many measurements, whereas the SNR for the *S*-wave usually approached 10 or more. As a result of this behavior, *P*-wave identification was generally easier for the explosive source, *S*-wave for the mechanical source.

The second difference between signatures from the two sources involved the frequency content of the signals. It was generally observed that the explosive source gave somewhat higher *S*-wave frequencies (90 to 170 Hz) than the mechanical source (75 to 130 Hz). The water table had no effect

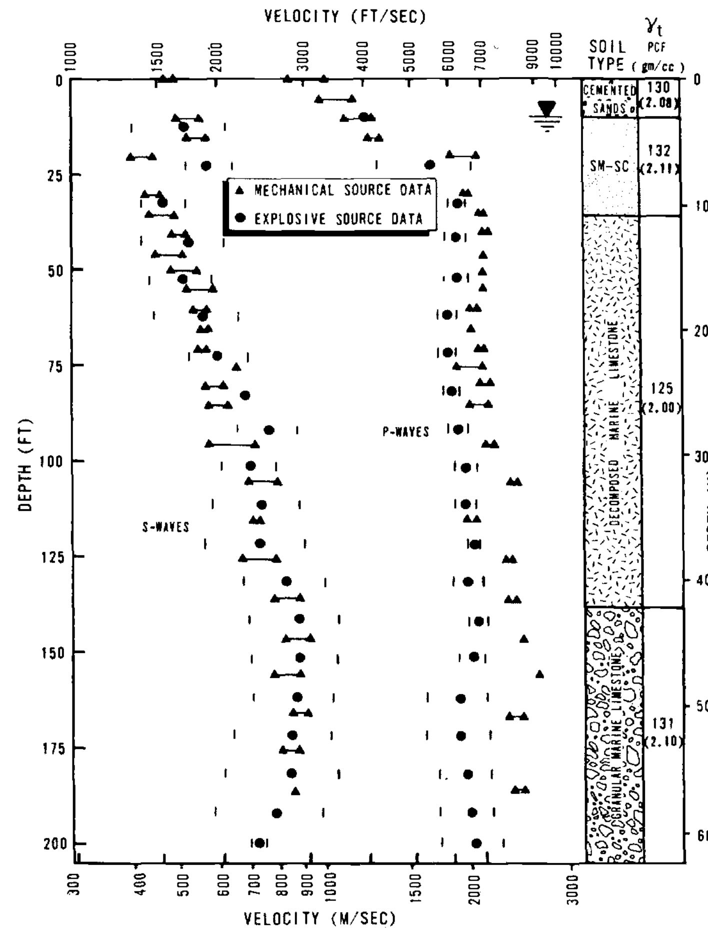

FIG. 16—*Seismic velocities obtained from Survey E (1 ft = 0.305 m).*

on this observation. Frequencies of *P*-waves for each source were about the same above the water table but were higher for the explosive source below the water table. It is believed that above the water table *P*-wave frequencies from the explosive source initially may have been higher, but these motions had attenuated prior to the first recordings at the closest receiving hole.

Certain factors were also observed to enhance the quality of the recorded seismic wave. For the explosive source, the quality of the *S*-wave improved with distance from the source. This was due to the decreasing effects of the earlier arriving *P*-waves; thus the SNR improved with distance. It was also observed that the SNR for the *S*-wave was improved as the size of the

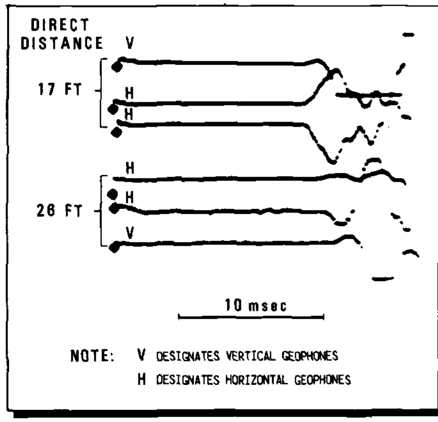

FIG. 17—*Seismogram from mechanical source showing* P-*wave arrival on vertical and horizontal geophones* (*1 ft* = *0.305 m*).

explosive shot decreased and as the hydrostatic pressure (confinement) increased. For both source mechanisms, it was found that *P*-wave detection improved when a horizontally oriented geophone was used. The horizontal geophone sensed a *P*-wave arrival which was larger in magnitude and slightly ahead of that recorded by a vertically oriented geophone, as illustrated in Fig. 17. Finally, for both source mechanisms, the *P*- and *S*-wave quality improved with depth. One factor which did not seem to affect the quality of seismic wave arrivals was the type of casing used in the receiving hole. No differences were noted with sensors in plastic or steel casing.

General Considerations

The comparative study described in the previous sections showed that both source mechanisms gave generally comparable results. It is believed that the close comparison resulted because the field programs were planned giving consideration to a number of factors that would limit the test variables, thereby enabling a realistic evaluation of the explosive and mechanical source mechanism.

Number of Borings

The minimum number of borings that could be used to perform a crosshole survey is two, one for the source and one for the receiver. Surveys involving just two holes are, however, generally discouraged because the accuracy of the *P*- and *S*-wave velocities are absolutely dependent on the accuracy of determining (1) the instant of energy generation, (2) the initial arrival of energy at the receiver, and (3) the length of the wave travel path.

Unfortunately, inaccuracies introduced by these factors are difficult to detect in a two-boring array. Such an array also lacks statistical reliability (in terms of average general soil conditions at a site) because only material along a single travel path is sampled. As observed in this study, the reliability of velocities was increased by using four to five borings in the cross-hole survey and by using more than one boring as an energy hole. The importance of this procedure is demonstrated by the fact that, in the comparative study, velocities from a given depth but for different travel paths differed by 10 percent or more in some cases. Single velocity measurements could, therefore, have contained considerable error.

Boring Spacing

Because the stiffness of soils normally increases with depth, first wave arrivals can result from refraction to lower but stiffer soil layers [*10,13,17*]. The consequence of this refraction phenomenon is that apparent *P*- and *S*-wave velocities may be defined, and these velocities may be higher than true velocities at the depth of the test. In general, refraction effects increase with greater boring spacing and may become particularly significant when spacing exceeds 12 to 15 m (39 to 49 ft) (for velocities which increase gradually with depth) or at even smaller spacing in the vicinity of large velocity discontinuities. Although shorter travel paths are desired from the refraction standpoint, negative aspects do arise. Inaccuracy in distance and time measurements becomes more significant for short travel paths [*18*]. Furthermore, as the length of the travel path decreases, the zone sampled also decreases; thus variations in velocities due to heterogeneities in the soil profiles also increase. The quality of measurements in this study was enhanced by using a variety of travel path distances and then using time-distance plots to determine whether or not refraction occurred.

Arrangement of Borings

Receiving holes can be arranged in many patterns. One of the more desirable patterns in terms of velocity determination is a linear pattern of borings. The linear pattern is arranged so that the energy from the source passes through one receiver on the way to the succeeding receivers. A primary benefit of the linear array is that the interval time between receivers can be used to obtain a measurement of velocity even if the instant of energy generation is not recorded. Furthermore, some later correlative portion of the wave, such as a peak or trough, can be used as a means for establishing a velocity if the wave onset is not clear. A linear arrangement of borings also provides a means of analyzing refraction effects or verifying the accuracy of time breaks or both. The disadvantage of a single linear array is that it cannot provide information on horizontal anisotropy.

Few cases of horizontal anisotropy are cited in the literature, however, and there is little reason for the process of sedimentation to produce them. If anisotropy is expected, velocity observations along at least three orientations should be planned to verify and define it. Linear arrays should be used for each of the observations. For the surveys described herein, preliminary site studies indicated that horizontal anisotropy did not occur; hence linear arrays were used in all but one of the surveys.

Depth Interval

The depth interval between *P*- and *S*-wave measurements should be chosen for the same reasons used when selecting intervals for soil sampling. Measurements should be made at sufficiently close spacing such that no layers of significance to the engineering analysis are missed. This may require a smaller interval in zones where variations in soil type or properties occur than in zones of thick homogeneous materials. The soil profiles at each of the survey sites were developed before commencing the crosshole tests, thereby enabling specific layering characteristics to be investigated.

Verticality

The accuracy of *P*- and *S*-wave velocity measurements varies directly with the accuracy of the travel path distance [*18*]. If the borings are not vertical, distances measured between them at the surface will not be representative of distances at depth. In order to obtain reliable velocity values, the direction and amount of deviation from the vertical (drift) in each boring must be known. The distance between the borings then must be calculated at each level where data are taken. This drift from vertical may cause the receivers in a linear array to become sufficiently far out of line that the concept of interval velocity is no longer valid.

In general, verticality corrections become significant below 15 m (49 ft). A study of 63 borings indicated that the average drift was 0.2 m at 15 m (0.6 ft at 49 ft). The data in Table 1 illustrate that drift becomes much larger at greater depths.

Coupling

To enhance signal detection, it is desirable to provide firm mechanical contact between the soil and the casing and between the sensor and the casing. Coupling the soil to the casing was normally achieved in these surveys by grouting the annulus between the soil and the casing. In another crosshole survey outside of this study, testing was initiated with ungrouted casings, but terminated when the recordings were generally poor. The casing was then grouted into the holes and the survey was repeated and successfully completed.

Orientation of Sensors

Most crosshole surveys including the ones described herein utilize sensor packages that contain three geophones oriented at right angles to each other. One of the sensors is aligned parallel to the axis of the boring, or approximately vertical, and the other two are approximately horizontal. Ideally the horizontal geophones are oriented such that the one geophone is transverse to the source so that it can detect horizontally polarized *S*-waves and the other is radially oriented so that it is positioned most favorably for detecting *P*-waves and vertically polarized *S*-waves. Arrival detection can be enhanced by using oriented horizontal geophones. However, when the horizontal geophones are not oriented, the least favorable orientation possible occurs when both are at 45 deg to the desired orientation. Such orientations still permit reasonable response to the *S*- and *P*-waves, although with reduced amplitude. In cases of weak energy, reduced amplitudes can result in the times of arrival being picked slightly late.

Furthermore, the vertically oriented geophone can provide accurate determination of the *S*-wave arrival as long as the *S*-wave is vertically polarized. Because *S*-waves were of primary interest to those surveys and because predominant *S*-waves were vertically polarized, no attempt was made to orient the horizontal geophones.

Filters

Electronic filters have been used at times to lower the level of background noise or to accentuate certain frequencies in the record. Unfortunately, electronic filters usually introduce time delays which vary with the frequency of the input signal; hence, unfiltered signals are generally preferred and were used during this study. If filtering is felt to be necessary, the same filter settings should be used for all traces, and velocity calculations should be based on interval times between geophones. In addition, at least one set of unfiltered traces should be obtained for reference at each test level.

Instant of Energy Generation

The instant of energy generation is often used as a basis for determining all or part of the time required for the seismic wave to travel from the source to the receiver. If receiving geophones are distributed radially around the source, or if only a single recovery geophone is used, the instant of energy generation must be accurately defined.

When using explosives, time is generally measured from the instant at which a small voltage is supplied by a blaster as a capacitive circuit is closed. However, this is the instant that current is applied to the cap, which is prior to the actual detonation that transfers kinetic energy to the soil. Delays between time instant and energy transfer are generally less than 0.5 ms, as long as "seismic-caps" are used. For measurements made at 7 m (23 ft) spacing in typical soil materials, time break inaccuracies of less than 0.5 ms would cause less than a 10 percent variation in *P*-wave velocity and 3 percent variation in *S*-wave velocity. Other types of blasting caps produce delays of up to several milliseconds and these delays may vary randomly from cap to cap. Velocities determined from these caps must therefore be based on interval times between receivers. Even when using seismic caps, delays may occur if long, high-resistance firing lines (circuit wire from cap to surface) are used with low-voltage blasters, because the current which reaches the cap is too low. Several procedures can be used to record more accurate time breaks or to check the time breaks. One technique involves monitoring the current in the cap leads so that time is recorded the instant the bridge wire separates [*19*]. Another technique is to monitor a current passing through a thin wire wrapped around the cap. At detonation, the wire is broken, thereby marking the instant of detonation.

For mechanical systems the timing process is normally initiated either by the completion of a circuit when a metal hammer contacts the source mechanism or by the response of an inertial system such as a velocity transducer [*9*]. The closure of an electrical circuit is generally preferred because the rise time of the signal is very rapid. The velocity transducer depends on the movement of a mass in a coil-magnet system and, therefore, trigger times vary with factors such as sharpness of the blow to the system or damping of the system. Travel time corrections must be made if the point of hammer contact or inertial system is located a substantial distance from the point of energy transfer. The difference between the instant of time and energy transfer can be determined either by placing a sensor at the bottom of the rod to record the time required for the rod wave to reach the bottom of the hole or by connecting and laying out a number of lengths of rod along the ground and measuring the average velocity of seismic waves in the rod. Hoar and Stokoe [*20*] provide additional details about problems associated with timing delays in mechanical source systems recording equipment.

In this study, inaccuracies associated with timing delays were minimized by using "interval times" to compute *P*- and *S*-wave velocities. For mechanical surveys a geophone was placed at the bottom of the source boring to indicate the time of energy transfer.

Conclusions

The results from the five sets of crosshole surveys evaluated in this comparative study permit the following conclusions to be made:

1. Average *P*- and *S*-wave velocities generated by explosive and mechani-

cal methods are similar when care is used in performing each type of test. Scatter in *P*- and *S*-wave velocities about the average value is generally greater for the explosive source, particularly when materials are heterogeneous in consistency.

2. *P*-wave arrivals are more readily identifiable with the explosive source whereas *S*-wave arrivals are more identifiable from the mechanical source. The onset of *S*-waves from both sources is obscure at times due to *P*-wave interference, but later portions of the *S*-wave are generally definable for both sources. *P*-wave interference is usually much more significant for the explosive source, but some of this interference can be eliminated in explosive surveys by using small explosive charges and by maintaining a hydrostatic head over the charge. Also, identification of *P*-wave arrivals can be enhanced by using horizontal geophones.

3. The ability to derive velocities for both sources is improved by utilizing a linear arrangement of receiving holes and then evaluating velocities on the basis of interval travel times and distances. This approach avoids some of the inaccuracies associated with defining the instant of energy generation and the onset of wave arrivals.

4. The overall quality and accuracy of crosshole surveys are improved by using multiple borings, multiple tests per level, variable boring spacing, linear survey arrays, verticality surveys, and, if casing is used, grouting the casing in the boring.

The favorable comparison of velocity data from the two-source crosshole surveys should be encouraging to practicing engineers and geophysicists. Because the surveys were performed under strict quality-assurance and control procedures, confidence in the results is quite high. In addition, the velocity values from one source mechanism in each survey set appear to confirm the reliability of values from the other mechanism. Obviously, reliable crosshole results depend heavily on proper field and analysis techniques during the survey. In the development of future ASTM standards on crosshole surveys, it is suggested that techniques such as those discussed herein be considered for inclusion. The suggestions of other practicing geophysicists and engineers should also be solicited and considered in order to develop meaningful procedures which can produce reliable velocity determinations for use in engineering analyses.

Acknowledgments

Financial support for compilation of data and presentation of velocity comparisons was provided by the Fugro Technical Development Program.

References

[1] Richart, F. E., Jr., Hall, J. R., Jr., and Woods, R. D., *Vibrations of Soils and Foundations*, Prentice-Hall, Englewood Cliffs, N.J., 1970, p. 414.

[2] "Soil Behavior Under Earthquake Loading Conditions: State of the Art, Evaluation of Soil Characteristics for Seismic Response Analyses," a joint venture of Shannon & Wilson, Inc. and Agbabian-Jacobsen Associates, Jan. 1972.
[3] "Seismic Design of Nuclear Power Plants—An Assessment," prepared for Electric Power Research Institute by the Applied Nucleonics Co., Research Project 273, 1087-2A, June 1975, p. 261.
[4] "The Air Force Manual for Design on Analysis of Hardened Structures," Air Force Weapons Laboratory, AFWL-TR-74-102, Oct. 1974, p. 1118.
[5] Isenberg, J., "Nuclear Geoplosics, A Sourcebook of Underground Phenomena and Effects of Nuclear Explosions; Part 2: Mechanical Properties of Earth Materials," Defense Nuclear Agency Report DNA 1285H2, Nov. 1972, p. 150.
[6] Swiger, W. F. in *Proceedings*, Conference on Analysis and Design in Geotechnical Engineering, Austin, Texas, Vol. 2, June 1974, pp. 79-92.
[7] Riggs, E. D., *Geophysics*, Vol. 20, No. 1, Jan. 1955, pp. 53-67.
[8] Geyer, R. and Martner, S., *Geophysics*, Vol. 34, No. 6, Dec. 1969, pp. 893-905.
[9] Stokoe, K. H., II, and Woods, R. D., *Journal of the Soil Mechanics and Foundations Division*, American Society of Civil Engineers, Vol. 98, No. SM5, May 1972, pp. 443-460.
[10] Schwartz, S. D. and Musser, J. M. in *Proceedings*, International Conference on Microzonation for Safer Construction, Research and Application, Seattle, Wash., Vol. 2, 1972, pp. 593-608.
[11] Murphy, V. J. in *Proceedings*, International Conference on Microzonation for Safer Construction, Research and Application, Seattle, Wash., Vol. 2, 1972, pp. 131-159.
[12] Mooney, H. M., *Journal of the Geotechnical Engineering Division*, American Society of Civil Engineers, Vol. 100, No. GT8, Aug. 1974, pp. 905-923.
[13] Ballard, R. F., *Journal of the Geotechnical Engineering Division*, American Society of Civil Engineers, Vol. 102, No. GT12, Dec. 1976, pp. 1261-1273.
[14] "*In Situ* Impulse Test, an Experimental and Analytical Evaluation of Data Interpretation Procedures," U.S. Nuclear Regulatory Commission Report NUREG-0028, prepared by a joint venture of Shannon & Wilson, Inc. and Agbabian-Jacobsen Associates, Sept. 1976.
[15] Swain, R., *Geophysics*, Vol. 27, No. 2, 1962, pp. 237-241.
[16] McLamore, V. R., "Compressional and Shear Wave Velocities," VUF 2500, Defense Atomic Support Agency, Washington, D.C., 1964.
[17] Haupt, W. A., Discussion of Stokoe and Woods, *Journal of the Soil Mechanics and Foundations Division*, American Society of Civil Engineers, Vol. 99, NO. SM2, Feb. 1973, pp. 224-228.
[18] Anderson, D. G. and Woods, R. D. in *Proceedings* Conference on *In Situ* Measurement of Soil Properties, Raleigh, N.C., Vol. 1, 1974, pp. 69-92.
[19] McLamore, V. R., "Seismic Velocity Determination and Distance Measurements in a Salt Dome," VUF 3015, Defense Atomic Support Agency, Washington, D.C., 1964.
[20] Hoar, R. J. and Stokoe, K. H., II, this publication, pp. 3-29.

C. T. Statton,[1] *B. Auld,*[2] *and A. Fritz*[3]

In Situ Seismic Shear-Wave Velocity Measurements and Proposed Procedures

REFERENCE: Statton, C. T., Auld, B., and Fritz, A., "***In Situ* Seismic Shear-Wave Velocity Measurements and Proposed Procedures,**" *Dynamic Geotechnical Testing, ASTM STP 654,* American Society for Testing and Materials, 1978, pp. 56–65.

ABSTRACT: Determination of dynamic shear modulus *in situ* has been an increasingly important source of data for ground response analysis for earthquake design studies. Historically, shear modulus is calculated from *in situ* measurement of seismic shear-wave velocity. A downhole impact energy source has been developed which maximizes the shear-wave energy produced and minimizes compressional-wave energy for purposes of crosshole *in situ* seismic shear-wave velocity measurements. The geometry of the energy source permits reversal of the polarity of shear-wave arrivals without changing the polarity of compressional-wave arrivals.

The energy source is described and *in situ* measurement data are presented. Based on more than three years experience using the downhole source, a procedure for *in situ* measurement of seismic shear-wave velocity is suggested.

KEY WORDS: earthquakes, measurements, velocity, shear stress, soils

Determination of dynamic shear modulus, G, *in situ* has become an increasingly important factor of late in ground response analysis for earthquake design studies. Historically, the shear modulus is calculated from *in situ* measurement of the seismic shear-wave velocity, V_S, and has been empirically related to the mean principal effective stress, σ'_m, or confining pressure, through the general relation for sands (after Seed and Idriss [*1*][4])

$$G = \rho V_S{}^2 = 1000\, K_2\, (\sigma'_m)^{1/2}$$

where

[1]Project engineer-geologist, Woodward-Clyde Consultants, New York, N.Y.
[2]Project geophysicist, Woodward-Cycle Consultants, San Francisco, Calif.
[3]President, Bison Instruments, Inc., Minneapolis, Minn.
[4]The italic numbers in brackets refer to the list of references appended to this paper.

$$\sigma_m{}' = \frac{\sigma_1{}' + \sigma_2{}' + \sigma_3{}'}{3}$$

and

K_2 = parameter used in defining shear modulus as a function of shear strain and confining pressure,
$\sigma_1{}' + \sigma_2{}' + \sigma_3{}'$ = principle stresses, and
ρ = density.

The modulus was determined at very low strain (for example, 1×10^4 to 1×10^7) to the variation in modulus with strain through relations presented by Hardin and Drnevich [*2*] and Seed and Idriss [*1*]. Based on such relations, the modulus determined can be seen to affect directly subsequent analyses of ground response.

Seismic shear-wave velocity measurement techniques historically have included: (1) surface measurements of either shear-wave or Raleigh-wave-phase velocity, and (2) borehole techniques commonly termed downhole, uphole, and crosshole methods. All techniques employ either pulse sources (that is, an explosive or mechanical pulse) or a continuous-signal source. A review of shear-wave velocity measurement techniques, theory, and use is presented by Mirafuente et al [*3*], Mooney [*4*], Stokoe and Woods [*5*], and Ballard and McLean [*6*].

One difficulty encountered in shear-wave velocity measurement is recognition of the signature of the shear-wave phase within the arriving wave train. Several methods of filtering, scaling, and sometimes back-calculating shear-wave velocity data have been utilized by investigators in attempts to provide reasonable results from sometimes ambiguous data at best. This often results in a reluctance to publish or produce actual records of data, and often only numerical results or conclusions are presented with no detail of the interpretation methods.

To overcome the difficulty in recognition of the shear-wave phase arrival, recent efforts have tended to examine the energy source. While explosive energy sources provide strong compressional wave and weak shear wave output, mechanical impulse sources have been developed which provide a strong polarized energy output. The advantage of the polarization of the source energy is in the generation of motions which are predominantly those sought. The additional advantage of the polarized energy source is that a symmetric reversal of input energy results in the reversed arrival of the polarized wave at the recording station. Reversal of the polarized wave is unique, and does not occur for other waves generated in the wave train and background noise in the area. Based on such an approach, even in high noise environments, shear-wave phase arrivals can be recognized as seismic shear-wave arrivals, while the background noise is random with respect to discrete specimens in time.

Measurement System and Procedure

The general mechanics of a suitable measurement system include: (1) an energy source, capable of producing vertically polarized seismic energy that can be coupled to the walls of a borehole so that the energy can be transmitted efficiently to the surrounding soil or rock material; (2) a directional borehole geophone, capable of being coupled to the borehole walls, to receive the source signal; and (3) a storage oscilloscope or seismograph to display signals received, equipped with a camera for obtaining permanent records of the measurements.

The energy source, or "shear-wave hammer," illustrated in Fig. 1, consists simply of (1) a reaction mass that can be coupled to the borehole

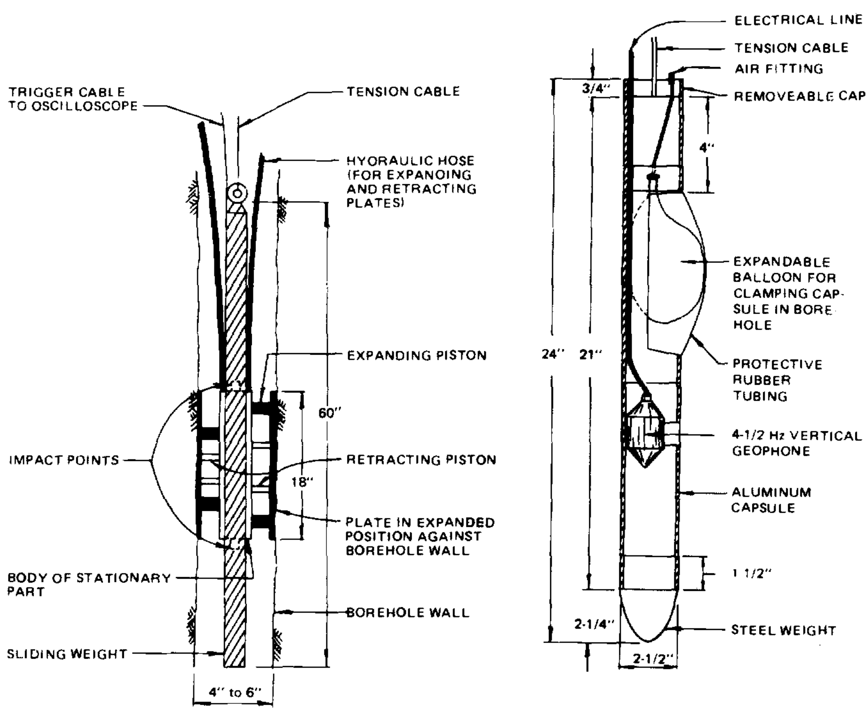

FIG. 1—*Schematic diagram of downhole shear-wave hammer and borehole geophone clamping devices (1 in. = 2.54 cm).*

walls by means of a hydraulic jacking system, and (2) a slide weight weighing approximately 4.5 to 20.25 kg (10 to 45 lb) or more, cable operated, capable of imparting uniaxial impact to the reaction mass along the axis of the borehole. The slide weight was designed such that impacts can be symmetrically imparted in both upward and downward directions.

The geophones are directionally sensitive along the axis of the adjacent boreholes. The motion received is primarily that of the vertically polarized shear wave. Geophones are coupled to the borehole walls at the same elevation of the downhole hammer by means of inflatable pneumatic diaphragms; see Fig. 1. A cross section showing borehole locations and instrument arrangement is presented in Fig. 2. Travel time can be measured as simply the time difference between arrival times at two adjacent geophone holes.

The measurement system utilizes a multichannel storage oscilloscope or seismograph for trace display and recording purposes. Advantages of the oscilloscope or storage screen display seismographs are the time resolution with accurate display to read time to a tenth of a millesecond and the capability to display both initial and subsequent reversal of shear-wave arrivals on the same photographic record. Using this technique and equipment, measurements have been made both near the surface and to depths of 152 m (500 ft), providing results in materials ranging from hard rock to relatively soft sand and clay.

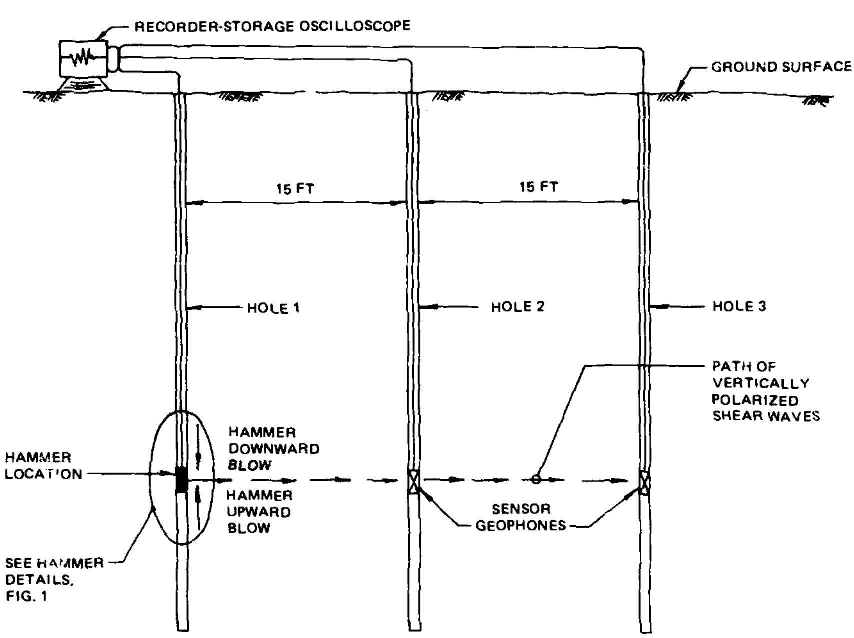

FIG. 2—*Cross section showing typical instrument arrangement in boreholes.*

The measurement technique consisted of recording signals received in adjacent boreholes from the impact energy transmitted from the hammer borehole. Traces for a given impact were recorded on the upper half of the split-screen oscilloscope display, and traces from the directionally reversed impact were recorded on the lower half of the display screen. Four examples are presented in Fig. 3. As shown in the figures, the shear-wave phase

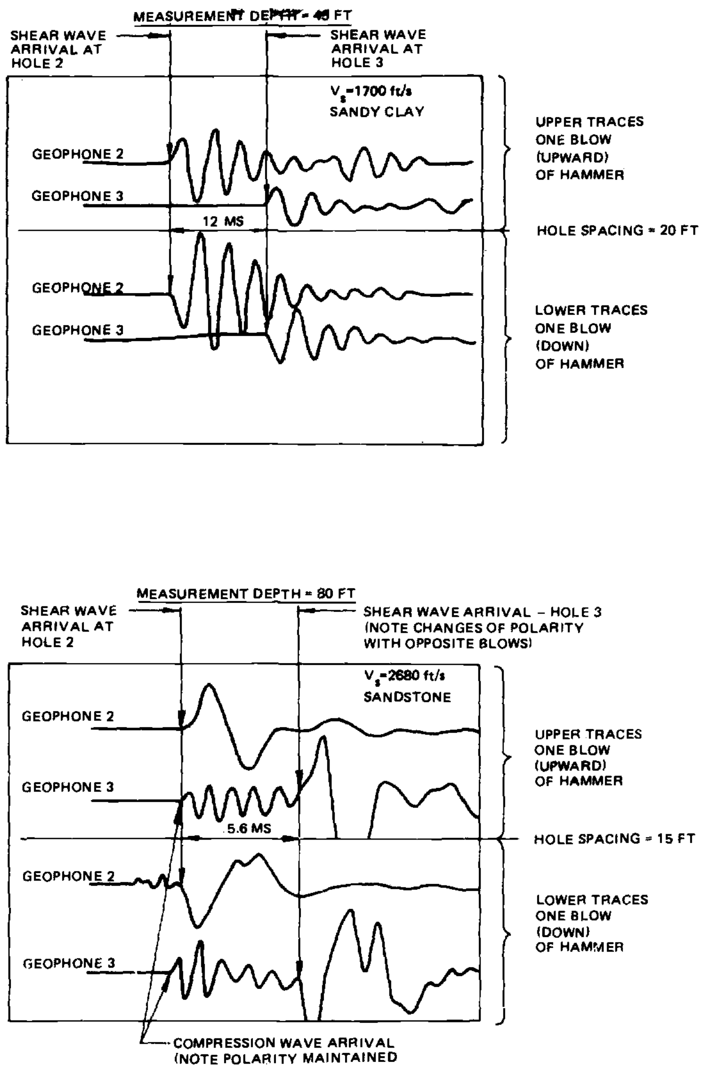

FIG. 3a—*Examples of seismic wave arrivals traced from oscillograph screen photographs (1 ft = 0.3048 m).*

arrival is distinguished by a reversal in polarity with reversed impact direction. Background noise and other wave types produced retain a generally constant polarity.

To facilitate measurement efficiency, the borehole used as the energy source of downhole hammer hole was prepared by grouting in place a steel

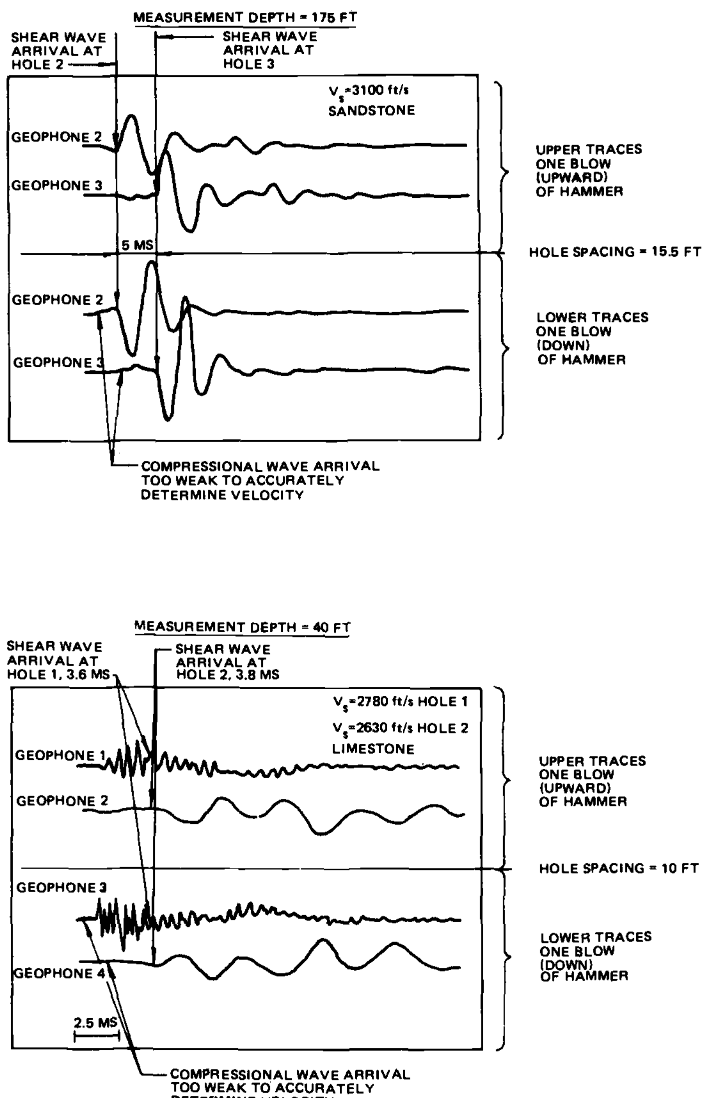

FIG. 3b—*Examples of seismic wave arrivals traced from oscillograph screen photographs (1 ft = 0.3048 m).*

casing with an inside diameter of 100 to 127 mm (4 to 5 in.) The annular space between the outside casing wall and the surrounding ground was fully grouted. Grouting is generally accomplished by filling the borehole with cement grout (pumped in from bottom to top), and the steel casing, with a watertight wooden end plug installed, can be lowered into the grout-filled borehole. Lowering the casing displaces the grout, and reasonably ensures a complete grouting of the casing in place.

Casing of the signal receiving holes, or geophone holes, is not generally required. Geophone holes can remain filled with drilling mud, however, to ensure that significant sloughing of the borehole walls does not occur.

Measurements have been made in two adjacent arrays, one array fully grouted, and one array uncased and ungrouted to compare results. Preliminary data indicate that grouting of geophone holes does not affect measured shear-wave arrival times. Such measurements have been made only in clay deposits, however, and more permeable granular deposits have not been tested.

Once the boreholes are drilled, and the casing installed in the downhole hammer hole, borehole deviation survey measurements are made. Distances between boreholes, calculated from the results of the deviation survey, are compiled in tabular form for each of the deviation measurement stations. Deviation measurement locations are typically on 1.5 m (5 ft) centers down the length of each borehole.

Seismic shear-wave velocity values are calculated at the time of the measurements. The oscilloscope screen is photographed upon completion of both directional hammer impacts (see Fig. 3), arrival times are scaled off the Polaroid photographs, and velocity values calculated in the field. This permits immediate data examination, and any data discrepancies or peculiarities can be discovered and checked before proceeding with further measurements.

Determinations of the shear-wave phase arrivals are made at the two geophone locations. Seismic shear-wave velocities are calculated using the time difference between phase arrivals at the two geophones, and the distance between boreholes. Uniformity of the velocity is checked by using total phase arrival time measured from the zero time provided by the impact triggers on the downhole hammer.

Aside from the obvious advantages and improved accuracy of the foregoing measurements, care must be taken in planning measurement programs. Usually, subsurface investigation data indicate horizontal continuums, with layer boundaries defined by material changes and, in some cases, strong density changes. Velocity boundaries potentially corresponding to these layers are generally not well defined, although significant velocity boundaries may be represented by material changes.

Accurate measurement of shear-wave velocity is dependent on optimum measurement location. Measurements in low-velocity materials near high-velocity boundaries, for example, can result in intermediate velocity values of a refracted wave path. Borehole specimen classification procedures are not always adequate to identify velocity differences of materials, and typically do not.

Uncertainty with regard to subsurface velocities can be resolved by defining the subsurface in terms of compressional wave velocity layers. A subsurface velocity profile may be prerequisite to obtaining reliable shear-wave measurement data. Existing specimen boreholes and boreholes for geophysical measurements can be utilized for purposes of velocity profiling by uphole shooting techniques. Uphole shooting techniques are illustrated in Fig. 4, which presents theoretical and actual data obtained by this technique. Advantages of velocity profiling by uphole shooting in comparison with more usual seismic refraction studies include (1) more accurate depth determinations, (2) definition of low-velocity layers, and (3) higher resolution for defining intermediate velocity layers. Explosive sources in boreholes and surface geophones, or borehole geophone and explosive or mechanical surface energy sources, provide a means of defining the subsurface in terms of velocity layers. Such data can be obtained using standard seismic refraction equipment. Compressional wave arrival times at surface geophones can be plotted at the cross-sectional depth of the borehole source as shown in Fig. 4*a*. This empirical method of isoarrival contouring has successfully indicated the subsurface velocity profile (Fig. 4*c*).

Based on uphole velocity profile data, distances between adjacent boreholes can be selected for subsequent shear-wave velocity measurements. Distances are governed by the thickness of the low-velocity layers; that is,

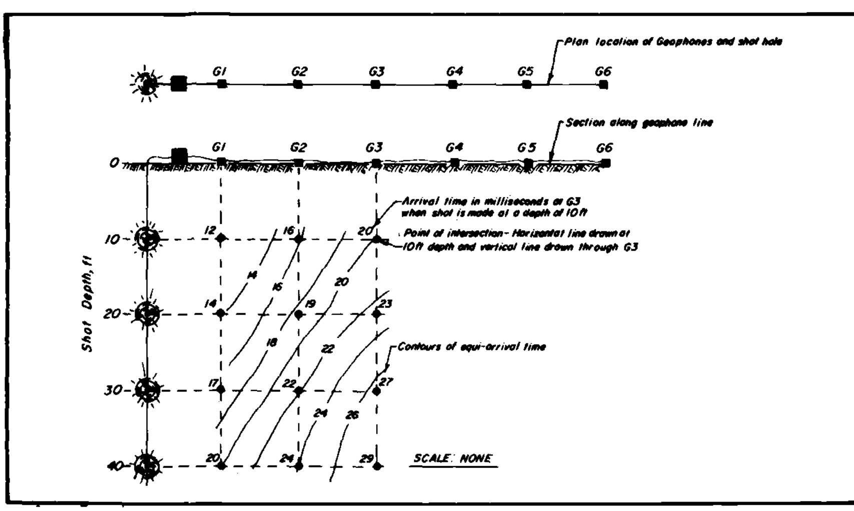

FIG. 4*a*—*Procedure for analysis of uphole data (1 ft = 0.3048 m).*

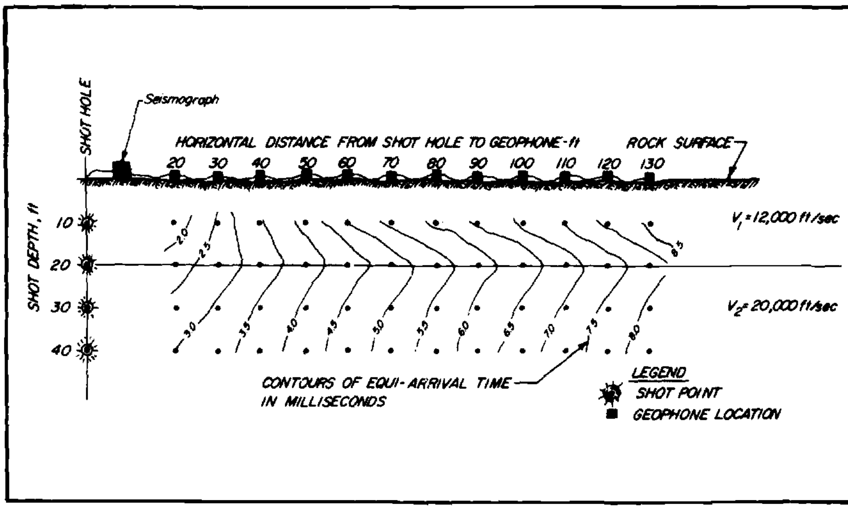

FIG. 4b—*Theoretical contours of equi-arrival time for two velocity layer case (1 ft = 0.3048 m).*

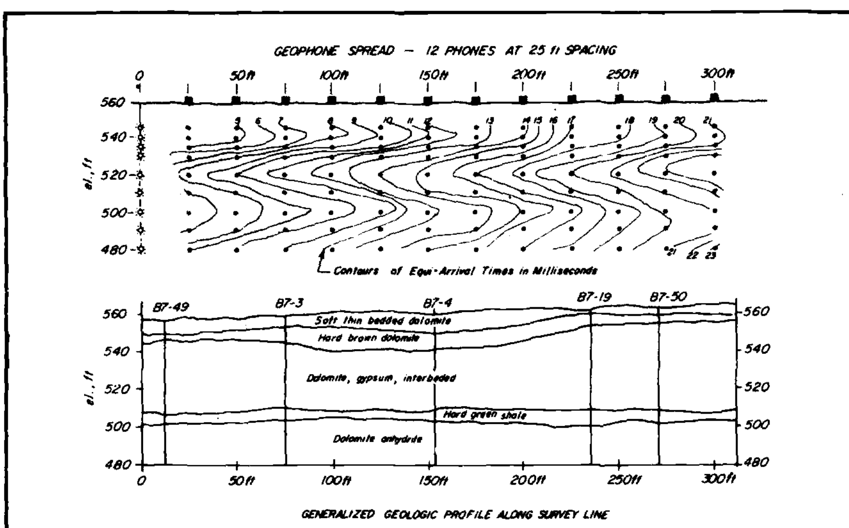

FIG. 4c—*Results of uphole method on bedded dolomite (1 ft = 0.3048 m).*

the controlling factor is the thickness of the thinnest low-velocity layer in which measurements are to be made. Assuming that the impulse source and receiver can be accurately located in the middle of the low-velocity layer, the spacing between holes generally should not exceed the layer thickness; somewhat greater distances can be tolerated provided velocity ratios between adjacent velocity layers can be estimated prior to the drilling of geophysical boreholes.

While the foregoing requirements may indicate close spacing of holes, measurement accuracy is not impaired. Time resolution within the measurement system (using the oscilloscope) far exceeds measurement requirements of closely spaced boreholes. In general, the spacing need not be greater than 3 to 7.5 m (10 to 25 ft) for most applications. The accuracy of the borehole inclinometer, used in the deviation survey for determining the exact hole spacing, is typically much greater than data requirements of the overall system.

Conclusion

The development of the borehole impulse energy source producing highly polarized seismic-wave energy has eliminated the difficulties in shear-wave velocity measurements made *in situ*. The general method described eliminates possible ambiguity in interpretation of shear-wave velocity data, and provides for a permanent photographic record of data recorded. The validity of shear-wave velocity measurements must be evaluated, however, in terms of measurement location. An accurate uphole velocity profile of subsurface conditions can improve the shear-wave velocity measurement system by providing supporting data to guide selected measurement location intervals; high-quality shear-wave measurement data improve subsequent calculation of shear modulus. Reliable results depend upon both the knowledge of what is being measured and the accuracy and integrity of the measurements themselves.

References

[*1*] Seed, H. and Idriss, I. M., "Soil Moduli and Damping Factors for Dynamic Response Analyses," Report EERC 70-10, Earthquake Engineering Research Center, University of California at Berkeley, 1970.

[*2*] Hardin, B. O. and Drnevich, V. P., *Journal of the Soil Mechanics and Foundations Division,* American Society of Civil Engineers, Vol. 98, No. SM6, 1972, pp. 667-692.

[*3*] Mirafuente, N. T., Zurflueh, E. G., and Statton, C. T., "Improved Shear-Wave Measurement Technique for Better Earthquake-Resistant Design," Woodward-Clyde Consultants Geotechnical/Environmental Bulletin, Vol. 7, No. 2, 1974.

[*4*] Mooney, H. M., *Journal of the Geotechnical Engineering Division,* American Society of Civil Engineers, Aug. 1974, pp. 905-923.

[*5*] Stokoe, K. H. and Woods, R. D., *Journal of the Soil Mechanics and Foundations Division,* American Society of Civil Engineers, Vol. 98, No. SM5, 1972, pp. 443-460.

[*6*] Ballard, R. F. and McLean, F. G., "Seismic Field Methods for *In Situ* Moduli," Soils and Pavements Laboratory, U.S. Army Engineer Waterways Experiment Station, Vicksburg, Miss., Miscellaneous Paper, S-75-10, 1975.

D. G. Anderson[1] *and K. H. Stokoe II*[2]

Shear Modulus: A Time-Dependent Soil Property

REFERENCE: Anderson, D. G. and Stokoe, K. H., II, **"Shear Modulus: A Time-Dependent Soil Property,"** *Dynamic Geotechnical Testing, ASTM STP 654,* American Society for Testing and Materials, 1978, pp. 66–90.

ABSTRACT: Dynamic shear moduli determined at low shearing strain amplitudes ($<10^{-3}$ percent) during sustained-pressure, resonant-column tests are shown to increase with time of confinement. The time-dependent modulus increase is characterized by two phases: (1) an initial phase which results from primary consolidation, and (2) a second phase which occurs after completion of primary consolidation, called the "long-term time effect." The duration of primary consolidation and the magnitude of the long-term time effect vary with factors such as soil type and stress conditions. Although shapes of the modulus-time relationships differ depending on whether the soil is primarily fine- or coarse-grained, all soils exhibit a long-term time effect. The long-term time effect is also shown to occur at higher shearing strains (0.001 to 0.1 percent) for moduli determined at the onset of cyclic loading. On the basis of these results, confinement time is shown to be an important parameter which must be properly accounted for in the laboratory measurement of shear moduli and which must be considered when interpreting laboratory moduli in terms of *in situ* response.

KEY WORDS: clays, dynamics, dynamic response, geotechnical engineering, laboratory tests, cyclic loading, resonant-column test, sands, shear modulus, time-effect, torsion shear tests, vibration, soils

Dynamic shear moduli of undisturbed and recompacted soils can be determined by a variety of laboratory testing methods. The most widely used methods are cyclic triaxial shear, cyclic simple shear, cyclic torsional shear, and resonant column. Moduli determined by these testing methods are influenced by factors such as confining pressure, stress history, shearing strain amplitude, number of cycles of loading, degree of saturation and drainage conditions. One other factor, *duration of the confining pressure,* is also of fundamental importance in laboratory evaluations of shear modulus by any of these test methods. Unfortunately this factor is often either neglected or misunderstood. This oversight can easily result in mis-

[1] Project engineer, Fugro, Inc., Long Beach, Calif. 90807.
[2] Assistant professor of civil engineering, The University of Texas, Austin, Tex. 78712.

interpretation of test data and failure to derive maximum benefit from a testing program.

The objective of this paper is to provide quantitative information about the effect of time at constant confining pressures on shear moduli of sands and clays. Previous research on time effects is reviewed. Procedures to measure modulus change with time are described, after which typical results from laboratory tests are shown. On the basis of these data, general guidelines are given for determining the time at which shear moduli should be evaluated during laboratory tests. Furthermore, a rationale is established for adjusting shear moduli measured in the laboratory at various shearing strain amplitudes to probable *in situ* moduli at corresponding shearing strains. Finally, the general concepts are illustrated by presenting two examples in which initial and long-term phases of modulus-time response are incorporated.

Background

The effect of confinement duration (at a constant pressure) on the magnitude of shear moduli was reported as early as 1961 [*1*].[3] In the following years other researchers [*2-5*] observed that when specimens were confined at a constant confining pressure, shear moduli measured at shearing strain amplitudes below 0.001 percent (commonly referred to as low-amplitude moduli) increased with time of specimen confinement. As a result of these general observations, a number of individuals [*6-9*] performed more detailed studies of the time-dependent modulus change. These studies showed that shear moduli of artificially prepared soil specimens indeed increased with time of specimen confinement. More recently, sustained-pressure studies on undisturbed specimens of sands and clays determined that this time-dependent behavior was also characteristic of natural soils as well [*10-15*].

Table 1 summarizes some studies in which the effect of long-term confinement on low-amplitude dynamic shear moduli has been evaluated. As shown in the table, time effects have been recorded for a variety of materials, ranging from clean sands which were prepared in the laboratory to natural clays from the Gulf of Mexico. Time effects have been observed over a wide range in confining pressures, 35 kN/m^2 (5 psi) to more than 700 kN/m^2 (100 psi), and for a wide range in shear moduli, 14 000 kN/m^2 (2030 psi) to more than 200 000 kN/m^2 (28,990 psi). Although the rate of modulus change varied from study to study, all soils exhibited an increasing shear modulus with increasing time of confinement.

Previous sustained-pressure studies indicate that for most soils the time-dependent behavior at low strain levels can be characterized by an

[3] The italic numbers in brackets refer to the list of references appended to this paper.

TABLE 1—*Typical values of* I_G *and* N_G.

Soil Type	Specimen Type	Confining Pressure (kN/m²)[c]	Low-Amplitude Shear Modulus G_{1000} (kN/m²)[c]	Typical I_G (kN/m²)[c]	Typical N_G[b] (%)	Reference
EPK Kaolinite	vacuum extruded	200 to 300	140 000 to 190 000	24 000 to 35 000	17 to 18	[4]
Ottawa sand Quartz sand Quartz silt Dry clay	compacted by raining and tamping	70 to 280	50 000 to 180 000	1400 to 5500	1 to 11	[6]
Kaolinite Bentonite	vacuum extruded	70 to 550	4000 to 170 000	1000 to 8500	5 to 25	[8]
Agsco sand Ottawa sand Air-dried EPK Kaolinite	compacted by raining and tamping	70 to 280	50 000 to 110 000	2000 to 10 000	1 to 17	[9]
Saturated EPK Kaolinite	vacuum extruded					
Silty sand Sandy silt Clayey silt Shale	undisturbed[d]	70 to 220	80 000 to 2 600 000	2000 to 22 900	1 to 14	[10,11]
Boston blue clay	undisturbed[d]	70 to 700	32 500 to 54 000	≃7000	15 to 18	[12]
9 Clays 1 Silt	undisturbed[d]	35 to 415	13 000 to 235 000	26 000 to 23 500	2 to 40	[13,26]
Clay fills	undisturbed[d]	35 to 70	50 000 to 200 000	4200 to 15 000	7 to 14	[14]
Decomposed marine limestone	undisturbed[d]	325 to 830	365 000 to 1 300 000	28 000 to 102 000	3 to 4	[15]
San Francisco bay mud	undisturbed[d]	17 to 550	7600 to 150 000	725 to 32 000	8 to 22	[18]
Dense silty sand	undisturbed[d]	220 to 620	45 000 to 180 000	5000 to 17 000	4 to 10	[31]
Stiff OC[e] clay	undisturbed[d]	1280 to 1300	300 000 to 320 000	14 000 to 26 000	4 to 8	[31]

[a] I_G defined by Eq 1.
[b] N_G defined by Eq 2.
[c] 1 kN/m² = 0.145 psi.
[d] Nominally undisturbed.
[e] Overconsolidated.

initial phase when modulus changes rapidly with time followed by a second phase when modulus increases about linearly with the logarithm of the time. This response is illustrated in Fig. 1. For the most part, the initial phase results from void ratio changes during primary consolidation. The initial phase is, therefore, referred to as "primary consolidation." The second phase, in which modulus increases about linearly with the logarithm of time, is believed to result largely from a strengthening of physical-chemical bonds in the case of cohesive soils [*13*] and an increase in particle contact for cohesionless soils [*16*]. This phase is referred to as the "long-term time effect." The long-term effect represents the increase in modulus with time which occurs after primary consolidation is completed.

Two methods are used to describe the long-term effect. The long-term time effect is expressed in an absolute sense as a coefficient of shear modulus increase with time, I_G

$$I_G = \Delta G/\log_{10}(t_2/t_1) \tag{1}$$

where

t_1, t_2 = times after primary consolidation, and
ΔG = change in low-amplitude shear modulus from t_1 to t_2 as shown in Fig. 1.

Numerically, I_G equals the value of ΔG for one logarithmic cycle of time. The long-term time effect is also expressed in relative terms by the normalized shear modulus increase with time, N_G

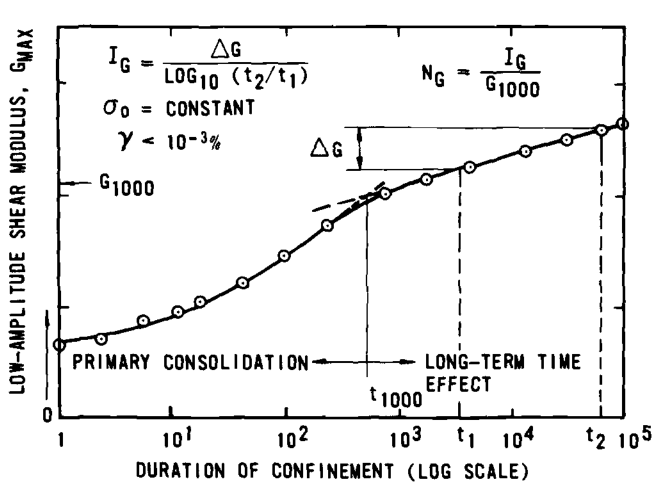

FIG. 1—*Phases of modulus-time response.*

$$N_G = \left(\frac{\Delta G}{\log_{10}(t_2/t_1)}\right)\left(\frac{1}{G_{1000}}\right) 100\% = \frac{I_G}{G_{1000}} 100\% \qquad (2)$$

where G_{1000} = shear modulus measured after 1000 min of constant confining pressure (must be after completion of primary consolidation). The purpose of this normalization is to remove some of the influence of confining pressure and to provide a common basis for reporting modulus data. Values of N_G are particularly helpful when trying to estimate the magnitude of *in situ* modulus change with time when long-term laboratory tests have not been conducted.

The duration of primary consolidation and the magnitude of the long-term time effect vary with factors such as soil type, initial void ratio, undrained shearing strength, confining pressure, and stress history. Figure 2 shows typical time-dependent modulus responses for different soils. Typical values of I_G and N_G are given in Table 1.

Significance

The time dependency of modulus has significant implications. In the first place, it means that duration of confinement at a constant confining pressure must be considered when performing laboratory tests. As evident from Fig. 2, the modulus of a clay determined after ten minutes of confinement could differ by 20 percent or more from a modulus measured after two days of confinement. The obvious conclusion is, therefore, that if

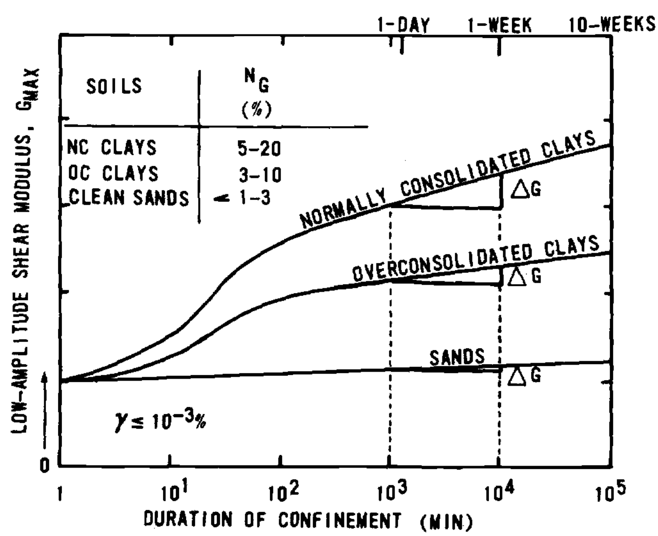

FIG. 2—*Effect of confinement time on shear modulus.*

laboratory values of modulus of a given soil are to be compared, they should be compared after equal confinement times for similar drainage conditions, and these times should be equal to or greater than the time of primary consolidation. In addition, for laboratory tests in which moduli are measured, times for primary consolidation of the specimens and, if possible, magnitudes of the long-term time effect, I_G, should be reported.

This time-dependent behavior is of even more fundamental importance. It means that time must be considered when estimating shear moduli of *in situ* soils from laboratory measurements. For example, a question arises as to whether *in situ* moduli should be represented by laboratory shear moduli determined at the appropriate confining pressure after ten minutes, ten hours, ten days, or some other time. In this case the problem involves engineering judgment which could have a significant effect on the satisfactory performance of a project.

Testing Methods

The effect of confinement time on shear modulus can be conveniently evaluated in the resonant-column test. The primary advantage of this testing method is that high-quality moduli measurements can easily be made at very small shearing strains (strains less than 0.001 percent). As long as shearing strains are less than 0.001 percent, moduli values can be obtained from the same soil specimen at different intervals of time without introducing the effects of previous measurements at that pressure. The added advantage of some resonant-column test devices is that moduli values can be determined at higher shearing strain levels (0.01 to 1.0 percent).

Equipment and Test Setup

The primary resonant-column systems which have been used by the authors and others to conduct time-dependent moduli studies are the Drnevich, Hall, Hardin, and Stokoe devices. Each device consists essentially of a coil-magnet drive system, an accelerometer or velocity transducer to monitor the motion of the drive system, a linear variable differential transformer (LVDT) or other displacement transducer to detect vertical height change of the soil specimen, and a confining chamber. Additional details of the mechanics of these systems are described elsewhere [*3,16–18*].

In the test setup the coil-magnet drive system is attached to a top cap which is seated on a membrane-encased, cylindrical soil specimen. The soil specimen can be either hollow [*3,18*] or solid [*16,17*], depending on the capabilities of the particular test device. The base pedestal, upon which the specimen is placed, is connected to a drainage line. Filter paper strips may be used along the length of the specimen to accelerate specimen consolidation. The top cap and bottom pedestal are usually serrated or roughened in some manner to assure good mechanical coupling between the soil and equipment. The system is generally set up such that only a hydrostatic confining pressure is applied, although the Hardin device [17] is capable of applying anisotropic load conditions.

An electrical system is used to operate and monitor resonant-column equipment. To obtain accurate shear wave velocity measurements, it is necessary to use electronic equipment such as shown in Fig. 3. In this system, a signal generator supplies a sinusoidal voltage to the coils in the coil-magnet drive system. The magnetic field induced by the current in the coils interacts with the magnetic field from the permanent magnet, thereby resulting in torsional oscillation of the drive cap and specimen. By varying the frequency of the input signal, the amplitude of vibration varies. An accelerometer (or velocity transducer) located on the top cap generates a voltage proportional to the amplitude of vibration of the soil top-cap system. This signal is conditioned and then viewed on the oscilloscope. A voltmeter and digital counter are used to monitor the amplitude and frequency, respectively, of the signal at resonance, and an LVDT is used to monitor specimen-height change.

The object of the test is to vibrate the soil-top-cap system at first-mode resonance. First-mode resonance is defined as the frequency at which maximum top-cap motion is obtained during a sweep of frequencies (usually starting at about 20 Hz). At first-mode resonance, material in a cross section at every elevation vibrates in phase with the top of the specimen. Shear

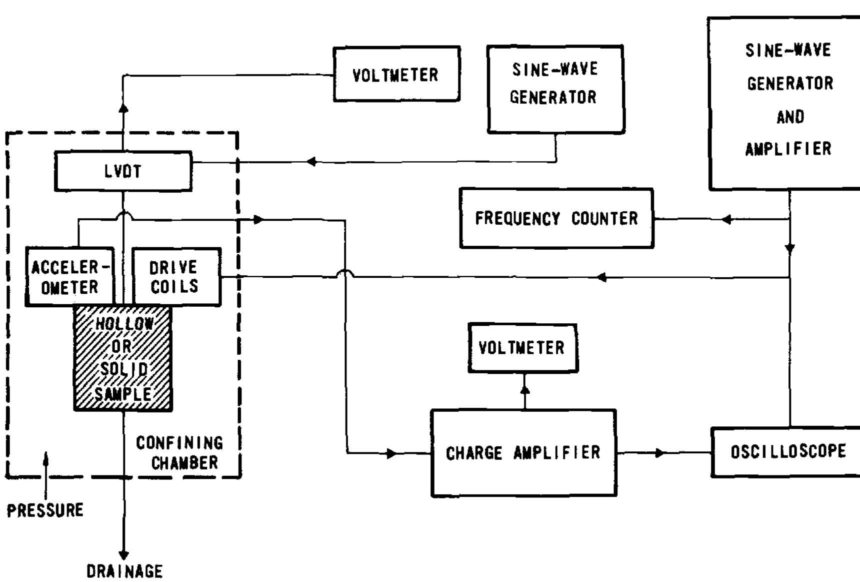

FIG. 3—*Typical electronics for resonant-column device.*

wave velocity and shear modulus are then determined on the basis of system constants and the size, shape, and weight of the soil specimen [*19*].

Low-Amplitude Test Procedure

In time-dependent, resonant-column studies, moduli are determined at various times after application of the confining pressure. The actual recording sequence is analogous to that used during an odeometer test; that is, moduli are measured at 1, 2, 4, 8, 15 ... minutes after the pressure is applied during the first day. Measurements are then made about twice a day thereafter.

Figure 4 illustrates a typical test sequence. Each recording requires about 30 to 60 s of vibration to determine the resonant frequency. Levels of deformation are such that shearing strains are less than 0.001 percent (hence, a low-amplitude test). It should be noted that duration of vibration is immaterial at these shearing strain levels. Whether the specimen is vibrated continuously or for only a few seconds has no influence on that measurement or on subsequent measurements. Only when strains exceed about 0.001 percent does duration of vibration affect moduli determination [*18,20,21*].

The entire low-amplitude test sequence is performed with drainage. It is not necessary to close drainage valves during vibration, as is typically done during cyclic triaxial testing, because levels of deformation are far below those levels required to generate excess pore-water pressures [*22,23*]. Specimens can be back-pressure saturated if desired; however, due to air migration, it is difficult to maintain a completely saturated state.

Low-amplitude measurements are performed until the slope of the re-

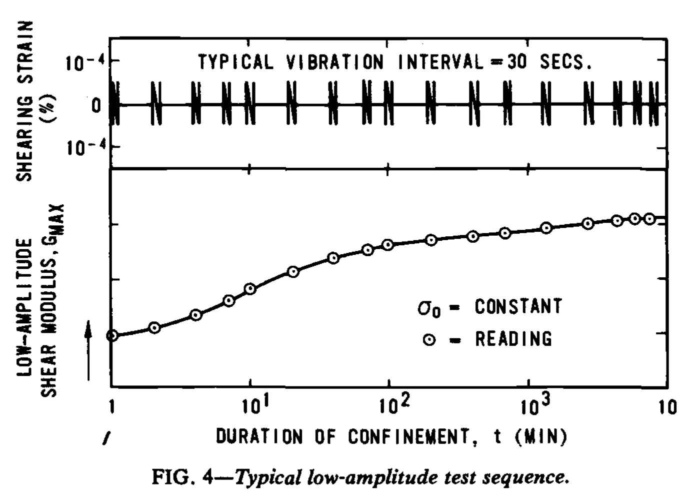

FIG. 4—*Typical low-amplitude test sequence.*

lationship for long-term modulus increase with time, I_G, is well defined. For most soils a one- to three-day period is sufficient to define I_G if the test pressure is part of an increasing confining pressure sequence. Experimental test results indicate that a longer period, up to as much as a week, may be required if the test pressure is part of a decreasing confining pressure sequence.

Upon completion of moduli measurements at one confining pressure, either the pressure is removed and the device disassembled, or the pressure is changed to the next pressure in the sequence. Once again amplitudes of vibration are so low that vibration at the previous pressure has no effect on moduli at the present confining pressure; therefore, a new modulus-time measurement sequence can be conducted at the higher confining pressure on the same specimen. However, modulus measurements are affected by stress history for the decreasing pressure sequence.

High-Amplitude Test Procedure

Measurement of shear moduli at shearing strains above 0.001 percent is not performed during primary consolidation, because of the unknown effective stress condition and because vibration at strains above this level might alter pore-water pressure and soil structure during this phase. Although high-amplitude measurements (above a shearing strain of 0.001 percent) could be performed immediately after primary consolidation, these modulus measurements are most meaningfully performed after the long-term time effect has been well defined at low-amplitude shearing strains.

High-amplitude modulus measurements are usually performed by increasing the amplitude of torsional vibration in several steps, and after each step the low-amplitude moduli are again determined. The low-amplitude moduli are used as reference values to determine if any specimen change has occurred as result of high-amplitude cycling [*18,21*]. The following is a typical high-amplitude measurement sequence given in terms of shearing strain amplitudes at which moduli were determined: 0.001, 0.004, 0.001, 0.01, 0.001, 0.02, 0.001, 0.04, 0.001, 0.07, 0.001, 0.10, 0.001, 0.20, and 0.001 percent. Figure 5 shows this sequence. About 30 to 40 s of high-amplitude vibration are required at each strain level, and usually a one-minute rest time is used between all measurements. Drainage valves are closed during the high-amplitude measurement sequence and opened during the rest interval.

After high-amplitude moduli measurements are completed, a rest period of several days follows during which the specimen remains under constant confining pressure with drainage. During this rest period the low-amplitude modulus should be monitored with time. The low-amplitude modulus may initially have a different value than that measured before the high-

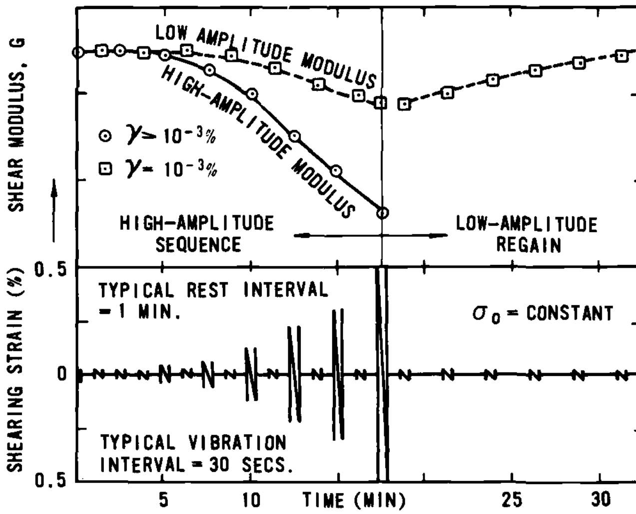

FIG. 5—*Typical high-amplitude test sequence for clay.*

amplitude sequence. For example, in clays a decrease in low-amplitude moduli typically occurs after high-amplitude cycling. This decrease in modulus is temporary, and the low-amplitude modulus regains with time to the value predicted by the long-term time effect [*18,21*]. If the low-amplitude modulus regains to the long-term time effect value, permanent alteration of the specimen characteristics is assumed not to have occurred, and another high-amplitude test sequence can be performed on the "undisturbed" specimen. If complete regain of the low-amplitude modulus does not occur, then subsequent modulus measurements will no longer be representative of initial specimen characteristics.

Evaluation

Resonant frequencies are converted to shear wave velocities and shear moduli by utilizing one-dimensional wave propagation formulas [*19,24*]. Correct specimen volume and weight at the measurement time should be used in these calculations. Results are typically plotted showing the variation in velocity or modulus as a function of the logarithm of time at a constant pressure. It should be noted that *velocity* most closely follows a linear increase with the logarithm of time [*18*]. Because modulus is determined from the square of the velocity, a slightly nonlinear variation in moduli results with increasing time. For most cases this variation is small, and the increase in modulus can be assumed linear.

Low-Amplitude, Time-Dependent Shear Moduli

The shape of the low-amplitude modulus-time response at a constant confining pressure depends primarily on whether the soil is predominantly fine-grained (silts and clays) or coarse-grained (sands).

Fine-Grained Soils

Figure 6*a* illustrates typical changes in shear modulus with time at a constant confining pressure for a clay on the loading sequence. The two distinct phases of modulus-time response are very evident in this figure. First,

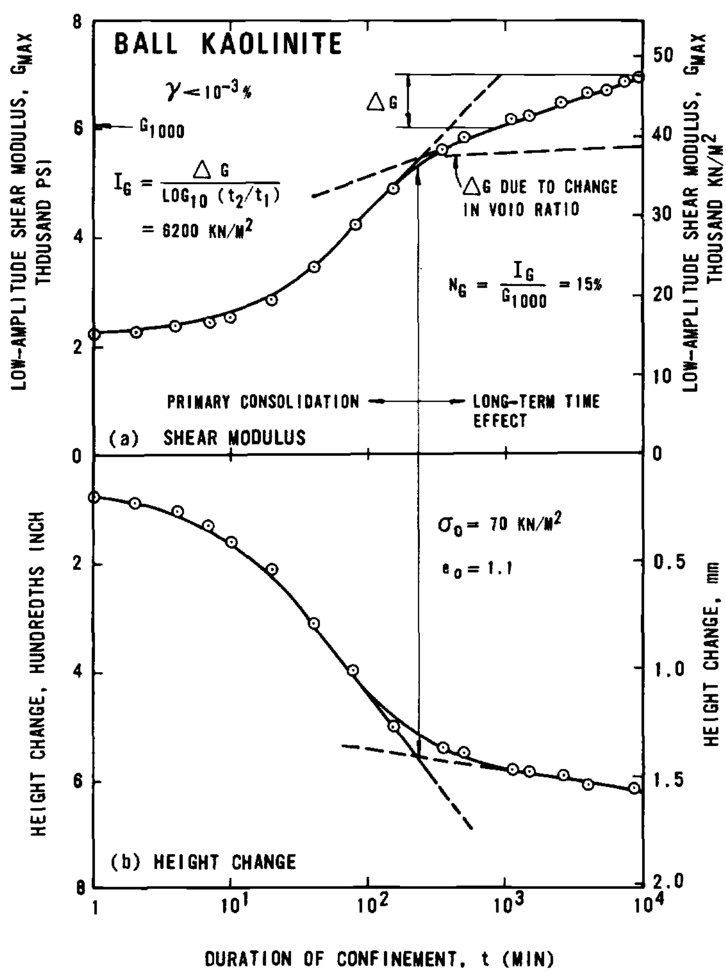

FIG. 6—*Typical modulus and height changes with time for clay at constant confining pressure.*

during primary consolidation, values of the shear modulus are initially constant, then increase rapidly and finally begin to level off. Second, during the long-term time effect, values of the modulus increase linearly with the logarithm of time.

Figure 6*b* shows the vertical height change of the clay specimen during this constant-pressure confinement. By comparing the height change results with the modulus-time response, it is evident that the end of the initial phase in the modulus-time response coincided with the end of primary consolidation. The point of transition in the modulus-time response for this loading sequence is defined as the end of primary consolidation. Therefore, modulus values determined at confinement times before the end of the primary consolidation phase will be at an effective stress less than that assumed because excess pore-water pressures still exist in the specimen.

During the long-term time-effect phase of modulus response, shear modulus increased about linearly with the logarithm of time. In Fig. 6*a*, this increase was monitored for 10 000 min or about one week. For another study of a fine-grained soil [25], a similar modulus-time response was monitored over periods as long as 20 weeks. In Fig. 6*a* the coefficient of shear modulus increase with time, I_G, is about 6200 kN/m^2 (900 psi), and the normalized shear modulus increase with time, N_G, is about 15 percent.

Several factors appear to affect values of I_G and N_G. The value of I_G generally increases as the confining pressure increases. Values of N_G decrease with increasing undrained shearing strength and increase with increasing void ratio for fine-grained soils [26]. Stress history also affects values of I_G and N_G. Figure 7 shows this effect for a series of modulus-time tests conducted on one specimen. Values of the modulus were determined over approximately a one-week period of confinement at each pressure in the following pressure sequence: 117, 235, 414, 235, and 117 kN/m^2 (17, 34, 60, 34, and 17 psi). It can be observed that, in the overconsolidated state, values of I_G and N_G were reduced relative to value of I_G and N_G in the normally consolidated state. Finally, N_G increases as the mean grain diameter, D_{50}, decreases, as shown in Fig. 8.

Coarse-Grained Soils

A typical modulus-time response of a coarse-grained soil is illustrated in Fig. 9. It can be observed that the shape of the modulus-time response for the cohesionless soil differs significantly from that of the fine-grained soil shown in Fig. 6. For the sand shown in Fig. 9, the primary consolidation phase is not evident. Rather, the long-term time effect had begun by the time the first measurement was made. The long-term time effect is, however, similar to that which occurs for clays, that is, a straight line on a semilogarithmic plot of modulus versus time.

No evidence of primary consolidation should have been expected in this

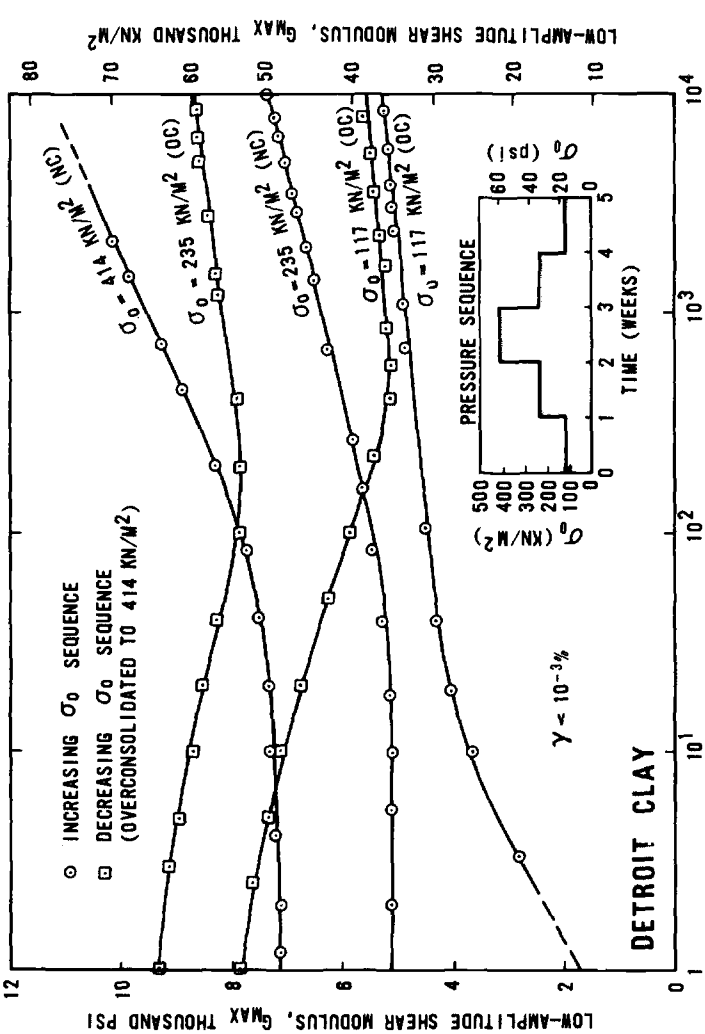

FIG. 7—*Effect of stress history on shear modulus-time relationship.*

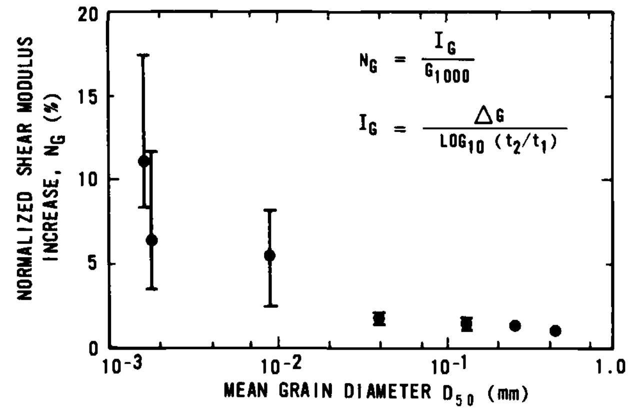

FIG. 8—*Effect of D_{50} on normalized modulus increase.* I_G (*Ref* 9).

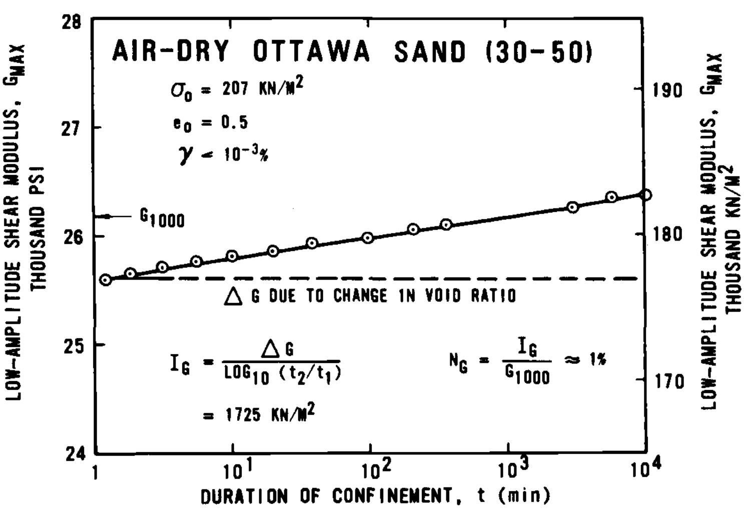

FIG. 9—*Typical modulus change with time for sand (data from Ref* 18).

clean sand because pore pressure changes and elastic deformations occurred prior to the first modulus measurement. If fines had inhibited drainage, some primary consolidation would have occurred. It should not, however, be interpreted that the initial phase of the modulus-time response in a sand is strictly a pore-pressure, elastic deformation process. In view of the high stresses at points of particle contact, some viscoelastic adjustments might occur depending on the crystalline structure of the soil grains. Therefore, a nonlinear response might be recorded initially.

In Fig. 9 the linear increase in modulus with the logarithm of time was monitored for about 10 000 min. Other results have been presented [6] in which this response was monitored for as many as 60 weeks in crushed, air-dried sand (Agsco No. 2). Values of I_G and N_G for the results shown in Fig. 9 are 1725 kN/m^2 (250 psi) and 1.0 percent, respectively. These values are much smaller than those shown for the clays in Fig. 6*a*.

In contrast to the behavior of fine-grained soils, the magnitude of the long-term time effect in coarse-grained soils seems to be relatively independent of D_{50} until values of D_{50} are less than about 0.05 mm (0.002 in.), as shown in Fig. 8. It should be noted, however, that Fig. 8 was developed on the basis of measurements made on relatively uniform sands. Other unpublished data indicate that N_G in sands increases as the proportion of fine-grained material increases; that is, a silty sand will exhibit a higher N_G than a clean sand even though both materials have the same D_{50}.

High-Amplitude, Time-Dependent Shear Moduli

Variations in modulus with time of confinement at a constant pressure are not limited to low shearing strain amplitudes. Recent studies [*13,18,27*] indicate that moduli measured at shearing strain amplitudes between 0.001 and 0.1 percent also increase with time.

At present (1977), only the long-term time effect of high-amplitude response for fine-grained soils has been investigated extensively. Typical results for a soft marine clay are presented in Fig. 10. It can be observed in this figure that the modulus increase with time at 0.1 percent shearing strain was only slightly below the rate recorded at low-amplitude shearing strains. These modulus increases at larger strains were noted at the onset

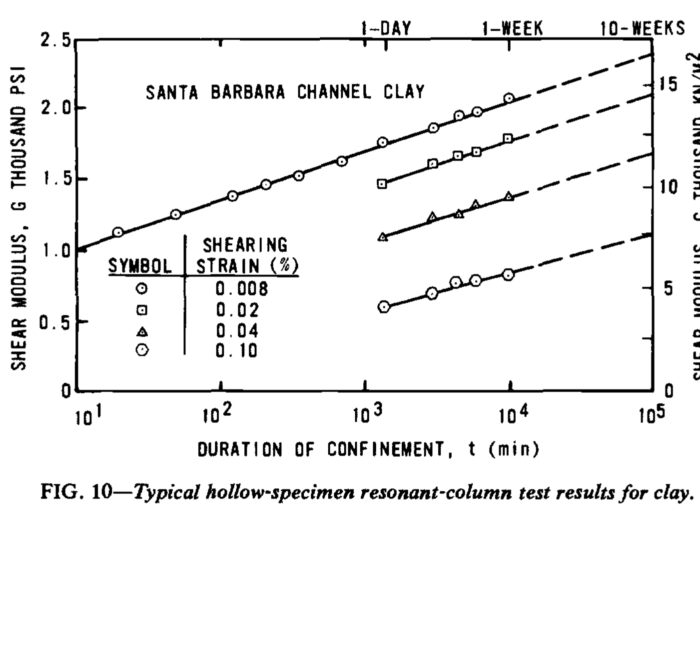

FIG. 10—*Typical hollow-specimen resonant-column test results for clay.*

of high-amplitude cycling, before pore pressure buildup and modulus degradation became a factor.

A number of tests [*18*] have been performed which also show that long-term modulus increases occur at low to intermediate strain levels (0.001 to 0.1 percent) for stiffer clays. Preliminary results from long-term, high-amplitude moduli tests on sand seem to indicate that long-term moduli increases occur in clean, dry sands at strain amplitudes to 0.1 percent as well. These results are consistent with those noted by others [*28-30*] where strength (a high-strain behavior) was also found to be time dependent.

Because of the general similarity between the increase in moduli with time at low- and high-shearing strain amplitudes, it seems reasonable to conclude that many of the factors which affect the low-amplitude modulus time response also affect the high-amplitude, modulus-time response (at the start of high-amplitude cycling).

Interpretation of Time-Dependent Shear Moduli

The time-dependent behavior of shear modulus has fundamental importance in planning and executing a laboratory testing program. Evaluation and understanding of this time-dependent behavior is also important in the prediction of *in situ* shear moduli from laboratory measurements.

Primary Consolidation

Primary consolidation should be completed before defining low-amplitude modulus or initiating a high-amplitude test sequence. If primary consolidation is not complete, then excess pore-water pressures exist, and modulus values are defined at an unknown state of effective stress. In general, drained confinement for one day before measurement is adequate for sands and clays (for specimens sizes up to 7 cm (2.8 in.) in diameter with radial and end drainage).

Because primary consolidation occurs in less than one day for most specimens, a one-day measurement of shear modulus will include some increase in modulus from the long-term time effect. One might speculate that the contribution of the long-term time effect would be most significant in coarse sands because primary consolidation occurs so rapidly in these materials [three or more log cycles of time (in minutes) elapse between the end of primary consolidation and the one-day reading]. However, the long-term time effect in coarse sands is generally quite small, so that differences in modulus introduced by including some long-term time increase are generally small. This is not necessarily the case for clays, particularly if significant time elapses between the end of primary consolidation and the measurement. For example, consider a clay specimen which is confined on Friday and tested on Monday rather than on Saturday. The modulus measured on Monday may be 10 percent or more greater than the modulus which would have been measured on Saturday. This difference would be even more important if measurements were made on a soft marine specimen where long-term modulus increases can be very large.

Low-Amplitude Moduli

Evaluation of the long-term time effect serves a very useful function if shear moduli have not been determined *in situ*. It has been shown [10-14] that laboratory shear wave velocities and shear moduli determined after one day of confinement are typically less than those occurring *in situ*. However, when long-term modulus increases are properly introduced into the comparison, much closer agreement between field and laboratory moduli results. The amount of long-term time effect which should be incorporated in the laboratory measurement is believed to be related to the geological age and geological history of the material.

To estimate low-amplitude moduli where *in situ* data do not exist, the following procedure can be used. First, measure the low-amplitude shear modulus at the end of primary consolidation, $G_{\text{max primary}}$. Then evaluate the long-term time effect, I_G, from resonant-column tests or from empirical relationships [9,26]. With I_G, add to $G_{\text{max primary}}$ the long-term time effect estimated to have occurred in the field. This procedure can be expressed mathematically as

$$G_{\text{max field}} = G_{\text{max primary}} + F_A * I_G \tag{3}$$

where

$G_{\text{max field}}$ = predicted *in situ* low-amplitude shear modulus, and
F_A = age factor for site.

The age factor of a site is estimated from

$$F_A = \log_{10}(t_c/t_p) \tag{4}$$

where

t_c = time since start of most recent *significant* change in stress history at the site, and
t_p = time to complete primary consolidation at site as a result of stress change.

The time to complete primary consolidation, t_p, will vary with soil type, thickness of the deposit, drainage conditions, etc. For sand deposits, t_p is usually assumed to be small, say equal to 100 or 1000 min, whereas for clays t_p may be on the order of years. Typical values of F_A might range from 4 to 8, which corresponds to site ages of 20 and 200 000 years, respectively (assuming primary consolidation was completed in a day or less).

As an example, consider a site composed of a 6-m-thick (20 ft) layer of sand overlying a 3-m-thick (10 ft) layer of overconsolidated clay which is underlain by bedrock. The water table is at the interface between the sand and clay. The average age of the sand is estimated to be 55 000 years, and the average age of the clay is estimated to be 2.5 million years. The object is to predict the low-amplitude *in situ* shear modulus at the center of the clay layer as the deposit presently exists. From laboratory tests, it was determined that

$$G_{\text{max primary}} = 125\,000 \text{ kN/m}^2 \text{ (18 120 psi)} \tag{5}$$

$$I_G = 14\,000 \text{ kN/m}^2 \text{ (2030 psi)} \tag{6}$$

$$t_p = 1000 \text{ days} \tag{7}$$

If it is assumed that the most recent significant stress change in the clay resulted from the loading imposed by the sand, then

$$t_c \simeq 55\,000 \text{ years} \tag{8}$$

$$F_A = \log\left(\frac{55\,000 \text{ years} \times 365 \text{ days/year}}{1000 \text{ days}}\right) = 4.3 \tag{9}$$

The estimated *in situ* shear modulus is

$$\begin{aligned} G_{\text{max field}} &= 125\,000 \text{ kN/m}^2 \text{ (18 120 psi)} + 4.3 * 14\,000 \text{ kN/m}^2 \text{ (2030 psi)} \\ &= 185\,200 \text{ kN/m}^2 \text{ (26 840 psi)} \end{aligned} \tag{10}$$

This estimating procedure does not take into account modulus variations due to effects such as specimen disturbance and incorrect laboratory representation of field confinement. In the case of clays and dense sands, moduli estimated by this procedure most likely represent a lower bound. However, for loose sands sampling may actually increase the stiffness and, in that case, the estimated moduli may represent an upper bound.

It is important to recognize that in this extrapolation method the time for primary consolidation and time of the most recent significant stress change are usually very difficult to estimate. For example, a sudden change in water table or an earthquake may cause enough stress change to destroy the previous effects of long-term confinement. Laboratory test data indicate that changes in effective confining pressure as small as 70 kN/m² (10 psi) may alter long-term effects in normally consolidated soils [*9*]. However, this threshold is expected to differ according to the soil type and the stress history at the site. For instance, a heavily overconsolidated clay may require far more than a 70 kN/m² (10 psi) change to alter long-term time effects. In view of these unknown factors, any estimate of field moduli can at best be shown as a range in expected values.

In situ *High-Amplitude Moduli*

Results in Fig. 10, which show shear moduli increasing with time at low to intermediate shearing strain amplitudes (0.001 to 0.1 percent), suggest that the modulus-versus-strain curve would continually shift upward until the low-amplitude laboratory modulus coincided with the seismic modulus if tests were conducted for a long enough time (neglecting sampling disturbance, etc.). This concept is shown in Fig. 11. The expected field modulus-strain curve at the point where the lab and seismic moduli coincide would be represented mathematically by

$$G_{\text{field}} = G_{\text{lab}} + A_r \tag{11}$$

where A_r is simply the difference between $G_{\max\,\text{field}}$ and $G_{\max\,\text{lab}}$.

It is worthwhile noting that the modulus-strain curve predicted on this basis differs considerably from the curve commonly used in the engineering profession today. In the commonly used procedure, shear moduli are increased by a constant percentage, that is

$$G_{\text{field}} = G_{\text{lab}} * P_r \tag{12}$$

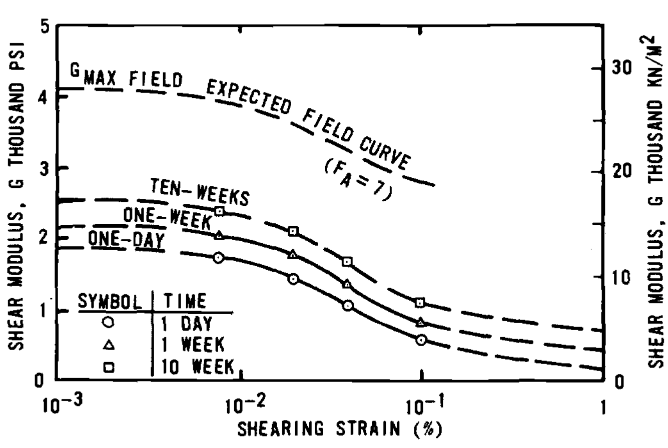

FIG. 11—*Effect of time on shear modulus versus shearing strain relationship.*

where P_r is the ratio of $G_{\max\ \mathrm{field}}$ to $G_{\max\ \mathrm{lab}}$. This procedure is perhaps more easily recognized as

$$G_{\mathrm{field}} = \left(\frac{G}{G_{\max}}\right)_{\mathrm{lab}} * G_{\max\ \mathrm{field}} \tag{13}$$

but has the same meaning.

The two approaches are shown schematically in Fig. 12. Note that at lower strains (less than 0.01 percent) the two procedures give similar values of shear modulus, but as shearing strains increase the difference between modulus values predicted by the two methods increases. In the 0.01 to 0.1 percent range the two values may differ by 50 percent or more, with the value predicted by the arithmetic method being higher than that predicted by the percentage method.

To demonstrate the arithmetic-prediction procedure, consider the previous example of the sand-clay-bedrock site for which $G_{\max\ \mathrm{field}}$ at the center of the clay layer was predicted. The object is now to predict the *in situ* shear modulus at the center of the clay layer at a shearing strain of 0.1 percent at the start of cyclic loading. For this example, assume that $G_{\max\ \mathrm{field}}$ has been determined by seismic methods and is equal to 205 000 kN/m^2 (29 710 psi) [which if, in fact, were true would be considered to be in very good agreement with the predicted lower bound of 185 200 kN/m^2 (26 840

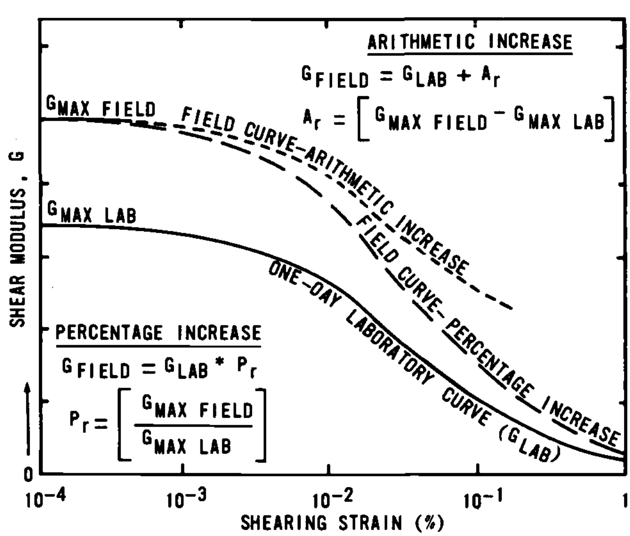

FIG. 12—*Field curve predicted by arithmetic and percentage increase in moduli (Ref 26).*

psi)]. From high-amplitude laboratory tests, it was determined that at the end of primary consolidation

$$G_{\text{lab at } \gamma = 0.1\%} = 38\,000 \text{ kN/m}^2 \text{ (5510 psi)} \tag{14}$$

Then by the arithmetic method

$$\begin{aligned} G_{\text{field}} &= 38\,000 \text{ kN/m}^2 \text{ (5510 psi)} \\ &+ [205\,000 \text{ kN/m}^2 \text{ (29 710 psi)} - 125\,000 \text{ kN/m}^2 \text{ (18 120 psi)}] \\ &= 118\,000 \text{ kN/m}^2 \text{ (17 100 psi)} \end{aligned} \tag{15}$$

and by the percentage method

$$\begin{aligned} G_{\text{field}} &= 38\,000 \text{ kN/m}^2 \text{ (5510 psi)} \\ &\times [205\,000 \text{ kN/m}^2 \text{ (29 710 psi)}/125\,000 \text{ kN/m}^2 \text{ (18 120 psi)}] \\ &= 62\,320 \text{ kN/m}^2 \text{ (9030 psi)} \end{aligned} \tag{16}$$

The concept of an arithmetic increase also implies that the shape of the modulus ratio, G/G_{max}, versus shearing strain curve is not unique but changes with time. In fact, G/G_{max} will vary with the magnitude of the low-amplitude modulus as well as the coefficient of shear modulus increase with time, I_G, and age factor of the site, F_A. Figure 13 indicates that the most significant differences occur for soft soils (low G_{max}) exhibiting a large long-term time effect, such as a marine clay, and that the least difference occurs for stiff soils (large G_{max}) with a small long-term time effect, such as dense sands and highly overconsolidated clays. In Fig. 13 the upper bound of the long-term time-effect band represents a site age of about 200 000 years and the lower bound about 20 years (assuming a short period of primary consolidation).

Because laboratory test results are time dependent, the G/G_{max} versus shearing strain curve cannot be unique. Therefore, the percentage increase procedure based on measurements made after one day of specimen confinement will be at best a lower bound. Due to the impracticality of conducting extremely long-term tests, a question exists regarding the best location for the field curve. Whether the actual curve will be equal to the arithmetically corrected curve or will fall between the two can be verified only by conducting high-amplitude *in situ* tests and comparing results with results predicted on either basis. Although laboratory data suggest that results will more closely resemble the arithmetic correction at strains less than 0.1 percent (Eq 11), it would probably be prudent at this stage

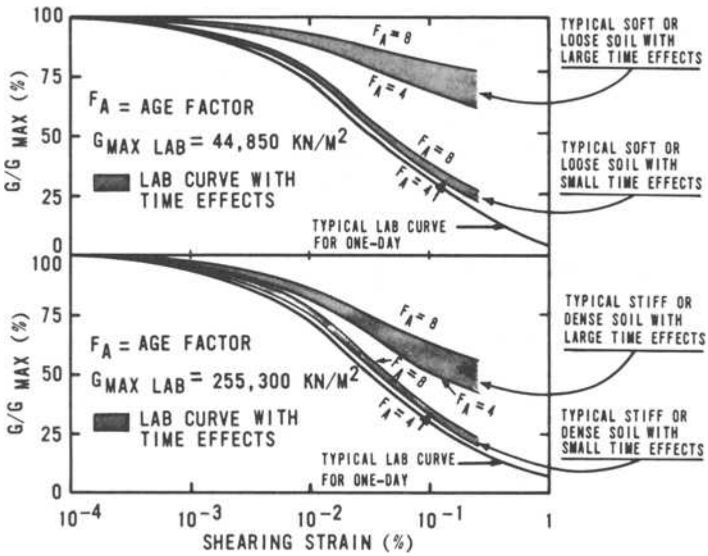

FIG. 13—*Effect of time on modulus ratio curves* (*Ref* 28).

to use both methods and evaluate the consequences of the different bounds on the project of concern.

Conclusions

On the basis of information presented, the following conclusions can be made:

1. Shear moduli of sands, silts, and clays vary with time of confinement at a constant confining pressure. Time, therefore, must be considered when reporting and interpreting shear moduli data from laboratory tests.

2. The time-dependent response of shear modulus at shearing strains less than or equal to 0.001 percent is characterized by two phases: an initial phase which is due mainly to primary consolidation, and a second phase in which modulus increases about linearly with the logarithm of time. The second phase is referred to as the long-term time effect. Fine-grained soils exhibit both phases when tested, whereas coarse-grained soils usually exhibit only the long-term time effect.

3. Increase in shear modulus with duration of confinement also occurs at shearing strains from 0.001 to 0.1 percent. This increase in high-amplitude modulus is equal to or slightly less than that which occurs at low-amplitude shearing strains. As a result, the shape of the G/G_{max} versus shearing strain curve is not unique but changes with time. This nonunique-

ness is most significant for soft soils which exhibit a large long-term time effect.

4. High-amplitude shear moduli should be determined by an increasing shearing-strain amplitude test sequence similar to that shown in Fig. 5. The low-amplitude modulus should be used as a reference value to evaluate possible permanent specimen changes resulting from high-amplitude cycling.

5. To estimate *in situ* low-amplitude shear moduli from laboratory tests, the increase in modulus with time should be taken into account in a manner shown by Eq 3.

6. To estimate *in situ* high-amplitude shear moduli from laboratory tests, the arithmetic increase shown by Eq 11 represents a possible upper bound and the percentage increase shown by Eq 12 represents a reasonable lower bound.

Recommendations

In view of the general importance of the time-dependent behavior of shear modulus, it is recommended that ASTM procedures for performing resonant-column and other dynamic tests incorporate a provision for assuring that shear moduli are evaluated after primary consolidation has been completed, as determined by monitoring the change in low-amplitude shear modulus, height change, or volume change with time. Moreover, such ASTM procedures should require that a statement be included with the test results which documents the duration of confinement (at each confining pressure) and the time for primary consolidation. It is further recommended that the long-term time effect for a representative number of specimens be determined if *in situ* moduli are to be predicted. It is also recommended that comparisons of laboratory values of shear moduli be made either at the end of primary consolidation or after equal intervals of the long-term time effect. Finally, it is recommended that if the long-term time effect is to be determined at high shearing strain amplitudes, procedures outlined in this discussion be followed.

Acknowledgments

The authors would like to thank F. E. Richart, Jr., and R. D. Woods for their guidance, stimulation, and encouragement over the past ten years. Funding from the Department of Civil Engineering and the College of Engineering at The University of Michigan, the Bureau of Engineering Research and the University Research Institute at the University of Texas, National Science Foundation Grants GK-37443 and GK-21455 and U.S. Geological Survey Grant No. 14-08-001-G-194 are greatly appreciated.

Support provided by the Fugro Technical Development Program for the preparation of this paper is also gratefully acknowledged.

References

[1] Richart, F. E., Jr., Closure to "Foundation Vibrations," *Journal of the Soil Mechanics and Foundation Division*, American Society of Civil Engineers, Vol. 87, No. SM4, Part 1, Aug. 1961, pp. 169-178.

[2] Lawrence, F. V., Jr., "Ultrasonic Wave Velocities in Sand and Clay," Report No. 23, Response of Soils to Dynamic Loadings, Massachusetts Institute of Technology, Cambridge, Mass., 1965.

[3] Drnevich, V. P., "Effects of Strain History on the Dynamic Properties of Sand," thesis presented in partial fulfillment for Ph.D., The University of Michigan, Ann Arbor, Mich., 1967, p. 151.

[4] Hardin, B. O., and Black, W. L., *Journal of the Soil Mechanics and Foundations Division*, American Society of Civil Engineers, Vol. 94, No. SM2, March 1968, pp. 353-368.

[5] Humphries, W. K. and Wahls, H. E., *Journal of the Soil Mechanics and Foundations Division*, American Society of Civil Engineers, Vol. 94, No. SM2, March 1968, pp. 371-389.

[6] Afifi, S. E. A. and Woods, R. D., *Journal of the Soil Mechanics and Foundations Division*, American Society of Civil Engineers, Vol. 97, No. SM10, Oct. 1971, pp. 1445-1460.

[7] Gray, D. H. and Kashmeeri, N. A., *Journal of the Soil Mechanics and Foundations Division*, American Society of Civil Engineers, Vol. 97, No. SM1, Jan. 1971. pp. 193-207.

[8] Marcuson, W. F., III, and Wahls, H. E., *Journal of the Soil Mechanics and Foundations Division*, American Society of Civil Engineers, Vol. 98, No. SM12, Dec. 1972, pp. 1359-1373.

[9] Afifi, S. E. A. and Richart, F. E., Jr., *Soils and Foundations* (Japan), Vol. 13, No. 1, March 1973, pp. 77-95.

[10] Stokoe, K. H., II, and Richart, F. E., Jr. in *Proceedings*, Fifth World Conference on Earthquake Engineering, Rome, Vol. 1, 1973a, pp. 356-359.

[11] Stokoe, K. H., II, and Richart, F. E., Jr. in *Proceedings*, Eighth International Conference on Soil Mechanics and Foundation Engineering, Moscow, Vol. 1, Part 2, 1973b, pp. 403-409.

[12] Trudeau, P. J., Whitman, R. V., and Christian, J. T., *Journal of the Boston Society of Civil Engineers*, Vol. 61, No. 1, Jan. 1974, pp. 12-25.

[13] Anderson, D. G. and Woods, R. D., *Proceedings*, *In Situ* Measurement of Soil Properties, American Society of Civil Engineers, Raleigh, N.C., Vol. 1, 1975, pp. 66-92.

[14] Stokoe, K. H., II, and Abdel-razzak, K. G., *Proceedings*, *In Situ* Measurement of Soil Properties, American Society of Civil Engineers, Raleigh, N.C., Vol. 1, 1975, pp. 422-447.

[15] Yang, Z. and Hatheway, A. W., *Journal of the Geotechnical Engineering Division*, American Society of Civil Engineers, Vol. 102, No. GT2, Feb. 1976, pp. 123-138.

[16] Afifi, S. E. A., "Effects of Stress History on the Shear Modulus of Soils," thesis presented in partial fulfillment for Ph.D., The University of Michigan, Ann Arbor, Mich., 1970, p. 209.

[17] Hardin, B. O. and Music, J. in *Instruments and Apparatus for Soil and Rock Mechanics, ASTM STP 392*, American Society for Testing Materials, 1965, pp. 55-74.

[18] Lodde, P. J., "Shear Moduli and Material Damping Ratios of San Francisco Bay Mud," thesis to be presented in partial fulfillment for M.Sc., The University of Texas, Austin, Tex. (in preparation).

[19] Drnevich, V. P., Hardin, B. O., and Shippy, D. H., this publication, pp. 91-125.

[20] Hardin, B. O. and Drnevich, V. P., *Journal of the Soil Mechanics and Foundations Division*, American Society of Civil Engineers, Vol. 98, No. SM6, June 1972, pp. 603-624.

[21] Anderson, D. G. and Richart, F. E., Jr., *Journal of the Geotechnical Engineering Division*, American Society of Civil Engineers, Vol. 102, No. SM9, Sept. 1976, pp. 975-987.

[22] Drnevich, V. P., *Journal of the Soil Mechanics and Foundation Division,* American Society of Civil Engineers, Vol. 98, Aug. 1972, pp. 807-825.
[23] Silver, M. C. and Park, T. K., *Journal of the Geotechnical Engineering Division,* American Society of Civil Engineers, Vol. 101, No. GT10, Oct. 1975, pp. 1060-1083.
[24] Richart, F. E., Jr., Hall, J. R., Jr., and Woods, R. D., *Vibrations of Soils and Foundations,* Prentice-Hall, Englewood Cliffs, N.J., 1970.
[25] Anderson, D. G., "Dynamic Modulus of Cohesive Soils," dissertation presented in partial fulfillment for Ph.D., The University of Michigan, Ann Arbor, Mich., June 1974.
[26] Anderson, D. G. and Woods, R. D., *Journal of the Geotechnical Engineering Division*, American Society of Civil Engineers, Vol. 102, No. GT5, May 1976, pp. 525-537.
[27] Richart, F. E., Jr., Anderson, D. G., and Stokoe, K. H., II, *Proceedings,* Sixth World Conference on Earthquake Engineering, New Delhi, Vol. 6, Jan. 1977, pp. 159-164.
[28] Mitchell, J. K., *Journal of the Soil Mechanics and Foundation Division,* American Society of Civil Engineers, Vol. 86, No. SM3, June 1960, pp. 19-52.
[29] Bjerrum, L. A. and Ko, K. Y., *Geotechnique,* Vol. 13, No. 2, June 1963, pp. 147-157.
[30] Lee, K. L., "Formation of Adhesion Bonds in Sands at High Pressures," UCLA Report No. 7586, University of California, Los Angeles, Oct. 1975, p. 12.
[31] Fugro, Inc., "Sustained-Pressure Studies," Fugro Technical Development Program, unpublished, 1977.

V. P. Drnevich,[1] *B. O. Hardin,*[1] *and D. J. Shippy*[1]

Modulus and Damping of Soils by the Resonant-Column Method

REFERENCE: Drnevich, V. P., Hardin, B. O., and Shippy, D. J., "**Modulus and Damping of Soils by the Resonant-Column Method,**" *Dynamic Geotechnical Testing, ASTM STP 654,* American Society for Testing and Materials, 1978, pp. 91–125.

ABSTRACT: The resonant-column method, a relatively nondestructive test employing wave propagation in cylindrical specimens, is used to obtain modulus and damping of soils as functions of vibratory strain amplitude and other factors such as ambient confining stress and void ratio. Descriptions of the apparatus, calibration procedures, testing procedures, and aids for data reduction are given for apparatus which propagate either rod compression waves or shear waves or both. Data reduction aids include graphs for a wide range of apparatus conditions and include a computer program that covers all admissable boundary conditions.

KEY WORDS: resonant column, soil testing, soil dynamics, laboratory testing, modulus, damping, stresses, strains, test apparatus, wave propagation, resonance, viscoelastic, vibration, testing procedures, data reduction, computer programs, nondestructive testing, soils

The methods discussed herein cover the determination of the shear modulus, shear damping, rod modulus (commonly referred to as Young's modulus), and rod damping for solid cylindrical specimens of soil in the undisturbed and remolded conditions by vibration using the resonant column. The vibration of the specimen may be superposed on a controlled ambient state of stress in the specimen. The vibration apparatus and specimen may be enclosed in a triaxial chamber and subjected to an all-around pressure and axial load. In addition, the specimen may be subjected to other controlled conditions (for example, pore-water pressure, degree of saturation, temperature). These methods of modulus and damping determination are considered nondestructive when the strain amplitudes of vibration are less than 10^{-4} rad (10^{-4} in./in.), and many measurements may be made on the same specimen and with various states of ambient stress.

[1] Associate professor, professor, and associate professor, respectively, Department of Civil Engineering, University of Kentucky, Lexington, Ky. 40502.

These methods cover only the determination of the modulus and damping, the necessary vibration, and specimen preparation procedures related to the vibration, etc., and do not cover the application, measurement, or control of the ambient stress. The latter procedures may be covered by, but are not limited to, the ASTM Test for Unconfined Compressive Strength of Cohesive Soils D 2166, or the ASTM Test for Unconsolidated Undrained Strength of Cohesive Soils in Triaxial Compression (D 2850).

Significance

The modulus and damping of a given soil, as measured by the resonant-column technique herein described, depend upon the strain amplitude of vibration, the ambient state of effective stress, and the void ratio of the soil as well as other, less significant factors such as temperature and time. Since the application and control of the ambient stresses and the void ratio are not prescribed in these methods, the applicability of the results to field conditions will depend on the degree to which the application and control of the ambient stresses and the void ratio, as well as other parameters such as soil structure, duplicate field conditions. The techniques used to simulate field conditions depend on many factors and it is up to the engineer to decide on which techniques apply to a given situation and soil type.

Definitions

Resonant-Column System

The resonant-column system consists of a cylindrical specimen or column of soil that has platens attached to each end as shown in Fig. 1. A sinusoidal vibration excitation device is attached to the active-end platen. The other end is the passive-end platen. It may be rigidly fixed (the criterion for establishing fixity is given later) or its mass and rotational inertia must be known. The vibration excitation device may incorporate springs and dashpots connected to the active-end platen, where the spring constants and viscous damping coefficients are known. Vibration excitation may be longitudinal or torsional. A given apparatus may have the capability of applying one or the other, or both. The mass and rotational inertia of the active-end platen and portions of the vibration excitation device moving with it must be known. Transducers are used to measure the vibration amplitudes for each type of motion at the active end and also at the passive end if it is not rigidly fixed. The frequency of excitation will be adjusted to produce resonance of the system, composed of the specimen and its attached platens and vibration excitation device.

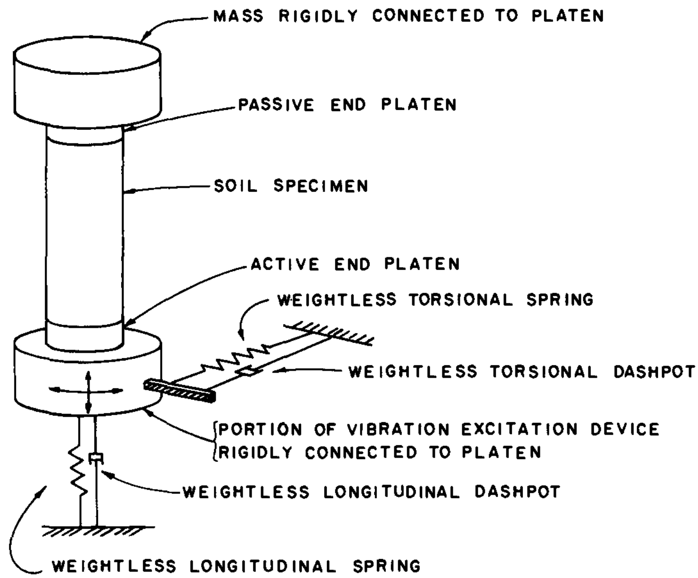

FIG. 1—*Resonant-column schematic.*

System Resonant Frequency

The definition of system resonance depends on both apparatus and specimen characteristics. For the case where the passive-end platen is fixed, motion at the active end is used to establish resonance, which is defined as the lowest frequency for which the sinusoidal excitation force (or moment) is in phase with the velocity of the active-end platen. For the case where the passive-end platen mass (or passive end platen rotational inertia) is greater than 100 times the corresponding value of the specimen and is not rigidly fixed, resonance is the lowest frequency for which the sinusoidal excitation force (or moment) is 180 deg out of phase with the velocity of the active-end platen. Otherwise, motion at the passive end is used to establish resonance, which is the second lowest frequency for which the sinusoidal excitation force (or moment) is in phase with the velocity of the passive-end platen. (The lowest frequency for this condition is not used because it does not produce significant strains in the specimen.) In general, the system resonant frequency for torsional excitation will be different from the system resonant frequency for longitudinal excitation.

Ambient Stress

These are stresses applied to the specimen, during the test, that do not result from the vibration strains. These methods of test do not cover the application and measurement of ambient stresses; however, the ambient stress at the time of measurement of the system resonant frequency and system damping shall be measured and recorded in accordance with the final section of the paper.

Moduli and Damping Capacities

Young's modulus (herein called rod modulus), E, is determined from longitudinal vibration, and the shear modulus, G, is determined from torsional vibration. The rod and shear moduli shall be defined as the elastic moduli of a uniform, linearly viscoelastic (Voigt model) specimen of the same mass density and dimensions as the soil specimen necessary to produce a resonant column having the measured system resonant frequency and response due to a given vibratory force or torque input. The stress-strain relation for a steady-state vibration in the resonant column is a hysteresis loop. These moduli will correspond to the slope of a line through the end points of the hysteresis loop. The section on calculations provides for computation of rod and shear moduli from the measured system longitudinal and torsional resonant frequencies. The energy dissipated by the system is a measure of the damping of the soil. Damping will be described by the rod damping ratio, D_L, and the shear damping ratio, D_T, which are analogous to the critical viscous damping ratio, c/c_r, for a single-degree-of-freedom system. The damping ratios shall be defined by

$$D_L = 0.5(\eta\omega/E)$$

where

η = viscous coefficient for rod motion [N-s/m^2],
ω = circular resonant frequency [rad/s], and
E = rod modulus [Pascal's].

and by

$$D_T = 0.5(\mu\omega/G)$$

where

μ = viscous coefficient for torsional motion [N-s/m^2], and
G = shear modulus [Pascal's].

Values of damping determined in this way will correspond to the area of the stress-strain hysteresis loop divided by 4π times the elastic strain energy stored in the specimen at maximum strain. Methods for determining damping ratio are prescribed later. In viscoelastic theory, it is common to use complex moduli to express both modulus and damping. The complex rod modulus is given by

$$E^* = E(1 + 2iD_L)$$

and the complex shear modulus is given by

$$G^* = G(1 + 2iD_T)$$

where

$i = \sqrt{-1}.$

Specimen Strain

For longitudinal motion, the strain, ϵ, is the average axial strain in the entire specimen. For torsional motion, the strain, γ, is the average shear strain in the specimen. In the case of torsion, shear strain in each cross section varies from zero along the axis of rotation to a maximum at the perimeter of the specimen, and the average shear strain for each cross section occurs at a radius equal to two-thirds the radius of the specimen. Methods for calculating specimen strain are given later in the Calculations section.

Apparatus Model and Constants

The rigidity and mass distribution of the resonant column shall be as required in the following section in order for the resonant-column system to be accurately represented by the model shown in Fig. 1. The apparatus constants are the mass of the passive-end platen, M_P, including the mass of all attachments rigidly connected to it; the rotational inertia of the passive-end platen, J_P, including the rotational inertia of all attachments rigidly connected to it; similar mass, M_A, and rotational inertia, J_A, for the active-end platen and all attachments rigidly connected to it, such as portions of the vibration excitation device; the spring and damping constants for both longitudinal and torsional springs and dashpots [K_{SL}, K_{ST}, ADC_L, ADC_T); the apparatus resonant frequencies for longitudinal vibration, f_{OL}, and torsional vibration, f_{OT}; the force/current constant, *FCF*, relating applied vibratory force to the current applied to the longitudinal excitation device; the torque/current constant, *TCF*, relating applied vibratory torque to the current applied to the torsional excitation device; and the motion transducer calibration factors (LCF_A, RCF_A, LCF_P, RCF_P) relating the transducer outputs to active- and passive-end longitudinal and rotational motion.

Apparatus

General

The complete test apparatus includes the platens for holding the specimen in the pressure cell, the vibration excitation device, transducers for measuring the response, the control and readout instrumentation, and auxiliary equipment for specimen preparation.

Specimen Platens

Both the active-end and passive-end platens shall be constructed of noncorrosive material having a modulus at least ten times the modulus of the material to be tested. Each platen shall have a circular cross section and a plane surface of contact with the specimen, except that the plane surface of contact may be roughened to provide for more efficient coupling with the ends of the specimen. The diameter of platens shall be equal to or greater than the diameter of the specimen. The construction of the platens shall be such that their stiffness is at least ten times the stiffness of the specimen. The active-end platen may have a portion of the excitation device, transducers, springs, and dashpots connected to it. The transducers and moving portions of the excitation device must be connected to the platen in such a fashion that they are to be considered part of the platen and have the same motion as the platen for the full range of frequencies to be encountered when testing soils. The theoretical model used for the resonant-column system represents the active-end platen, with all attachments, as a rigid mass that is attached to the specimen; this mass may also have weightless springs and dashpots attached to it as shown in Fig. 1. If weightless springs are used, the excitation device and active-end platen (without the specimen in place) form a two degree-of-freedom system (one-degree-of-freedom system for devices designed for only longitudinal or only torsional motion) having undamped natural frequencies for longitudinal motion, f_{0L}, and torsional motion, f_{0T}. The device shall be constructed such that these modes of vibration are uncoupled. The passive-end platen may have a mass and transducers rigidly attached to it or it may be rigidly fixed. The passive-end platen may be assumed to be rigidly fixed when the inertia of it and the mass(es) attached to it provide a dimensionless frequency factor within one percent of the dimensionless frequency factor for the passive-end inertia ratio equal to infinity. (Use Fig. 2 and the Calculations section to get the dimensionless frequency factor.)

Vibration Excitation Device

This shall be an electromagnetic device capable of applying a sinusoidal longitudinal vibration or torsional vibration or both to the active-end platen to which it is rigidly coupled. The frequency of excitation shall be adjustable and controlled to within 0.5 percent. The excitation device shall have a means of measuring the current applied to the drive coils that has at least a 5 percent accuracy. The voltage drop across a fixed, temperature-and-frequency-stable power resistor in series with the drive coils may be used for this purpose. The force/current and torque/current factors for the vibration excitation devices must be linear within 5 percent for the entire range of operating frequencies anticipated when testing soils.

Sine Wave Generator

The sine wave generator is an electric instrument capable of producing a sinusoidal current with a means of adjusting the frequency over the entire range of operating frequencies anticipated. This instrument shall provide sufficient power to produce the required vibration amplitude, or its output may be electronically amplified to provide sufficient power. The total distortion of the signal applied to the excitation device shall be less than 3 percent.

Vibration Measuring Devices and Readout Instruments

The vibration measuring devices shall be acceleration, velocity, or displacement transducers that can be attached to and become a part of the active- and passive-end platens. On each platen, one transducer shall be mounted to produce a calibrated electrical output that is proportional to the longitudinal acceleration, velocity, or displacement of that platen (not required for torsion-only apparatus). The other transducer shall be mounted to produce a calibrated electrical output that is proportional to the rotational acceleration, velocity, or displacement (not required for longitudinal-only apparatus). The readout instrument and transducers shall have a sensitivity such that a displacement of 2.5×10^{-6} m (10^{-4} in.) and a rotation of 10^{-5} rad can be measured with 10 percent accuracy for the entire range of frequency anticipated. It is also necessary to have an x-y-time oscilloscope available for observing signal waveforms and for establishing the system resonant frequency. This oscilloscope must have at least one amplifier (vertical or horizontal) with sufficient gain to observe the motion transducer output over the entire range of output voltages and frequencies anticipated. For measurement of damping by the free-vibration method, and for calibration of the apparatus damping, the readout instrument shall be capable of recording the decay of free vibration. Either a strip-chart recorder with appropriate response time and chart speed or an oscilloscope and camera may be used for this purpose.

Support for Vibration Excitation Device

For the special case where the passive end of the specimen is rigidly fixed and the vibration excitation device and active-end platen are placed on top of the specimen, it may be necessary to support all or a portion of the weight of the platen and excitation device to prevent excessive axial stress or compressive failure of the specimen. This support may be provided by a spring, counterbalance weights, or pneumatic cylinder as long as the supporting system does not prevent axial movement of the active-end platen and as long as it does not alter the vibration characteristics of the excitation device.

Temporary Platen Support Device

The temporary support may be any clamping device that can be used to support one or both end platens during attachment of vibration excitation device to prevent specimen disturbance during apparatus assembly. This device is to be removed prior to the application of vibration.

Vernier Caliper

The caliper shall be suitable for measuring the physical dimensions of the specimen to the nearest 0.25 mm (0.01 in.).

Weighing Device

The weighing device shall be suitable for weighing soil specimens as well as weighing portions of the device during calibration. All weighings should be accurate to 0.1 percent.

Specimen Preparation and Triaxial Equipment

These methods of test cover specimen preparation and procedures related to the vibration of the specimen and do not cover the application and control of ambient stresses. Any or all of the apparatus described in ASTM Methods D 2166 or D 2850 may be used for specimen preparation and application of ambient stresses. Additional apparatus may be used for these purposes as required.

Miscellaneous Apparatus

The miscellaneous apparatus consist of specimen trimming and carving tools, a membrane expander, remolding apparatus, moisture content cans, and data sheets as required.

Apparatus Calibration

Motion Transducers

Motion transducers shall be calibrated with each other and with an independent method to ensure calibration accuracy within 5 percent. Linear motion transducers whose axes are located fixed distances from the axis of rotation may be used to measure rotational motion if the cross-axis sensitivities of the transducers are less than 5 percent. For this case the distance between the axis of rotation and the transducer axes shall be known to within 5 percent. The calibration factors for longitudinal motion shall be expressed in terms of peak-meters/peak-volt. The calibration factors for rotational motion shall be expressed in terms of peak-radians/peak-volt. This means that for velocity and acceleration transducers the vibration frequency shall be included as a term in the calibration factor. For velocity transducers, the calibration factors are given by

$$\text{Displacement calibration factor} = \text{Velocity calibration factor}/(2\pi f)$$

where

f = frequency, Hz.

For acceleration transducers, the calibration factors are given by

$$\text{Displacement calibration factor} = \text{Acceleration calibration factor}/(2\pi f)^2$$

Thus, for velocity and acceleration transducers, the calibration factors will not be constants but will vary with measured frequency, f. Calibration factors for longitudinal motion are given by the symbol LCF with a subscript A or P denoting whether the transducer is located on the active-end platen or passive-end platen. Likewise, the calibration factors for rotational motion will be given by the symbol RCF and will have subscripts A or P depending on their location.

Passive-End Platen Mass and Rotational Inertia

The mass and rotational inertia of the passive-end platen shall be determined with all transducers and other rigid attachments securely in place. The mass, M_P, is calculated from

$$M_P = W_P/g$$

where

W_P = weight of passive-end platen and its attachments, and
g = acceleration of gravity.

The rotational inertia of the concentric solid cylindrical components of the passive-end platen and its attachments is given by

$$(J_P)_i = \frac{1}{8g} \sum_{i=1}^{n} W_i d_i^2$$

where

W_i = weight of ith solid cylindrical component,
d_i = diameter of ith solid cylindrical component, and
n = number of solid cylindrical components.

Transducers and other masses attached to this platen can be accounted for by

$$(J_P)_2 = \frac{1}{g} \sum_{i=1}^{n} W_i r_i^2$$

where

W_i = weight of ith component,
r_i = distance from the platen axis to center of mass for ith component, and
n = number of components attached to passive-end platen and not covered in determination of (J_P)

The total rotational inertia for the passive end is given by

$$J_P = (J_P)_1 + (J_P)_2$$

Active-End Platen Mass and Rotational Inertia

The mass, M_A, and rotational inertia, J_A, of the active-end platen shall be determined with all transducers and rigid attachments, including attached portions of the vibration excitation device, securely in place. The equations just given may be used to obtain the mass and rotational inertia. For rotational inertia, if all components do not have simple geometry, an alternative procedure that involves a metal calibration rod of known torsional stiffness may be used. One end of the rod shall be rigidly fixed and the other end shall be rigidly fastened to the active-end platen. Since it may be very difficult to fasten the calibration rod to the platen without adding rotational inertia, it is recommended that the calibration rod be permanently fastened by welding, etc., to an auxiliary platen. If the auxiliary platen is not identical to the one to be used in testing, the difference between its rotational inertia and that of the platen for soil testing must be taken into account by use of aforementioned equations. (For example, suppose that the value of the active-end rotational inertia with the calibration rod was $J1$ and the rotational inertia of the calibration rod platen was $J2$. If the rotational inertia of the platen for testing soil is $J3$, then the value of J_A would be given by $J_A = J1 - J2 + J3$.) The torsional stiffness of the calibration rod should be chosen such that the system resonant frequency with the calibration rod in place is near the middle of the range of system resonant frequencies anticipated for soil testing. Several calibration rods may be necessary to account for different specimen sizes. With the calibration rod in place, determine the low-amplitude system resonant frequency for torsional vibration, $(f_{rod})_T$. The rotational inertia of the active end platen system is calculated from

$$J_A = \frac{(K_{rod})_T}{(2\pi)^2\,[(f_{rod})_T^{\,2} - f_{oT}^{\,2}]}$$

where

$(K_{rod})_T$ = torsional stiffness of calibration rod,
= $(I_p G)/L$,
I_p = polar moment of inertia of calibration rod,
= $(\pi d^4)/32$,
d = calibration rod diameter,
G = shear modulus for calibration rod material, and
f_{oT} = apparatus torsional resonant frequency as described in the following subsection.

The foregoing equations assume that the rotational inertia of the calibration rods is much less than the corresponding values for the active-end platen system. A second alternative procedure is to couple the metal calibration rod to the platens in place of the specimen and then use the procedures of the Calculations section to backfigure the active end inertias from the known moduli of the rod.

Apparatus Resonant Frequencies, Spring Constants, and Damping Constants

Apparatus resonant frequencies and spring constants are defined only for those apparatus that have springs attached to the active-end platen system. To determine the resonant frequencies, set up the apparatus complete with active-end platen and O-rings but no specimen. Vibrate at low amplitude and adjust the frequency of vibration until the input force is in phase with the velocity of the active-end platen system. For longitudinal vibration, this apparatus resonant frequency is f_{oL} and for torsional vibration it is f_{oT}. The longitudinal and torsional apparatus spring constants (K_{SL}, K_{ST}) may be calculated from

$$K_{SL} = (2\pi f_{oL})^2 M_A$$

$$K_{ST} = (2\pi f_{oT})^2 J_A$$

where M_A and J_A are defined in the previous subsection.

To measure the damping constants for the apparatus, attach the same masses as used for the determination of apparatus resonant frequencies. For apparatus without springs attached to the active-end platen, insert the calibration rod described in the previous subsection. With the apparatus vibrating at the resonant frequency, cut off the power to the excitation device and record the decay curve for the vibration of the apparatus. From the decay curve, compute the logarithmic decrement, δ, as follows

$$\delta = \frac{1}{n} \ln \frac{A_1}{A_{n+1}}$$

where

A_1 = amplitude of vibration for first cycle after power is cut off, and
A_{n+1} = amplitude for $(n + 1)$th cycle.

The apparatus damping coefficient, ADC_L, from longitudinal vibration shall be given by

$$ADC_L = 2 f_L M_A \delta_L$$

where

f_L = longitudinal motion resonant frequency measured during apparatus damping determination,
M_A = active-end platen mass from previous subsection, and
δ_L = logarithmic decrement for longitudinal motion.

For torsional motion, the apparatus damping coefficient, ADC_T, is given by

$$ADC_T = 2 f_T J_A \delta_T$$

where

f_T = torsional motion resonant frequency measured during apparatus damping determination,
J_A = active-end rotational inertia from previous subsection, and
δ_T = logarithmic decrement for torsional motion.

Force/Current and Torque/Current

For apparatus without springs attached to the active-end platen, insert the calibration rod as described earlier. Determine the resonant frequency of this single-degree-of-freedom system consisting of the active-end platen and apparatus spring (or calibration rod) by use of the same procedure as described later in the Procedures section. Then set the frequency to 0.707 times the resonant frequency and apply sufficient current to the vibration excitation device so that the vibration transducer output to the readout device has a signal of at least ten times the signal due to ambient vibrations and electrical noise when no power is applied to the excitation device. Read and record the output of both the vibration transducer and the current measuring instrument. Next, set the frequency to 1.414 times the system resonant frequency and obtain the vibration transducer and current instrument readings in a similar fashion to those at 0.707 times the resonant frequency. Calculate C_1 and C_2 from

$$C_1 = \frac{(VTCF)\,(TO1)}{2(CR1)}$$

$$C_2 = \frac{(VTCF)\,(TO2)}{CR2}$$

where

$VTCF$ = active-end vibration transducer calibration factor (LCF or RCF) depending on whether vibration is longitudinal or torsional,
$TO1$ = active-end transducer output at 0.707 times resonant frequency,
$CR1$ = current instrument reading at 0.707 times resonant frequency,
$TO2$ = active-end transducer output at 1.414 times resonant frequency, and
$CR2$ = current instrument reading at 1.414 times resonant frequency.

C_1 and C_2 should agree within 10 percent. By use of C_1 and C_2 from longitudinal vibration, the force/current calibration factor, FCF, is obtained from

$$FCF = 0.5(C_1 + C_2)K$$

where

K = apparatus spring constant (or for apparatus without springs, the calibrating rod spring constant) for longitudinal motion.

By use of C_1 and C_2 from torsional vibration, the torque/current calibration factor, TCF, is obtained from

$$TCF = 0.5(C_1 + C_2)K$$

where

K = apparatus spring constant (or for apparatus without springs, the calibrating rod spring constant) for torsional motion.

Test Specimens

General

These methods cover only the special specimen preparation procedures related to the vibration and resonant-column technique. Since the resonant-column test may be conducted in conjunction with controlled ambient stresses, the provisions for preparation of specimens in ASTM Methods D 2166 or D 2850 may be applicable or may be used as a guide in connection with other methods of application and control of ambient stresses.

Specimen Size

Specimens shall be of uniform circular cross section with ends perpendicular to the axis of the specimen. Specimens shall have a minimum diameter of 33 mm (1.3 in.). The largest particle contained within the test specimen shall be smaller than one tenth of the specimen diameter except that, for specimens having a diameter of 70 mm (2.8 in.) or larger, the largest particle size shall be smaller than one sixth of the specimen diameter. If, after completion of a test, it is found that larger particles than permitted are present, indicate this information in the report of test data under "Remarks." The length-to-diameter ratio shall be not less than 2 (this may be changed to 1 for torsional vibration only) nor more than 7 except that, when an ambient axial stress greater than the ambient lateral stress is applied to the specimen, the ratio of length to diameter shall be between 2 and 3. Measure the length at three locations and average the values. Measure two diameters at each of three elevations and average the values. Determine the weight of the test specimen. For determination of moisture content [ASTM Test for Laboratory Determination of Moisture

Content of Soil (D 2216-71)], secure a representative specimen of the cuttings from undisturbed specimens, or of the extra soil for remolded specimens, placing the specimen immediately in a covered container.

End Coupling for Torsion

For torsional motion, complete coupling of the ends of the specimen to the specimen cap and base must be assured. Complete coupling for torsion may be assumed if the mobilized coefficient of friction between the end platens and the specimen is less than 0.2 for all shear strain amplitudes. The coefficient of friction is approximately given by

$$\text{Coefficient of friction} = \gamma G/\sigma_a'$$

where

γ = shear strain amplitude (see Calculations section),
G = shear modulus (see Calculations section), and
σ_a' = effective axial stress.

When this criterion is not met, other provisions such as the use of adhesives must be made in order to assure complete coupling. In such cases, the effectiveness of the coupling provisions shall be evaluated by testing two specimens of the same material but of different length. The lengths of these specimens shall differ by at least a factor of 1.5. The provisions for end coupling may be considered satisfactory if the values of the shear modulus for these two specimens of different length do not differ by more than 10 percent.

Procedure

Test Setup

The exact procedure to be followed during test setup will depend on the apparatus and electronic equipment used and on methods used for application, measurement, and control of the ambient stresses. However, the specimen shall be placed in the apparatus by procedures that will minimize the disturbance of the specimen. Particular care must be exercised when attaching the end platens to the specimen and when attaching the vibration excitation device to the platens. A temporary support as discussed earlier may be needed. For cases where ambient isotropic stresses are to be applied to a membrane-enclosed specimen, liquid- or air-confining media may be used for dry or partially saturated specimens. For tests where complete saturation is important, a liquid-confining medium should be used. Where the vibration excitation device is located within the pressure chamber, an air-liquid interface is acceptable as long as the liquid covers the entire membrane that encloses the specimen.

Electric Equipment

Connect the vibration excitation device to the sine wave generator (with amplifier, if required). The power supplied to the vibration excitation device should be very low in order not to exceed the amplitude of vibration prescribed later. Connect the vibration transducers to the readout instruments for the type of motion (longitudinal or torsional) to be applied. Adjust the readout instruments according to the instruction manuals for these instruments.

Measurement of Resonant Frequency

The procedure for measuring system resonant frequency is the same for both longitudinal and torsional vibration except that the longitudinal motion transducer is used for longitudinal motion and the rotational motion transducer is used for torsional motion. If the passive end is fixed or if $P > 100$ (see the Calculations section for definition of P), motion of the active-end platen is used to establish resonance. Otherwise, motion of the passive-end platen is used. With the power as low as practical, increase the frequency of excitation from a very low value (for example, 10 Hz) until the system resonant frequency is obtained. The phase relationship describing resonance can be established by observing the Lissajous figure formed on an x-y oscilloscope with the voltage proportional to the driving current applied to the horizontal amplifier and the output from the transducer applied to the vertical amplifier. If a velocity transducer is used for vibration measurement, the system resonant frequency occurs when the figure formed is a straight, sloping line. If a displacement or acceleration transducer is used, the frequency should be adjusted to produce an ellipse with axes vertical and horizontal. (Refer to the Definitions section to establish which resonant frequency should be recorded.) It is recommended that the frequency be measured with a digital electronic frequency meter and be recorded to at least three significant figures. The system resonant frequency for longitudinal motion shall be designated f_L and that for torsional motion shall be designated f_T.

Measurement of Strain Amplitude

The strain amplitude measurements shall be made only at the system resonant frequencies. Thus, for a given current applied to the excitation device, the vibration motion transducer outputs recorded at the system resonant frequency give sufficient information to calculate strain amplitude. To increase or decrease strain amplitude, the current to the vibration excitation device must be increased or decreased. After making a change in current applied to the vibration excitation device, the procedure of the previous subsection must be followed to establish the corresponding system resonant frequency before the transducer outputs can be used to establish the new strain amplitude value.

Measurement of System Damping

Associated with each strain amplitude and system resonant frequency is a value of damping. Two methods are available for measuring system damping: the steady-state vibration method and the amplitude decay method. Theoretically, both methods should give identical results. In practice, results of each method are usually close to each other. The steady-state method is easier and quicker. It is generally always used and the amplitude decay method is used for occasional spot-checking. The procedures for both methods are independent of whether longitudinal or torsional motion is under consideration. For the steady-state method, the active-end or the passive-end vibration transducer output (depending on which end is used to establish resonance) and the current applied to the vibration excitation device must be measured at each resonant frequency. The calculations are outlined in the following section. For the free-vibration method, with the system vibrating at the system resonant frequency, cut off the power to the vibration excitation device and record the output of the transducer used in establishing resonance as a function of time. This gives the decay curve for free vibration. The calculations for damping are also outlined in the following section.

Calculations

General

Calculations require the apparatus calibration factors and the physical dimensions and weight of the specimen. In addition, for each ambient stress condition, one data set is required for each vibration strain amplitude. A data set consists of the type of vibration (longitudinal or torsional), duration of vibration (this time can be used to calculate the number of vibration cycles), system resonant frequency, active- or passive-end transducer outputs (depending on which end is used to establish resonance), the reading associated with the current applied to the vibration excitation device, and the free-vibration amplitude decay curve (if the amplitude decay method of measuring damping is also going to be used).

Soil Mass Density

The soil mass density, ρ, is given by

$$\rho = \frac{W}{Vg}$$

where

W = total weight of specimen,
V = volume of specimen, and
g = acceleration of gravity.

Specimen Rotational Inertia

The specimen rotational inertia about the axis of rotation is given by

$$J = \frac{Wd^2}{8g}$$

where

d = diameter of specimen.

Active-End Inertia Factors

The active-end inertia factor for longitudinal motion, T_L, is calculated from

$$T_L = \frac{M_A g}{W}\left[1 - \left(\frac{f_{oL}}{f_L}\right)^2\right]$$

where

M_A = mass of active-end platen system as calculated earlier,
f_{oL} = apparatus resonant frequency for longitudinal motion (for apparatus without springs attached to the active end platen, this term is zero), and
f_L = system resonant frequency for longitudinal motion.

The active-end inertia factor for torsional motion, T_T, is given by

$$T_T = \frac{J_A}{J}\left[1 - \left(\frac{f_{oT}}{f_T}\right)^2\right]$$

where

J_A = rotational inertia of active-end platen system as calculated earlier,
J = specimen rotational inertia as calculated earlier,
f_{oT} = apparatus resonant frequency for torsional motion (for apparatus

without springs attached to the active-end platen, this factor is zero), and

f_T = system resonant frequency for torsional motion.

Passive-End Inertia Ratios

For longitudinal motion, the passive-end inertia ratio, P_L, is given by

$$P_L = \frac{M_p g}{W}$$

where

M_p = mass of passive-end platen system as described earlier.

For torsional motion, the passive-end inertia ratio, P_T, is given by

$$P_T = \frac{J_p}{J}$$

where

J_P = rotational inertia of passive-end platen system as calculated earlier.

For the special case where the passive end of the specimen is rigidly fixed, P_L and P_T are equal to infinity.

Apparatus Damping Factors

For longitudinal motion, the apparatus damping factor, ADF_L, is calculated from

$$ADF_L = ADC_L/[2\pi f_L (W/g)]$$

where

ADC_L = apparatus damping coefficient for longitudinal motion as described earlier.

For rotational motion, the apparatus damping factor, ADF_T, is calculated from

$$ADF_T = ADC_T/[2\pi f_T J]$$

where

ADC_T = apparatus damping coefficient for torsional motion as described earlier.

Dimensionless Frequency Factor

The dimensionless frequency factor, F, is used in calculating modulus. It is a function of system factors T, P, and ADF and of specimen damping ratio, D. Values of F are provided by the computer program in the Appendix, which is written in FORTRAN IV. For cases where ADF is zero and specimen damping ratio is less than 10 percent, values of F can be obtained from Fig. 2. Figure 2*b* is similar to Fig. 2*a* except that the range of T is different. This figure is independent of which end of the specimen is used to determine resonance.

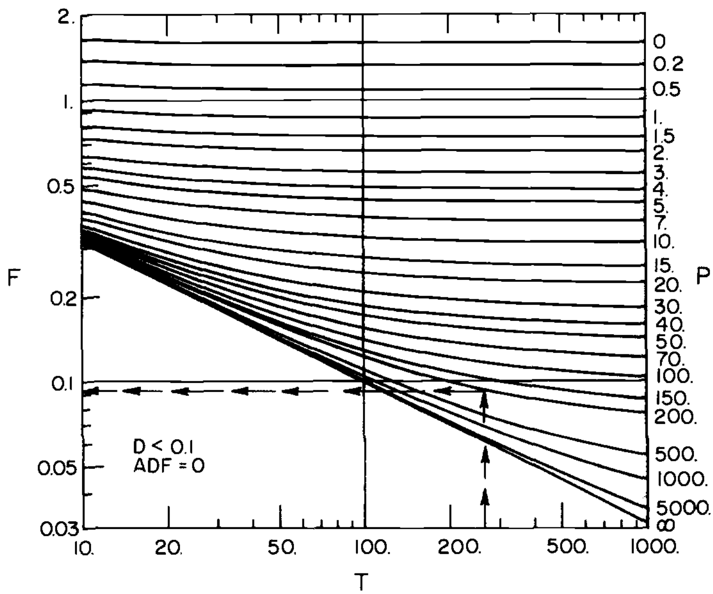

FIG. 2*a*—*Dimensionless frequency factors.*

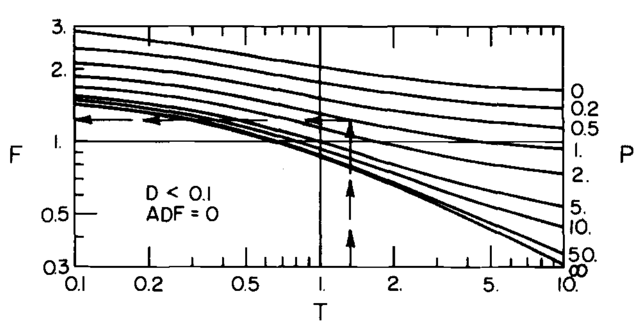

FIG. 2*b*—*Dimensionless frequency factors.*

Magnification Factors

These factors are used in calculating damping. For longitudinal motion, the magnification factor is calculated from

$$MMF_L = [(LCF)(LTO)/(FCF)(CR_L)](W/g)(2\pi f_L)^2$$

where

LCF = longitudinal motion transducer calibration factor for transducer used in establishing resonance,
LTO = longitudinal motion transducer output of transducer used in establishing resonance,
FCF = force/current factor given earlier, and
CR_L = current reading to longitudinal excitation system.

For torsional motion, the magnification factor is calculated from

$$MMF_T = [(RCF)(RTO)/(TCF)(CR_T)]J(2\pi f_T)^2$$

where

RCF = rotational transducer calibration factor for transducer used in establishing resonance,
RTO = rotational transducer output for transducer used in establishing resonance,
TCF = torque/current factor given earlier, and
CR_T = current reading to torsional excitation system.

Moduli

The rod modulus is calcualted from

$$E = \rho(2\pi L)^2\ (f_L/F_L)^2$$

where

ρ = specimen mass density given earlier,
f_L = system resonant frequency for longitudinal motion given earlier,
F_L = dimensionless frequency factor given earlier, and
L = specimen length.

The shear modulus is calculated from

$$G = \rho(2\pi L)^2\ (f_T/F_T)^2$$

where

f_T = system resonant frequency for torsional motion given earlier, and
F_T = dimensionless frequency factor given earlier.

Strain Amplitude

The average rod strain amplitude, ϵ, for longitudinal vibration shall be calculated from

$$\epsilon = (LCF)(LTO)(SF/L)$$

where

LCF = longitudinal motion transducer calibration factor for the transducer used in establishing resonance,
LTO = longitudinal transducer output for the transducer used in establishing resonance,
SF = strain factor calculated by program in the Appendix or, for cases of ADF = 0 and specimen damping equal to 10 percent, it may be obtained from Fig. 3. For other values of specimen damping ratio, values from Fig. 3 are only approximately correct. (Note that Fig. 3*a* is for the case where resonance is established by phase measurement between input force and motion at the active end and Fig. 3*b* is for the case where resonance is established by phase measurement between input force and motion at the passive end), and
L = specimen length.

For torsional motion, the average shear strain amplitude, γ, shall be calculated from

$$\gamma = (RCF)(RTO)(SF)[d/(3L)]$$

where

RCF = rotational motion transducer calibration factor for transducer used in establishing resonance,
RTO = rotational transducer output for transducer used in establishing resonance,
SF = strain factor determined in same manner as described for rod strain amplitude, and
d = specimen diameter.

Damping Ratio from Steady-State Vibration

If the computer program in the Appendix is used, the damping ratio of the specimen is established as part of the output. Manual calculation of

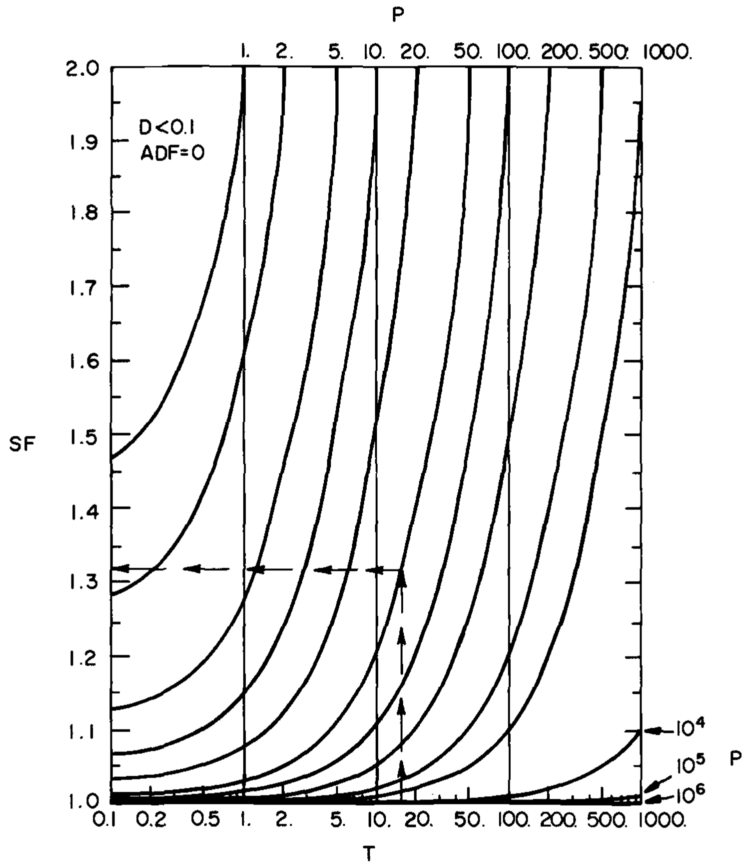

FIG. 3*a*—*Strain factors for resonance determined from motion at active end.*

damping ratio may be done for cases where the apparatus damping factor, *ADF*, is zero or may be assumed to be zero (definition of *ADF* given earlier). The procedure requires that Fig. 4*a* be used if resonance is established by phase measurement between input force (or torque) and the longitudinal (or rotational) motion at the active-end platen. Figure 4*b* is used for the case where resonance is established by phase measurement between the input force (or torque) and the longitudinal (or rotational) motion at the passive-end platen. The damping ratio, D, is calculated from

$$D = 1/[A(MMF)]$$

where

A = value from Fig. 4, and
MMF = magnification factor given earlier.

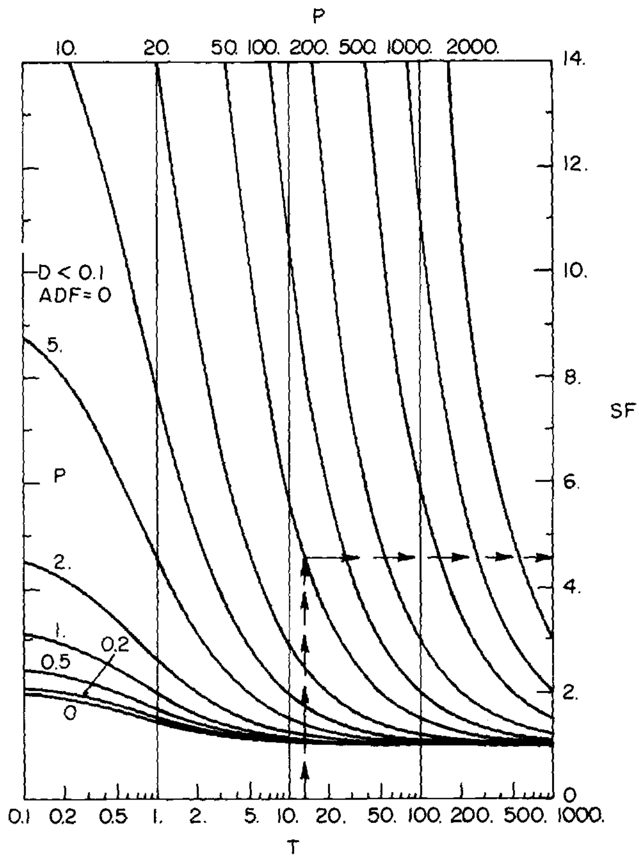

FIG. 3b—Strain factors for resonance determined from motion at passive end.

Damping ratios obtained from longitudinal vibration are not the same as damping ratios obtained from torsional vibration. Subscripts L and T should be used to relate the damping ratios to the type of vibration used in their determination.

Damping Ratio from Free Vibration

This procedure is theoretically exact for apparatus where the passive end can be assumed to be rigidly fixed. For the cases where the passive end is not rigidly fixed, irrespective of which end of the specimen is used in establishing resonance, this method is approximate. The same transducer that is used to determine resonance must be used to obtain the amplitude decay curve. For the case where resonance is established by use of the passive transducer, values of T and P should both be greater than 10 when

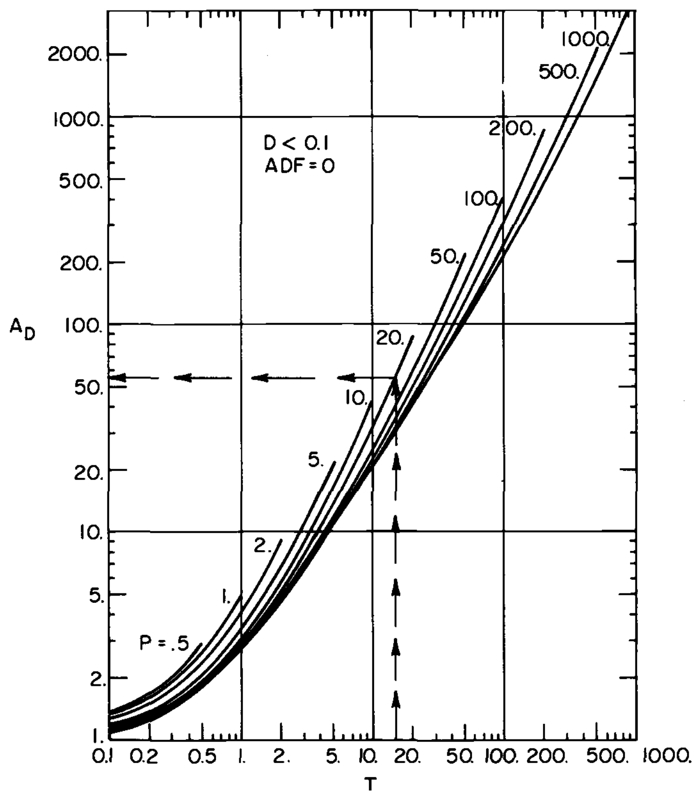

FIG. 4a—*Damping factors for resonance determined from motion at active end.*

amplitude decay is used. For apparatus where the active-end platen is restrained by a spring, a system energy ratio must be calculated. For other apparatus, this factor is zero. For longitudinal motion, this ratio is calculated from

$$S_L = (M_A g/W)(f_{oL} F_L/f_L)^2$$

and for torsional motion from

$$S_T = (J_A/J)(f_{oT} F_T/f_T)^2$$

where

F_L, F_T = dimensionless frequency factors for longitudinal and torsional motion, respectively, from Fig. 2.

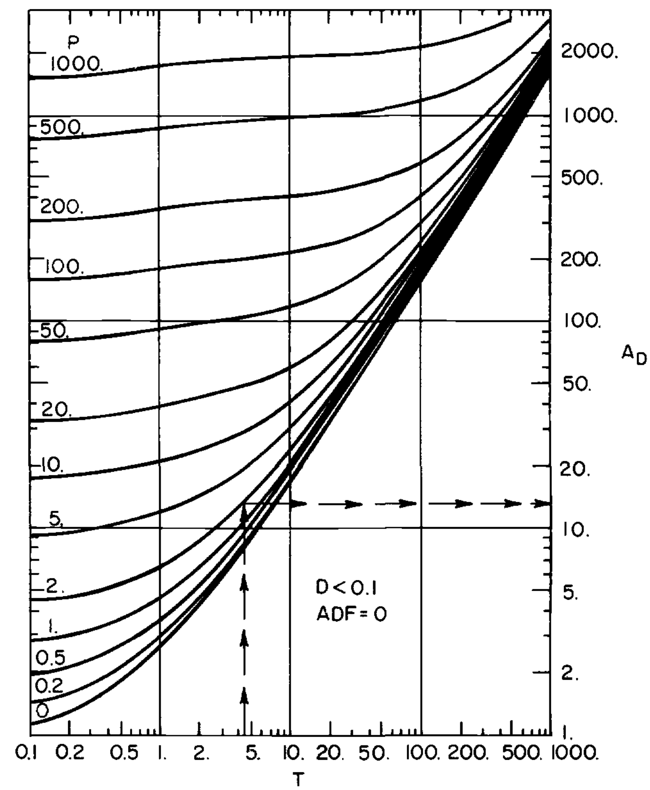

FIG. 4b—*Damping factors for resonance determined from motion at passive end.*

Compute the system logarithmic decrement from the free-vibration decay curve (as obtained in the previous section) from

$$\delta_s = (1/n) \ln (A_1/A_{1+n})$$

where

A_1 = amplitude of vibration for first cycle after power is cut off,
A_{n+1} = amplitude of vibration for $(n + 1)$th cycle of free vibration, and
n = number of free vibration cycles which must be 10 or less.

Finally, calculate the damping ratio from

$$D = [\delta_s(1 + S) - S\delta]/(2\pi)$$

where

$D = D_L$ or D_T depending on whether vibration is longitudinal or torsional,

δ_s = δ_{sL} or δ_{sT} depending on whether vibration is longitudinal or torsional,
S = S_L or S_T depending on whether vibration is longitudinal or torsional, and
δ = δ_L or δ_T, apparatus logarithmic decrement given earlier.

Report

General

The report shall include characteristics of the apparatus, specimen, ambient test conditions, and the results for each data set.

Apparatus Characteristics

The following apparatus characteristics shall be included: apparatus name, model number, and serial number; active-end and passive-end masses and rotational inertias (M_A, M_P, J_A, J_P); longitudinal and torsional apparatus resonant frequencies (f_{oL}, f_{oT}); longitudinal and torsional apparatus logarithmic decrements (δ_L, δ_T); the force/current and torque/current constants (*FCF*, *TCF*); and the applicable motion transducer calibration factors (LCF_A, LCF_P, RCF_A, RCF_P). (Note that if the passive end is fixed, inertias and transducers are not needed for the passive end. Likewise, if only one type of motion, longitudinal or torsional, is used, then only factors and inertias for that type need be given.)

Specimen Characteristics

A visual description and origin of the soil shall be given, including name, group symbol, and whether undisturbed or remolded. Initial and final specimen weight, dimensions, void ratio, water content, and degree of saturation shall also be given. Specimen preparation procedures and test setup procedures should be outlined.

Ambient Test Conditions

A complete description of the ambient stress conditions shall be given, including total stresses and pore water pressures, drainage conditions, and the procedures used to measure applied stresses, pore pressures, length change, and volume change.

Results for Each Data Set

For each data set, the following items shall be reported: approximate time of vibration at this strain amplitude, cell pressure, back or pore pressure, axial stress, specimen length and volume, type of vibration, system resonant frequency, strain amplitude, modulus, and damping ratio.

APPENDIX

```
C.   COMPUTER PROGRAM FOR RESONANT COLUMN DATA REDUCTION
C
C
C-------------DEFINITIONS OF INPUT-OUTPUT VARIABLES-------------------
C
C  ADF        APPARATUS DAMPING FACTOR (ADF > 0.)
C  D          SPECIMEN DAMPING RATIO (0.01% < D < 35%)
C  EPSD       ERROR CRITERION FOR D (DEFAULT VALUE:  0.0001)
C  EPSF       ERROR CRITERION FOR F (DEFAULT VALUE:  0.01)
C  F          FREQUENCY FACTOR
C  ITERD      MAXIMUM NUMBER OF ITERATIONS ALLOWED FOR D (DEFAULT
C               VALUE:  40)
C  ITERF      MAXIMUM NUMBER OF ITERATIONS ALLOWED FOR F (DEFAULT
C               VALUE:  40)
C  JPA        INDICATOR OF END WHERE MEASUREMENTS WERE TAKEN:
C                JPA = 0 FOR MEASUREMENTS AT THE ACTIVE END;
C                JPA = 1 FOR MEASUREMENTS AT THE PASSIVE END.
C  MMF        MODIFIED MAGNIFICATION FACTOR (MMF > 0.)
C  P          PASSIVE-END INERTIA RATIO (P > 0.;  IF JPA = 0, THEN
C               P > 100. AND P > T)
C  SF         STRAIN FACTOR
C  T          ACTIVE-END INERTIA FACTOR (T > -10.)
C
C----------------------------------------------------------------------
C
C         GIVEN VALUES OF T, P, ADF, MMF, AND JPA, THIS PROGRAM CALCU-
C  LATES VALUES OF F, D, AND SF AND WILL PRINT VALUES OF ALL THESE
C  PARAMETERS.
C
C---------------DATA INPUT INSTRUCTIONS--------------------------------
C
C         VALUES OF EPSF, ITERF, EPSD, AND ITERD MAY BE SPECIFIED ON THE
C  FIRST DATA CARD ACCORDING TO THE FORMAT 2(F10.0,7X,I3).  THESE
C  PARAMETERS ARE REQUIRED IN THE ITERATIVE SOLUTION PROCEDURE TO CON-
C  TROL ACCURACY AND LIMIT THE NUMBER OF ITERATIONS.  THIS DATA CARD
C  MAY BE LEFT BLANK IF THE USER CHOOSES TO USE THE DEFAULT VALUES
C  SPECIFIED BY THE PROGRAM.  (SEE THE LIST OF DEFINITIONS OF INPUT-
C  OUTPUT VARIABLES.)  THE DEFAULT VALUES WILL GIVE GOOD RESULTS IN MOST
C  CASES INVOLVING SMALL APPARATUS DAMPING.  FOR LARGE APPARATUS DAMPING
C  OR TO CHECK RESULTS OBTAINED WITH THE DEFAULT VALUES, SMALLER VALUES
C  OF ITERF AND ITERD SHOULD BE USED.  (HOWEVER, IN SOME CASES OF LARGE
C  APPARATUS DAMPING, ACCURATE CALCULATION OF D IS IMPOSSIBLE.)
C
C         EACH SUBSEQUENT DATA CARD SHOULD CONTAIN A VALUE OF EACH OF THE
C  PARAMETERS P, T, ADF, MMF, AND JPA ACCORDING TO THE FORMAT 4F10.0,
C  9X,I1.  THUS, EACH OF THESE CARDS CORRESPONDS TO ONE SET OF EXPERI-
C  MENTAL TEST DATA.  SEE THE LIST OF DEFINITIONS OF INPUT-OUTPUT
C  VARIABLES FOR THE RANGES OF THESE VARIABLES ALLOWED BY THE PROGRAM.
C  THE DATA CARDS SHOULD BE TERMINATED WITH A BLANK CARD.
C
C----------------------------------------------------------------------
C
C
      DIMENSION C(4),UP(11)
      REAL MMF,MMFCAL
      INTEGER OD
      COMMON /VALS/P,T,ADF,MMF,JPA,AMP,D,F /DLIM/DL,DR
      COMMON /ALARM/KALARM /EPSIT/EPSF,ITERF,EPSD,ITERD
      COMMON /PAR/PL,QL,C
      COMMON /CRIT/MMFCAL,PHASE
      EXTERNAL DELAMP
1000 FORMAT(4F10.0,9X,I1)
1005 FORMAT(2(F10.0,7X,I3))
1110 FORMAT(49H * * * * *   W A R N I N G   * * * * *   POSSIBLY,
   1    23H NOT ENOUGH ITERATIONS )
1115 FORMAT(50H TO OBTAIN SPECIFIED ACCURACY FOR D WITH THE ABOVE,
   1    18H PARAMETER VALUES.)
1117 FORMAT(30H  TRY A LARGER VALUE OF ITERD.)
1120 FORMAT(46H * * * * *   E R R O R   * * * * *   THE VALUE,
   1    19H OF D FOR THE ABOVE)
1125 FORMAT(46H PARAMETERS LIES OUTSIDE THE ALLOWABLE RANGE, ,
   1    14H0.001 TO 0.35.)
```

```
1140 FORMAT(31H    THE ERROR CRITERION FOR F IS,E12.2/)
1150 FORMAT(52H    THE MAXIMUM NUMBER OF ITERATIONS ALLOWED FOR F IS,
   1    I4/)
1160 FORMAT(31H    THE ERROR CRITERION FOR D IS,E12.2/)
1170 FORMAT(52H    THE MAXIMUM NUMBER OF ITERATIONS ALLOWED FOR D IS,
   1    I4///)
1210 FORMAT(5X,1HT,9X,1HP,8X,3HADF,6X,3HMMF,4X,3HJPA,3X,1HF,8X,2HDM,
   1 8X,2HSF,6X,9HMMF(CALC),3X,5HPHASE/)
1220 FORMAT(3(1X,F9.4),1X,F9.5,1X,I1,2(1X,F9.6),1X,1PE9.3,
   1    2(1X,0PF9.5))
1230 FORMAT(53H * * * * *   E R R O R   * * * * *   P MUST BE .GE.0.)
1240 FORMAT(50H * * * * *   E R R O R   * * * * *   IF(JPA.EQ.0) ,
   1    19H P MUST BE .GE.100.)
1250 FORMAT(50H * * * * *   E R R O R   * * * * *   IF(JPA.EQ.0) ,
   1    17H P MUST BE .GE. T)
1260 FORMAT(55H * * * * *   E R R O R   * * * * *   T MUST BE .GE.-10.)
1270 FORMAT(55H * * * * *   E R R O R   * * * * *   ADF MUST BE .GE.0.)
1280 FORMAT(54H * * * * *   E R R O R   * * * * *   MF MUST BE .GT.0.)
1310 FORMAT(49H * * * * *   W A R N I N G   * * * * *   POSSIBLY,
   1    23H NOT ENOUGH ITERATIONS )
1315 FORMAT(50H TO OBTAIN SPECIFIED ACCURACY FOR F WITH THE ABOVE,
   1    12H PARAMETERS.)
1317 FORMAT(30H  TRY A LARGER VALUE OF ITERF.)
1320 FORMAT(48H * * * * *   E R R O R   * * * * *   THERE IS NO,
   1    10H RESONANCE)
1330 FORMAT(51H  (DISPLACEMENT ONE-QUARTER CYCLE OUT OF PHASE WITH,
   1    19H FORCING FUNCTION) )
1340 FORMAT(25H FOR THE ABOVE PARAMETERS)
1350 FORMAT(51H * * * * *   W A R N I N G   * * * * *   BECAUSE OF,
   1    16H LARGE APPARATUS)
1360 FORMAT(49H  DAMPING, THE CALCULATED AMPLITUDE IS RELATIVELY,
   1    15H INSENSITIVE TO)
1365 FORMAT(49H  SPECIMEN DAMPING.  CONSEQUENTLY, THE CALCULATED,
   1 17H SPECIMEN DAMPING)
1367 FORMAT(37H  RATIO ABOVE MAY BE VERY INACCURATE.)
C  SET INPUT AND OUTPUT DEVICE CODES
      ID = 5
      OD = 6
      READ(ID,1005) EPSF,ITERF,EPSD,ITERD
      IF(EPSD.EQ.0.)  EPSD = 1.E-4
      IF(ITERD.EQ.0)  ITERD = 40
      IF(EPSF.EQ.0.)  EPSF = 1.E-2
      IF(ITERF.EQ.0)  ITERF = 40
      WRITE(OD,1140) EPSF
      WRITE(OD,1150) ITERF
      WRITE(OD,1160) EPSD
      WRITE(OD,1170) ITERD
      WRITE(OD,1210)
   10 READ(ID,1000) T,P,ADF,MMF,JPA
      IF(MMF.EQ.0.)  GO TO 190
     MAL = 0
     IF(P.GE.0.)  GO TO 20
     MAL = MAL + 1
     IF(MAL.EQ.1)  WRITE(OD,1220) P,T,ADF,MMF,JPA
     WRITE(OD,1230)
  20 IF(JPA.EQ.1.OR.P.GE.100.)  GO TO 30
     MAL = MAL + 1
     IF(MAL.EQ.1)  WRITE(OD,1220) P,T,ADF,MMF,JPA
     WRITE(OD,1240)
  30 IF(JPA.EQ.1.OR.T.LE.P)  GO TO 40
     MAL = MAL + 1
     IF(MAL.EQ.1)  WRITE(OD,1220) P,T,ADF,MMF,JPA
     WRITE(OD,1250)
  40 IF(T.GE.-10.)  GO TO 50
     MAL = MAL + 1
     IF(MAL.EQ.1)  WRITE(OD,1220) P,T,ADF,MMF,JPA
     WRITE(OD,1260)
  50 IF(ADF.GE.0.)  GO TO 60
     MAL = MAL + 1
     IF(MAL.EQ.1)  WRITE(OD,1220) P,T,ADF,MMF,JPA
     WRITE(OD,1270)
  60 IF(MMF.GT.0.)  GO TO 70
     MAL = MAL + 1
     IF(MAL.EQ.1)  WRITE(OD,1220) P,T,ADF,MMF,JPA
     WRITE(OD,1280)
  70 IF(MAL.NE.0)  GO TO 10
     KALARM = 0
```

```
      DL = 0.0001
      DR = .35
      CALL RTMI2(D,AMPDEL,DELAMP,DL,DR,EPSD,ITERD,IER)
      IF(KALARM.NE.1)  GO TO 80
      MAL = MAL + 1
      IF(MAL.EQ.1)  WRITE(OD,1220) P,T,ADF,MMF,JPA
      WRITE(OD,1320)
      WRITE(OD,1330)
      WRITE(OD,1340)
      GO TO 10
   80 IF(IER.NE.2)  GO TO 90
      MAL = MAL + 1
      IF(MAL.EQ.1)  WRITE(OD,1220) P,T,ADF,MMF,JPA
      WRITE(OD,1120)
      WRITE(OD,1125)
      GO TO 10
   90 CONTINUE
      DO 180 I=1,11
      XR = (I-1)/10.
      QLX = QL*XR
      PLX = PL*XR
      CC = COSH(QLX)*COS(PLX)
      SC = SINH(QLX)*COS(PLX)
      SS = SINH(QLX)*SIN(PLX)
      CS = COSH(QLX)*SIN(PLX)
      UP(I) = C(1)*(-PL*CS+QL*SC) + C(2)*(-PL*SS+QL*CC) +
     1   C(3)*(PL*SC+QL*CS) + C(4)*(PL*CC+QL*SS)
  180 CONTINUE
      GAM = (UP(1)+UP(11)+4.*(UP(2)+UP(4)+UP(6)+UP(8)+UP(10))
     1   +2.*(UP(3)+UP(5)+UP(7)+UP(9)))/30.
      SF = ABS(GAM*F**2/MMF)
       D = D*100.
      WRITE(OD,1220) T,P,ADF,MMF,JPA,F,D,SF,MMFCAL,PHASE
      IF(IER.NE.1)  GO TO 110
        WRITE(OD,1110)
        WRITE(OD,1115)
        WRITE(OD,1117)
  110 IF(KALARM.NE.2)  GO TO 120
        WRITE(OD,1350)
        WRITE(OD,1360)
        WRITE(OD,1365)
        WRITE(OD,1367)
  120 IF(KALARM.NE.4)  GO TO 140
        WRITE(OD,1310)
        WRITE(OD,1315)
        WRITE(OD,1317)
  140 CONTINUE
        GO TO 10
  190 STOP
        END
C************************
        FUNCTION DELAMP(D)
C************************
        COMMON /VALS/P,T,ADF,MMF,JPA,AMP,DD,F /DLIM/DL,DR
        COMMON /ALARM/KALARM /EPSIT/EPSF,ITERF,EPSD,ITERD
        EXTERNAL VFCN
        INTEGER OD
        REAL MMF
        OD = 6
        DD = D
        IF(T.LT.0.)  GO TO 30
        AA = -48*T*P - 7*(T+P) - 1
        BB = 48*T*P + 20*(T+P) + 5
        CC = -4*(T+P) - 4
        BD2A = BB/(2*AA)
        F = SQRT(12*(-BD2A-SQRT(BD2A**2-CC/AA)))
        FL = .8*F
        FR = 1.2*F
        GO TO 60
   30   IF(T.LT.-.1)  GO TO 40
        FL = 1.4
        FR = 1.5*FL
        GO TO 60
   40   FL = 1.75
        FR = 1.5*FL
   60   CONTINUE
        CALL RTMI(F,V,VFCN,FL,FR,EPSF,ITERF,IER)
```

```
      IF(IER.NE.2)  GO TO 70
      FL = .99*FR
      FR = 1.5*FR
      IF(FL.LE.8.)  GO TO 60
      KALARM = 1
      GO TO 120
   70 IF(IER.EQ.1)  KALARM = 4
   90 CONTINUE
      V = VFCN(F)
      A   = AMP
      AM   = MMF/F**2
      DELAMP = A - AM
      IF(D.EQ.DL)  DELL = DELAMP
      IF(D.EQ.DL)  AML = A
      IF(D.NE.DR)  GO TO 120
      DELR = DELAMP
      AMR = A
      DIF = AML - AMR
      RELDIF = DIF/AML
      IF(RELDIF.LE.0.20)  KALARM = 2
  120 CONTINUE
      RETURN
      END
C************************
      FUNCTION VFCN(F)
C***********************
      DIMENSION A(4,4),C(4)
      REAL MMFCAL
      COMMON /VALS/P,T,ADF,MMF,JPA,AMP,D,FP
      COMMON /PAR/PL,QL,C
      COMMON /CRIT/MMFCAL,PHASE
      BETA = SQRT(1.+(2.*D)**2)
      PL = F*SQRT((BETA+1.)/2.)/BETA
      QL = F*SQRT((BETA-1.)/2.)/BETA
      SNHQ = SINH(QL)
      CSHQ = COSH(QL)
      SNP = SIN(PL)
      CSP = COS(PL)
      CS = CSHQ*SNP
      SC = SNHQ*CSP
      SS = SNHQ*SNP
      CC = CSHQ*CSP
      CSSC = -PL*CS + QL*SC
      SSCC = -PL*SS + QL*CC
      SCCS = PL*SC + QL*CS
      CCSS = PL*CC + QL*SS
      PF2 = P*F**2
      A(1,1) = T*F**2
      A(1,2) = QL - 2*D*PL
      A(1,3) = - ADF*F**2
      A(1,4) = PL + 2*D*QL
      A(2,1) = -A(1,3)
      A(2,2) = -A(1,4)
      A(2,3) = A(1,1)
      A(2,4) = A(1,2)
      A(3,1) = CSSC - 2.*D*SCCS - PF2*CC
      A(3,2) = SSCC - 2.*D*CCSS - PF2*SC
      A(3,3) = SCCS + 2.*D*CSSC - PF2*SS
      A(3,4) = CCSS + 2.*D*SSCC - PF2*CS
      A(4,1) = -A(3,3)
      A(4,2) = -A(3,4)
      A(4,3) = A(3,1)
      A(4,4) = A(3,2)
      C(1) = 0
      C(2) = -1.
      C(3) = 0
      C(4) = 0
      EPS = 1.E-5
      NN = 4
      CALL  GELG(C,A,NN,1,EPS,IER,NN*NN,NN)
      U0 = C(1)
      V0 = C(3)
      AMPL0 = SQRT(U0**2 + V0**2)
      PHASE0 = ATAN2(V0,U0)
      IF(PHASE0.LT.0.)  PHASE0 = PHASE0 + 6.283185
      UL = C(1)*CC + C(2)*SC + C(3)*SS + C(4)*CS
      VL = C(3)*CC + C(4)*SC - C(1)*SS - C(2)*CS
```

```
      AMPLL = SQRT(UL**2 + VL**2)
      PHASEL = ATAN2(VL,UL)
      IF(JPA.EQ.0)   VPCN = PHASEO - 3.141593
      IF(JPA.NE.0)   VPCN = PHASEL
      IF(JPA.EQ.0)   AMP = AMPLO
      IF(JPA.NE.0)   AMP = AMPLL
      MMFCAL = AMP*F**2
      PHASE = VPCN
      RETURN
      END
C*****************************************************************
      SUBROUTINE RTMI2(X,F,FCT,XLI,XRI,EPS,IEND,IER)
C*****************************************************************
      COMMON /ALARM/KALARM
      IER=0
      XL=XLI
      XR=XRI
      X=XL
      TOL=X
      F=FCT(TOL)
      IF(KALARM.EQ.1)   RETURN
      IF(F)1,16,1
    1 FL=F
      X=XR
      TOL=X
      F=FCT(TOL)
      IF(KALARM.EQ.1)   RETURN
      IF(F)2,16,2
    2 FR=F
      IF(SIGN(1.,FL)+SIGN(1.,FR))25,3,25
    3 I=0
      TOLF=100.*EPS
    4 I=I+1
      DO 13 K=1,IEND
      X=.5*(XL+XR)
      TOL=X
      F=FCT(TOL)
      IF(KALARM.EQ.1)   RETURN
      IF(F)5,16,5
    5 IF(SIGN(1.,F)+SIGN(1.,FR))7,6,7
    6 TOL=XL
      XL=XR
      XR=TOL
      TOL=FL
      FL=FR
      FR=TOL
    7 TOL=F-FL
      A=F*TOL
      A=A+A
      IF(A-FR*(FR-FL))8,9,9
    8 IF(I-IEND) 17,17,9
    9 XR=X
      FR=F
      TOL=EPS
      A=ABS(XR)
      IF(A-1.) 11,11,10
   10 TOL=TOL*A
   11 IF(ABS(XR-XL)-TOL) 12,12,13
   12 IF(ABS(FR-FL)-TOLF) 14,14,13
   13 CONTINUE
      IER=1
   14 IF(ABS(FR)-ABS(FL)) 16,16,15
   15 X=XL
      F=FL
   16 RETURN
   17 A=FR-F
      DX=(X-XL)*FL*(1.+F*(A-TOL)/(A*(FR-FL)))/TOL
      XM=X
      FM=F
      X=XL-DX
      TOL=X
      F=FCT(TOL)
      IF(KALARM.EQ.1)   RETURN
      IF(F)18,16,18
   18 TOL=EPS
      A=ABS(X)
      IF(A-1.) 20,20,19
   19 TOL=TOL*A
```

```
   20 IF(ABS(DX)-TOL)21,21,22
   21 IF(ABS(F)-TOLF)16,16,22
   22 IF(SIGN(1.,F)+SIGN(1.,FL))24,23,24
   23 XR=X
      FR=F
      GO TO 4
   24 XL=X
      FL=F
      XR=XM
      FR=FM
      GO TO 4
   25 IER=2
      RETURN
      END
C*********************************************
      SUBROUTINE GELG (R,A,M,N,EPS,IER,MM,NM)
C*********************************************
      DIMENSION A(MM), R(NM)
      IF(M)23,23,1
    1 IER=0
      PIV=0.
      MM=M*M
      NM=N*M
      DO 3 L=1,MM
      TB=ABS(A(L))
      IF(TB-PIV)3,3,2
    2 PIV=TB
      I=L
    3 CONTINUE
      TOL=EPS*PIV
      LST=1
      DO 17 K=1,M
      IF(PIV)23,23,4
    4 IF(IER)7,5,7
    5 IF(PIV-TOL)6,6,7
    6 IER=K-1
    7 PIVI=1./A(I)
      J=(I-1)/M
      I=I-J*M-K
      J=J+1-K
      DO 8 L=K,NM,M
      LL=L+I
      TB=PIVI*R(LL)
      R(LL)=R(L)
    8 R(L)=TB
      IF(K-M)9,18,18
    9 LEND=LST+M-K
      IF(J)12,12,10
   10 II=J*M
      DO 11 L=LST,LEND
      TB=A(L)
      LL=L+II
      A(L)=A(LL)
   11 A(LL)=TB
   12 DO 13 L=LST,MM,M
      LL=L+I
      TB=PIVI*A(LL)
      A(LL)=A(L)
   13 A(L)=TB
      A(LST)=J
      PIV=0.
      LST=LST+1
      J=0
      DO 16 II=LST,LEND
      PIVI=-A(II)
      IST=II+M
      J=J+1
      DO 15 L=IST,MM,M
      LL=L-J
      A(L)=A(L)+PIVI*A(LL)
      TB=ABS(A(L))
      IF(TB-PIV)15,15,14
   14 PIV=TB
      I=L
   15 CONTINUE
      DO 16 L=K,NM,M
      LL=L+J
   16 R(LL)=R(LL)+PIVI*R(L)
```

```
   17 LST=LST+M
   18 IF(M-1)23,22,19
   19 IST=MM+M
      LST=M+1
      DO 21 I=2,M
      II=LST-I
      IST=IST-LST
      L=IST-M
      L=A(L)+.5
      DO 21 J=II,MM,M
      TB=R(J)
      LL=J
      DO 20 K=IST,MM,M
      LL=LL+1
   20 TB=TB-A(K)*R(LL)
      K=J+L
      R(J)=R(K)
   21 R(K)=TB
   22 RETURN
   23 IER=-1
      RETURN
      END
C*************************************************
      SUBROUTINE RTMI(X,F,FCT,XLI,XRI,EPS,IEND,IER)
C*************************************************
      IER=0
      XL=XLI
      XR=XRI
      X=XL
      TOL=X
      F=FCT(TOL)
      IF(F)1,16,1
    1 FL=F
      X=XR
      TOL=X
      F=FCT(TOL)
      IF(F)2,16,2
    2 FR=F
      IF(SIGN(1.,FL)+SIGN(1.,FR))25,3,25
    3 I=0
      TOLF=100.*EPS
    4 I=I+1
      DO 13 K=1,IEND
      X=.5*(XL+XR)
      TOL=X
      F=FCT(TOL)
      IF(F)5,16,5
    5 IF(SIGN(1.,F)+SIGN(1.,FR))7,6,7
    6 TOL=XL
      XL=XR
      XR=TOL
      TOL=FL
      FL=FR
      FR=TOL
    7 TOL=F-FL
      A=F*TOL
      A=A+A
      IF(A-FR*(FR-FL))8,9,9
    8 IF(I-IEND)17,17,9
    9 XR=X
      FR=F
      TOL=EPS
      A=ABS(XR)
      IF(A-1.)11,11,10
   10 TOL=TOL*A
   11 IF(ABS(XR-XL)-TOL)12,12,13
   12 IF(ABS(FR-FL)-TOLF)14,14,13
   13 CONTINUE
      IER=1
   14 IF(ABS(FR)-ABS(FL))16,16,15
   15 X=XL
      F=FL
   16 RETURN
   17 A=FR-F
      DX=(X-XL)*FL*(1.+F*(A-TOL)/(A*(FR-FL)))/TOL
      XM=X
```

```
      FM=F
      X=XL-DX
      TOL=X
      F=FCT(TOL)
      IF(F) 18,16,18
   18 TOL=EPS
      A=ABS(X)
      IF(A-1.) 20,20,19
   19 TOL=TOL*A
   20 IF(ABS(DX)-TOL) 21,21,22
   21 IF(ABS(F)-TOLF) 16,16,22
   22 IF(SIGN(1.,F)+SIGN(1.,FL)) 24,23,24
   23 XR=X
      FR=F
      GO TO 4
   24 XL=X
      FL=F
      XR=XM
      FR=FM
      GO TO 4
   25 IER=2
      RETURN
      END
```

W. F. Marcuson III[1] *and H. E. Wahls*[2]

Effects of Time on Damping Ratio of Clays

REFERENCE: Marcuson, W. F., III, and Wahls, H. E., "**Effects of Time on Damping Ratio of Clays**," *Dynamic Geotechnical Testing, ASTM STP 654,* American Society for Testing and Materials, 1978, pp. 126–147.

ABSTRACT: Laboratory tests with a Hardin oscillator were used to study the time-dependent characteristics of the damping ratio of isotropically consolidated specimens of kaolinite and calcium bentonite. Damping was determined using a steady-state method and from the decay of free vibrations. After completion of primary consolidation, the dynamic response was studied as a function of time for both drained and undrained conditions.

The damping ratio decreased approximately 12 percent for kaolinite and 25 percent for bentonite per logarithmic cycle of a dimensionless time ratio during secondary compression. To evaluate the effects of time in clay soils, at least one test should be continued to five to ten times the time at the end of primary consolidation.

Errors due to diffusion of air into the specimen were eliminated by using a mercury jacket around the specimen. The apparatus damping constant was found to vary significantly from test to test because of minor variations in the apparatus setup, and hence the apparatus must be recalibrated for each test.

KEY WORDS: clays, damping ratio, resonant-column tests, time effects, soils

Nomenclature

- d Damping ratio
- d_{fv} Damping ratio determined by free vibration method
- e Void ratio
- G Shear modulus
- T_r Dimensionless time ratio
- μ Viscous coefficient for shear
- ω Circular frequency

[1] Research civil engineer, Earthquake Engineering and Vibrations Division, Soils and Pavements Laboratory, U. S. Army Engineer Waterways Experiment Station, Vicksburg, Miss. 39180.

[2] Professor, Department of Civil Engineering, North Carolina State University, Raleigh, N. C. 27607.

The new advanced dynamic techniques for computing the response of soils subjected to seismic forces require that the stress-strain properties of the soil be known. These stress-strain properties are not unique for a given soil but are functions of various other soil and load parameters. Many studies have contributed to the understanding of shear modulus and how it varies with material and load parameters; however, the energy-absorbing characteristics of the soil are still not adequately understood.

The purpose of this study was to evaluate the effects of time on the damping capacity of clay soils. It was a laboratory study of the fundamental behavior of material properties which provides information to be used in theories covering soil-structure interaction. The resonant-column technique was used to study the dynamic response of two cohesive soils, a kaolinite and a bentonite, under various test conditions. The damping ratio, d, was determined, and is defined as

$$d = 0.5 \frac{\mu \omega}{G}$$

where

μ = viscous coefficient for shear,
ω = circular frequency, and
G = shear modulus.

The damping ratio was studied as a function of time, void ratio, consolidation pressure, and strain amplitude of resonant oscillation.

Materials

Two different materials were used in this investigation, kaolinite and bentonite.

Kaolinite—The kaolinite used was Burgess Pigment No. 10, purchased in a powdered state from the Burgess Pigment Company, Sanderville, Ga. It has a liquid limit of 66 percent and a plasticity index of 35 percent. The specific gravity is 2.65. Specimens were extruded through a Vac Air extruder at an average moisture content of approximately 52 percent.

Bentonite—The bentonite used is known as Panther Creek bentonite and was obtained from the American Colloid Company, Skokie, Ill. This is a calcium montmorillonite, which has a liquid limit of 120 percent and a plasticity index of 60 percent. The specific gravity is 2.72 and the water content of extruded specimens was approximately 102 percent.

Testing Apparatus and Procedures

The values of damping ratio were determined by the steady-state method and apparatus developed by Hardin [1].[3] The equipment is described by Hardin and Music [2] and shown schematically in Humphries and Wahls [3].

In this investigation, specimens 36 mm (1.4 in.) in diameter and approximately 76 mm (3 in.) long were subjected to isotropic consolidated pressures of approximately 70, 140, 280, and 560 kPa (10, 20, 40, and 80 psi). Drained (D) and consolidated undrained (CU) tests were conducted. When primary consolidation was completed, steady-state sinusoidal torsional oscillation was applied to the top of the specimen, while the bottom of the specimen remained fixed. The test procedure is described in more detail in Marcuson and Wahls [4].

Damping was studied primarily by recording the current providing the driving sinusoidal force for three vibration amplitudes, namely, 0.00015, 0.0003, and 0.0006 rad, peak-to-peak and calculating the damping ratio. These correspond to average shear strain amplitudes of 0.0012, 0.0024, and 0.0048 percent, respectively. For the vibration amplitudes of 0.0006 rad, free vibration damping, d_{fv}, also was determined by recording and measuring vibration amplitude decay, after the driving force was removed. Damping was studied as a function of time, void ratio, pressure, and amplitude.

In order to study the effect of time of consolidation, a dimensionless time factor or T-ratio was used. This T-ratio, T_r, is defined as any time, t, divided by the time to 100 percent primary consolidation. For this study, all damping data were obtained when T_r was equal to or greater than one, that is, after the completion of primary consolidation.

Effects of Mercury as a Chamber Fluid

Because the drive system of the resonant-column equipment is electrically powered, it is mandatory that it remain dry. Thus, an air-fluid interface must be maintained inside the triaxial cell chamber. When the cell is pressurized with air under high pressure, air is forced into solution with the water. During long-term tests, this air, in solution, diffuses through the latex rubber membrane. Once inside the membrane, it is at a lower pressure and can come out of solution. Bubbles may form and cause the water level in the burette to change, thus indicating an erroneous volume change. Also, the degree of saturation of the specimen may change.

The magnitude of this effect was very significant for the test durations employed in the investigation (about one week). To alleviate this problem, mercury was used as a substitute fluid because air does not diffuse into mercury at the pressures used in this study. This required the same equipment modification as discussed in Marcuson and Wahls [4].

The use of mercury as a chamber fluid was studied in Test 7, which was

[3] The italic numbers in brackets refer to the list of references appended to this paper.

performed on kaolinite. During this test, the specimen was consolidated to 100 percent primary consolidation using mercury as a chamber fluid. The specimen was then vibrated and data were recorded. Holding the cell pressure constant, the mercury was drained out, the specimen was vibrated in air, and data were recorded. With the pressure still constant, the chamber was again filled with mercury and the next pressure increment was applied. Primary consolidation at the next higher confining stress was allowed and the foregoing procedure was repeated. This was done for pressures of 70, 140, 280, and 560 kPa (10, 20, 40, and 80 psi).

Based on the results of Test 7, which are presented in Table 1, it appears that the damping ratio was slightly less in air than in mercury. However, this difference was only 10 percent or less. The damping ratio cannot be determined to such accuracy that a 10 percent or less reduction would be significant. Therefore, the effect of mercury as a chamber fluid may be ignored.

TABLE 1—*Results of mercury and air calibration test.*

Pressure, psi[a] (1)	Void Ratio (2)	Vibration Amplitude Peak-to-Peak (3)	Damping Ratio Mercury (4)	Damping Ratio Air (5)
10	1.281	0.0006	0.037	0.036
20	1.218	0.0006	0.032	0.030
40	1.154	0.0006	0.029	0.026
80	1.108	0.0006	0.024	0.023

[a] Metric conversion: 1 psi = 6.89 kPa.

Presentation and Analysis of Results

It was observed during the investigation that the apparatus damping constant was very sensitive to apparatus configuration. The apparatus logarithmic decrement sometimes changed by a factor of two between tests, which in turn changed the damping ratio approximately 20 percent. Among the factors that affected this change in apparatus damping were kinks or twists in the wiring and wires in contact with the apparatus. This apparatus sensitivity contributed to the scatter in the damping data from test to test. This variation is not important if the data for each test are considered separately, because the equipment remains unchanged throughout the duration of each individual test. For this reason, damping will be discussed in general terms, taking note of the trends that developed during each test.

Kaolinite

The damping data from Tests 1-4 are presented in Tables 2 through 5. It may seem that the damping ratio decreases with increasing stiffness; consequently, the damping ratio varies inversely with the shear modulus. During this testing program, a decrease in void ratio corresponds to an increase in consolidation pressure. It is not possible to isolate (decouple) the influence of changing void ratios from the influence of changing consolidation pressure on the damping ratio. It is believed that the effects of changing the consolidation pressure may be large enough to mask the effect of changing the void ratio; however, further research is needed to clarify this point. Consequently, no conclusions have been drawn concerning the influence of changing void ratio on damping.

Table 6 presents the damping ratio for Test 2 in terms of percentage of the average damping ratio for each void ratio, pressure, and time state. The data presented in this table, which are typical of the results obtained, show that the damping ratio generally varied less than ±12 percent for the range of strain amplitude studied.

At low pressures, damping was observed to increase with increasing amplitude. This is attributed to the strain-softening behavior exhibited by the soil with increasing displacement amplitude, which yields a decreasing shear modulus and an increasing damping ratio. As the pressure increased to the highest value considered in this study, the amplitude effect changed. At 560 kPa (80 psi) the damping ratio was higher at the extreme amplitudes and lower for the intermediate value, but the variation with amplitude decreased to approximately 5 percent. This decrease in variation might be explained by the decrease in the strain softening behavior of the soil at 560 kPa (80 psi). As the pressure was increased from 70 kPa (10 psi) to 560 kPa (80 psi), the void ratio decreased from 1.3 to 1.1 and the damping ratio decreased from approximately 0.04 to 0.02. The decrease in the damping ratio observed for the intermediate amplitude (0.0003 rad) is small. This could be due to experimental error; however, the trend appears too consistent for this.

Although the damping ratio decreased with increasing pressure, it did not increase with the slight decrease in effective stress caused by the pore pressure developed in the "consolidated-undrained" tests (see Tables 4 and 5). For the "drained" tests the overconsolidation ratio was always 1 and for the consolidated-undrained tests the overconsolidation ratio was less than 1.15. This overconsolidation was due only to pore pressure buildup during the test. This indicates that the preconsolidation pressure is actually the important stress when small overconsolidation is observed.

The data determined by the free-vibration method are lower than the values calculated by the steady-state method. This difference is greater at lower pressures for the drained conditions. At 70 kPa (10 psi) the difference

TABLE 2—*Damping data for kaolinite, Test 1, drained.*

			Damping Ratio, d				d_{fv}
			Amplitude,[b] rad Peak-to-Peak				Amplitude, rad Peak-to-Peak
Pressure psi[a] (1)	Void Ratio (2)	Time Ratio (3)	0.00015 (4)	0.0003 (5)	0.0006 (6)	Average (7)	0.0006 (8)
10	1.305	1.0	0.0371	0.0402	0.0506	0.0426	0.0387
	1.303	4.0	0.0354	0.0388	0.0484	0.0408	0.0375
	1.302	7.0	0.0339	0.0376	0.0467	0.0394	0.0357
	1.300	13.0	0.0332	0.0363	0.0438	0.0378	0.0349
	1.299	25.0	0.0330	0.0364	0.0451	0.0382	0.0351
	1.297	40.0	0.0327	0.0359	0.0435	0.0374	0.0345
	1.296	70.0	0.0283	0.0335	0.0425	0.0348	0.0334
20	1.251	1.0	0.0328	0.0346	0.0467	0.0380	0.0334
	1.247	3.0	0.0313	0.0315	0.0375	0.0334	0.0307
	1.246	5.0	0.0305	0.0306	0.0347	0.0319	0.0301
	1.243	9.0	0.0295	0.0294	0.0337	0.0309	0.0293
	1.241	17.0	0.0276	0.0283	0.0318	0.0292	0.0277
	1.240	25.0	0.0271	0.0271	0.0306	0.0283	0.0280
	1.237	48.0	0.0250	0.0266	0.0300	0.0272	0.0278
40	1.182	1.0	0.0261	0.0249	0.0286	0.0265	0.0264
	1.179	2.5	0.0242	0.0234	0.0256	0.0244	0.0239
	1.178	4.0	0.0234	0.0226	0.0252	0.0237	0.0237
	1.176	7.0	0.0229	0.0216	0.0246	0.0230	0.0224
	1.173	13.0	0.0214	0.0212	0.0230	0.0219	0.0213
	1.171	35.5	0.0207	0.0206	0.0221	0.0211	0.0211
80	1.114	1.0	0.0205	0.0200	0.0227	0.0211	0.0199
	1.110	2.0	0.0187	0.0194	0.0203	0.0195	0.0194
	1.109	3.0	0.0183	0.0181	0.0199	0.0188	0.0181
	1.106	5.0	0.0180	0.0176	0.0198	0.0185	0.0176
	1.104	9.0	0.0171	0.0166	0.0192	0.0176	0.0152
	1.102	13.0	0.0164	0.0160	0.0182	0.0169	0.0167
	1.100	24.0	0.0176	0.0160	0.0178	0.0171	0.0163

[a] Metric conversion: 1 psi = 6.89 kPa.
[b] These amplitudes correspond to a shear strain amplitude of 0.0012, 0.0024, and 0.0048 percent, respectively.

132 DYNAMIC GEOTECHNICAL TESTING

TABLE 3—*Damping data for kaolinite, Test 2, drained.*

			Damping Ratio, d				d_{fv}
			Amplitude,[b] rad Peak-to-Peak				Amplitude, rad Peak-to-Peak
Pressure, psi[a] (1)	Void Ratio (2)	Time Ratio (3)	0.00015 (4)	0.0003 (5)	0.0006 (6)	Average (7)	0.0006 (8)
10	1.288	1.0	0.0317	0.0293	0.0383	0.0331	0.0281
	1.286	4.0	0.0289	0.0286	0.0365	0.0313	0.0287
	1.286	7.0	0.0289	0.0309	0.0368	0.0322	0.0285
	1.285	13.0	0.0280	0.0301	0.0353	0.0311	0.0275
	1.285	25.0	0.0280	0.0296	0.0349	0.0308	0.0271
	1.284	40.0	0.0268	0.0278	0.0328	0.0291	0.0328
	1.284	70.0	0.0263	0.0275	0.0325	0.0288	0.0251
20	1.241	1.0	0.0275	0.0278	0.0329	0.0294	0.0263
	1.239	3.0	0.0256	0.0269	0.0311	0.0279	0.0233
	1.237	5.0	0.0244	0.0257	0.0287	0.0263	0.0223
	1.235	9.0	0.0230	0.0237	0.0276	0.0248	0.0213
	1.233	17.0	0.0221	0.0230	0.0262	0.0238	0.0201
	1.233	25.0	0.0212	0.0225	0.0255	0.0231	0.0202
	1.231	46.0	0.0207	0.0214	0.0248	0.0223	0.0197
40	1.177	1.0	0.0213	0.0230	0.0267	0.0237	0.0206
	1.175	2.5	0.0201	0.0222	0.0258	0.0227	0.0188
	1.173	4.0	0.0193	0.0216	0.0253	0.0221	0.0189
	1.171	7.0	0.0190	0.0210	0.0249	0.0216	0.0178
	1.169	13.0	0.0189	0.0208	0.0233	0.0210	0.0178
	1.168	19.0	0.0181	0.0202	0.0227	0.0203	0.0168
	1.167	35.5	0.0177	0.0198	0.0223	0.0199	0.0176
80	1.108	1.0	0.0253	0.0260	0.0248	0.0253	0.0236
	1.104	2.0	0.0237	0.0227	0.0230	0.0231	0.0225
	1.103	3.0	0.0224	0.0214	0.0227	0.0222	0.0217
	1.101	5.0	0.0219	0.0207	0.0222	0.0216	0.0206
	1.099	9.0	0.0215	0.0200	0.0219	0.0211	0.0199
	1.098	13.0	0.0207	0.0198	0.0223	0.0209	0.0197
	1.096	24.0	0.0203	0.0194	0.0213	0.0203	0.0193

[a] Metric conversion: 1 psi = 6.89 kPa.
[b] These amplitudes correspond to a shear strain amplitude of 0.0012, 0.0024, and 0.0048 percent, respectively.

MARCUSON AND WAHLS ON EFFECTS OF TIME 133

TABLE 4—*Damping data for kaolinite, Test 3, undrained.*

Pressure, psi[a] (1)	Void Ratio (2)	Time Ratio (3)	Damping Ratio, d — Amplitude,[b] rad Peak-to-Peak 0.00015 (4)	0.0003 (5)	0.0006 (6)	Average (7)	d_{fv} — Amplitude, rad Peak-to-Peak 0.0006 (8)
9.4	1.290	1.0	0.0229	0.0245	0.0300	0.0258	0.0250
9.1		4.0	0.0227	0.0232	0.0289	0.0249	0.0236
9.1		7.0	0.0227	0.0232	0.0227	0.0229	...
9.1		13.0	0.0213	0.0225	0.0312	0.0250	0.0218
9.0		25.0	0.0211	0.0225	0.0312	0.0249	0.0226
9.0		37.0	0.0210	0.0221	0.0305	0.0245	0.0221
9.0		70.0	0.0206	0.0216	0.0306	0.0243	0.0228
19.8	1.236	1.0	0.0259	0.0276	0.0335	0.0290	0.0225
19.0		3.0	0.0252	0.0250	0.0312	0.0271	0.0260
19.0		5.0	0.0252	0.0246	0.0308	0.0269	0.0267
18.9		9.0	0.0245	0.0241	0.0298	0.0261	0.0269
18.3		17.0	0.0248	0.0239	0.0294	0.0260	0.0256
18.0		26.5	0.0248	0.0236	0.0288	0.0257	0.0233
18.0		47.0	0.0245	0.0231	0.0284	0.0253	0.0252
40.0	1.176	1.0	0.0208	0.0205	0.0285	0.0233	0.0202
39.0		2.5	0.0187	0.0197	0.0269	0.0218	0.0180
38.5		4.0	0.0188	0.0196	0.0269	0.0218	0.0187
37.9		7.0	0.0179	0.0184	0.0247	0.0203	0.0174
37.0		13.0	0.0175	0.0179	0.0246	0.0200	0.0178
36.9		19.0	0.0169	0.0176	0.0246	0.0197	0.0169
36.4		35.5	0.0164	0.0171	0.0235	0.0190	0.0147
60.0	1.139	1.0	0.0186	0.0200	0.0249	0.0212	0.0143
58.9		2.2	0.0168	0.0180	0.0233	0.0194	0.0171
57.9		3.4	0.0152	0.0171	0.0224	0.0182	0.0164
56.9		5.8	0.0152	0.0170	0.0223	0.0182	0.0158
56.4		10.6	0.0152	0.0170	0.0221	0.0181	0.0154
55.0		15.4	0.0151	0.0170	0.0219	0.0180	0.0160
54.0		28.6	0.0149	0.0167	0.0215	0.0177	0.0149

[a] Metric conversion: 1 psi = 6.89 kPa.
[b] These amplitudes correspond to a shear strain amplitude of 0.0012, 0.0024, and 0.0048 percent, respectively.

TABLE 5—*Damping data for kaolinite, Test 4, undrained.*

			Damping Ratio, d				d_{fv}
			Amplitude,[b] rad Peak-to-Peak				Amplitude, rad Peak-to-Peak
Pressure, psi[a] (1)	Void Ratio (2)	Time Ratio (3)	0.00015 (4)	0.0003 (5)	0.0006 (6)	Average (7)	0.0006 (8)
9.6	1.291	1.0	0.0254	0.0275	0.0329	0.0286	0.0291
9.3		4.0	0.0252	0.0270	0.0315	0.0279	0.0309
9.0		7.0	0.0246	0.0258	0.0307	0.0270	0.0296
9.0		13.0	0.0243	0.0257	0.0303	0.0268	0.0289
8.9		25.0	0.0242	0.0252	0.0301	0.0265	0.0287
8.9		37.0	0.0241	0.0252	0.0297	0.0263	0.0289
8.9		70.0	0.0234	0.0254	0.0289	0.0259	0.0282
19.7	1.240	1.0	0.0262	0.0262	0.0297	0.0274	0.0259
19.0		3.0	0.0241	0.0241	0.0276	0.0253	0.0314
18.8		5.0	0.0233	0.0233	0.0265	0.0244	0.0241
18.4		9.0	0.0231	0.0232	0.0265	0.0243	0.0230
18.0		17.0	0.0230	0.0231	0.0258	0.0240	0.0229
17.9		25.0	0.0221	0.0225	0.0250	0.0232	0.0222
17.9		47.0	0.0213	0.0219	0.0249	0.0227	0.0219
39.8	1.170	1.0	0.0216	0.0235	0.0269	0.0240	0.0224
38.5		2.5	0.0215	0.0231	0.0258	0.0235	0.0216
37.5		4.0	0.0209	0.0229	0.0254	0.0231	0.0221
37.0		7.0	0.0209	0.0228	0.0251	0.0230	0.0213
36.0		13.0	0.0209	0.0223	0.0255	0.0229	0.0218
35.9		19.0	0.0206	0.0221	0.0245	0.0224	0.0214
35.0		35.5	0.0204	0.0219	0.0242	0.0222	0.0202
59.9	1.126	1.0	0.0222	0.0238	0.0236	0.0232	0.0216
58.7		2.2	0.0219	0.0223	0.0220	0.0221	0.0196
57.9		3.4	0.0209	0.0213	0.0213	0.0212	0.0185
57.2		5.8	0.0206	0.0211	0.0208	0.0208	0.0178
56.2		10.6	0.0203	0.0205	0.0206	0.0205	0.0177
56.0		15.4	0.0195	0.0203	0.0207	0.0202	0.0178
54.8		31.6	0.0189	0.0200	0.0201	0.0197	0.0182

[a] Metric conversion: 1 psi = 6.89 kPa.
[b] These amplitudes correspond to a shear strain amplitude of 0.0012, 0.0024, and 0.0048 percent, respectively.

TABLE 6—*Damping data as a percentage of average damping for kaolinite, Test 2, drained.*

			Damping Ratio / Average Damping Ratio		
			Amplitude,[b] rad Peak-to-Peak		
Pressure, psi[a] (1)	Void Ratio (2)	Time Ratio (3)	0.00015 (4)	0.0003 (5)	0.0006 (6)
10	1.288	1.0	95.8	88.5	115.7
	1.286	4.0	92.3	91.4	116.6
	1.286	7.0	89.8	95.0	114.3
	1.285	13.0	90.0	96.8	113.5
	1.285	25.0	90.9	96.1	113.3
	1.284	40.0	92.1	95.5	112.7
	1.284	70.0	91.3	95.5	112.8
20	1.241	1.0	93.5	94.6	111.9
	1.239	3.0	91.8	96.4	111.5
	1.237	5.0	92.8	97.7	109.1
	1.235	9.0	92.7	95.6	111.3
	1.233	17.0	92.9	96.6	110.1
	1.233	25.0	91.8	97.4	110.4
	1.231	46.0	92.8	96.0	111.2
40	1.177	1.0	89.9	97.0	112.7
	1.175	2.5	88.5	97.8	113.7
	1.173	4.0	87.3	97.7	114.5
	1.171	7.0	88.0	97.2	115.3
	1.169	13.0	90.0	99.0	111.0
	1.168	19.0	89.2	99.5	111.8
	1.167	35.0	88.9	99.5	112.1
80	1.108	1.0	100.0	102.8	98.0
	1.104	2.0	102.6	98.3	99.6
	1.103	3.0	100.9	96.4	102.3
	1.101	5.0	101.4	95.8	102.8
	1.099	9.0	101.9	94.8	103.8
	1.098	13.0	99.0	94.7	106.7
	1.096	24.0	100.0	95.6	104.9

[a] Metric conversion: 1 psi = 6.89 kPa.
[b] These amplitudes correspond to a shear strain amplitude of 0.0012, 0.0024, and 0.0048 percent, respectively.

is approximately 30 percent, while at 560 kPa (80 psi) the difference is less than 10 percent. For the consolidated-undrained tests, the data exhibit more scatter; however, the same general trends appear. The damping decreases with increasing pressure and time.

Figures 1 and 2 are plots of average damping ratio, d, versus logarithm of T-ratio, T_r, for drained Test 1 and consolidated-undrained Test 3,

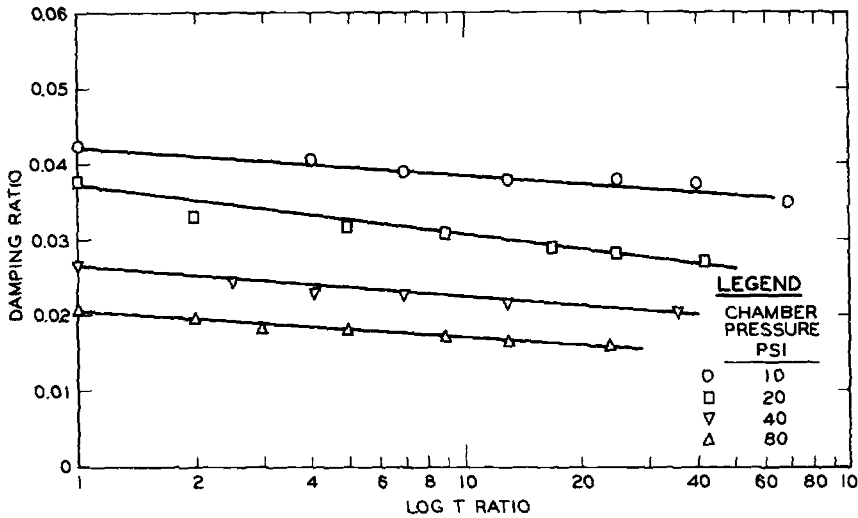

FIG. 1—*Average damping ratio versus logarithm of* T-*ratio for kaolinite, Test 1-D (1 psi = 6.89 kPa).*

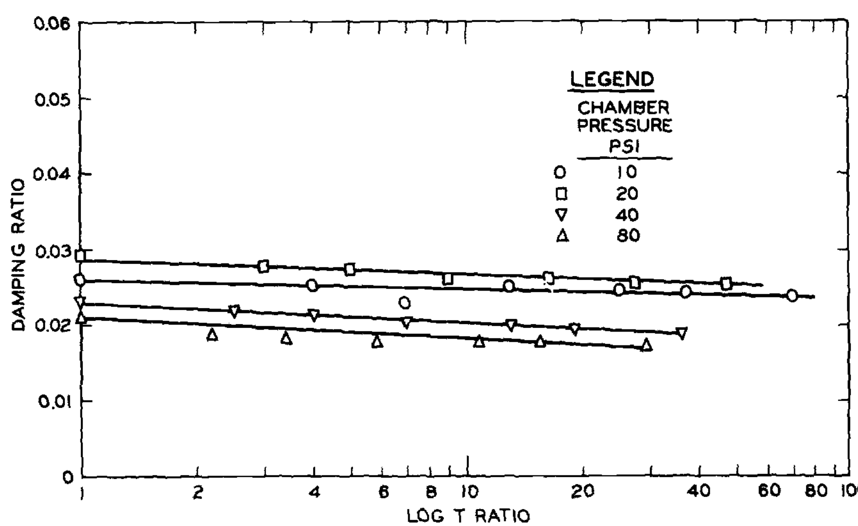

FIG. 2—*Average damping ratio versus logarithm of* T-*ratio for kaolinite, Test 3-CU (1 psi = 6.89 kPa).*

respectively. The decrease in average damping ratio is greater in Test 1 than in Test 3. The reason for this is that in Test 3 the void ratio was held constant and in Test 1 the void ratio decreased with time; thus, Fig. 1 has the effects of both void ratio and time. From Fig. 1 it appears that damping ratio decreases approximately 0.003 per logarithmic cycle of T_r, which represents a change in damping ratio of between 7.5 and 15 percent. This decrease in damping with time might also have been predicted due to structural changes causing a stiffening of the specimen and a corresponding increase in the shear modulus [*4,5*].

Bentonite

Because of the very high void ratios at low chamber pressures, damping for the bentonite was calculated only at chamber pressures of 280 kPa (40 psi) and above.

The damping data on Tests 5, 6 and 8–13 are presented in Tables 7–10. These data indicate that damping decreases with increasing pressure and with time, as was the case for the kaolinite tests.

Whitman and Richart [*6*] observed that the damping ratio for small strains was generally less than 0.05. Their observation was based largely on data obtained from cohesionless soil. The data obtained during this investigation confirm their observation for soil with a void ratio less than 1.5. However, these data indicate that as the void ratio approaches 2.0, the damping ratio approaches 0.1 for small strains.

The free-vibration method of calculating damping yields a lower value than the steady-state method. The difference in the two methods is less than 30 percent. For the bentonite data, the foregoing statement is applicable to both drained and consolidated-undrained test results.

Table 11 presents the damping ratio for each amplitude as a percentage of the average damping ratio for each pressure, void ratio, and time state. These data are from Tests 6 and 12, which were considered typical. A review of this table shows that for bentonite the effect of amplitude on the damping ratio is almost random and generally less than 3 percent. Because the effect is small, this could merely be an error induced in changing the sensitivity range on the recording equipment (oscilloscope).

Figures 3 and 4 present the average damping ratio versus logarithm of T-ratio for Tests 6 and 10, respectively. In both drained and undrained conditions, the damping decreases almost linearly with increasing logarithm of time. The damping ratio decreases approximately 25 percent during the first logarithmic cycle of T-ratio. These results do not agree with the results of Humphries [*7*]. The reason for the discrepancy is believed to be directly associated with the different mathematical models used to reduce the raw data [*5,7*].

Discussion of Results

For both the kaolinite and the bentonite, the damping ratio decreases with increasing pressure. There also is a strong correlation between damping

TABLE 7—*Damping data for bentonite, Tests 5 and 6, drained.*

				Damping Ratio, d				d_{fv}
				Amplitude,[b] rad Peak-to-Peak				Amplitude, rad Peak-to-Peak
	Pressure, psi[a] (1)	Void Ratio (2)	Time Ratio (3)	0.00015 (4)	0.0003 (5)	0.0006 (6)	Average (7)	0.0006 (8)
Test 5	40	1.869	1.0	0.0890	0.0859	0.0920	0.0890	0.0662
		1.863	1.2	0.0880	0.0860	0.0901	0.0880	0.0691
		1.858	1.3	0.0869	0.0849	0.0878	0.0865	0.0631
		1.852	1.6	0.0826	0.0808	0.0857	0.0830	0.0640
		1.844	2.2	0.0796	0.0798	0.0828	0.0807	0.0610
		1.833	3.8	0.0735	0.0744	0.0744	0.0741	0.0548
		1.824	5.1	0.0694	0.0694	0.0685	0.0691	0.0490
		1.817	7.2	0.0662	0.0662	0.0662	0.0662	0.0518
	80	1.621	1.0	0.0653	0.0629	0.0653	0.0645	0.0492
		1.618	1.1	0.0625	0.0608	0.0630	0.0621	0.0470
		1.615	1.2	0.0620	0.0608	0.0630	0.0619	0.0477
		1.610	1.3	0.0610	0.0593	0.0625	0.0609	0.0468
		1.599	2.2	0.0586	0.0564	0.0585	0.0578	0.0428
		1.595	2.5	0.0588	0.0551	0.0568	0.0569	0.0439
Test 6	40	1.890	1.0	0.0798	0.0777	0.0842	0.0806	0.0639
		1.881	1.2	0.0767	0.0767	0.0807	0.0780	0.0636
		1.876	1.3	0.0767	0.0757	0.0797	0.0774	0.0621
		1.868	1.6	0.0744	0.0738	0.0777	0.0744	0.0603
		1.858	2.2	0.0736	0.0726	0.0764	0.0744	0.0606
		1.848	3.4	0.0692	0.0674	0.0709	0.0692	0.0518
	80	1.635	1.0	0.0625	0.0601	0.0607	0.0611	0.0467
		1.631	1.1	0.0625	0.0602	0.0607	0.0611	0.0442
		1.629	1.2	0.0615	0.0591	0.0596	0.0601	0.0415
		1.624	1.3	0.0604	0.0586	0.0586	0.0592	0.0436
		1.616	1.7	0.0575	0.0562	0.0567	0.0568	0.0425
		1.611	2.7	0.0564	0.0548	0.0538	0.0550	0.0424
		1.605	3.8	0.0552	0.0531	0.0536	0.0540	0.0412
		1.599	5.2	0.0548	0.0528	0.0528	0.0535	0.0379

[a] Metric conversion: 1 psi = 6.89 kPa.
[b] These amplitudes correspond to a shear strain amplitude of 0.0012, 0.0024, and 0.0048 percent, respectively.

TABLE 8—*Damping data for bentonite, Tests 8 and 9, drained.*

				Damping Ratio, d				d_{fv}
				Amplitude,[b] rad Peak-to-Peak				Amplitude, rad Peak-to-Peak
	Pressure, psi[a] (1)	Void Ratio (2)	Time Ratio (3)	0.00015 (4)	0.0003 (5)	0.0006 (6)	Average (7)	0.0006 (8)
Test 8	40	1.880	1.0	0.0894	0.0907	0.0942	0.0914	0.0695
		1.871	1.2	0.0883	0.0908	0.0940	0.0910	0.0775
		1.864	1.3	0.0871	0.0883	0.0914	0.0889	0.0742
		1.854	1.6	0.0823	0.0850	0.0879	0.0851	0.0682
		1.843	2.2	0.0794	0.0794	0.0832	0.0807	0.0623
		1.834	3.3	0.0765	0.0765	0.0792	0.0774	0.0602
	80	1.637	1.0	0.0654	0.0680	0.0687	0.0674	0.0549
		1.634	1.1	0.0636	0.0667	0.0667	0.0657	0.0527
		1.629	1.2	0.0674	0.0668	0.0668	0.0670	0.0525
		1.620	1.3	0.0662	0.0650	0.0656	0.0656	0.0530
		1.613	1.7	0.0640	0.0639	0.0639	0.0639	0.0497
		1.603	3.1	0.0588	0.0578	0.0582	0.0583	0.0490
Test 9	40	1.853	1.0	0.0757	0.0767	0.0788	0.0771	0.0605
		1.845	1.1	0.0743	0.0757	0.0768	0.0756	0.0578
		1.838	1.3	0.0724	0.0724	0.0744	0.0731	0.0549
		1.824	1.8	0.0716	0.0716	0.0726	0.0719	0.0540
		1.817	2.2	0.0664	0.0681	0.0690	0.0678	0.0502
		1.808	2.8	0.0648	0.0648	0.0665	0.0654	0.0482
		1.802	3.7	0.0633	0.0633	0.0642	0.0636	0.0462
	80	1.606	1.0	0.0665	0.0665	0.0646	0.0659	0.0461
		1.601	1.1	0.0641	0.0653	0.0634	0.0643	0.0478
		1.596	1.2	0.0619	0.0624	0.0612	0.0618	0.0463
		1.591	1.3	0.0598	0.0613	0.0601	0.0604	0.0447
		1.581	1.7	0.0583	0.0588	0.0576	0.0582	0.0432
		1.566	3.3	0.0522	0.0530	0.0515	0.0522	0.0417

[a] Metric conversion: 1 psi = 6.89 kPa.
[b] These amplitudes correspond to a shear strain amplitude of 0.0012, 0.0024, and 0.0048 percent, respectively.

TABLE 9—*Damping data for bentonite, Tests 10 and 11, undrained.*

	Pressure, psi[a] (1)	Void Ratio (2)	Time Ratio (3)	Damping Ratio, d — Amplitude,[b] rad Peak-to-Peak 0.00015 (4)	0.0003 (5)	0.0006 (6)	Average (7)	d_{fv} — Amplitude, rad Peak-to-Peak 0.0006 (8)
Test 10	38.9	1.913	1.0	0.0707	0.0697	0.0707	0.0704	0.0493
	37.0		1.2	0.0681	0.0680	0.0698	0.0686	0.0458
	36.0		1.3	0.0681	0.0671	0.0663	0.0672	0.0466
	35.0		1.6	0.0664	0.0646	0.0663	0.0658	0.0514
	34.0		2.2	0.0656	0.0638	0.0638	0.0644	0.0456
	33.0		3.4	0.0618	0.0601	0.0600	0.0606	0.0414
	58.8	1.776	1.0	0.0604	0.0617	0.0610	0.0610	0.0452
	57.8		1.1	0.0598	0.0584	0.0598	0.0593	0.0435
	55.5		1.3	0.0586	0.0573	0.0585	0.0581	0.0423
	54.6		1.5	0.0581	0.0586	0.0580	0.0582	0.0436
	52.2		2.0	0.0553	0	0.0562	0.0558	0.0418
	52.2		2.4	0.0543	0.0548	0.0548	0.0546	0.0403
	51.2		3.5	0.0514	0.0528	0.0526	0.0623	0.0393
Test 11	39.0	1.907	1.0	0.0725	0.0725	0.0748	0.0733	0.0591
	38.0		1.2	0.0704	0.0714	0.0714	0.0711	0.0526
	36.5		1.3	0.0694	0.0714	0.0714	0.0707	0.0560
	35.0		1.6	0.0675	0.0675	0.0684	0.0678	0.0521
	34.3		2.2	0.0636	0.0653	0.0666	0.0652	0.0520
	34.0		4.0	0.0597	0.0612	0.0621	0.0610	0.0493
	33.0		5.9	0.0590	0.0597	0.0623	0.0603	0.0507
	59.0	1.783	1.0	0.0656	0.0656	0.0656	0.0656	0.0528
	57.2		1.1	0.0648	0.0656	0.0656	0.0653	0.0529
	56.0		1.2	0.0648	0.0648	0.0656	0.0650	0.0521
	55.0		1.5	0.0627	0.0634	0.0634	0.0632	0.0509
	53.4		2.0	0.0613	0.0620	0.0620	0.0618	0.0480
	51.0		4.3	0.0597	0.0590	0.0590	0.0592	0.0451

[a] Metric conversion: 1 psi = 6.89 kPa.
[b] These amplitudes correspond to a shear strain amplitude of 0.0012, 0.0024, and 0.0048 percent, respectively.

TABLE 10—*Damping data for bentonite, Tests 12 and 13, undrained.*

				Damping Ratio, d				d_{fv}
				Amplitude,[b] rad Peak-to-Peak				Amplitude, rad Peak-to-Peak
	Pressure, psi[a] (1)	Void Ratio (2)	Time Ratio (3)	0.00015 (4)	0.0003 (5)	0.0006 (6)	Average (7)	0.0006 (8)
Test 12	38.4	1.936	1.0	0.0791	0.0779	0.0780	0.0783	0.0554
	36.7		1.2	0.0757	0.0768	0.0768	0.0764	0.0569
	36.0		1.3	0.0757	0.0768	0.0768	0.0764	0.0547
	34.9		1.6	0.0737	0.0747	0.0747	0.0744	0.0542
	33.9		2.2	0.0745	0.0717	0.0727	0.0730	0.0522
	32.9		3.4	0.0687	0.0678	0.0678	0.0681	0.0497
	58.5	1.794	1.0	0.0734	0.0744	0.0753	0.0744	0.0559
	56.5		1.1	0.0726	0.0726	0.0726	0.0726	0.0541
	55.5		1.2	0.0710	0.0718	0.0710	0.0712	0.0542
	54.0		1.5	0.0687	0.0694	0.0694	0.0692	0.0542
	53.0		2.0	0.0672	0.0672	0.0672	0.0672	0.0518
	51.0		4.2	0.0631	0.0631	0.0624	0.0629	0.0474
Test 13	39.2	1.889	1.0	0.0823	0.0832	0.0920	0.0858	0.0625
	35.0		1.2	0.0787	0.0797	0.0880	0.0821	0.0587
	34.4		1.3	0.0745	0.0764	0.0888	0.0799	0.0593
	34.0		1.6	0.0760	0.0779	0.0864	0.0801	0.0573
	33.0		3.0	0.0695	0.0722	0.0795	0.0737	0.0547
	59.3	1.757	1.0	0.0749	0.0805	0.0855	0.0803	0.0581
	57.0		1.1	0.0715	0.0778	0.0825	0.0774	0.0573
	56.2		1.2	0.0691	0.0752	0.0807	0.0750	0.0560
	55.2		1.5	0.0669	0.0736	0.0790	0.0732	0.0436
	54.2		2.0	0.0648	0.0705	0.0784	0.0712	0.0740
	53.0		3.9	0.0783	0.0677	0.0738	0.0733	0.0504

[a] Metric conversion: 1 psi = 6.89 kPa.
[b] These amplitudes correspond to a shear strain amplitude of 0.0012, 0.0024, and 0.0048 percent, respectively.

TABLE 11—*Damping data as a percentage of average damping for bentonite, Tests 6 and 12.*

				Damping Ratio		
				Average Damping Ratio		
				Amplitude,[b] rad Peak-to-Peak		
	Pressure, psi[a] (1)	Void Ratio (2)	Time Ratio (3)	0.00015 (4)	0.0003 (5)	0.0006 (6)
Test 6—drained	40	1.890	1.0	99.0	96.4	104.5
		1.881	1.2	98.3	98.3	103.5
		1.876	1.3	99.1	97.8	103.0
		1.868	1.6	100.0	99.2	104.4
		1.858	2.2	98.9	97.6	102.7
		1.848	3.4	100.0	97.4	102.5
	80	1.635	1.0	102.3	98.4	99.3
		1.631	1.1	102.3	98.5	99.3
		1.629	1.2	102.3	98.3	99.2
		1.624	1.3	102.0	99.0	99.0
		1.616	1.7	101.2	98.9	99.8
		1.611	2.7	102.5	99.6	97.8
		1.605	3.8	102.2	98.3	99.3
		1.599	5.2	102.4	98.7	98.7
Test 12—undrained	38.4	1.936	1.0	101.0	99.5	99.6
	36.7		1.2	99.1	100.5	100.5
	36.0		1.3	99.1	100.5	100.5
	34.9		1.6	99.1	100.4	100.4
	33.9		2.2	102.1	98.2	99.6
	32.9		3.4	100.9	99.6	99.6
	58.5	1.749	1.0	98.7	100.0	101.2
	56.5		1.1	100.0	100.0	100.0
	55.5		1.2	99.7	100.8	99.7
	54.0		1.5	99.3	100.3	100.3
	53.0		2.0	100.0	100.0	100.0
	51.0		4.2	100.3	100.3	99.2

[a] Metric conversion: 1 psi = 6.89 kPa.
[b] These amplitudes correspond to a shear strain amplitude of 0.0012, 0.0024, and 0.0048 percent, respectively.

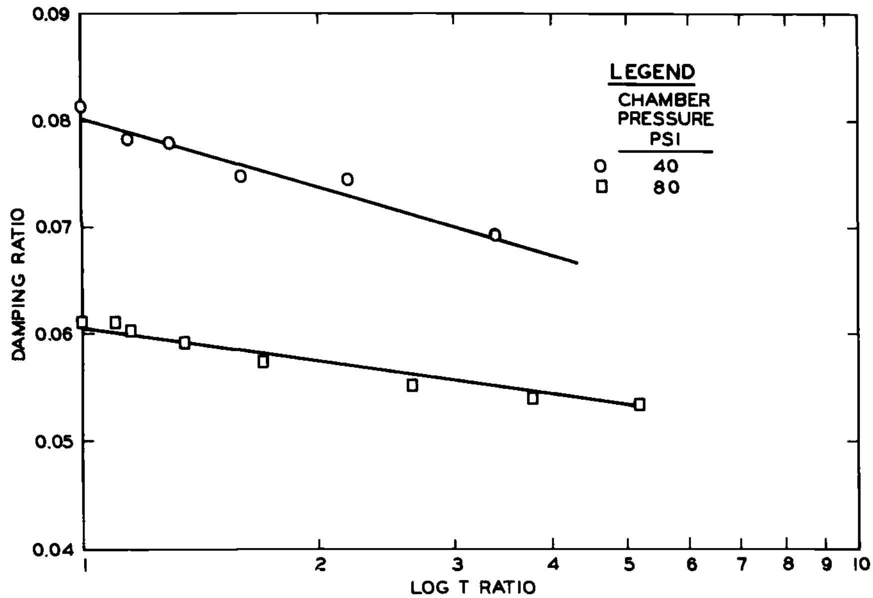

FIG. 3—*Average damping ratio versus logarithm of* T*-ratio for bentonite, Test 6-D (1 psi = 6.89 kPa).*

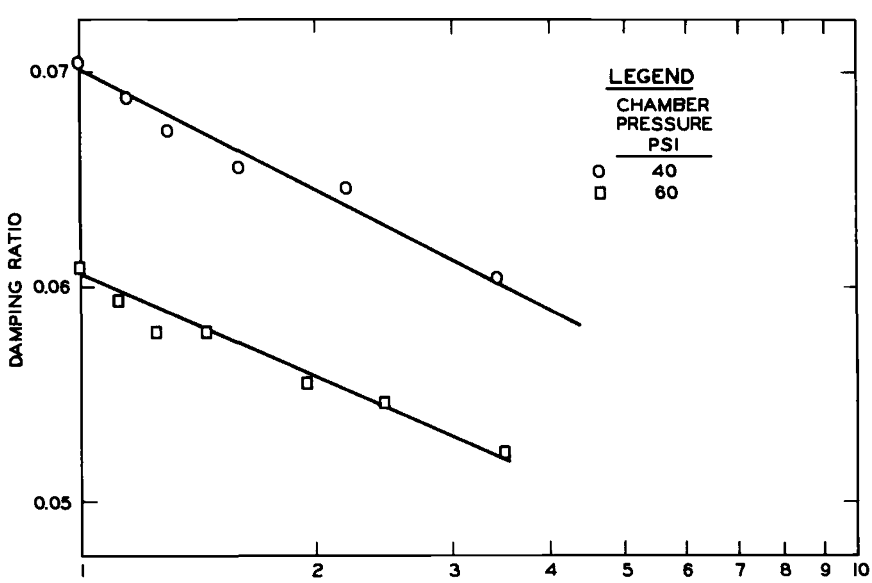

FIG. 4—*Average damping ratio versus logarithm of* T*-ratio for bentonite, Test 10-CU (1 psi = 6.89 kPa).*

ratio and shear modulus; that is, the damping ratio decreases as the shear modulus increases. These effects are well recognized in the literature [*3, 5, 7*].

The effects of vibration amplitude were relatively small in this investigation. Seed and Idriss [*8*] have presented damping ratios as a function of shear strain for saturated clays (see Fig. 5). The shear strain in Fig. 5 is zero-to-peak and is expressed as a percentage. This plot presents most of the damping data for clay available in the published literature. These data are for various confining pressures and do not generally include secondary consolidation or time effects. Superimposed on Fig. 5 are the ranges of damping ratios obtained in this study for a T-ratio of 1 at various confining pressures. These kaolinite data generally fall within the damping range developed by Seed and Idriss; however, the bentonite data lie above their curves. This is probably because of the high (large) void ratio of this particular soil. The lower range of our bentonite data lies just above the upper range of Seed's curves, which are based on one data point obtained by Hardin and Drnevich [*9*].

The data presented herein indicate that the damping ratio may decrease significantly with time at constant effective stress. The kaolinite exhibited a decrease in damping of 20 to 30 percent as the T-ratio increased from 1 to about 35, which corresponds to a decrease of approximately 12 percent

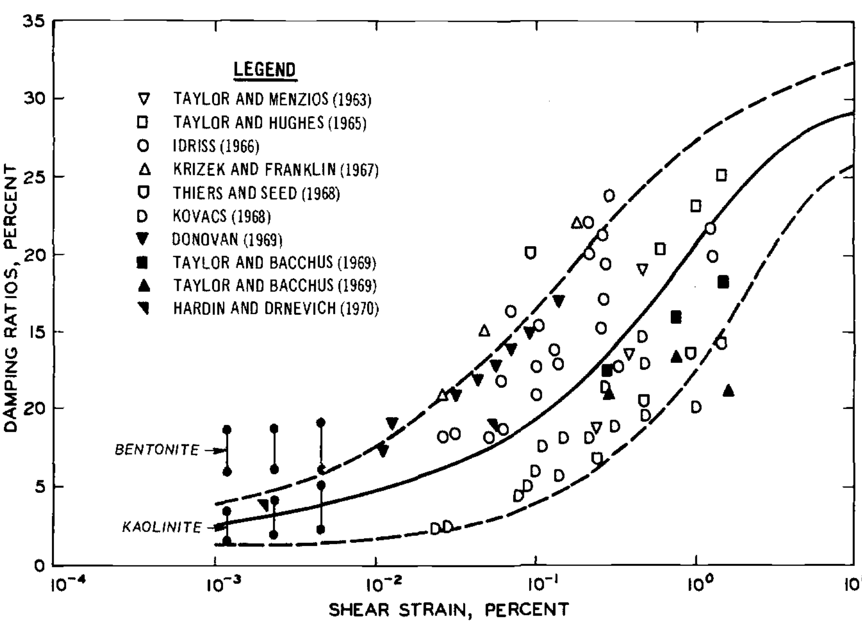

FIG. 5—*Damping ratios for saturated clays (after Seed and Idriss* [*8*]) (*1 psi = 6.89 kPa*).

per logarithmic cycle of T_r. The bentonite exhibited a decrease in damping of 10 to 30 percent as the T-ratio increased from 1 to about 5, which corresponds to a decrease of approximately 25 percent per logarithmic cycle of T_r. This is in general agreement with the data presented by Hardin and Drnevich [*9*] for Lick Creek silt, which exhibited a decrease in damping ratio of 25 to 30 percent over a period of 15 h.

It is currently the authors' opinion that this decrease in damping with time is due to time-dependent changes in the soil structure of the material. This structure may not be destroyed by vibrations which produce shear strains on the order of 10^{-4}. However, excitation levels producing shear strain on the order of 10^{-1} may sufficiently remold the material so as to erase the effects of time. For this reason the authors also feel that the effects of time on damping properties of the soil are more important at low strain levels.

Research at the University of Michigan [*10,11*] has indicated that shear moduli determined by resonant-column tests at the end of primary consolidation may significantly underestimate the field shear modulus. Anderson and Woods [*11*] suggest that extrapolation of the laboratory modulus to a time of 20 years will provide reasonable agreement with field measurements. Similar comparisons of laboratory and field data are not available for damping ratio. However, because of the demonstrated relations between damping and shear modulus, it is likely that laboratory resonant-column tests at the end of primary consolidation may overestimate the field damping ratio.

Implications to Testing Procedures

The results of the long-term tests conducted in this investigation have several implications regarding testing procedures for evaluating damping from laboratory resonant-column tests. First, because the damping ratio of some clays may decrease significantly with time, laboratory testing procedures should include provisions for evaluating the effects of time. This could be accomplished by performing at least one test in which damping is measured at the end of primary consolidation (T_r = 1.0) and at several additional times while secondary compression is taking place. It is suggested that the test be continued until T_r is 5 to 10. If the damping decreases linearly with the logarithm of T-ratio, the results may be extrapolated to longer time periods.

The study also indicates two potential sources of error in the evaluation of damping from resonant-column tests. It was observed that the apparatus damping constant, which is required for computation of the soil damping ratio, is sensitive to relatively minor variations in the position and stiffness of the electric wires connected to the vibration head of the resonant-column apparatus. The importance of this effect should be evaluated for other resonant-column equipment. If the effect is significant for a particular apparatus, it may be necessary to recalibrate the apparatus at the start of each test series.

For long-term tests to investigate time effects in clays, an air-water interface in the test chamber may allow air to diffuse into the specimen, which will affect volume change and void ratio measurements. In this study, diffusion was prevented by introducing a mercury jacket around the specimen. It was demonstrated that the mercury had little effect on the measured damping values.

Finally, the damping values obtained from the decay of free vibrations were consistently lower than those determined by the steady-state method. No explanation is available for this observation, and it is recommended that this effect should be investigated further.

Conclusions and Recommendations

The primary objective of this study was to determine the effects of time, void ratio, and pressure on the damping ratio of clay soils. A kaolinite, which exhibits very little secondary compression, and a calcium bentonite, which exhibits relatively large secondary compression, were studied. The more significant conclusions regarding the behavior of these materials are:

1. The damping ratio decreases with time at constant effective stress after completion of primary consolidation. The percentage decrease is larger for bentonite than for kaolinite.

2. The damping ratio of both soils decreases with increasing stiffness and increasing pressure.

As a result of this investigation, the following recommendations are made regarding resonant column testing procedures for evaluating damping:

1. The effects of time should be considered for clay soils by continuing at least one test to T-ratios of 5 to 10.

2. For long-term tests, precautions should be taken to prevent diffusion of air into the specimen. The use of a mercury jacket around the specimen is suggested for this purpose; however, the researcher is encouraged to take all safety precautions when using mercury.

3. The effects of equipment setup details (position of lead wires, etc.) on the apparatus damping constant should be investigated. If the apparatus is sensitive to this effect, the damping constant should be reevaluated at the start of each test.

Acknowledgments

The investigation reported herein constituted a part of the study conducted by W. F. Marcuson III, under the supervision of H. E. Wahls, at North Carolina State University, Raleigh, N. C., in partial fulfillment of the requirements for the degree of doctor of philosophy. The senior author gratefully acknowledges the financial support of the National Science Foundation and the Ford Foundation during his graduate studies. Special thanks are due Vincent P. Drnevich, University of Kentucky, for his constructive review.

References

[1] Hardin, B. O. in *Special Procedures for Testing Soil and Rock for Engineering Purposes, ASTM STP 479,* American Society for Testing and Materials, 1970, pp. 516–529.

[2] Hardin, B. O. and Music, J. in *Symposium on Instrumentation and Apparatus for Soils and Rocks, ASTM STP 392,* American Society for Testing and Materials, 1965, pp. 55–73.

[3] Humphries, W. K. and Wahls, H. E., *Journal of Soil Mechanics and Foundations Division,* American Society of Civil Engineers, Vol. 94, No. SM2, March 1968, pp. 371–389.

[4] Marcuson, W. F., III, and Wahls, H. E., *Journal of Soil Mechanics and Foundations Division,* American Society of Civil Engineers, Vol. 98, No. SM12, 1972, pp. 1359–1373.

[5] Marcuson, W. F., III, "The Effects of Time on the Dynamic Shear Modulus and Damping Ratio of Clay Soils," thesis presented in partial fulfillment for Ph.D., University of North Carolina, Raleigh, N. C., 1970.

[6] Whitman, R. V. and Richart, F. E., Jr., *Journal of Soil Mechanics and Foundations Division,* American Society of Civil Engineers, Vol. 93, No. SM6, Nov. 1967, pp. 169–193.

[7] Humphries, W. K., "The Effects of Stress History on the Dynamic Response of Clay Soils," thesis presented in partial fulfillment for Ph.D., University of North Carolina, Raleigh, N.C., 1966.

[8] Seed, H. B. and Idriss, I. M., "Soil Modulus and Damping Factors for Dynamic Response Analyses," Earthquake Engineering Research Center Report No. EERC 70-10, University of California at Berkeley, 1970.

[9] Hardin, B. O. and Drnevich, V. P., *Journal of Soil Mechanics and Foundations Division,* American Society of Civil Engineers, Vol. 98, No. SM6, 1972, pp. 667–692.

[10] Stokoe, K. H., II, and Abdel-razzak, K. G., *Proceedings,* American Society of Civil Engineers Conference on *In Situ* Measurement of Soil Properties, Raleigh, N. C., Vol. 1, June 1975, pp. 422–449.

[11] Anderson, D. G. and Woods, R. D., *Proceedings,* American Society of Civil Engineers Conference on *In Situ* Measurement of Soil Properties, Raleigh, N. C., Vol. 1, June 1975, pp. 69–92.

C. K. Shen,[1] *K. Sadigh,*[2] *and L. R. Herrmann*[1]

An Analysis of NGI Simple Shear Apparatus for Cyclic Soil Testing

REFERENCE: Shen, C. K., Sadigh, K., and Herrmann, L. R., **"An Analysis of NGI Simple Shear Apparatus for Cyclic Soil Testing,"** *Dynamic Geotechnical Testing, ASTM STP 654,* American Society for Testing and Materials, 1978, pp. 148–162.

ABSTRACT: A numerical analysis parametric study was conducted to determine the stress and strain states within an idealized soil specimen enclosed by a wire-reinforced rubber membrane and tested in the Norwegian Geotechnical Institute (NGI) simple shear apparatus. The computations were performed utilizing a finite-element program applicable to three-dimensional elastic analysis of nonaxisymmetrically loaded axisymmetric solids. Orthotropic membrane elements were incorporated in the program to simulate the action of the wire-reinforced rubber membrane. A total of 14 cases was analyzed using different combinations of material properties, membrane stiffness, specimen geometry, and boundary displacements. In general, for the values of the parameters studied, the uniformity of shear strain distribution improves as (1) the specimen height-to-diameter ratio is decreased, (2) the percent of wire-reinforcement is increased, (3) the elastic modulus of the soil decreases, (4) the Poisson's ratio of the soil decreases, and (5) the applied horizontal displacement is increased.

KEY WORDS: simple shear, NGI apparatus, soils, cyclic testing, finite elements, linear elastic analysis, reinforced membrane, stress and strain

During the past few years there has been a growing interest in simple shear devices for cyclic liquefaction testing and determination of dynamic soil properties. The simple shear devices developed by the Swedish Geotechnical Institute (SGI) [*1*],[3] the Norwegian Geotechnical Institute (NGI) [*2*], and Cambridge University [*3,4*] are potentially capable of imposing static and cyclic simple shear loading and allow the application of appreciable normal loads to specimens. The stress conditions within the specimen tested in the Cambridge device were first studied theoretically by Roscoe [*3*], and later by Duncan and Dunlop [*5*] using the finite-element

[1] Associate professor and professor, respectively, Department of Civil Engineering University of California, Davis, Calif. 95616.

[2] Senior project engineer, Woodward-Cycle Consultants, San Francisco, Calif. 94111.

[3] The italic numbers in brackets refer to the list of references appended to this paper.

method of analysis. Prevost and Hoeg [6] recently presented a detailed discussion of the stress conditions in connection with simple shear soil testing.

The NGI apparatus was designed to apply simple shear loading to a thin cylindrical specimen [typically 2 cm (0.8 in.) high and 8 cm (3.2 in.) in diameter]. This apparatus was developed so as to constrain the specimen to a constant diameter while undergoing shear deformation. To achieve this constraint, the specimen is enclosed by a wire-reinforced rubber membrane. Because of the relatively complex boundary of the specimen-membrane system, as well as the nonsymmetric loading condition, very few attempts have been made to date to determine the states of stress and strain in the soil specimen tested in the NGI device. Lucks et al [7] and Sadigh [8] conducted linear elastic finite-element analyses to study the stress conditions in the NGI simple shear test. The analyses by Lucks et al [7] appear to assume that upon application of the initial vertical load there is no lateral restraint due to friction between the testing platens and the specimen, and thus possible initial static shear strains due to end effects are not included. Furthermore, analyses by Lucks et al did not include the confining effect of the wire-reinforced membrane. In the finite-element analyses by Sadigh [8] the wire-reinforced rubber membrane was represented using thin conical shell elements. These analyses were limited to cases involving application of shearing displacements only.

This paper presents the results of a numerical study conducted to determine the stress and strain states within a soil specimen enclosed by a wire-reinforced rubber membrane and tested in the NGI device. The membrane effect and the combined effects of initial vertical and horizontal displacements are incorporated in the analyses.

Problem Formulation

The study was formulated by assuming that the soil specimen is a linear-elastic isotropic cylindrical solid enclosed in a wire-reinforced rubber membrane. The rather gross approximation of modeling the soil as linear elastic was made in order to render the analyses economically feasible; while it is recognized that this approximation introduces quantitative error, it is felt that the results give a good qualitative measure of the relative effects of the several parameters. A uniform vertical displacement was applied on the top surface of the specimen to simulate the vertical load that is applied to insure a perfect bonding at both the top and bottom platens. The vertical displacement is followed by the application of a uniform horizontal displacement on the same surface to simulate the simple shear action. The complete boundary conditions of the system and the finite-element mesh are shown in Fig. 1.

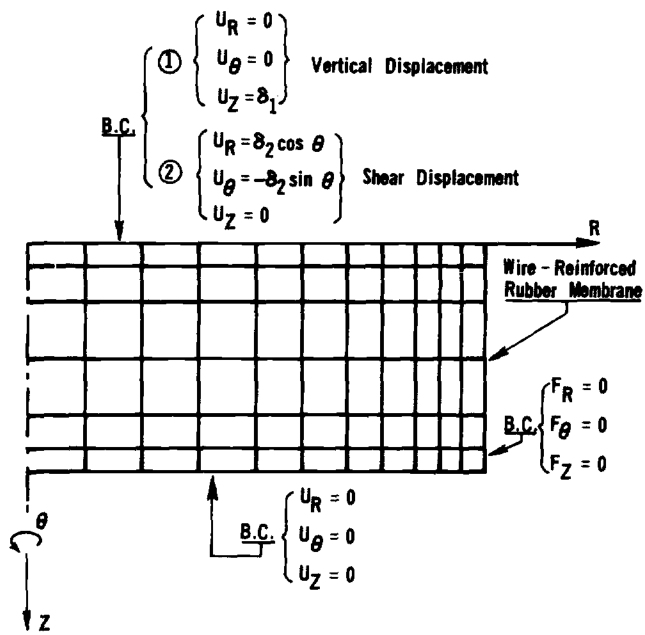

FIG. 1—*Boundary conditions and finite-element representation.*

Analyses and Parameters Studied

Analyses were performed using a finite-element computer program developed by Herrmann [*9,10*]; the analysis is similar to that reported in [*11*]. Orthotropic membrane elements were incorporated in this program to capture the action of the wire-reinforced rubber membrane. The membrane element is developed by using linear approximations for the membrane displacements. The composite orthotropic properties of the wire-reinforced membrane are found by treating it as a composite material [*12*]. The program is capable of performing three-dimensional linear elasticity analysis of nonaxisymmetrically loaded axisymmetric solids. It utilizes a complete Fourier expansion of the θ dependence.

A total of 14 cases was analyzed using different combinations of material properties (E and ν), membrane stiffness (A_s/A), specimen geometry (H/D), and boundary displacement (δ_1 and δ_2). A summary of these cases is listed in Table 1. A set of parameters taken as the basis for comparison is given as follows (Case 3 in Table 1):

E = Young's modulus of soil specimen = 29 480 kN/m^2 (4272 psi),

ν = Poisson's ratio of soil specimen = 0.4,

A_s = cross-sectional area of reinforcing wire in R-Z plane = 0.05 mm²/mm,
A = total cross-sectional area of rubber membrane in R-Z plane = 0.5 mm²/mm,
E_r = Young's modulus of rubber = 2070 kN/m² (300 psi),
E_w = Young's modulus of reinforcing wire = 107 × 10⁶ kN/m² (16 × 10⁶ psi),
H = height of soil specimen = 20 mm (0.8 in.),
D = diameter of soil specimen = 80 mm (3.2 in.),
$\delta_1 = H\epsilon_z$ = uniform vertical displacement applied to soil specimen to cause 0.25 percent vertical strain, and
$\delta_2 = H\gamma_{RZ}$ = uniform horizontal displacement applied to soil specimen to cause 0.5 percent shear strain.

In all 14 cases analyzed, A, E_r, E_w, and D were assumed to be constants, these values were measured and reported by Sadigh [8].

TABLE 1—*Summary description of cases analyzed.*

Case	H/D	A_s/A	ϵ_z, %	γ_{RZ}, %	E (g/mm²)[a]	ν
1	1/4	0.1	0.25	0	3 000	0.4
2	1/4	0.1	0	0.5	3 000	0.4
3	1/4	0.1	0.25	0.5	3 000	0.4
4	1/2	0.1	0.25	0.5	3 000	0.4
5	1/8	0.1	0.25	0.5	3 000	0.4
6	1/4	0.1	0.25	0.5	300	0.4
7	1/4	0.1	0.25	0.5	30 000	0.4
8	1/4	0.1	0.25	1	3 000	0.4
9	1/4	0.1	0.25	0.25	3 000	0.4
10	1/4	0	0.25	0.5	3 000	0.4
11	1/4	0.05	0.25	0.5	3 000	0.4
12	1/4	0.2	0.25	0.5	3 000	0.4
13	1/4	0.1	0.25	0.5	3 000	0.3
14	1/4	0.1	0.25	0.5	3 000	0.49

[a] 1 g/mm² = 9.83 kN/m².

Results

For a given θ-position the finite-element analysis yields the node point displacements, and the stress and strain states in all elements. The relative influence of different parameters on the stress and strain distribution within a circular soil mass was compared by examining the vertical stress (σ_Z) and the shear strain (γ_{RZ}) developed in the R-Z plane at the θ = 0 deg position.

Using the linear elastic formulation, it was possible for a given set of system parameters to superimpose solutions of different boundary displacements (such as Cases 1 and 2) to obtain the solution of the combined boundary displacements (Case 3) as shown for the stresses in Fig. 2 and strains in Fig. 3. In Case 1, shear strain is developed in the specimen due to a uniform vertical displacement; its distribution is rather nonuniform with larger magnitudes occurring at or near the boundaries. On the other hand, in Case 2, the distribution of shear strain due to horizontal displacement is relatively uniform throughout the specimen except near the vertical boundaries. It is important to mention that an axis of symmetry exists at mid-height of the specimen for the shear strain distribution developed by the horizontal displacement (Case 2, Fig. 3); however, in the case of vertical displacement the induced shear strains maintain opposite signs on both sides of the mid-height axis (Case 1, Fig. 3).

Because the properties are constant for linear elastic materials, the shear strains induced by the initial vertical displacement would not affect the measured shear modulus for such materials. However, for nonlinear materials (such as soil) these initial shear strains cause the incremental (incremental tangent) properties, which define the soil behavior when the subsequent horizontal displacement is applied, to vary throughout the specimen; the measured modulus would then be the average of this distribution.

Figures 4–8 show the influence of the various parameters listed in Table 1 (Case 3 through Case 14) on the distribution and magnitude of shear strain in the R-Z plane (θ = 0 deg). In all the 12 cases studied, a vertical displacement causing a vertical strain of 0.25 percent was first applied for the simulation of a perfect bonding required for simple shear testing. This, in conjunction with the horizontal displacement conditions applied in the individual cases, resulted in a nonuniform shear strain distribution throughout the circular specimen.

In studying the effect of each individual parameter on the shear strain distribution, one must examine the influence of the vertical as well as the horizontal displacements. As shown in Fig. 3, for example, the application of a vertical displacement can result in a rather nonuniform shear distribution throughout the specimen, whereas the induced shear state due to a horizontal displacement is relatively uniform except near the outer vertical boundaries. Coded zones are used in the figures to show the percentage of shear strain deviation from a uniform distribution (that is, the assumed input shear strain). The percentage of deviation is negative for elements in the upper half of the specimen and near the outer vertical boundaries; for most of the lower half of the specimen, the percentage of deviation is positive. A typical example of such a distribution is shown in Case 3 of Fig. 3.

Figure 4 shows the effect of height-to-diameter ratio on the shear strain distribution. Since the standard NGI specimen has a diameter of 8 cm (3.2 in.) and a height of 2 cm (0.8 in.) (H/D = 1/4), it was decided that the H/D ratios of 1/2, 1/4, and 1/8 would be studied. In all cases the

Case 1

14.94										14.76
15.08										12.01
15.19										11.44
15.19	15.14	15.03	14.84	14.60	14.31	13.97	13.55	13.05	12.31	11.44
15.08	15.0	14.86	14.65	14.38	14.05	13.70	13.38	13.10	13.23	12.01
14.94	14.84	14.68	14.44	14.13	13.76	13.36	13.01	12.82	12.59	14.76

Case 2

0.0038										(-) 13.14
0.0041										(-) 7.78
0.0019										(-) 2.74
(-) 0.0019	(-) 0.0082	(-) 0.023	(-) 0.048	(-) 0.070	(-) 0.025	0.16	0.64	1.41	2.09	2.74
(-) 0.0041	(-) 0.016	(-) 0.044	(-) 0.089	(-) 0.12	(-) 0.023	0.36	1.35	2.92	5.64	7.78
(-) 0.0038	(-) 0.015	(-) 0.035	(-) 0.063	(-) 0.056	0.093	0.55	1.60	3.39	5.7	13.14

Case 3

14.94	14.85	14.72	14.51	14.19	13.67	12.81	11.40	9.43	6.89	1.62
15.08	15.01	14.91	14.74	14.50	14.07	13.34	12.03	10.18	7.59	4.23
15.19	15.15	15.05	14.88	14.67	14.33	13.81	12.91	11.65	10.22	8.70
15.19	15.13	15.00	14.79	14.53	14.28	14.13	14.19	14.56	14.40	14.17
15.07	14.98	14.82	14.56	14.26	14.03	14.06	14.74	16.20	18.87	19.80
14.93	14.82	14.65	14.38	14.08	13.85	13.91	14.61	16.21	18.29	27.91

FIG. 2—*Distribution of vertical normal stresses* (σ_{zz}) *in* g/mm^2 (θ = *0 deg*) (*Note: 1* g/mm^2 = *9.83* kN/m^2).

Case 1

											(-)
0.01	0.04	0.07	0.11	0.15	0.19	0.23	0.24	0.22	0.12	0.03	
0.03	0.09	0.17	0.26	0.36	0.47	0.59	0.69	0.75	0.71	0.26	(+)
0.04	0.12	0.21	0.33	0.45	0.60	0.75	0.92	1.10	1.36	1.61	

Case 2

2.50										1.98
2.50										0.82
2.50										0.54
2.50	2.50	2.51	2.54	2.58	2.61	2.58	2.40	2.02	1.41	0.54
2.50	2.50	2.50	2.50	2.48	2.45	2.40	2.31	2.15	1.87	0.82
2.50	2.50	2.50	2.47	2.42	2.33	2.18	2.02	1.88	1.92	1.98

Case 3

2.46	2.38	2.28	2.15	1.97	1.73	1.44	1.10	0.79	0.56	0.37
2.47	2.41	2.33	2.24	2.13	1.96	1.81	1.62	1.41	1.17	0.56
2.49	2.47	2.45	2.43	2.43	2.42	2.35	2.16	1.80	1.29	0.51
2.51	2.54	2.58	2.64	2.72	2.80	2.81	2.64	2.24	1.53	0.56
2.53	2.60	2.67	2.75	2.84	2.92	2.98	3.0	2.90	2.58	1.08
2.54	2.62	2.71	2.80	2.88	2.92	2.93	2.93	2.98	3.28	3.58

FIG. 3—*Distribution of horizontal shear strain* ($\frac{1}{2}\gamma_{RZ} \times 10^{-1}$) *in percent* ($\theta = 0$ *deg*).

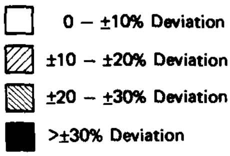

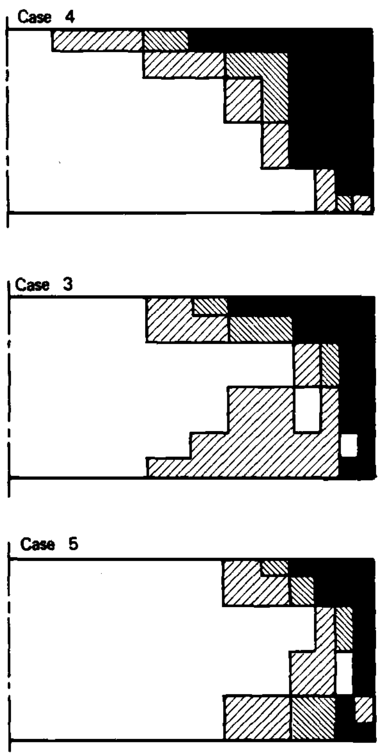

FIG. 4—*Effect of height-to-diameter ratio on shear strain distribution in the* R-Z *plane* (θ = *0 deg*).

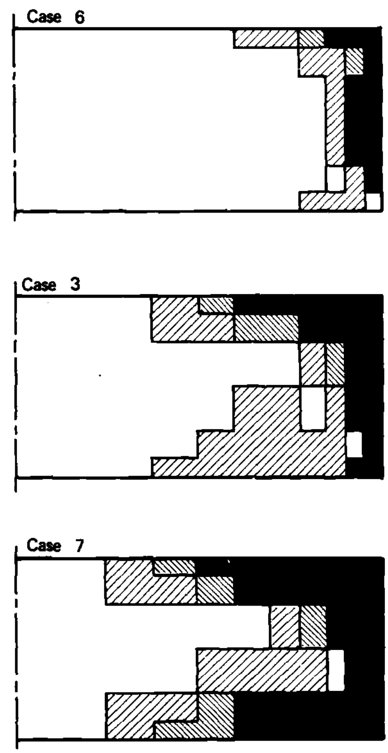

FIG. 5—*Effect of soil modulus on shear strain distribution in the* R-Z *plane* (θ = *0 deg*).

diameter of the specimen was assumed to be 8 cm (3.2 in.). It can be seen that a thinner specimen (H/D = 1/8, Case 5) yields a more uniform shear strain distribution than the thicker specimen (H/D = 1/2, Case 4). This is due to the fact that for the same amount of horizontal displacement given to each specimen, a larger external moment is developed in the thicker specimen, consequently creating a more nonuniform shear state. A similar general observation has been reported by Kovacs [*13*] in studying the effect of specimen configuration in simple shear testing, wherein he concluded that the effect of specimen size on the test results diminishes as the length-to-height ratio increases.

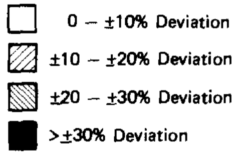

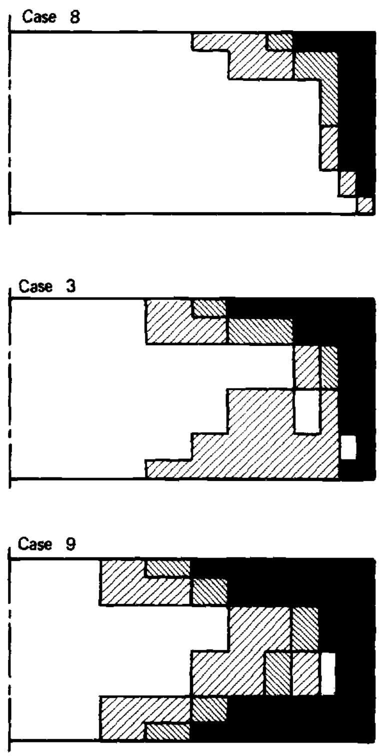

FIG. 6—*Effect of applied horizontal shear displacement on shear strain distribution in the* R-Z *plane* (θ = *0 deg*).

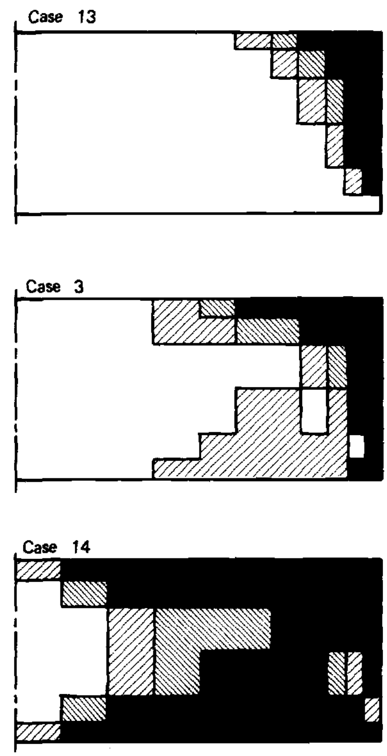

FIG. 7—*Effect of soil Poisson's ratio on shear strain distribution in the* R-Z *plane* (θ = *0 deg*).

Figure 5 illustrates the effect of soil modulus on the shear strain distribution. It is important to mention that in this study the elastic modulus of the rubber membrane was assumed to be a constant of 2070 kN/m^2 (300 psi). So, by varying the soil modulus, it would give a different ratio of the relative stiffness of the soil and the rubber membrane. Soil moduli of 2948, 29 480, and 294 800 kN/m^2 (427, 4272, and 42 724 psi) were assumed for Cases 6, 3, and 7, respectively. It is clearly indicated that the percentage of deviation decreases as the stiffness ratio approaches unity. This implies that boundary effects are minimized when the soil and the rubber membrane have similar elastic properties.

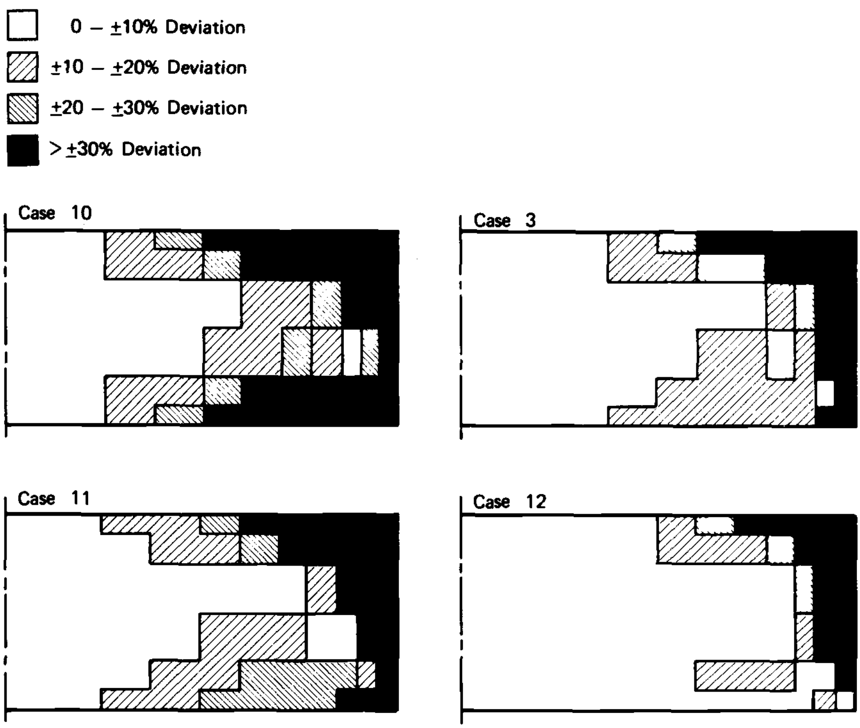

FIG. 8—*Effect of percent of wire reinforcement on shear strain distribution in the* R-Z *plane* (θ = *0 deg*).

The effect of shear strain amplitude on the uniformity of shear distribution is shown in Fig. 6. Here, shear strains of 0.25, 0.5, and 1.0 percent were applied to identical specimens. Because the nonuniform shear distribution in the specimen is the result of a combined effect of the vertical and horizontal displacements, for the same amount of vertical displacement a large horizontal displacement (thus a larger shear strain amplitude) seems to have an overriding effect in minimizing the nonuniform shear distribution due to vertical displacement (Case 8).

The effect of Poisson's ratio was studied as presented in Fig. 7. Values of 0.3, 0.4, and 0.49 were assumed for Cases 13, 3, and 14, respectively. A lower Poisson's ratio (Case 13) is associated with less lateral volume change under vertical loading, thus causing less shear strain in the specimen. Figure 7 shows that, under the same loading conditions, specimens having different Poisson's ratios have significantly different shear strain distributions. The uniformity of shear strain distribution increases as the Poisson's ratio of the specimen decreases.

Finally, the amount of wire reinforcement was studied by assuming the values of the A_s/A ratio to be 0, 5, 10, and 20 percent, in Cases 10, 11, 3, and 12, respectively. As the A_s/A ratio increases, the wire-reinforced membrane becomes stronger in resisting lateral expansion due to vertical loading, and consequently it reduces the amount of shear distortion in the specimen. As shown in Fig. 8, the higher the A_s/A ratio, the more uniform is the shear strain distribution in the specimen.

Based on the discussion given in the preceding paragraphs, it may be stated that in general, for the values of the parameters studied, the uniformity of shear strain distribution improves as (1) the specimen height-to-diameter ratio (H/D) is decreased; (2) the percent of wire reinforcement, A_s/A, is increased; (3) the elastic modulus of the soil, E, decreases; (4) the Poisson's ratio, ν, of the soil decreases; and (5) the applied horizontal displacement amplitude, $H\gamma_{RZ}$, is increased. It should be noted that for a given element the stress and strain components vary with θ; the distributions shown in Figs. 4–8 are for the θ = 0-deg condition. Figure 9 shows the shear strain components (γ_{RZ}) of Case 3 projected on the plane parallel to the direction of shearing for θ values of 0, 45, and 90 deg, respectively. Furthermore, the percentage of deviation, for a given element, is not directly proportionate to the area of the element in the R-Z plane. This is due to the fact that the size of a circular volume formed by the rotation of the area of an element depends upon not only the dimension in the R-Z plane but also on its distance from the axis of rotation.

It is recognized that the selection of parameters for this study has been at best arbitrary, and that the nonlinearity of the soil has not been included. Interpretation of the numerical results from this study, therefore, should be done with caution. However, the information provided by this study clearly illustrates the importance of the various parameters and the edge effects resulting from the selected test configuration. This information can be most helpful in assessing the suitability and limitations of the NGI simple shear apparatus for cyclic soil testing.

Discussion

Based on the present study, the following observations are made concerning the stress and strain distribution in a circular soil mass subjected to cyclic testing in the NGI simple shear apparatus.

1. It has been shown that the shear stress or strain distribution developed in the NGI simple shear apparatus is far from uniform. Furthermore, in many instances the externally "applied strain" may not be representative of the actual strain experienced by the bulk soil mass in the specimen.

2. The present study seems to indicate that the nonuniform stress and strain distribution in a specimen results from the two boundary conditions associated with the NGI simple shear apparatus; namely, the application of a uniform horizontal displacement and a vertical loading (causing a

Case 3

$\theta = 0°$ plane

2.46	2.38	2.28	2.15	1.97	1.73	1.44	1.10	0.79	0.56	0.37
2.47	2.41	2.33	2.24	2.13	1.96	1.81	1.62	1.41	1.17	0.56
2.49	2.47	2.45	2.43	2.43	2.42	2.35	2.16	1.80	1.29	0.51
2.51	2.54	2.58	2.64	2.72	2.80	2.81	2.64	2.24	1.53	0.56
2.53	2.60	2.67	2.75	2.84	2.92	2.98	3.00	2.90	2.58	1.08
2.54	2.62	2.71	2.80	2.88	2.92	2.93	2.93	2.98	3.28	3.58

Case 3

$\theta = 45°$ plane

2.47	2.42	2.35	2.26	2.14	1.98	1.79	1.58	1.37	1.22	1.10
2.48	2.43	2.38	2.32	2.24	2.14	2.03	1.90	1.78	1.66	1.41
2.49	2.47	2.46	2.45	2.44	2.43	2.40	2.28	2.10	1.83	1.41
2.51	2.53	2.56	2.60	2.67	2.70	2.71	2.63	2.41	2.00	1.45
2.52	2.57	2.62	2.68	2.74	2.80	2.86	2.88	2.84	2.66	1.78
2.53	2.59	2.65	2.72	2.78	2.82	2.84	2.87	2.92	3.13	3.37

Case 3

$\theta = 90°$ plane

2.50	2.50	2.50	2.50	2.49	2.47	2.45	2.43	2.42	2.43	2.50
2.50	2.50	2.50	2.50	2.50	2.49	2.49	2.48	2.47	2.45	2.38
2.50	2.50	2.50	2.51	2.52	2.53	2.53	2.52	2.49	2.43	2.33
2.50	2.50	2.50	2.51	2.52	2.53	2.53	2.52	2.49	2.43	2.33
2.50	2.50	2.50	2.50	2.50	2.49	2.49	2.48	2.47	2.45	2.38
2.50	2.50	2.50	2.50	2.49	2.47	2.45	2.43	2.42	2.43	2.50

FIG. 9—*Shear strain distribution* ($\frac{1}{2}\gamma_{RZ} \times 10^{-1}$) *in percent projected in planes parallel to the direction of shearing—Case 3.*

uniform vertical displacement) to the circular specimen. Figure 10 shows the creation of an external moment due to the horizontal displacement. To balance this moment, additional stresses must be generated in the soil specimen, particularly near the vertical boundaries as indicated in Case 2 (Fig. 2). For a given soil and membrane, the magnitude of the moment is a function of the horizontal displacement and the height of the specimen. The larger the displacement, the thicker the specimen, the more significant the influence of the moment on the stress and strain states in the specimen. Furthermore, shear stress and strain can also be introduced to the soil mass by the uniform vertical displacement as discussed previously. Therefore, the combination of the two essential boundary conditions of the simple shear apparatus leads to significant nonuniform stress and strain distributions in the soil specimen.

3. It may be reasoned according to Cases 1 and 2 of Fig. 3 that the shear strain due to the vertical displacement amounts only to a very small fraction of the shear strain induced by the horizontal displacement and that therefore the existence of the former may be ignored for all practical purposes. However, simple shear testing has been used to determine dynamic soil properties at much lower strain amplitudes than the 1/2 percent assumed in this study (1×10^{-1} to 1×10^{-3} percent shear strain), thus inducing shear strains of the same order of magnitude as those developed by the vertical displacement. For such cases there is some question as to whether or not the externally "applied strain" can be used as the basis to determine the dynamic response of a nonlinear soil mass.

4. The assumption of perfect bonding developed between the soil and the top and bottom platens in simple shear testing is worthy of close examination. This is most significant when large horizontal displacement amplitudes are applied. At those levels of strain, the shear stresses developed at the contact surface may exceed the available frictional resistance at the soil-platen interface, particularly when high pore water pressure is built up inside a saturated granular soil specimen.

5. The application of a uniform cyclic horizontal displacement would result in the reversal of the induced shear stresses as well as strains in the soil specimen. However, the shear stresses and strains due to a vertical displacement are unidirectional. The overall shear stress and strain states in a soil specimen are therefore not only nonuniform, as previously dis-

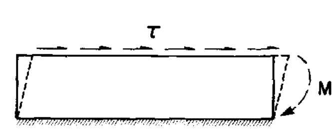

FIG. 10—*Creation of external moment due to applied shear displacement.*

cussed, but also complicated by the nonsymmetrical loading cycles experienced by every soil element as depicted in Fig. 11. The existence of a baseline static shear strain contradicts the general belief that uniform and symmetrical shear states exist in NGI simple shearing testing. It is possible, however, that progressive incremental slippage between the top and bottom platens and the specimen would cause a gradual relief of the static shear strain produced by the initial vertical load; such behavior is suggested in Fig. 12. Further analytical investigation is needed to determine whether or not such a shakedown phenomenon actually occurs.

Conclusion

Laboratory soil testing is vitally important to geotechnical engineering practice, since only good and reliable soil characterization can ensure accurate prediction of soil behavior in the field. In recent years, substantial progress has been made in numerical solutions of complex foundation and earth structure problems; however, our ability to develop simple and reliable testing techniques for proper soil characterization has been slow, particularly in the area of dynamic property determination of soils. During the past few years, a growing interest has been directed toward the use of the NGI simple shear apparatus for dynamic testing. Based on the analysis reported in this paper, observations are offered concerning the nature and the distribution of shear states developed in the NGI simple shear apparatus. The analysis reported in the preceding pages is not intended to directly evaluate the available NGI test results, but rather to study the apparatus and its associated boundary effects on the test results. It is hoped that futher discussion and exploration of the NGI simple shear apparatus may improve our knowledge in searching for a simple, reliable, and yet versatile dynamic soil testing apparatus.

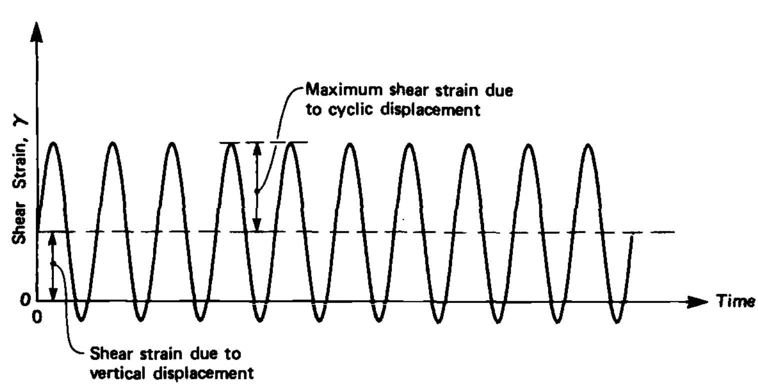

FIG. 11—*State of shear strain within the specimen due to combined effects of initial vertical displacement and cyclic shear displacement.*

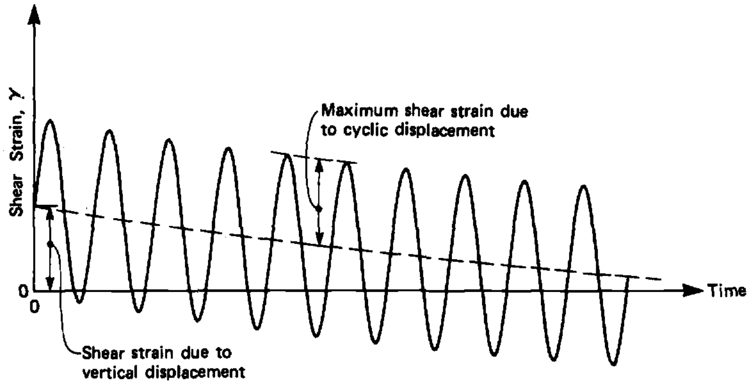

FIG. 12—*Changes in state of shear strain due to possible progressive incremental slippage.*

Acknowledgment

The authors wish to express their appreciation to Richard Fragaszy, who helped in performing the computer solutions, and to the reviewers, whose comments and suggestions have helped in preparing the final manuscript.

References

[1] Kjellman, W., *Geotechnique,* Vol. 2, No. 3, 1951, pp. 225-235.
[2] Bjerrum, L. and Landva, A., *Geotechnique,* Vol. 26, No. 1, 1966, pp. 1-20.
[3] Roscoe, K. H. in *Proceedings,* 3rd International Conference on Soil Mechanics and Foundation Engineering, Vol. 1, Session 2, 1953, pp. 259-278.
[4] Roscoe, K. H., *Geotechnique,* Vol. 20, No. 2, 1970, pp. 129-170.
[5] Duncan, J. M. and Dunlop, P. in *Proceedings,* 7th International Conference on Soil Mechanics and Foundation Engineering, Mexico, Vol. 1, 1969, pp. 101-109.
[6] Prevost, J. H. and Hoeg, K., *Canadian Geotechnical Journal,* Vol. 13, No. 4, 1976, pp. 418-429.
[7] Lucks, S. A., Christian, J. T., Brandow, G. E., and Hoeg, K., Technical Note, *Journal of Soil Mechanics and Foundations Division,* American Society of Civil Engineers, Vol. 98, No. SM1, 1972, pp. 155-160.
[8] Sadigh, K., "Characterization of Soft Saturated Clays for Dynamic Analyses," Ph.D. Dissertation, University of California, Davis, Calif., 1972, p. 354.
[9] Herrmann, L. R., "Three-Dimensional Elasticity Analysis of Non-Axisymmetrically Loaded Solids of Revolution," Department of Civil Engineering Report No. 68-12-1, University of California, Davis, Calif. 1968.
[10] Herrmann, L. R., "Analysis of Solids of Revolution Subjected to Non-Axisymmetric Loads," Department of Civil Engineering Report No. 74-10-1, University of California, Davis, Calif., 1974.
[11] Wilson, E. L., *American Institute of Aeronautics and Astronautics Journal,* Vol. 3, No. 12, 1965, pp. 2269-2274.
[12] Ashton, J. E., Halpin, J. C., and Petit, P. H., *Primer on Composite Materials: Analysis,* Technomic Publishing Co., Stanford, Conn., 1969.
[13] Kovacs, W. D. in *Proceedings,* Symposium on the Behavior of Earth and Earth Structures Subjected to Earthquakes and Other Dynamic Loads, Roorkee, India, Vol. 1, 1973, pp. 82-86.

K. L. Saucier[1] *and L. Carpenter*[2]

Dynamic Properties of Mass Concrete

REFERENCE: Saucier, K. L. and Carpenter, L., "**Dynamic Properties of Mass Concrete,**" *Dynamic Geotechnical Testing, ASTM STP 654,* American Society for Testing and Materials, 1978, pp. 163–178.

ABSTRACT: The objective of this study was to determine the tensile strength, cyclical behavior, and stress-strain relationships for concrete under loading conditions (1 to 10 Hz) such as could be produced by an earthquake.

Dynamic direct tension tests and stress-reversal tests were conducted on core specimens from two concrete mixtures representative of mass concrete. Test procedures were developed for cyclical loading and loading to failure in 0.25 to 0.025 s, which represent one fourth of a cycle having a frequency of 1 to 10 Hz. Stress-strain measurements were made on selected specimens. The procedures used could be modified to become ASTM test methods for direct-tension and stress-reversal tests of rock.

The tests indicated that there was no significant difference in tensile strength determined statically or dynamically on dry specimens. A 30 percent increase in strength was indicated for wet specimens tested dynamically. Very little hysteresis was evident in the tensile stress-strain curves. The results should be useful in studies conducted to determine the earthquake resistance of mass-concrete structures.

KEY WORDS: concrete testing, tensile strength, dynamic tensile strength, mass concrete, soils

Prediction of the dynamic response of a structure under loading such as could be caused by an earthquake requires a working knowledge of the mechanical properties of the material used in construction of the structure. Specifically, tensile strength, cyclic behavior, and stress-strain relationships appear to be of primary importance. Gravity dams are often constructed of mass concrete. A considerable amount of attention has been given to the compressive-stress parameter of concrete with the resulting recommendation *[1]*[3] that the dynamic compressive strength used in an analysis be assumed as 125 percent of the static compressive strength, that is, f'_c, for dynamic loading conditions. Information on tensile strength, stress-

[1] Research civil engineer, Waterways Experiment Station, Vicksburg, Miss. 39180.
[2] Research structural engineer, U.S. Bureau of Reclamation, Denver, Colo. 80225.
[3] The italic numbers in brackets refer to the list of references appended to this paper.

strain relationships, and effects of cyclic loading in the range of seismic loading (1 to 10 Hz) appears to be meager [2,3].

The objective of this study was to determine the tensile strength, cyclical behavior, and stress-strain relationships for concrete under seismic loading conditions (1 to 10 Hz).

Procedure

Mixtures

Two typical mass concrete mixtures selected for study are given in Table 1. Batches of concrete 0.76 m^3 (15 ft^3) were mixed from each mixture and used to cast blocks 400 mm (16 in.) high. The blocks were cured for 28 days and then cored to secure nominal 200 by 400-mm (8 by 16 in.) cores. The cores were stored in air until the date of the test.

Test Methods

The dearth of test data on the direct tensile strength of concrete indicated that equipment to conduct such tests would likely not be readily available. When this premise proved correct, plans were made to modify the equipment available at the Waterways Experiment Station (WES) to conduct dynamic monotonic (single stroke) and cyclical tensile-strength tests on mass-concrete test specimens. Contact with the U.S. Bureau of Reclamation (USBR) revealed that a rapid-loading test machine at their Denver laboratory could possibly be used to conduct stress-reversal tests through the tensile-compressive range in question on large specimens. To assure that some reliable information was developed, the test schedule was formulated to use both machines. Also, if useful data were obtained using both machines, comparisons could be made between direct tension tests and stress-reversal tests.

The absence of a standard test led to the development and use of a

TABLE 1—*Mass concrete mixtures.*

	Mixture 1	Mixture 2
Nominal maximum size aggregate, mm (in.)	75 (3)	75 (3)
Type of fine and coarse aggregate	limestone	limestone
Cement factor; kg/m^3 (lb/yd^3)	(254) (151)	(400) (237)
W/C ratio; by weight	0.80	0.51
S/A ratio; by volume	0.31	0.29
Air content, %	5	5
Slump, mm (in.)	50 (2)	50 (2)
Compressive strength, MPa (psi)	21 (3000)	41 (6000)
Test age	90 days	1 year

method of test for direct tensile strength of concrete patterned after the ASTM Standard Method of Test for Direct Tensile Strength of Intact Rock Core Specimens (D 2936-71). Two diametrically opposed electrical-resistance strain gages were used on selected specimens to provide longitudinal stress-strain information. The test arrangement is shown in Figure 1. The procedure for the stress-reversal tests is similar to that for direct tensile strength. Specimens used were companion cores to those tested for direct tensile strength. Specimens were cut to proper length, gaged, and shipped to the USBR only after the concrete had reached 90 days of age. The test configuration for the stress-reversal test is shown in Fig. 2. Preparation consisted of placing the specimen in the test frame with end pieces attached by epoxy. The epoxy was allowed to harden overnight. Prior to test the specimen was cycled statically to 5-MPa (700 psi) compression for the purpose of securing proper seating of all components.

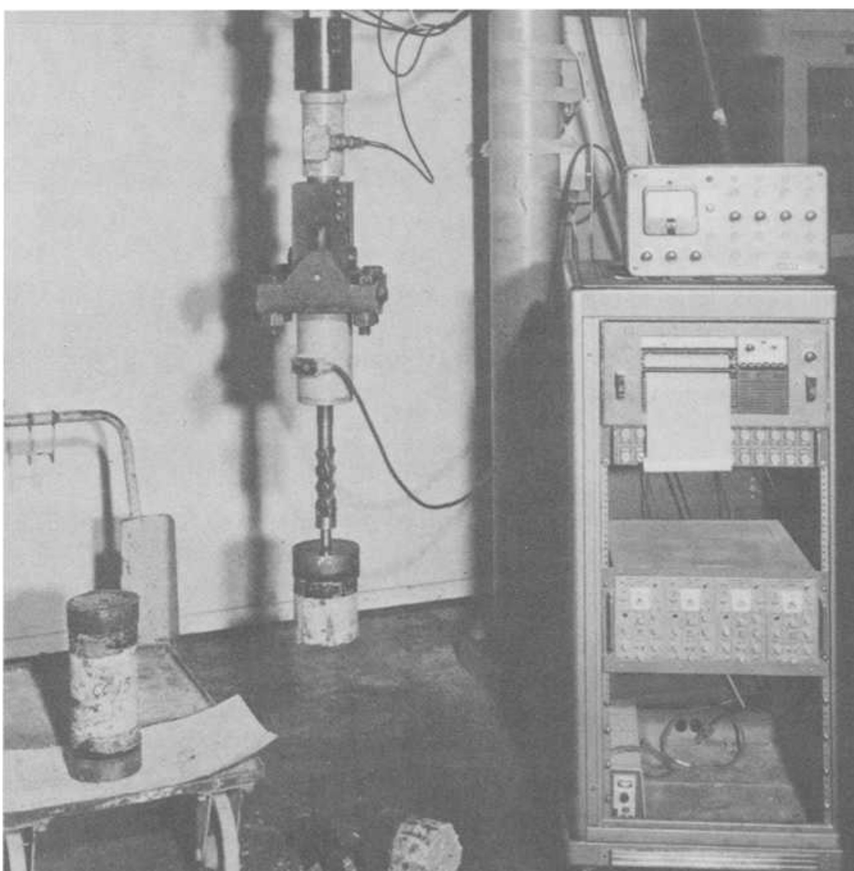

FIG. 1—*Direct-tension test apparatus.*

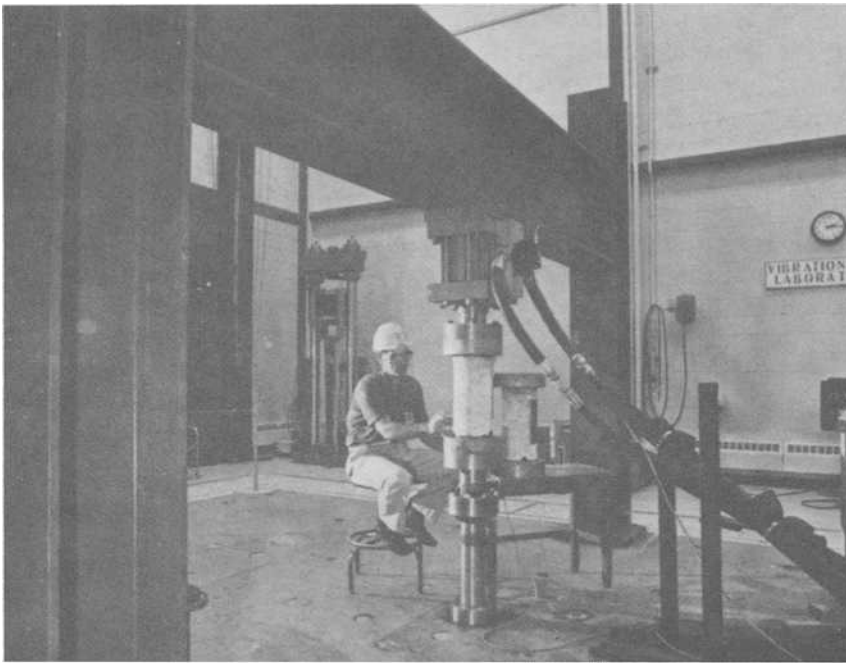

FIG. 2—*Test configuration, stress-reversal tests.*

Rapid load tests were then conducted either through a cyclic phase or monotonically, both starting with a preload of 1.4-MPa (200 psi) compression. Figure 3 gives typical strain-time curves for a specimen undergoing cyclical loading.

Test Program

The large energy input to concrete gravity dams is to be most likely in the range of 1 to 10 Hz. The test program was thus established to include tests to failure within a time frame based on this frequency. Since there are four distinct parts of an earthquake loading pulse, namely, (1) tension loading and (2) unloading, and (3) compression loading and (4) unloading, the time to tensile failure should be one fourth of the cycle time. Thus, the time to failure (rise time) for 1-, 5-, and 10-Hz tests would be 0.25, 0.05, and 0.025 s, respectively. There is, of course, no way of knowing the strength beforehand; the rise times achieved in the actual tests varied somewhat from those desired, generally ± 20 percent.

In order to investigate the effects of monotonic stress reversal and cyclical loading and difference in moisture content on mass concrete, several types of loading conditions were used:

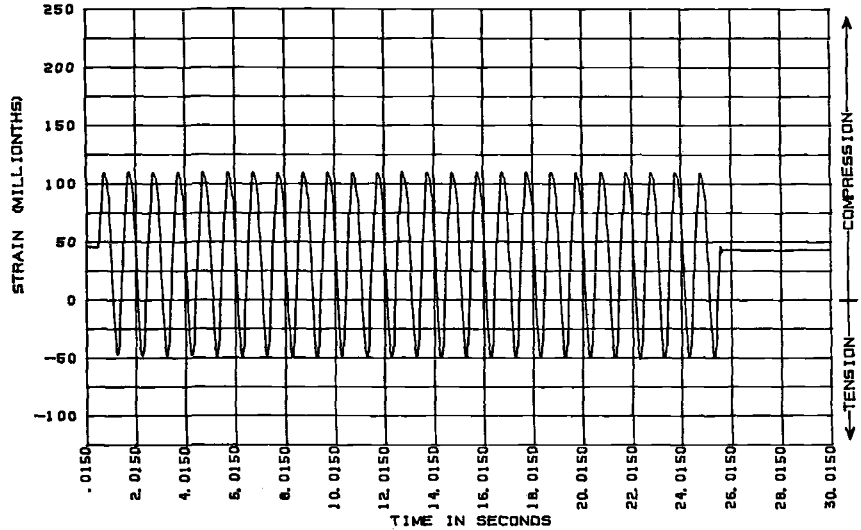

FIG. 3—*Typical strain-time record.*

1. *Direct-tension tests* cycled to either 60 or 80 percent of ultimate strength for approximately 25 cycles, then loaded to failure at the rate used during cycling.
2. *Stress-reversal tests* cycled to 80 percent of ultimate tensile strength for approximately 25 cycles, then loaded to tensile failure at the rate used during cycling.
3. *Monotonic (single stroke) direct-tension tests* in which the failure load is applied so that the specimen fails during the first and only pulse of a dynamic loader at a peak load occurring at one fourth of the cycle time.
4. *Monotonic stress-reversal tests* in which the failure load is applied so that the specimen fails in tension during the first and only tensile pulse following the compressive portion of the cycle. The tensile failure stress is caused to occur at one fourth of the complete cycle time.
5. *Monotonic direct-tension static tests* in which failure is produced in approximately 60 s of loading time.

Experimental Work (Results)

Cyclical Tests

Cyclical tests were conducted on 34 specimens from Mixture No. 1 to determine the effect of repetitive loading on the ultimate strength of mass concrete. Specimens were loaded through approximately 25 cycles for a predetermined percentage of the estimated ultimate tensile strength at three

TABLE 2—*Results of cyclical tensile on tests, Mixture No. 1.*

Type Test	Specimen No.	Rate of Load, Hz	No. of Cycles	Cycled to Tension psi	(MPa)	Broke During Cycling	Remarks
Direct tension 60% level	4	1	22	160	(1.1)	no	
	10	1	24	140	(1.0)	no	
	11	1	24	40	(1.0)	no	
	12	1	25	140	(1.0)	no	
	13	1	26	160	(1.1)	no	
Direct tension 80% level	2	1	20	200	(1.4)	no	
	14	1	24	185	(1.3)	no	
	15	1	26	200	(1.4)	no	
	18	1	5	200	(1.4)	yes	failed 5th cycle
	20	1	14	215	(1.5)	yes	failed 14th cycle
Stress reversal	CE-1	1	25	200	(1.4)	no	
	CE-2	1	1	210	(1.4)	yes	failed 1st cycle
	CE-3	1	25	160	(1.1)	no	
	CE-4	1	25	170	(1.2)	no	
	CE-6	1	25	170	(1.2)	no	
	3-11	1	50	180	(1.2)	no	
	3-12	1	25	190	(1.3)	no	
	3-13	1	25	200	(1.4)	no	
Stress reversal	CE-13	5	25	200	(1.4)	no	
	CE-14	5	12	160	(1.1)	no	
	CE-15	5	25	180	(1.2)	no	
	CE-16	5	25	180	(1.2)	no	
	CE-17	5	25	180	(1.2)	no	
	3-8	5	27	110	(0.8)	no	
	3-9	5	28	180	(1.2)	no	
	3-10	5	5	230	(1.6)	yes	failed 5th cycle
Stress reversal	CE-7	10	25	150	(1.0)	no	
	CE-8	10	9	175	(1.2)	yes	failed 9th cycle
	CE-9	10	25	180	(1.2)	no	
	CE-10	10	25	180	(1.2)	no	
	CE-11	10	25	170	(1.2)	no	
	3-5	10	2	160	(1.1)	yes	failed 2nd cycle
	3-7	10	20	170	(1.2)	yes	failed 20th cycle
	3-14	10	25	180	(1.2)	no	

TABLE 3—*Cycling failure specimens.*

Type of Test	Specimen No.	Rate of Load, Hz	Failed on Cycle No.	Tensile Strength, psi	(MPa)
Direct tension	18	1	5	200	(1.4)
Direct tension	20	1	14	215	(1.5)
Stress reversal	CE-2	1	1	210	(1.4)
Stress reversal	3-10	5	5	230	(1.6)
Stress reversal	CE-8	10	9	175	(1.2)
Stress reversal	3-5	10	2	160	(1.1)
Stress reversal	3-7	10	20	170	(1.2)

different rates of loading. The specimens which did not fail during cycling were then loaded to failure monotonically. Results are given in Table 2. Seven of the 34 specimens that failed during cycling are listed in Table 3.

The ultimate monotonic tensile strength of virgin specimens from Mixture No. 1 was found to be approximately 1.62 MPa (235 psi) (Table 4). Indications are, therefore, that some failures may be expected under cyclical loading at approximately 70 to 90 percent of the ultimate tensile strength.

Monotonic Tests

Monotonic (single stroke) tests were conducted on representative virgin specimens from each mixture and on specimens which did not fail during cycling. Both direct-tension and stress-reversal tests were conducted at different loading rates and results compared where feasible. Results of tests on the virgin specimens are given in Table 4. Although the data are somewhat limited, indications are that the rate of loading has no effect on the tensile strength for either mixture up to 10 Hz. Using the data from Table 5, it may be noted that the tensile strength of Mixture No. 1 is approximately 8 percent of the compressive; however, for Mixture No. 2, the tensile strength is only 5 percent of the compressive strength.

Those specimens which did not fail during cyclical loading (Table 2) were subsequently tested to failure monotonically. Twenty-seven specimens from Mixture No. 1 were so tested. Results are given in Table 4. Again, no significant difference is indicated between rapid tensile strength and static tensile strength up to 10-Hz loading rate. The slight increase in average strength of the previously cycled specimens may be explained by the elimination of the weaker specimens during cyclical testing. Also of relevance is a comparison of the test methods. At the 1-Hz rate there is apparently no significant difference in the ultimate tensile strength obtained by the two methods, rapid direct and stress-reversal.

Statistical treatment of the data developed for the two types of tests and various rates of loading would be desirable. The pertinent information for

TABLE 4—*Results of monotonic tests.*

Type Test	Mixture No.	No. of Specimens	Rate of Load, Hz	Tensile Strength psi	Tensile Strength (MPa)	Standard Deviation psi	Standard Deviation (MPa)
Virgin Specimens							
Static direct tensile	1	5	0.02	235	(1.6)	13.5	(0.09)
Rapid direct tensile	1	5	1	230	(1.6)	23.6	(0.16)
Static direct tensile	2	5	0.02	305	(2.0)	29.5	(0.20)
Rapid direct tensile	2	5	5	315	(2.2)	19.5	(0.13)
Stress reversal	2	5	10	310	(2.1)	32.5	(0.22)
Previously cycled specimens							
Rapid direct tensile	1	8	1	255	(1.8)	17.5	(0.13)
Stress reversal	1	7	1	270	(1.9)	39.8	(0.27)
Stress reversal	1	7	5	250	(1.7)	37.9	(0.26)
Stress reversal	1	5	10	265	(1.8)	25.4	(0.18)

TABLE 5—*Moisture effects tests—monotonic loading—5 Hz.*

Static Compressive Strength			Static Direct Tensile Strength			Rapid-Load Direct Tensile Strength		
Specimen No.	psi	(MPa)	Specimen No.	psi	(MPa)	Specimen No.	psi	(MPa)
			Dry Cores					
M1	3630	(25.02)	M7	225	(1.55)	M17	250	(1.72)
M2	3410	(23.51)	M8	265	(1.83)	M18	260	(1.79)
M3	3200	(22.06)	M9	220	(1.52)	M19	230	(1.59)
			M10	235	(1.62)	M20	265	(1.83,
			M11	240	(1.65)	M21	245	(1.69)
Avg	3410	(23.51)		235	(1.62)		250	(1.72)
			Inundated Cores					
M4	2760	(19.03)	M12	185	(1.28)	M22	270	(1.86)
M5	2790	(19.24)	M13	195	(1.34)	M23	280	(1.93)
M6	2890	(19.93)	M14	180	(1.24)	M24	260	(1.79)
			M15	220	(1.52)	M25	255	(1.76)
			M16	190	(1.31)	M26	240	(1.65)
Avg	2810	(19.37)		195	(1.34)		260	(1.79)

TABLE 6—*Failure test data for Mixture No. 1.*

Type of Test	Rate of Load, Hz	No. of Specimens	Average Strength, psi	(MPa)	Standard Deviation, psi	(MPa)
Direct tensile[a]	0.02	10	238	(1.64)	15	(0.10)
Direct tensile[a]	1 to 5	10	241	(1.66)	20	(0.14)
Direct tensile	1	8	254	(1.75)	17	(0.12)
Stress reversal	1	7	269	(1.85)	40	(0.28)
Stress reversal	5	7	249	(1.72)	38	(0.26)
Stress reversal	10	5	267	(1.84)	25	(0.17)

[a] Virgin specimens, all others cycled specimens.

the failure tests of Mixture No. 1 is given in Table 6. Due to the limited data, the closeness of the averages, and the relatively large standard deviations, detailed statistical analyses would serve no useful purpose. A cursory examination of the average strengths and standard deviations is sufficient to reveal that there is no significant difference in the various test methods or loading rates. There is less variation in results of the direct-tension tests than in the stress-reversal tests which, in the absence of other considerations, would provide a basis for selection of the direct-tension test as the standard method of test for evaluation of concrete under earthquake-type loading conditions.

The predominant effect in all the tension tests was probably the alignment of the large aggregate with respect to the stress field. The interface of the aggregate and the paste was obviously the weakest portion of the concrete conglomerate. Large pieces of aggregate were exposed in most specimens after failure, as shown in Fig. 4. The random alignment of these interfaces apparently determines the stress level at which a specimen will fail. Thus, one with a large critically positioned, smooth surface would fail at a much lower stress than one on which the bond interface was rough or was not required to resist a high tensile stress.

Moisture Effects Tests

A suite of tests was conducted on specimens from Mixture No. 1 to determine the effects of moisture on the rapid loading strength of mass concrete. Half of the test specimens were inundated for 28 days prior to test while the other half remained in air storage. Direct-tension tests were conducted when the concrete was approximately one year old. Considerable difficulty was experienced in affixing the end caps to the wet cores; 18 tests were required to secure the 10 usable pieces of data for the wet specimens.

Results of the moisture effects tests are given in Table 5. Again, no difference is indicated in static and rapid loading-direct tensile strength of dry specimens. However, an appreciable increase, apparently 30 percent,

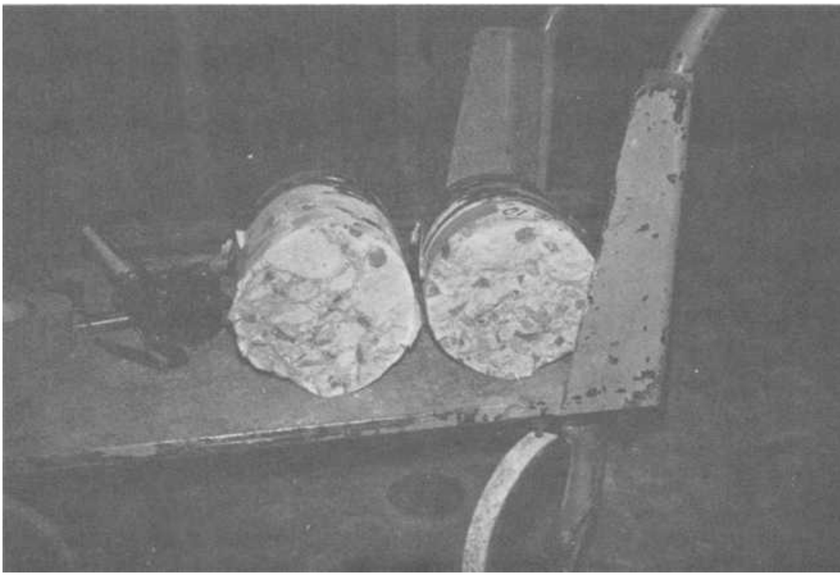

FIG. 4—*Typical failure surface of a tension test specimen.*

in strength is indicated between the static and rapid loading strength of wet specimens. Thus the effect of rate of straining appears to be significant when moisture is present. Not unexpected is the decrease in static strength, both compressive and tensile, when test specimens are saturated. It should also be noted that no difference is indicated in the rapid-loading direct tensile strength of concrete whether tested wet or dry.

Tests of Jointed Specimens

It is recognized that a massive unreinforced concrete structure will likely contain both joints and cracks due variously to construction requirements, temperature and volume changes in the mass, and foundation movement. These joints or cracks or both will have strength values varying between 0 and 100 percent of the mass. Obviously tests are not required to determine that direct tensile strength of an open discontinuity is nonexistent. Joints, however, can be tested for strength as intact specimens if jointed cores are secured without breakage. During the course of the investigation, core specimens of both massive and jointed concrete taken from a gravity dam were received for test. The massive intact concrete compared favorably with that of Mixture No. 2 [compressive strength, 41 MPa (6000 psi); rapid direct tensile strength, 2 MPa (300 psi)]. Significantly, the strength of the construction joints was indicated to be approximately one third [0.7 MPa (100 psi)] that of the concrete mass.

Stress-Strain Relationships

The stress-strain relationships were determined on selected specimens from 152-mm (6 in.)-long electrical resistance strain gages affixed to the specimens. A typical strain-time, stress-time record for a stress reversal test is shown in Fig. 3. Stress-strain curves were plotted from these results. A typical stress-strain curve for a specimen undergoing cyclical loading is given in Fig. 5. Given in Fig. 6 is a stress-strain curve for a test to failure. Significantly, stress-strain relationships were essentially identical in tension and compression for the stress-reversal tests. Very little hysteresis was noted in any of the tests. Apparently the compressive stress was not large enough

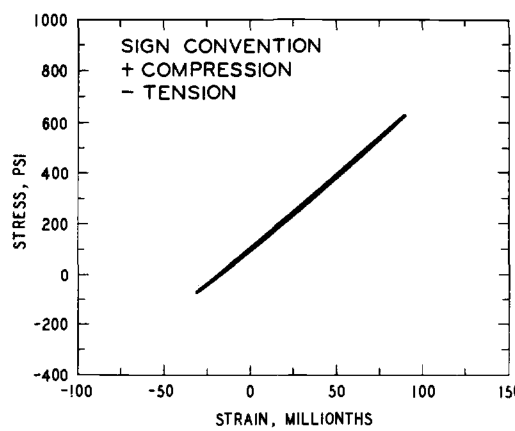

FIG. 5—*Dynamic stress-reversal studies, cyclical test.*

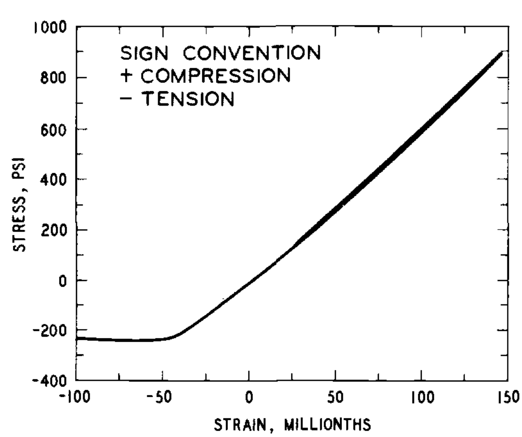

FIG. 6—*Dynamic stress-reversal studies, failure test.*

to induce microfracturing with the resulting hysteresis. Tensile failure of a brittle material is usually the result of one crack rather than a series of small fractures which result in nonrecoverable deformation. Indications were that tensile cracking of dry specimens began at approximately 90 percent of ultimate strength and progressed very sharply during final failure loading.

Discussion

According to a recent review of the applicable literature [*3*], significant gaps in knowledge remain relative to the earthquake resistance of mass concrete. The areas most in need of study were cited to be:

1. The effect of strain rate on dynamic properties, particularly tensile strength.
2. The effect of stress reversal on mechanical properties, including hysteretic behavior.
3. The effect of biaxial stress conditions.

The significant parameter is, of course, the tensile fracture mechanism of concrete. There are two predominant failure theories for concrete [*4,5*], each of which has almost equal support: the Griffith theory and the strain-energy release theory. However, very few pure tension tests of concrete have been reported, and therefore the theories are of limited values for practical application. Hopefully, the information reported herein will help to narrow the gap between theory and practice.

The fact that approximately 20 percent of the tensile specimens failed during cycling at 70 to 90 percent of the indicated tensile strength is probably more the result of strength variation between specimens than fatigue effect. The fatigue effect at 25 cycles would likely not be great. Conversely, the failure of many specimens around large, critically oriented pieces of aggregate and the resulting high variability of the test results would account for some failures at lower than expected loads. Due to the heterogeneous composition of concrete, especially mass concrete, the large variation in test results might well be representative of the nature of the material.

The most significant information developed in the study is related to the effect of rate of load on mass concrete specimens. Essentially, no significant difference in tensile strength was noted for concrete of two strength levels stressed to failure at times ranging between 60 s (static) and 0.025 s (10 Hz). In terms of dynamic testing, a time to failure of 0.025 s is relatively slow. It is known that, the more brittle a material, the less the effect of rate of load. Apparently mass concrete in a dry condition is sufficiently brittle to escape the effect of load rate on strength in the range relevant to earthquake loading.

Also of significance is the effect of rate of load on strength of wet concrete specimens. Although the data are somewhat limited, there appears to be an increase of approximately 30 percent in tensile strength of wet concrete between static testing and rapid loading to failure at a rate of 5 Hz. This indication agrees substantially with the results of the only two studies discovered which dealt with dynamic tensile strength of concrete, by Hatano [6] and Takeda [7]. Hatano's tests were conducted on wet specimens, but the moisture condition of Takeda's specimens was not defined. Apparently wet concrete, being less brittle than dry, is susceptible to strain-rate effects in the range of earthquake loading.

The indication that the ratio of tensile to compressive strength decreases as the concrete strength increases is not surprising. Previous work [8,9] on the static test range supports this finding. The information secured from tests of jointed cores is significant. The joints tested appeared to be excellent construction joints, yet developed only one-third the tensile strength of comparable mass concrete. Reversal of stresses within test specimens apparently had no effect on the tensile strength or stress-strain relationships of dry concrete. Compared with the stress reversal test, the direct-tension test is easier to conduct and would appear to be acceptable for use as a method of determining the relevant properties of earthquake-susceptible concrete.

Several important aspects of the stress-strain relationships were developed: (1) the linearity of the stress-strain ratio up to approximately 80 percent of the ultimate strength; (2) the similarity of the stress-strain curves in tension and compression; (3) the noneffect of stress reversal; and (4) the lack of applicable hysteresis. Yerlici [10] has reported substantiating data for Point 1 above and Hughes and Chapman [11] for Point 2. The lack of effect of stress reversal (Point 3) may be new but not surprising information. The aforementioned points are related and should be useful in analyzing the stress-strain relationships for concrete under earthquake-type loading conditions.

Probably the most significant point is the almost perfect elasticity and consequent absence of hysteresis in the stress-strain curves. The interest in the hysteresis loop arises from the fact that its area represents an irreversible energy of deformation. The loop may be used to calculate a value of hysteretic damping. Obviously the deformability of a material such as the concrete tested herein will be nominal.

The effect of biaxial stress conditions on the strength or durability of mass concrete was not addressed in this study. Reportedly the parameter of biaxial tension is of importance in earthquake analysis [3]. Of interest is some recent work on the area of biaxial tension as given in Ref *12*. Indications are that concrete strength in biaxial tension is essentially equal to, but no greater than, the uniaxial tensile strength. It follows then that the rapid-loading biaxial strength of dry concrete should approximate the direct tensile strength as determined in this investigation. Biaxial tension tests may be required to determine the effect of multiaxial stresses on the strength of wet concrete.

Conclusions

Based on the results of this investigation, the following conclusions appear warranted:

1. Some failures may be expected under cyclical tensile loading of mass concrete specimens at 70 to 90 percent of the indicated ultimate tensile strength.
2. Rate of loading has no effect on the tensile strength of dry, virgin, mass-concrete specimens up to a loading rate of 10 Hz.
3. For conventional concrete the tensile strength is approximately 7.5 percent of the compressive strength; for high-strength concrete the tensile strength is 5 percent of the compressive strength.
4. No difference is indicated between static tensile strength and rapid tensile strength up to 10-Hz loading rate for previously cycled specimens.
5. There is apparently no significant difference in the results obtained, and therefore the two test methods used herein, rapid direct and stress reversal, are equally useful.
6. The effect of alignment within the test specimens of large aggregate pieces is critical and probably contributes to the high variability of the test results.
7. An increase in tensile strength of approximately 30 percent is indicated between static and rapid loading tests of wet concrete specimens.
8. The strength of representative construction joints in direct tension may be only about one-third that of the concrete mass.
9. Stress-strain relationships for dry mass concrete are essentially identical in tension and compression, and the tensile curve is linear up to approximately 80 percent of ultimate strength.
10. Very little hysteresis is evident in stress reversal tests of mass up to 30 percent of the compressive stress and 80 percent of the tensile stress.

References

[1] *Design of Structures to Resist Nuclear Weapons Effects*, American Society of Civil Engineers, Manual No. 42, 1961.

[2] Hughes, B. P. and Gregory, R., *Magazine of Concrete Research*, Vol. 24, No. 78, March 1972, pp. 25–36.

[3] Pal, N., "Nonlinear Earthquake Response of Concrete Gravity Dams," Report No. EERC 74-14, University of California, Berkeley, Calif., Dec. 1974.

[4] Popovics, Sandor, *Journal of the Engineering and Mechanics Division*, American Society of Civil Engineers, June 1969, pp. 531–544.

[5] Glucklich, Joseph, *Journal of the Engineering and Mechanics Division*, American Society of Civil Engineers, Dec. 1963, pp. 127–138.

[6] Hatano, Tadashi, "Dynamical Behavior of Concrete Under Impulsive Tensile Load," Technical Report C-6002, Central Research Institute of Electric Power Industry, Tokyo, 1960.
[7] Takeda, J. and Tachikawa, H. in *Proceedings*, International Conference on Mechanical Behavior of Materials, Japan, 1971, Vol. 4, pp. 267-277.
[8] Kadleck, V. and Spetta, Z., *Journal of Materials*, Vol. 2, No. 4, Dec. 1967, pp. 749-767.
[9] Grieb, W. E. and Werner, G. in *Proceedings*, American Society for Testing and Materials, Vol. 62, 1962, pp. 972-995.
[10] Yerlici, V. A., *Journal of the American Concrete Institute*, Aug. 1965, pp. 987-991.
[11] Hughes, B. P. and Chapman, G. P., "The Complete Stress-Strain Curve for Concrete in Direct Tension," RILEM Bulletin No. 30, International Union of Testing and Research Laboratories to Materials and Structures, March 1966, pp. 95-97.
[12] Kupfer, H., Hilsdorf, H. K., and Rusch, H., *Journal of the American Concrete Institute*, Vol. 66, No. 8, Aug. 1969, pp. 656-666.

R. W. Stephenson[1]

Ultrasonic Testing for Determining Dynamic Soil Moduli

REFERENCE: Stephenson, R. W., "**Ultrasonic Testing for Determining Dynamic Soil Moduli,**" *Dynamic Geotechnical Testing, ASTM STP 654,* American Society for Testing and Materials, 1978, pp. 179–195.

ABSTRACT: Determination of dynamic *E*- and *G*-moduli of a silty clay material were made by measuring directly the velocity of both ultrasonic longitudinal and shear waves transmitted through the material. The equipment, developed at the University of Missouri-Rolla, allows dynamic, nondestructive testing of soil materials to be conducted rapidly and easily.

KEY WORDS: dynamic testing, ultrasonic testing, soil dynamics, soils

A consideration of the dynamic behavior of a soil-rock system is becoming a very important part of geotechnical design practice. Not only are soil dynamics important in aseismic design, but also in the design of foundations subjected to machine vibrations and in subgrade and base courses of pavement. It is obvious that the design techniques used for static analyses are not always applicable to field conditions, because these techniques are based upon static, destructive test methods. These methods do not accurately model the actual dynamic loading conditions occurring in the field.

Testing methods have been sought which evaluate the strength parameters of soil and rock materials as they undergo the actual strain levels that will occur in the field. The parameters of Young's modulus (*E*), shear modulus (*G*), and Poisson's ratio (μ) are required in certain mathematical models used to evaluate soil-structure response.

Elastic theory has been used in the afore-mentioned models. Since soil material response conforms reasonably well with elastic theory for low strain levels associated with machine vibrations, the use of elastic moduli may be justified.

[1] Associate professor of civil engineering, University of Missouri-Rolla, Rolla, Missouri 65401.

[2] The italic numbers in brackets refer to the list of references appended to this paper.

The high interest in soil response to earthquake loadings has added to the need for an even more rational design theory. One of the theories being considered involves viscoelastic modeling of the system. The theory behind this model utilizes the strength parameters previously mentioned plus a measure of the damping capacity of the material. Thus a single testing method which would evaluate these material characteristics dynamically would be very useful in dynamic response analysis.

As a result of this reasoning, numerous testing methods have been developed that attempt to measure the needed design parameters. The test methods most desirable are those where the actual field conditions are most closely approximated. The ideal test should also be nondestructive, thus allowing the testing of a single specimen under a variety of loading conditions.

In this study, a test technique involving the generation and detection of ultrasonic waves in soil specimens has been used to measure the parameters in question. These values were determined by measuring nondestructively the propagation velocity of the ultrasonic waves through the test material. The equipment required in this study has been developed at the University of Missouri-Rolla. It has been the main purpose of this study to further the knowledge of this testing technique in the area of soil materials. In particular, an ultrasonic probe more suitable for attenuation measurements has been developed.

Theory of Ultrasound

The theory of ultrasound is very similar to that of audible sound. Sound is the result of mechanical disturbance of a material, that is, a vibration. In general, three types of waves are generated by a source vibration: compression waves, shear waves, and Rayleigh waves.

Using elastic theory, a relationship between the speed of propogation and wave amplitude of these waves and certain properties of the media through which they are traveling can be determined as follows

$$E = V_c^2 \rho \frac{(1 + \mu)(1 - 2\mu)}{(1 - \mu)} \tag{1}$$

$$G = V_s^2 \rho \tag{2}$$

$$\mu = \frac{1 - \frac{1}{2}(V_c/V_s)^2}{1 - (V_c/V_s)^2} \tag{3}$$

and

$$\delta = \frac{2.302}{n} \log_{10} \frac{A_0}{A_n} \tag{4}$$

where

V_c = velocity of compression wave,
V_s = velocity of shear wave,
μ = Poisson's ratio,
E = Young's modulus,
G = shear modulus,
ρ = mass density = γ/g,
δ = logarithmic decrement (attenuation per cycle),
A_0 = initial value of amplitude, and
A_n = amplitude after n oscillation.

In this study, the method of direct transmission of ultrasonic waves was used to evaluate V_c, V_s and A. The "elastic" constants were calculated from these measurements.

Instrumentation and Materials

Electronic Equipment

The electronic equipment used in this study was previously used and partially developed at the University of Missouri-Rolla [*1*].[2] The equipment necessary for conducting the tests includes a pulse generator, an oscilloscope, and two ultrasonic probes (transmitter and receiver). The construction and design of these probes are discussed later.

The pulse generator delivers a variable-voltage direct-current pulse to the transmitting probe simultaneously with a 7-V trigger pulse to the time base of the oscilloscope. The generator is also designed such that the pulse interval and pulse width can be varied. Voltages may be varied from 100 to 1100 V, pulse intervals from 1 to 99 ms and pulse widths from 1 to 100 μs.

Crystal Selection

The design of an ultrasonic probe suitable for dynamic evaluation of heterogeneous mixtures is hindered by various complications. The development of a probe that effectively overcomes these complications thus became a major part of this investigation. Various crystal characteristics have therefore been investigated and are discussed.

Crystal Polarity—Compressional crystals (primarily thickness expanders) were chosen to be used in the first probes constructed due to their superior acoustic characteristics. This choice evolved from the fact that shear waves tend to be scattered by inhomogenities (for example, aggregate particles) to a greater degree than compressional waves. Acoustic coupling is also much easier to obtain, on rough surfaces, with compressional wave crystals than with shear wave crystals. It should be stressed that these considerations are the result of the character of the material being tested (nonhomogeneous and rough surface texture). In other applications (for example, with metals), the shear wave crystals may prove satisfactory.

Crystal Materials—Different materials, from quartz to certain ceramics, possess piezoelectric properties. A desirable crystal characteristic is a short ringing time. Ringing time is the time period involved in the decay of crystal vibrations after the initial excitation of the crystal. Unfortunately, crystals with short ringing times have lower sensitivity than those with longer ringing times. The result is the sacrifice of some sensitivity for the advantage of a crystal which resonates only a few cycles.

Another desirable crystal characteristic is a low Poisson's ratio. Crystals with lower Poisson's ratios will vibrate less in unwanted modes.

The piezoelectric ceramics initially used in this study were compressional disks made of lead zirconate titanate (PZT). These crystals were chosen primarily due to their availability. It should be noted that crystals with different properties are now commercially available and may demonstrate the superior qualities of a shorter ringing time and lower Poisson's ratio.

Directional Characteristics—The size of the ceramic disks chosen for a particular testing program depends upon various factors. One of these is the directional characteristics of the crystal. The amount of mode conversion at the probe-specimen interface is a factor that is related to crystal size and wavelength in the specimen. The wavelength-to-diameter ratio of a particular crystal controls the intensity of secondary waves transmitted into the specimen. It is observed that for testing techniques where the existence of strong secondary waves is a hindrance, the wavelengths of the compressional wave in the specimen should be considerably smaller than the crystal diameter. The diameter of the crystal should thus be chosen large enough that divergence of the ultrasonic beam is minimized.

Near-Field Effects—The amount of mode conversion can also be decreased by choosing larger-diameter crystals. The choice of a large-diameter crystal increases the length of the field while simultaneously decreasing the amount of mode conversion from reflections at the specimen boundaries.

Infinite Media Assumption—To assume "infinite media" or to be able to ignore the effects of specimen size, the wavelength of the ultrasonic pulse in the specimen should be as small as possible compared to the specimen dimensions. This criterion sets an upper limit of wavelength for a particular-size specimen. For a material with known wave velocity, this maximum wavelength corresponds to a minimum crystal frequency according to the equation

$$\lambda_{\max} = vT_{\max} = \frac{v}{f_{\min}} \tag{5}$$

where

λ_{max} = maximum wavelength acceptable to assume infinite media,
v = wave velocity in material being tested,
T_{max} = period length corresponding to λ_{max}, and
f_{min} = minimum frequency corresponding to λ_{max}.

Material Grain Size—Scattering of the ultrasonic wave increases greatly as the wavelength in the specimen approaches the grain diameter of the specimen. A minimum wavelength acceptable for testing in a particular material is thus set by the grain diameter. By using equations identical to Eq 5, a maximum crystal frequency is calculated corresponding to the minimum wavelength set by the grain size.

Crystal Requirements

In summary, the size of a compressional wave crystal should conform to the following requirements:

1. To limit the intensity of secondary waves (shear waves and compression waves)

$$\lambda_s \ll 2a \tag{6}$$

where

λ_s = wavelength of compressional wave in specimen, and
a = radius of transmitting crystal.

2. To stay within the near field and thus to limit excessive divergence of the compression waves

$$L_s < \frac{a^2}{\lambda_s} \tag{7}$$

where

L_s = length of specimen in direction of wave propagation.

3. To assume "infinite media"

$$\lambda_s \ll L_p \tag{8}$$

where

L_p = minimum dimension of specimen perpendicular to wave propagation.

4. To reduce scattering

$$\lambda_s \ll D_{max} \tag{9}$$

where

D_{max} = maximum grain diameter of specimen.

Requirements 1 and 2 set lower limits upon the crystal diameter where Requirements 3 and 4 set an upper and lower limit upon the wavelength in the specimen. As mentioned earlier, the wavelength is related inversely to the crystal frequency by the velocity of sound in the material. For longitudinal wave crystals, the thickness of the crystal controls the frequency. Requirements 3 and 4 therefore set upper and lower limits on the crystal thickness.

The crystals initially used were 2.5-cm-diameter PZT thickness expanders manufactured by Gulton Industries. The resonant frequency of these crystals is approximately 308 kHz in the thickness mode. The strain generated by the crystal deformations was less then 10^{-4} percent.

The next crystals used (also 2.54 cm in diameter) were primarily radial expanders (shear mode) manufactured by Clevite. The crystal material was PZT and has been identified as PZT-4 by the manufacturer. These crystals had a resonant frequency in the radial mode of 90 kHz and in the thickness mode of 640 kHz.

It should be stressed that the crystals just described were used primarily due to their availability. Some of their characteristics (for example, diameter) do not meet the specifications calculated by the theories presented earlier in this section. These specifications were computed on the basis of crystal use in the investigation of asphaltic concrete. They may be suitable for use with other materials possessing different characteristics (for example, different wave velocity and grain size). Although they did not fit specifications, the crystal behavior with respect to various operating conditions was expected to be informative. These conditions are discussed in the following section.

Probe Construction

Previous works have been published on the design of ultrasonic probes for flaw detection in metals [*2,3*]. The basic characteristics of the probes used in flaw detection coincide with the properties of the probes used for ultrasonic testing in asphaltic concrete. Three of the main features considered in the probe design were (*a*) crystal selection, (*b*) mechanical damping of the crystals, and (*c*) concentration of ultrasonic waves in one direction.

Mechanical Damping—In addition to selection of a crystal material which results in a short ringing time, the crystal may also be mechanically damped. Mechanical damping is often accomplished by cementing a backing material onto the crystal. This material helps to restrain the vibrations of the crystal after its initial excitation.

Concentration of Ultrasound—The crystal backing also serves another purpose. An ultrasonic probe design has been suggested by Washington [*3*] where the backing acts as an absorbent layer. This layer of absorbent material not only damps the crystal vibrations, but decreases the intensity of ultrasound radiating from the back of the crystal. The result of this behavior is the concentration of energy in one direction from the probe.

The backing material suggested by Washington and used in this study is a mixture of tungsten powder and casting resin (Araldite). The tungsten-Araldite ratio suggested was a 2:1 by weight mixture. Figure 1 shows a section of the probe as built. Figure 2 is a photograph of two probes.

Probe Characteristics—Two additional advantages have resulted from the construction of the ultrasonic probe just described. The first is that the probe design offers complete electronic shielding. This results in the elimination of "noise" (for example, from lighting fixtures) that often hinders ultrasonic measurements. The second and probably most practical advantage of the probe design is the increase in durability of the probe system. Piezoelectric crystals can and have been successfully used by themselves, but, due to their cost and delicate nature, their uses are often limited. The probe design results in the possibility of greater pressure between probe and specimen and less chance of breakage during normal laboratory handling. The use of these probes underwater is also possible due to the impermeable characteristics of the probe design.

Materials

The soil used in this investigation was a processed silty clay of low plasticity. The material has a liquid of 25 percent, a plastic limit of 15 percent, a shrinkage limit of 13 percent, and a specific gravity of 2.67. Hydrometer

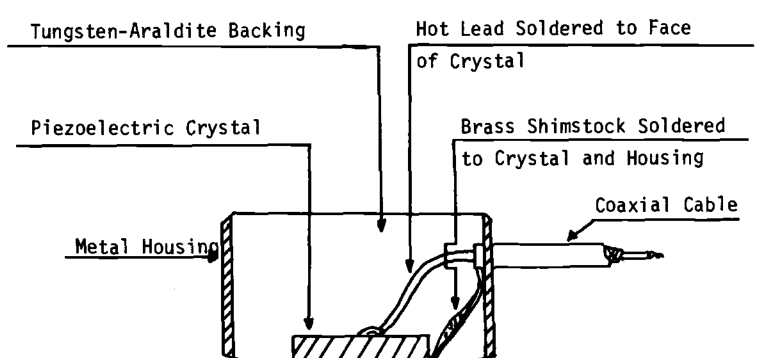

FIG. 1—*Section of probe assembly.*

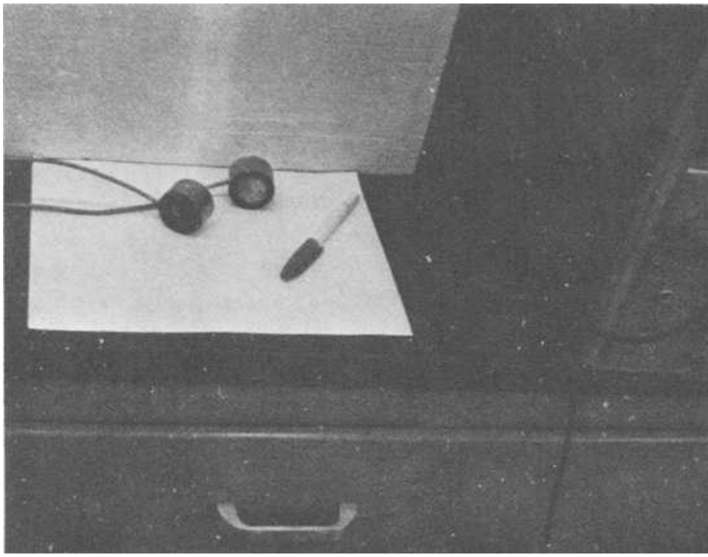

FIG. 2—*Ultrasonic probes.*

analyses indicate 80 percent finer than 0.05 mm and 35 percent finer than 0.005 mm.

Specimen Preparation

Specimens were prepared to predetermined void ratios and degrees of saturation. The amount of material needed to produce a given void ratio in a standard 100-mm (4 in.) compaction mold was determined. The required amount of water was added to the soil to produce the desired degree of saturation for that void ratio. The material and water were compacted. Compaction to a uniform void ratio was accomplished by compacting the specimen in five layers. Each layer was the same weight (the sum total was the original amount of soil plus water) and was compacted in layers with equal compacted thicknesses (the total height was the height of the lower section of a compaction mold). Compaction was accomplished by use of a 2.4- or 4.5-kg (5.5 or 10 lb) compaction hammer dropped various times and from various heights to obtain the specified height of layer. The specimen was then wrapped in cellophane, waxed, and stored for later use.

Void ratios were varied from 0.30 to 0.60 in 0.05 increments and the degrees of saturation were varied from 30 to 100 percent in 10 percent increments. It was found that specimens with water contents less than about 6 percent could not be adequately compacted; specimens with water contents less than this amount cracked and broke at interfaces between layers. Therefore, specimens with lower degrees of saturation could not be made for soil specimens with void ratios lower than 0.45.

Testing Techniques

The advantages of ultrasonic testing methods lie primarily in that the method is nondestructive, dynamic, and is easily and rapidly performed. In addition, the imparted strains (10^{-4} percent or less) are small enough such that the material approximates elastic behavior. As previously noted, Sheeran, Baker, and Krizek [*4*] used pulse velocity techniques for moisture content and density relationships. Similar results were found by Leslie [*5*]. Manke and Galloway [*6*] made use of the pulse technique to generate longitudinal waves through the soil. Lawrence [*7*] used pulse techniques in the investigation of various parameters on the effect of shear wave velocity.

Since little information on pulse testing could be found, and also since the performance of the apparatus developed at the University of Missouri-Rolla was unknown, it was necessary to investigate the effect of specimen size, pulse width, rate of repetition of the pulse, pulse amplitude, and pulse frequency on the transmitted pulse.

It should be noted that the ultrasonic testing techniques employed in this study made use of the direct-transmission method. The use of this method was necessary due to the significant amount of scatter associated with the multiple reflections and longer path lengths typical of other methods.

Specimen-Supporting Devices and Acoustic Coupling

The specimen-supporting device initially employed in this study was a testing frame normally used for unconfined compressive strength tests of soils. The proving ring normally used for load measurement was replaced by a much lighter ring constructed from Plexiglass. This smaller ring was used in obtaining constant pressure between the probes and the test specimen. The load-deformation characteristics of the ring were determined, and a constant-contact load between specimen and probes was obtained by raising the load platen, specimen, and probes until the ring compressed a specified distance.

The main advantages of this specimen holding device is its simplicity. Specimens can be mounted, tested, and removed quickly and with little effort. The constant pressure obtained using this device is also advantageous, minimizing any deviations due to changes in coupling pressures.

As in other studies [*1,8*], pressure coupling of the probes to the specimens did not always prove adequate. Better-quality results were obtained through the use of an intermediate coupling material. Silicone grease was employed as a coupling medium and proved adequate for measurements involving velocity determination.

Specimen Size—Tests were conducted on specimens with void ratios of 0.45 and 0.50 and degrees of saturation of 85 and 77 percent, respectively. Specimens 10.2 and 5.1 cm in diameter with lengths varying from 1.3 to 7.6 cm, in 1.0-cm increments, were studied. It was generally found that specimens 10.2 cm in diameter provided more clearly defined wave forms at all pulse widths than those 5.1 cm in diameter. From these tests it was also concluded that a length of 6.25 cm provided optimum transmission results.

Typical results are shown in Fig. 3. This tracing is from a specimen with a void ratio of 0.50 and a degree of saturation of 77 percent.

Point A on the trace represents the arrival of the compression wave. Defining the arrival of the P-wave is usually not a problem, as can be seen in the figure, since the wave arrival is quite sharp.

Point B is the arrival of the shear wave. The arrival of the shear wave as shown in Fig. 3 and most of the other 10.2 cm specimens was defined as being the point where a strong change of pulse direction was noted, after which there occurred numerous smaller peaks representing the resonant frequency of the crystal in the shearing mode. Points C and D in Fig. 3 represent one cycle of a wave at the resonant frequency. The computed frequency of these waves is about 96 kHz, which corresponds closely to the manufacturer's specification of 90 kHz.

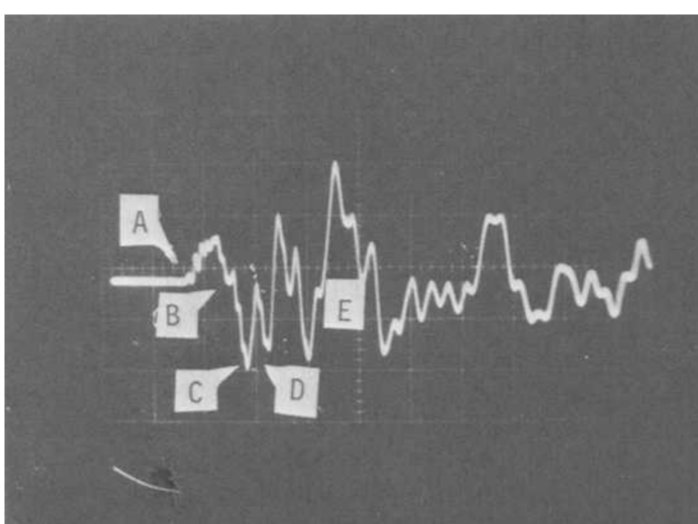

FIG. 3—*Typical wave trace.*

Point E represents the arrival of the Rayleigh wave. The Rayleigh wave is usually characterized by a long period and large amplitude.

Pulse Width and Interval—Once specimen length and diameter were determined, optimum pulse width and pulse interval needed to be investigated. Tests conducted on a specimen with a void ratio of 0.54 and degree of saturation of 70 percent determined that a pulse width of 5 to 7 μs and a pulse interval of 2 ms obtained optimum wave forms. Interference from previous waves was nonexistent.

Pulse Amplitude—The amplitude of generated and received pulses is a function of the voltage applied to the generating crystal. It is desirable to use a combination of voltage from the pulse generator and oscilloscope magnification factor to obtain an oscilloscope trace that uses the full height of the oscilloscope scale but yet keeps noise levels low and maintains as narrow a trace as possible. An amplitude of 600 V was usually adequate for wave transmission, but occasionally voltages up to 1100 V combined with large magnification factors had to be used.

Pulse Frequency—Limitations on frequency as well as the frequencies of the crystals used in this investigation have been discussed previously. The 0.37-mm crystal was not used when testing soils; a combination of the pressure required for coupling, the roughness of the surface, and the delicacy of the crystal prohibited its use.

The 3.18-cm crystal was used in this investigation and had a frequency such that the crystal in both the radial and thickness mode had wavelengths larger than most of the grain sizes. However, since attenuation does increase as wavelength approaches grain size, some scattering could be attributed to the frequency of the crystals. Also dependent upon wavelength is the length of the near field, which has an effect on mode conversion. The 6.35-cm-length specimens are within the near field.

Velocity and Damping Measurements—As previously stated, measurement of longitudinal wave velocity allows the calculation of several important dynamic material parameters that are descriptive of the dynamic nature of the test material. In addition, measurement of different arrival times of a given wave could possibly be made and a measure of the wave attenuation properties of the media ascertained.

When a piezoelectric crystal is excited, all three types of wave forms are generated (compression, shear, and surface). The first wave to arrive at the receiver will be that with the greatest velocity, namely, compression waves. Since shear wave velocity and Rayleigh wave velocity are approximately equal, the arrival times may be about the same and some difficulty distinguishing waves may result. Identification is usually not much trouble, however, because the Rayleigh wave has a much larger amplitude than the shear wave. These waves may be distorted by reflected and refracted longitudinal waves due to longer path lengths.

A portion of the wave energy is lost at the specimen/receiver interface.

As a result, some of the energy is reflected back to the source crystal and back to the receiver crystal. The travel time of this wave is about three times the time required for the first wave to arrive. The arrival of this wave is important in attenuation measurements and may distort arrivals of other wave forms. Measurement of the difference in amplitude between the first and second arrival of the P-wave divided by the travel distance between first and second arrivals gives the amount of attenuation per unit length.

Test Results and Discussion

Any testing technique is of value if and only if results are indicative of the actual properties of the material being tested. It is believed that the results of the test method used in this investigation satisfy these criteria, yield behavioral patterns as expected, and are compatible with results obtained by other investigators using the same or a similar technique. The test results reported here, although not conclusive, compare favorably with the results of other investigators who used different investigative methods. The influence of void ratio, and degree of saturation upon compression and shear wave velocity, and hence Young's modulus, shear modulus, and Poisson's ratio, were of primary concern in this study. Of equal significance in this study was the evaluation of a high-voltage pulse generator for ultrasonic testing developed at the University of Missouri-Rolla. The results presented herein are to be considered indicative only of the material tested.

Dynamic Material Properties

Forty-eight tests of compacted soil at seven void ratios and eight varying degrees of saturation were made in this study. As stated previously, some specimens with lower degrees of saturation were not tested for void ratios below 0.45.

The dynamic material parameters studied and their relationship to void ratio and degree of saturation are presented and discussed in the following subsections.

Young's Modulus—Figure 4 shows a plot of E-modulus versus void ratio for given ranges of degree of saturation. For clarity, the actual data points have not been shown, but it should be noted that a scatter of data points was present. The lines shown in Fig. 4 represent equations obtained by linear regression analysis. The data had correlation coefficients between -0.88 and -0.98.

As expected, Young's modulus decreases with increasing void ratio for all degrees of saturation. Since moduli values are dependent on velocity, it should follow that the moduli of a soil would behave as the velocity with respect to void ratio. However, moduli values are also influenced by the den-

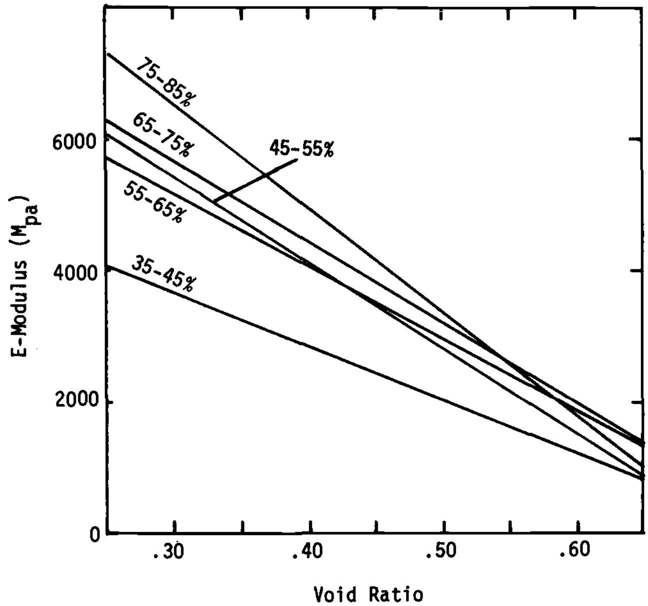

FIG. 4—*Modulus versus void ratio.*

sity of a soil, which will result in minor deviations of linear plots when compared against velocity data.

It can be seen that the data have approximately the same slope except for the 35 to 45 percent degree-of-saturation range line. This deviation is attributed to the difficulty in obtaining good coupling between specimen and transducer for soil specimens in this range. This coupling difficulty also explains lower compression wave velocities for the 35 to 45 percent saturation range which are reflected in moduli values.

Increasing the degree of saturation at a given void ratio generally increases the moduli values. A slight discrepancy occurs between the degree of saturation range of 45 to 55 percent and 55 to 65 percent. However, the difference between the two curves is small and may be attributed to coupling or oscilloscope normal data reading scatter.

Shear Modulus—A plot of the linear regression analysis of shear modulus versus void ratio is shown in Fig. 5. Correlation coefficients are between −0.90 and 0.91.

Since shear wave velocity decreases as void ratio increases, it is not surprising that shear moduli exhibit a similar tendency. The decrease of moduli for increase in void ratio can be explained by the fact that, as a rule, for the same material with an identical stress history, an increase in the amount of voids will decrease the shearing resistance for a given amount of strain and consequently reduce the shear modulus. A similar explana-

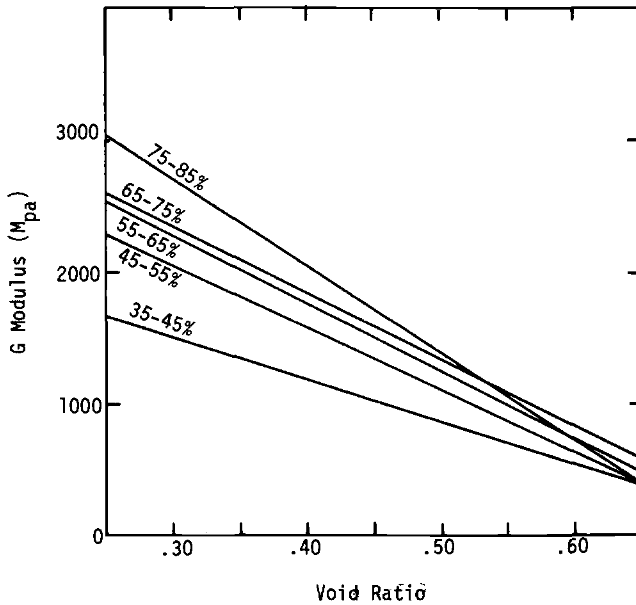

FIG. 5—*Modulus versus void ratio.*

tion can account for the decrease of Young's modulus with increase of void ratio.

For a given void ratio, shear moduli increase with degree of saturation. As was explained earlier, shear wave velocity for an increase in degree of saturation at a given void ratio should remain constant. Because of the way in which shear modulus is defined in Eq 2, any variation in shear modulus should be due to an increase in unit weight, which increases with degree of saturation. One would therefore expect shear modulus to increase at a given void ratio for an increase of degree of saturation. Additional increase of shear modulus can be attributed to variation of shear wave velocity.

Values of shear moduli obtained in this text and another investigation are shown in Fig. 6. The data of Hardin and Black [9] were obtained from tests performed on a clay material by means of a modified triaxial apparatus for pressures of 138 to 690 kPa (20 to 100 psi). Differences of results are due to variation of material, parameters studies, and ranges of strain encountered.

Poisson's Ratio—Results of Poisson's ratio were too scattered to reveal any definite relationship. However, when several data points are deleted, a relationship of decreasing Poisson's ratio with increasing void ratio can be noted. At a given void ratio, an increase in degree of saturation gave a slight decrease in Poisson's ratio. The scatter of Poisson's ratio can be attributed to the fact that calculation of Poisson's ratio is highly sensitive to

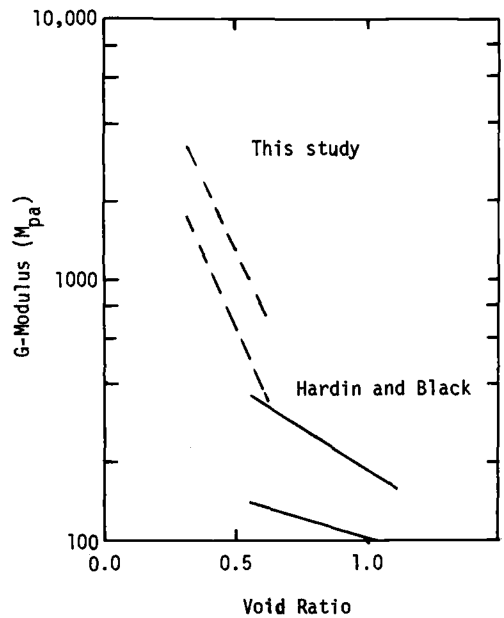

FIG. 6—*Comparison of moduli values.*

velocity changes. A 10 percent change in velocity may change Poisson's ratio by as much as 100 percent.

Damping

Measurements of material damping could not be made with the test setup used. In order for the damping of a wave to be measured, it is necessary to detect the first arrival of a wave form and also the wave that is reflected and arrives at a time three times the first arrival. This could not be done because of large surface waves which were encountered at three times the first arrival. These surface waves masked all other wave forms. Recommendations for damping measurements are made later.

Conclusions

Of primary importance in this study was the investigation of the possibility of evaluating Young's modulus, shear modulus, Poisson's ratio, and damping for a soil by use of a pulse velocity technique. This test would be of value because it would provide a quick, nondestructive method of determining soil parameters appropriate for dynamic analysis at strain ranges smaller than tests presently available.

From test data described herein, it can be said that it is possible to measure ultrasonic wave velocities through soil, and the testing procedure employed for the determination of wave velocities can be used to define the dynamic properties of interest. The possibility also exists that parameters as determined by this testing technique can have some application in the design, control, and investigation of soils subject to small-strain dynamic loadings such as machine vibrations, microtremors, and vehicular traffic vibrations.

One technique of evaluating dynamic soil moduli subjected to earthquake-level strains is to conduct dynamic-triaxial or resonant-column tests, determine the moduli at that strain level, and then apply a reduction factor to approximate the moduli at the higher strains [*10*]. The ultrasonic technique could substitute quite easily and readily for the triaxial or resonant-column test methods.

The ultrasonic tests were conducted only on unconfined specimens of cohesive soils. Other researchers have suggested that the ratio of dynamic modulus [*6*] to undrained shear strength (s_u) does not vary widely from one soil to another [*10*]. Plots of this ratio for varying strain levels allow extrapolation from low-strain tests to large-strain moduli values.

No ultrasonic tests were conducted on cohesionless soils. It is recognized that the dynamic moduli of sands are strongly influenced by confining pressure, and modification of a triaxial compression chamber to allow ultrasonic testing under multidirectional loading, while expected to be relatively simple to do, has not been done at this time.

The following conclusions are based on the material and test procedure outlined in the paper. Testing of a wider range of materials needs to be done before general conclusions can be made.

1. It is possible to generate and detect ultrasonic compression and shear waves in a soil material with equipment developed at the University of Missouri-Rolla.

2. Specimen size does affect velocity measurements; length affects the intensity of a wave at the receiver; and diameter directly influences the arrival of the large-amplitude Rayleigh wave. There exists a specimen geometry that results in optimum testing conditions.

3. Optimum pulse duration, interval, amplitude, and frequency vary within a soil and it is suspected that these parameters will differ from soil to soil.

4. Compression and shear wave velocity tends to decrease with an increase of void ratio for a given band of degree of saturation. Shear wave velocities do not decrease as rapidly with increase of void ratio as compression wave velocities.

5. At a constant void ratio, wave velocity generally increases with degree of saturation.

6. Young's modulus and shear modulus have behaviors similar to that of

the corresponding velocity. As with velocity measurements, G-modulus did not decrease as rapidly as Young's modulus.

7. Data points of Poisson's ratio versus void ratio were widely scattered, but a general trend of a decreasing Poisson's ratio with increasing void ratio was noted.

8. Damping could not be determined with the test procedure used. However, tests on an asphalt-aggregate specimen using these techniques have been able to measure relative attenuation. It is believed that crystals selected with dampling movements foremost in mind would allow such measurements to be made in soil materials. In such techniques, the attenuation of the wave through the test material could be related to the attentuation in a reference material.

References

[1] Eckelkamp, R. M., "Laboratory Evaluation of Dynamic Soil Properties by Ultrasonic Testing Methods," unpublished M.S. thesis, University of Missouri-Rolla, Mo., 1974.

[2] Walker, D. C. B. and Lamb, R. F., *Applied Materials Research*, Vol. 3, 1964, pp. 176-183.

[3] Washington, A. B. G. *British Journal of Non-Destructive Testing*, TRG Report 17(c), Vol. 3, 1961, pp. 56-63.

[4] Sheenan, D. E., Baker, W. H., and Krizek, R. J., "Experimental Study of Pulsed Velocities in Compacted Soils," presented at 47th Annual Meeting of the Highway Research Board, 1967.

[5] Leslie, J. R. in *Proceedings*, American Society for Testing and Materials, Vol. 50, 1950, pp. 1314-1323.

[6] Manke, P. G. and Galloway, B. M., *Highway Research Board Record 131*, 1961, pp. 128-153.

[7] Lawrence, F. V., "The Response of Soils to Dynamic Loadings," Report No. 23: *Ultrasonic Shear Wave Velocity in Sand and Clay*, Research Report R65-05, U.S. Army Engineer Waterways Experiment Station, Vicksburg, Miss., 1964.

[8] Stephenson, R. W. "Ultrasonic Testing of Asphalt-Aggregate Mixtures," Ph.D. dissertation, Oklahoma State University, Norman, Okla., May 1971.

[9] Hardin, B. O. and Black, W. L., *Journal of Soil Mechanics and Foundations Division*, American Society of Civil Engineers, Vol. SM-2, March 1968.

[10] SW-AJA, "Soil Behavior Under Earthquake Loading Conditions—State of the Art Evaluation of Soil Characteristics for Seismic Response Analysis," prepared for U.S. Atomic Energy Commission, Jan. 1972.

T. S. Vinson,[1] *T. Chaichanavong,*[2] *and J. C. Li*[3]

Dynamic Testing of Frozen Soils Under Simulated Earthquake Loading Conditions

REFERENCE: Vinson, T. S., Chaichanavong, T., and Li, J. C., "**Dynamic Testing of Frozen Soils Under Simulated Earthquake Loading Conditions,**" *Dynamic Geotechnical Testing, ASTM STP 654,* American Society for Testing and Materials, 1978, pp. 196–227.

ABSTRACT: Engineers concerned with the development of Alaska and other highly seismic areas underlain by permafrost must have knowledge of dynamic properties of frozen soils under earthquake loading conditions. In response to this need, a cyclic triaxial test system and test methods have been developed to evaluate the dynamic Young's modulus and damping ratio of artificially frozen soils over a range of test conditions which simulate earthquake loadings of permafrost deposits.

The test system developed represents a coupling of conventional closed-loop cyclic triaxial equipment to evaluate the dynamic properties of unfrozen soils with conventional temperature control equipment to evaluate static properties of frozen soils. On-line, real-time data processing has been achieved by coupling a minicomputer to the test system. With the test system, the dynamic Young's modulus and damping ratio can be determined over a range of axial strain amplitudes from 3×10^{-3} to 10^{-1} percent, temperatures from -1 to $-10°C$ (30 to 14°F), frequencies from 0.3 to 5.0 Hz, and confining pressures from 0 to 1400 kN/m^2 (200 psi). An extensive laboratory program was undertaken to establish suitable methods of specimen preparation, specimen installation, and testing for artificially frozen specimens of clay, silt, sand, and ice.

At present there is no standard test procedure to evaluate dynamic properties of frozen soils under simulated earthquake loading conditions. The material presented provides a basis for the development of a standard test procedure.

KEY WORDS: cyclic loading, damping, dynamics, earthquakes, frozen soils, geotechnical engineering, ice, permafrost, triaxial tests, Young's modulus, soils

Alaska is located in one of the world's most active seismic zones. Nearly 500 earthquakes of Richter Magnitude 6 or greater have occurred there

[1]Associate professor, Department of Civil Engineering, Oregon State University, Corvallis, Ore. 97331.

[2]Instructor, Kasetsart University, Bangkok, Thailand.

[3]Graduate research assistant, Division of Engineering Research, Michigan State University, East Lansing, Mich. 48824.

since the 1800's [*1*].[4] Further, 85 percent of Alaska lies within a permafrost region, that is, a region of perennially or permanently frozen ground [*2*]. The need to evaluate the dynamic properties of frozen soils under simulated earthquake loading conditions for seismic studies in Alaska is apparent.

Dynamic properties of frozen soils have been evaluated from geophysical field studies [*3-13*] and from forced-vibration [*14,15*], ultrasonic [*16-25*], and resonant-column tests [*26,27*] in the laboratory. The results from these studies, however, do not simulate earthquake loadings of permafrost deposits. Specifically, little or no work has been done to evaluate dynamic properties of frozen soils under the following test condition parameters:

1. temperature in the range of -4 to 0°C (25 to 32°F),
2. confining pressure,
3. shear strains greater than 10^{-3} percent, and
4. frequency over a range of 1 to 5 Hz.

These parameters are of particular significance in studies concerned with ground motion predictions of permafrost deposits during earthquakes. The mean annual air temperature (MAAT) over a considerable portion of Alaska is in the range 0 to -6°C (32 to 21°F) [*2*]. In general, the MAAT is about 0.5°C (1°F) higher than the mean annual ground temperature (MAGT) at the surface [*28*]. (This is due to the heat absorbed in the process of surface evaporation.) Therefore, a considerable portion of Alaska will have MAGT's between -0.5 and -6.5°C (31 and 20°F). The temperature in permafrost increases from close to the MAGT to 0°C (32°F) at some depth below the surface, on an average thermal gradient of 0.033°C/m [*28*]. Consequently, over a considerable portion of Alaska much of the permafrost should be in a range of -4 to 0°C (25 to 32°F). For deposits where the MAGT is -4°C (25°F) or higher, the entire deposit will be in this range. For deposits where the MAGT is -6.5°C (20°F) and the average thermal gradient is 0.033°C/m, approximately two thirds of the deposit will be in the range -4 to 0°C (25 to 32°F).

Ground motion analyses for unfrozen soil deposits are conducted for a wide range of depths of deposit, generally associated with the depth to bedrock. Where the soil deposit is particularly deep, the deposit is often assumed to extend to a depth of approximately 200 m (600 ft). In either case, it is apparent that there will be a significant variation in confining pressure which should be considered in the determination of dynamic properties. While it might be difficult to determine the actual value of confining pressure in a permafrost deposit, it is reasonable to assume that the confining pressure would vary significantly over the depth associated with a ground motion analysis. Therefore, the dynamic properties of the

[4]The italic numbers in brackets refer to the list of references appended to this paper.

frozen soils should also be evaluated over a range of confining pressures to establish if there is a strong dependence on confining pressure.

The dynamic properties of frozen soils have been evaluated from very low shear strains up to about 10^{-3} percent by previous investigators [*29*]. Within this range, Stevens [*27*] states that the effect of strain (dynamic stress) on the dynamic modulus is, in general, small. It should be noted, however, that up to 10^{-3} percent, the effect of strain on dynamic properties of unfrozen soils is also small. At greater strains associated with moderate to strong motion earthquakes, the dynamic modulus drops off sharply, while material damping increases. Similar behavior might be expected for frozen soils, particularly if they are in the temperature range -4 to 0°C (25 to 32°F).

Earthquake loadings can be thought of as a composite of harmonic oscillations, each with its own frequency and amplitude. As either distance or magnitude of the shock increases, the greater will be the proportion of low-frequency components. It is generally felt that strong motion earthquakes can be represented by frequencies of loading in the range of 1 to 5 Hz.

Purpose and Scope of Studies

The purpose of the work described herein was to develop a testing system and test methods to evaluate dynamic properties of frozen soils over a range of test conditions which simulate earthquake loadings of permafrost deposits. The scope of the work reported includes (1) a discussion of the selection of the test system from several alternatives, (2) a description of the test system, (3) a discussion of the specimen preparation techniques and test procedures, (4) a presentation of representative test results, and (5) a discussion of the application of the results of the work to the development of a standard test procedure to evaluate dynamic properties of frozen soils under simulated earthquake loading conditions.

Selection of Test System

Given the test condition parameters just mentioned, the criteria for the development of a test system to evaluate dynamic properties of frozen soils were considered to be

1. temperature control over a range 0 to -10°C[5] (14°F) ± 0.1°C (0.2°F),
2. control of confining pressure over a range 0 to 1400 kN/m^2 (200 psi) ± 10 kN/m^2 (1.5 psi),
3. control of strain amplitude over a range 10^{-3} to 1 percent, and
4. control of frequency over a range 1 to 5 Hz.

At the onset of the research work it was decided to couple existing equipment to evaluate the dynamic properties of unfrozen soils with existing temperature control equipment to evaluate the static properties of frozen soils. It was felt that this approach would significantly expedite the development of a test system to evaluate the dynamic properties of frozen soils.

The strain amplitude and frequency range of interest in the test program dictate that only three dynamic test devices be considered:

1. cyclic triaxial,
2. cyclic simple shear, and
3. cyclic torsional shear.

In the cyclic triaxial test a cylindrical specimen is placed in a triaxial cell and confined to an initial isotropic stress state, as shown in Fig. 1*a*. An axial load is cycled on the specimen, causing a reversal of shear stresses in the specimen which are a maximum on 45-deg planes. The axial load produces a deviator stress in the specimen, that is major principal stress minus minor principal stress, $\sigma_1 - \sigma_3$. Typical test results expressed in these terms for one cycle of loading are shown in Fig. 1*a*. From this record, the dynamic Young's modulus, E_d, and damping ratio, λ, may be calculated as follows

$$E_d = \frac{\sigma_{\text{max deviator}}}{\epsilon_{\text{max axial}}} \tag{1}$$

$$\lambda = \frac{A_L}{4\pi A_T} \tag{2}$$

with the terms as defined in Fig. 1*a*. A_L represents the total dissipated energy per cycle and A_T the work capacity per cycle.

In cyclic simple shear testing, an axial load is applied to a specimen which is not allowed to move in the lateral direction. This establishes an initial anisotropic state of stress as shown in Fig. 1*b*. A cyclic horizontal load is applied to the top (or base) of the specimen which causes a reversal of shear stresses on both the horizontal and vertical planes as shown in Fig. 1*b*. The resulting symmetric shear stress versus shear strain relationship is shown in Fig. 1*b*. The shear modulus, G, and damping ratio are calculated as follows

$$G = \frac{\tau_{\max}}{\gamma_{\max}} \tag{3}$$

[5] −10°C (14°F) was selected as the lower limit of temperature because (1) it is felt that most of the water in the voids of a frozen soil would be frozen at this temperature if it would freeze at all; and (2) this is close to the lower limit of temperatures at which permafrost deposits exist.

$$\lambda = \frac{A_L}{4\pi A_T} \tag{4}$$

with the terms as defined in Fig. 1*b*. Two types of simple shear devices are presently available. The Cambridge device uses specimens with a square cross section which are completely surrounded by a steel container. The Norwegian Geotechnical Institute (NGI) device (or modifications of it) uses a specimen with a round cross section surrounded by a wire-reinforced rubber membrane which prevents lateral expansion of the specimen during shear.

In a typical torsional shear test, a hollow cylinder of soil is subjected to an initial anisotropic state of stress and the specimen is cyclically twisted to subject it to a reversal of shear stress as shown in Fig. 1*b*. If the fre-

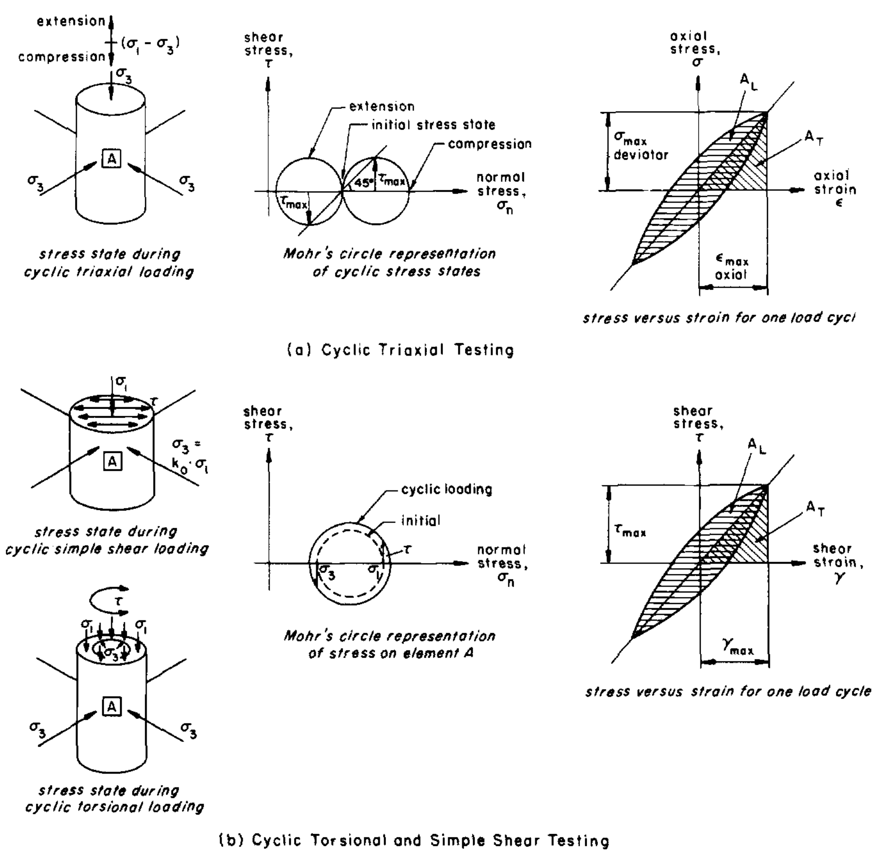

FIG. 1—*Stress state and stress versus strain for cyclic loading tests.*

quency of loading is slow enough, then inertia forces will not be significant and the load-deformation relationship measured at the specimen top cap will represent the load-deformation relationship for the specimen. The shear stress and shear strain vary with radius in the test specimen. However, acceptable results are obtained when the behavior is correlated with the average strain in the specimen. Shear modulus and damping ratio are calculated as in the cyclic simple shear test.

During an earthquake, in many cases, the main forces acting on soil elements in the ground are due to the upward propagation of shear waves from underlying rock formations. Before the earthquake an element of soil in the ground is in an anisotropic stress state. During an earthquake the element will be deformed through the development of shear stresses on horizontal and vertical planes [*30*]. The stress conditions on an element of soil before and during an earthquake are represented in principle in the cyclic torsional and simple shear test (see Fig. *1b*), but not by the cyclic triaxial test (see Fig. *1a*). Accordingly, the shear modulus obtained in a cyclic torsional or simple shear test can be used to predict ground surface motions during earthquakes using presently available analytic techniques [*31*], whereas the dynamic Young's modulus obtained in a cyclic triaxial test must be converted to a shear modulus by employing

$$G = \frac{E_d}{2(1 + \mu)} \tag{5}$$

where

μ = Poisson's ratio.

Temperature control of frozen soils during testing can be achieved by employing any one of three methods:

1. placing the test equipment (all or part) in a cold room or environmental chamber,
2. circulating a coolant in a cold bath around a cell containing the frozen soil specimen and noncirculating coolant, or
3. circulating coolant through a coil placed around the frozen soil specimen which is inside a cell containing a noncirculating coolant.

The latter two techniques are shown in Fig. 2.

The use of a cold room to control temperature has four disadvantages:

1. a high initial and operating cost,
2. personnel conducting the tests have to work at subfreezing temperatures,
3. temperature fluctuations can easily be greater than ± 0.1°C (0.2°F), and

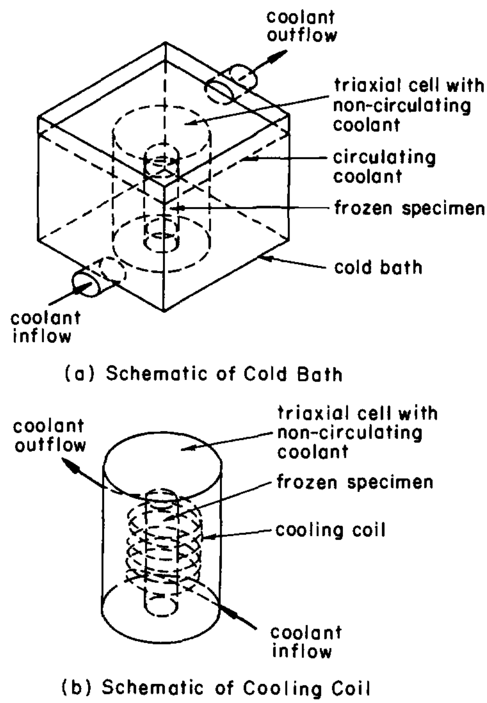

FIG. 2—*Laboratory temperature control devices.*

4. the dynamic equipment must operate at subfreezing temperatures since it would (in all probability) be inside the cold room.

The first, second, and third disadvantages were considered serious enough to rule out the use of a cold room in the test program. An environmental chamber has the first and third disadvantages and was eliminated on this basis.

Given the fact that a cold room or environmental chamber would not be used, it was recognized that coupling a cyclic simple shear device with either of the temperature control devices shown in Fig. 2 would be an extremely difficult task. Further, if the Cambridge device was used, it would be difficult to prepare the test specimens. If the NGI device was used, it was doubtful that the wire-reinforced rubber membrane would perform well at cold temperatures and prevent lateral expansion of the specimen during shear. Therefore, the cyclic simple shear device was eliminated from further considerations.

A cold bath with a coolant circulating around a cell containing a frozen soil specimen and nonciruculating coolant is a relatively simple, inexpensive temperature-control system. It has a slight advantage over a cooling coil system in that it is easier to install a specimen in a triaxial cell in a cold bath. On this basis the cold bath was chosen over the cooling coil.

At this point only two test system configurations are possible:

1. Cyclic triaxial test equipment coupled with a cold bath.
2. Cyclic torsional shear test equipment coupled with a cold bath.

The cyclic triaxial device has the advantage of being a more conventional piece of test equipment than the torsional shear device. A greater backlog of information exists for this test device than for the cyclic torsional shear device. This could prove to be a valuable asset in the overall research program. Further, it would be easier to prepare an artificially frozen solid cylindrical specimen than it would be to prepare a hollow cyclindrical specimen. Naturally frozen core specimens could be tested directly with the cyclic triaxial equipment, whereas the cores would have to be hollowed out for the torsional shear device. For these reasons, it was decided to couple the cyclic triaxial test equipment with the cold bath to evaluate the dynamic properties of frozen soils.

Description of Cyclic Triaxial Test Equipment

Figure 3*a* and *b* shows a schematic diagram of the cyclic triaxial test system developed in the research program. The test system consists of four basic components:

1. An electrohydraulic closed-loop test system (actuator, servovalve, hydraulic power supply, servovalve controller, hydraulic controller, and function generator) which applies a cyclic axial load (deviator stress) to the frozen specimen.
2. A triaxial cell which contains the specimen and noncirculating coolant.
3. A refrigeration unit and cold bath which circulates the coolant around the triaxial cell.
4. Transducers, and output recording and monitoring devices (load cell, spring-actuated gage head with a linear variable differential transformer (LVDT), thermistors, strip-chart recorder, digital multimeter, and storage oscilloscope) to monitor the load (stress) and displacement (strain).

Electrohydraulic Closed-Loop Test System

The heart of the test setup is the electrohydraulic closed-loop test system. It consists of a commercially available 0.010 m^3/min (6.0 gpm), 20700 kN/m^2 (3000 psi) hydraulic power supply, a hydraulic control unit with a function generator, a servovalve controller with command and feedback signal conditioning, and a 5000 kg (11 kip) actuator with a 0.057 m^3/min (15 gpm) servovalve. Referring to Fig. 3*c*, the system operates as follows:

1. A command signal (voltage) from the function generator or other external source is input to the servovalve control unit where it is compared

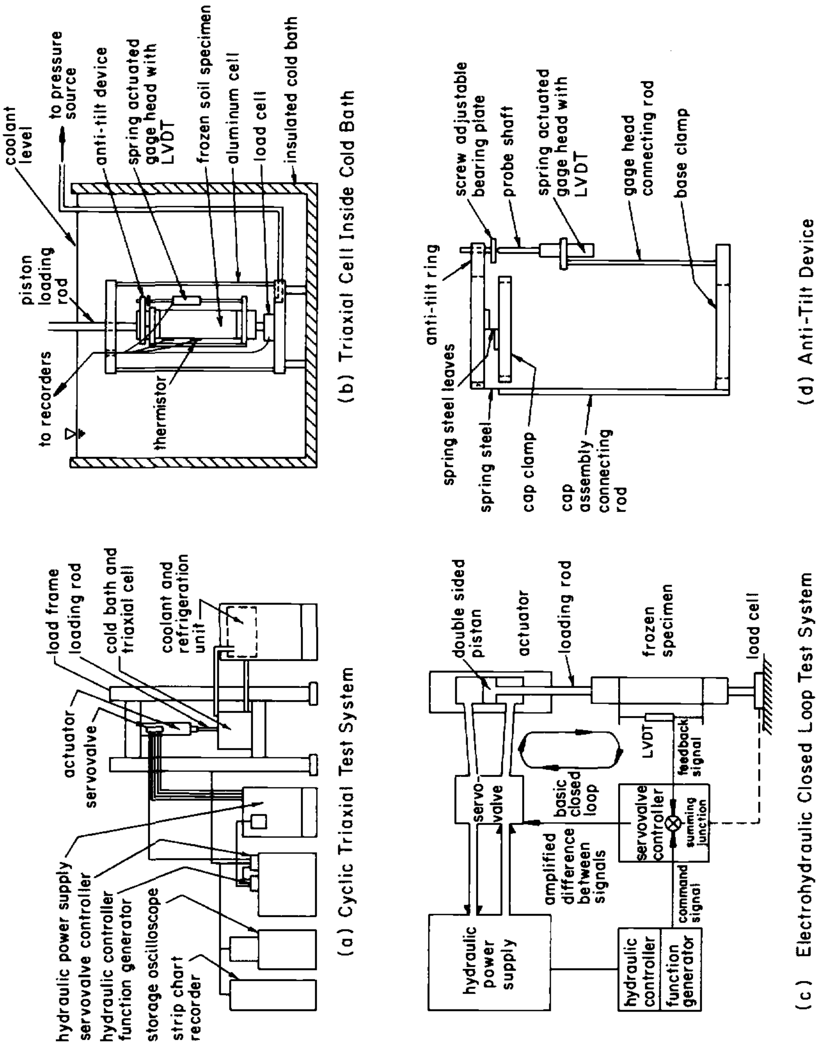

FIG. 3—*Schematic of cyclic triaxial test system.*

with the feedback signal (voltage) from a transducer (a load cell or LVDT) monitoring the response of the specimen in the closed loop.

2. The difference (error) between the two signals is amplified and applied to the torque motor in the servovalve coupled to the actuator.

3. The torque motor drives a pilot stage which in turn drives a power stage of the servovalve, which directs hydraulic fluid under pressure to one side or the other of the double-sided actuator piston to cause the actuator to move.

4. The movement of the actuator causes the specimen to respond in such a way that the transducer monitoring the specimen "feeds back" a signal equal to the command signal.

The speed at which these steps are executed causes the specimen, for all practical purposes, to be subjected to a loading equal to the command signal. A more complete treatment of electrohydraulic closed-loop testing theory is given by Johnson [*32*].

Triaxial Cell

A schematic of the triaxial cell inside the cold bath is shown in Fig. *3b*. The cell is 180 mm (7.2 in.) in diameter and 350 mm (14 in.) high. An aluminum cell was chosen over steel or Lucite for three reasons:

1. It has sufficient strength to allow testing at high confining pressure (compared with Lucite).

2. It is lightweight for ease of handling (compared with steel).

3. It has a higher thermal conductivity (compared with steel and particularly with Lucite) to insure that the noncirculating coolant inside the bath remains at a temperature approximately equal to the coolant circulating outside the bath.

Two thermistors were attached to the 71-mm-diameter (2.8 in.) and 178-mm-high (7.1 in.) specimen to monitor its temperature during the test. An LVDT in a spring-actuated precision-gage head was attached across the specimen to the cap and base to monitor displacement. The output of this LVDT was also the feedback signal in the closed loop. A load cell attached to the base plate of the cell monitors the load.

When the spring-actuated gage head LVDT is mounted at the side of the specimen, care must be taken to insure that tilting of the specimen cap or base does not influence the LVDT displacement reading. A device developed in this research program to eliminate any error associated with tilting is shown in Fig. *3d*. It consists of three basic components:

1. A base clamp (attached to the specimen base) with a connecting rod for the gage head body and a connecting rod to the cap assembly.

2. An antitilt ring connected to the cap assembly connecting rod with a piece of spring steel. The antitilt ring has a diameter 6.3 mm (0.25 in.)

greater than the specimen cap to allow free movement about the cap. It has a screw-adjustable bearing plate which contacts the gage head probe shaft.

3. A cap clamp (attached to the specimen cap) attached to the antitilt ring with two springs steel leaves.

The spring steel leaves between the antitilt ring and the cap clamp act as a pivot point. Any (slight) tilt of the specimen cap will not be transmitted through the spring steel. As the specimen cap moves, the probe shaft of the gage head in contact with the bearing plate is forced to move because the antitilt ring is fixed to the base clamp with the cap assembly connecting rod. The movement at the pivot point causes the displacement measured at the gage head to be twice that of the specimen at the centerline. (This is another advantage of the antitilt assembly ... it effectively doubles the output of the LVDT for a given specimen displacement.)

The two thermistors used to monitor temperature of the specimen were calibrated with a laboratory thermometer with a scale division of 0.1°C (0.2°F). The thermistors were capable of reading to the nearest 0.1°C (0.2°F). The temperature of a specimen was obtained by averaging the readings of the two thermistors.

Cooling System

The cold bath is approximately 0.35 by 0.35 by 0.46 m (1.1 by 1.1 by 1.5 ft) and contains 0.048 m^3 (1.7 ft^3) of circulating coolant, excluding the volume of the triaxial cell. The bath was constructed so that the coolant enters at the bottom and returns to the refrigeration unit from a line at the top of the bath. This is shown in Fig. 2*a*. It is important to insulate the top of the cold bath as this represents a potential source of heat loss in the cell (and specimen through the cell top plate). Two 25-mm-thick (1 in.) sheets of styrofoam were used for this purpose. In addition, coolant was "washed" across the top plate of the cell through an auxiliary circulating line. With these precautions it was found that the temperature inside the cell adjacent to the specimen did not vary appreciably along the length of the specimen.

To ensure that thermal equilibrium had been reached in the specimen and the coolant surrounding it in the cell, temperature measurements were made at the center of ice and frozen clay specimens and adjacent to the specimen, as shown in Fig. 4. The figure illustrates the variation of temperature as a function of time for three test conditions. In one test (Fig. 4*a*) an ice specimen and stainless steel cap and base were at an initial temperature of −16°C (3°F) and the coolant inside the cell was at a temperature of −12°C (10°F). After approximately one hour, the temperature of the specimen (measured with a thermistor frozen in the center of the specimen) and the coolant inside the cell were equal and remained constant. Similar results were obtained when an aluminum cap and base were used

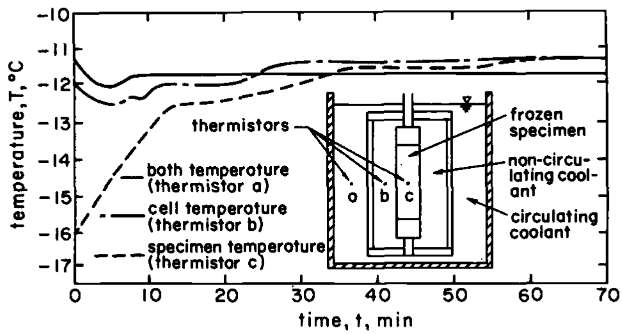

(a) Variation of Temperature Using Steel Cap and Base - Ice

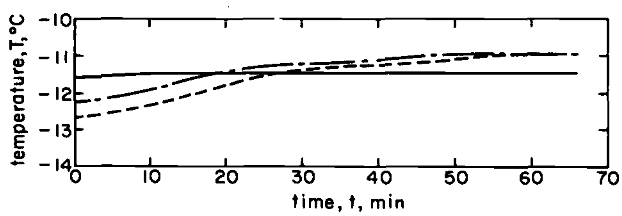

(b) Variation of Temperature Using Aluminum Cap and Base - Ice

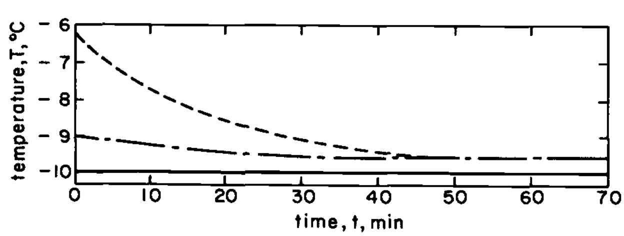

(c) Variation of Temperature Using Steel Cap and Base - Clay

FIG. 4—*Specimen temperature versus time for different test conditions.*

with an ice specimen (Fig. 4*b*) and when a stainless steel cap and base were used with a clay specimen (Fig. 4*c*).

The temperature of the coolant in the refrigeration unit was controlled by a mercury thermometer thermostat submerged in the coolant. The temperature difference between the cold bath and refrigeration unit was approximately 0.5°C (1°F) as shown in Fig. 4*a*, *b*, and *c*. Therefore, it was possible to set the thermostat in the refrigeration unit and obtain any test temperature desired with reasonable accuracy. The average temperature in the specimen did not vary by more than ± 0.1°C (0.2°F) during a test.

Output Recording and Monitoring

The dynamic Young's modulus and damping ratio were calculated from Eqs 1 and 2. The maximum deviator stress and axial strain were evaluated by measuring the amplitude of the load and displacement trace on the strip-chart recording obtained during a test, and dividing by the cross-sectional area and length of the specimen, respectively. The damping ratio was evaluated from the photographic record of load versus displacement obtained with the storage oscilloscope. Specifically, the area of the hysteresis loop, A_L, was measured with a planimeter from an enlargement of the photographic record, and the work capacity per cycle was determined by measuring the amplitude of load and displacement from the enlarged record. A digital multimeter was used to monitor the voltage output from the load cell and LVDT and thermistor resistance during the test as required.

The frequency response of the strip-chart recorder was checked and it was determined there was no variation in the amplitude of the input signal when the frequency was varied from 0.05 to 50 Hz. There is no variation in the amplitude of the input signal to the storage oscilloscope over a much greater range of frequency. In this respect the storage oscilloscope has a great advantage over an *x-y* recorder for which there can be significant mechanical hysteresis for frequencies greater than 0.3 Hz.

The signal from the load cell and LVDT has "noise" at very low voltage output. This "noise" was not visible on the traces on the strip-chart recorder; however, it was recorded on the storage oscilloscope. To eliminate the "noise," the input signals to the storage oscilloscope were filtered. Extreme care was taken to avoid any "phase offset" between the channels. However, the filtering caused some attenuation of the input signals. The attenuation appeared to be somewhat dependent on frequency. Consequently, the dynamic Young's modulus could not be determined from the hysteresis loop recorded with the storage oscilloscope without many calibrations. To avoid these calibrations, only damping ratio was determined from the hysteresis loops recorded. This could be done because damping ratio is a nondimensional parameter.

During the latter stages of development of the test system a minicomputer was used for on-line, real-time data processing. As expected, this afforded significant time savings in the data reduction effort. For example, it took one day's computational effort to reduce and check the test results "by hand"; it took ½ h of additional testing time to reduce and check the test results with the minicomputer. However, the strip-chart recorder and storage oscilloscope are still employed to obtain permanent records of the analog output from the load cell and LVDT.

Specimen Preparation and Specimen Coupling Device

Cylindrical specimens 71 mm (2.8 in.) in diameter and 178 mm (7.1 in.) in height were tested in the research program. All of the specimens tested were reconstituted materials artificially frozen in the laboratory. A description of the specimen preparation techniques for (1) fine-grained soil specimens, (2) dense coarse-grained soil specimens, (3) loose coarse-grained soil specimens, and (4) ice are given in Table 1. To date, specimens of frozen clay, frozen silt, dense and loose frozen sand, and ice at two densitites

TABLE 1—*Specimen preparation techniques.*

A. Fine-Grained Soil Specimens

1. The air-dried, fine-grained materials previously crushed and screened through a No. 40 sieve were thoroughly mixed with distilled water to a water content slightly greater than their liquid limit; the resultant slurry was stored under constant moisture conditions for a period of one week (silts) to one month (clays)
2. The slurry was taken from the constant-moisture environment and isotropically consolidated in a triaxial cell to a cylindrical shape approximately 100 mm (4 in.) in diameter and 200 mm (8 in.) long. (Differences in the water content of the specimens could be obtained by consolidating the slurry to different confining pressures)
3. The consolidated specimen was taken from the cell and trimmed to a diameter slightly smaller than the inside diameter of a hollow trifluoroethylene mold
4. The specimen was placed in the trifluoroethylene mold, and the cap and base, with the coupling device (see Fig. 5*b*), were forced into the two ends of the mold. (Material trimmed from the specimen was previously packed tightly around the coupling on the cap and base)
5. The mold and specimen were placed in a freezer maintained at a temperature of -30 ± 1°C (-22 ± 2°F) for approximately 24 h; the frozen specimen was then extruded from the mold

B. Dense Coarse-Grained Soil Specimens

1. A hollow cylindrical trifluoroethylene mold, with the specimen base inserted in one end, and the specimen cap was placed in a freezer maintained at a temperature of -30 ± 1°C (-22 ± 2°F) for approximately one hour. Both the cap and the base have a coupling device (see Fig. 5*b*)
2. The trifluoroethylene mold was filled to within 50 mm (2 in.) from the top with a mixture of precooled coarse-grained soil and water
3. The specimen cap was forced into contact with the coarse-grained soil/water mixture. The excess water was released through a small hole in the cap. The mold was vibrated to achieve a high density
4. The mold and specimen were placed in a freezer maintained at a temperature of -30 ± 1°C (-22 ± 2°F) for approximately 24 h; the frozen specimen was then extruded from the mold

C. Loose Coarse-Grained Soil Specimens

1. A hollow cylindrical trifluoroethylene mold, with the specimen base inserted in one end, and the specimen cap was placed in a freezer maintained at a temperature of -30 ± 1°C (-22 ± 2°F) for approximately one hour. Both the cap and the base have a coupling device (see Fig. 5*b*)
2. The trifluoroethylene mold was filled to within 50 mm (2 in.) from the top with a mixture of precooled coarse-grained soil and loose dry clean snow. Precooled distilled water, close to 0°C was poured into the coarse-grained soil/snow mixture from the top
3. The specimen cap was forced into contact with the coarse-grained soil/snow/water mixture. The excess was released through a small hole in the cap
4. The mold and specimen were placed in a freezer maintained at a temperature of -30 ± 1°C (-22 ± 2°F) for approximately 24 h; the frozen specimen was then extruded from the mold

TABLE 1—*Continued.*

D. Ice Specimens

1. A hollow cylindrical trifluoroethylene mold, with the specimen base inserted in one end, and the specimen cap was placed in a freezer maintained at a temperature of -30 ± 1°C (-22 ± 2°F) for approximately one hour. Both the cap and the base have a coupling device (see Fig. 5*b*)
2. The trifluoroethylene mold was filled to within 50 mm (2 in.) from the top with loose, dry clean snow passing the No. 4 sieve
3. Precooled distilled water, close to 0°C (32°F), was poured into the snow from the top of the mold up to 50 mm (2 in.) from the top for high-density ice specimens. (Precooled carbonated water was used for low-density ice specimens)
4. The specimen cap was forced into contact with the snow-water mixture. The excess water was released through a small hole in the cap
5. The mold and specimen were placed in a freezer maintained at a temperature of -30 ± 1°C (-22 ± 2°F) for approximately 24 h; the frozen specimen was then extruded from the mold

have been prepared using the procedures given in Table 1. The characteristics and a description of these specimens are given in Table 2.

A cohesive unfrozen soil can be subjected only to a very small tensile stress and a cohesionless soil cannot be subjected to any tensile stress. Consequently, cyclic triaxial tests on unfrozen soils are always performed with the specimen in a compressive state of stress. In contrast to this, frozen soils and ice can be subjected to relatively high tensile stresses before failing. Consequently, it is possible during strain- (or stress) controlled cyclic triaxial testing for the specimen to go into tension.

Two possible devices to couple the specimen to the cap and base to achieve a tensile state of stress were considered in the research program. The "screw" coupling shown in Fig. 5*a* consists of four screws 6.4 mm (0.25 in.) in diameter in the cap and base. The "screw and metal plate" coupling shown in Fig. 5*b* is essentially the same as the "screw" coupling except that an aluminum plate, 54 mm long (2.16 in.), 25.4 mm (1 in.) wide, and 6.4 mm (0.25 in.) thick, was attached to two of the screws in the cap and base. The clearance between the cap and the aluminum plate was set at 12.7 mm (0.50 in.).

Figure 6 shows a comparison of the hysteresis loops obtained for an ice specimen without a coupling and for an ice specimen with the "screw" and "screw and metal plate" couplings. The hysteresis loop for the specimen without a coupling is highly nonsymmetric. This is reasonable since the specimen can be subjected only to compressive stresses. The hysteresis loop for the specimen with the "screw" coupling is also highly nonsymmetric. This indicates that (1) the specimen failed, (2) the dynamic modulus in compression is much greater than that in tension, or (3) the coupling was not sufficient to resist the tensile force applied. Inspection of the specimens from the tests with this coupling indicated they had not failed. In the

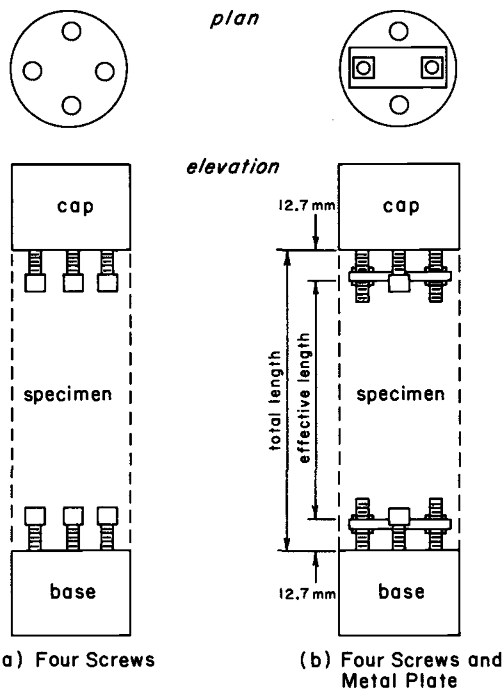

FIG. 5—*Coupling devices used in cyclic triaxial testing (1 mm = 0.04 in.).*

authors' opinion, there is no reason to believe that the modulus in tension for ice is significantly different from the modulus in compression at the low strain levels associated with cyclic triaxial testing. Thus, the hysteresis loop could not be explained on this basis. It was concluded, therefore, the coupling did not provide sufficient resistance to the tensile force.

The hysteresis loop for the specimen with the four screws and metal plate shown in Fig. 6c is symmetric and indicates that a resistance to the tensile force was developed which allowed the specimen to be subjected to a tensile stress. This coupling was selected for use in the research program. It is obvious that with the "screw and metal plate" coupling the effective length of the specimen used to calculate dynamic properties would be slightly less than the total length of the specimen. The effective length of the specimen is extremely difficult to calculate because it is dependent on the dynamic elastic moduli of the specimens. For practical purposes, the effective lengths were assumed to be 25.4 mm (1 in.) shorter than the full length, owing to a reduction of 12.7 mm (0.50 in.) from the cap and 12.7 mm (0.50 in.) from the base. If the estimate of effective length is slightly in error, it would result in only a small error in the evaluation of the dynamic modulus and axial strain. The lengths of the specimens were

TABLE 2—*Characteristics and description of frozen soil and ice specimens.*

Soil Group	Name	Identification Symbol	Unified Soil Classification	Specific Gravity of Solids	Void Ratio	Density,[a] kg/m^3	Index Properties	Description
Fine-grained	Ontonagon clay	OC	CH	2.74	1.50	1620	liquid limit = 61; plastic limit = 24	the frozen clay specimens were classified as CH, V_r [33]. They had a random orientation of ice lenses whose thicknesses varied from 0.8 to 2 mm[b]. There was a thin film of ice surrounding the specimens caused by water movement toward the outside of the specimens during the freezing process
	Montmorillonite-Ontonagon clay	MOC	CH	2.74	1.56	1660	liquid limit = 97; plastic limit = 37	
	Hanover silt	HS	ML	2.74	0.60	2030	nonplastic; D_{50} = 0.035 mm	the frozen silt specimens were classifed as ML, Nbn. There was a thin layer of silt with ice lenses surrounding the specimens
	Alaska silt	AS	ML	2.70	0.59	2090	nonplastic; D_{50} = 0.02 mm	

Dense coarse-grained	high-density Ottawa sand	OSH	SP	2.65	0.49	2000	coefficient of uniformity = 1.1; coefficient of curvature = 1.1; D_{50} = 0.7 mm	the OSH specimens were classified as Sp, Nb
Loose coarse-grained	low-density Ottawa sand	OSL	SP	2.65	3.73	1290	coefficient of uniformity = 1.1; coefficient of curvature = 1.1; D_{50} = 0.7 mm	the OSL specimens were classified as Sp, V_s. They had a transverse layered structure
Ice	low-density ice	LDI	...	...	...	770	...	the ice specimens were polycrystalline and cloudy and bubbly in appearance. There was a slight radial pattern of ice crystals visible in some specimens when they were broken apart and examined in cross section
	high-density ice	HDI	...	...	...	904	...	

NOTE—All frozen soil specimens tested were at a degree of ice saturation close to 100 percent.
[a] 1 kg/m^3 = 0.062 lb/ft^3.
[b] 1 mm = 0.04 in.

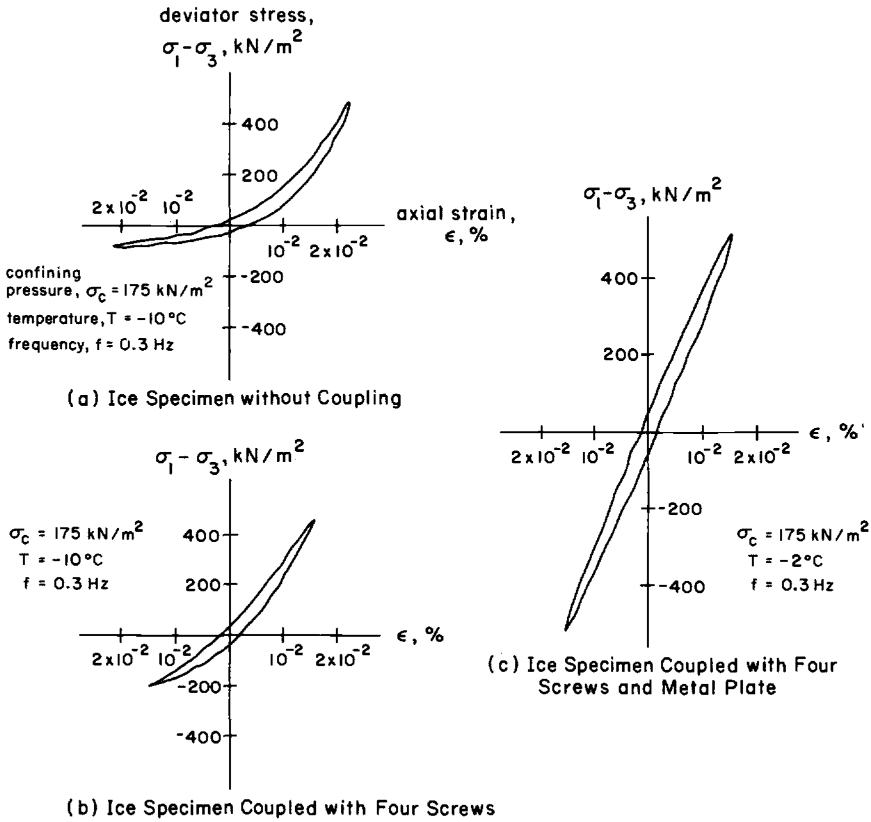

FIG. 6—*Typical hysteresis loops of ice specimens with different coupling devices (1 kN/m^2 = 0.145 psi).*

approximately 180 mm (7.2 in.) with corresponding effective lengths of 155 mm (6.2 in.). If the assumed effective length was ± 10 mm (0.4 in.) in error, the error in the dynamic modulus would be about ± 6.5 percent and in the strain about ± 7 percent.

Test Procedure

The frozen specimens were stored in a freezer at −20°C (−4°F) ± 1°C (2°F) after they were jacketed with two rubber membranes, each with a wall thickness of 0.5 mm (0.02 in.). Prior to testing, the base clamp of the antitilt device was fastened to the specimen base (see Figs. 3*d* and 5*b*). The specimen was immersed in the cold bath and the base was fastened to the load cell (see Fig. 3*b*). The antitilt device was assembled as follows:

1. The gage head body was attached to the connecting rod of the base clamp.

2. The cap clamp was fastened to the specimen cap in a position such that the screw-adjustable bearing plate on the antitilt ring bore on the probe shaft and caused the output from the LVDT to be close to zero.

3. The antitilt ring (in a horizontal position) was connected to the spring steel extending from the base clamp; the bearing plate was screw adjusted to move the probe shaft to its null (zero voltage output) position.

After the antitilt device was attached to the specimen, a collar pressing the thermistors to the side of the specimen was placed around the specimen. The aluminum triaxial cell cylinder was placed on the base plate of the cell. Finally, the top plate was tightened down on the cell cylinder and the piston loading rod was connected to the cap by inserting it through a ball-bushing loading collar. Care must be taken when attaching the piston rod. If the torque applied in tightening the piston rod is too great, the specimen will fail. After the piston rod was attached, the specimen assembly could be checked by manually applying a cyclic vertical load to the piston rod and observing the hysteresis loop. If the loop did not exhibit the symmetric shape shown in Fig. 6c the specimen assembly was not good.

The voltage output from the gage head LVDT attached across the specimen to the cap and base was the feedback signal to the servovalve controller. With the LVDT in this position, deformations associated with loose connections, elastic deformations of the piston loading rod, or the load frame were eliminated.

When the specimen assembly was satisfactory, the cold bath was covered with styrofoam and an auxiliary coolant line was placed on the top plate of the triaxial cell. A small increase in temperature was usually experienced during the installation of the specimen. Therefore, the specimens were left in the cell for at least two hours to ensure temperature equilibrium in the triaxial cell and specimen before a dynamic test was conducted. The temperature of the specimen was controlled by the mercury thermometer thermostat in the refrigeration unit. The two thermistors attached to the side of the specimen were monitored to obtain the temperature to within ± 0.1°C (0.2°F). If the temperature was not correct, the thermostat was readjusted and the test was delayed two hours to ensure that a temperature equilibrium condition was reached.

After the specimen was installed in the triaxial cell, a test was conducted employing the following procedure:

1. The LVDT in the actuator was used as the feedback signal to move the actuator ram to within 12 mm (0.5 in.) of the piston loading rod. The hydraulic power supply was turned off and a valve at the supply port of the hydraulic manifold of the actuator was closed to prevent fluid movement.

2. The feedback signal was changed from the LVDT in the actuator to the LVDT on the antitilt device. The actuator and the piston loading rod were connected with a split-ring connector, and a confining pressure of

approximately 350 kN/m² (50 psi) was applied to the specimen to prevent disturbance caused by the movement of the actuator during the reapplication of hydraulic pressure to the actuator. The servovalve stability adjustments for the closed-loop test system were strongly dependent on the strength of the specimens and "snugness" of the connection. For practical purposes, they were readjusted whenever the movement of the actuator observed on the strip-chart recorder deviated from the command sine wave form.

3. The hydraulic pressure was applied and the valve at the supply port of the hydraulic manifold was opened. The actuator was now controlled by the LVDT on the antitilt device.

4. Following Steps 1, 2, and 3 an axial load was generally induced in the specimen. This axial load was monitored on a digital voltmeter. The specimen was returned to a zero axial load (deviator stress) condition by adjusting the command signal voltage level to the LVDT on the antitilt device. The LVDT voltage output after this adjustment was nonzero. A voltage offset was used to bring the net LVDT output close to zero so it would stay "on scale" on the output recording devices.

5. The sensitivities of the recording devices were set for the range of frequencies and voltage outputs anticipated during testing. The setting for the load cell could be made from experience after testing a number of specimens.

6. The desired strain (displacement) amplitude and frequency for the test was selected. A sinusoidal wave form was selected as the command signal.

Test History Effects on Evaluation of Dynamic Properties

Owing to the number of test condition parameters to be considered when evaluating the dynamic properties of a given specimen, it was believed that as much data as possible should be collected with a single experimental setup. It was recognized, however, that the "test history" a specimen experienced might influence the dynamic properties measured. By test history is meant (1) the sequence in which the test condition parameters considered in the test program (temperature, confining pressure, frequency, strain amplitude, and number of cycles) were applied to the specimen and (2) the magnitude of the parameters considered following a given sequence. Many tests were conducted to establish an acceptable test history. The results for ice specimens may be summarized as follows:

1. Temperature: Individual specimens were tested through a range of temperatures. It was found that the dynamic properties were comparable to those of specimens tested at a single temperature if the specimens were tested from high (−1°C) (30°F) to low (−10°C) (14°F) temperature. When the tests were performed from low (−10°C) (14°F) to high (−1°C) (30°F) temperature, the specimens were disturbed, apparently at the

coupling, even if they were left in the cell at a new test temperature for 24 h prior to testing. The disturbance could be observed from the hysteresis loop. (Specifically, a loop similar to those shown in Fig. 6*a* or *b* was observed.) Melting between the specimens and the caps was found when the specimens were taken out of the cell. It was observed that if the temperature was decreased and the specimen was allowed to readjust to the new temperature for a 24-h period, it would "erase" any disturbance effects that might have occurred at the higher temperature.

2. Strain amplitude: Individual specimens were tested from low to high strain amplitude at a given confining pressure. If the specimens were retested at the lowest strain amplitude, it was observed that the damping ratio of the latter test was greater than the damping ratio of the former at the lowest strain amplitude by about 50 percent. The dynamic Young's modulus appeared to be equal in magnitude.

3. Confining pressure: When the specimens were subjected to a high confining pressure [greater than 700 kN/m^2 (100 psi)], they deformed rapidly. The rate of deformation decreased with time, and the volume of the specimens appeared to decrease, which would cause the density to increase. This effect was demonstrated by testing a specimen at a low confining pressure, subjecting it to a high confining pressure, then retesting at the low confining pressure. The dynamic Young's modulus of the specimen after it was subjected to a high confining pressure was slightly greater than the dynamic Young's modulus of the specimen before experiencing the high confining pressure. To avoid this problem, the specimens were subjected to the highest confining pressure [1400 kN/m^2 (200 psi)] used in the test sequence for at least 20 min before a test was performed. The rate of deformation of the specimens was very small for subsequent applications of confining pressure after employing this procedure.

4. Frequency: Variations in the frequencies of testing from 0.05 to 5 Hz did not appear to cause specimen disturbance.

5. Number of cycles: The dynamic properties of the specimens did not appear to be influenced by the number of cycles a specimen was subjected to provided the number of cycles of loading did not exceed approximately 20 per one test. Several specimens were found to be disturbed when they were subjected to more than 100 cycles per one test.

Based on these results, acceptable test histories for frozen specimens could be established. Acceptable test histories for ice and the frozen clay specimens tested are given in Table 3. The test sequence starts at the lowest axial strain amplitude and frequency and highest confining pressure. It proceeds with increases in frequency, then a reduction in confining pressure and frequency, followed by increases in frequency, etc. The strain amplitude is increased after the specimen is tested at the lowest confining pressure and highest frequency. The range of test conditions was chosen to include the field conditions and loadings anticipated for permafrost deposits sub-

TABLE 3—*Acceptable test histories.*

(*a*) Ice			(*b*) Frozen Clay		
Axial Strain Amplitude, ϵ_A, %	Confining Pressure,[a] σ_c, kN/m^2	Frequency, f, Hz	Axial Strain Amplitude, ϵ_A, %	Confining Pressure, σ_c, kN/m^2	Frequency, f, Hz
3×10^{-3}	→ 1400 →	0.3 → 1.0 → 5.0	3.2×10^{-3}	→ 1400 →	0.3 → 1.0 → 5.0
↓			↓		
3×10^{-3}	→ 700 →	0.3 → 1.0 → 5.0	3.2×10^{-3}	→ 700 →	0.3 → 1.0 → 5.0
↓			↓		
3×10^{-3}	→ 350 →	0.3 → 1.0 → 5.0	3.2×10^{-3}	→ 350 →	0.3 → 1.0 → 5.0
↓			↓		
3×10^{-3}	→ 175 →	0.3 → 1.0 → 5.0	3.2×10^{-3}	→ 175 →	0.3 → 1.0 → 5.0
↓			↓		
3×10^{-3}	→ 0 →	0.3 → 1.0 → 5.0	3.2×10^{-3}	→ 0 →	0.3 → 1.0 → 5.0
↓			↓		
9×10^{-3}	→ 1400 →	0.3 → 1.0 → 5.0	1.0×10^{-2}	→ 1400 →	0.3 → 1.0 → 5.0
↓			↓		
9×10^{-3}	→ 700 →	0.3 → 1.0 → 5.0	1.0×10^{-2}	→ 700 →	0.3 → 1.0 → 5.0

↓			↓		
9×10^{-3}	→ 350 →	0.3 → 1.0 → 5.0	1.0×10^{-2}	→ 350 →	0.3 → 1.0 → 5.0
↓			↓		
9×10^{-3}	→ 175 →	0.3 → 1.0 → 5.0	1.0×10^{-2}	→ 175 →	0.3 → 1.0 → 5.0
			↓		
			1.0×10^{-2}	→ 0 →	0.3 → 1.0 → 5.0
↓			↓		
2×10^{-2}	→ 1400 →	0.3 → 1.0 → 5.0	5.6×10^{-2}	→ 1400 →	0.3 → 1.0 → 5.0
↓			↓		
2×10^{-2}	→ 700 →	0.3 → 1.0 → 5.0	5.6×10^{-2}	→ 700 →	0.3 → 1.0 → 5.0
			↓		
			5.6×10^{-2}	→ 350 →	0.3 → 1.0 → 5.0
			↓		
			1.0×10^{-1}	→ 1400 →	0.3 → 1.0 → 5.0
			↓		
			1.0×10^{-1}	→ 700 →	0.3 → 1.0 → 5.0

NOTE—Testing sequence is horizontal (→), then vertical (↓).
[a] 1 kN/m^2 = 0.145 psi.

jected to strong motion earthquakes. If at any time in the sequence of testing the specimen became disturbed, it was easily recognized from the hysteresis loop. At this time the test was abandoned.

The maximum and minimum strain amplitudes of testing given in Table 3 depend on the stiffness and strength of the frozen specimen. The minimum strain amplitude of testing is associated with the lowest amplitude of displacement command signal attainable with the present test system. The maximum strain amplitude is associated with a tensile failure of the specimen or significant specimen disturbance. Before a specimen was subjected to the acceptable test history, the cell pressure was increased to 1400 kN/m^2 (200 psi) for approximately 20 min. Following this, the dynamic Young's modulus was evaluated at a strain amplitude of approximately 10^{-2} percent and a frequency of 0.3 Hz. The value obtained from this test was compared with that obtained during the course of the test history as another check on the disturbance of the specimen. If they were found to be in good agreement, the test was presumed to be acceptable.

A test procedure employing a test history sequence such as that given in Table 3 is often referred to as "multistage" testing. In contrast to this, "single-stage" tests can be employed to determine dynamic properties. In single-stage testing of frozen materials, a specimen is tested at only one strain amplitude, confining pressure, temperature, and frequency. Single-stage tests were performed on several frozen soil specimens and the results were compared with those obtained during the course of multistage testing. In all cases the dynamic properties were within 15 percent of each other, and generally much closer. An error of this magnitude could be attributable to differences in the structure of the specimens being compared and slight differences in the test temperatures.

Influence of Cycle Number on Evaluation of Dynamic Properties

It is generally believed by researchers conducting cyclic triaxial tests on unfrozen soils that the dynamic properties associated with the 5th or 10th cycle are the most appropriate for predicting ground motions during earthquakes. To assess the influence of the choice of the cycle number on dynamic properties of frozen soils and ice, the variation of the ratio (E_d at Nth cycle/E_d at 10th cycle) and (λ at Nth cycle/λ at 10th cycle) with the number of cycles at different frequencies, confining pressures, strain amplitudes, and temperature was determined. These ratios are given for ice and frozen clay specimens at 1, 5, 10, and 20 cycles in Table 4. There appears to be no significant variation in the dynamic Young's modulus with number of cycles for different frequencies, confining pressures, strain amplitudes, and temperatures. At the greatest, the dynamic Young's modulus at the Nth cycle for ice or frozen clay is approximately 6.0 percent different from the modulus at the 10th cycle. Further, the damping ratio does not appear to vary with the number of cycles for different frequencies, confining pressures, strain amplitudes, and temperatures. The damping ratio at the *N*th cycle is at the greatest about 14 percent different from the damping ratio at the 10th cycle for ice and 12 percent different from the damping ratio at the 10th cycle for clay. The damping ratios used to determine the ratios given in Table 4 were determined by planimetering the area of the hysteretic load versus displacement relationship. The error in the ratios shown associated with planimetering can be as great as 5 percent.

Typical Test Results

The dynamic properties of frozen sand (OSH), frozen clay (OC), and ice (HDI) specimens evaluated with the cyclic triaxial test system, specimen preparation techniques, and test procedure discussed in the preceding sections are presented in Fig. 7. The characteristics and a description of these specimens are given in Table 2. The results shown indicate that there is a decrease in the dynamic Young's modulus with (1) ascending temperature, (2) increasing axial strain amplitude, and (3) decreasing frequency, and an increase in damping ratio with (1) ascending temperature and, in general, with (2) increasing axial strain amplitude, and (3) decreasing frequency. The dynamic Young's modulus for the coarse-grained cohesionless soil tested and ice increased with increasing confining pressure, whereas the dynamic Young's modulus for the fine-grained soil does not change with confining pressure. Damping ratio does not change with confining pressure for the soil specimens tested. The relationship between damping ratio and confining pressure for ice specimens is not clearly defined at this time. The values of the dynamic Young's modulus for the soil specimens in the frozen state are approximately two orders of magnitude greater than the values of the dynamic Young's modulus for the materials in the unfrozen state. The values of damping ratio for the materials in the frozen state are close to the values of damping ratio for the materials in the unfrozen state. A phenomenological explanation of the results obtained is outside the scope of this paper. The interested reader is referred to Vinson and Chaichanavong [*34*] and Vinson et al [*35*] for this discussion.

Conclusions and Application of Test Results to Development of Standard Test Procedure

A testing system and test methods have been developed to evaluate dynamic properties of frozen soils over a range of test conditions which simulate earthquake loadings of permafrost deposits. Several aspects of the work described herein warrant emphasis, namely:

1. Displacements of the specimen during cyclic loading were measured across the specimen cap and base; this eliminated errors in the displace-

TABLE 4—*Influence of cycle number on evaluation of dynamic properties.*

(*a*) Dynamic Properties of Ice

Variable	Temperature, T °C	Axial Strain Amplitude, ϵ_A %	Confining Pressure, σ_c kN/m^2	Frequency, f Hz	$\frac{E_d \text{ at } N\text{th cycle}}{E_d \text{ at 10th cycle}}$ Cycle Number, N 1	5	10	20	$\frac{\lambda \text{ at } N\text{th cycle}}{\lambda \text{ at 10th cycle}}$ Cycle Number, N 1	5	10	20
Frequency	−4	0.00287	350	0.05	0.988	1.003	1.0	0.995	0.909	0.860	1.0	0.871
	−4	0.00287	350	0.3	1.035	1.014	1.0	1.020	1.029	1.035	1.0	0.994
	−4	0.00287	350	1.0	0.981	1.012	1.0	1.024	...	...	...	...
	−4	0.00287	350	5.0	1.002	1.008	1.0	0.989	...	...	...	...
Confining pressure	−4	0.00287	1400	0.3	0.992	1.014	1.0	1.015	0.944	0.958	1.0	1.007
	−4	0.00287	350	0.3	1.035	1.014	1.0	1.020	1.029	1.035	1.0	0.994
	−4	0.00287	0	0.3	1.033	1.001	1.0	0.987	0.970	0.965	1.0	0.970
Strain amplitude	−4	0.00127	1400	0.3	1.015	1.038	1.0	1.063	0.990	0.962	1.0	0.942
	−4	0.00287	1400	0.3	0.992	1.015	1.0	1.014	0.944	0.958	1.0	1.007
	−4	0.0093	1400	0.3	1.005	1.003	1.0	1.005	0.973	0.965	1.0	1.013
	−4	0.0192	1400	0.3	0.996	0.995	1.0	0.984	0.996	1.021	1.0	1.000
Temperature	−1	0.00287	350	0.3	1.000	1.008	1.0	1.013	0.955	0.977	1.0	1.008
	−4	0.00287	350	0.3	0.992	1.015	1.0	1.014	1.029	1.035	1.0	0.994
	−10	0.00287	350	0.3	1.034	1.011	1.0	1.019	1.103	1.000	1.0	1.046

(*b*) Dynamic Properties of Frozen Ontonagon Clay

Frequency	−4	0.01	350	0.05	0.987	1.000	1.0	0.996	1.075	0.987	1.0	0.965
	−4	0.01	350	0.3	1.004	1.019	1.0	0.989	0.953	0.985	1.0	1.031
	−4	0.01	350	1.0	1.009	1.005	1.0	1.019	...	...	...	...
	−4	0.01	350	5.0	0.987	0.996	1.0	1.000	...	...	...	...
Confining Pressure	−4	0.01	0	0.3	1.009	1.005	1.0	1.001				
	−4	0.01	175	0.3	1.004	0.995	1.0	0.989	0.992	0.969	1.0	1.016
	−4	0.01	350	0.3	1.004	1.019	1.0	0.989	0.953	0.985	1.0	1.031
	−4	0.01	700	0.3	1.019	0.995	1.0	0.987	1.022	1.000	1.0	1.029
	−4	0.01	1400	0.3	1.012	1.000	1.0	1.000	1.028	0.986	1.0	0.979
Strain amplitude	−4	0.00316	350/700[b]	0.3	0.993	0.993	1.0	0.980	1.022	1.022	1.0	1.055
	−4	0.01	350/700	0.3	1.004	1.019	1.0	0.989	1.022	1.000	1.0	1.029
	−4	0.056	350/700	0.3	1.025	1.000	1.0	0.994	1.000	1.000	1.0	1.000
	−4	0.10	350/700	0.3					1.122	1.000	1.0	0.977
Temperature	−1	0.01	350	0.3	1.018	1.009	1.0	0.999	0.957	1.000	1.0	1.000
	−4	0.01	350	0.3	1.004	1.019	1.0	0.989	0.953	0.985	1.0	1.031
	−10	0.01	350	0.3	1.010	1.012	1.0	0.995	1.114	1.000	1.0	1.029

[a] 1 kN/m^2 = 0.145 psi.

[b] The variation of the ratio (E_d at the Nth cycle/E_d at the 10th cycle) was evaluated at σ_c = 350 kN/m^2 whereas (λ at the Nth cycle/λ at 10th cycle) was evaluated at σ_c = 700 kN/m^2.

°C = $\frac{5}{9}$ (°F − 32).

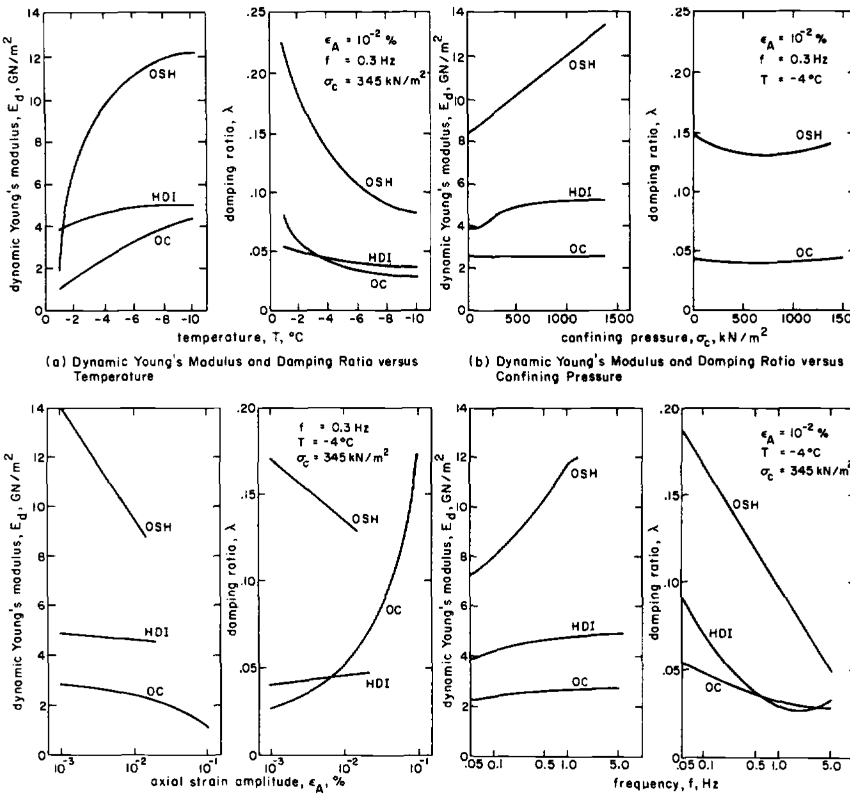

(a) Dynamic Young's Modulus and Damping Ratio versus Temperature

(b) Dynamic Young's Modulus and Damping Ratio versus Confining Pressure

(c) Dynamic Young's Modulus and Damping Ratio versus Axial Strain Amplitude

(d) Dynamic Young's Modulus and Damping Ratio versus Frequency

FIG. 7—*Dynamic properties of frozen sand, frozen clay, and ice.*

ment measurement associated with deformations in the load train and load frame.

2. Measurement across the cap and base was accomplished by mounting an LVDT at the side of the specimen to the cap and base; an antitilt device (see Fig. 3*d*) was used to eliminate any error in the displacement measurement associated with tilt of the specimen cap or base.

3. A coupling device was used to allow the specimen to be subjected to a tensile state of stress (see Fig. 5*b*) during the extension cycle of loading; if this device was not used, incorrect test results were obtained.

4. During the latter stages of development of the test system, a minicomputer was used to reduce the experimental data; this afforded substantial time savings in the data reduction effort.

5. "Multi-stage" testing of frozen soil specimens is necessary if all of the field or test condition parameters or both are to be considered; the

sequence in which the various physical parameters considered in the test program and the magnitude of the parameters considered following a given sequence can be established in a preliminary test program.

At present there is no standard test procedure to evaluate dynamic properties of frozen soils under simulated earthquake loading conditions. The material presented herein provides a basis for the development of a standard test procedure. There are several test variables yet to be investigated, however, before a standard procedure can be recommended. These include:

1. Influence of the specimen height-to-diameter ratio on measured soil properties,
2. Influence of coupling device on measured soil properties,
3. Influence of specimen preparation technique on measured soil properties,
4. Influence of the thermal history a specimen is subjected to prior to testing on measured soil properties,
5. Time-dependence of dynamic properties of frozen soils, and
6. Relationship between the dynamic properties of artificially frozen soils and those of naturally frozen soils.

Finally, there are several cases cited in the literature where observed unfrozen ground response during earthquake loadings has been compared with the ground response predicted with presently available analytic techniques using soil properties measured in the laboratory. The comparisons are quite favorable, which would tend to support both the use of the analytic techniques and the soil properties measured in the laboratory. Similar comparisons have not been made for permafrost deposits subjected to earthquake loadings. A favorable comparison represents the ultimate validation of a recommended standard test procedure to evaluate dynamic properties of frozen soils.

Acknowledgments

The studies described herein were supported by Grant No. ENG74-13506 from the National Science Foundation for the project entitled "Shear Moduli and Damping Factors in Frozen Soils." The support of the Foundation is gratefully acknowledged.

References

[1] Meyers, H., "A Historical Summary of Earthquake Epicenters in and Near Alaska," NOAA Technical Memorandum EDS NGSDC-1 April 1976.

[2] Brown, R. J. E. and Pewe, T. L. in *Proceedings*, North American Contribution to the Second International Conference on Permafrost, National Academy of Science, 1973, pp. 91–100.

[3] Barnes, D. F. in *Proceedings*, First International Conference on Permafrost, National Academy of Sciences, National Research Council, Publication No. 1287, 1963, pp. 349–355.

[4] Bell, R. A. I., *Journal of Glaciology*, Vol. 6, No. 44, 1966, pp. 209–221.
[5] Gagne, R. M. and Hunter, J. A. M., Geological Survey of Canada, Paper 75-1B, 1975, pp. 13–18.
[6] Hobson, G. D., Report of Activities Nov. 1965 to April 1966, Geological Survey of Canada Paper 66-2, Ottawa, 1966, pp. 10–14.
[7] Hobson, G. D., *Geophysics*, Vol. 27, No. 2, 1962, pp. 253–273.
[8] Hunter, J. A. M. in *Proceedings*, North American Contribution to the Second International Conference on Permafrost, National Academy of Science, 1973, pp. 527–535.
[9] Hunter, J. A. M., Geological Survey of Canada, Paper 74-1, Part B, 1974, pp. 89–90.
[10] McGinnis, L. D., Nakao, K., and Clark, C. C. in *Proceedings*, North American Contribution to the Second International Conference on Permafrost, National Academy of Science, 1973, pp. 136–146.
[11] Roethlisberger, H., "Applicability of Seismic Refraction Soundings in Permafrost Near Thule, Greenland," Technical Report 81, United States Army Cold Regions Research and Engineering Laboratory, Hanover, N.H., Feb. 1961.
[12] Roethlisberger, H., "Seismic Exploration in Cold Regions," Technical Monograph II-A2a, United States Army Cold Regions Research and Engineering Laboratory, Hanover, N.H., Oct. 1972.
[13] Woolson, J. R., "Seismic and Gravity Surveys of Naval Petroleum Reserve No. 4 and Adjoining Areas, Alaska," U. S. Geological Survey, Professional Paper 304-A, 1963.
[14] Kaplar, C. W. in *Proceedings*, Permafrost International Conference, National Academy of Sciences, National Research Council Publication No. 1287, 1963, pp. 293–301.
[15] Kaplar, C. W., "Laboratory Determination of Dynamic Moduli of Frozen Soils and of Ice," Research Report 163, United States Army Cold Regions Research and Engineering Laboratory, Hanover, N.H., Jan. 1969.
[16] Dzhurik, V. I. and Leshchikov, F. H. in *Proceedings*, 2nd International Conference on Permafrost, Yakutsk, USSR, 1973, pp. 387–404.
[17] Inoue, M. and Kinosita, S., *Low Temperature Science, Series A, Physical Sciences*, Vol. 33, 1975, pp. 243–253.
[18] Khazin, B. G. and Goncharov, B. V., *Soil Mechanics and Foundation Engineering*, Vol. 11, No. 2, March-April, 1974, pp. 122–125.
[19] King, M. S., Bamford, T. S., and Kurfurst, P. J. in *Proceedings*, Symposium on Permafrost Geophysics, Calgary, Feb. 1974, pp. 35–42.
[20] Kurfurst, P. J., *Canadian Journal of Earth Sciences*, Vol. 13, 1976, pp. 1571–1576.
[21] Müller, G., *Gefreirshachten Geophysical Prospecting*, Vol. 9, No. 2, 1961, pp. 276–295.
[22] Nakano, Y. and Arnold, R., *Journal of Water Resources Research*, Vol. 9, No. 1, Feb. 1973, pp. 178–184.
[23] Nakano, Y., and Froula, N. H. in *Proceedings*, North American Contribution to the Second International Conference on Permafrost, National Academy of Science, 1973, pp. 359–369.
[24] Nakano, Y., Martin, R. J., and Smith, M., *Journal of Water Resources Research*, Vol. 8, No. 4, Aug. 1972, pp. 1024–1030.
[25] Zykov, Y. D. and Baulin, I. in *Proceedings*, 2nd International Conference on Permafrost, Yakutsk, USSR, Vol. 6, 1973.
[26] Stevens, H. W. in *Proceedings*, North American Contribution to the Second International Conference on Permafrost, National Academy of Sciences, 1973, pp. 400–409.
[27] Stevens, H. W., "The Response of Frozen Soils to Vibratory Loads," Technical Report 265, United States Army Cold Regions Research and Engineering Laboratory, Hanover, N.H., June 1975.
[28] Terzaghi, K., *Journal of the Boston Society of Civil Engineers*, Jan. 1952.
[29] Vinson, T. S. in *Geotechnical Engineering in Cold Regions*, Andersland and Anderson, Ed., McGraw-Hill, New York, 1978, Chapter 8.
[30] Seed, H. B. and Peacock, W. H., *Journal of the Soil Mechanics and Foundations Division*, American Society of Civil Engineers, Vol. 97, No. SM8, Aug. 1971, pp. 1099–1119.
[31] Seed, H. B. and Idriss, I. M., "Soil Modulus and Damping Factors for Dynamic Response Analyses," Report No. EERC 70-10, Earthquake Engineering Research Center, University of California, Berkeley, Dec. 1970.

[32] Johnson, H. C. in *Proceedings*, National Conference on Fluid Power, Vol. 18, Chicago, Oct. 1964, pp. 2–8.
[33] Linell, K. A. and Kaplar, C. W., "Description and Classification of Frozen Soils," Technical Report 150, United States Army Cold Regions Research and Engineering Laboratory, Hanover, N.H., Aug. 1966.
[34] Vinson, T. S. and Chaichanavong, T., "Dynamic Properties of Ice and Frozen Clay Under Cyclic Triaxial Loading Conditions," Report No. MSU-CE-76-4, Division of Engineering Research, Michigan State University, Lansing, Mich., Oct. 1976.
[35] Vinson, T. S., Czajkowski, R., and Li, J., "Dynamic Properties of Frozen Cohesionless Soils Under Cyclic Triaxial Loading Conditions," Report No. MSU-CE-77-1, Division of Engineering Research, Michigan State University, Lansing, Mich., Jan. 1977.

B. C. Haimson[1]

Effect of Cyclic Loading on Rock

REFERENCE: Haimson, B. C., "**Effect of Cyclic Loading on Rock,**" *Dynamic Geotechnical Testing, ASTM STP 654,* American Society for Testing and Materials, 1978, pp. 228–245.

ABSTRACT: Hard rocks are significantly weakened or fatigued when subjected to cyclic loading. In uniaxial tension and in uniaxial compression the fatigue strength for 10^5 cycles is 60 to 80 percent of the monotonic strength. In triaxial compression the fatigue strength rises as the confining pressure is increased. By far the most damaging cyclic load is the tension-compression type, its fatigue strength reaching 25 percent of the monotonic tensile strength. The strain-time behavior is not unlike that observed in static creep, with primary, steady-state, and tertiary stages. The accumulated cyclic creep in uniaxial compression for different upper peak cyclic stresses appears to be bounded by the complete stress-strain curve. Acoustic emission and specimen photomicrography suggest microfracturing as the principal mechanism of fatigue failure, with distinct differences between cyclic compression and cyclic tension. Acoustic emission is an excellent precursor of imminent cyclic failure. ASTM standardization of cyclic testing is recommended.

KEY WORDS: rocks, rock mechanical testing, rock fatigue, acoustic emission, cyclic compression, cyclic tension, cyclic tension-compression

The phenomenon of static fatigue—premature failure due to prolonged constant loading—has been observed in rock during creep testing, and subsequently has been taken into consideration in the design of structures in rock salt and other time-dependent rocks. However, the phenomenon of dynamic (cyclic) fatigue—premature failure due to cyclic or repetitive loading—has been all but ignored in rock despite growing evidence that such strength weakening is found in many man-made materials, and notwithstanding the common occurrence of such loading. Earthquakes, blasting, drilling, and traffic are but some of the sources of cyclic loading. Better understanding of the cyclic loading effect on rock could assist the engineer and scientist in a number of ways: toward improving rational design of rock structures, aid in earthquake prediction and control, and advance rock breaking methods.

[1]Professor of rock mechanics, Department of Mineral Engineering, University of Wisconsin, Madison, Wis. 53706

Very little research on cyclic loading in rock was published prior to this decade [*1,2*].[2] The most important work has been carried out since 1970. Hardy and Chugh [*3*] detected cyclic fatigue in three rock types under uniaxial compression. Saint-Leu and Sirieys [*4*] and Attewell and Farmer [*5*] emphasized in their studies rock deformational behavior under cyclic uniaxial compression.

At the University of Wisconsin we embarked in 1969 on a comprehensive investigation of the effect of cyclic loading on rock under uniaxial compression, uniaxial tension, triaxial compression, and uniaxial tension-compression, basically covering the more common loading modes [*6–14*]. The effect of repetitive stresses on strength, deformation, fabric, and acoustic emission were investigated in four rock types. This paper presents the major results of our research and points up how they can be applied in general, and with particular reference to developing new ASTM standards.

Experimental Program and Equipment

Four hard rock types (Tennessee marble, Indiana limestone, Berea sandstone, Westerly granite) were tested under uniaxial cyclic compression and uniaxial cyclic tension; one rock type (Westerly granite) was also tested under triaxial cyclic compression and uniaxial cyclic tension-compression. In each rock, specimens were cored in the same direction out of one block to prevent variability due to anisotropy or inhomogeneity. Specimen preparation followed the ASTM Test for Unconfined Compressive Strength of Intack Rock Core Specimens (D 2930-71a). However, specimen size was kept at 2.5 cm (1 in.) diameter and 6.3 cm (2.5 in.) long. A servo-controlled loading machine was used throughout.

In uniaxial cyclic compression tests, specimens were placed between a fixed platen and a platen connected to the loading machine through a swivel head. In uniaxial cyclic tension and in uniaxial cyclic tension-compression tests, specimens were epoxy cemented at both ends to threaded end-caps, carefully maintaining concentricity. The top end-cap was rigidly attached to the crosshead of the loading machine and the bottom end-cap fit loosely into a pot filled with "woods-metal," a material whose melting point is 70°C (158°F) (Fig. 1). By keeping the woods-metal in the liquid state when installing the specimen and then freezing it in position, alignment was ensured. Results indicate that very little bending took place since in most of the tests tensile rupture occurred away from specimen ends. The triaxial cyclic compression tests were run in a pressure-cell which enabled the confining oil to maintain its volume approximately constant throughout the vertical load fluctuations, thus keeping the horizontal pressure within ± 5 percent of its predetermined value. Specimens were kept dry using heat-shrinkable tubing jackets.

[2]The italic numbers in brackets refer to the list of references appended to this paper.

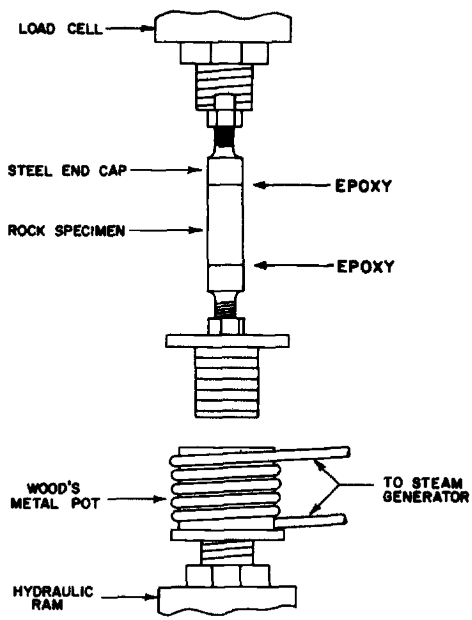

FIG. 1—*Jig for cyclic uniaxial tension.*

In each of the four loading configurations the basic cycle was stress-controlled (that is, stress was the independent variable), triangular in shape, and had a frequency of 1 Hz (equivalent to the frequency of large events in earthquakes and blasting). The lower peak stress was kept constant throughout the testing, at approximately 60 000 kPa (600 bars) compression in the cyclic tension-compression tests, and near zero in the other loading configurations. The upper peak stress was varied between tests. The number of loading cycles per test was limited to 10^5 or more. Strain was measured using strain-gage-instrumented cantilevers or linear variable differential transformers (LVDT's).

A Dunegan 3000 acoustic emission (AE) detecting system was used for monitoring acoustic signals during testing. It consisted of a pickup transducer (usually glued to the upper end-cap of specimen), a preamplifier, a speaker for audio monitoring, a band-pass filter set in our tests at 0.1 to 1 MHz, an amplifier, an outlet for oscilloscopic recording, a digital counter of events of amplitude higher than a set threshold, a digital-to-analog converter, and an oscillographic plotter. The latter was used to record accumulated events or noise rate versus time. A block diagram of the AE system is shown in Fig. 2.

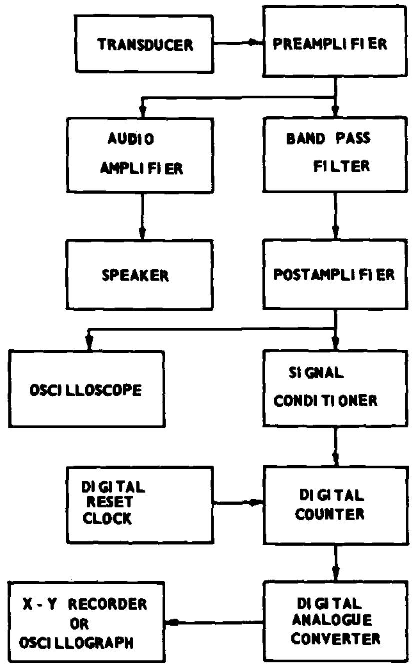

FIG. 2—*Block diagram of AE system.*

Cyclic Uniaxial Compression

The effect of cyclic uniaxial compression loading on rock strength appears to be rather significant. *S-N* curves showing the number of cycles (*N*) required to fail a specimen loaded to a certain upper peak stress (*S*) are illustrative of the continuous weakening of rock with the increase in number of cycles [*10*] (Figs. 3,4). This so-called fatigue effect is observed in each of the four rocks tested [*10,13*] (Fig. 5). The fatigue strength for the maximum number of cycles used varied between 60 and 80 percent of the respective uniaxial compression strength (C_o) as obtained by the ASTM Test D 2930-71a. This important result should be kept in mind when using values of laboratory-determined uniaxial compressive strengths in rock structure design.

The cyclic stress-strain behavior has been recorded in all four rocks. The common characteristic is the large hysteresis in the first cycle, followed by decreasing loops in the next few cycles, a narrowing of the loop to an almost constant shape in the following groups of cycles, and a reopening of the loops in the last cycles prior to failure [*10,13*] (Fig. 6). In very short

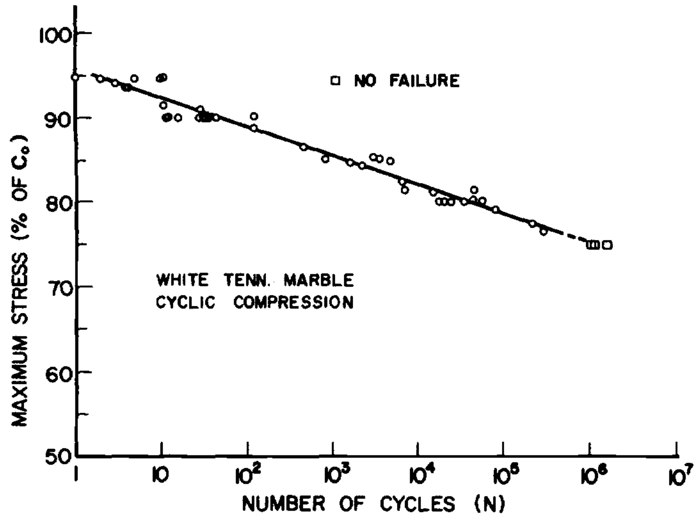

FIG. 3—*Experimental results and* S-N *curve for Tennessee marble under cyclic uniaxial compression* (C_0 *is the static uniaxial compressive strength*).

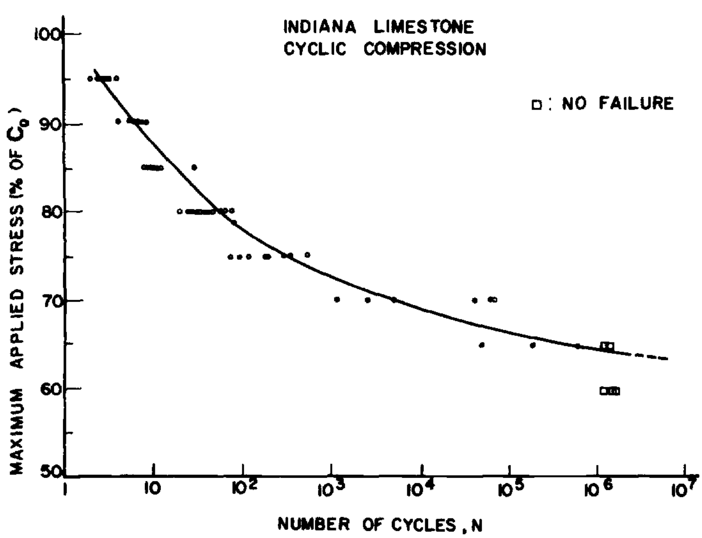

FIG. 4—*Experimental results and* S-N *curve for Indiana limestone under cyclic uniaxial compression* (C_0 *is the static uniaxial compressive strength*).

life tests (1 to 20 cycles), only the first and the last stages are apparent (Fig. 7).

The phenomenon of cyclic creep is generally observed in all loading types. For every stress level within the stress range of the cyclic loading, the strain

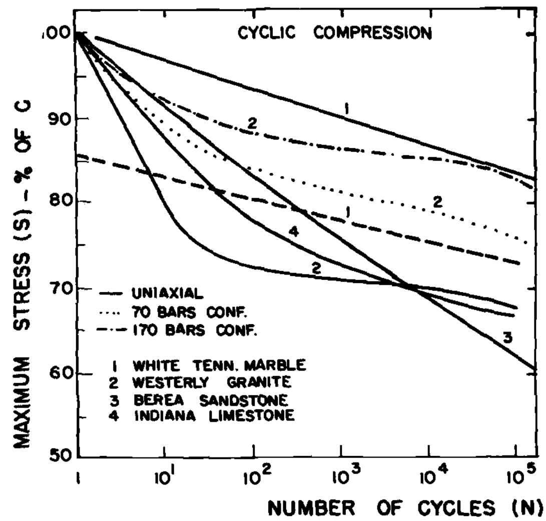

FIG. 5—*Average S-N curves in cyclic uniaxial and triaxial compression in terms of percentage of normalized monotonic compressive strength* (C) *(1 bar = 100 kPa).*

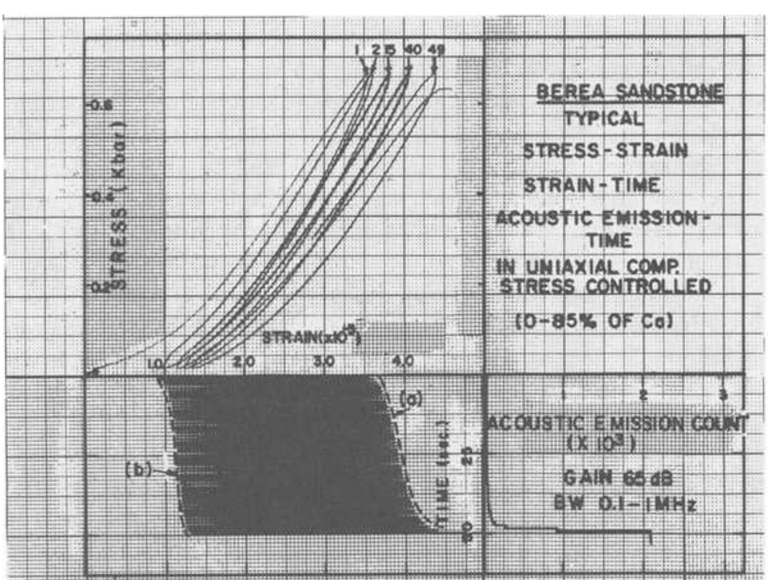

FIG. 6—*Typical stress-strain, strain-time, and cumulative AE behavior in rock under cyclic compression. Lines* (a) *and* (b) *outlining the curves shaped by the upper and lower peaks, respectively, of the strain-time cycles closely resemble static creep curves (1 kbar = 100 MPa).*

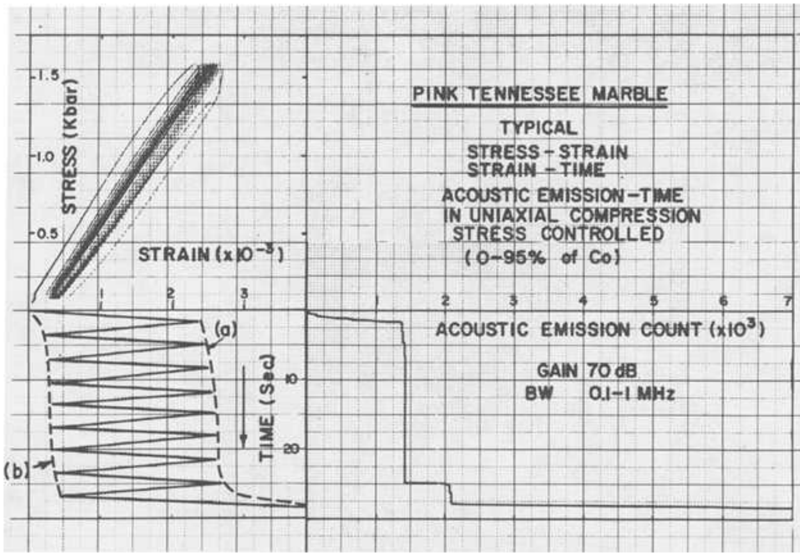

FIG. 7—*Typical stress-strain, strain-time, and cumulative AE behavior in rock under short-life cyclic compression. Lines* (a) *and* (b) *outlining the curves shaped by the upper and lower peaks, respectively, of the strain-time cycles closely resemble static creep curves (1 kbar = 100 MPa).*

increases with each cycle. Three cyclic creep stages are observed, directly related to the hysteresis loops: a primary stage in which the strain increases from cycle to cycle at a decelerating rate, followed by a steady stage of linear strain increase, and culminating in an accelerated strain increase stage up to failure. The line connecting all the peak strain points in a strain-time plot closely resembles that of a static creep curve (Figs. 6,7). The lower peak strain points define the amount of permanent deformation after each cycle. It is interesting to note that the permanent deformation after the first cycle is often 30 to 70 percent of the total permanent deformation just before failure. Hence, by loading a given rock through one cycle only, a fairly good estimate can be made of the total permissible permanent deformation. This could be used in conjunction with strain monitoring in rock structures to obtain a precursor of impending failure.

The cyclic creep of the upper peak strain between the first and the last cycles prior to failure was carefully measured in all the rocks loaded in uniaxial compression [*10,13*]. Invaribly the cyclic creep was found to be bounded by the complete stress-strain curve of the respective rock (for example, Fig. 8). This result is significant in that it reinforces the suggestion that the complete stress-strain curve defines for any stress level the range of allowable strain (bounded between the ascending and the descending portions of the curve). This important conclusion could be advantageously

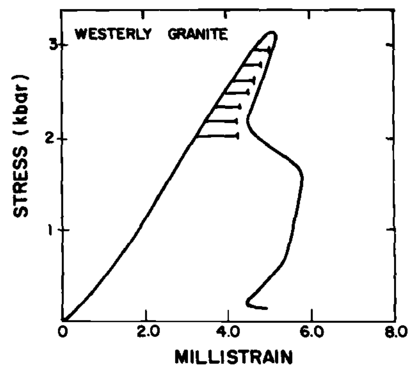

FIG. 8—*Complete stress-strain curve for Westerly granite in uniaxial compression and average cyclic creep of upper peak strains under cyclic loading (1 kbar = 100 MPa).*

used in structure design. Determining the complete stress-strain curve for a rock [*15*] is considerably less time-consuming than preparing an *S*-*N* curve. Monitoring the amount of accumulated strain at a particular stress level (whether in a laboratory specimen or an underground structure) and comparing it with the allowable quantity from the complete stress-strain curve could establish the stability condition and provide an estimate of the amount of cyclic loading that the rock can still withstand. The shape of the complete stress-strain curve could indicate the ranges of maximum stress for which the rock is more susceptible to fatigue effects. These are the regions of minimum allowable permanent strain, usually caused by the portions of the descending stress-strain curve having positive slopes. Such is, for example, the case of Westerly granite, whose *S*-*N* curve for uniaxial compression shows a very strong fatigue effect in the top 30 percent of the stress range corresponding to its positively sloped portion of the descending complete stress-strain curve [*13*] (Figs. 5,8). Below this, the slope of the descending stress-strain curve becomes negative and the number of cycles required to bring about fatigue failure increases considerably.

Using an AE system, microseismic activity was usually detected in the very first loading cycle since the upper peak load was always above the region of linear elastic behavior. In the next few cycles the acoustic emission continued to increase at a decelerating rate. During the steady-state stage, almost no new events were recorded. As fatigue failure was approached, the seismic activity picked up considerably, providing a valuable warning of incipient failure [*10,13*] (Figs. 6,7). This result strongly indicates that the deformational behavior and the mechanism of cyclic fatigue are determined by microfracturing, from which the acoustic emission emanates.

Photomicrography studies of selected specimens removed from the testing machine at different stages of cyclic loading supported the strong indications from deformation and AE results that cyclic fatigue is the result of a microfracturing process [10]. Fabric changes in uniaxial compression appeared to be dominated by grain boundary loosening and intergranular cracking in the first few cycles, followed by a stage at which no additional damage seemed to occur, although some crack extension probably did take place. Finally, crack coalescence, widening, and faulting resulting in fatigue failure were observed. The entire process of cumulative damage appeared to be evenly distributed throughout the entire specimen.

Cyclic Triaxial Compression

The behavior of Westerly granite subjected to cyclic triaxial compression (axial cyclic loading with constant confining pressure) is similar in every respect to that under uniaxial compression [13]. Figure 5 shows the *S-N* curves for Westerly granite under 7000 and 17 000 kPa (70 and 170 bars) confining pressure. The shape of the curve remains basically the same. The fatigue strength, however, increases from 65 percent in uniaxial loading to 75 percent at 7000 kPa (70 bars) and to 80 percent at 17 000 kPa (170 bars). In each case the percentage is of the respective compressive strength (*C*).

A typical stress-versus-time and AE rate in a test under triaxial compression is shown in Fig. 9. After an initial burst of emission in the first cycle (not shown), almost no activity is noticed until the last stage of the cyclic loading prior to failure. The noise rate appears to gradually increase as the last cycle to failure is approached [11]. This behavior could be utilized in field situations by monitoring acoustic emission in order to predict imminent failure.

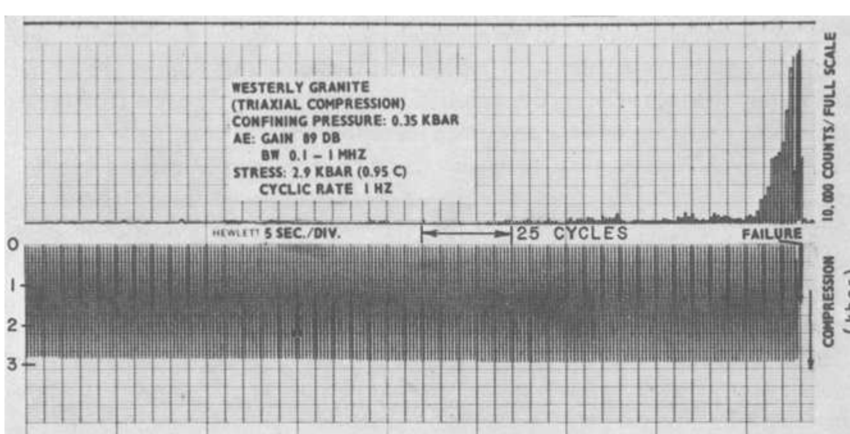

FIG. 9—*Typical AE rate versus time and stress versus time records in cyclic triaxial compression (AE = acoustic emission; BW = bandwidth) (1 kbar = 100 MPa).*

Cyclic Uniaxial Tension

All four rock types exhibited clear fatigue characteristics in uniaxial tension. The *S-N* curves for all rocks were linear and were represented approximately by the equation $S = 100 - 7 \log N$. They all showed a fatigue strength of approximately 65 percent of the monotonic strength at 10^5 cycles [*9,12*]. The *S-N* curve for Westerly granite is shown in Fig. 10.

A typical stress-strain curve in cyclic uniaxial tension is shown in Fig. 11. Its characteristics are a strongly nonlinear slope during the first loading cycle, a large permanent deformation after the first cycle (about 50 percent of the total permanent set), a straightening of the loading portion of the following cycles, and little change prior to final rupture. The latter observation could be due to a localized mechanism of crack extension to failure.

Acoustic emission followed the trend established in cyclic compression, with events recorded mainly in the first cycle, little or no emission during the bulk of the cycles (steady-state stage), and an increase in acoustic events in the last cycles prior to tensile rupture (Fig. 12). The number of cycles before failure during which acoustic emission was detected and the number of counts per cycle for the same rock (Westerly granite) are clearly fewer than in cyclic compression [*11*]. This is again interpreted as an indication that cyclic tensile failure is due to just one or a few microcracks (oriented normal to the tensile force direction) reaching their critical length beyond which they propagate until rock ruptures. Photomicrography has confirmed this indication. Other than the close vicinity of the tensile rupture plane, created apparently by the propagation of one critical crack, no

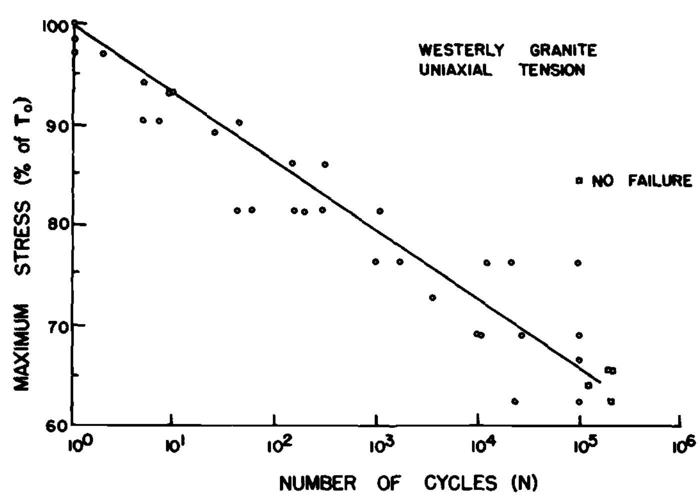

FIG. 10—*Experiment results and* S-N *curve for Westerly granite under cyclic uniaxial tension.*

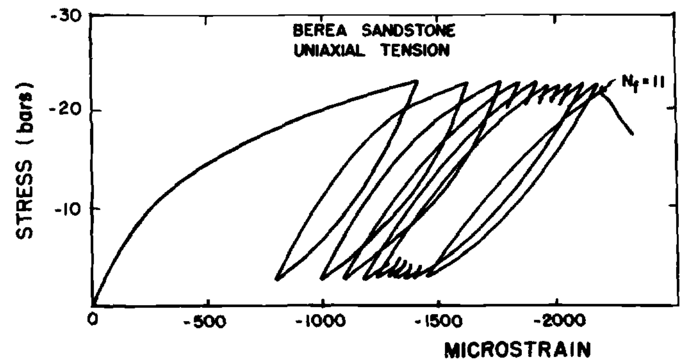

FIG. 11—*Typical stress-strain curve in uniaxial tension (1 bar = 100 kPa).*

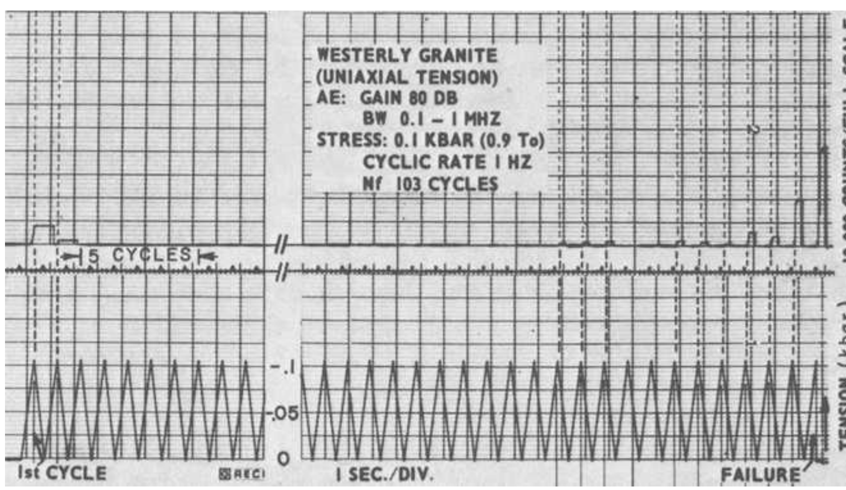

FIG. 12—*Typical AE rate versus time and stress versus time records in cyclic uniaxial tension—Westerly granite.* (N_f = *Number of cycles to failure*) *(1 kbar = 100 MPa).*

changes were observed in the internal structure of the rock [*9,12*]. In cyclic compression, on the other hand, both acoustic emission and photomicrography indicate that failure is a result of microfracture activity throughout the specimen [*10*]. In the more extreme case of cyclic tension applied to pink Tennessee marble, no warning whatsoever is given by the acoustic emission [*11*] (Fig. 13). Counts are recorded only in the first few cycles and in the failure cycle itself.

Cyclic Uniaxial Tension-Compression

The effect of cyclic compression on tensile fatigue in Westerly granite

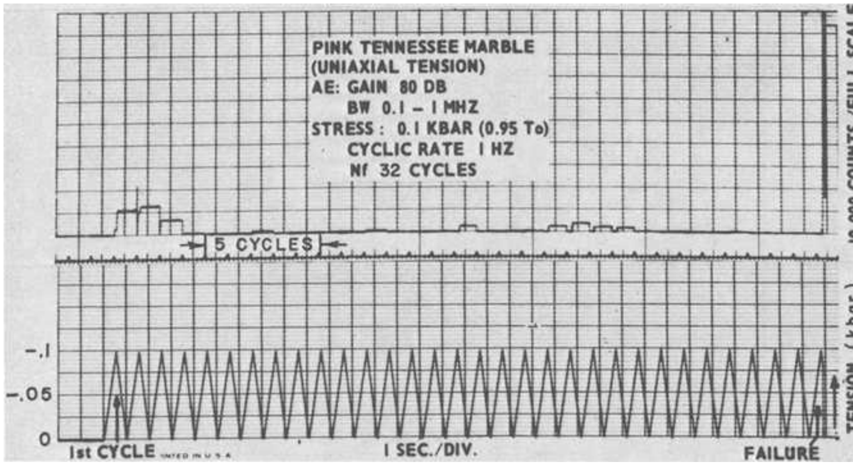

FIG. 13—*Typical AE rate versus time and stress versus time records in cyclic uniaxial tension—pink Tennessee marble (1 kbar = 100 MPa).*

was studied by applying a tension-compression cyclic load with the tension peak at 90 percent of the tensile strength (T_o) and the compression peak varying from test to test but kept within 0 to 20 percent of the compressive strength (C_o) [*12*]. Figure 12 shows the AE rate when the compression peak is zero (uniaxial tension). Figure 14 displays the AE rate for the case when the compression peak equals the tension peak ($\cong$ 3 percent of C_o). The emission rate in both cases is very similar: a burst in the first cycle, some activity in the next few cycles, and another burst in the last very few cycles. As the compression peak is increased, however, a marked increase in acoustic emission is observed, although the tension peak is still at the same level of 90 percent T_o. Figure 15 shows the AE rate when the compression peak is about 20 percent of C_o (well below the level of dilatancy onset in uniaxial compression). Acoustic emission was recorded in every cycle with a gradual increase in counts well before failure. Although emission occurred only near the tension peak, it was evident that it was affected by the compression loading. The peak compression load was low and could not have caused any shear microcracking, but it sufficiently aided the tensile crack opening mechanism to yield tangible acoustic emission during each and every cycle and bring about rapid fatigue failure. This cyclic behavior of rock could be exploited to facilitate drilling or breaking of rock, since it appears to be the most damaging type of loading.

An *S-N* curve for cyclic uniaxial tension-compression was obtained for a constant-compression cyclic peak [60 000 kPa (600 bars)] and a tension peak that varied from test to test. The linear relationship obtained (Fig. 16) exhibits by far the worst weakening effect of any cyclic load type tested. The fatigue strength at 10^5 cycles is no more than 25 percent of T_o [*12*].

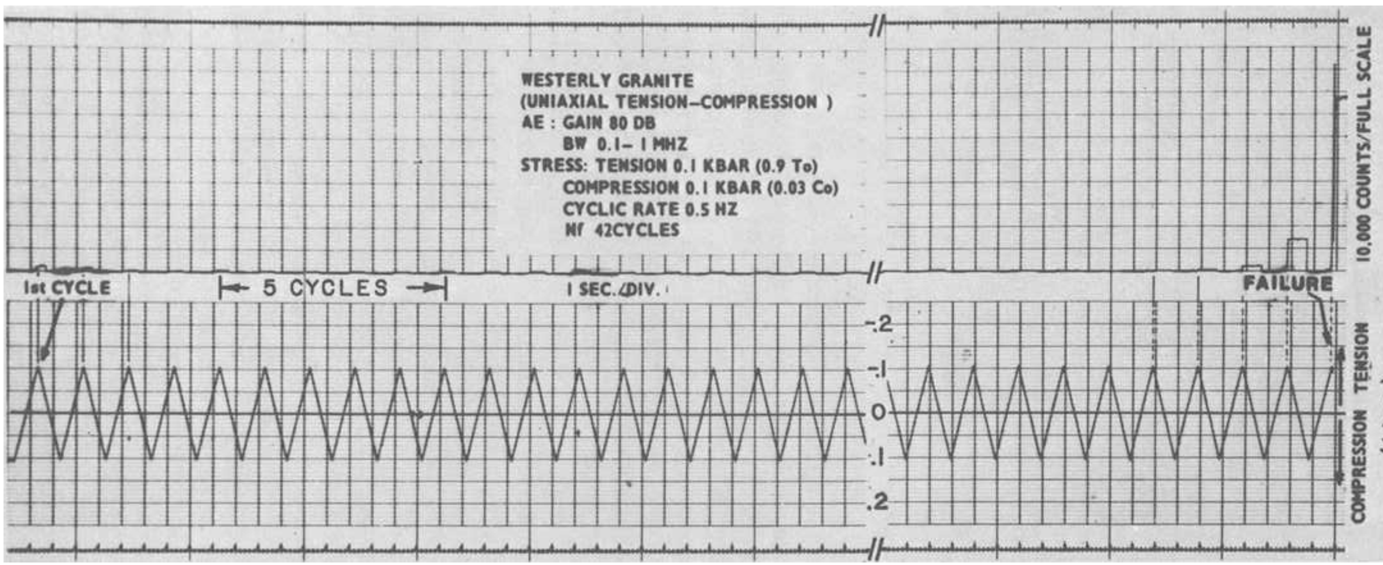

FIG. 14—*Typical AE rate versus time and stress versus time records in cyclic uniaxial tension-compression (loading ratio: tension = 1/compression = 1)—Westerly granite (1 kbar = 100 MPa).*

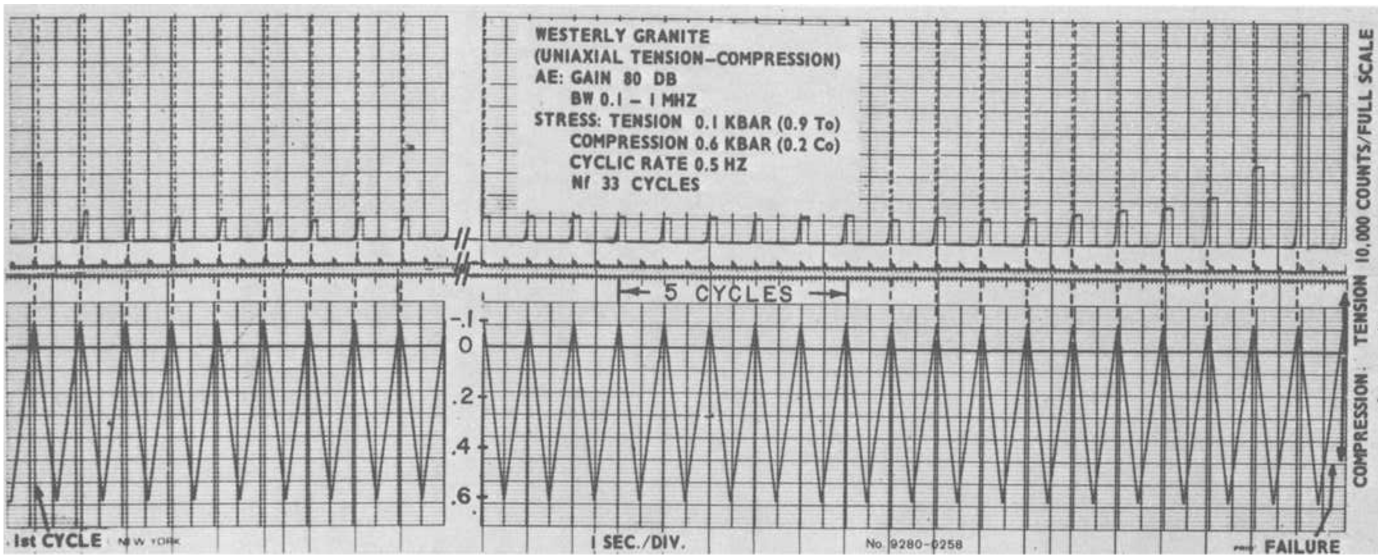

FIG. 15—*Typical AE rate versus time and stress versus time records in cyclic uniaxial tension-compression (loading ratio: tension = 1/compression = 6)—Westerly granite (1 kbar = 100 MPa).*

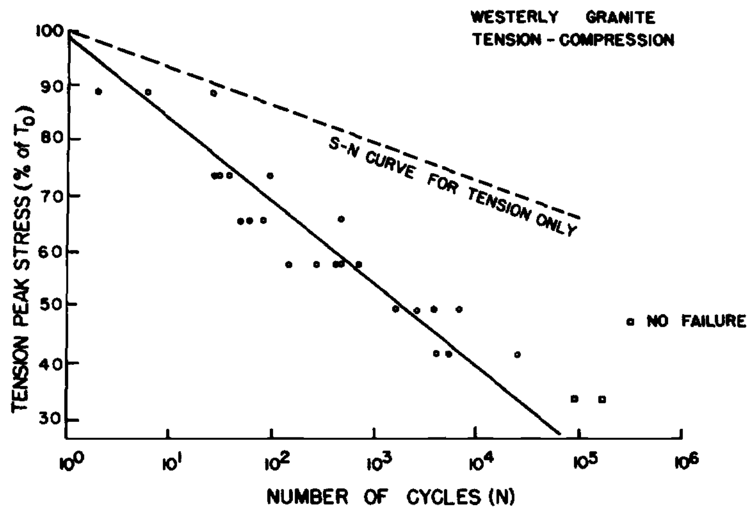

FIG. 16—*Experimental results and* S-N *curve for Westerly granite under cyclic uniaxial tension-compression (compression peak constant-tension peak varied from test to test). Comparison with* S-N *curve for uniaxial tension.*

The stress-strain curve in cyclic tension-compression (Fig. 17) for the case where the compression peak is 60 000 kPa (600 bars) ($\cong$ 20 percent of C_o) is useful in understanding the different effects that tension and compression have on rock [*12*]. In every cycle as the load shifts from compression into tension, there is a sharp drop in the elastic modulus, indicating the opening of the heretofore closed microcracks. In addition, the elastic modulus in tension drops with every cycle until it is reduced by 30 percent just before failure. This excessive "softening" is considerably higher than in other cyclic loading types and indicates continuous and partially irreversible opening of microcracks leading to a most premature failure (Fig. 17). It is clear from the figure that while the compression cyclic peak strain stays constant throughout because of the low level compressive stress, the tension cyclic peak strain goes through all three stages of cyclic creep. At the end of the first complete cycle, some 70 percent of the total permanent deformation has already occurred. Failure of cyclic tension-compression specimens occurs in tension along a plane approximately perpendicular to the line of load application.

Applications

The following are some of the practical applications resulting from the tests conducted:

1. In designing underground or surface structures, proper consideration

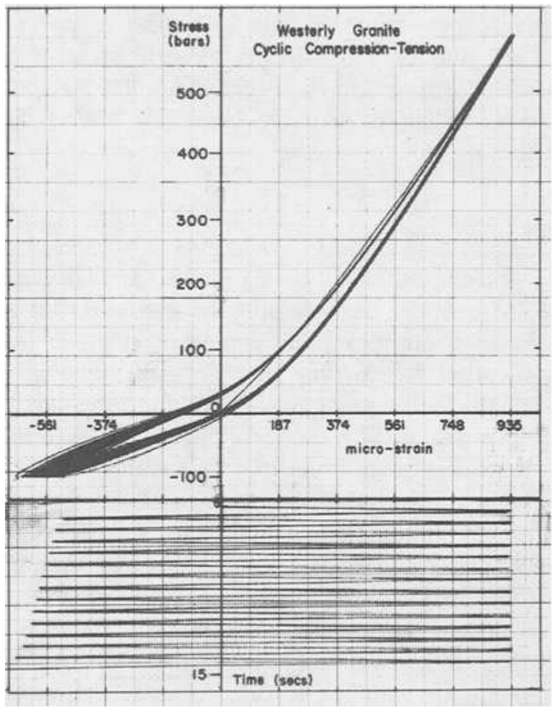

FIG. 17—*Typical stress-strain and strain-time curves recorded during uniaxial tension-compression cycling (1 bar = 100 kPa).*

should be given to the effect of cyclic loading due to activities such as earthquakes, blasting, drilling, and traffic. It is clear that repetitive loading of any type can weaken rock strength and results in premature failure.

2. *S-N* curves should be determined and used to establish more realistic compressive and tensile strengths of rock which could withstand both static and cyclic loading. The respective fatigue strengths at 10^5 cycles are recommended as more applicable strength values than the presently common compressive or tensile strengths.

3. The apparent relationship detected between the complete stress-strain curve and cyclic creep provides a quick means of determining total deformation prior to fatigue failure. If allowable deformation is the important parameter in a structure, or if deformation or strain are monitored closely, the complete stress-strain curve could be used to predict imminent failure or to prevent it by remedial action.

4. AE is probably the most effective precursor of rock failure and, in particular, of cyclic fatigue. It appears that AE is more useful in predicting compressive failure, although in some rocks it could be just as effective with respect to tension.

5. Cyclic tension-compression appears to be the most fatigue-inducing loading mode. Particular care should be taken in structures expected to be subjected to such loading. On the other hand, the weakening effect of tension-compression cycling could have beneficial effects if exploited in drilling and blasting methods.

ASTM Standards

Based on the reported results and their practical applications, it is recommended that ASTM consider the feasibility of setting testing standards for determining *S-N* curves for rock. The compression cyclic tests would require little modification to existing standards for uniaxial compression testing, except that the loading machine should have the capability of loading and unloading automatically between two set stress levels at a given frequency. *S-N* curve determinations in tension and tension-compression would require a rigid testing setup like the one shown in Fig. 1. This arrangement enables the application of both tension and compression. For triaxial compression cyclic testing, a pressure chamber similar to that used in static tests is sufficient. The requirement is, however, that the confining pressure be kept constant during axial load cycling. This could be achieved by use of an accumulator or by a servo-controlled electrohydraulic system. It is felt that a maximum number of 10^5 cycles are sufficient to simulate any field situation realistically.

The method of obtaining complete stress-strain curves for rock has been described by others (for example, Ref *15*). The standardization of this test would be extremely valuable in general, and most useful to predicting cyclic creep in particular.

The application of acoustic emission is another very important tool in rock mechanics in general and could and should be standardized. The usefulness of the method to understanding fatigue mechanism and predicting cyclic loading failure has been described in the body of this paper.

Acknowledgments

The work reported herein was carried out with the assistance of graduate students C. M. Kim, K. Kim, V. Rajaram, and T. Tharp, who conducted most of the experimental work. The research was supported in part by U.S. Bureau of Mines Contracts Nos. H0210004 and H0220041.

References

[*1*] Grover, H. J., Dehlinger, P., and McClure, G. M., "Investigation of Fatigue Characteristics of Rocks," Reported by Battelle Memorial Institute to Drilling Research, Incorporated, Nov. 30, 1950.

[2] Burdine, N. T., *Society of Petroleum Engineers Journal*, March 1963, pp. 1-8.
[3] Hardy, H. R. and Chugh, Y. P. in *Proceedings*, Sixth Canadian Symposium on Rock Mechanics, Montreal, 1970, pp. 33-47.
[4] Saint-Leu, C. and Sirieys, P. in *Proceedings*, Symposium on Rock Fracture of the International Society for Rock Mechanics, Nancy, France, 1971, Paper II-18.
[5] Attewell, P. B. and Farmer, I. W., *International Journal of Rock Mechanics and Mining Sciences*, Vol. 10, 1973, pp. 1-9.
[6] Haimson, B. C. and Kim, C. M. in *Proceedings*, Thirteenth Symposium on Rock Mechancis, American Society of Civil Engineers, 1972, pp. 845-864.
[7] Haimson, B. C., "Mechanical Behavior of Rock Under Cyclic Loading," Annual Technical Report to the Bureau of Mines, Contract H0210004, 1972.
[8] Haimson, B. C., "Mechanical Behavior of Rock Under Cyclic Loading," Final Technical Report to the Bureau of Mines, Contract H0220041, 1973.
[9] Tharp, T. M., "Behavior of Three Calcite Rocks Under Tensile Cyclic Loading," MS Thesis, University of Wisconsin, Madison, Wisc., 1973.
[10] Kim, C. M., "Fatigue Failure of Rock in Cyclic Uniaxial Compression," PhD. Thesis, University of Wisconsin, Madison, Wisc., 1973.
[11] Haimson, B. C. and Kim, K., in *Proceedings*, First Conference on Acoustic Emission in Geologic Structures and Materials, H. R. Hardy, Jr. and F. W. Leighton, Eds., Trans Tech Publications, Clausthal, Germany, 1977, pp. 35-55.
[12] Kim, K., "Deformation and Failure of Rock Under Monotonic and Cyclic Tension," Ph.D. Thesis, University of Wisconsin, Madison, Wisc., 1976.
[13] Rajaram, V., "Mechanical Behavior of Westerly Granite and Berea Sandstone Under Cyclic Compression," PhD Thesis, University of Wisconsin, Madison, Wisc., 1978.
[14] Haimson, B. C. in *Advances in Rock Mechanics* (*Proceedings*, 3rd Congress of the International Society for Rock Mechanics). National Academy of Sciences, Washington, D.C., 1974, Vol. 11, pp. 373-378.
[15] Rummel, F. and Fairhurst, C., *Rock Mechanics*, Vol. 2, 1970, pp. 189-204.

Kenji Ishihara,[1] *Masato Sodekawa,*[2] *and Yasuo Tanaka*[2]

Effects of Overconsolidation on Liquefaction Characteristics of Sands Containing Fines

REFERENCE: Ishihara, Kenji, Sodekawa, Masato, and Tanaka, Yasuo, "**Effects of Overconsolidation on Liquefaction Characteristics of Sands Containing Fines,**" *Dynamic Geotechnical Testing, ASTM STP 654,* American Society for Testing and Materials, 1978, pp. 246-264.

ABSTRACT: Two series of cyclic triaxial tests were performed on soils containing fines (passing #200 sieve) from 0 to 100 percent by weight. The first series included the testing of laboratory-prepared reconstituted specimens overconsolidated to overconsolidation ratio (OCR) values of 1.0 to 2.0. It was shown that the overconsolidation had an definite effect in strengthening the cyclic resistance of the specimens, and its effect became more pronounced as the content of the fines increased. The second in the series was concerned with the tests on undisturbed specimens from alluvial deposits in Tokyo as well as the tests on remolded specimens of the same soil. It was shown that the cyclic strength of the undisturbed specimens was about 15 percent greater than that of the reconstituted ones. Comparison of the results from this second series of tests appeared to show that the greater cyclic strength of the undisturbed specimens over that of the remolded specimens might have been caused by a slight overconsolidation which existed in the alluvial deposit of the sands containing the fines.

KEY WORDS: liquefaction, sands, fines, cyclic loads, triaxial tests, overconsolidation, specimens, soils

Field observations of loose saturated sand deposits that were liquefied during strong earthquakes have led to extensive laboratory studies on the liquefaction resistance of sands. Most of the studies on this subject, however, have been limited to granular materials such as clean sands or gravels containing little or no fines. On the other hand, gradation studies of soils in the field have disclosed the fact that soils containing some fines are far more frequently encountered than clean sands in the alluvial or reclaimed deposits where soil liquefaction often becomes of critical importance in

[1] Professor, Department of Civil Engineering, University of Tokyo, Bunkyo-ku, Tokyo, Japan.

[2] Civil engineer, Fudo Construction Company, Taito 1, Taito-ku, Tokyo, Japan.

assessing the stability of the ground during earthquakes. Moreover, there are many cases where the soils known to have liquefied were identified as silty sands or sandy silts containing 10 to 50 percent fines (Marsal, 1961 [*1*][3]; Ikehara, 1970 [*2*]; Yamanouchi et al, 1976 [*3*]).

In present practice, the liquefaction resistance of a given soil deposit is often determined roughly on the basis of the standard penetration resistance. It is generally recognized that the blow-count of the standard penetration test (SPT) strongly reflects the amount of fines present in the soils. It is also known that the blow-count value is influenced by the density of the clean sands as well. In other words, the decrease in blow-count can be caused either by an increase in fines present or by the low density of the soils. Therefore, if the blow-count value is low for a given soil, it can mean either of the two following soil conditions: (1) When the soil is clean sand, it may be low in density and susceptible to liquefaction; or (2) when some fines are present in the soil, it may also be low in density but less vulnerable to liquefaction due to the hardening effect of the fines. Since the blow-count implies two mutually opposite conditions in soils as stated in the foregoing, the determination of liquefaction resistance based on the N-values alone can be misleading, unless the effect of fines is properly considered.

It appears likely that soils in the alluvial deposit tend to be subjected to some degree of overconsolidation, and this may bring about the hardening effect on the soils and consequent increase in the cyclic strength. Shown in Fig. 1 is a diagram plotting the existing effective overburden pressure versus the preconsolidation pressure as determined from the usual consolidation curves for many clays prevailing in the alluvial deposit in the lowlying area of Tokyo, Japan. The plot shows that most of the clays were slightly overconsolidated to overconsolidation ratio (OCR) values of 1.0 to 2.0. Therefore, it may well be assumed that the same degree of overconsolidation exists also for the cohesionless soils in the same area, generally classified as silty sand or sandy silt, and that this accounts for some increase in liquefaction resistance of the soils as against the low N-values of this area.

The study described in the following pages presents the results of cyclic triaxial tests carried out to show the possible hardening effect that the overconsolidation may have and to provide an explanation for the increased resistance to liquefaction of the intact soil specimens based on the effect of overconsolidation.

In the first series of the test program, test specimens were reconstituted from remolded soils obtained from the alluvial deposit in Tokyo. Cyclic triaxial tests were performed on the specimens prepared with OCR-values of 1.0 to 2.0, and the effect of overconsolidation on the cyclic strength was investigated.

[3]The italic numbers in brackets refer to the list of references appended to this paper.

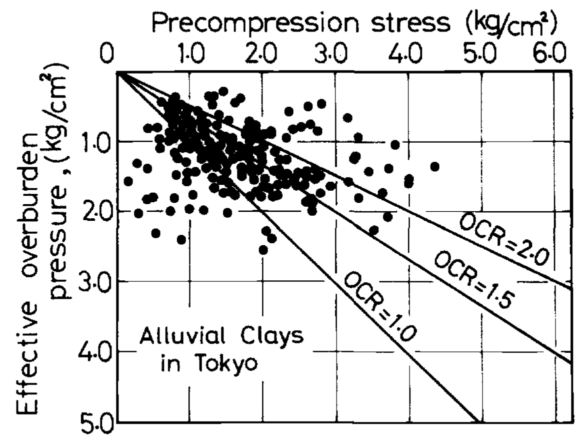

FIG. 1—*Degree of overconsolidation of soils in alluvial deposits in Tokyo.*

In the second test series, cyclic triaxial tests were performed on undisturbed specimens obtained by thin-wall tube samplers. The specimens were remolded afterwards and reconstituted by the same procedure as adopted in the first test series. They were then subjected to cyclic triaxial tests to compare the cyclic strengths of intact and reconstituted specimens.

Test Materials

The soils used for the present test program were silty sands and sandy silts obtained from the alluvial deposit in the low-land area of the Koto, Taito, and Katsushika wards in Tokyo, Japan. The soil specimens were secured from drilled holes by means of 7.62-cm-diameter thin-wall tube samplers. The sites of the borings were located within about 3 km of each other and the specimens obtained were considered to represent the general characteristics of the soils of alluvial origin prevailing in the low-land area of Tokyo.

The specimens obtained from the Koto and Katsushika wards were used for the tests of reconstituted specimens that were planned to investigate the effect of overconsolidation on the cyclic strength of soils. The grain-size curves of these soils are shown in Fig. 2. The gradation curves of Koto A soil containing 58 percent fines and Koto B soil containing 15 percent fines represent natural soils, whereas the other three represent artificially graded soils obtained from the same general area. Consistency tests made for the fine portions of the foregoing soils showed a liquid limit of about 60 and a plasticity index of about 20.

The thin-wall tube specimens secured from the Taito ward were used directly for the tests of undisturbed specimens. Three thin-wall tube speci-

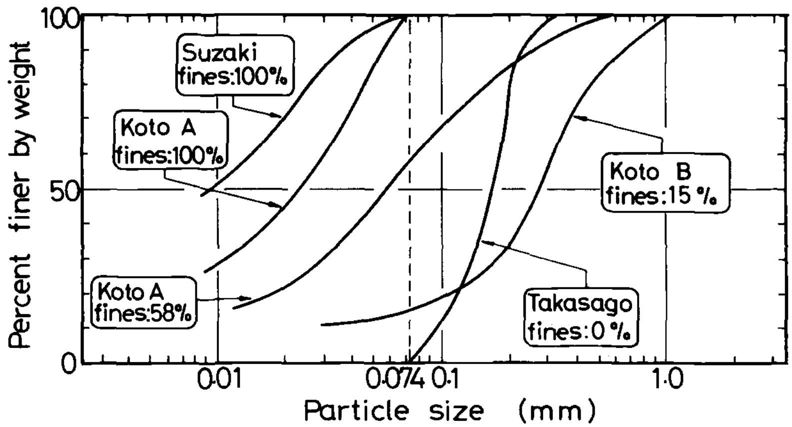

FIG. 2—*Grain-size distributions of soils used for tests of reconstituted specimens.*

mens were obtained continuously from the silty sand deposit at a depth of 3.5 to 5.0 m having the standard penetration resistance (*N*-value) of about 5. These specimens were labeled A1, A2, and A3 and their grain-size curves are shown in Fig. 3. Another specimen, labeled B1 was obtained from the soil of a nearby site at a depth of 6.0 m having the *N*-value of 6.

Method of Specimen Preparation

Preparation of Reconstituted Specimens

Reconstituted specimens for cyclic triaxial tests were prepared by sedimentation through de-aired water in a forming mold. To facilitate consolidation at a later stage, a piece of filter paper with several vertical slits was attached inside the forming mold. Then, the soil mixed with de-aired water was poured into the mold. When a soil contained more than 10 percent fines by weight, this procedure turned out to be undesirable because coarser grains tended to settle faster than finer particles, producing nonuniform layering in the structure of the specimens.

To avoid this segregation of particles, a special procedure as described in the following was adopted for preparing specimens for cyclic triaxial tests. First of all, the soils to be tested were sieved with the #200 mesh and separated into fine and coarse portions. Each portion was thoroughly mixed with distilled water to achieve full saturation. The slurry containing the fines was first poured into the forming mold and then the coarse material was deposited slowly by a spoon and made to settle through the slurry. When a specimen with a high content of fines was to be formed, heavy slurry was used. Light slurry with low concentration of fines was used to

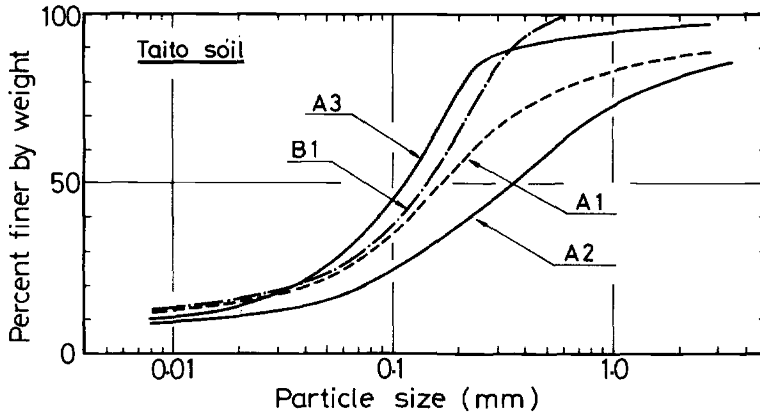

FIG. 3—*Grain-size distribution curves of soils used for tests of intact specimens.*

form a specimen with a low content of fines. The quality of the specimen in terms of segregation of grains that might have occurred during the sedimentation was checked by examining the grain size distributions at different sections of the specimen. After the specimen had been formed and consolidated, it was taken out of the triaxial cell. The specimen was then divided into three sections and a grain size analysis was made for each of these. The result of the sieve analyses made for Koto A soil containing 58 percent fines is shown in Fig. 4*a*, where it is noted that there are 5 percent more fines in the upper third of the specimen than in the lower third. Figure 4*b* shows the similar test result for Koto B soil containing 18 percent fines. It is also noted that there was about 5 percent difference in the fines present between the upper and lower third of the specimen. A number of similar sieve analyses made for the soils containing different percentages of fines showed that, for the specimens containing an amount of the fines either less than 30 percent or more than 80 percent, the method of sedimentation through slurry as adopted in this study proved generally useful in providing fairly uniform specimens as evidenced by only 5 percent difference in the content of fines throughout the length of the specimen. For the range of fines between 30 and 80 percent, the sedimentation procedure described in the foregoing failed to provide uniform specimens, and it was found that minor details in slurry handling had considerable effect on the uniformity of the specimens. Height and speed of pouring the coarse material needed to be carefully controlled to allow uniform sedimentation to take place through the slurry. The result of the sieve analyses shown in Fig. 4*a* is that the specimen with 58 percent fines formed most successfully with considerable precaution.

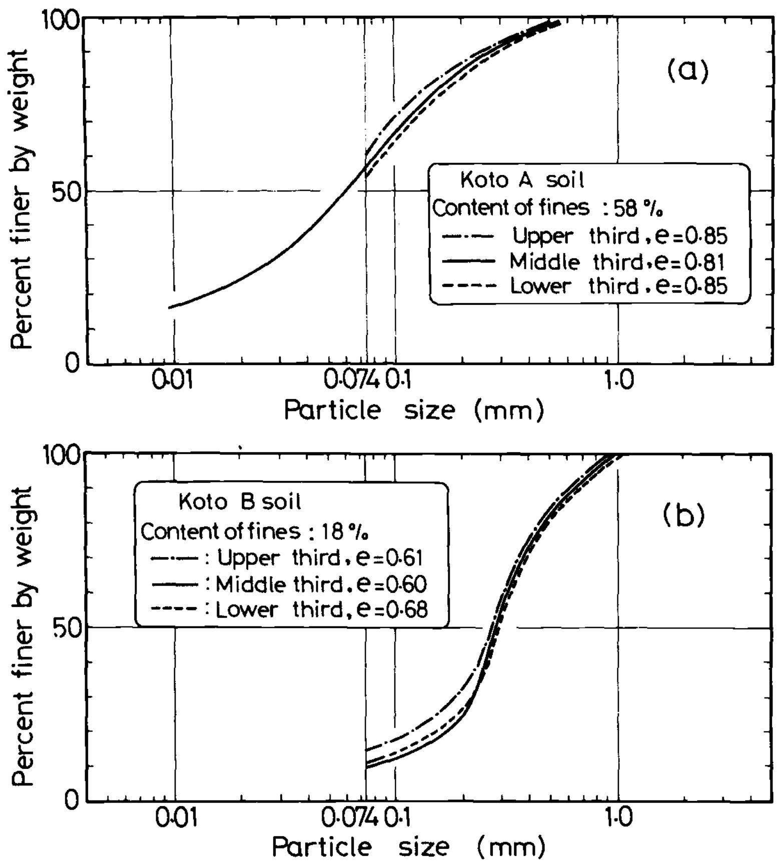

FIG. 4—*Grain-size distributions at different sections of reconstituted specimen.*

Handling of Undisturbed Specimens

Soil specimens in the thin-wall tube were carefully extruded out, as illustrated in Fig. 5, by pushing one end of the specimen by a specimen excluder, while the other end was pushed into an awaiting specimen holder which had a sharp cutting edge with a diameter smaller than that of the extruded specimen. The result was forming a 5-cm-diameter and 10-cm-length specimen for the cyclic triaxial tests inside the specimen holder. The specimen, now secured undisturbed inside the holder, was held by a split liner which was designed to provide smooth entry into the holder and temporary support. The details of the specimen holder are shown in Fig. 6. A rubber membrane was set inside the holder and kept tight against the inside wall of the holder by vacuum. After the specimen was pushed into the holder, it was turned upright and the split liner was pulled out. Immediately

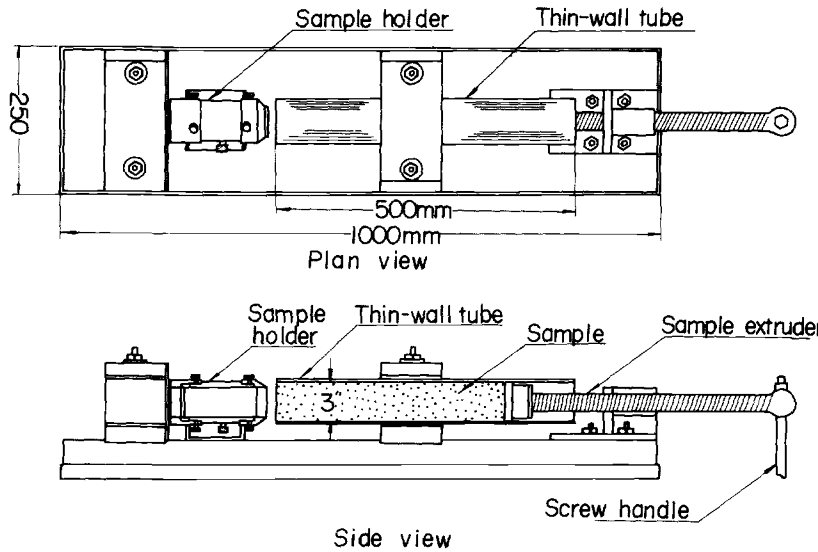

FIG. 5—*Cross sections of the specimen holder and specimen extruder.*

afterwards, the vacuum was released and the membrane was allowed to make a firm contact with the specimen. Elasticity of the membrane served to hold the weak specimen intact. Then, the specimen ends were trimmed and smoothened, and porous disks were put on both ends. The specimen, together with the holder, was put upright on the base of the triaxial test apparatus and the lower end of the rubber membrane was rolled down and fastened to the base with O-rings. The vertical loading piston was, then, lowered to the top of the specimen and the upper end of the membrane was rolled up and fastened to the loading piston with O-rings. A slight vacuum was applied to the specimen to mobilize the confining pressure. Then the specimen holder was removed. The foregoing procedure was considered to function satisfactorily for handling undisturbed specimens before they were set up in the triaxial apparatus.

Test Procedures

Cyclic Triaxial Tests on Reconstituted Specimens

Test specimens prepared by the aforementioned procedures were first saturated by circulating de-aired water through the specimens and then consolidated to a preconsolidation pressure of either 0.75 or 1.0 kg/cm^2. The confining pressure was then reduced to 0.5 kg/cm^2 to achieve a desired condition of overconsolidation of 1.5 or 2.0. In the tests on normally consolidated specimens, two confining pressures of 0.5 and 1.0 kg/cm^2

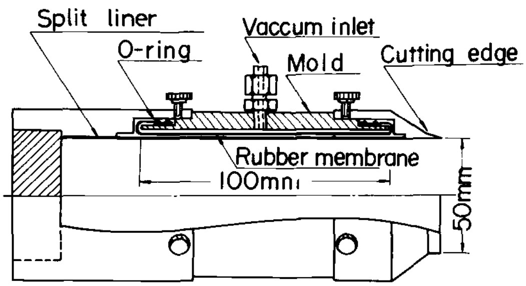

FIG. 6—*Cross section of the specimen holder.*

were employed. The time required for consolidation was varied from 1 to 24 h depending upon the amount of fines present in each specimen. Back pressures up to 2.0 kg/cm^2 were applied to the specimens to ensure almost full saturation. The specimens were subjected under undrained conditions to a constant-amplitude axial cyclic load until they developed the condition of initial liquefaction or excessive axial strains. The test equipment used in this study was the same as that used in the previous investigation (Ishihara and Yasuda, 1972 [*4*]).

Cyclic Triaxial Tests on Undisturbed Specimens

All the cyclic triaxial tests were performed with an effective confining pressure of 1.0 kg/cm^2, which corresponded to the normally consolidated state of the soil in the field. Back pressures were also used to saturate the specimens. After completing cyclic triaxial tests on undisturbed specimens, the specimens were completely remolded and used to prepare reconstituted specimens by the same procedures as described in the previous section. Therefore, cyclic triaxial tests were performed both on undisturbed and reconstituted specimens with approximately the same void ratios at the time of consolidation.

Test Results of Reconstituted Specimens

The results of the cyclic triaxial tests are plotted in Figs. 7-11 in terms of the cyclic stress ratio versus the number of cycles required to cause initial liquefaction or ± 2.5 percent axial strain. The cyclic stress ratio is defined as the ratio of the cyclic deviator stress, σ_{dl}, to twice the effective confining pressure, $2\sigma_0'$, at the time of consolidation. The initial liquefaction is a measure of failure of a specimen at which the developed pore water pressure becomes equal to the initial effective confining pressure. It has been shown, however, that for soils containing a larger percentage of fines, the pore pressure does not build up fully to become equal to the initial effective

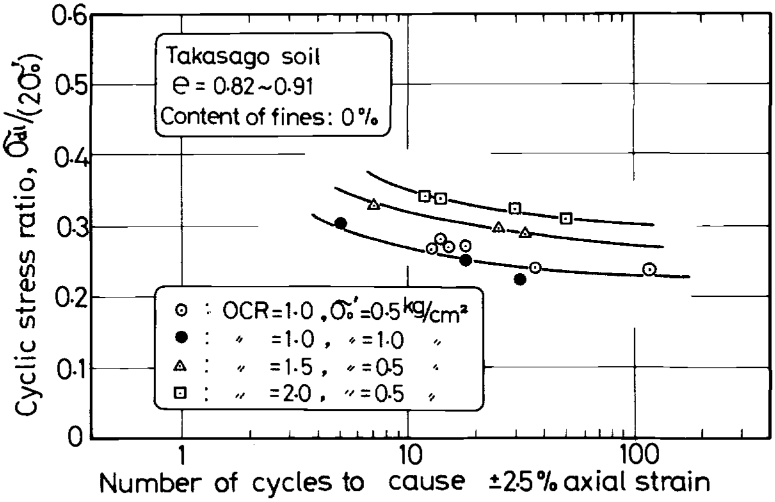

FIG. 7—*Cyclic stress ratio versus number of cycles.*

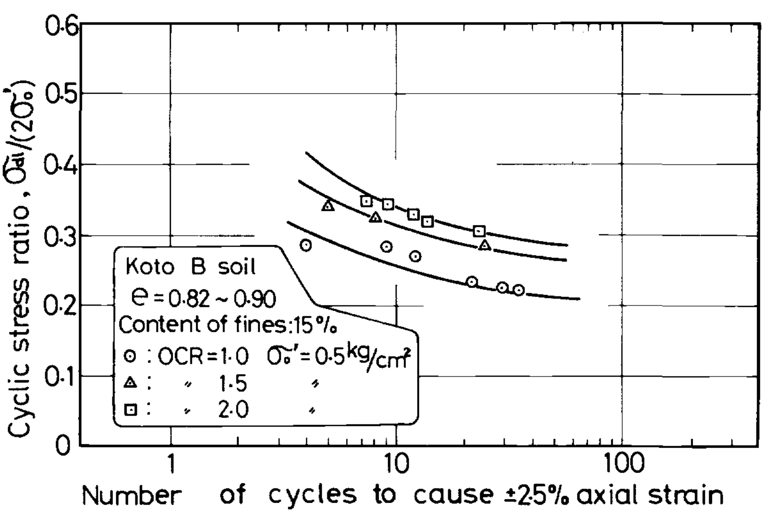

FIG. 8—*Cyclic stress ratio versus number of cycles.*

confining pressure, even though considerable axial strain may develop during cyclic loading. Shown in Fig. 12 is a summary of test results in which the maximum pore water pressures that developed as the result of application of an infinite number of cyclic loadings were plotted against the mean grain size, D_{50}, of the test specimens. The figure clearly shows that the smaller the mean grain size of the specimen, the lower was the

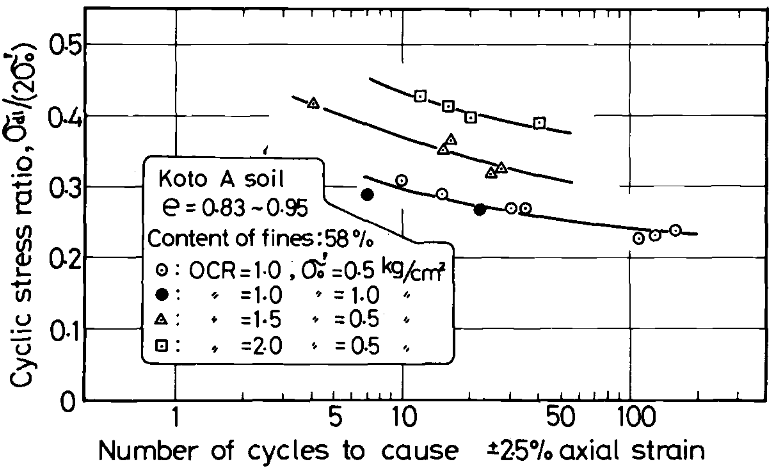

FIG. 9—*Cyclic stress ratio versus number of cycles.*

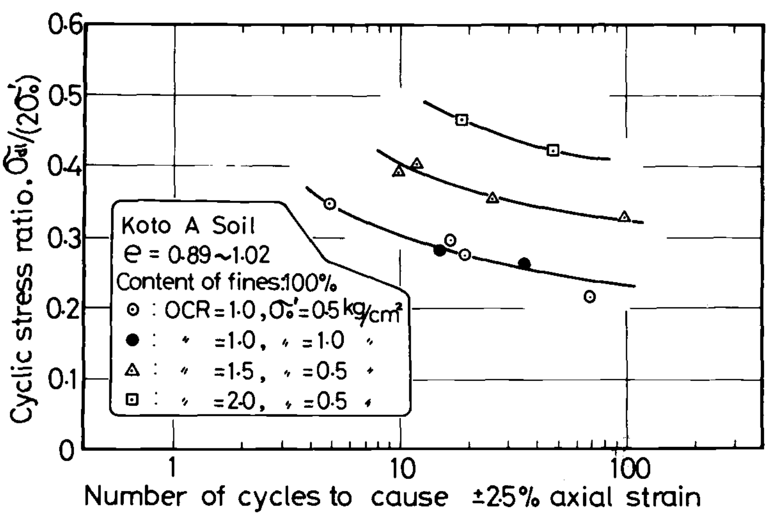

FIG. 10—*Cyclic stress ratio versus number of cycles.*

maximum pore water pressure developed. Therefore, it does not seem appropriate to use the concept of initial liquefaction as a failure criterion for a soil containing some fines. To provide a more common measure for evaluating the cyclic strength of soils embracing a wide range of fines, the use of ±2.5 or ±5.0 percent axial strain was suggested by Silver and Park (1976) [5]. A number of cyclic triaxial tests conducted on relatively clean sands in the present investigation, however, have shown that the number of

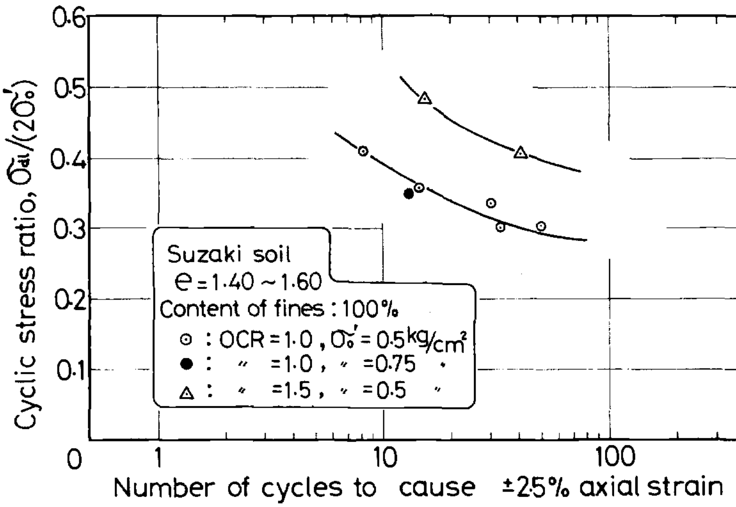

FIG. 11—*Cyclic stress ratio versus number of cycles.*

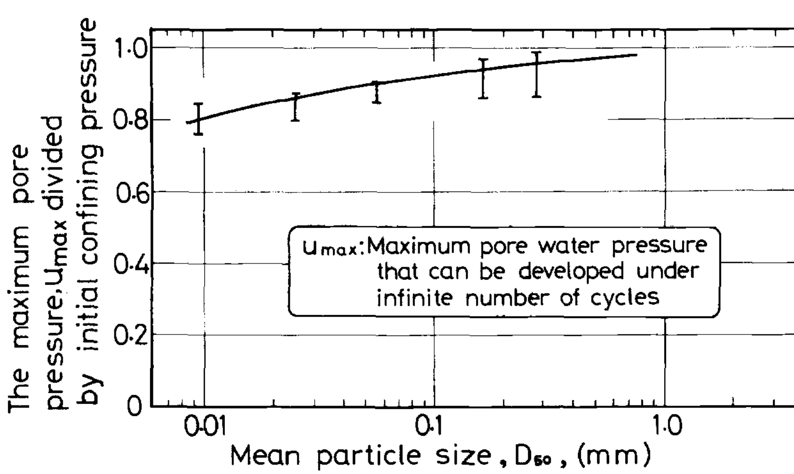

FIG. 12—*Maximum attainable pore water pressure versus mean particle size.*

cycles required to cause initial liquefaction in a specimen under a given cyclic stress ratio is almost equal—within an allowable limit of accuracy—to the number of cycles needed to produce ±2.5 percent axial strain. Thus, for the purpose of the uniformity of failure criterion, the test results shown in Fig. 7-11 are presented in terms of the number of cycles to cause ±2.5 percent axial strain.

Figure 7, the test results for reconstituted sand specimens of Takasago soil without fines, shows that the cyclic stress ratio required to cause ±2.5

percent axial strain (or equivalent or initial liquefaction) increased by about 30 percent with an increase in overconsolidation ratio from 1.0 to 2.0. For reconstituted specimens of Koto B soil, artificially graded soil containing 15 percent fines, the test results (Fig. 8) show that the rate of increase in cyclic strength due to an increase in overconsolidation ratio was somewhat more pronounced. However, all the more noticeable increase in cyclic strength due to overconsolidation was observed in the test results shown in Figs. 9-11, where specimens with successively higher contents of fines were tested. It should be noted particularly in Fig. 11 that the specimens with 100 percent fines with overconsolidation ratio of 2.0 showed almost twice as much increase in cyclic strength as the similar specimens normally consolidated.

In order to see the effect of overconsolidation more clearly, the cyclic stress ratio required to cause ±2.5 percent axial strain or initial liquefaction under 20 cycles of load application was read off from Figs. 7-11 and plotted in Fig. 13 versus the fines contained in the specimens. The same data on the cyclic stress ratio were also plotted in Fig. 14 versus the mean grain size, D_{50}, of the specimens. These figures clearly show that the rate of gain in cyclic strength due to overconsolidation increased with an increase in fines or a decrease in mean grain size of the soil specimens.

The characteristic manner in which overconsolidation causes a gain in cyclic strength may be more clearly visualized by examining the changes in cyclic strength caused by the changes in effective confining pressure. In Fig. 15-17, the cyclic deviator stress and the cyclic stress ratio required

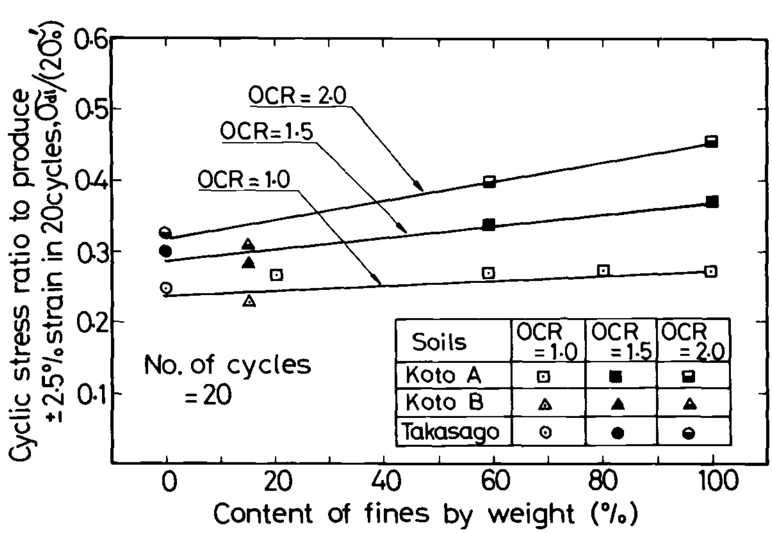

FIG. 13—*Relationship between cyclic strength and content of fines in soils.*

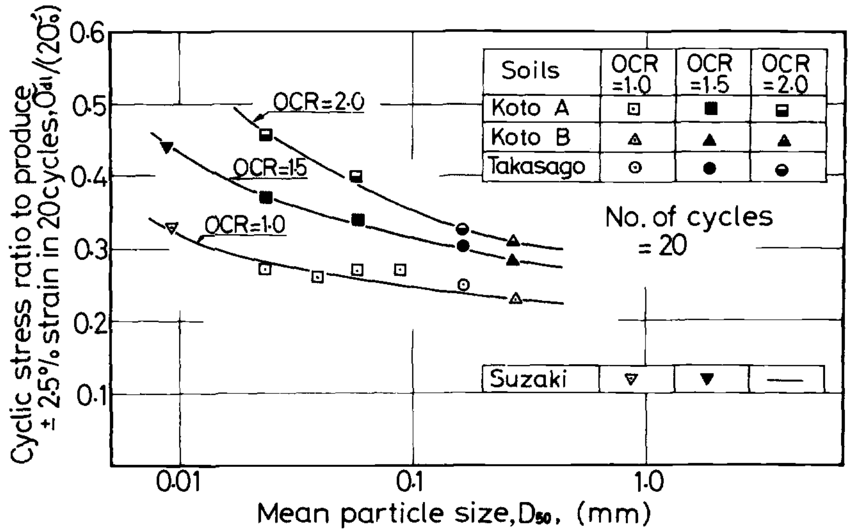

FIG. 14—*Relationship between cyclic strength and mean particle size of soils.*

to cause ±2.5 percent axial strain in 20 cycles of cyclic loading were plotted versus the effective confining pressure for the three soils containing 0, 58, and 100 percent fines. Also plotted versus the effective confining pressure were the corresponding changes in void ratio. The data points in these figures are the averaged values estimated from the original test data shown in Figs. 7, 9, and 10. In Fig. 15*b*, it is noted that the cyclic deviator stress required to cause ±2.5 percent axial strain in 20 cycles of normally consolidated specimens increased in proportion to the effective confining pressure, a fact that has been recognized based on many previous laboratory test results. However, when the tests were performed in the overconsolidated state, as Fig. 15*b* shows, the cyclic strength became larger than that required at the corresponding effective confining pressure in the normally consolidated state. These general characteristics are the same as those observed in the static strength of normally and overconsolidated clays. Because of these characteristics, an increase in the cyclic stress ratio was observed as shown in Fig. 15*c* in the unloading branches of the stress ratio-effective confining pressure curve. In Fig. 16 where the test result for the soil containing 58 percent fines is demonstrated, it is noted that a similar increase in cyclic stress ratio occurred in overconsolidated specimens in a more exaggerated manner. When the amount of fines in the specimen was increased further, up to 100 percent, the gain in cyclic strength with an OCR-value of 2.0 became as much as 70 percent, as shown in Fig. 17, of the cyclic strength in the normally consolidated state. It is also noted that the difference in void ratio between normally consolidated and overconsoli-

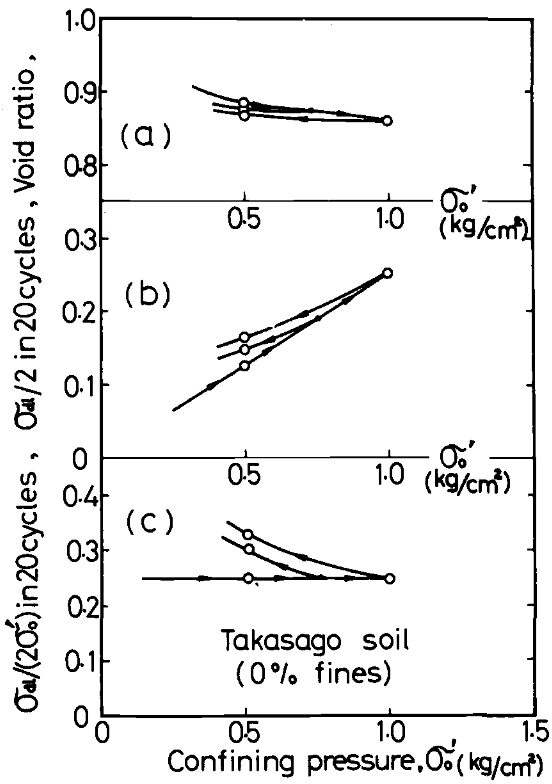

FIG. 15—*Void ratio and cyclic stress ratio versus confining pressure based on average values.*

dated specimens became more pronounced as the content of fines was increased.

Test Results of Undisturbed Specimens

The results of cyclic triaxial tests on undisturbed specimens are shown in Fig. 18-21, together with those on the specimens reconstituted afterwards. As indicated in the figures, there was no significant difference in the void ratio at the time of consolidation between the intact and reconstituted test specimens. These figures show consistently that the cyclic stress ratio required to induce failure in the specimens under a given number of cycles was greater for the undisturbed specimens than for the reconstituted specimens. To visualize more clearly the effect of specimen remolding, the ratios in the cyclic strength under 20 cycles between the undisturbed and reconstituted specimens were read off from the raw data in Figs. 18-21 and plotted in Fig. 22 versus the fines present in each soil tested. Figure 22

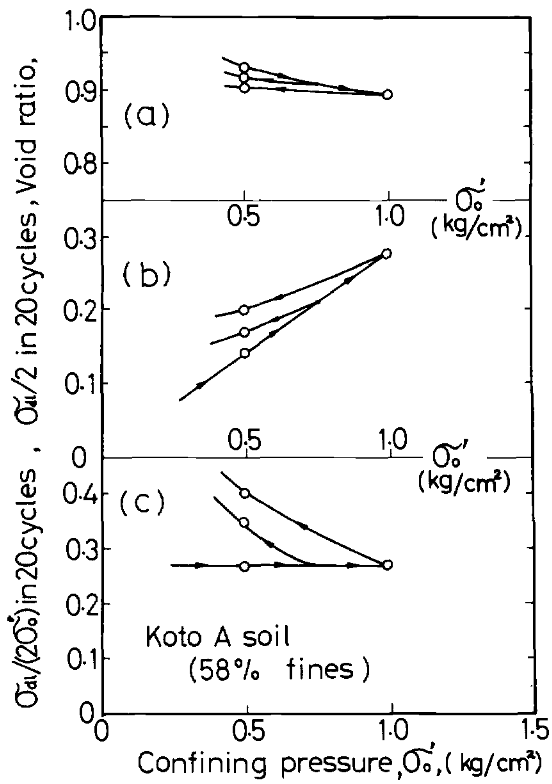

FIG. 16—*Void ratio and cyclic stress ratio versus confining pressure based on average values.*

shows that on the average about a 15 percent strength increase was observed in the intact specimens over the cyclic strength of the reconstituted specimens.

Discussions of Test Results

As demonstrated in Fig. 1, natural soil deposits which exist in an alluvial plane such as in the low-lying area of Tokyo are generally slightly overconsolidated to an overconsolidation ratio of 1.0 to 2.0. The effect of this order of magnitude of overconsolidation on the cyclic strength of soils was investigated in the first phase of the present test program by using reconstituted specimens. As the summary plot in Fig. 13 shows, it became apparent that the increase in cyclic strength due to overconsolidation became more pronounced as the specimen contained more fines. Therefore, if the naturally occurring soils containing a fair amount of fines exhibit higher cyclic strength than reconstituted specimens of the same soil, it may

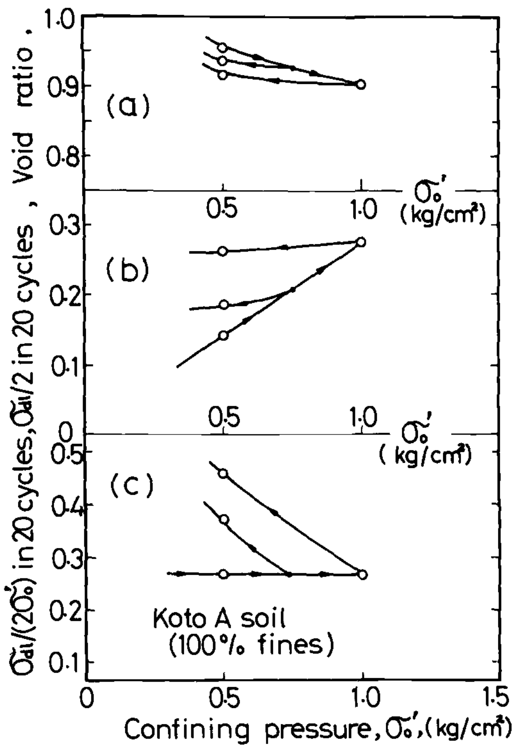

FIG. 17—*Void ratio and cyclic stress ratio versus confining pressure based on average values.*

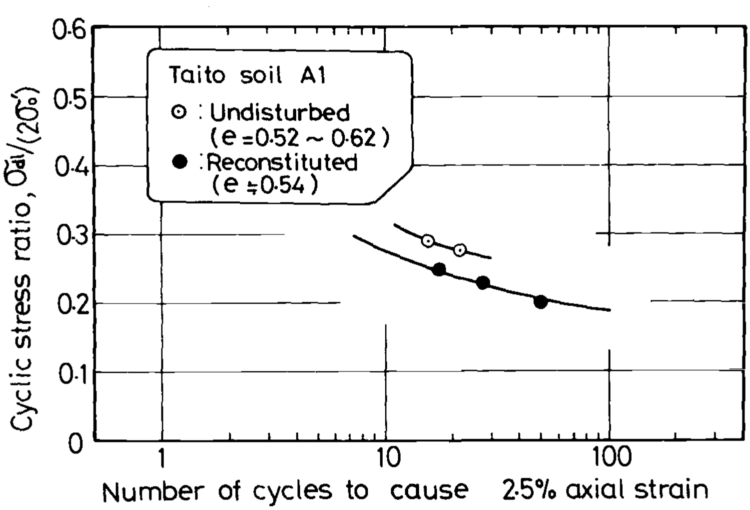

FIG. 18—*Cyclic stress ratio versus number of cycles.*

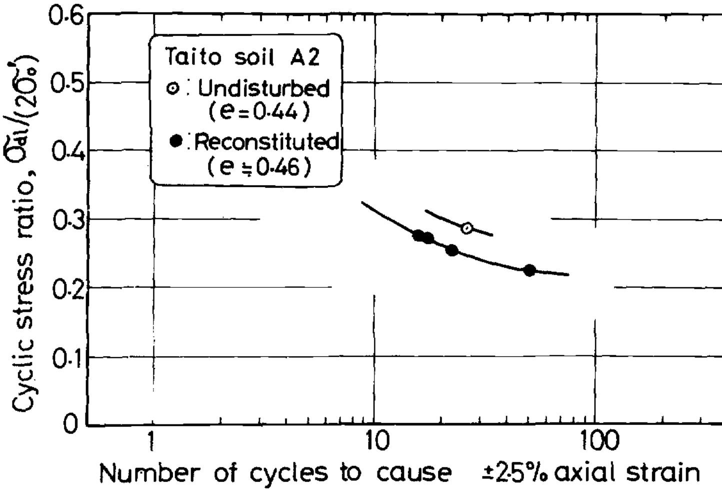

FIG. 19—*Cyclic stress ratio versus number of cycles.*

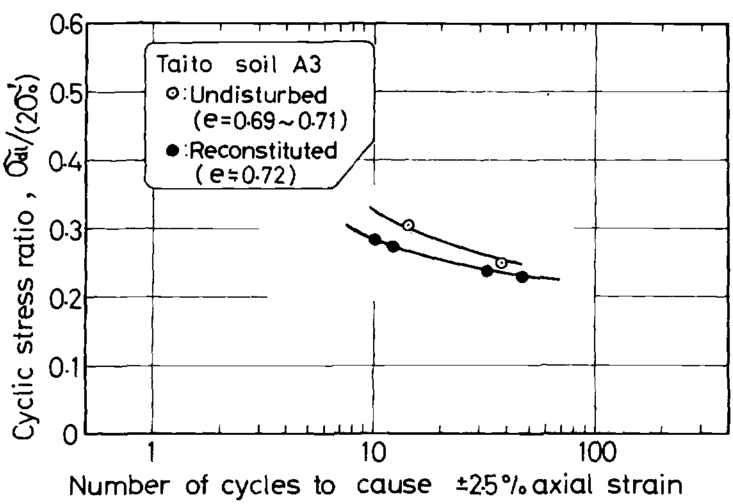

FIG. 20—*Cyclic stress ratio versus number of cycles.*

well be anticipated that the strength increase in natural soils is brought about by the overconsolidation which takes place in the deposit for a long period of time. To see the adequacy of this assumption, the ratio of cyclic strength of overconsolidated specimens to that of normally consolidated reconstituted specimens was calculated from the averaged results in Fig. 13 and this was superimposed on the diagram of Fig. 22, where the ratio of

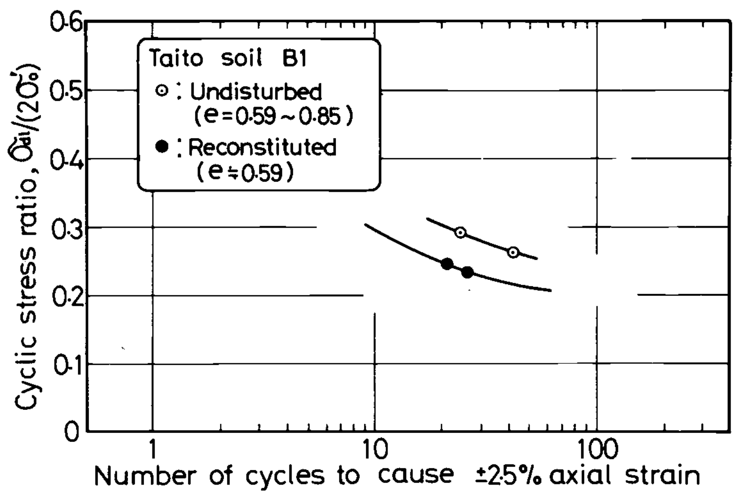

FIG. 21—*Cyclic stress ratio versus number of cycles.*

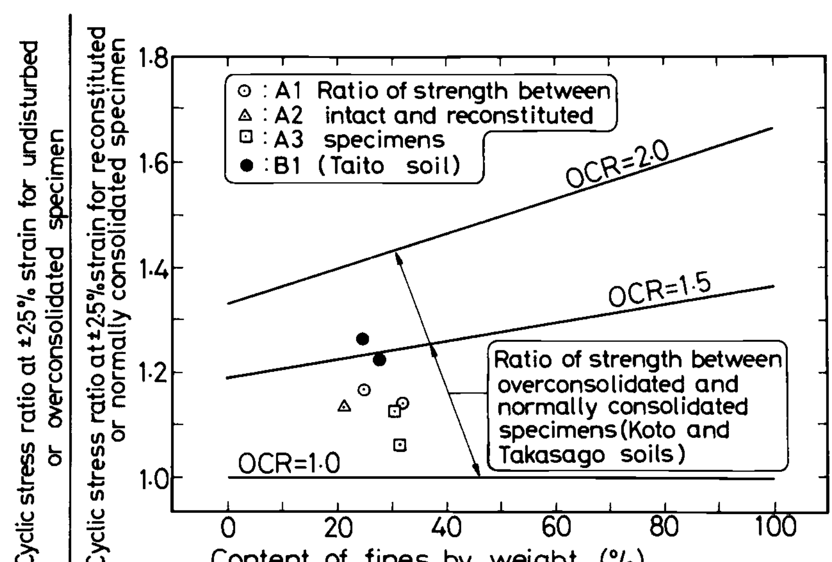

FIG. 22—*Comparison of cyclic strength of intact specimens with that of overconsolidated specimens.*

cyclic strength of undisturbed specimens to that of reconstituted specimens was plotted versus the fines contained. It is clearly demonstrated in Fig. 22 that the increase in cyclic strength of undisturbed specimens over that of reconstituted specimens agreed well with the increase in cyclic strength that could be attributed to a slight overconsolidation by a factor of 1.0 to 2.0.

Conclusions

A series of cyclic triaxial tests was performed on reconstituted specimens overconsolidated in varying degrees of overconsolidation ratios between 1.0 and 2.0. The test results showed that the overconsolidation ratio of 2.0 could increase the cyclic strength by 70 percent as much as the strength of normally consolidated specimens, and that the strength increase became less pronounced as the fines present in the specimen decreased. On the other hand, cyclic triaxial tests were performed on undisturbed specimens as well as on normally consolidated reconstituted specimens of identical soils. For the undisturbed specimens, about a 15 percent strength increase was observed over the strength of the reconstituted specimens. By comparing the two strength increases, the one in the intact state and the other in the overconsolidated reconstituted state, each having a comparable amount of fines, it was shown that the strength increase in intact soils might have been brought about by the hardening effect of overconsolidation with an OCR-value of 1.0 to 2.0. Since the strain history is also known to influence the cyclic strength, the exact cause of the strength increase has yet to be investigated.

Acknowledgments

The study described herein was carried out when the second and third authors were at the University of Tokyo from 1972 to 1974 on leave from Fudo Construction Company. The study was supported partly by a grant from the Japanese Ministry of Education.

References

[1] Marsal, R. J. in *Proceedings*, 5th International Conference on Soil Mechanics and Foundation Engineering, Paris, France, Vol. 1, 1961, pp. 229-234.
[2] Ikehara, T., *Soils and Foundations*, Vol. 10, No. 2, 1970, pp. 52-71.
[3] Yamanouchi, T., Koreeda, K., and Sakaguchi, O., *Tsuchi-to-Kiso*, Japanese Society of SMFE, Vol. 24, No. 7, 1976, pp. 25-32 (in Japanese).
[4] Ishihara, K. and Yasuda, S., *Soils and Foundations*, Vol. 12, No. 4, 1972, pp. 65-77.
[5] Silver, M. L. and Park, T. K. *Soils and Foundations*, Vol. 16, No. 3, 1976, pp. 51-65.

J. P. Mulilis,[1] *F. C. Townsend,*[2] *and R. C. Horz*[2]

Triaxial Testing Techniques and Sand Liquefaction

REFERENCE: Mulilis, J. P., Townsend, F. C., and Horz, R. C., "**Triaxial Testing Techniques and Sand Liquefaction,**" *Dynamic Geotechnical Testing, ASTM STP 654,* American Society for Testing and Materials, 1978, pp. 265–279.

ABSTRACT: This investigation examines effects of specimen preparation and testing techniques, that is, loading wave form, degree of saturation, and density variations, on the liquefaction behavior of Monterey No. 0 sand under cyclic loading. The test results indicate that specimen preparation greatly affects the cyclic strength. Specimens prepared moist were 38 to 58 percent stronger than specimens of comparable density prepared dry. Also, specimens prepared using a procedure of undercompaction were approximately 10 percent stronger than comparable specimens prepared without using variable compaction. Loading wave form, as well, affected cyclic strength, with sinusoidal wave forms exhibiting strengths 15 percent stronger than triangular-shaped and 30 percent stronger than rectangular-shaped loading wave forms. An increase in density of 20 kg/m^3 (1.2 lb/ft^3) caused a 22 to 30 percent increase in strength.

The results showed that changing the diameter of the compaction foot from 0.95 cm (0.375 in.) to 3.56 cm (1.4 in.) or the molding water content from 12.8 percent to 8.0 percent, or testing specimens after a *B*-value of either 0.98 or 0.91 had been obtained, had no significant effect on the cyclic strength of specimens.

KEY WORDS: sands, liquefaction, cyclic triaxial tests, testing techniques, specimen preparation, soil dynamics, soils

Recent investigations by Pyke [*1*],[3] Ladd [*2*], Mulilis et al [*3*], Marcuson and Townsend [*4*], and Mitchell et al [*5*] have provided clear evidence that the liquefaction characteristics of saturated sands under cyclic loading are significantly influenced by the method of specimen preparation or soil deposition. There is limited data available in the literature, however, on the effects of certain testing techniques or procedures or both on the liquefaction behavior of sands (for example, what range of *B*-values can be used without affecting the test results, and the effects of using triangular, rectangular, or sinusoidal loading wave forms). The following investigation

[1] Project engineer, Fugro Inc., 3777 Long Beach Blvd., Long Beach, Calif. 90807.

[2] Research civil engineer, and civil engineer, respectively, Soil Mechanics Division, Soils and Pavements Laboratory, U. S. Army Engineer Waterways Experiment Station, Corps of Engineers, Vicksburg, Miss. 39180.

[3] The italic numbers in brackets refer to the list of references appended to this paper.

was performed to provide additional information on the effects of specimen preparation, to study the effects of certain testing techniques or procedures or both on the liquefaction behavior of soils, and to assist in the establishment of ASTM standards for cyclic triaxial testing.

Material

The material used in this investigation was Monterey No. 0 sand, whose sand grains are rounded to subrounded. The physical properties and grain-size distribution are presented in Fig. 1.

Testing Equipment

Undrained isotropically consolidated cyclic triaxial tests were performed on remolded specimens of Monterey No. 0 sand, using two different pneumatic loading units.

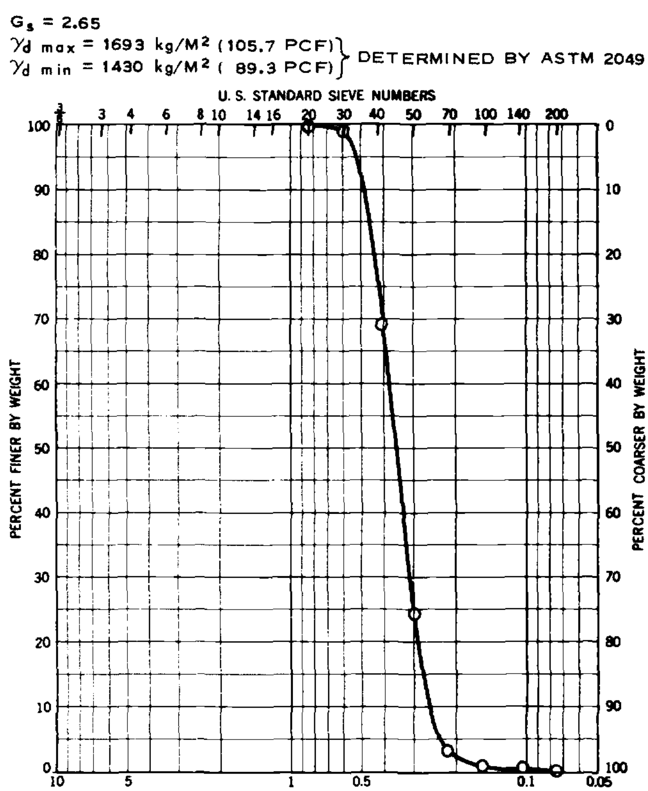

FIG. 1—*Grain size distribution for Monterey No. 0 sand.*

1. One of these units consists of regulators and solenoid valves to provide alternating air pulses to a double-acting load cylinder so that a load is cyclically applied from the load cylinder through the connecting piston to the specimen. This unit has the capability of applying cyclic loads in a rectangular wave form, a triangular wave form, or forms varying between rectangular and triangular.

2. The other unit is a sinusoidal loading system designed by Chan and Mulilis [*6*]. The main components of the system are a sine wave generator, a volume booster relay, and double-acting air piston. At the start of the test, when deformations are extremely small, the sine wave generator applies a cyclic air pressure to one side of piston while the pressure on the other side of the piston remains at a static value. As deformations become larger with the onset of liquefaction, the volume booster relay boosts the quantity of airflow required to keep the output pressure matching the signal pressure from the sine wave generator. This air boost enables the load on the specimen to remain constant during large strains, which generally is not the case in most other loading systems.

All cyclic triaxial tests were performed at a loading rate of 1 Hz, and for any one test, irrespective of the loading system used, four variables were monitored continuously during each test: axial load, axial deformation, pore pressure, and chamber pressure. The variables were monitored with a load cell, linear variable differential transducer (LVDT), and pressure transducers, respectively, and recorded using a high-speed continuous line recorder. The equipment was carefully calibrated prior to testing.

Specimen Preparation

The effects of specimen preparation were investigated by performing undrained cyclic triaxial tests on remolded specimens of Monterey No. 0 sand compacted to a relative density of approximately 60 percent by three tamping procedures. In addition, several tests were performed on specimens which were compacted by variations of a particular method. All specimens were compacted in six 2.54-cm (1 in.) layers inside a rubber membrane which was mounted on the base of the triaxial cell and supported by a split forming mold. A description of the three compaction procedures follows:

1. Dry Rodding—The desired weight of dry soil for the first layer was slowly poured into the mold, and a 0.95-cm-(3/8 in.) diameter rod was forced through the layer in a circular pattern until the layer decreased in thickness to the desired height. Subsequently, the height of each layer was determined to the nearest 0.025 cm (0.01 in.) by placing a straight edge across the top of the mold and measuring the distance from the top of the layer to the top of the mold with a scale. The procedure was then repeated for each succeeding layer, producing a specimen approximately 15.24 cm (6 in.) high by 7.11 cm (2.8 in.) in diameter.

2. Moist Rodding—The desired weight of dry soil for the first layer was placed in a beaker and enough deaired water was added to produce an arbitrarily selected moisture content of 12.8 percent. The soil and water were then thoroughly mixed and poured into the mold, and compacted in the identical manner previously described. The compacted layer was then scarified to a depth of about 0.25 cm (0.1 in.) and the procedure was repeated for each succeeding layer, producing a specimen approximately 15.25 cm (6 in.) high by 7.11 cm (2.8 in.) in diameter.

3. Moist Tamping—This method of preparation is identical to that previously described, except that the size of the tamping foot is different for this method. In this case, each layer of moist sand and (w = 12.8 percent) was compacted using a tamping rod with a tamping foot equal to one-half the specimen diameter.

After the specimen had been compacted by any one method and sealed by placing the top cap and securing the membrane with an O-ring, a vacuum of 10 in. Hg (33.8 kN/m^2 = 4.9 psi) was applied to the specimen through the top cap. Subsequently, the forming jacket was removed, and the specimen was supported by the vacuum while its height and diameter were measured. A straight edge was placed on the top cap of the specimen, and a scale was used to measure the height of the specimen to the nearest 0.025 cm (0.01 in.). The diameter of the specimen was originally measured with calipers to the nearest 0.002 cm (0.001 in.), two mutual perpendicular readings being taken at three equally spaced locations (approximately the quarter points) along the height of the specimen. A thin steel circumferential tape, which is wrapped around the specimen and calibrated to read the diameter directly, was used in the latter stages of the investigation. With a little practice and extreme care, it was found that the diameter computed from the average measurements obtained by the calipers agreed reasonably well with that obtained by use of the circumferential tape. However, since the circumferential tape measures the average diameter at any one location on the specimen, whereas the calipers measure a "two-point" diameter, the use of the circumferential tape will result in a more accurate measurement of the diameter.

After the specimen dimensions were recorded, the triaxial chamber was assembled and a chamber pressure of 34.5 kN/m^2 (5 psi) was gradually applied while the vacuum on the specimen was simultaneously reduced to zero. All specimens were then saturated by first allowing water to seep slowly into the specimen, and then by simultaneously increasing the chamber pressure and back pressure. Typically, complete saturation of the soil determined by Skempton's B parameter was obtained with a back pressure of 414 kN/m^2 (60 psi) to 690 kN/m^2 (100 psi). All specimens were then consolidated under an effective confining pressure of 100 kN/m^2 (14.5 psi) for approximately 20 min prior to testing. Additional details concerning testing equipment and specimen preparation are contained in Ref. 7.

Effects of Specimen Preparation Procedure

A comparison of cyclic stress ratio versus number of cycles to cause initial liquefaction (point at which peak pore pressure response equalled chamber pressure) for specimens prepared by dry rodding and moist rodding using rectangular wave loading is presented in Fig. 2; a summary of all the cyclic triaxial test results is presented in Table 1. The results in Fig. 2 clearly show that the specimens prepared by moist rodding were significantly stronger than those prepared by dry rodding; the increase in the cyclic stress ratio required to cause initial liquefaction is approximately 58 percent at 10 cycles and 38 percent at 30 cycles.

Similar results were observed by Mulilis et al [3] in performing undrained cyclic triaxial tests on specimens of Monterey No. 0 sand remolded to a relative density of 50 percent and tested at an initial effective confining pressure of 55.2 kN/m^2 (8 psi). They found that specimens prepared by moist rodding at a water content of 12 percent were approximately 20 percent stronger than those prepared by dry rodding when compared at the cyclic stress ratio required to cause initial liquefaction in 10 cycles. The difference in the magnitude of the increase in strength (58 percent versus 20 percent) could be due to the fact that their specimens were compacted to a lower relative density (50 percent versus 60 percent) and prepared in a slightly different manner. [After initially rodding each layer with a 0.94-cm (3/8 in.) rod to the approximate desired height, a cylindrical surcharge, 7.1 cm (2.8 in.) in diameter, was used to achieve a level surface and decrease the thickness of the layer to the final desired height.]

Figure 2 also presents the results of two tests prepared by moist rodding, but at a lower molding water content (8 percent versus 12 percent). These results show that, at high stress ratios, reducing the molding water content from 12.8 to 8.0 percent has virtually no effect on the cyclic strength of the material.

Effect of Tamping Foot Size

Figure 3 presents the results of tests conducted to evaluate the effects of tamping foot size, that is, moist rodding versus moist tamping. Based on the results of two tests performed on specimens compacted using a larger-diameter tamping foot, it may be seen that the size of the tamping foot had virtually no effect at high stress ratios on the strength of the soil. Since no effect of tamping foot size was observed, and since the moist rodding and moist tamping compaction procedures were otherwise identical, it was decided to use the moist tamping method of compaction to prepare the remaining test specimens. This decision was based on the fact that the moist tamping equipment provided closer control over the density of each layer.

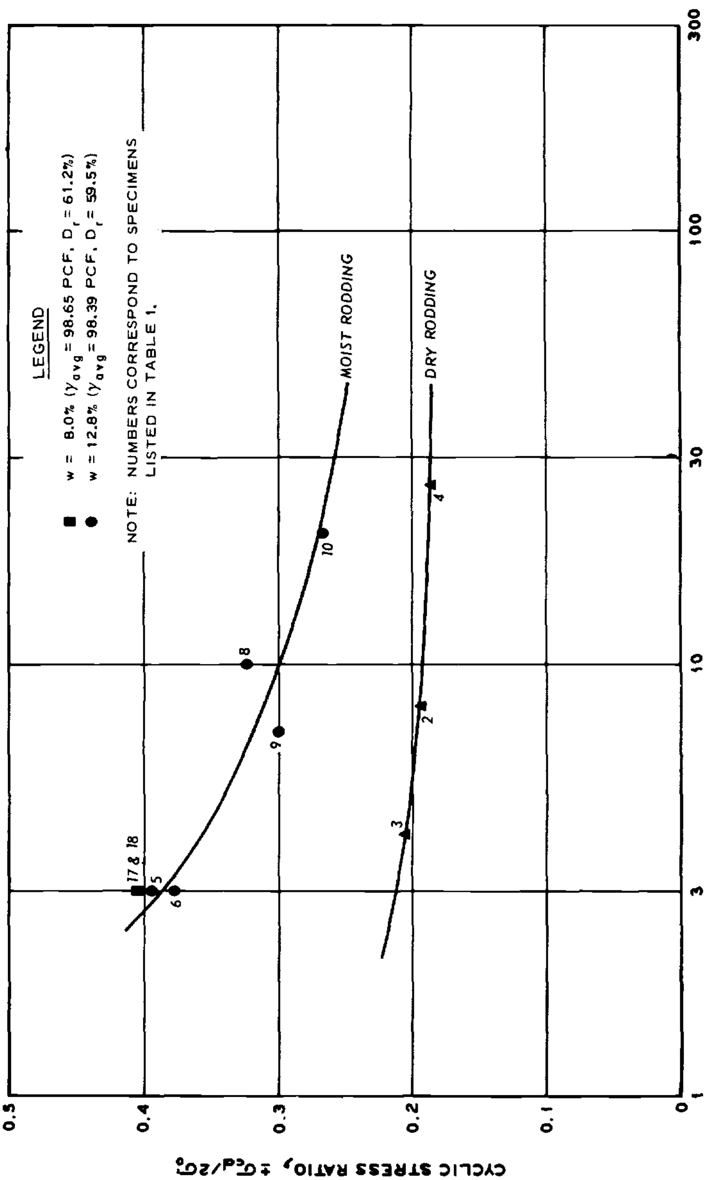

FIG. 2—*Effect of specimen preparation method and molding water content on number of loading cycles to cause initial liquefaction (rectangular wave) (1 lb/ft^3 = 16 kg/m^3).*

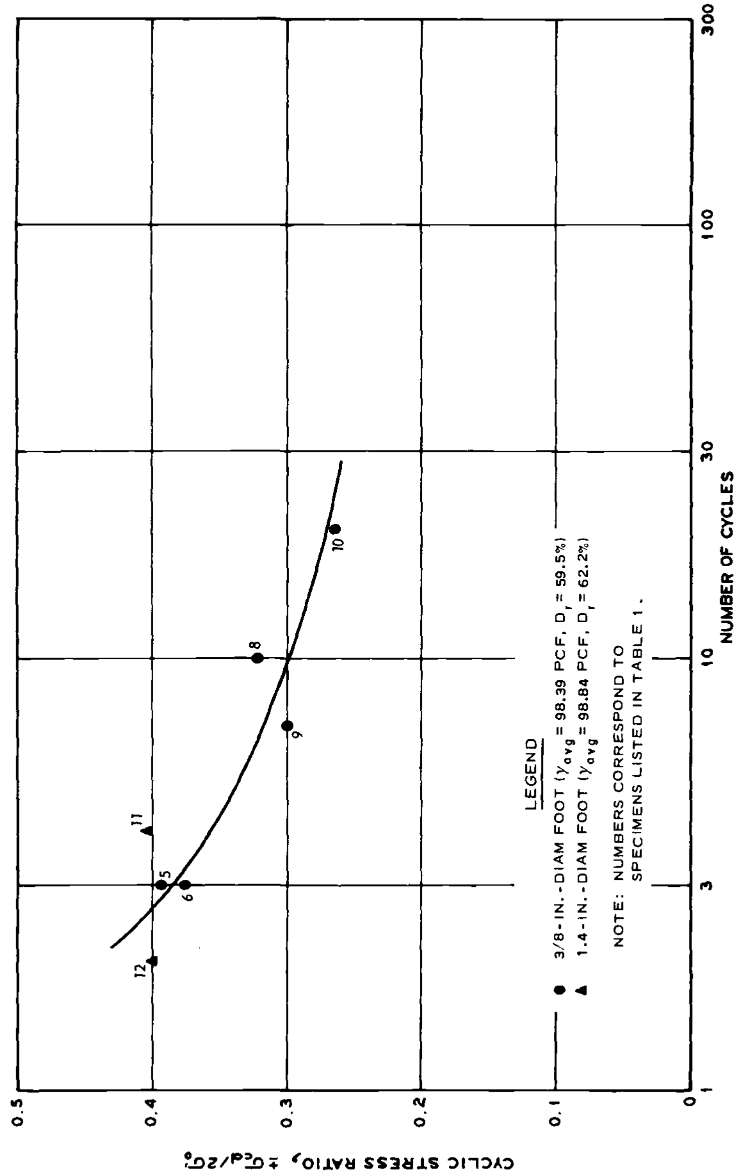

FIG. 3—*Effect of tamping foot on loading cycles to initial liquefaction (rectangular wave) (1 lb/ft^3 = 16 kg/m^3).*

Mulilis et al [3] also investigated the effects of tamping foot size on the cyclic triaxial strength of Monterey No. 0 sand molded to a relative density of 50 percent. They found that specimens prepared by moist tamping were approximately 10 percent stronger than specimens prepared by moist rodding. The small difference between the results of their investigation and the one described herein could be due to scatter or to the fact that their specimens were compacted to a lower relative density (50 percent versus 60 percent) and prepared in a slightly different manner. (The moist tamping methods of compaction were identical, and the differences in the moist rodding method of compaction were described previously.)

Effects of Variable Compaction and *B*-Value

When compacting a specimen in layers, each succeeding layer densifies the material in the layers below it. This fact was recognized by Chen [8] in 1948; hence, three tests were performed on specimens which were prepared using a procedure of variable compaction suggested by Silver et al [9]. The concept of variable compaction consists of preparing each layer at an initially looser density than the final desired value by a certain percentage. An optimum value of percent undercompaction is chosen for the first layer and each succeeding layer is prepared denser, or at a lower percent undercompaction, the result ideally being a uniform specimen with respect to density. Typically, the optimum value of percent undercompaction ranges between zero and about 20 percent, with the higher value being associated with very loose specimens. For the three specimens tested at 60 percent relative density, a value of 10 percent undercompaction as suggested by Ladd [10] was chosen.

In order to investigate the effect of the B-value on the strength of the soil, the three specimens were tested at B-values of only 0.91, 0.92, and 0.93, as opposed to the typical B-value of 0.97 or greater. Figure 4, comparing the effects of undercompaction and B-value, shows that specimens which were undercompacted and tested at a lower B-value were approximately 10 percent stronger. Thus, it may be concluded that using a procedure of variable compaction and testing at a lower B-value may result in somewhat higher strengths.

To throw some light on the subject, the degree of saturation was calculated for various B-values using the following relationship suggested by Black and Lee [11]:

$$S_i = \frac{1 - Z(1 - B)}{1 - ZQ}$$

where

$$Q = Bn_i \frac{C_w}{C_D}$$

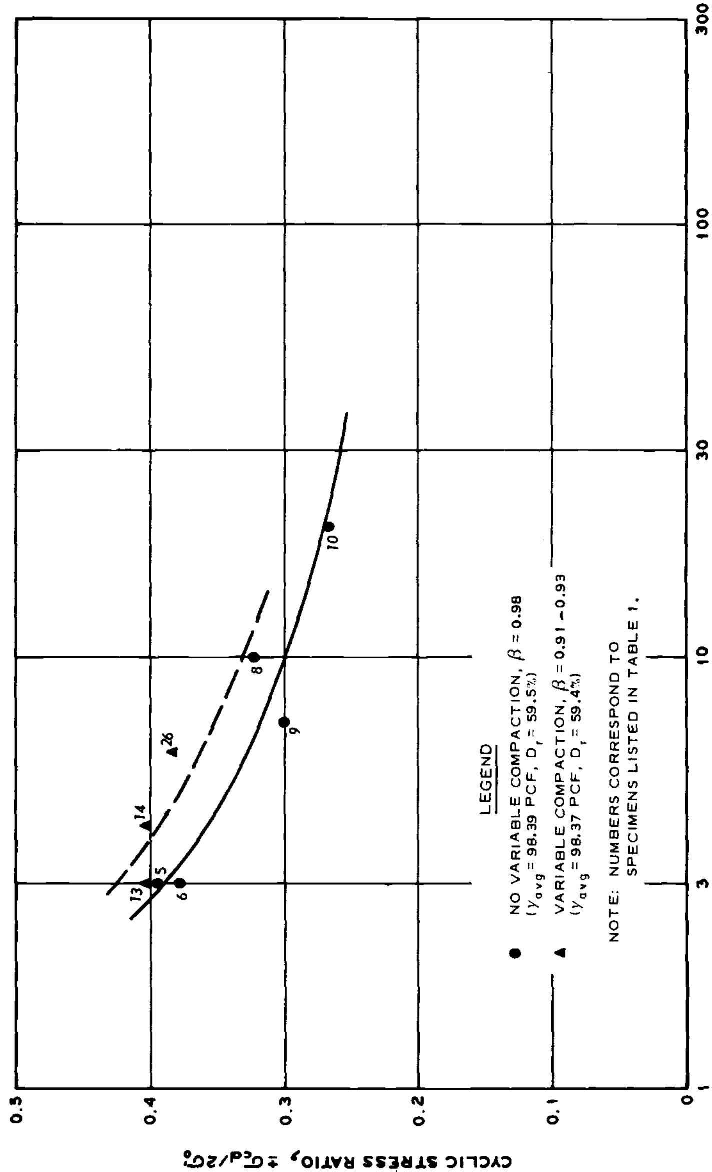

FIG. 4—*Effect of undercompaction and* B*-value on number of loading cycles to initial liquefaction (rectangular wave) (1 lb/ft^3 = 16 kg/m^3).*

$$Z = \frac{Y}{D}$$

$$Y = C_d \left(\frac{\Delta\sigma_3}{n_i}\right)$$

$$D = 1 - \left(\frac{P_i}{P_i + B\Delta\sigma_3}\right)$$

and

B = Skempton's parameter,
S_i = initial degree of saturation,
P_i = pressure corresponding to S [typically, 414 kN/m^2 (60 psi) for the lower B-values, and 414 kN/m^2 to 690 kN/m^2 (100 psi) for the higher B-values],
n_i = initial porosity (for a relative density of 60 percent, n_i = 0.405),
C_d = compressibility of soil structure (1.4 × 10^{-5} kN/m^2 = 10^{-4} psi) C_d is approximately equal to
c_w = compressibility of water (0.22 × 10^{-6} kN/m^2 = 3.2 × 10^{-6} psi)
$\Delta\sigma_3$ = change in chamber pressure (68.9 kN/m^2 = 10 psi)

The results of these calculations indicated that for the conditions used in this investigation, a measured B-value of 0.91 to 0.98 implied a degree of saturation of 99.9 percent. Thus it might be concluded that the increase in strength of the three specimens was probably due to the fact that the specimens were formed using a procedure of variable compaction, rather than to the fact that they were tested at a lower B-value. Support for this conclusion comes from studies by Ladd [*10*] which showed that the liquefaction characteristics of sands can be greatly influenced by the amount of undercompaction used in the specimen preparation procedure. Studies by Chaney [*12*], however, indicate that the measured cyclic strength of remolded specimens of sand tested at B-values ranging from 0.91 to 0.99 could vary significantly, depending on the soil type, the density, and the initial effective confining pressure. Thus the foregoing conclusions may be applicable only to Monterey No. 0 sand tested at a relative density of 60 percent and an initial effective confining pressure of 100 kN/m^2 (14.5 psi).

Effects of Loading Wave Form

The effects of loading wave form on the cyclic triaxial strength were investigated by conducting tests on specimens prepared by moist tamping using the procedure of variable compaction and a sine wave load form. In addition, two tests were performed on specimens compacted by moist tamping with no variable compaction using a nearly triangular loading wave. The results of the tests using a sine loading wave are shown in Fig. 5, along with a comparison of the results of tests using a sine loading wave (on specimens prepared using the variable compaction procedure), nearly triangular loading wave (on specimens prepared without using the variable compaction procedure), and rectangular loading wave (on specimens prepared without using the variable compaction procedure). Although only two tests were performed using the nearly triangular loading wave, and there is some scatter in the data, the following observations could be made regarding the effect of loading wave form on the strength of the soil (see Fig. 5):

1. Specimens which were tested using a nearly triangular loading wave were approximately 13 percent stronger at high stress ratios than specimens tested using a rectangular loading wave. Similar results were observed by Lee and Fitton [*13*], Seed and Chan [*14*], and Thiers [*15*].

2. Specimens which were tested using a sine loading wave were approximately 15 percent stronger than specimens tested using a nearly triangular loading wave and approximately 30 percent stronger than specimens tested using a rectangular loading wave; part of the difference in strength is probably due to the procedure of undercompaction as explained previously. Similar effects of loading wave shape were obtained by Silver et al [*9*] when using a rectangular wave with a fast rise time. If the rise time in the rectangular wave form was degraded such that the wave shape did not have a nearly instantaneous change of velocity in either the loading or unloading portion of the cycle, however, then the strength of specimens which were tested using the degraded wave form was approximately the same as that of specimens which were tested using the sine wave form. The shape of the rectangular loading wave used in this investigation was in between the shapes of the degraded rectangular loading wave and the severe rectangular loading wave used by Silver et al [*9*].

Effects of Density

While it is generally agreed that the liquefaction potential of a soil decreases with increasing density (other factors being equal), the degree to which a small change in density affects the liquefaction potential of a particular soil is not so well known. Since it is nearly impossible to consistently prepare specimens to an exact density, a tolerance of ± 2 percent relative density (± 5.3 kg/m^3 = 0.33 lb/ft^3) was arbitrarily chosen in this investigation. However, to investigate the effect of a small change in density on the strength of the soil, three specimens were compacted to a somewhat higher density; the average relative density of these specimens was 66.4 percent (1595 kg/m^3 = 99.54 lb/ft^3). The results of tests performed on these specimens are presented in Fig. 6, together with the results of similar

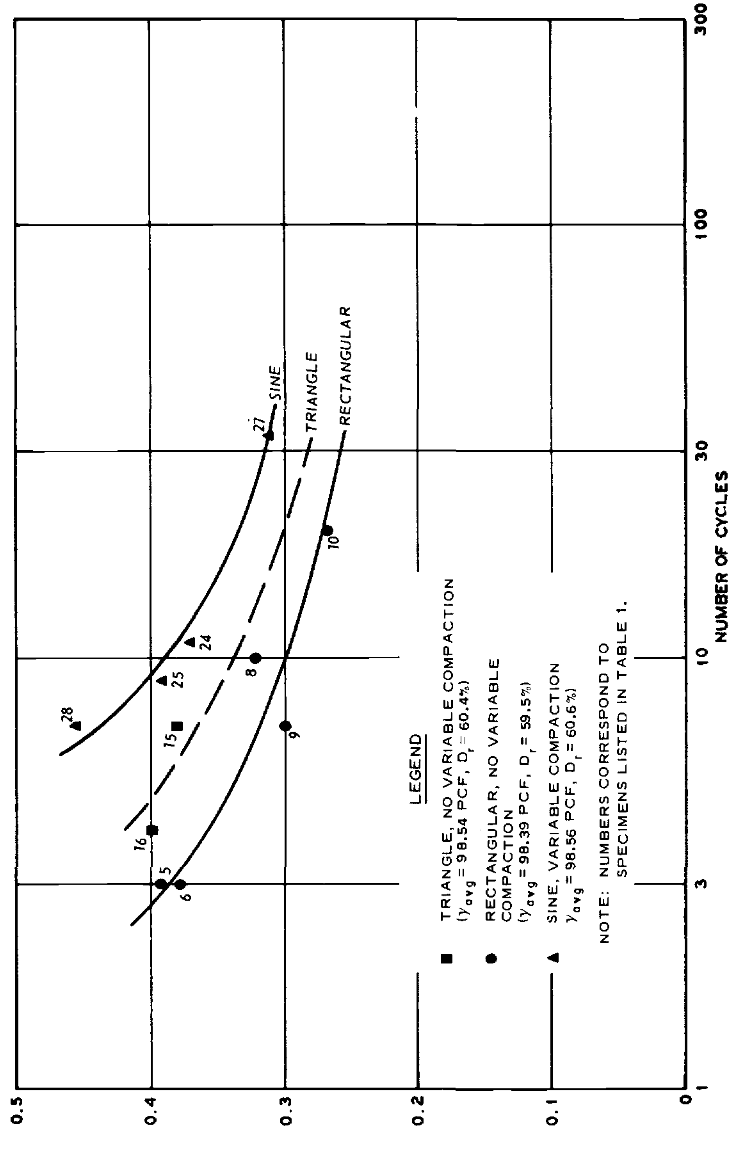

FIG. 5—*Effect of loading wave form on cycles to initial liquefaction for moist-tamped specimens (1 lb/ft^3 = 16 kg/m^3).*

tests performed on five specimens whose average relative density was 59.5 percent (1576 kg/m^3 = 98.39 lb/ft^3). It may be observed in Fig. 6 that the slightly denser specimens were significantly stronger; the increase in the cyclic stress ratio required to cause initial liquefaction is approximately 30 percent at 10 cycles and 22 percent at 30 cycles. Thus it can be concluded that for Monterey No. 0 sand, an increase in relative density of about 12 percent (20 kg/m^3 = 1.2 lb/ft^3) can cause an increase in strength of approximately 22 to 30 percent.

Conclusions

The investigation [7] described in the foregoing was performed to determine the effects of certain testing techniques or procedures or both on the liquefaction characteristics of sands. Although some of the variables were investigated to only a limited degree, the following conclusions regarding the undrained cyclic triaxial strength of Monterey No. 0 sand may be drawn:

1. The cyclic strength of specimens prepared by moist rodding was approximately 38 to 58 percent greater than that of comparable specimens prepared by dry rodding.
2. Specimens tested using a sinusoidal loading wave form and variable compaction exhibited higher strengths than specimens tested using either a nearly triangular or square loading wave form and no variable compacting. Specimens tested using a nearly triangular loading wave form exhibited higher strengths than specimens tested using a square wave form.
3. An increase in the relative density of a specimen of approximately 12 percent (20 kg/m^3 = 1.2 lb/ft^3) may cause a 22 to 30 percent increase in the strength of the specimen.
4. Changing the diameter of the compaction foot from 0.95 cm (0.375 in.) to 3.56 cm (1.4 in.), or the molding water content from 12.8 to 8.0 percent, or testing specimens after a B-value of either 0.98 or 0.91 has been obtained, appeared to have no significant effect at high stress ratios on the strength of the specimens.
5. Specimens prepared using a procedure of undercompaction were approximately 10 percent stronger than comparable specimens formed without using a procedure of variable compaction.

Based upon the results of this investigation and supporting conclusions from the literature, it is obvious that extreme care must be used in preparing remolded sand specimens, and special attention paid to testing techniques in order to obtain reproducible test results. In particular, the method of specimen preparation, the shape of the loading wave form, and the preciseness of density determinations greatly affect cyclic strength. Hence, development of ASTM standards for cyclic triaxial testing should include consideration of these factors and the results of this investigation.

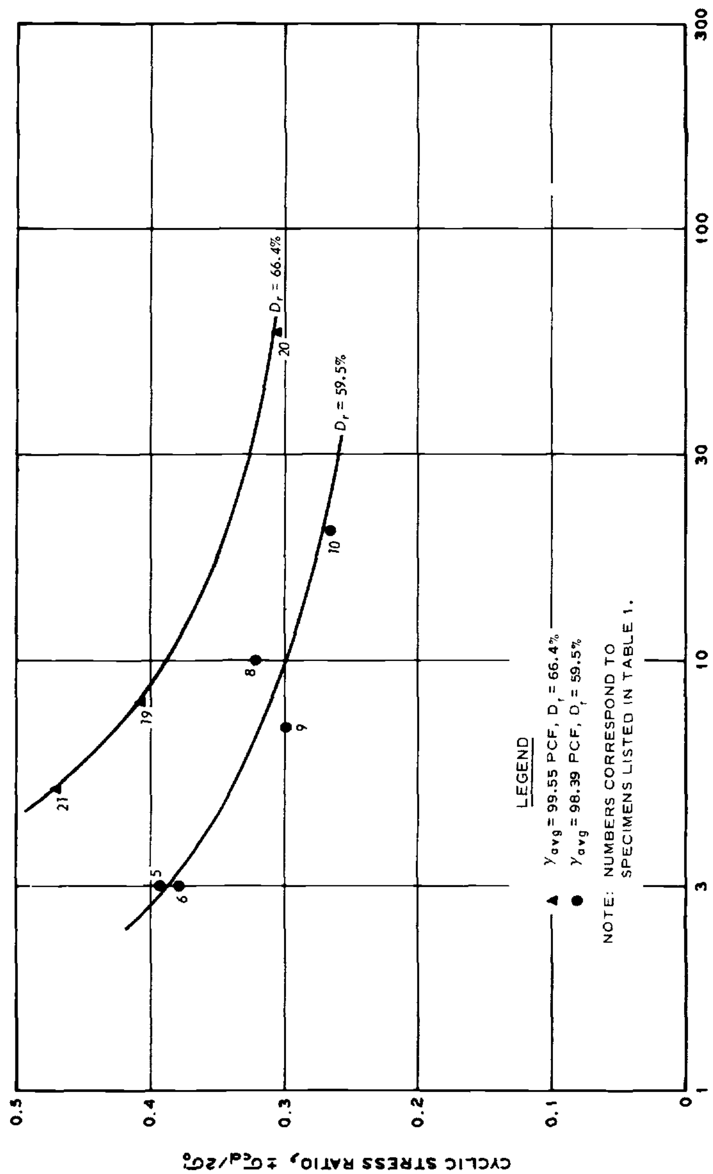

FIG. 6—*Effect of density on number of square wave loading cycles to cause initial liquefaction for moist-tamped specimens (rectangular wave) (1 lb/ft^3 = 16 kg/m^3).*

Acknowledgments

The study described in this paper was performed at the U. S. Army Engineer Waterways Experiment Station and sponsored by Project 4A161102B52E, Task 04, Research in Military Construction. The support and work of Mr. G. D. Abel, who conducted the laboratory tests, is gratefully acknowledged.

References

[*1*] Pyke, R. M., "Settlement and Liquefaction of Sands Under Multi-Directional Loading," Ph.D. dissertation, University of California, Berkeley, 1973.

[*2*] Ladd, R. S., Technical Note, *Journal, Geotechnical Engineering Division,* American Society of Civil Engineers, Vol. 100, No. GT10, Oct. 1974, pp. 1180–1184.

[*3*] Mulilis, J. P. et al, *Journal, Geotechnical Engineering Division,* American Society of Civil Engineers, Vol. 103, No. GT2, Feb. 1977, pp. 91–108.

[*4*] Marcuson, W. F., III, and Townsend, F. C., "Effects of Specimen Reconstitution on Cyclic Triaxial Results," Miscellaneous Paper S-76-5, U. S. Army Engineer Waterways Experiment Station, Corps of Engineers, Vicksburg, Miss., 1976.

[*5*] Mitchell, J. K., Chatoian, J. M., and Carpenter, G. C., "The Influences of Sand Fabric on Liquefaction Behavior," Contract Report S-76-5, U. S. Army Engineer Waterways Experiment Station, Corps of Engineers, Vicksburg, Miss., June 1976.

[*6*] Chan, C. K. and Mulilis, J. P., "A Pneumatic Sinusoidal Loading System," *Journal, Geotechnical Engineering Division,* American Society of Civil Engineers, Vol. 102, No. GT3, March 1976, pp. 277–281.

[*7*] Mulilis, J. P., Horz, R. C., and Townsend, F. C., "The Effects of Cyclic Triaxial Testing Techniques on the Liquefaction Behavior of Monterey No. 0 Sand," Miscellaneous Paper S-76-6, U. S. Army Engineer Waterways Experiment Station, Corps of Engineers, Vicksburg, Miss., April 1976.

[*8*] Chen, L. S. in *Proceedings,* Second International Conference, Soil Mechanics and Foundation Engineering, Vol. 5, Rotterdam, 1948.

[*9*] Silver, M. L. et al, "Cyclic Triaxial Strength of a Standard Test Sand," *Journal, Geotechnical Engineering Division,* American Society of Civil Engineers, Vol. 102, No. GT5, May 1976, pp. 511–524.

[*10*] Ladd, R. S., "Preparing Test Specimens Using Undercompaction," submitted for publication to the *Journal of the Geotechnical Engineering Division,* American Society of Civil Engineers, 1976.

[*11*] Black, D. K. and Lee, K. L., *Journal, Soil Mechanics and Foundations Division,* American Society of Civil Engineers, Vol. 99, No. SM1, Jan. 1973, pp. 75–93.

[*12*] Chaney, R. C., "Deformations of Earth Dams Due to Earthquake Loading," Ph.D. thesis, University of California, Los Angeles, 1976.

[*13*] Lee, K. L. and Fitton, J. A. in *Vibration Effects of Earthquakes on Soils and Foundations, ASTM STP 450* American Society for Testing and Materials, 1969, pp. 71–95.

[*14*] Seed, H. B. and Chan, C. K., "Pulsating Loading Tests on Samples of Clay and Silt from Anchorage, Alaska," Report on Anchorage Area Soil Studies to U. S. Army Engineer District, Anchorage, Alaska, Aug. 1964.

[*15*] Thiers, G. R., "The Behavior of Saturated Clay Under Seismic Loading Conditions," Ph.D. dissertation, University of California at Berkeley, 1965.

D. A. Sangrey,[1] *W. S. Pollard,*[1] *and J. A. Egan*[2]

Errors Associated with Rate of Undrained Cyclic Testing of Clay Soils

REFERENCE: Sangrey, D. A., Pollard, W. S., and Egan, J. A., "**Errors Associated with Rate of Undrained Cyclic Testing of Clay Soils,**" *Dynamic Geotechnical Testing, ASTM STP 654,* American Society for Testing and Materials, 1978, pp. 280–294.

ABSTRACT: A wide range of cyclic testing rates can be applied to specimens of clay soil depending on the particular test objective. A group of factors which influence the results of these tests is identified and the significance of these factors on test results is demonstrated. Undrained creep effects and air diffusion through membranes surrounding the test specimen are major factors, and methods are described to correct or control these errors. Nonuniform conditions within the test specimen are also significant in some tests. Illustrations of the potential errors and corrections are presented.

There is no cyclic loading rate which has a clear advantage over other rates, although for particular purposes there is a clear preference.

KEY WORDS: laboratory testing, cyclic triaxial tests, pore pressures, earthquake engineering, creep, diffusion, dynamic properties of soils, soils

Nomenclature

- d Empirical parameter used in prediction of pore pressure errors due to diffusion
- k Empirical parameter used in prediction of pore pressure errors due to creep
- m Empirical parameter used in describing creep as a rate process
- p Mean normal effective stress, $(\sigma_1' + \sigma_2' + \sigma_3')/3$
- p_s Specimen pore fluid pressure predicted using diffusion model
- p_c Cell pressure in diffusion model
- q Principal stress difference, $\sigma_1 - \sigma_3$
- t Time

[1]Associate professor and research assistant, respectively, School of Civil and Environmental Engineering, Cornell University, Ithaca, N.Y. 14853.

[2]Engineer, Woodward-Clyde Consultants, Houston, Tex.

t_0, t_1, t_{100}	Specific reference times
Δu	Excess pore pressure
Δu_T	Total excess pore pressure
Δu_q	Excess pore pressure due to applied stress difference, q
Δu_p	Excess pore pressure due to mean normal stress, p
Δu_{cyc}	Excess pore pressure due to cyclic loading
A	Strain rate at time t_1
D	Creep deviator stress
$\dot{\epsilon}$	Strain rate
α	Constant in creep rate prediction

The rate of applying cyclic or repeated loading to clay soils can vary over a wide range of periods. In actual field situations, loading can be a result of earthquakes with a loading period of less than one second per cycle, through wind and wave loading with a period of several seconds, to live loading of structures having a period of several months per cycle. Undrained conditions can apply to all these problems because of the low permeability of clay soils and the time required for drainage of excess pore pressures in the field.

In some cases attempts are made to conduct laboratory tests at a rate appropriate to actual field loading. More frequently, however, testing convenience controls the rate of load application. This is especially important if accurate pore pressure measurements are required (effective stress methods), in which case the rate of testing may be quite slow. Effective stress methods, and testing procedures appropriate to effective stress methods, will become more common. This trend is clearly indicated by evolving practice and government regulation, in Northern Europe, for example, and in general for offshore applications. Consequently, the two conflicting factors, a desire to test at rates similar to actual loading and testing convenience or requirements, must be weighed when selecting a laboratory testing rate. The underlying question, however, is, What influence does the rate of testing have on the response of clay soils subjected to cyclic loading and what errors are associated with different rates?

There is no generally accepted method for conducting cyclic loading tests on clays, although several methods have been described as part of research on the fundamental mechanism of behavior of these soils *[1-3]*.[3] For sands there is an extensive literature describing the influence of many testing variables, and systematic testing procedures have been proposed *[4-6]*. However, most of this work was done using relatively rapid rates of loading since the practical application of the results was to earthquakes. The significance of cyclic loading rate has been noted for selected studies on both sands and clays *[1,7-9]*. In summary, these studies have shown

[3]The italic numbers in brackets refer to the list of references appended to this paper.

that under a rapid cyclic loading rate it usually takes more cycles to achieve a particular result, either failure or some level of strain, than for an identical test run under a slower loading rate. On the basis of these studies it is not clear whether failure will occur under some loading rates but not others for a particular stress level. One reason for this uncertainty is that testing errors have not been separated from testing effects.

In this paper the results of a comprehensive study on the influence of testing rate are presented and both testing errors and soil response effects are identified. Each major factor is discussed in a separate section, followed by a discussion and recommendations to account for these factors. As a basis for this study it is appropriate to summarize the response of a clay soil subjected to undrained cyclic loading. Figure 1 applies to a saturated contractive, or normally consolidated soil which develops cumulative positive pore pressures during cyclic loading. The illustration is for a triaxial compression test loaded one way from an initial condition of no applied

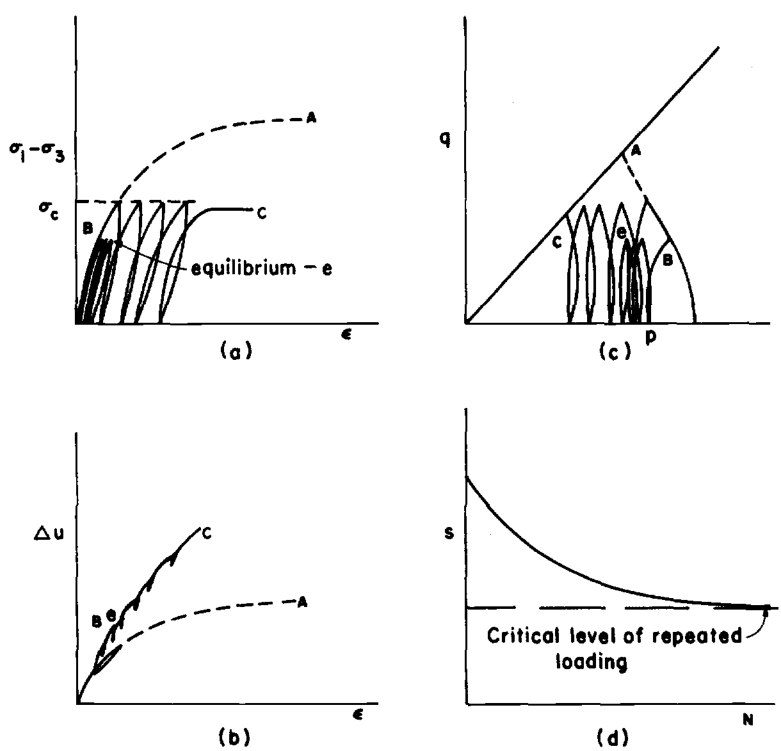

FIG. 1—*Summary of the response of saturated soils to repeated loading: Curve A—monotonic loading to failure; Curve B—low-level cyclic loading; Curve C—higher-level cyclic loading.*

stress difference. As such, it may not be particularly relevant to a field condition but it is a common and simple example of laboratory behavior.

The magnitude of pore pressure change and strain in a cyclic loading test depends primarily on the level of cycled stress along with other factors. When the cycled stress level is high, Curve C in Fig. 1, pore pressure will accumulate to the point that an effective stress failure occurs. At lower levels of cycled stress, Curve B, there is a different behavior. The pore pressure and strain increase only up to a point after which a large number of loading cycles produces no significant change in strain or effective stress, and no failure. This condition is termed nonfailure equilibrium [2] and must represent a common situation for soils which perform satisfactorily under large numbers of cycled stresses in actual applications. The behavior of soils under undrained cyclic loading has been summarized using illustrations such as Fig. 1*d*, in which the level of cycled stress, S, is plotted against the number of cycles at that stress level, N, necessary to cause failure. The highest level of nonfailure equilibrium stress corresponds to the limit of failure, the critical level of repeated loading.

Special attention is directed herein to the condition of nonfailure equilibrium, especially to the unique relationship between cycled stress level and the pore pressure at this condition, Fig. 2*a*. Sangrey et al [2] have used the unique relationship between pore pressure and cycled stress level to define a locus of nonfailure equilibrium in a stress space, Fig. 2*b*. This locus, or equilibrium line, is defined by the effective stress state at the peak of a loading cycle when nonfailure equilibrium has been achieved (Point "e" on Curve B in Fig. 1). Nonfailure equilibrium can be used as a reference for many of the errors and rate of loading effects introduced during cyclic loading tests. The ultimate effect of most of these testing errors and effects is a pore pressure different from that at the ideal nonfailure equilibrium condition. For example, a possible testing error is a leak from the pore pressure measuring system, leading to a drop in pore pressure. The expression of this error would be an equilibrium effective stress condition falling to the right of the equilibrium locus in Fig. 2*b*. In contrast, a leak through the membrane would cause an increase in pore pressure within the test specimen and an effective stress state to the left of the equilibrium conditions. A testing error of this type might ultimately result in failure of the specimen.

The data used to define the nonfailure equilibrium condition in Fig. 2 were obtained from tests on a soil which had no significant undrained creep potential and using test methods which minimized the effect of errors. In the following sections, these two factors are described as the most significant ones affecting undrained cyclic load tests on clay soils. The example in Fig. 2 has been carefully selected to be a best reference for the ideal behavior of undrained cyclic loading of a clay soil with a minimum of errors.

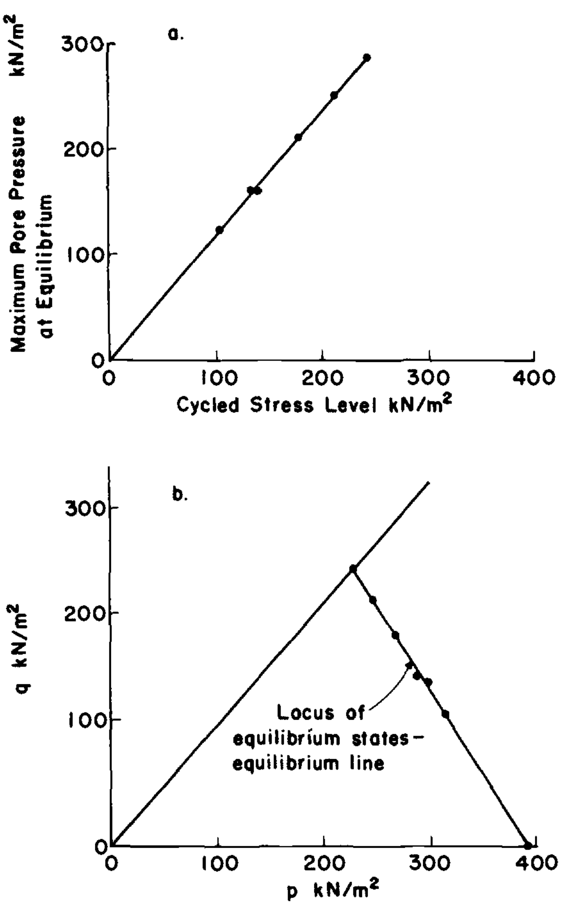

FIG. 2—(a) *Relationship of equilibrium pore water pressure to the level of cycled stress.* (b) *Locus of nonfailure equilibrium stress states.*

Effects of Undrained Creep

Creep is the phenomenon of continued long-term strain under drained conditions, or pore pressure buildup and strain under undrained conditions when a soil is subjected to a sustained stress. Creep has been studied and described in terms of strain rate [*10,11*] and pore pressure buildup [*12-14*] for conventional triaxial test conditions. Effective stress testing of soils subjected to cyclic loading requires separation of pore pressure effects due to creep from those due to load cycling for rational prediction of field behavior. This paper proposes a method to accomplish this separation.

It is appropriate to separate creep effects because they will be very different in a test specimen compared with the field condition. In almost any field situation a soil will have existed under a particular stress state for a long period of time and all significant creep effects will be over. In contrast, the laboratory specimen is consolidated for only a relatively short time, and creep, particularly undrained creep, will continue after the undrained testing begins.

The classical contribution to the study of stress-strain-time effects under sustained deviator stress is reported by Singh and Mitchell [*10*] and by Mitchell, Campanella, and Singh [*11*]. Their work proposed the generalized equation describing creep as a rate process

$$\epsilon = A\left(\frac{t_1}{t}\right)^m e^{\alpha D} \tag{1}$$

Soils exhibiting creep susceptibility were related to m values less than 1, where m equals the slope of logarithmic strain rate versus time. The mechanism proposed to account for the creep effect involved development of adequate activation energy to overcome barriers corresponding to bonding forces within the soil. Creep would occur only if the barriers could be overcome in a preferred manner such that the net effect would be one of breaking soil bonds. This preferential orientation was to be brought about by application of a shearing force, that is, a nonzero deviator stress.

Another approach was taken by Arulanandan, Shen, and Young [*13*], who produced a series of experimental curves showing pore pressure buildup with time under undrained conditions at various deviator stress levels including zero. They concluded that the buildup of pore pressure during creep resulted from the arrest of secondary consolidation under the mean normal stress, p.

A more detailed analysis of these data was reported by Holzer, Hoeg, and Arulanandan [*14*]. By subtracting the quantity of pore pressure generated at a given time in a creep test with zero deviator stress, $q = o$, from the total pore pressure produced at the same elapsed time in a similar creep test with $q > o$, the remaining pore pressure was shown to be approximately constant after an initial period of pore pressure equilization. The authors concluded that time dependency of pore pressure during creep was solely a function of the initial consolidation stress or mean normal stress, p.

Since pore pressure increase under undrained creep may be divided into a time-dependent portion which is a function of p-level and a time-independent portion which is a function of q-level, it is proposed that a third portion could be attributed to cyclic loading. The total pore pressure generated during cyclic load tests on a creep sensitive soil could then be described as

$$(\Delta u)_T = (\Delta u)_p + (\Delta u)_q + (\Delta u)_{\text{cyc}} \tag{2}$$

A stress state plot of a series of these tests would take the form of Fig. 3. Subtraction of Δu_p from the total pore pressures, Δu_T, of tests which had reached equilibrium would allow the plot of an equilibrium line, Fig. 2.

A single creep test at the consolidation conditions to be used in the testing program could be used to generate the Δu_p data. For isotropic testing, an appropriate test would be a zero deviator stress creep test from p_o. For testing anisotropically consolidated soils, a creep test from the consolidation stress state would be preferred.

Experimental Program

To investigate the proposed model of pore pressure behavior, a series of triaxial tests on San Francisco Bay Mud was conducted. Undrained cyclic load tests, creep tests, and conventional deformation controlled tests on specimens trimmed to 3.56 cm (1.42 in.) diameter from 7.62 cm (3 in.) piston cores were run from an anisotropic consolidation state approximating *in situ* conditions. Specimens were consolidated for 72 h before the drainage valve was closed; this consolidation period was approximately three times t_{100}, as defined by a log-time plot. Cyclic loading was done at a rate of one or two cycles per day so that pore pressures could be measured accurately. The general procedure for cyclic load tests at the various q levels was to continue cycling until strain and pore pressure reached apparent

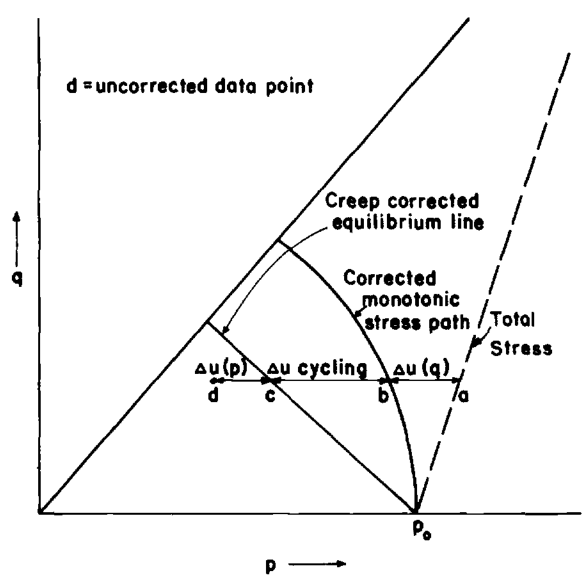

FIG. 3—*Effective stress conditions for cyclic loading tests illustrating the contribution to pore pressure by creep,* Δu_p, *cyclic loading,* Δu_{cyc}, *and applied stress difference,* Δu_q.

equilibrium values (characterized by nearly closed hysteresis loops for several cycles) or failure occurred. After reaching an apparent nonfailure equilibrium condition, the test was monotonically loaded to failure. An undrained creep test was done by following the consolidation scheme just described, then closing the drainage valve at the end of the consolidation period and measuring pore pressures for a given length of time thereafter.

Results are shown in Fig. 4 both as uncorrected and as creep-corrected data. The creep correction to pore pressure involved subtracting the amount of pore water pressure, Δu_p, generated at a given time in the creep test, from the pore pressure, Δu_T, measured at the same time in the cycled test. The net effect of the correction was to increase p by Δu_p while leaving q unchanged. A simplification would involve linearizing the Δu_p versus log time plot of creep data to provide a computational rather than graphical method of determining Δu_p. The actual curve, Fig. 5, can readily be linearized in the time range of interest for most testing with minimal loss of accuracy

$$\Delta u_p = k \log (t - t_0) \tag{3}$$

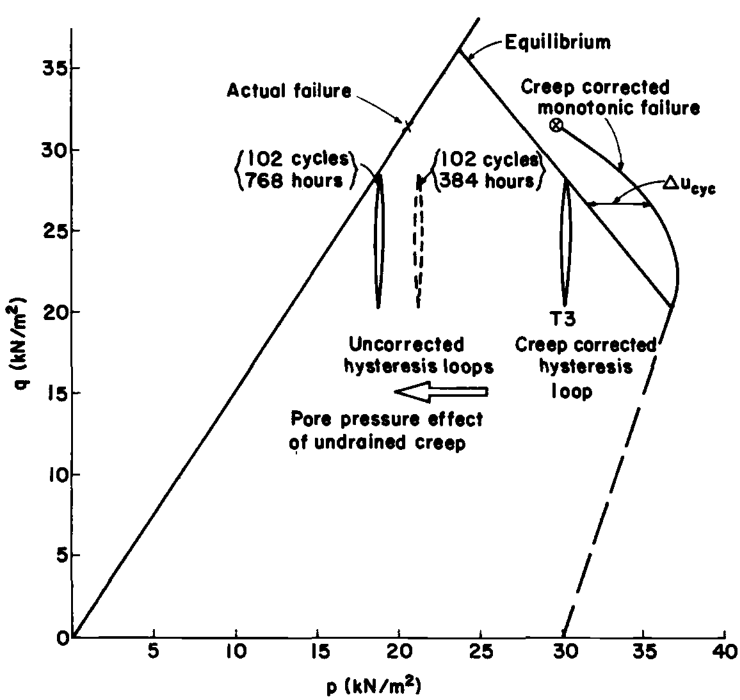

FIG. 4—*Illustration of the correction of pore pressures (Test T3) to account for undrained creep in San Francisco Bay mud; correction moves hysteresis to equilibrium line.*

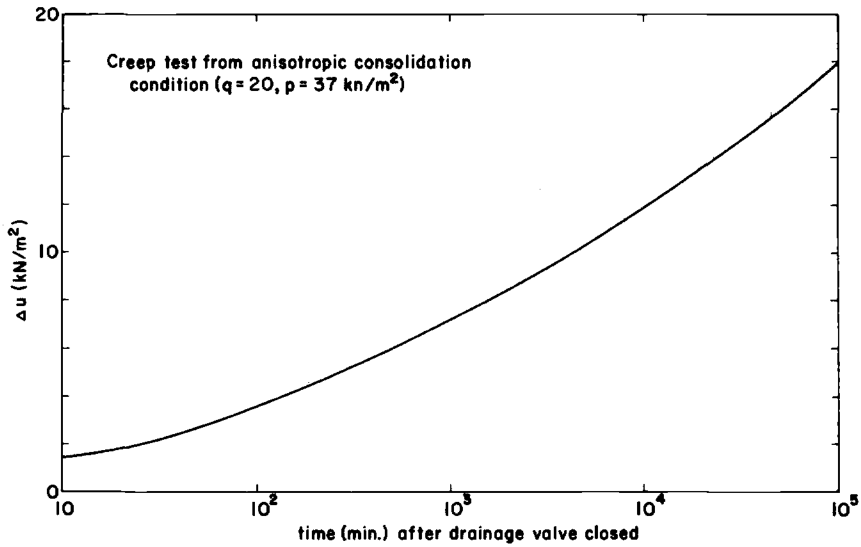

FIG. 5—*Pore water pressure due to undrained creep in San Francisco Bay mud.*

where

k = empirical parameter for a given test condition.

When the test data are corrected for undrained creep, the nonfailure equilibrium conditions define an equilibrium locus much like the reference illustrated in Fig. 2 for a soil where creep was not significant. It should be emphasized again that *in situ* soils will have a negligible potential for undrained creep and so a correction to laboratory tests is appropriate if test results are to be meaningful when applied to a field situation.

Without the creep correction it is difficult to interpret the results of cyclic loading tests, because the pore pressures are not just a function of the cyclic loading but also a function of the rate of loading and the total time of the test. Since specimen behavior is dependent on the effective stress state during the test, the amount of strain and whether failure occurs or not will depend on the rate of testing and time as well as the level of cycled stress. This is illustrated in Fig. 4 for Test T3. The uncorrected hysteresis corresponds to 102 cycles of loading and an elapsed testing time of 768 h. The specimen is on the verge of an effective stress failure, but primarily due to the pore pressures Δu_p. If the same number of cycles, 102, was applied at twice the loading rate, the amount of pore pressure due to creep, Δu_p, would bring the effective stress state only to the position indicated by the dashed hysteresis loop. Similarly, if the rate of cycling was halved, the pore pressures due to creep, Δu_p, would result in failure even though only 51 cycles of loading had been applied. Many of the conflicting conclusions reported in earlier studies of cyclic loading of clays can be explained by this correction.

Experimental Errors in Cyclic Loading Tests

Conducting an accurate cyclic loading test requires, as a minimum, all of the care and control necessary in normal soil testing [*15*]. In addition, there are several rate-dependent factors which can introduce significant errors in cyclic tests. The most important of these are pore pressure measurement and equilization problems and the effects of air diffusion.

A fundamental question is whether the triaxial test, or any laboratory test, is a reasonable model of the stress and deformation conditions applied to a soil *in situ* during actual cyclic loading. Even if the initial state of stress *in situ* can be applied to a test specimen, the real cyclic loading will involve fluctuations in normal stress and shear stress and will usually involve rotation of principal stresses. These conditions cannot be duplicated with conventional testing equipment. Consequently, any test involves simplification even without considering the problems of duplicating the time history of cyclic loading. Several studies have been concerned with these problems [*3,5,8*].

Pore Pressure Measurement and Equilization

While it is generally accepted that pore pressure changes are a principal consequence of undrained cyclic loading, there are many situations when these pore pressures are not measured. An effective stress analysis cannot be done using such data, but other useful information can be obtained. Especially when tests are run at faster loading rates, it may be impossible to measure meaningful pore pressures in clay soils because of the time lag required to register on a measuring system, even on a small-volume compliance transducer. The need to allow sufficient time for measuring pore pressures in laboratory tests is well known [*15*]; however, the related problem of pore pressure equilization may be significant in rapid cyclic loading tests.

The distribution of stress within a test specimen is not uniform, which leads to nonuniform pore pressure distribution within the test specimen [*15*]. Since the behavior of a cyclic loading test depends on the maximum value of pore pressure, whether measured or not, the nonuniform pressure distribution within the specimen will control its behavior. If the cyclic loading is run at a rate so rapid that equilization of pore pressure within the specimen cannot take place, then the behavior in the cyclic test is a consequence of the test procedure. Several factors are involved which cannot be predicted or corrected at present, including the nonuniform stress distribution and pore pressure equalization rates. Bishop and Henkel [*15*] have shown data where the difference in pore pressures within an undrained specimen was 50 percent of the maximum value after more than 1000 min in a conventional undrained compression test. Similar conditions are certainly produced during cyclic loading of clay soils, but there is no method to account for these errors when interpreting the data. Sangrey et al [*2*] among others have used slower loading rates for cyclic testing of clay soils, so that the effects of nonuniform pore pressures can be minimized.

Air Diffusion Through Membranes

Leaks in the pore pressure system or through the membrane surrounding a specimen must obviously be eliminated for accurate undrained cyclic testing. Diffusion through the membrane will also affect pore pressures. A common testing arrangement for cyclic loading of soils utilizes compressed air as a pressure source for the cell fluids. In this arrangement the diffusion of air through the membrane and into the test specimen can cause major errors [*16*]. The potential for this problem is most significant when an air-water interface is established within the testing chamber itself. This is a common arrangement when high-frequency cycling is applied because the air acts to cushion the rapid pressure changes resulting from the loading ram moving in and out of the cell.

Pollard et al [*16*] have considered the diffusion process and its influence on pore pressures within the specimen. An approximate equation to describe the phenomenon is

$$P_s = P_c(1 - e^{-d(t-t_0)}) \tag{4}$$

where

P_s = specimen pore pressure,
P_c = cell pressure, and
t = time.

In this equation, d is an empirical diffusion parameter which may be approximately constant but varies with pressure, the degree of cell fluid saturation by air, and several less important factors. The parameter t_0 is an initial reference time depending on initial conditions, particularly the degree of air saturation in the cell and pore fluids. Until time t_0 there is no pore pressure error due to the air diffusion. However, these errors can become very significant in a short time after t_o, as illustrated in Fig. 6. For this test specimen all applied loading was held constant. Due to air diffusion, however, the pore pressure was equal to 80 percent of the cell pressure 200 h after the test began and 150 h after t_o.

Air diffusion errors can be controlled in most tests by increasing the time t_o. This can be done by using special seals around the test specimen or by using cell fluids other than water [*14*]. The convenience of using water in routine tests is often an important consideration, however, and in this case a satisfactory solution is to use a remote air-water interface connected to the test chamber using a long section of small-diameter tubing. This arrangement will not be satisfactory if an air cushion within the test chamber is necessary because of very rapid loading rates. In this case the consolidation phase of the test up to the time when loading begins should be done without the air cushion. Some cell water is then removed and

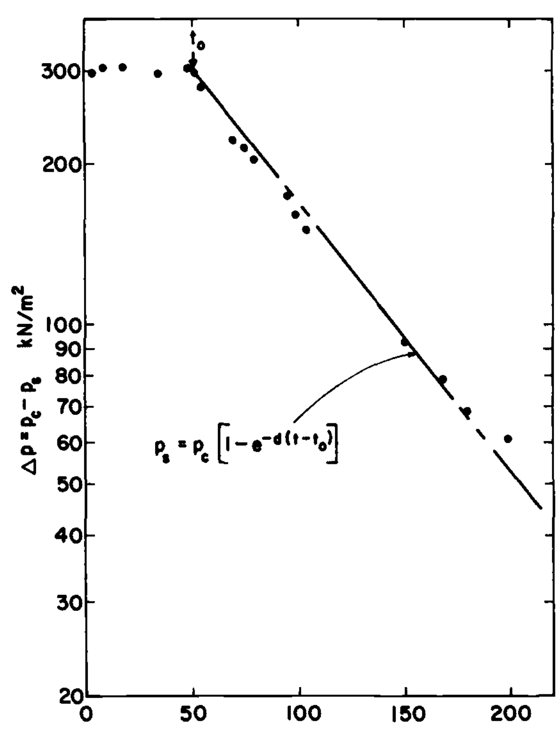

FIG. 6—*Typical membrane air diffusion data for test on Concord blue clay illustrating pore pressure change with time. The specimen had been isotropically consolidated to 300 kN/m^2 (43 psi). There was no change in the applied load during the test.*

replaced by air. Under this condition the test must be completed before t_0 if pore pressure errors are to be avoided.

Discussion

The rate of testing clay soils under cyclic loading conditions will have an important influence on test results. Several major factors are involved which cannot be avoided and there is no preferred testing rate to minimize errors and undesirable effects. There are advantages to running tests very slowly but this presents several major disadvantages as well. The same can be said for running tests at rapid rates. The influence of testing rate on the cyclic behavior of clays can be summarized as follows:

Slow Cycling Rates

Advantages:
- a. Pore pressures can be measured.
- b. Uniform pore pressures within the specimen.

Disadvantages:
- a. Creep effects (can be corrected).
- b. Air diffusion through membrane.

Rapid Cycling Rates

Advantages:
- a. May be more representative of actual loading rates for earthquakes, wind, and waves.
- b. Cost and convenience.

Disadvantages:
- a. Nonuniform pore pressure conditions within test specimen.
- b. Creep effects (can be corrected).
- c. Air diffusion through membrane.

Depending on a particular situation, some of these factors may be more important than others. Certainly if effective stress analysis is considered important, a slower testing rate must be used. For routine commercial, testing, rapid rates may be more practical. In any case, the effects of creep and air diffusion must be considered and, at least for the case of undrained creep, it is appropriate to make corrections.

The significance of two factors is not clear at present. If the nonuniformity of pore pressure within the specimen is as large as some data indicate [*15*], then there is a serious question whether any rapid rate of loading test is at all meaningful when applied to *in situ* conditions. Even though pore pressures are not measured in these tests, the fact that the test specimen is nonuniform in an unpredictable way that depends on test conditions presents serious questions about the validity of rapid tests on soils of low permeability. The other unanswered question is the importance of tests being done at the same rate as will be applied in the field. Many engineering properties of soil such as stress-strain behavior and undrained strength are significantly influenced by the rate of loading in a monotonic mode [17]. There is no clear evidence at present whether this is also the case under repeated loading.

This paper is not concerned with cyclic loading of sands, but a brief comment about the application of the results presented in this study of clays is appropriate. Most tests on sand can be done in a relatively short period of time, even for many cycles of loading. Permeability is high and the potential for undrained creep is low. Consequently, the only factor which might introduce a testing error is air diffusion through the membrane and this will depend on the time t_o for the particular test.

Conclusions

A number of factors have a significant influence on the behavior of clay soils subjected to various rates of loading. Among the most important are the effects of undrained creep, nonuniform pore pressures within the test specimen, and errors due to air diffusion through the membrane. The effects of undrained creep can be corrected and the errors resulting from most other factors can be controlled.

There is no cyclic loading rate which has a clear advantage over other rates although for particular purposes there is a clear preference.

Acknowledgments

The research described in this paper was done as part of a program supported by the National Science Foundation under Grant AEN-75-03217. The authors appreciate the work of Mr. W. R. Sawbridge, who assisted in the research and in the preparation of drawings.

References

[1] Seed, H. B. and Chan, C. K., *Journal of the Soil Mechanics and Foundations Division*, American Society of Civil Engineers, Vol. 92, No. SM2, March 1966, pp. 53-78.
[2] Sangrey, D. A., Henkel, D. J., and Esrig, M. I., *Canadian Geotechnical Journal*, Vol. 6, No. 3, Aug. 1969, pp. 241-252.
[3] Lee, K. L. and Focht, J. A., Jr., *Marine Geotechnology*, Vol. 1, No. 4, 1976, pp. 305-325.
[4] Lee, K. L. and Fritton, J. A. in *Vibration Effects of Earthquakes on Soils and Foundations*, ASTM STP 450, American Society for Testing and Materials, 1969, pp. 71-95.
[5] Seed, H. B. and Peacock, N. H., *Journal of the Soil Mechanics and Foundations Division*, American Society of Civil Engineers, Vol. 97, No. SM8, Aug. 1971, pp. 1099-1273.
[6] Seed, H. B., "Evaluation of Soil Liquefaction Effects on Level Ground During Earthquakes," Liquefaction Problems in Geotechnical Engineering, American Society of Civil Engineers National Convention, Sept. 1976, pp. 1-105.
[7] Thiers, G. R. and Seed, H. B. in *Vibration Effects of Earthquakes on Soils and Foundations, ASTM STP 450*, American Society for Testing and Materials, 1969, pp. 3-56.
[8] Krizek, R. J. and Franklin, A. G. in *Vibration Effects of Earthquakes on Soils and*

Foundations, ASTM STP 450, American Society for Testing and Materials, 1969, pp. 96-113.

[9] Arango, I. and Seed, H. B., *Journal of the Geotechnical Engineering Division,* American Society of Civil Engineers, Vol. 100, No. GT2, Feb. 1974, pp. 139-156.

[10] Singh, A. and Mitchell, J. K., *Journal of the Soil Mechanics and Foundations Division,* American Society of Civil Engineers, Vol. 94, No. SM1, Jan. 1968, pp. 21-46.

[11] Mitchell, J. K., Campanella, R. G., and Singh, A., *Journal of the Soil Mechanics and Foundations Division,* American Society of Civil Engineers, Vol. 94, No. SM1, Jan. 1968, pp. 231-253.

[12] Walker, L. K., *Journal of the Soil Mechanics and Foundations Division,* American Society of Civil Engineers, Vol. 95, No. SM1, Jan. 1969, pp. 167-188.

[13] Arulanandan, K., Shen, C. K., and Young, R. B., *Geotechnique,* Vol. 21, No. 4, Dec. 1971, pp. 359-375.

[14] Holtzer, T. L., Höeg, K., Arulanandan, K., *Canadian Geotechnical Journal,* Vol. 10, No. 1, Feb. 1973, pp. 12-24.

[15] Bishop, A. W. and Henkel, D. J., *The Measurement of Soil Properties in the Triaxial Test,* Edward Arnold, London, 1962.

[16] Pollard, W. S., Sangrey, D. A., and Poulos, S. J., *Journal of the Geotechnical Engineering Division*, American Society of Civil Engineers, Vol. 103, No. nGT 10, 1977, pp. 1169-1173.

[17] Casagrande, A. and Wilson, S. D., "Investigation of Effect of Long-Time Loading on the Strength of Clays and Shales at Constant Water Content," Harvard University Report, Cambridge, Mass., July 1949.

S. D. Wilson,[1] *F. R. Brown, Jr.,*[1] *and S. D. Schwarz*[1]

In Situ Determination of Dynamic Soil Properties

REFERENCE: Wilson, S. D., Brown, F. R., Jr., and Schwarz, S. D., "***In Situ* Determination of Dynamic Soil Properties**," *Dynamic Geotechnical Testing ASTM STP 654*, American Society for Testing and Materials, 1978, pp. 295–317.

ABSTRACT: Geophysical procedures used to determine the shear modulus for soils are reviewed and the more recent improvements in each technique are discussed. The two most commonly used methods are identified and shear wave velocities by both methods are compared for nine different sites. Considering all of the variables involved in both the test procedures and the soil types, the agreement is considered good. Two newly developed large-strain procedures for obtaining soil properties *in situ* are also presented. One method is an impulse test which determines with closely spaced waveform measurements the change in shear wave velocity both as a function of depth and strain. The other method is a back-calculation procedure which corrects assumed model properties until agreement is reached between the calculated and field-measured response. Both methods offer promise for the future development of better large-strain field procedures for conducting more complex seismic studies.

KEY WORDS: geophysics, soil dynamics, seismic velocities, shear moduli, field tests, large-strain tests, soils

Great progress has been made in recent years in the development and improvement of analytical procedures for evaluating the response of soils under dynamic loading. As the analytical methods are refined to solve more complex problems, procedures must also be improved to provide more realistic parameters for defining stress and strain properties for use in these models. In cases where there are no permanent soil displacements and where loading is primarily in shear, the response to a specific input vibration is determined primarily by the shear modulus and corresponding damping of the soils through which these vibrations must pass. Because these properties for soils are nonlinear, a single cycle of simple shear loading, and unloading, as produced by an earthquake on a soil deposit, follows a curvilinear stress-strain path having the form of a long, narrow, closed

[1]Executive vice president, senior associate engineer, and vice president, respectively, Shannon & Wilson, Inc., Seattle, Wash. 98103.

loop (hysteresis loop). The shape and orientation of the loop change as the amplitude of strain changes.

These loops can be obtained in the laboratory at both low and high strain levels and show that the soil is not only nonlinear but that it also is capable of absorbing a considerable amount of energy. At small strains, the fact that the stress-strain characteristics are more nearly linear and elastic is also evident.

For convenience and simplicity in performing dynamic response analyses, this hysteretic behavior for soils is currently expressed as equivalent linear shear moduli and damping ratios. These values account for the hysteretic loop for each cyclic pulse during a defined period of shaking. In addition to laboratory determinations, the shear modulus is currently being determined in the field at small strains using geophysical wave propagation methods. These geophysical methods together with recent successes in extending these procedures and measurements to larger strains are treated in this paper.

Damping can be measured in the field by observing the rate of decay of amplitude of wave motion with distance from a large energy source such as an actual earthquake or blast. Unfortunately these sources are neither predictable nor routinely available. Smaller sources such as vibration generators have produced microtremors to study damping at low strain levels. Energy dissipation from these sources results from geometric damping as well as from internal (hysteretic) damping. It is very difficult at this time to distinguish between the two, either at high or low strains.

Because of these difficulties in distinguishing hysteretic damping from total damping *in situ*, there are no field tests that are routinely performed for determining this property. For practical application, emphasis is placed on studying and measuring this property in the laboratory. Even though the field determination of damping appears elusive and difficult, the authors greatly encourage future research on this important property. For lack of field methods for determining this property, emphasis in this paper is placed on field procedures for evaluating the shear modulus.

Geophysical Techniques

Geophysical techniques are normally used to determine the dynamic Young's modulus (E) or shear modulus (G) of the soil through measurement of the compression wave (V_p) and shear wave (V_s) velocities, respectively. Since compression wave velocities are strongly influenced by the presence of water, emphasis for engineering problems continues to be placed on the determination of shear wave velocities and converting these values to G directly and then to E through the assumption or determination of Poisson's ratio.

There are three primary field methods routinely utilized to measure the shear wave velocity: (1) the downhole, (2) crosshole, and (3) surface refraction methods. It is not the intent of this paper to describe in detail the procedures of these methods or how to identify first arrival times, as this has been adequately covered elsewhere [*1-6*].[2] Instead, it is intended to (1) point out the more significant advancements in the field in recent years, (2) describe briefly the most suitable procedures for carrying out the tests, and (3) describe the unique features and shortcomings of each method. From these discussions, guidance is also provided for selecting the best method or methods for obtaining adequate data for given site conditions.

In general, all of these geophysical techniques have a common limitation: they provide velocity measurements only at low strain levels (generally less than 10^{-4} percent). Therefore, the velocities (or moduli) determined by these procedures must often be scaled downward appropriately to account for the strain dependency of this property. This is usually done through the use of data from laboratory resonant-column or cyclic triaxial tests [*2,7*] or by using empirical relationships [*2,8*].

Downhole Method

The downhole method involves the generation of seismic waves rich in shear energy with an impulse source at the ground surface adjacent to a borehole. The travel time of the downward-propagating shear wave is measured at one or more multi-axis geophones clamped in the borehole at various elevations. A simplified diagram of the procedure is shown in Fig. 1. The travel times are then plotted with depth, the slope of which corresponds to the shear wave velocity.

The procedure is well developed, simple in principle, and therefore has not undergone many significant recent advancements. Probably the most significant advancement is the development of a stronger impulse system [*4*]. This high-energy reversible bi-directional energy source has been used for detecting shear waves by the surface refraction technique in sea-bottom sediments. However, it probably would make an excellent surface strong-energy source (18 800 m·kg) (68 ft-tons) for downhole work, especially when measurements are required at great depths [greater than 152 m (500 ft)]. However, there presently is not much demand for shear wave velocity measurements at these depths.

Another improvement in the procedure is that as more sophisticated multichannel recorders become available, more geophones are being placed in a borehole at one time (two or three multidirectional geophones), enabling more simultaneous readings to be taken with a single impulse. This not

[2]The italic numbers in brackets refer to the list of references appended to this paper.

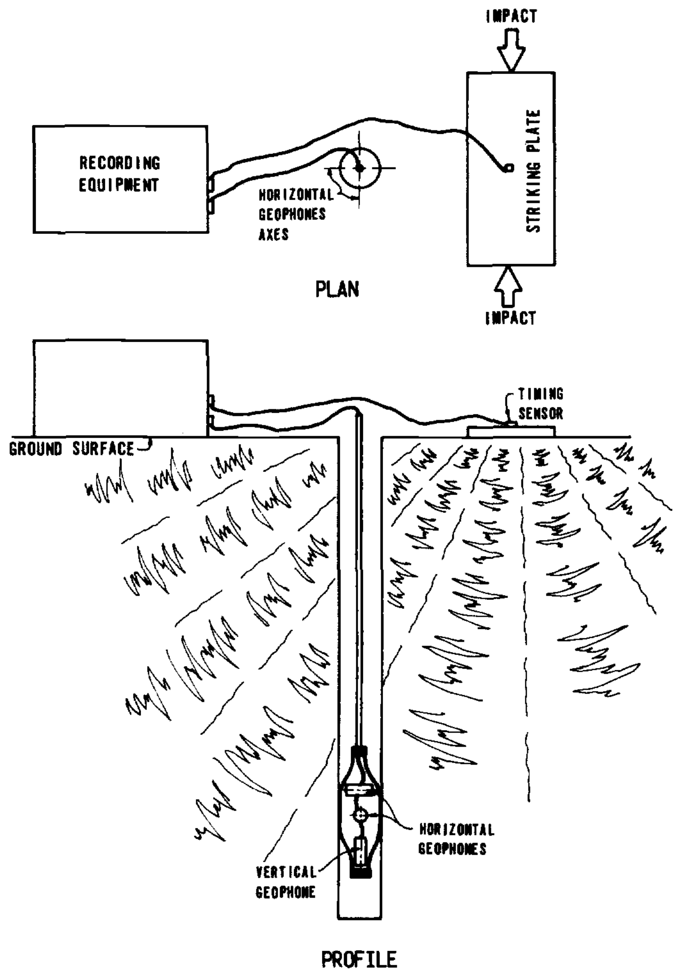

FIG. 1—*Schematic diagram of downhole method.*

only enables the measurements to be taken more quickly, but also provides for measuring time differences between respective geophones as well as from the energy source.

Another important advancement has been the development of the multichannel signal-enhancement seismograph. With this equipment, not only two or more downhole transducer packages can be used as just described to measure incremental as well as total travel times, but stacking or signal enhancement can be used to increase the signal-to-noise ratio, thereby providing data with improved clarity. A variation of this technique involves alternately reversing both the polarity of the energy source and of the geophone for repeated applications of the mechanical source. In this way the shear wave signal is cumulatively added and compressional wave energy and random noise are cancelled out.

The most widely used downhole approach currently involves using a rich source of reversible shear wave energy and good coupling between the geophones and the walls of the borehole. The most common energy source consists of striking a post, buried plate or plank, or embedded concrete block (Fig. 1) with a sledgehammer. By reversing the direction of the impact and by taking two records at each depth, the polarity of the shear wave reverses while the compression wave characteristics in the wave pattern remain unchanged. The two records can then be overlaid and the true arrival time determined. Although not common practice, it is the authors' opinion that in all downhole work more than one in-hole geophone should be used and that time differences between respective in-hole geophones should be recorded as well as arrival times with respect to a time zero (impact). Using this approach, a single average velocity can be determined between each set of geophones (generally spaced 1.5 or 3 m (5 or 10 ft) apart) and plotted with depth as a point rather than as a straight-line segment over an interval. This not only gives a more realistic velocity depth profile, but also with the points plotted the investigator is able to have a better view for the possible scatter in the test results. Also, by recording incremental intervals of time between in-hole geophones, the many difficulties associated with triggering are eliminated. This subject is well discussed by Hoar and Stokoe [*9*] elsewhere in this volume.

The unique features of the downhole test include:

1. Low cost. It requires only one hole, utilizes a simple energy source, and does not require support or standby time of men and equipment.
2. Ease and ability to reverse the polarity.
3. Generation of S_H waves which travel (in most cases) perpendicular to layer interfaces, keeping reflected and refracted V_p and V_s components to a minimum [*10*].
4. Determination of average shear wave velocities in horizontally stratified media and identification of relatively thick low-velocity zones.
5. Applicability in limited space areas.
6. Workability in noisy areas with stacking or signal enhancement.

The major shortcoming of the test is that the small strains produced make the signal-to-noise ratio low in many cases. This condition is especially difficult to handle in heavy traffic areas, around machinery or electrical works where seismic noise is likely to be significant. Special variable filter systems and variable gain amplifiers, and often late night work, are usually required to keep noise levels within tolerable limits. Along with this specialized equipment, an experienced geophysicist is also needed. This geophysicist will not only know the "art" of minimizing noise, but also how to set the amplifiers and filters and apply the proper impact to accentuate the shear wave characteristics in the complex train of waves generated. This expertise is needed when conducting the conventional test to depths greater than 30 m (100 ft), especially if casing is used. These difficulties have been largely eliminated with the recently developed signal stacking or enhancement types of signal conditioning equipment.

Crosshole Method

The crosshole method involves generating a seismic wave in one borehole and at the same depth in one or more adjacent boreholes measuring the average time for the wave to travel between respective geophones or between a single geophone and the source. A simplified diagram of the method is shown in Fig. 2. Once the distance between the boreholes and first shear wave arrival time are determined, shear wave velocities at that depth can be calculated.

One of the most simplified and practical approaches by this procedure was described by Stokoe and Woods [*11*]. A major shortcoming of this and other crosshole procedures involved determining first shear wave arrival times, especially when explosive charges were being used. The difficulties of determining correct arrival times from a single event, such as an explosion, is especially well illustrated elsewhere in this volume [*12*]. Records from explosions are complex, because large shearing and compression components are both generated. In the past five years, considerable research has been conducted toward improving crosshole procedures primarily by developing more repeatable energy sources and better techniques for identifying shear wave arrival times. These same investigators [*13*] improved upon their basic method [*11*] by striking up as well as down on their embedded pipe or sampler. More recently other researchers [*9*] experimented with energy sources by applying torsional loads in opposite directions in a borehole. These procedures produced a reversal in polarity of the shear wave arrivals, enabling arrival times to be clearly identified by the same basic procedures used for the downhole test. References *14* and *15* describe case histories of the successful use of this reversal method.

Investigators [*16*] also have suggested a skewed crosshole test for measuring S_H waves, again using a reversal in polarity procedure to identify the first arrival of S_H waves. This procedure appears reasonable for shallow depth; at significant depths and steep angles, however, both sensors in the adjacent boreholes could just as easily be placed in a single borehole. This procedure would then be the same as the conventional downhole method.

Since 1969, researchers [*17*] at the Waterways Experiment Station have been studying crosshole procedures using a vibropacker system for inducing steady-state, vertically polarized shear waves. At that time the procedures

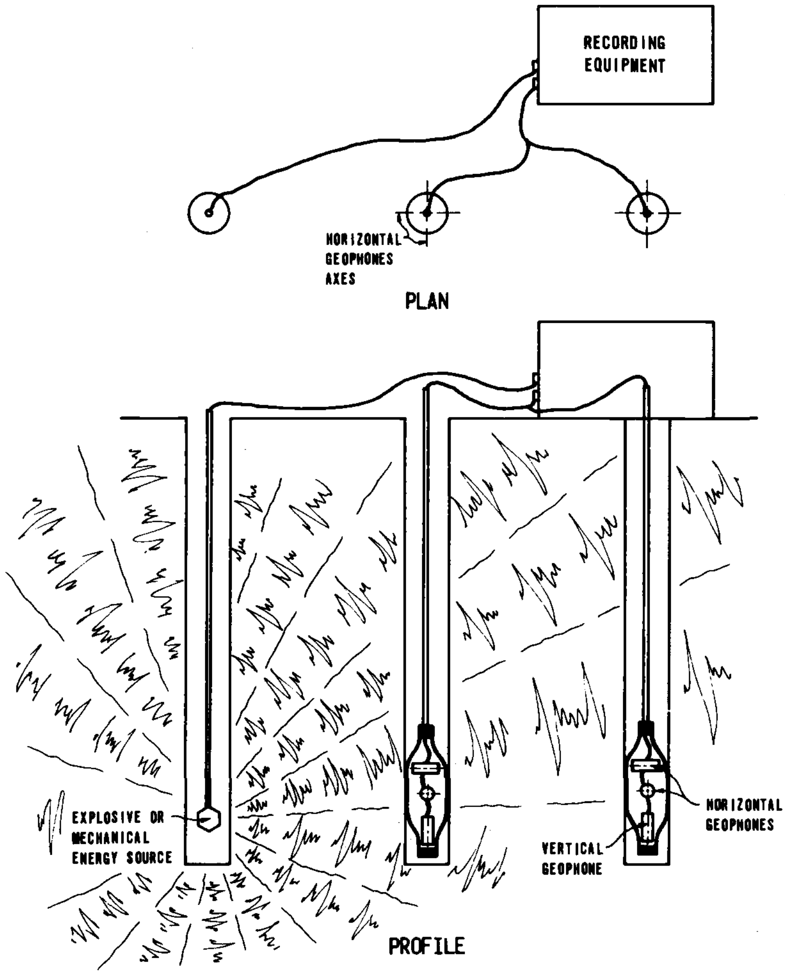

FIG. 2—*Schematic diagram of crosshole method.*

showed promise with the advantages of applying a controlled energy source over a period of time, as well as providing constant coupling of the energy source to the borehole wall. More recently they have made greater improvements in this method [*18*]. An electromagnetic vibrator placed on a rod which is attached to an oriented, spring-wedged geophone is used as the source. The vibrator can pulse a controlled number of cycles at a predetermined frequency. Enhancing equipment is then used which sums successive signals and displays processed data on the premise that true signals are additive and random noise self-cancelling. The procedure with a controlled source gives repeatable results which, with the enhancing unit, provide much better data than obtained using explosives or other non-repeatable sources.

The foregoing investigators [*18*] also improved upon the crosshole procedures by decreasing the spacing between the boreholes. Stokoe and Woods [*11*] used two boreholes spaced 1.5 to 4.5 m (5 to 15 ft) apart [typically 2.4 to 3.7 m (8 to 12 ft)] while Ballard [*18*] suggests that the first two boreholes have maximum spacings of less than 6.1 m (20 ft). At these close spacings, wave bending [*19*] and reflecting of waves are minimized because the travel path is also minimized. When large borehole spacings are used, the wave can travel over a different path through a more competent layer, producing, in effect, a higher and incorrect velocity. In decreasing the spacing, the authors have found that the boreholes should always be surveyed to assure accurate distance measurements and thus velocity calculations. Boreholes are rarely, if ever, drilled truly vertical, especially if gravels are present. Figure 3 presents the survey results of 12 boreholes advanced at three different sites. These 11.4-cm (4.5 in.)-diameter closely spaced boreholes were all advanced using the same drilling equipment [rotary using a 3 m (10 ft)-long drill collar], taking special precautions to advance the boreholes as nearly vertical as possible. One can imagine the error involved had the distances between the boreholes been assumed and not surveyed. Similar survey results have also been obtained using hollow-stem augers. Differences in distance of this magnitude, if not accounted for, can produce misleading velocity results and, therefore, should receive equal attention as the determination of best arrival points on the velocity histories. One procedure for surveying the boreholes is given in Ref *20*.

Because of the relatively short distances used between boreholes for crosshole measurements, travel times are comparatively small, and small timing errors in the initiation of shear wave energy or determination of shear wave arrivals can cause unacceptable errors in velocity calculations when zero time is used. This can be remedied by paying particular attention to the method of determining time zero or by using two or more adjacent boreholes and measuring elapsed time between similar points on a waveform recorded at two or more adjacent geophone sets [*12*].

The best geophysical crosshole procedure to use at a given site is largely controlled by the available seismic recording equipment. The procedure suggested by Stokoe and Woods [*11*], incorporating the reversal in polarity technique and using closely spaced boreholes, appears especially desirable because of its simplicity, its minimal equipment requirements, and the need for only two borings. In recent years, investigators have been recommending the use of more than two boreholes to improve on the quality of the measurements. The procedure by Ballard appears equally suitable; however, more specialized equipment would be required.

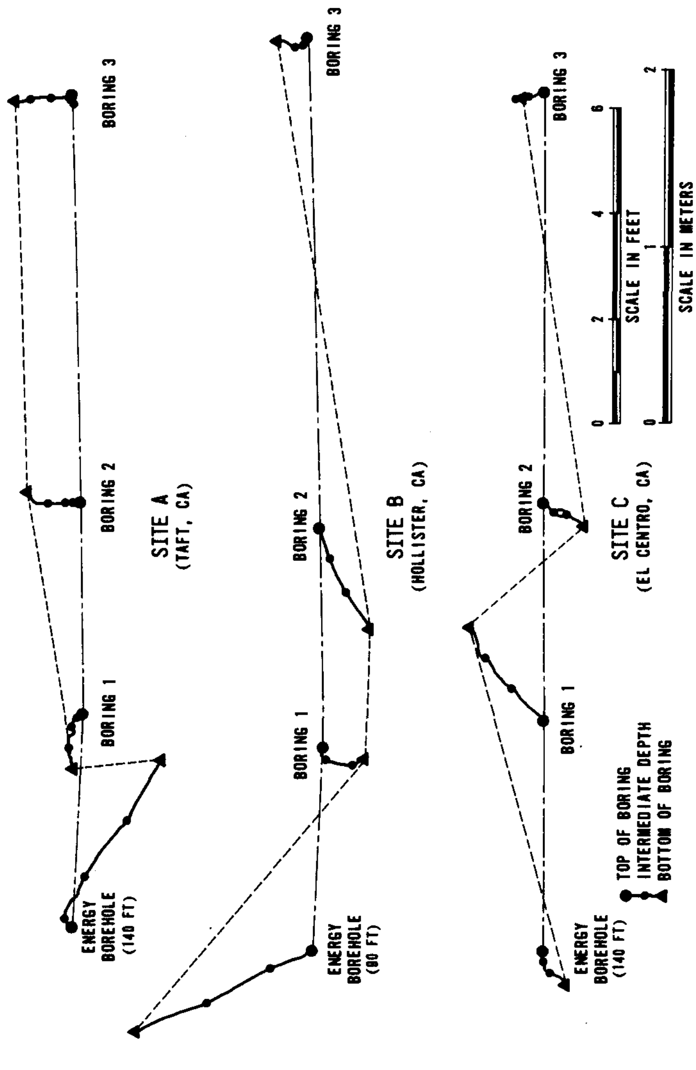

FIG. 3—*Plan view of three sites showing drift of boreholes with depth.*

As with the downhole procedure, data can be improved with the use of multichannel stacking or signal-enhancement equipment.

With these recent improvements, the unique features of the crosshole test now include:

1. The ability to reverse the polarity or produce a greatly enhanced shear wave signal from a repeatable energy source.
2. A test simple to perform, requiring, in some cases, relatively low-cost recording equipment.
3. A test generally unaffected by casing (if plastic casing is used).
4. Its workability in limited space areas.
5. Its workability in noisy areas where there is a high ambient seismic background.
6. Its workability in layered soils (if close borehole spacings are used).

The major shortcomings of the test are that more than one borehole is needed, and support or standby time for a drill rig is sometimes required. These are cost considerations. Also, there is the potential in layered soils that the wave may reflect or refract and travel the fastest path through more competent layers. This may cause thin low-velocity layers to be missed or may produce, in effect, upper-bound velocity values rather than average values.

Shear Wave Refraction Method

The procedure for making shear wave velocity measurements from the surface without the use of boreholes is similar to the procedure for making conventional seismic refraction measurements, except that horizontal geophones are employed with the sensitive axis of the sensors aligned in a horizontal plane transverse to the direction of wave travel. A simplified diagram of the method is shown in Fig. 4. Detailed procedures and typical results are provided in Refs *4, 6,* and *26.*

Little, if any, advancements in the procedure have developed recently, except for possibly the use of a larger energy source [*4*]. The procedure is not widely used or discussed in the literature. Especially in the refraction procedure, data can be greatly improved through the use of multichannel stacking or signal-enhancement recording equipment. Alternate reversing of the energy source and geophones causes a sequential summing of shear wave energy and cancellation of compressional wave energy and random noise.

The unique features of the procedure include the following:

1. It is a low-cost test.
2. Information can be obtained without the use of boreholes.
3. It provides a wider-area coverage than in-hole methods.
4. It provides good data for preliminary planning purposes and feasibility studies.

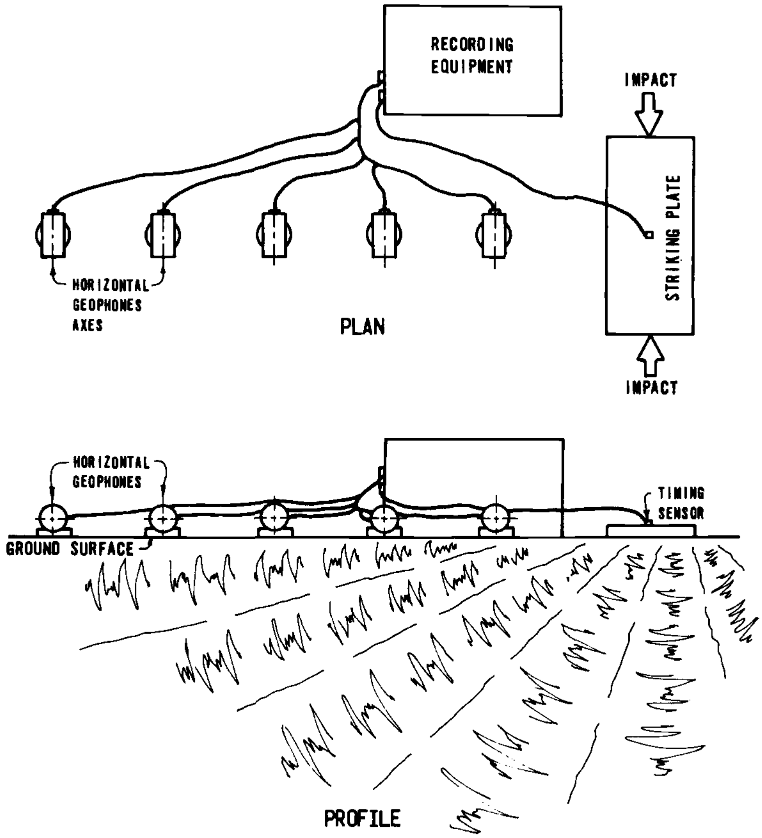

FIG. 4—*Schematic diagram of refraction method.*

The shortcomings of the test are:

1. It is accurate only under conditions where velocities increase with depth; even then it averages rather than shows variations within a given soil zone.
2. Low-velocity stratum below high-velocity stratum is not detected and errors are introduced.
3. It requires large energies to achieve penetration.
4. The quality of data decreases with depth.
5. Data become complicated in multilayered deposits.

Direct Shear Wave Velocity Measurements

This is a procedure that is extremely simple and has received little attention in the literature as opposed to other more complicated procedures.

Its use, however, is limited to exposures of rock or soil where only one seismic layer is known to exist. A single or multigeophone array is placed on the exposure, generally at short geophone spacings [less than 3 m (10 ft)]. The geophones are of the conventional vertical rather than horizontal type. Velocity measurements are made by striking the outcrop vertically with a hammer at the ends of the array. The seismic wave generated is a vertically polarized shear wave which is measured by the adjacent vertical geophones. If more than one seismic layer exists, refraction will occur and the second layer velocity will become converted to compressional waves. This procedure can be used only in the single-layer case.

Other Methods

Other less-common methods for determining the low-strain shear wave velocity or modulus include (1) uphole procedures, (2) surface vibrator procedures, and (3) static and vibratory plate bearing tests. The test procedures for these methods are described in Ref *2*. Uphole procedures are not commonly used, because explosives are usually required in the test. With explosives, the hole is usually damaged and the recorded signal is nonpolarized and therefore difficult to evaluate. The other two procedures are more applicable for working at shallow depths. The surface vibrator procedure also has the same shortcomings as the refraction method described previously.

Conclusions

Of the three major geophysical tests, the downhole and crosshole techniques are the most accepted methods in practical use for determining the *in situ* shear modulus variation with depth, even though both have different limitations. Shear wave refraction methods suffer for lack of detailed results and because they can produce errors in other situations. Of the two most accepted methods, the choice of one procedure over the other is largely one of preference by the firm making the measurements. With the more recent advancements discussed previously, both downhole and crosshole methods are considered suitable techniques for obtaining positive shear wave arrival times. Because only a limited number of studies have been made comparing the results of the two techniques at given sites (generally at nuclear power plant sites), a number of questions have been raised about both techniques:

1. How do the results compare?
2. Is one better than the other?
3. Which gives the most representative values for earthquake analyses?
4. When should one procedure be used over the other?
5. Do anisotropic stress conditions sometimes account for differences in results between the two methods?

6. How does layering affect the methods?

Figure 5 shows a comparison of downhole and crosshole measurements accomplished at nine different sites in California and Washington. A full range of soil types, including sands, silts, clays, and gravels, is among the data. Some materials are normally consolidated, others slightly preconsolidated, and others heavily preconsolidated, and have been deposited under many different geological conditions. The tests were conducted using the same holes at each site but in many cases using different recording equip-

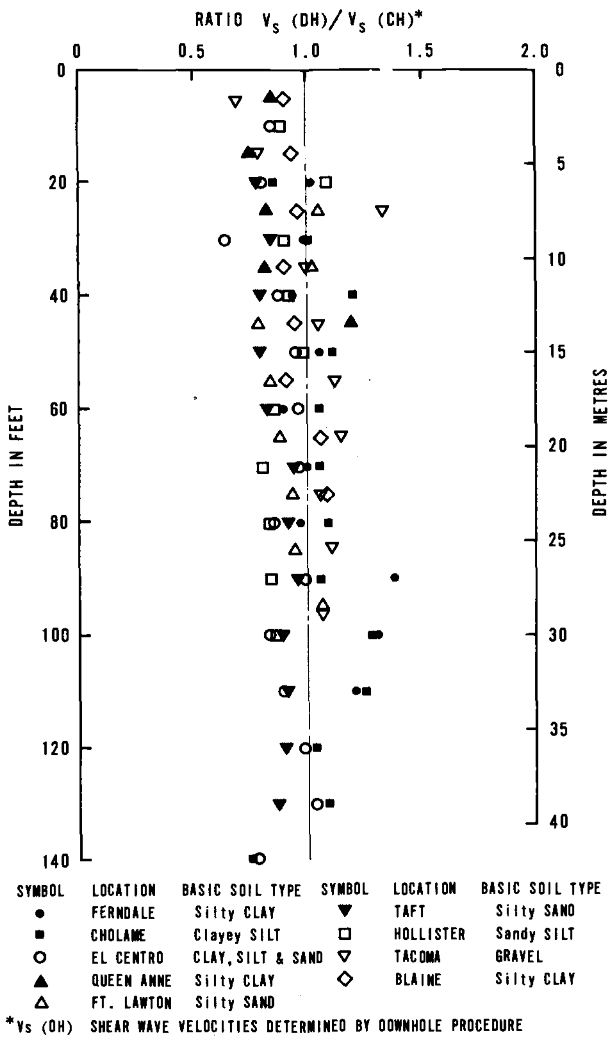

FIG. 5—*Comparison of test results from downhole and crosshole methods.*

ment. In both test procedures, maximum spacing of any two sensors in the boreholes rarely exceeded 3 m (10 ft). Also, in all cases the boreholes used in the crosshole procedures were surveyed. At three of the sites, 7.6-cm (3 in.) plastic casing was installed in the 10 to 12.7-cm (4 to 5 in.)-diameter boreholes and the annular space around the casing was grouted. At the other sites, tests were conducted in uncased boreholes.

While trends are obvious from these data and can be attributed to layering effects, anisotropic conditions, and geology, the scatter can also be attributed to errors in interpretation, significant layer changes, etc. With all the different soil types and site conditions present in the data, it is amazing that the data scatter is not more pronounced. The ratio values in most cases range from 0.8 to 1.15 with an approximate average value of 0.95. This would tend to indicate that downhole shear wave velocities are slightly lower (5 percent or less) than crosshole velocities. The authors believe that at these sites the slight difference is due to the influence of layering. Shear waves (S_H) in the downhole tests propagate vertically through hard and soft layers, in effect averaging the velocities between the geophones. In the crosshole procedure, the shear waves travel fastest through the more competent layers, producing a slightly higher than average velocity. Regardless of the causes, however, the small difference would tend to indicate that these effects and the effects of anisotropic conditions, except in special materials [*21*], are not large and that equally satisfactory results can be obtained with either procedure. More comparisons of this type using the latest advances in procedures and equipment are encouraged.

Modified Crosshole Impulse Techniques

Since conventional geophysical methods produce velocity or modulus values at low strains, laboratory tests must be carried out on undisturbed specimens to define the strain-dependent modulus characteristics of the material. In recent years, at least three research efforts have been undertaken in an attempt to measure *in situ* the strain-dependent dynamic soil properties [*20, 22, 23*]. All methods used a modified crosshole procedure. The first method [*22*] involved cyclically loading the ground with an in-hole anchor connected by heavy pipe to a large surface vibrator. Equipment design difficulties and other factors made the technique unfeasible. Two other methods have been more extensively developed and show more promise and, therefore, are described in the following sections.

In Situ *Impulse Test*

The *in situ* impulse test [*20*] is similar in many respects to the conventional crosshole technique in that it is based on the generation and recording of shear waves that propagate through a mass of soil between two or more boreholes. A diagram of the test, Fig. 6, includes an in-hole generating source and three recording stations with vertically oriented velocity geophones arranged along a single line in a horizontal plane at a given depth, inside vertical boreholes.

The primary difference between this test and other crosshole impulse-type tests is in the spacing of the boreholes and the generation of controlled shear waves. The desired larger strains are obtained by decreasing the spacing between the generating source and the boreholes. For achieving large strains (10^{-3} to 10^{-1} percent), geophones are generally positioned on the energy source and 1.2, 2.4, and 4.9 m (4, 8, and 16 ft) from the energy source. High strains (about 10^{-1} percent) are recorded at the energy source while 1.2 m (4 ft) away the strains are near 10^{-2} percent. Beyond 1.2 m

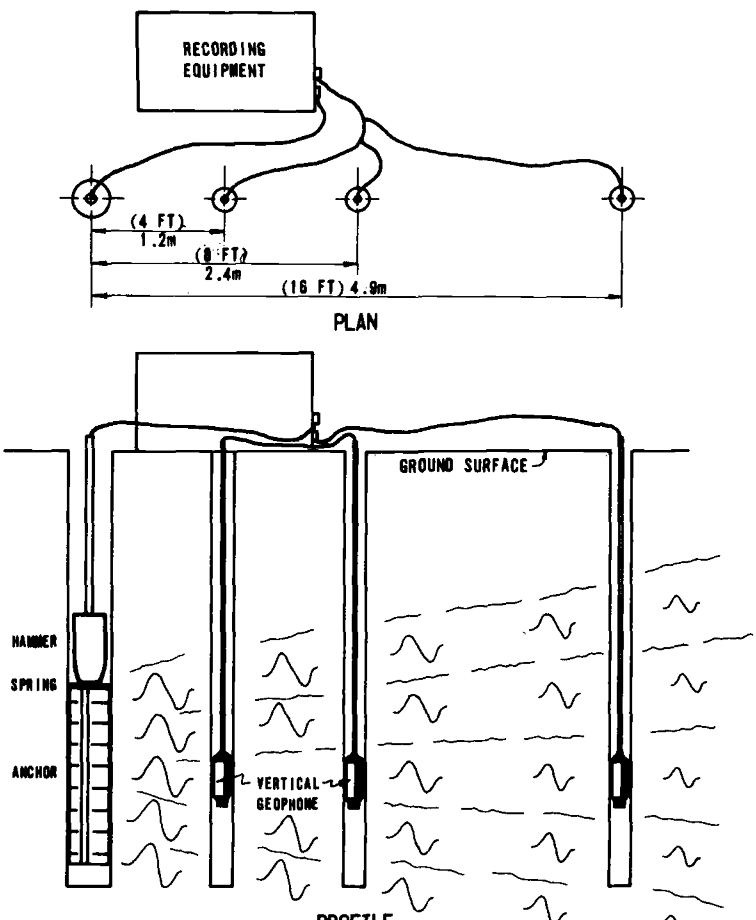

FIG. 6—*Schematic diagram of* in situ *impulse test method.*

(4 ft), the strains are much smaller and largely dependent on the stiffness of the medium. The close spacing of the boreholes minimizes wave bending and waves reflecting over paths greatly different than assumed.

A large controlled in-hole energy source is used to produce a single dominant shear pulse rather than a more complex train of body waves. The energy source (Fig. 7*a*) is formed by three aluminum curved plate segments which, when activated by a 22 700-kg (25 ton) central ram, expand outward, pressing tightly against the walls of the borehole. The in-hole hammer shown (Fig. 7*a*) weighs about 68 kg (150 lb) and when dropped about 30 cm (1 ft) produces a dynamic force on top of the anchor of the order of 9090 kg (20 000 lb). Unlike other in-hole mechanical systems, this

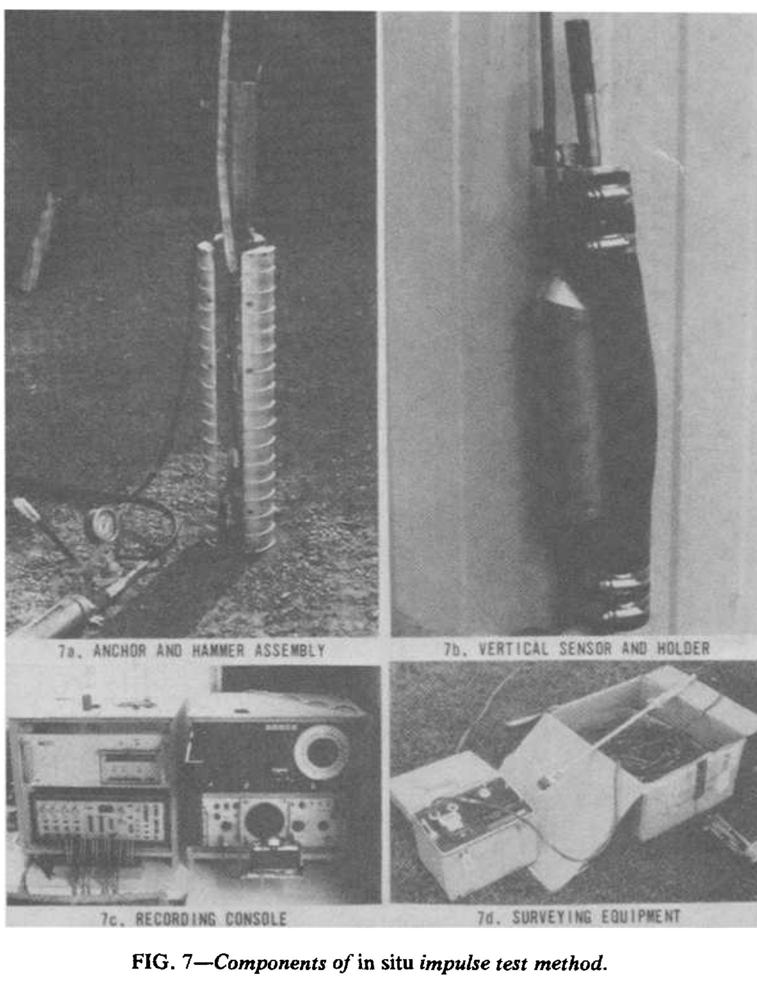

FIG. 7—*Components of* in situ *impulse test method.*

force is applied directly on top of each plate segment, producing a large shearing force at the anchor-soil interface. A Belleville spring with a stiffness of about 53 700 kg/cm (300 000 lb/in.) is placed between the hammer and the anchor plates to control the period and shape of the impulse wave produced in the surrounding soil.

In a typical test, the time history of the single pulse generated is measured simultaneously by four vertical velocity transducers, one fixed directly to the anchor and the others to sensor holders (Fig. 7*b*) in the adjacent boreholes. The holders are rubber packers which, when inflated, achieve firm coupling of the sensors with the borehole walls. With firm coupling the transducers can move in high compliance with the soil. The velocity-time data from an impact are first recorded in memory in a waveform recorder (Fig. 7*c*) and then replayed into an oscilloscope for field assessment. If the data are observed to be acceptable, they are recorded on digital computer tape directly from the recorder.

Simultaneous velocity-time records obtained in four different types of soils at four different sites are shown in Fig. 8. The characteristic shapes shown are easy to identify, clear, unfiltered, and completely repeatable. Background noise is also negligible because at high strains the voltage output from the transducers is over a thousand times larger than an equivalent noise level. If each basic S-shaped pulse is integrated, the resultant particle displacement will appear as a single down-up motion. Because this motion resembles the input (that is, the impact causes the anchor and the soil to move down and then back up to its starting point), the recorded shear pulse at each sensor has physical significance. Therefore, rather than picking a low strain time of first arrival point, the velocity of the wave form can be given by using an identifiable point on each time history which corresponds to a point in time after which peak strain has occurred at that sensor. The most easily identifiable point on the velocity-time signature is the zero crossing point between the two large peaks of the S-shaped pulse. Actually peak strain occurs near the first positive peak and therefore this also is an equally acceptable point.

The arrival time data are then plotted versus the measured distance at each sensor from the anchor (Fig. 9). The slope of the curve at each sensor is the shear wave velocity at that location. The corresponding shear strain can be computed as the ratio of the particle velocity amplitude to the computed shear wave velocity. By plotting the four values of velocity versus time, the variation of velocity with strain for each test depth interval can be defined. By repeating the test at regular depth intervals, the velocity or (modulus) variation with both strain and depth can be established for a given soil profile.

Velocity-time histories obtained at the anchor are more complicated than indicated in the foregoing and require special data reduction procedures to account for slippage at the interface, radial jack stress conditions, and

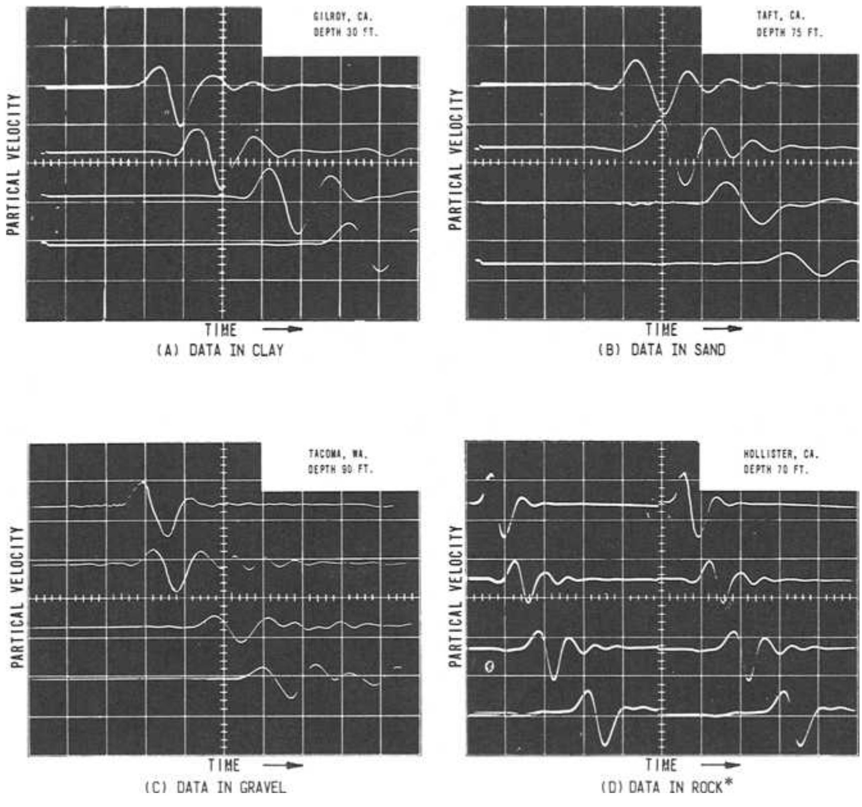

* DATA IS BEING DISPLAYED ON AN OSCILLOSCOPE FROM A MEMORY BANK IN THE RECORDING SYSTEM. THE TIME SCALE ON THIS RECORD IS SET SUCH THAT EACH SIGNAL IS BEING REPEATED (OR DISPLAYED TWICE).

FIG. 8—*Velocity-time records from four sites.*

other factors. Processing of this data, discussed further in Ref *20*, is semi-empirical and requires further study.

The unique features of the test are that clear, consistent, repeatable records are obtained in all types of soils and, unlike conventional geophysical tests, large controlled strains are produced *in situ*, providing velocities or equivalent moduli both as a function of strain and depth.

Also, the test does have limitations, which are discussed in detail in Ref *24*. The most significant limitation is cost. Extra boreholes must be drilled, sophisticated in-hole recording and borehole surveying equipment (Fig. 7*d*) is needed, and drill rig support is required. The test is also limited by the

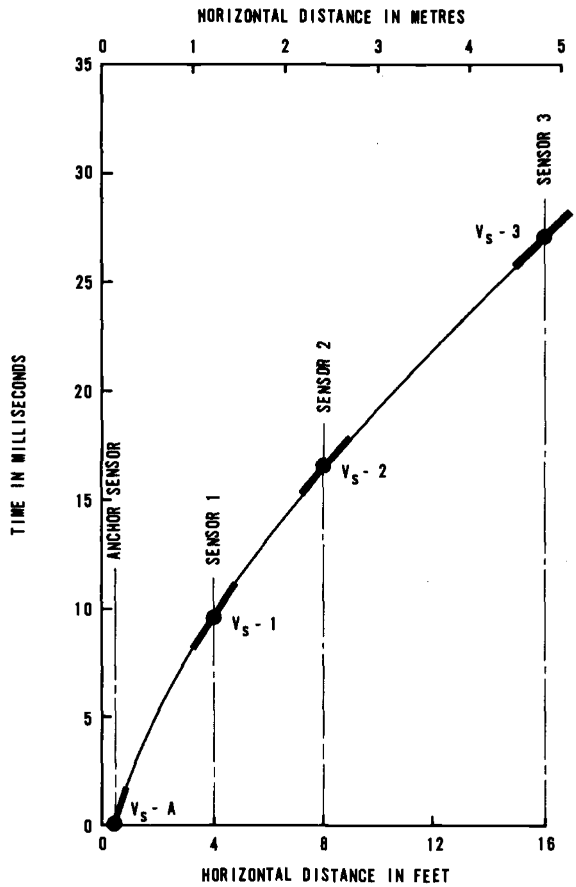

FIG. 9—*Time-distance plots.*

ability to advance boreholes at the indicated close spacings to great depths without having them interconnect. Typically, testing by this procedure can be conducted without undue difficulty to a depth of 46 to 61 m (150 to 200 ft) in most types of soil.

Cylindrical In Situ *Test* (*CIST*)

This procedure was developed in 1971 by the Air Force Weapons Laboratory to provide an *in situ* technique for determining response of soils to dynamic blast loads. As shown in Fig. 10, the test is in many ways like the impulse test, described previously, in that it utilizes crosshole procedures, closely spaced boreholes, and wave propagation measurement procedures.

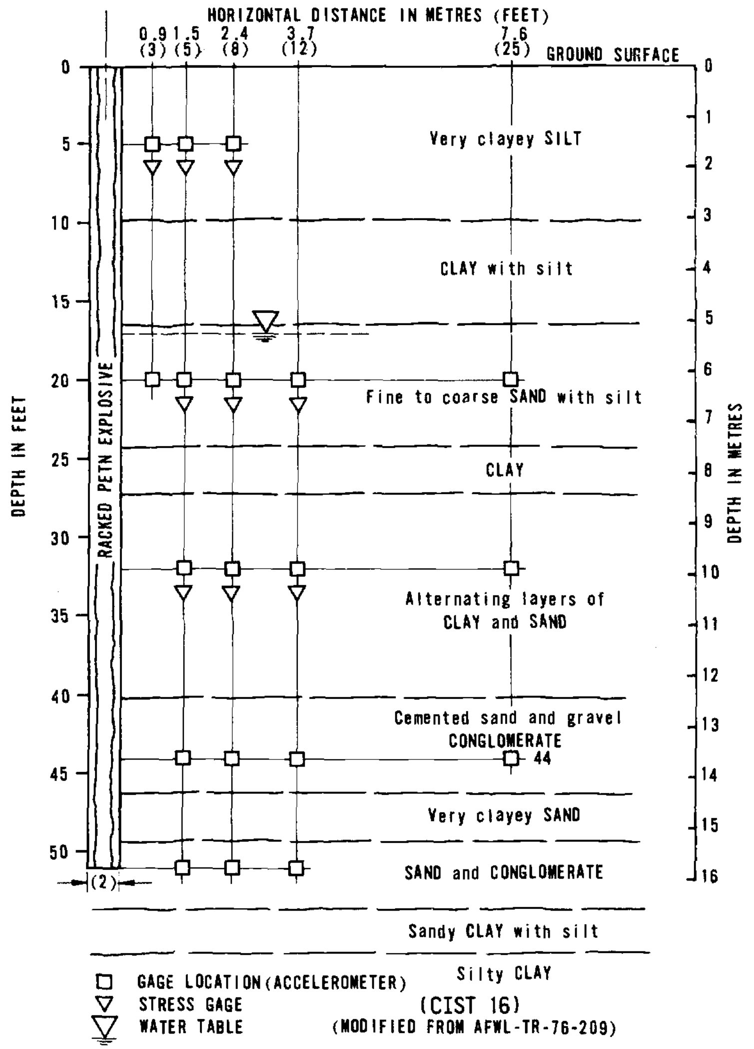

FIG. 10—*Schematic diagram of CIST method.*

The approach and procedures are different in that the objective is to obtain experimental data which are then used to develop a material model that describes the dynamic behavior of the site material. The principle of the test follows procedures used in Ref *25* to define shear modulus and damping from earthquake data recorded at sites with multilevel stations. While these procedures provide data on the combined effects of the shear or elastic modulus and damping, certain assumptions are normally necessary to evaluate the contribution of each.

The test utilizes a large explosive source which is detonated in a 0.6-m (2 ft)-diameter vertical cylindrical cavity. Free field measurements of acceleration are taken simultaneously at 30 or more locations at various ranges and depths within the various soil layers being tested. Input pressure forces reaching 472 kg/cm^2 (6700 psi) are determined with cavity pressure transducers. Once the field measurements are obtained, the material model is developed through an iterative technique of matching calculated results with measured time histories. The acceleration records are integrated and data are studied in terms of velocity. The model parameters are revised until all aspects of the particle velocity wave forms are reproduced. These include arrival time, time of peak velocity, magnitude of peak velocity, rise time, maximum positive phase duration, slope of the time history, and attenuation of the peak with range. The finalized parameters may then be used to calculate free field response to high-explosive and nuclear shock.

Instrument installation involves grouting accelerometers permanently at various depths using grout with a density close to that of the soil. Significant expertise is required when placing and arranging for delays in shot times to produce the desired effect from one blast. This, together with sophisticated instrumentation for recording 30 or more channels of data at one time, would no doubt be an extremely costly procedure to carry out routinely as a conventional test procedure. The test currently is used for blast and shock studies and is not yet applicable to earthquake engineering problems. We understand that because this procedure has produced much better results than when laboratory parameters are used, the developers of this test intend to adapt the principle of the test and procedures to study earthquake problems by generating largely shear rather than compression energies. Because this approach allows for back-calculation of all of the needed soil properties, further study of this technique is supported.

Conclusions

Significant advances made in the field of earthquake engineering, which resulted from the requirement to assure safe design of nuclear power plants, established a need to determine accurate shear moduli as a function of depth and shearing strain amplitude. This need has led to the development of greatly improved energy sources, recording and triggering equipment, and data reduction procedures. Both vibratory and mechanical impulse sources have been developed and tested and they produce clear, controlled, repeatable signals. Shear reversal techniques and enhancing equipment have been used to enable more positive identification of first arrival times. With these improvements, better and more accurate results are being obtained using the two most common methods: crosshole and downhole procedures. Nine sites were tested using both downhole and crosshole procedures, and the results show good agreement when considering all the different variables of each method. The authors conclude, therefore, that either method is acceptable and will give reasonably comparable velocity or modulus results, especially if controlled repeatable energy sources are employed, along with enhancement equipment or possibly wave reversal techniques to identify shear wave arrival times.

Two other modified crosshole techniques are also discussed which extend existing geophysical procedures by testing at higher strains. A unique feature of the *in situ* impulse test is that a clear controlled pulse is propagated through the ground, producing a simple repeatable wave form which has physical significance. This enables time measurements to be defined at different known strains rather than using first-arrival-time techniques. It is also unique in that the same basic wave shape or signature is produced at all sites, at all depths, and in all types of material, enabling positive determination of correct arrival times. Further research on waveform analysis procedures such as these is strongly recommended as it will enable, for the first time, the field study of wave propagation in soils which are subjected to dynamic stresses and strains in the nonlinear range.

The CIST test achieves its high strains through a large blast and was developed for modeling blast or shock phenomena. The unique advantage of CIST is that the soil's full dynamic behavior can be represented. However, it is a back-calculation procedure which relies on basic assumptions regarding its modeling and has not been extended to shear behavior. Further research on this basic procedure is encouraged as it may provide a better understanding of dynamic nonlinear soil behavior and may lead to field measurement methods for the development or representation of soil properties to satisfy some of the more complex analytical models of the future.

References

[1] Duke, C. M. in *Proceedings*, 4th World Conference on Earthquake Engineering, Santiago, Chile, 1969, pp. 39-54.

[2] Shannon & Wilson, Inc. and Agbabian-Jacobsen Associates, "Soil Behavior Under Earthquake Loading Conditions: State of the Art, Evaluation of Soil Characteristics for Seismic Response Analyses," Jan. 1972.

[3] Murphy, V. J. in *Proceedings*, International Conference on Microzonation for Safer Construction, Research and Application, Seattle, Wash., Vol. 2, 1972, pp. 131-159.

[4] Schwarz, S. D. and Musser, J. M., *Proceedings*, International Conference on Microzonation for Safer Construction, Research and Applications, Seattle, Wash., Vol. 2, 1972, pp. 593-608.

[5] Ballard, R. F., Jr., and McLean, F. G. in *Proceedings*, Conference on *In Situ* Measurement of Soil Properties, American Society of Civil Engineers, Raleigh, N.C., Vol. 1, June 1975, pp. 121-150.

[6] Viksne, A., "Evaluation of In Situ Shear Wave Velocity Measurement Techniques," REC-ERC-76-6, U.S. Bureau of Reclamation, April 1976.

[7] Anderson, D. G. and Richart, F. R., Jr., *Journal of the Geotechnical Engineering Division*, American Society of Civil Engineers, Vol. 102, No. GT9, Sept. 1976, pp. 975-987.

[8] Hardin, B. O. and Drnevich, V. P., *Journal of the Soil Mechanics and Foundations Division*, American Society of Civil Engineers, Vol. 98, No. SM7, July 1972, pp. 667-692.
[9] Hoar, R. J. and Stokoe, K. H., II, this publication, pp. 3-29.
[10] Mooney, H. M., *Journal of the Geotechnical Engineering Division*, American Society of Civil Engineers, Vol. 100, No. GT8, Aug. 1974, pp. 905-924.
[11] Stokoe, K. H., II, and Woods, R. D., *Journal of the Soil Mechanics and Foundations Division*, American Society of Civil Engineers, Vol. 98, No. SM5, May 1972, pp. 443-460.
[12] McLamore, V. R., Anderson, D. G., and Espana, C., this publication, pp. 30-55.
[13] Stokoe, K. H., II, and Woods, R. D., Closure of "In Situ Shear Wave Velocity by Cross-hole Method," *Journal of the Soil Mechanics and Foundations Division*, American Society of Civil Engineers, Vol. 99, No. SM11, Nov. 1973, pp. 1014-1016.
[14] Anderson, D. G. and Woods, R. D. in *Proceedings*, Conference on *In Situ* Measurement of Soil Properties, American Society of Civil Engineers, Raleigh, N.C., Vol. 1, June 1975, pp. 69-92.
[15] Stokoe, K. H., II, and Abdel-rassak, K. G. in *Proceedings*, Conference on *In Situ* Measurement of Soil Properties, American Society of Civil Engineers, Raleigh, N.C., Vol. 1, June 1975, pp. 422-449.
[16] Tanimoto, K. and Kurzeme, M., Discussion of "In Situ Shear Wave Velocity by Cross-hole Method," *Journal of the Soil Mechanics and Foundations Division*, American Society of Civil Engineers, Vol. 99, No. SM4, April 1973, pp. 351-353.
[17] Ballard, R. F., Jr., and Leach, R. E., "Development of a Vibropacker System for Inducting Polarized Shear Waves and Compression Waves at Depths," Miscellaneous Paper S-69-30, U.S. Army Engineer Waterways Experiment Station, Corps of Engineers, Vicksburg, Miss., July 1969.
[18] Ballard, R. F., Jr., *Journal of the Geotechnical Engineering Division*, American Society of Civil Engineers, Vol. 102, No. GT12, Dec. 1976, pp. 1261-1273.
[19] Haupt, W. A., Discussion of "In Situ Shear Wave Velocity by Cross-hole Method," *Journal of the Soil Mechanics and Foundations Division*, American Society of Civil Engineers, Vol. 99, No. SM2, Feb. 1973, pp. 224-228.
[20] Shannon & Wilson, Inc. and Agbabian Associates, "*In Situ* Impulse Test: An Experimental and Analytical Evaluation of Data Interpretation Procedures," Report No. NUREG-0028, Nuclear Regulatory Commission, Sept. 1976.
[21] Jolly, R. N., *Geophysics*, Vol. 21, No. 4, Oct. 1956, pp. 905-938.
[22] Miller, R. P. and Brown, F. R., Jr. in *Proceedings*, International Conference of Microzonation for Safer Construction, Research and Application, Seattle, Wash., Vol. 1, 1972, pp. 545-558.
[23] "Cylindrical *In-Situ* Test at Selected Nuclear and High-Explosive Test Sites," AFWL-TR-76-709, Air Force Weapons Laboratory, Kirtland Air Force Base, N.M. Feb. 1977.
[24] Shannon & Wilson, Inc. and Agbabian Associates, "Technical Manual, Operation and Equipment Instructions for *In Situ* Impulse Test," Draft Report, Nuclear Regulatory Commission, June 1977.
[25] Seed, H. B. and Idriss, I. M., *Bulletin of the Seismological Society of America*, Vol. 60, Feb. 1970, No. 1, pp. 125-136.
[26] Schwarz, S. D. and Conwell, F. R. in *Proceedings* of the Sixth Annual Offshore Technology Conference, No. OTC 2014, May 1974, pp. 755-762.

W. F. Marcuson III[1]

Determination of *In Situ* Density of Sands

REFERENCE: Marcuson, W. F., III, "**Determination of *In Situ* Density of Sands**," *Dynamic Geotechnical Testing, ASTM STP 654*, American Society for Testing and Materials, 1978, pp. 318–340.

ABSTRACT: The use of undisturbed samples to evaluate *in situ* density and the Standard Penetration Test (SPT) to estimate *in situ* relative density is reviewed. A procedure for obtaining high-quality undisturbed samples of sands and the influence of this sampling procedure on the *in situ* relative density are discussed. The use of radiographs to evaluate sample quality is examined.

As a result of studies reviewed, it is concluded that the SPT is not sufficiently accurate to be recommended for final evaluation of the density or relative density of a site unless site specific correlations are developed. High-quality undisturbed samples of sands may be obtained using a fixed-piston sampler and drilling mud. This sampling procedure yields very good samples in deposits of medium-dense sands; however, the procedure tends to densify samples of loose sands and loosen samples of dense sands.

KEY WORDS: *in situ* density, relative density, sand, undisturbed sampling, Standard Penetration Test, X-radiographs, soils

The accurate and reliable determination of *in situ* density and *in situ* relative density of cohesionless soil deposits has plagued civil engineers for decades. These determinations are currently made by direct or indirect techniques. In direct techniques the soil weight and volume are measured quantities and the *in situ* density is directly calculated. The discussion of these methods presented herein is limited to the use of undisturbed samples to determine *in situ* density and the influence of the sampling procedure on the density determined in the laboratory. Indirect techniques refer to empirical correlations between index values and relative density. The discussions presented herein are limited to correlations between Standard Penetration Test (SPT) *N*-values and relative density.

[1]Research civil engineer, Earthquake Engineering and Vibrations Division, Soils and Pavements Laboratory, U. S. Army Engineer Waterways Experiment Station, Vicksburg, Miss. 39180.

Throughout this paper, reference is made to *in situ* density and *in situ* relative density. Whenever possible, *in situ* density is discussed because of the many problems inherently associated with relative-density determinations. Indications [*1–7*][2] are that even if the *in situ* density of a soil deposit is known, the accuracy with which the relative density can be obtained is of the order of ±20 percent. This scatter is associated with difficulties in obtaining accurately the minimum and maximum densities required to compute the relative density. As a matter of practice, the U. S. Army Engineer Waterways Experiment Station (WES) uses *in situ* density whenever possible, and resorts to the use of *in situ* relative density only when it is necessary to compare different materials or different sites.

Indirect Determination of *In Situ* Relative Density

The Bureau of Reclamation has reported results [*8,9*] which correlate relative density with SPT *N*-values and overburden pressure. These correlations were based on data obtained from laboratory penetration tests conducted in tanks filled with sand. Bazaraa [*10*] also developed correlations between SPT *N*-values, overburden pressure, and relative density. These correlations were based on field data and are more conservative than the curves developed by Gibbs and Holtz [*8*]. In the interest of brevity, a discussion on the history of the use of the SPT to estimate relative density has been omitted. If the reader is interested in this, he is referred to deMello [*11*]. However, a brief summary of the results obtained at WES in a recent laboratory study of the SPT is included. The details are presented elsewhere [*12–15*].

During this WES study, SPT's were performed on 1.2-m (4 ft) diameter by 1.8-m (6 ft) high samples of four sands (Reid Bedford Model sand, Ottawa sand, Platte River sand, and Standard Concrete sand) at various relative densities under overburden pressures up to 552 kN/m^2 (80 psi). Figure 1 shows the grain size distribution curve and other pertinent data for each of these sands. Figure 2 is a plot of *N*-values versus relative density obtained by WES for the Reid Bedford Model and Ottawa sands. Data points are plotted on this figure for overburden pressures of 69, 276, and 552 kN/m^2 (10, 40, and 80 psi) and overconsolidation ratios (OCR) of 1 and 3. This figure depicts the spread of data for three overburden pressures under ideal laboratory conditions. As can be seen, for a given overburden pressure and *N*-value, the spread in the relative density is about ±15 percent. Figure 3 presents the same data spread with the Gibbs and Holtz and Bazaraa curves superposed for comparison purposes.

Figure 4 is a plot of *N*-values versus relative density for WES tests on Platte River and Standard Concrete sands. Figures 2–4 indicate that a

[2] The italic numbers in brackets refer to the list of references appended to this paper.

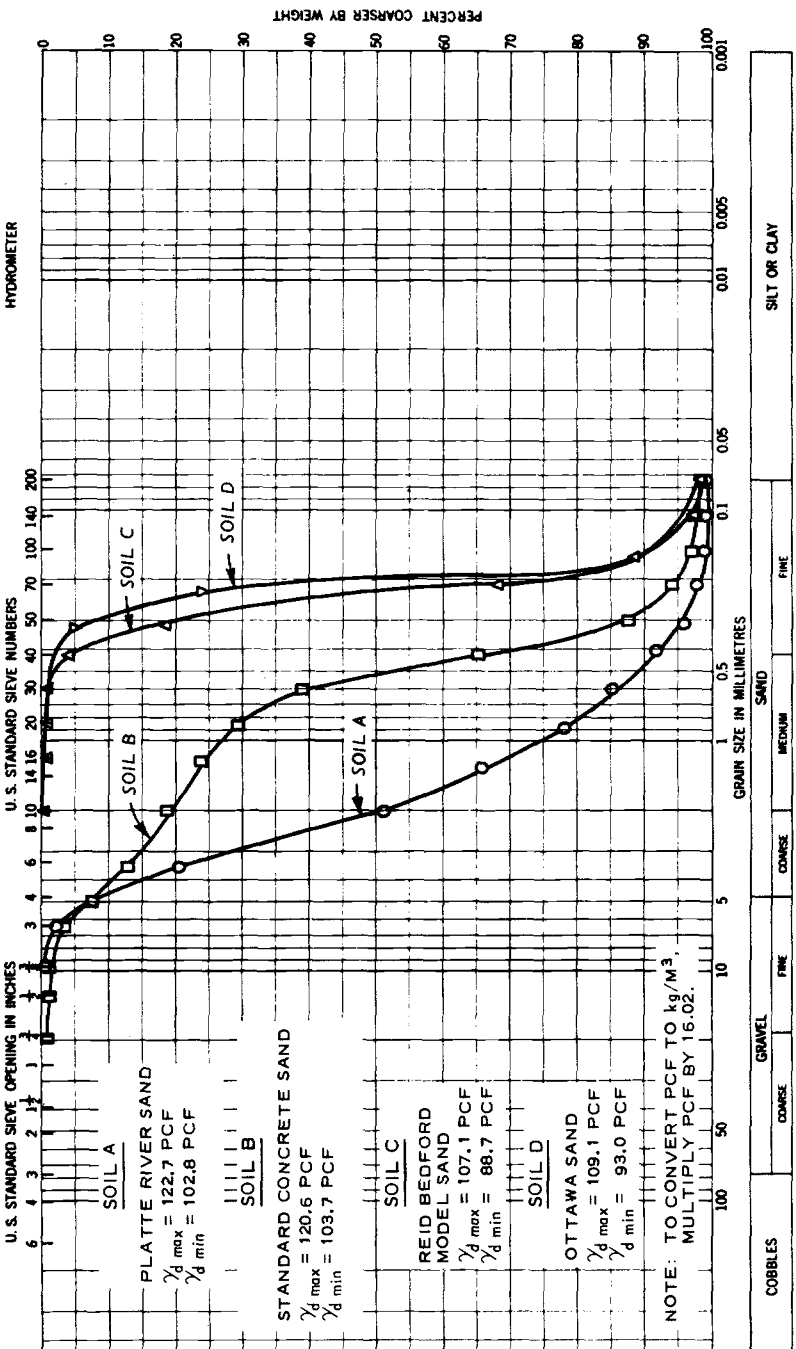

FIG. 1—*Mechanical analyses and density values for Platte River, Standard Concrete, Reid Bedford Model, and Ottawa sands.*

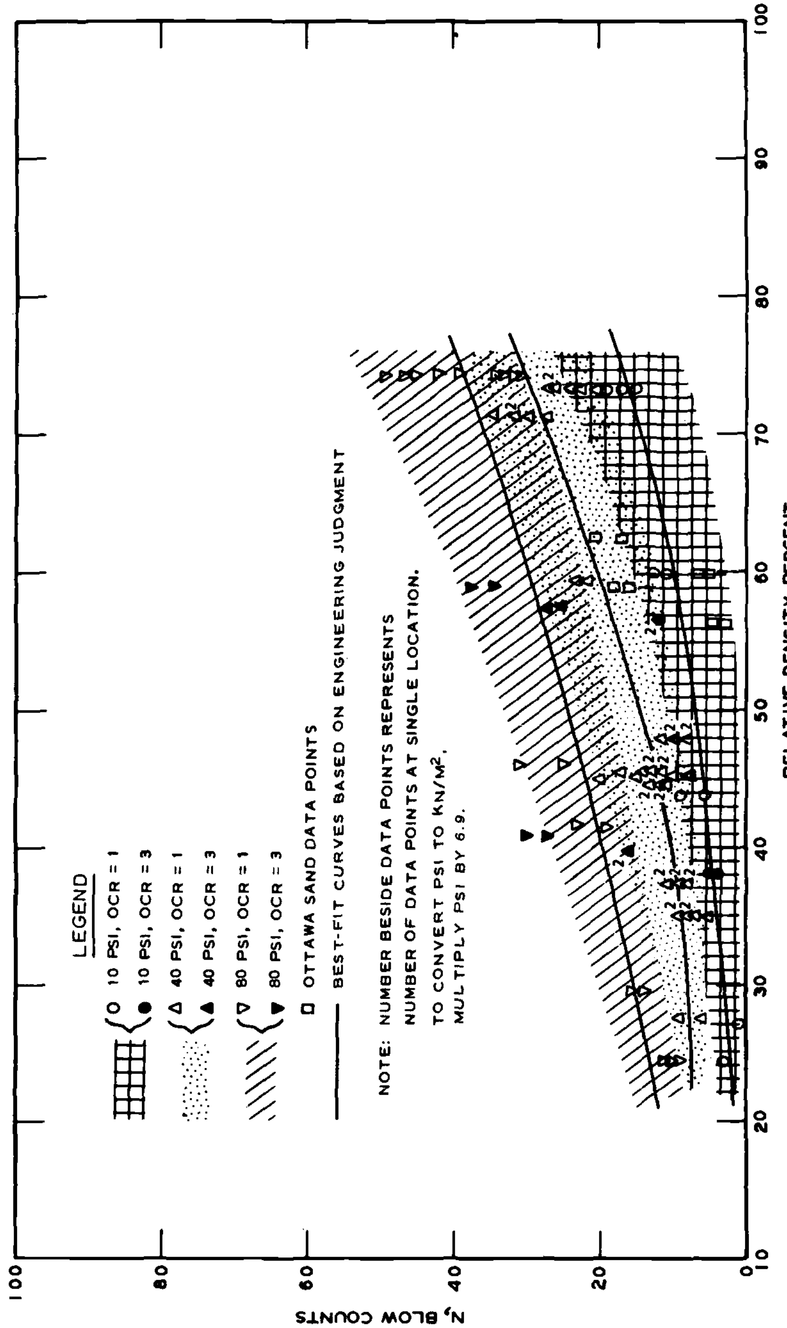

FIG. 2—*WES SPT data for Reid Bedford Model sand and Ottawa sand for three overburden pressures.*

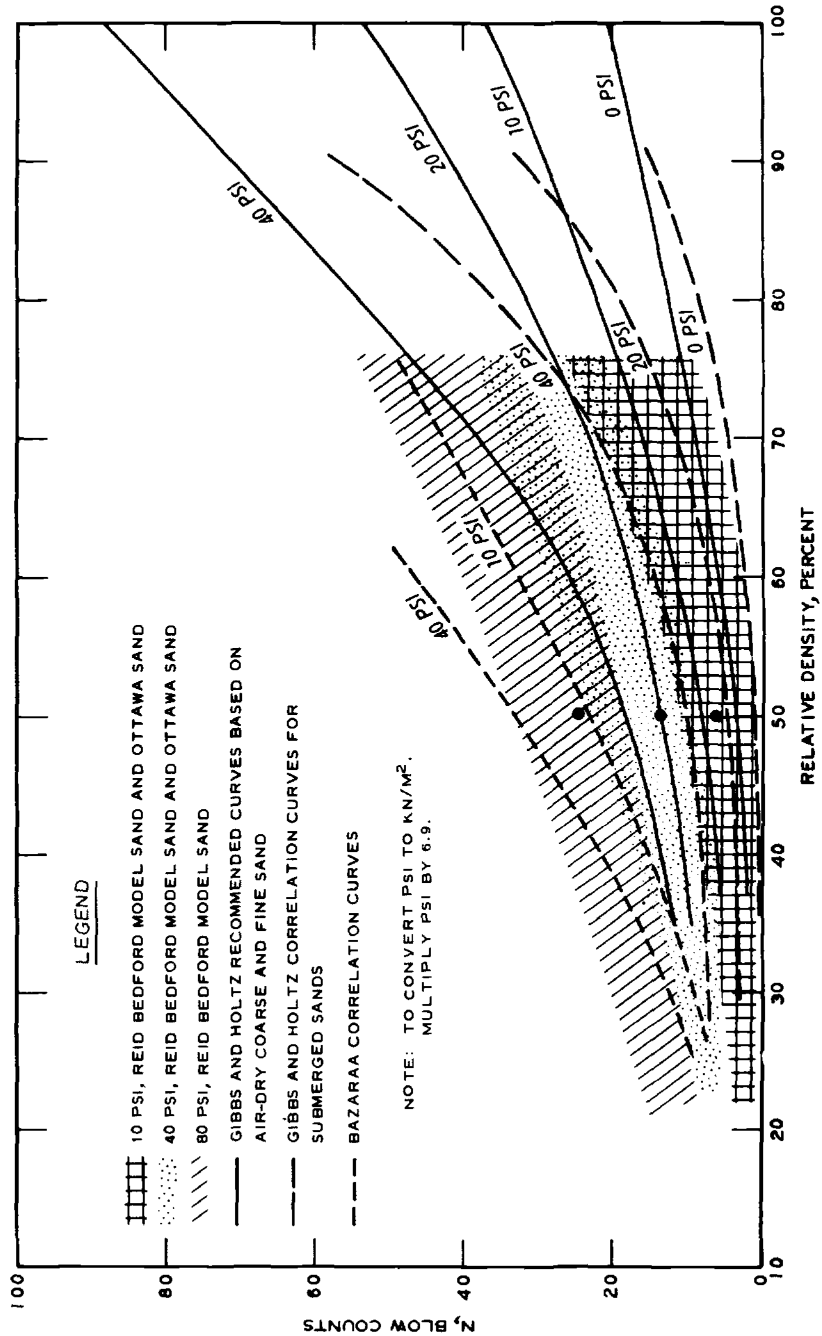

FIG. 3—*Comparison of WES data, Gibbs and Holtz correlation curves, and Bazaraa curves.*

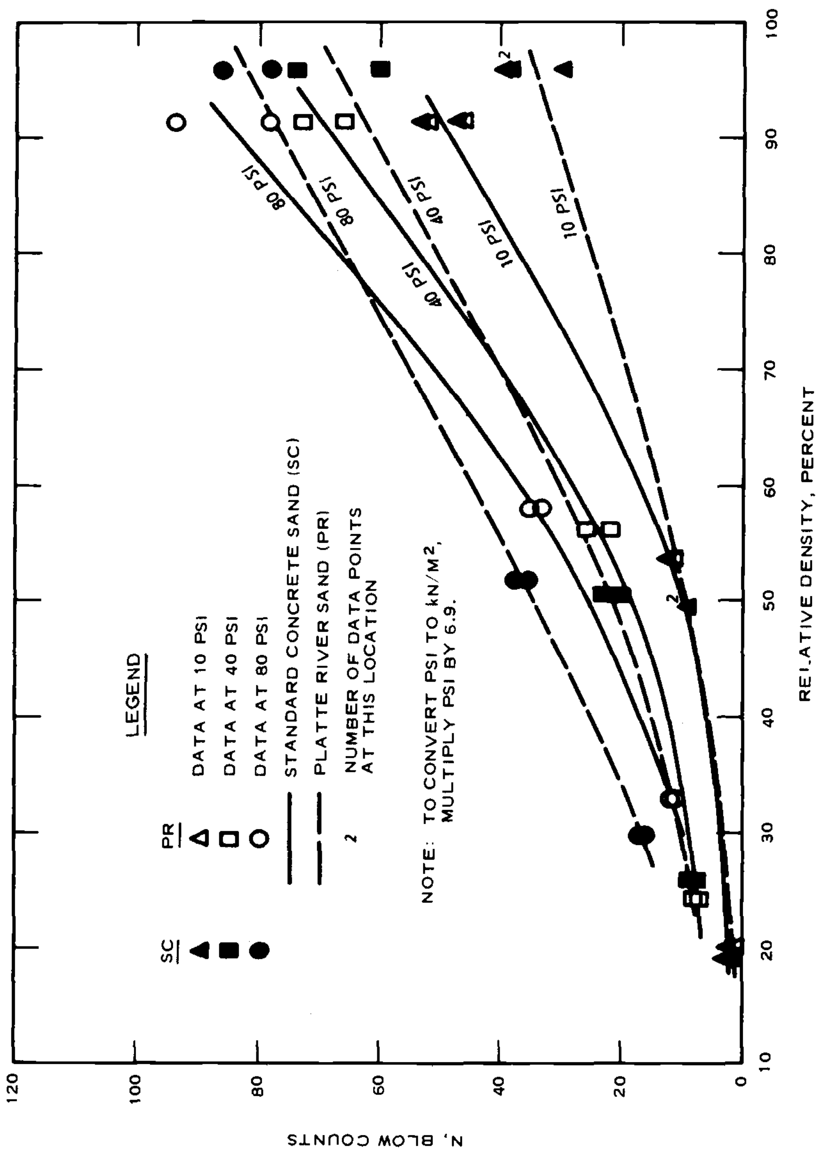

FIG. 4—WES SPT data for Platte River and Standard Concrete sands.

simple family of curves relating SPT N-values, overburden pressure, and relative density for all sands under all conditions is not valid.

After discarding unreliable data, a statistical analysis was performed on data obtained from testing all four sands. The equation developed to best describe the data is

$$D_r = 11.7 + 0.76\,[|(222)N + 1600 - 53(\bar{\sigma}_v) - 50(C_u)^2|]^{1/2}$$

where

D_r = relative density, percent,
N = SPT blow counts, blows per foot,
$\bar{\sigma}_v$ = effective overburden pressure, psi, and
C_u = coefficient of uniformity.

This equation fits the data obtained on normally consolidated material with a coefficient of correlation (r^2) of 0.85 and a standard deviation ($\pm\sigma$) of 8.3 percent.

The significant conclusions reached in this laboratory penetration test study were as follows:

1. Based on a comparison between the correlations presented by Bazaraa, Gibbs and Holtz, and WES, it was concluded that the SPT is not sufficiently accurate to be recommended for final evaluation of the density or relative density at a site, unless site-specific correlations are developed. However, the SPT does have value in planning the undisturbed sampling phase of the subsurface investigation and in comparing different sites.

2. Sand type and specimen preparation technique influence penetration resistance.

3. The spread of data derived from testing four sands under optimum laboratory conditions suggests that a simplified family of curves correlating SPT N-values, relative density, and overburden pressure for all cohesionless soils under all conditions is not valid.

4. The expression derived from the statistical analysis is based on data obtained under laboratory conditions and therefore has limited application. It does not adequately address the variability of subsurface conditions found in the field. Water table conditions, overconsolidation, length and weight of drill rods, and dynamic interaction of the drive-sampling system were either not intensively studied or were not investigated. Additional research is required to evaluate these factors.

Direct Determination of *In Situ* Density

As previously defined, direct determination of *in situ* density means a process in which the weight and volume of the soil are measured and density is easily calculated. It is generally accepted that there is no such thing as a truly undisturbed sample of soil. Samples that are routinely referred to as "undisturbed" samples are high-quality samples obtained with minimal disturbance. The question that remains is: How does this minimal disturbance affect the density determinations based on weight and volume measurements made in the laboratory?

Development of the Sampling Procedure

Over the past three decades, WES has conducted various studies with the objective of evaluating various sampling techniques for determination of *in situ* density [*16–20*]. During the late 1940's a drilling, sampling, and handling procedure was developed which yields high-quality undisturbed samples [*16*]. The drilling procedure uses a fishtail bit with baffles. These baffles are welded on the bit below the jets to block the downward flow of drilling mud which might otherwise disturb the sand to a considerable depth below the bit. The sampling procedure involves the use of a fixed-piston-type sampler known as the Hvorslev sampler. The drilling and sampling procedures, including starting and advancing the boring, sampling, withdrawal operation, and treatment of samples, are described in detail in Ref *16*. Using this procedure, the sample is withdrawn from the borehole, held in a vertical position, and the sampler and 7.62-cm (3 in.) inside-diameter thin-walled sampling tube are disconnected. The tube is maintained in a vertical position while a perforated expanding-end packer is placed in the bottom of the sample tube. The tube is placed in a rack in the vertical position and allowed to drain. The time required for proper drainage varies from 24 to 48 h depending on the amount and character of fines in the soil samples. After drainage is completed, an expanding end packer is placed in the top of the sample tube. If the sample is to be used only for density determinations, it is rotated into the horizontal position and placed in a cradle. The top of the tube is marked and the top side of each tube is then struck 50 light blows with a rubber hammer, starting at one end of the tube and working toward the other with 25 blows and then reversing the procedure, thereby consolidating the sand and preventing possible liquefaction and flow of any loose particles of sand in the tube during transportation to the laboratory. The tubes are prevented from rotating during transportation. In the laboratory, samples are cut into 7.62-cm (3 in.) increments with a band saw and unit weight determinations are made by conventional methods for each increment of sample. The total volume of the section of tube from which the sample increment is removed is used as the basic volume for the sample increment in all unit weight determinations.

It is important to note that once the sample is extracted from the borehole, its treatment depends on whether an undisturbed sample of the material is desired for laboratory testing or whether *in situ* density is the only desired end product. Only if *in situ* density is the desired end product is the sample tapped, thus disturbing the soil sample.

This sampling procedure is used routinely by WES and has been used effectively during the subsurface investigations for at least three building sites in Canada [*21*].

First Investigation

The density changes caused by the foregoing sampling procedure were studied at WES in the early 1950's [*17*]. In this study, two sands, one medium (MR-1) and one fine (MR-2), were placed in a 0.75-m (2½ ft) diameter by 1.8-m (6 ft) deep drum at high and low initial densities. The grain size distributions are shown in Fig. 5. The sand was sampled using a fixed-piston-type sampler with lacquered, thin-walled, seamless-steel Shelby tubes. These samples were not tapped but were carefully transported to the laboratory, where incremental distribution of density within the sample was determined using all possible precautions to avoid additional disturbance of the sample.

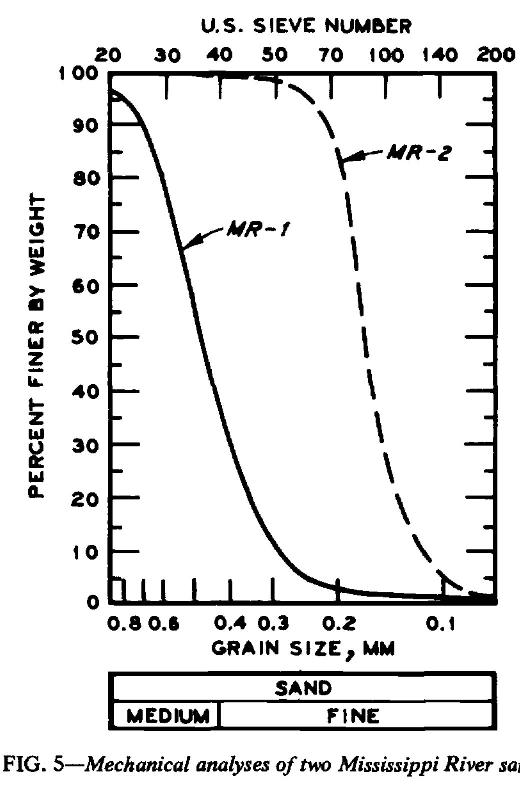

FIG. 5—*Mechanical analyses of two Mississippi River sands.*

The average density changes obtained are illustrated in Fig. 6. The change in density versus initial density is plotted in Fig. 6*a*. The greatest density changes were obtained in the first series of tests using the medium sand (MR-1). The samples were taken with a 7.3-cm (2.875 in.) diameter sampler having comparatively large clearances. High rates of penetration, depths of penetration equal to 0.6 to 0.7 m (2 to 2.3 ft) and no surcharge loads were used. The same sand was used in the second series of tests, but the clearance was reduced to 0.50 percent and penetration was stopped when settlements appeared to be excessive. The resulting disturbance was much less than in the first series. No trends which can be attributed to the controlled variation of equipment or procedures, or both, exist in the density changes obtained in the second series. A fine sand (MR-2) was used in the third series and samples were taken with a 7.62-cm (3 in.) diameter sampler having variable clearances and using a constant rate of penetration. The average density changes are similar to those obtained in the second series of tests. No trends exist in the density changes which can be attributed to variation in sampler clearance. In comparison with the second series, the greater length of drive in the third series appears to result in a greater disturbance of the loose material. Statistical correlations were made of the results of the second and third series. The results of these correlations appear to be reasonable even though based on limited data. The scatter of the data about the line of regression, as measured by the standard error of estimate, S, is in the order of ± 8.0 to ± 11.2 kg/m^3 (± 0.5 to ± 0.7 lb/ft^3). This scatter corresponds to the average density changes caused by the laboratory density determination procedures discussed earlier. It seems reasonable to assume that the scatter obtained in the second and third series of tests was caused by inherent errors in laboratory procedures and is large enough to mask any density changes caused by controlled variation in sampling equipment and procedures.

The results of all tests are plotted in Fig. 6*b* as changes in relative density versus initial relative density. The combined effects of sampling and testing tended to cause a decrease in average density for initial relative densities of greater than 77 percent and an increase in relative density for lesser initial values in the second and third series. The scatter expressed as a standard error of estimate, S, amounts to ± 3.5 percent (in terms of relative density). The change in average relative density is large, 10 to 15 percent, at extremely high and low values of initial relative density.

Second Investigation

Because the influence of overburden pressure was not adequately addressed in the first study, a second investigation was conducted at WES during the late 1950's [*18*]. During this study, two Mississippi River sands

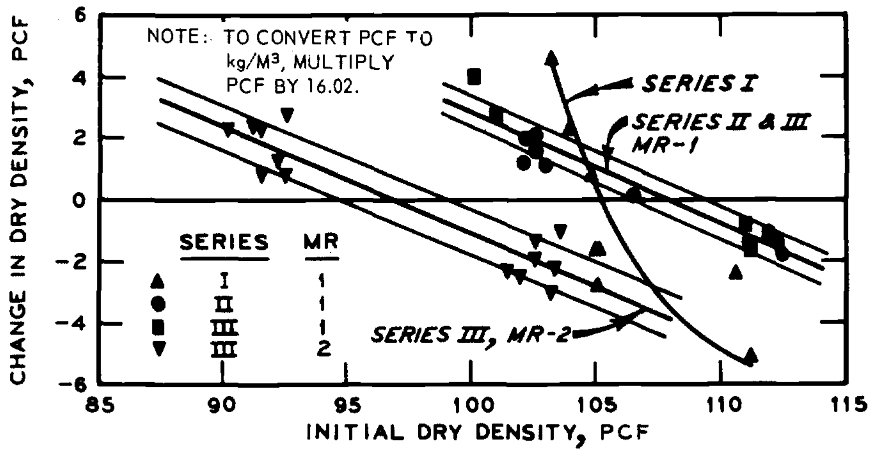

a. CHANGE IN DENSITY VERSUS DRY DENSITY

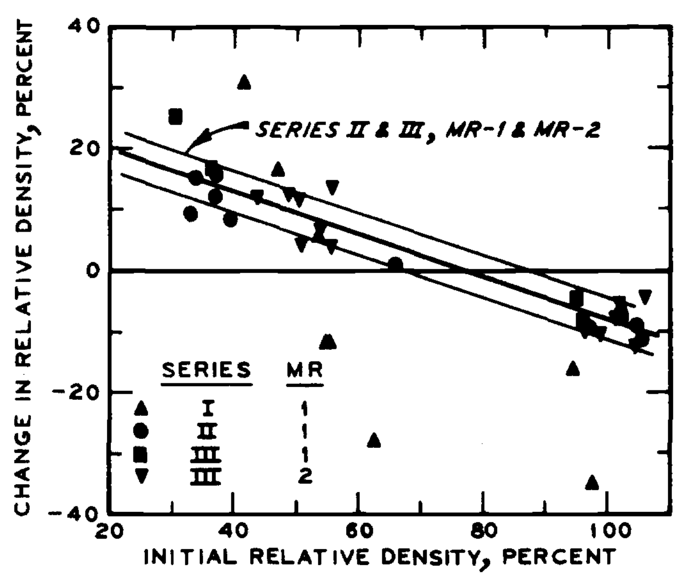

b. CHANGE IN RELATIVE DENSITY VERSUS INITIAL RELATIVE DENSITY

FIG. 6—*Average density changes caused by sampling.*

(Sands 1 and 2 in Fig. 7) were placed in a 1.07-m (3½ ft) diameter by 1.98 m (6½ ft) deep cylindrical tank at relative densities of approximately 20 and 90 percent. Surcharge pressures of 207, 414, and 690 kN/m² (30, 60, and 100 psi) were applied to the samples. After consolidation, 7.62-cm (3 in.) undisturbed samples were taken using the Hvorslev fixed-piston

MATERIAL	SPECIFIC GRAVITY	DRY DENSITY, PCF	
		MAX	MIN
SAND 1	2.65	104.2	87.2
SAND 2	2.66	111.6	95.6

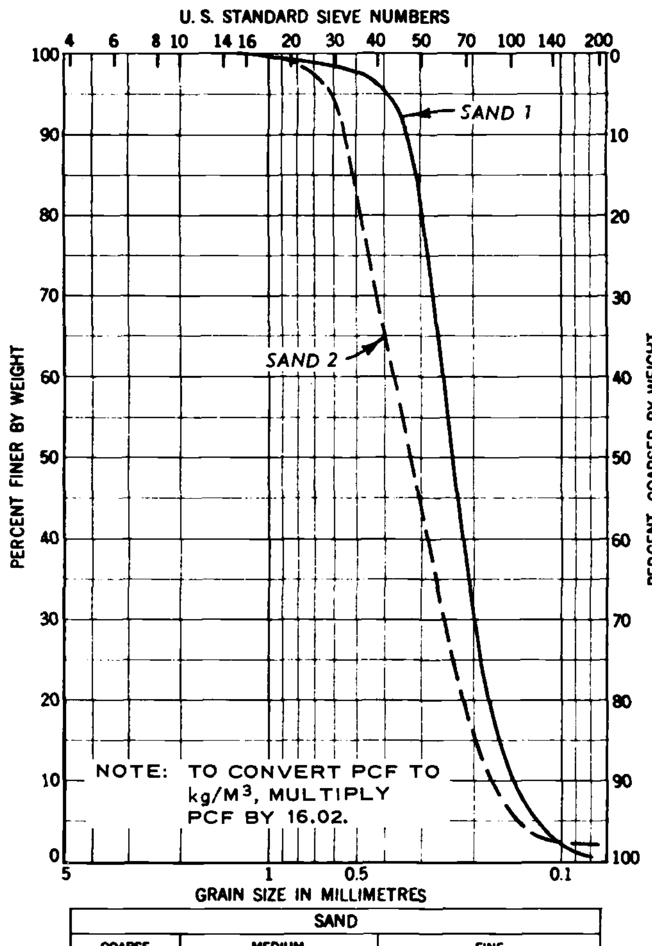

FIG. 7—*Mechanical analyses and density values for Sands 1 and 2.*

sampler. Figure 8 summarizes the pertinent results and gives corrections for the change in density caused by sampling. The correction factor curves are plotted in Fig. 8*a*. Lines shown to indicate the correction factors for relative density at 10 percent intervals between 30 and 86 percent were spaced by linear proportion. The plot of density correction for overburden pressure indicates that at overburden pressures ranging from 138 to 345 kM/m^2 (20 to 50 psi), the density corrections for Sand 1 at a measured relative density of 30 percent range from -19.2 to -25.6 kg/m^3 (-1.2 to -1.6 lb/ft^3) and for a measured relative density of 86 percent the corrections range from $+11.2$ to $+14.4$ kg/m^3 ($+0.7$ to $+0.9$ lb/ft^3). At a measured relative density of about 60 percent, which is common in the field, the density correction is almost zero.

The density was also dependent on the location of the increment in the sample tube. The correction was determined by the following procedure:

1. The measured change in density of each sample increment was corrected for overburden pressure by entering Fig. 8*a* at the pressure equal to the vertical pressure for the increment and reading horizontally across to either the 30 or 86 percent correction factor curve, depending on the measured density of the sample increment, and then reading vertically down to the average density correction scale. The difference between the total change in density of the increment and the correction determined for the effect of overburden pressure is considered to be the change in density effected by the location of the increment in the sample tube.

2. The change in density for the location in the sample tube was then plotted for each increment, with sign reversed, against the height of the increment from the bottom of the sample tube. The plot of increments from the 30 percent measured relative density specimen is shown in Fig. 8*b* and the plot of increments from the 86 percent measured relative density specimen is shown in Fig. 8*c*.

3. Smooth curves were drawn through the points. These smooth curves were then combined in a single plot, shown in Fig. 8*d*, and curves for measured relative densities of 40, 50, 60, 70, and 80 percent were drawn by linear proportion between the 30 and 86 percent relative density curves. The corresponding dry densities are given for each relative density curve.

The plot of density correction for location of increment in the sample tube, for Sand 1 at a measured relative density of 30 percent, indicates that at heights greater than about 61 cm (24 in.) in the tube, the density change is rather large and the data are quite scattered. This fact suggests that densities of increments at heights greater than 61 cm (24 in.) in the tube should not be considered reliable. Also, although density changes in the bottom 15.2 cm (6 in.) of the 76.2-cm (30 in.) long sample tubes were not excessive, it must be pointed out that the samples of the tank specimens were not pulled from the tank immediately after the sampler drive had ended, but were removed from the specimen after all three sample tubes

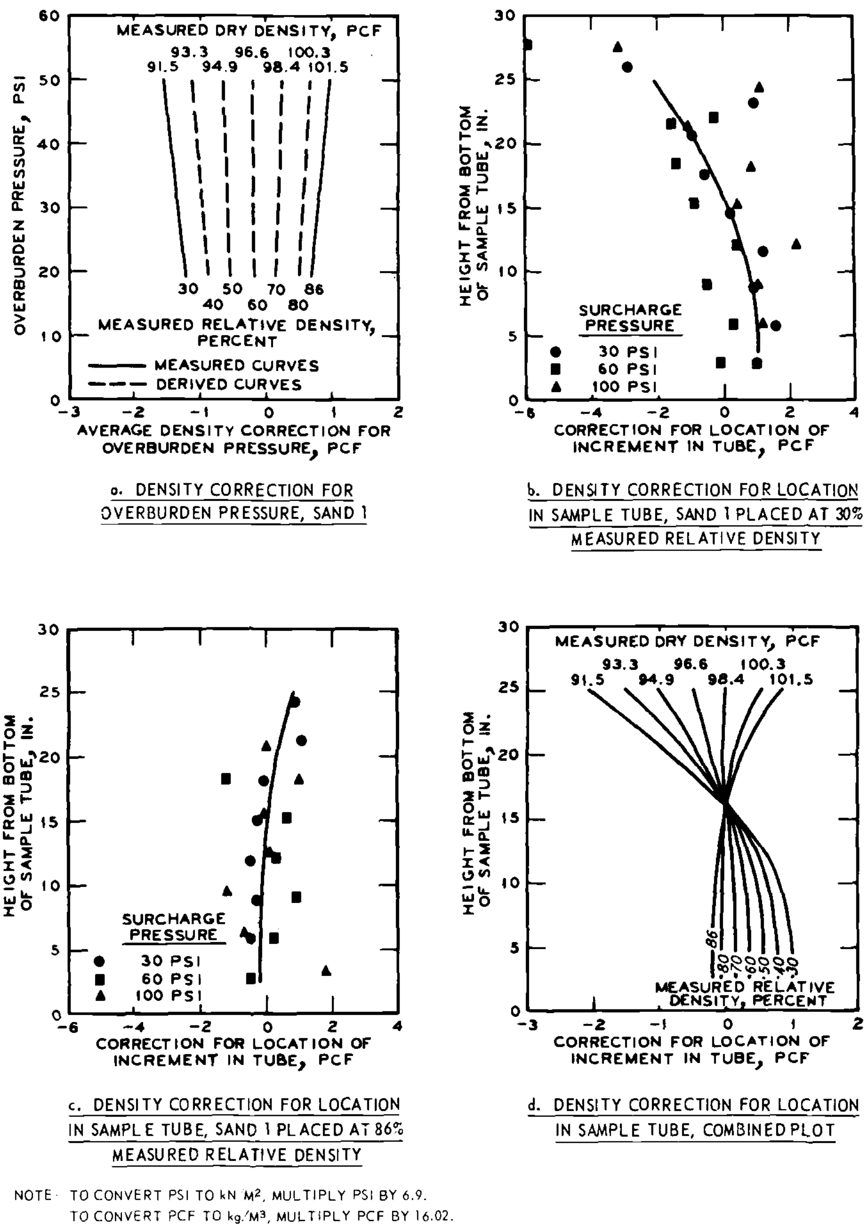

FIG. 8—*Corrections for change in density caused by sampling for Sand 1.*

had been pushed and the material excavated from around the tubes. If the sample tubes had been pulled out immediately, as is necessary in the field, it is believed that the density changes in the bottom 15.2 cm (6 in.) would have been larger because of stress changes in the vicinity of the bottom of the sampling tube. Therefore, in the analysis of density measurements on samples obtained in the field, data from heights greater than 61 cm (24 in.) and lower than 15.2 cm (6 in.) should be disregarded and only data from the central 45.7 cm (18 in.) should be used for determining densities.

The combined plot of density corrections for locations of increments in the sample tube for Sand 1 (Fig. 8*d*) indicates that at heights from 15.2 to 61 cm (6 to 24 in.) in the sample tube, the density correction for 30 percent measured relative density ranges from $+16$ to -28.8 kg/m^3 ($+1.0$ to -1.8 lb/ft^3), and for 86 percent measured relative density the correction ranges from -3.2 to $+11.2$ kg/m^3 (-0.2 to $+0.7$ lb/ft^3). At a measured relative density of 60 percent, a density commonly found in the field, the density correction depending on height in the tube ranges from $+4.8$ to -8.0 kg/m^3 ($+0.3$ to -0.5 lb/ft^3).

Considering density corrections for both overburden pressure and location in sample tube, the total density correction could be as large as -54.5 kg/m^3 (-3.4 lb/ft^3) for a measured relative density of 30 percent at an overburden pressure of 345 kN/m^2 (50 psi) and height of 61 cm (24 in.) in the sample tube, and as large as $+27.2$ kg/m^3 ($+1.7$ lb/ft^3) for a measured relative density of 86 percent at an overburden pressure of 345 kN/m^2 (50 psi) and a height of 61 cm (24 in.) in the sample tube. However, for conditions which are commonly encountered in the field [for example, relative densities ranging from 30 to 80 percent, and overburden pressures ranging from 138 to 276 kN/m^2 (20 to 40 psi)], with heights of increments in the tubes ranging from 15.2 to 50.8 cm (6 to 20 in.), the maximum total density corrections would range from -36.9 to $+12.8$ kg/m^3 (-2.3 to $+0.8$ lb/ft^3), with a more common average correction range of -19.2 to 9.6 kg/m^3 (-1.2 to 0.6 lb/ft^3).

Since the difference between maximum and minimum densities as determined by laboratory tests generally ranges from about 256.3 to 320.4 kg/m^3 (16 to 20 lb/ft^3) for various sands, a density correction of approximately 16 kg/m^2 (1.0 lb/ft^3) would amount to a change in relative density of about 5 to 6 percent. Based on a limited evaluation of results of tests on Sand 2, it appears that correction factors for other sands might be approximately 16 kg/m^3 (1 lb/ft^3) greater than correction factors for Sand 1 [that is, an average of about 32 kg/m^3 (2 lb/ft^3)].

Third Investigation

Recently (1974–76) another series of tests was conducted on Reid Bedford Model sand in a 1.2-m (4 ft) diameter by 1.8-m (6 ft) high stacked-ring facility [*19,20*]. The purpose of the stacked rings is to significantly reduce sidewall friction so that the sand sample has a more realistic stress gradient. Dry sand was placed in a stacked-ring facility, submerged, and then an overburden pressure was applied. Finally the sand was sampled using the WES procedure. Figure 9 is a comparison of placed density, corrected for the effects of consolidation under the applied vertical loadings, with sampled density. These data show considerable scatter and are difficult to interpret. The linear regression fit to the data is aligned fairly close to the line of perfect sampling, and crosses the perfect sampling line at a

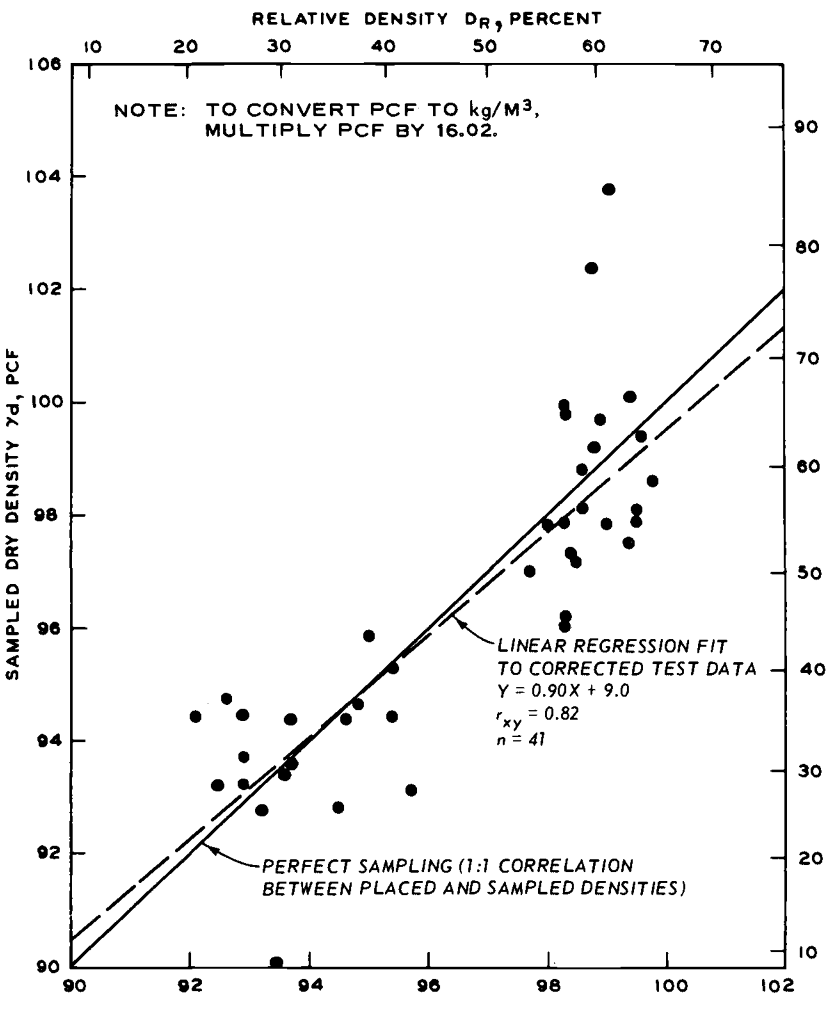

FIG. 9—*Comparison of placed density corrected for applied overburden pressure with sampled density.*

relative density of about 36 percent, which is considerably less than the relative density of 77 percent reported in Ref *17* and shown in Fig. 6, but the trend is the same. This variation may be attributed to (1) scatter in the data which made precise interpretation impossible, (2) differences in the sands tested (such as gradation, percent fines, and angularity), and (3) differences in the methods of sample preparation. The principal results and conclusions drawn from this study [*19*] are:

1. It was noted that the placed density at the time of sampling probably varied from +46.4 to −24 kg/m^3 (+2.9 to −1.5 lb/ft^3) from the measured values.

2. The sampled versus placed density comparisons presented suggest that sampling accuracy using the techniques described is within ±54.5 kg/m^3 (±3.4 lb/ft^3) for 95 percent of the sampling conducted at relative densities ranging from 20 to 60 percent. However, it can also be concluded that a more meaningful assessment of the sampling accuracy could have been made had it been possible to exercise better placed-density control during the study. It is very probable that in this event the apparent accuracy of sampling would have shown corresponding improvements.

Despite the uncertainties cited, this and the preceding studies indicate that sampling with a tube sampler tends to densify loose sand and to loosen dense sands. More definitive conclusions regarding the influence of tube sampling on the accuracy of density determinations cannot be advanced because of the uncertainty associated with the placed-density results uncovered in this study, and which probably existed in the previous studies.

Use of Test Pits

The results of all the studies discussed in the foregoing indicate that good samples can be taken in medium-dense material. However, the sampling procedure causes significant disturbance in either loose or dense deposits. Consequently, it may appear desirable to obtain undisturbed samples from test pits instead of boreholes whenever an extremely loose or dense deposit is encountered. The reader is cautioned that consolidation caused by the lowering of the groundwater table and shear stresses imposed during excavation may have an influence on the density that is larger than that experienced by sampling. Settlement markers should always be installed prior to excavation so that the effects of lowering the groundwater table may be evaluated. The equipment shown in Fig. 10 lends itself to obtaining high-quality undisturbed samples in test pits. This equipment, developed by Geotechnical Engineers Incorporated (GEI), Winchester, Mass., consists of a tripod holder and a 7.6-cm (3 in.) diameter brass Denison tube. The details of its use and operation are presented in Ref *22*. The sampling procedure involves trimming the soil carefully for a distance of about 0.3 to 0.6 cm (⅛ to ¼ in.) ahead of the tube to a diameter

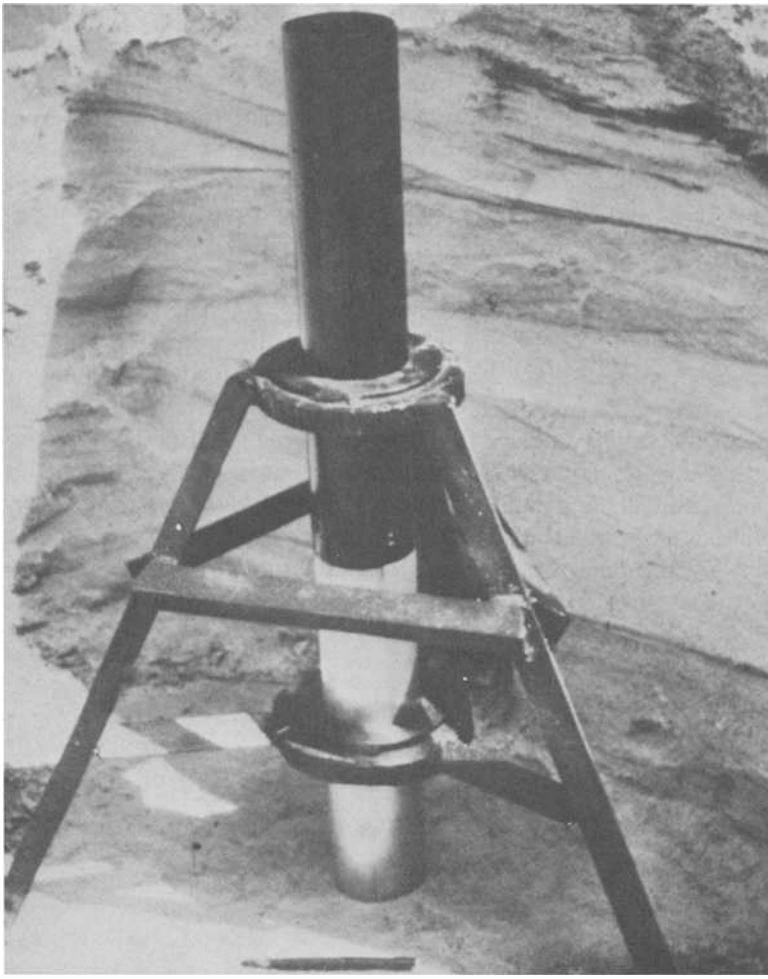

FIG. 10—*Undisturbed sampler being used in a test pit (courtesy of GEI).*

slightly larger than that of the tube. Then light (a few pounds) vertical pressure by hand is used to advance the tube, and the cutting edge shaves off the excess soil. This procedure is repeated until the desired sample length is recovered. Indications are that this sampling procedure also tends to loosen dense materials by an average of about 32 kg/m^3 (2 lb/ft^3) with extreme values as large as 64 kg/m^3 (4 lb/ft^3). Thus when a dense and possibly a loose deposit is encountered, test pits may not provide better undisturbed samples than borings; however, they do provide high-quality additional data unobtainable from borings. For this reason, test pits may be desirable.

Evaluation of Sample Quality

If one assumes a uniform thickness of sample tube and a uniform thickness of a homogeneous sample, then the density of the sample is roughly proportional to the film density of an X-ray; compare Krinitzsky [*23*]. Figure 11 shows a radiograph of an alluvial sand sample obtained with a Hvorslev fixed-piston sampler. Also shown is a plot of film density through the centerline of the core. This technique has been employed in several studies by WES [*24–26*] to evaluate qualitatively sample variation, layering, and disturbance.

Figure 12 shows radiographs of both high-quality and low-quality undisturbed samples. Notice that in the high-quality samples the bedding planes can be seen all the way to the sample edge. In the low-quality sample these planes are contorted, indicating disturbance. Visual observation of these radiographs indicate layering of the deposit, and the tubes can be marked at layer boundaries and cut so that the density of various layers can be determined. In general, WES avoids using relative density whenever possible; however, when relative density is required it is critical that layers be kept independent, because the mixing of materials will change the

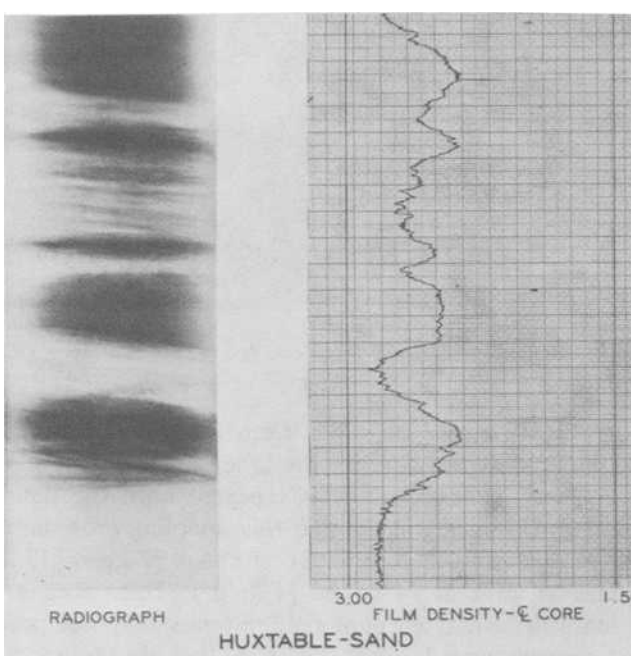

FIG. 11—*Use of X-radiograph film density to determine the density of soil samples.*

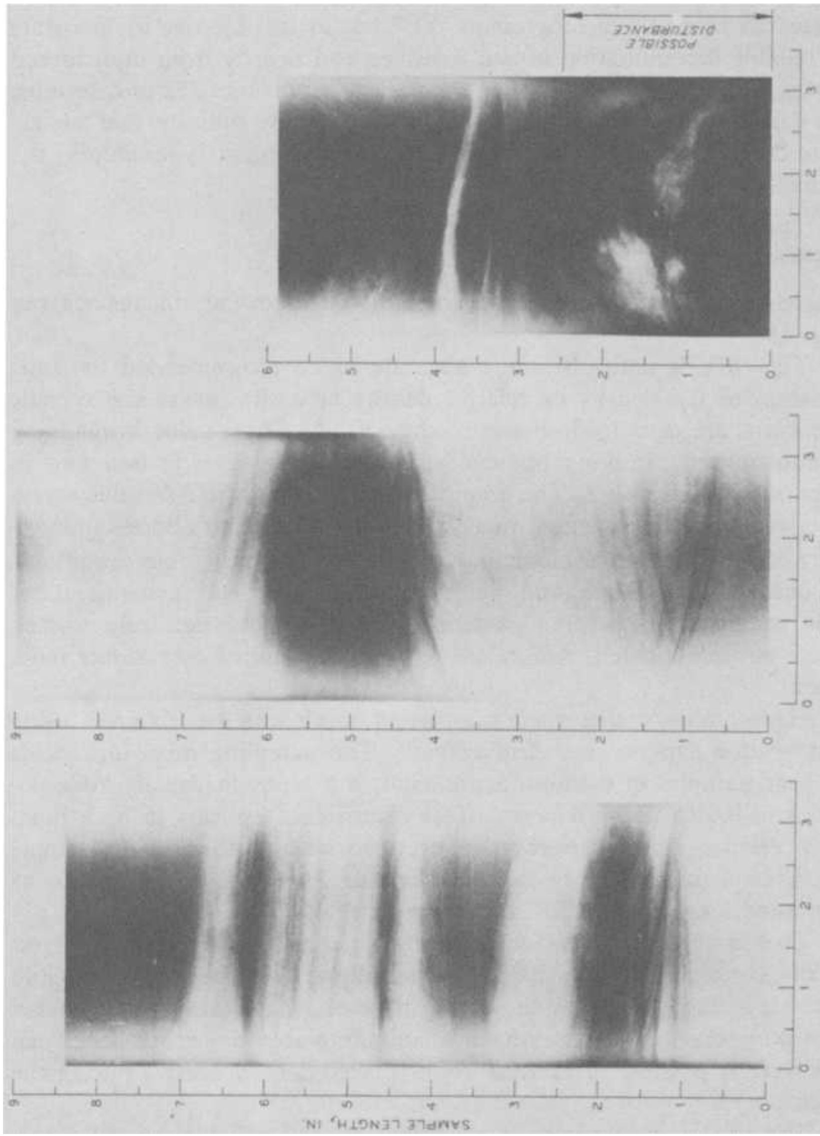

FIG. 12—*Use of X-radiography to evaluate sample disturbance.*

gradation and this can change the maximum and minimum density determinations considerably [27].

Research currently in progress at WES has as its objective the accurate and reliable determination of soil moisture and density from undisturbed samples [28]. The process involves the use of Californium 252 to determine bulk density and water content. Preliminary results indicate that an accurate determination of bulk density and water content is feasible in the forseeable future.

Conclusions

Based on the work summarized herein, the following conclusions can be drawn:

1. The SPT is not sufficiently accurate to be recommended for final evaluation of the density or relative density at a site unless site specific correlations are developed. However, the SPT does have value in planning the undisturbed sampling phase of the subsurface investigation and in comparing different sites. The empirical correlation of SPT *N*-value versus D_r derived from the statistical analysis does not adequately address the variability of subsurface conditions found in the field. Water table conditions, overconsolidation, length and weight of drill rods, and dynamic interaction of the drive-sampling system were either not intensively studied or were not investigated. Additional research is required to evaluate these factors.
2. High-quality undisturbed samples of sands can be obtained using a fixed-piston sampler and drilling mud. This sampling procedure yields very good samples of medium-dense sand, but tends to densify loose deposits and loosen dense deposits. This disturbance appears to be a function of relative density, overburden pressure, and position in the sample tube. This disturbance may cause the sample density to be in error by as much as 64.1 kg/m^3 (4 lb/ft^3) in extreme cases.
3. The sampled versus placed-density comparisons presented suggest that the sampling accuracy using the techniques described is within ± 48 kg/m^3 (± 3 lb/ft^3) most of the time; however, it can also be concluded that a more meaningful assessment of sampling accuracy could have been made were it possible to exercise better placed-density control during the studies.
4. The use of radiographs is an adequate and reliable way of determining the layering of the sample inside the tube and the degree of sample disturbance.

Acknowledgments

It is appropriate to acknowledge Messrs A. A. Maxwell, T. B. Goode, P. K. Garber, R. F. Reuss, R. W. Cunny, and W. E. Strohm, Jr., for their contribution to the early WES investigations [*16–18*]. Grateful appreciation is expressed to those colleagues at WES who offered constructive criticism as well as moral support during the writing of the paper. In addition, the support of the Office of the Chief of Engineers, U. S. Army, which funded many of the WES studies on which this paper is based, is gratefully acknowledged.

References

[*1*] Holtz, W. G. in *Evaluation of Relative Density and Its Role in Geotechnical Projects Involving Cohesionless Soils, ASTM STP 523,* American Society for Testing and Materials, June 1972, pp. 5–17.

[*2*] Holtz, W. G., Discussion, *Evaluation of Relative Density and Its Role in Geotechnical Projects Involving Cohesionless Soils, ASTM STP 523,* American Society for Testing and Materials, June 1972, p. 376.

[*3*] Lacroix, Y. and Horn, H. M. in *Evaluation of Relative Density and Its Role in Geotechnical Projects Involving Cohesionless Soils, ASTM STP 523,* American Society for Testing and Materials, June 1972, pp. 251–280.

[*4*] Selig, E. T. and Ladd, R. S. in *Evaluation of Relative Density and Its Role in Geotechnical Projects Involving Cohesionless Soils, ASTM STP 523,* American Society for Testing and Materials, June 1972, pp. 487–504.

[*5*] Tavenas, F. A., Discussion to deMello, *Fourth PanAmerican Conference on Soil Mechanics and Foundation Engineering,* Puerto Rico, Vol. 3, 1971, p. 64.

[*6*] Tavenas, F. A., Ladd, R. S., and LaRochelle, P. in *Evaluation of Relative Density and Its Role in Geotechnical Projects Involving Cohesionless Soils, ASTM STP 523,* American Society for Testing and Materials, June 1972, pp. 18–60.

[*7*] Youd, T. L., *Evaluation of Relative Density and Its Role in Geotechnical Projects Involving Cohesionless Soils, ASTM STP 523,* American Society for Testing and Materials, June 1972, pp. 98–112.

[*8*] Gibbs, H. J. and Holtz, W. G. in *Proceedings,* Fourth International Conference on Soil Mechanics and Foundation Engineering, London, Vol. 1, 1957, pp. 35–39.

[*9*] Gibbs, H. J. and Merriman, J., "Progress Report on Research on Penetration Resistance Method for Subsurface Exploration," U. S. Department of Interior, Bureau of Reclamation, Earth Laboratory Reports No. EM314 and EM356, Denver, Colo., 1952–1953.

[*10*] Bazaraa, A. R. S. S., "Use of the Standard Penetration Tests for Estimating Settlements of Shallow Foundations on Sand," Ph.D. thesis, University of Illinois, Urbana, 1967.

[*11*] deMello, V. F. B. in *Proceedings,* Fourth PanAmerican Conference on Soil Mechanics and Foundation Engineering, Puerto Rico, Vol. 1, June 1971, pp. 1–87.

[*12*] Bieganousky, W. A. and Marcuson, W. F., III, "Liquefaction Potential of Dams and Foundations; Report 1, Laboratory Standard Penetration Tests on Reid Bedford Model and Ottawa Sand," Research Report S-76-2, U. S. Army Engineer Waterways Experiment Station, Corps of Engineers, Vicksburg, Miss., Oct. 1976.

[*13*] Bieganousky, W. A. and Marcuson, W. F., III, "Liquefaction Potential of Dams and Foundations; Report 2, Laboratory Standard Penetration Tests on Platte River Sand and Standard Concrete Sand," Research Report S-67-2, U. S. Army Engineer Waterways Experiment Station, Corps of Engineers, Vicksburg, Miss., Feb. 1977.

[*14*] Marcuson, W. F., III, and Bieganousky, W. A., *Journal, Geotechnical Engineering Division,* American Society of Civil Engineers, Vol. 103, No. GT6, June 1977, pp. 565–587.

[*15*] Marcuson, W. F., III, and Bieganousky, W. A., *Journal, Geotechnical Engineering Division,* American Society of Civil Engineers. Vol. 103, No. GT11, Nov. 1977, pp. 1295–1309.

[*16*] "Undisturbed Sand Sampling Below the Water Table," Bulletin No. 35, U. S. Army Engineer Waterways Experiment Station, Corps of Engineers, Vicksburg, Miss., June 1950.

[17] "Density Changes of Sand Caused by Sampling and Testing," Potamology Investigations Report No. 12-1, U. S. Army Engineer Waterways Experiment Station, Corps of Engineers, Vicksburg, Miss., June 1952.
[18] "Rotary Cone Penetrometer Investigations," U. S. Army Engineer Waterways Experiment Station, Potamology Investigations Report No. 18-1, Vicksburg, Miss., June 1962.
[19] Cooper, Stafford S., "Laboratory Investigations of Undisturbed Sampling of Cohesionless Material Below the Water Table," Research Report S-76-1, U. S. Army Engineer Waterways Experiment Station, Corps of Engineers, Vicksburg, Miss., Oct. 1976.
[20] Marcuson, W. F., III, Cooper, S. S., and Bieganousky, W. A. in *Proceedings*, Ninth International Conference on Soil Mechanics and Foundation Engineering, Specialty Session No. 2, Soil Sampling, Tokyo, Japan, July 1977, pp. 15–22.
[21] Tavenas, F., Capelle, J. F., and LaRochelle, P., *Canadian Geotechnical Journal*, Vol. 7, Feb. 1970, pp. 37–53.
[22] Preliminary Safety Analysis Report, Pilgrim Station, Appendix 2A.2-4, Report on Test Pit Investigation and Laboratory Testing, Pilgrim Nuclear Station No. 600, Unit 2, Boston Edison Co., Submitted to Bechtel Power Corp., 5 March 1976.
[23] Krinitzsky, E. L., *Radiography in the Earth Sciences and Soil Mechanics*, Plenum Publishing Co., New York and London, 1970.
[24] Marcuson, W. F., III, and Gilbert, P. A., "Earthquake Liquefaction Potential at Patoka Dam, Indiana," Miscellaneous Paper S-72-42, U. S. Army Engineer Waterways Experiment Station, Corps of Engineers, Vicksburg, Miss., Dec. 1972.
[25] Marcuson, W. F., III, and Krinitzsky, E. L., "Dynamic Analysis of Fort Peck Dam," Technical Report S-76-1, U. S. Army Engineer Waterways Experiment Station, Corps of Engineers, Vicksburg, Miss., March 1976.
[26] Marcuson, W. F., III, "The Earthquake Analysis of the W. G. Huxtable Pumping Plant Site," Miscellaneous Paper S-76-8, U. S. Army Engineer Waterways Experiment Station, Corps of Engineers, Vicksburg, Miss., April 1976.
[27] Castro, Gonzalo, *Journal of the Geotechnical Engineering Society*, Vol. 101, No. GT6, June 1975, pp. 551–570.
[28] Lewis, Jack T., "Use of Californium 252 in Laboratory Testing for Moisture and Density of Soils," Miscellaneous Paper S-76-18, U. S. Army Engineer Waterways Experiment Station, Corps of Engineers, Vicksburg, Miss., Sept. 1976.

J. H. Schmertmann[1]

Use the SPT to Measure Dynamic Soil Properties?—Yes, But..!

REFERENCE: Schmertmann, J. H., "**Use the SPT to Measure Dynamic Soil Properties?—Yes, But . .!**" *Dynamic Geotechnical Testing, ASTM STP 654,* American Society for Testing and Materials, 1978, pp. 341–355.

ABSTRACT: The author briefly reviews the factors important to the blowcount (N) values obtained from the standard penetration test (SPT), and describes the dynamics of the SPT in terms of wave transmission theory and measurements. The SPT appears to correlate well qualitatively with sand liquefaction potential, with N proportional to the factor of safety against liquefaction. The SPT can also provide the basis for the field-model determination of the J_s and J_p damping coefficients in the wave equation analysis of pile-driving problems. An example indicates it may also correlate locally with shear wave velocity in sands. Because of its current variability, however, the profession needs an improved, possibly alternative ASTM standard before we use the SPT in important dynamic design problems. The author suggests using a mechanized hammer drop system producing a fixed energy content in the first compression wave in the rods, and the use of rotary drilling with the hole filled with drilling mud at all times.

KEY WORDS: standard penetration test, dynamics, wave equation, liquefaction, shear wave velocity (or shear modulus), ASTM standard, energy, soils, design

Worldwide interest in the standard penetration test (SPT) has increased greatly in the past five years, primarily as a result of the great economic importance of SPT data for the evaluation of possible liquefaction behavior when siting major onshore and offshore structures. Perhaps deMello [*1*][2] started this renewed interest through his exhaustive but frustrating state-of-the-art paper on the SPT. "Frustrating" because he found, despite an exhaustive search, virtually no carefully controlled research on the SPT. Since then the present author and others have performed controlled research involving both the statics and dynamics of the SPT, which has led to important new insight into what happens during the SPT.

[1] Professor, Department of Civil Engineering, University of Florida, Gainesville, Fla. 32611.
[2] The italic numbers in brackets refer to the list of references appended to this paper.

The author believes that understanding the SPT first requires an understanding of its dynamics. It then becomes clear that the SPT blowcount measurement, or N-value, results from the dynamic interactions between hammer, rods, sampler, and soil. In principle, a dynamic test such as the SPT should model a dynamic structure-soil interaction problem or at least sense some dynamic behavior properties of the soil sampled.

The SPT models the pile-driving problem and there exists a good theoretical connection between SPT behavior and the damping coefficients, J_p and J_s, very important in any wave equation analysis of pile-driving problems. Seed [*2*] showed that SPT N-values also appear to correlate well, at least qualitatively, with liquefaction behavior. Also, as shown subsequently by an example, the SPT N-values may correlate well empirically with shear wave velocity, V_s. The dynamic SPT should, in principle, correlate better with dynamic soil behavior than with any static or quasi-static test such as the Dutch cone penetration test (CPT).

Unfortunately, before any of these important dynamic soil property correlations can reach a quantitatively useful point of reliability and reproducibility, matching what we usually expect from our engineering tests, the profession must make important modifications to the present ASTM Penetration Test and Split-Barrel Sampling of Soils (ASTM D 1586) standard. This paper includes suggestions for such modifications.

A Minisurvey of New Research Knowledge

Schmertmann [*3*] showed in a discussion to deMello [*1*] that soil friction or adhesion along the inside and outside surfaces of the SPT sampler could account, and probably did account, for a major portion of the total static and dynamic soil resistance against sampler penetration. The percentage of side shear to total resistance usually increases as the cohesiveness of the soil increases. This means that a major portion of the energy of the sampling goes into shear. As a practical demonstration of this fact, Stokoe and Woods [*4*], found the SPT an acceptable way of introducing waves rich in shear energy in their crosshole shear wave velocity measurements.

Reasoning that the variables that affect the CPT would likely affect the SPT in a similar manner, Schmertmann [*3*] pointed out the probable major importance of the *in situ* horizontal effective stresses in determining the N-value in a soil. Zolkov and Weisman [*5*] had already suggested this possibility in their study of sand overconsolidated by the removal of overburden. Rodenhauser [*6*], working in a triaxial test chamber at Duke University, obtained SPT results in a dry sand, indicating N proportional to the octahedral stress to the $2/3$ power. Marcuson and Bieganousky ([*7*] Fig. 10) report a marked increase in N at overconsolidation ratio (OCR)

= 3 compared with the same sand at OCR = 1, presumably due to the greater lateral stresses after overconsolidation. From all of this it seems clear that *in situ* horizontal stresses play a major role, perhaps a dominant role, in determining N.

N-values have played an important role in the field evaluation of liquefaction potential. Seed and Idriss [*8*] used N-values to estimate relative density, then compared field liquefaction and no-liquefaction cases with relative density and earthquake acceleration, and then finally prepared N-value and depth charts to indicate the likelihood of liquefaction. The first step in this reasoning, estimating D_r from N, received severe criticism at the time [*9–11*]. More recently, the controlled N-D_r study recently completed by the Waterways Experiment Station and reported by Marcuson and Bieganousky [*7*] tends to further discredit the quantitative use of any such correlation unless made specifically for a given site. Although the Seed and Idriss double use of N-values reduces the importance of the N-D_r first step, Seed has responded to such criticism and to new research knowledge and has now eliminated this step entirely by suggesting the direct use of N-values without an intermediate correlation with relative density. With this new method, the factor of safety against liquefaction varies linearly with the N-value. Thus, a 100 percent error in N would result in a 100 percent error in factor of safety.

Only recently have researchers begun to delve into the question of understanding the dynamics of the SPT. Kovacs et al [*12,13*] have made direct measurements of the velocity of the 63.5-kg (140 lb) SPT hammer at the instant of impact with the anvil-rod system. Their research has demonstrated quantitatively what others, such as Frydman [*4*], Zolkov [*11,15*], and Serota and Lowther [*16*], showed only via the gross measurement of blowcount ratios—the large variations in N due to different hammer-drop systems. Their data showed definite trends from which they deduced that increasing the energy in the hammer at impact would decrease N, with some preliminary indications of N proportional to the inverse of hammer energy.

Schmertmann [*17*] reported on perhaps the first experimental investigation of the dynamic behavior involved when an SPT sampler penetrates the soil in response to the stress waves generated by the SPT hammer blow. The following section of this paper discusses in a summary way some of the findings from this research. The reader interested in details can consult the Ref *17*. This research involved a coordinated study of dynamic force-time measurements obtained just below the hammer and just above the sampler, resistance measurements during the quasi-static penetration of an SPT sampler, associated quasi-static friction-cone penetration tests, and computer simulations using the one-dimensional wave equation. Figure 1 shows some photos from the research.

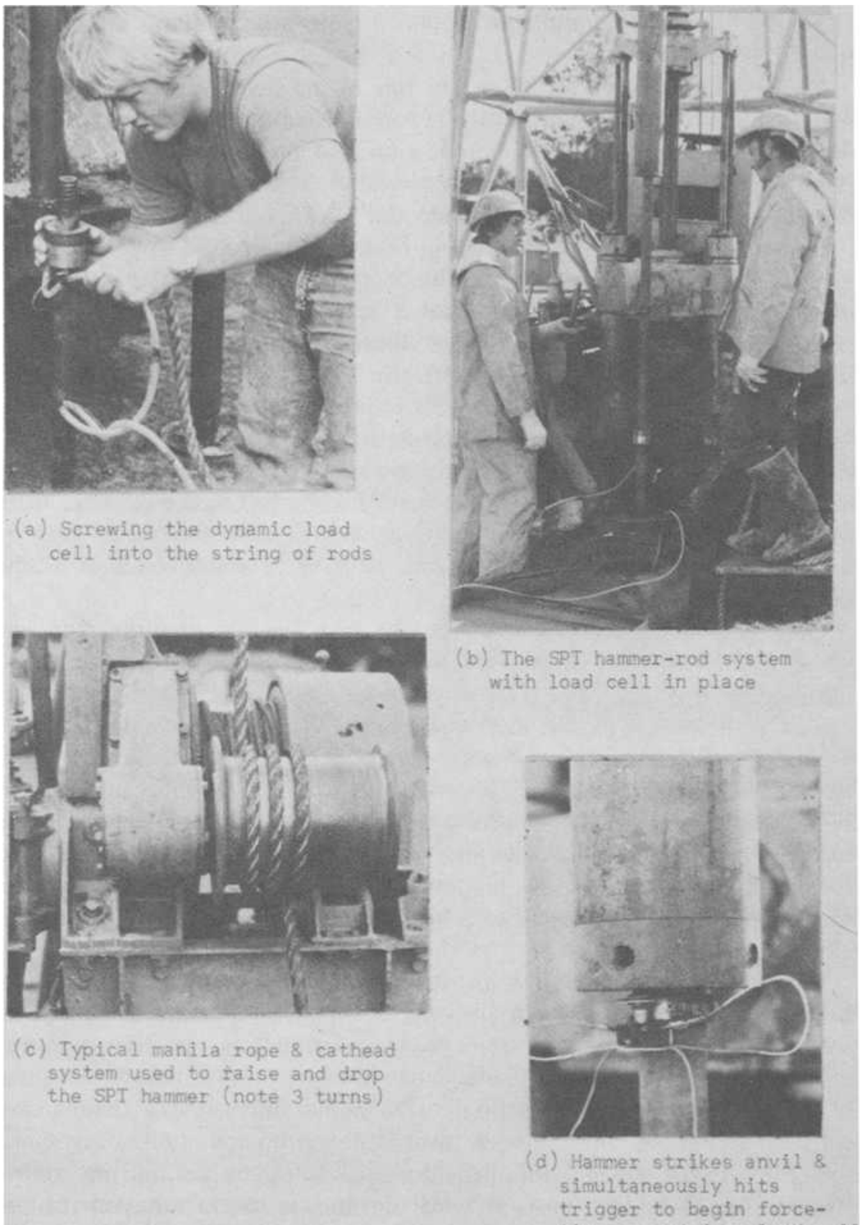

FIG. 1—*Measuring the dynamic energy input into the SPT rods for research or calibration or both.*

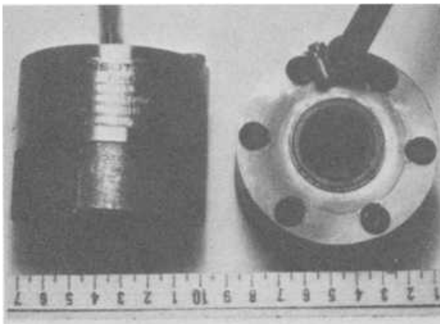

(e) The hollow dynamic load cell, 40,000 lb capacity, custom made by Sensotec Co.

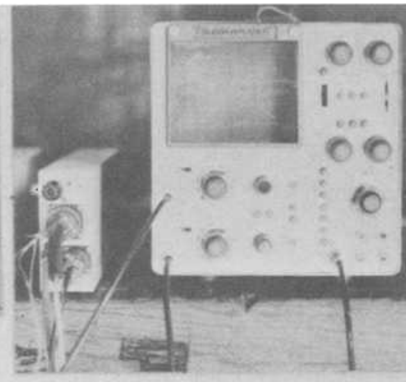

(f) The load cell signal then put on a storage oscilloscope, photographed, digitized, and integrated for energy content

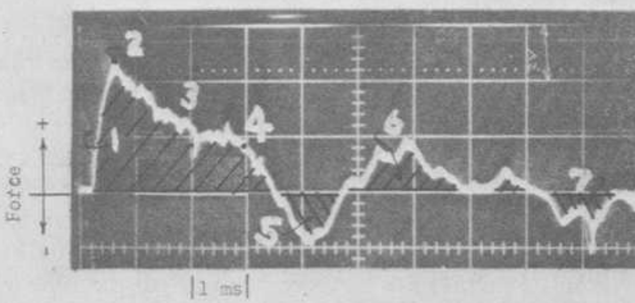

(g) Typical oscilloscope force-time record from a single SPT hammer blow. Numbers indicate:

1) Rapid rise of force in initial compression wave.
2) Peak force in this wave - about 21,000 lb.
3) Force decays with successive wave traverses in hammer.
4) Time at which the tension wave reflected from the sampler reaches the load cell. Rods then pull away from the hammer and hammer energy transfer stops.

Note: $E_i \sim \int_1^4 F^2 \, dt$

5) The first tension wave.
6) The second compression wave after reflection of the tension wave at the top of rods (note reduced energy content compared to first compression wave)
7) The second tension wave, etc.

FIG. 1—*Continued (1 lb = 0.45 kg).*

Review of Dynamics of SPT Sampler Penetration

From the coordinated research study at the University of Florida mentioned earlier, the author found that the following sequence of events takes place during a single SPT blow:

1. The hammer falls impeded by rope-cathead friction and any other energy-absorbing features of the hammer drop system. At the moment of rod impact it has anywhere from about 30 to 80 percent of its supposed energy of 63.5 kg by 76.2 cm (140 lb by 30 in.) = 4840 cm-kg (4200 in.-lb) = E^*.

2. Compression waves start simultaneously in the rods and hammer, traveling about 5030 m/s (16 500 ft/s) in both. They reflect as waves of opposite sign (compression-tension-compression, etc.) each time they come to the bottom or top of the rods or hammer. Because of its short length, many more wave traverses take place in the hammer than in the rods. Each time the compression wave pulse in the hammer reaches the hammer-rod contact, some of the hammer wave energy transfers to the rods, with a gradual and stepped decay in the amount per transfer.

3. The aforementioned energy transfer manifests itself in the rods as a compression wave with a short (approximately 0.6 ms) rise time to a peak compression stress of about 110 320 kPa (16 000 psi). Then its magnitude decays stepwise with time. These wave properties depend on the rod and hammer materials (steel in cases investigated) but not on rod cross-sectional area. The compression wave then reflects at the sampler and returns as a tension wave but with a net loss of energy to the sampler. When this first tension wave reaches the hammer, the rods pull away from the hammer and the energy input, E_i, from the hammer stops. With the rope-cathead hammer drop system we find great variability in E_i, with an average E_i equal about 50 percent of E^* [*18,19*]. The longer the rods, the greater the hammer-rod contact time and the more hammer energy that enters the rods for possible sampler penetration. Rod lengths less than 6 m (20 ft) cause progressively more significant reductions in hammer energy input because of the progressively earlier separation of rods from the hammer.

4. The compression wave entering the rod depends only on the hammer-rod system. It does not depend on the soil strength properties and therefore does not depend on *N*. For rod lengths exceeding 6 m (20 ft), 90+ percent of the compression wave energy has already entered the rods before the hammer senses any effect from the soil around the sampler. Soil resistance at the sampler, and therefore the *N*-value, has virtually no effect on determining E_i. Because of inevitable energy loss to heat during hammer impact as well as some energy always getting trapped in the anvil, the energy in the hammer at impact must exceed E_i. The energy loss from the impact can equal about 10 to 20 percent of E^* [*18,19*].

5. The sampler does not begin its penetration until the first compression

wave reaches the bottom of the sampler. Then it accelerates in about 0.5 ms to a maximum velocity of about 4.5 m/s (15 ft/s), afterward reducing velocity as the wave passes and its force level reduces. The sampler penetrates in decaying surges or cycles of suddenly increased and then decreasing velocity, synchronous with the wave cycles in the rods. The number of such cycles increases with decreasing N because the time required for penetration increases as N decreases, and with decreasing rod length because the time per cycle decreases. By the time the sampler has penetrated to 90 percent of its final set, the average sampler penetration velocity *during* this 90 percent has reduced to about 1.2 m/s (4 ft/s), with the average velocity when *at 90 percent* reduced to about 0.45 m/s (1.5 ft/s) [*17,20*].

6. The time for the sampler to reach 90 percent of its final set under each blow varies inversely with N, taking approximately 10 ms when N = 20 and 40 ms when N = 5.

7. The set/blow, equal to 30 cm/N' (12 in./N'), decreases steadily over the 15 to 45 cm (6 to 18 in.) total penetration to measure N. The set per blow at 45 cm (18 in.) of sampler penetration reduces compared with the set of 15 cm (6 in.) in the same soil and when using the same hammer system delivering the same E_i. This decrease results from the steadily increasing side-friction soil resistance against the sampler. Note that N = N' at 30-cm (12 in.) penetration.

8. To accomplish its penetration, the sampler uses about 80 percent of the rod input energy, E_i, to overcome dynamic soil resistance. The other 20 percent partly radiates away in soil "quake" and partly gets trapped and dissipates in the rods. N' varies inversely with the energy used, and therefore also approximately inversely with E_i—as expressed by Equation 1.

9. Equation 1, which results from wave equation simulation [*17,20*] of five typical SPT blows obtained by Palacios [*18*], expresses the average total end bearing and side-friction dynamic soil resistance to sampler penetration, F_{td}, during its penetration

$$F_{td}\,(\text{lb}) \simeq 280 \left(\frac{E_i}{E^*}\right) N\,(\text{blows/ft}) \tag{1}$$

The total quasi-static soil resistance at the sampler at our University of Florida research site averaged about 50 percent of the total dynamic resistance in clays and sandy clays but increased to as high as 90 percent in sands.

What Dynamic Soil Properties Can We Hope to Measure With the SPT?

It seems to the author that we can only hope to measure those dynamic soil properties where the SPT provides either a direct model of the problem at hand, or the factors that control the behavior of the SPT also similarly control the dynamic property we wish to correlate against. The author suggests the following possibilities.

The Wave Equation Soil Damping Coefficients J_p *and* J_s

The driving of the SPT sampler gives us a field test for the driving of a pile. Both involve hammer impact on a one-dimensional rod system to produce a pulsed or cyclic penetration of either pile or sampler into the soil, with the penetration behavior controlled by the stress wave traverses in the pile or sampling rods and the dynamic resistance response of the soil. Many investigators have shown the validity of using the one-dimensional wave equation to analyze real pile-driving problems. Others, notably Adam [*21*] and McLean et al [*22*], have recognized that we can also model the SPT behavior with the wave equation. Gallet [*20*] also did so and had the advantage of having dynamic SPT field data against which to adjust and validate his wave equation model for the SPT. After so doing, and demonstrating that the soil quake generated at the SPT sampler represented a negligible quantity, he could solve the SPT penetration problem with the wave equation and evaluate J_p and J_s. Gallet determined these damping coefficients for a number of SPT blows and obtained values within the range of values usually assumed in pile-driving analyses. The method looks viable.

The J damping coefficients represent major variables in the pile-driving simulation using the wave equation method. More-accurate, site-specific values of J might prove very useful in many applications. In principle, one can estimate these from the SPT using only the ordinary SPT data and the stress wave recorded by a dynamic load cell placed in the string of rods. This load cell should be close to the anvil, but at least 5 rod diameters below it, to allow the wave to recover from the effects of the area reduction from anvil to rods. It can usually be placed above ground level for convenience, as shown in Fig. 1*a* and 1*b*.

Correlation with Factor of Safety Against Liquefaction

We now know from field experience, and in some cases from controlled laboratory research [*2*], that all the variables we know of that increase the safety factor against liquefaction occurring also increase dynamic SPT or quasi-static cone penetration resistance. Table 1*a* summarizes these variables.

The results from the University of Florida research on the dynamics of the SPT can provide additional qualitative arguments to support the possible applicability of the dynamic SPT for the prediction of dynamic liquefaction behavior. Table 1*b* lists these additional arguments. The

TABLE 1*a*—*Qualitative comparison of soil penetration resistance with resistance to liquefaction.*

	Effect on	
Factor (after Seed [2])	N-Value	Liquefaction Factor of Safety
1. Greater relative density	+	+
2. Greater depth (vertical efficiency stress)	+	+
3. Greater horizontal efficiency stresses (OCR or roller compaction)	+	+
4. Cementation, aging phenomena	+	+
5. Vibration prestraining	+	+
	(+ denotes increase)	

TABLE 1*b*—*Some additional dynamic advantages of the SPT for evaluating liquefaction.*

6. Dynamic test to model dynamic behavior.
   (*a*) Rapid penetration: average 1.2 m/s (4 ft/s), 90 percent in 200/N ms
   (*b*) Pulsed penetration: decays with frequency 8000/depth (ft) Hz
7. Essentially undrained.
8. High percentage shear wave energy

Metric conversion: 1 ft = 0.3048 m.

SPT produces a pulsed sampler penetration and decaying cycles of loading. The penetration occurs very quickly and must be essentially undrained in all but very coarse soils. The sampler also introduces primarily shear strains into the soil—to match the primarily shear wave propagation assumed to occur under earthquake loading.

Considering the great qualitative similarity between penetration resistance and factor of safety against liquefaction, plus the dynamic and cyclic penetration of the SPT sampler and the dynamic and cyclic production of the liquefaction phenomenon, it seems quite reasonable to expect at least some useful degree of correlation between the SPT N-value and the factor of safety against liquefaction.

Correlation with Shear Wave Velocity

The shear wave velocity depends on the shear modulus, which in turn depends on the dynamic stress-strain properties of the soil and the level of strain in the traveling shear waves. Because the SPT sampler penetration involves primarily dynamic soil shear behavior, at the failure reference level of shear strain and modulus one can argue that it would be reasonable to expect a correlation between N-values and shear wave velocities at the other reference level of very low strain and maximum modulus.

Figure 2 shows an example from a research site in Florida that indicates such a correlation may exist—at least for a specific site. These data come from Heller [23].

The research site consisted of fine sands, above the water table. Figure 2 shows shear wave velocity profiles with depth using different determination methods and the average N-value profile as determined by Waterways Experiment Station equipment and personnel. It appears we can say that, approximately, V_s (ft/s) = 50 N at this site. The author understands that

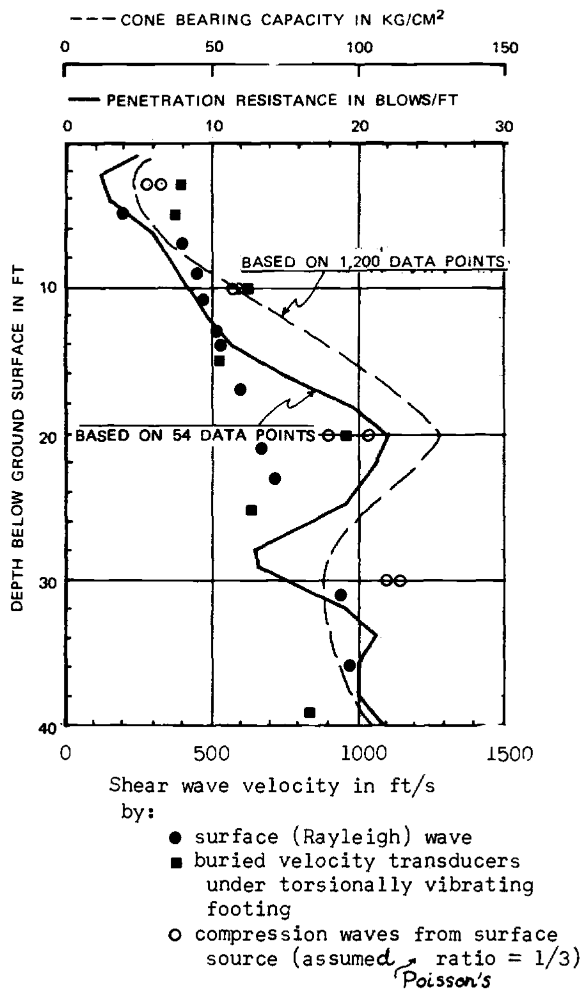

FIG. 2—*Correlation between SPT blowcount, CPT bearing capacity and shear wave velocity in a fine sand above the water table at a site in Northwest Florida (from Heller* [23]) *(1 kg = 2.2 lb; 1 cm² = 0.16 in.²; 1 ft/s = 0.3 m/s).*

the Waterways Experiment Station currently has an active project to more thoroughly explore the possibility of a more general correlation between V_s and N.

As a matter of general interest, Figure 2 also includes the average q_c profile from a large number of Begemann friction-cone penetration tests at the same site. It seems that one could also develop a site correlation between V_s and the static cone bearing capacity, q_c.

First Need to Restandardize the SPT

From only the previous section of this paper the reader would perhaps reach an optimistic conclusion about the possible use of SPT N-value data to make useful quantitative predictions of those dynamic soil properties discussed, and perhaps of others not discussed. Unfortunately, the SPT, as practiced in the United States under ASTM Method D 1586, suffers from a perhaps fatal or near-fatal flaw. Practicing engineers know all too well that the test and its N-values have a poor reproducibility and great variability between different operators and equipment. Many investigators, as mentioned earlier, have pointed out this major flaw and given one or more reasons to help explain it. See Schmertmann [*24*] for a broader discussion of the variability problem.

One need not look far to see why in practice we have such great variability in the test. The author has attempted in Table 2 to organize his digest of the literature and personal opinions as to the causes and magnitude of this variability. He believes that the major causes fall into two categories: variability in the energy that actually enters the sampling rods and travels to the sampler in the form of the first compression wave, and variability in the effective stress conditions at the bottom of the borehole during drilling and sampling.

As Table 2 indicates, these causes can produce major effects which can easily change N by 100 percent. Note that this would also change the factor of safety against liquefaction by 100 percent when using the SPT field method for evaluating the factor of safety. The author considers this an unacceptable situation. The present system negates almost any rational use of the SPT as a quantitative design tool in dynamic as well as in static problems. If we want to use the SPT to its potential for design in problems involving dynamic soil behavior, we must first establish and enforce logical standards for the performance of the SPT. The author offers the following suggestions.

Standardize Energy Entering Rods

The various works cited earlier have shown convincingly that the energy delivered by the drop weight system presents a major variable in deter-

TABLE 2—*Some factors in the variability of standard penetration test* N.

Cause: Basic	Cause: Detailed	Estimated % by Which Cause Can Change N
Effective stresses at bottom of borehole (sands)	1. use drilling mud versus casing and water	+100%
	2. use hollow-stem auger versus casing and water and allow head imbalance	±100%
	3. Small-diameter hole (3 in.) versus large diameter (18 in.)	50%
Dynamic energy reaching sampler (All Soils)	4. 2 to 3 turn rope-cathead versus free drop	+100%
	5. Large versus small anvil	+50%
	6. Length of rods	
	Less than 10 ft	+50%
	30 to 80 ft	0%
	more than 100 ft	+10%
	7. Variations in height drop	±10%
	8. A-rods versus NW-rods	±10%
Sampler design	9. Larger ID for liners, but no liners	−10% (sands) −30% (insensitive clays)
Penetration interval	10. $N_{0\text{ to }12\text{ in.}}$ instead $N_{6\text{ to }18\text{ in.}}$	−15% (sands) −30% (insensitive clays)
	11. $N_{12\text{ to }24\text{ in.}}$ versus $N_{6\text{ to }18\text{ in.}}$	+15% (sands) +30% (insensitive clays)

Metric conversions: 1 ft = 0.3048 m; 1 in. = 2.54 cm.

mining N. The work at the University of Florida has shown convincingly that N varies inversely with the compression wave energy that actually enters the sampling rods. We must develop a standard system that introduces a specified compression wave energy into the rods, and that is repeatable all day long in normal operation. It seems obvious that this requires a mechanized drop system that remains independent of operator techniques. With such a system the engineer can adjust the drop height to obtain a fixed amount of compression wave energy, E_i, as determined by appropriate integration of the force-time wave pulse measured by a load cell placed in the rod system a short distance below the hammer. Figure 1 illustrates how researchers at the University of Florida have measured E_i.

Of course, the idea of using a mechanized hammer drop system did not originate here. Some countries have already adopted a mechanized free-drop system as their standard. The paper by Kovacs et al [*13*] strongly supports the idea of using a mechanized drop system in the United States and details the impact velocity calibration results from such a system presently marketed by a national U.S. distributor.

The author already has some experience with trying to calibrate SPT rigs using the common rope-cathead hammer drop system so as to introduce a standard amount of wave energy delivered into the rods. However, even under the somewhat artificial, especially attentive conditions of a field calibration at a university site, the University of Florida researchers found [*19*] a ratio of high/low E_i energy delivered from blow to blow by the same operator using his own rig that varied from 1.53 to 1.10, and averaged 1.28 for 10 rigs when considering a random sampling of 5 blows. The author believes that any rig using a rope-cathead hammer drop system remains too operator-dependent to permit its use under a standardized SPT test procedure intended to produce N-values for quantitative design.

Need to Use Drilling Mud

In the author's opinion, as a practical matter the use of rotary drilling methods with the hole continuously filled with drilling mud to the surface offers the only present way to assure that the effective stress conditions in the sampling zone immediately below the borehole remain as little disturbed as possible by the borehole.

Possible Dual-Standard SPT

In recognition of the practical difficulties of suddenly adopting a much more rigorous standard for the SPT, involving new equipment with unfamiliar dynamic calibration and possibly unfamiliar drilling techniques, perhaps the profession should again consider a transition period with a dual standard. Chairman Frank Steiger of the SPT task committee for ASTM Committee D-18.02 already proposed a dual standard several years ago.

An SPT performed to say a "Class B" standard would use a calibrated, fully mechanized hammer drop system, and use only rotary drilling and drilling mud. This class would serve for testing in which the engineer intended to use the N-values for important quantitative design, or for research and establishing correlations intended for other than local use. "Class A" SPT work would fall under the continued present standard and allow the great local variability to accommodate local equipment, preferences and correlations.

Conclusions

1. The profession now has an important new insight into the statics and dynamics of the standard penetration test. Any full understanding of the SPT must include stress wave analysis.

2. A properly standardized SPT has a reasonable, already partly demon-

strated potential for quantitative correlations with a factor of safety against liquefaction, with the *J* damping coefficients in pile-driving problems, and perhaps with high- and low-strain shear wave velocity.

3. The profession needs to establish and enforce an alternative ASTM Method D 1586 standard that requires a mechanized hammer drop, a calibrated energy content in the first compression wave in the rods, and the use of rotary drilling in a hole kept continuously full with drilling mud.

Acknowledgments

Mr. Alejandro Palacios, Ph.D. student in civil engineering at the University of Florida, performed most of the initial theoretical, equipment development, and field research that led to the successful understanding and measurement of wave and energy phenomena in the SPT. Mr. Alain Gallet, former masters student in civil engineering, made the wave equation simulations of our field SPT data. Dr. David Crapps, former University of Florida (UF) student in civil engineering, assisted Mr. Gallet with the computer simulations. Mr. William J. Whitehead, Assistant in Civil Engineering, provided valuable field technician support. Mr. Julio Palacios, also a UF student, extensively assisted his brother with the field work.

The Florida Department of Transportation and the UF Engineering and Industrial Experiment Station provided the financial support to initiate and complete the research that provides the basis for this paper. The Florida DOT, Universal Engineering and Testing Company, Gainesville, Florida, and Florida Testing Laboratories, Inc., St. Petersburg, Florida, generously donated SPT rigs and crews for the field testing.

References

[1] deMello, V. in *Proceedings*, Fourth Pan American Conference on Soil Mechanics and Foundations Engineering, Puerto Rico, Vol. 1, 1971, pp. 1-86.

[2] Seed, H. B., Preprint 2752, from Speciality Session on Liquefaction Problems in Geotechnical Engineering, Philadelphia, 1976, pp. 1-104, Table 2.

[3] Schmertmann, J., Discussion to deMello in *Proceedings*, Fourth Pan American Conference on Soil Mechanics and Foundations Engineering, Puerto Rico, Vol. 3, 1971, pp. 90-98.

[4] Stokoe, K. H., II, and Woods, R. D., *Journal of the Soil Mechanics and Foundations Division*, American Society of Civil Engineers, Vol. 98, No. SM5, May 1972, Case Study III, p. 455.

[5] Zolkov, E. and Wiseman, G., in *Proceedings*, Sixth International Conference of Soil Mechanics and Foundations Engineering, Montreal, Vol. 1, 1965, p. 134.

[6] Rodenhauser, J., "The Effect of Mean Normal Stress on the Blow-count of the SPT in Dense Chattahoochee Sand," Project Report to the Department of Civil Engineering, Duke University, Raleigh, N.C., 1974.

[7] Marcuson, W. F., III, and W. A. Bieganousky, *Journal of the Geotechnical Engineering Division*, American Society of Civil Engineers, Vol. 103, No. GT6, June 1977, pp. 565-588.

[8] Seed, H. B. and Idriss, I. M., *Journal of the Soil Mechanics and Foundations Division*, American Society of Civil Engineers, Vol. 93, No. SM3, Sept. 1971, pp. 1249-1273.
[9] Schmertmann, J., Discussion in *Journal of the Soil Mechanics and Foundations Division*, American Society of Civil Engineers, Vol. 98, No. SM-4, 1972, pp. 430-433.
[10] Tavenas, F., Discussion in *Journal of the Soil Mechanics and Foundations Division*, American Society of Civil Engineers, Vol. 98, No. SM-4, 1972, pp. 433-436.
[11] Zolkov, E., Discussion in *Journal of the Soil Mechanics and Foundations Division*, American Society of Civil Engineers, Vol. 98, No. SM-4, 1972, p. 436.
[12] Kovacs, W. D., Evans, J. C., and Griffith, A. H., "A Comparative Investigation of the Mobile Drilling Company's Safe T-Driver with the Standard Cathead with Manila Rope for the Performance of the Standard Penetration Test," Report from the School of Civil Engineering, Purdue University, Lafayette, Ind., 1975.
[13] Kovacs, W. D., Griffith, A. H., and Evans, J. C., "An Alternate to the Cathead and Rope for the SPT," *Geotechnical Testing Journal*, Vol. 1, No. 2, American Society for Testing and Materials, June 1978.
[14] Frydman, S., Discussion of Ireland et al, *Géotechnique* Vol. 20, No. 4, 1970, p. 454.
[15] Zolkov, E., *Journal of Materials*, American Society for Testing and Materials, Vol. 7, No. 3, 1972, pp. 336-344.
[16] Serota, S. and Lowther, G., *Ground Engineering*, Vol. 6, No. 1, Jan. 1973, pp. 20-22; see also *Geotechnique*, Vol. 23, No. 1, 1973, pp. 301-03.
[17] Schmertmann, J., "Interpreting the Dynamics of the Standard Penetration Test," Final Report on Project D-636 to the Florida Department of Transportation, Research Division, Waldo Road, Gainesville, Fla. 32601, 1976.
[18] Palacios, A., "The Theory and Measurement of Energy Transfer During Standard Penetration Test Sampling," Ph.D. Dissertation to the University of Florida, Gainesville, Fla., 1977.
[19] Schmertmann, J. H. and Smith, T. V. "A Summary of SPT Energy Calibration Services Performed for the Florida DOT under Service Contract 99700-7150-010, University of Florida, College of Engineering, Final Research Report 245*D73, Gainesville, Fla., Sept. 1977.
[20] Gallet, A. J., "Use of the Wave Equation to Investigate Standard Penetration Test Field Measurements," Master's Degree Report, Department of Civil Engineering, University of Florida, Gainesville, Fla., 1976.
[21] Adam, J., Discussion of deMello in *Proceedings*, Fourth Pan American Conference on Soil Mechanics and Foundations Engineering, Puerto Rico, Vol. 3, 1971, pp. 82-84.
[22] McLean, F. G., Franklin, A. G., and Dahlstrand, T. K. in *Proceedings*, Speciality Conference on *In Situ* Measurement of Soil Properties, American Society of Civil Engineers, Raleigh, N.C., Vol. 1, 1975, pp. 287-318.
[23] Heller, L. H. "The Particle Motion Field Generated by the Torsional Vibration of a Circular Footing on Sand," U.S. Army Waterways Experiment Station Technical Report S-71-14, Report 2, Vicksburg, Miss., Corps of Engineers, April 1972.
[24] Schmertmann, J. H. in *Proceedings*, Specialty Conference on the *In Situ* Measurement of Soil Properties, American Society of Civil Engineers, Raleigh, N.C., June 1975, Vol. 2, Section 2 on the SPT, pp. 61-78.

F. C. Townsend[1]

A Review of Factors Affecting Cyclic Triaxial Tests

REFERENCE: Townsend, F. C., "**A Review of Factors Affecting Cyclic Triaxial Tests,**" *Dynamic Geotechnical Testing, ASTM STP 654,* American Society for Testing and Materials, 1978, pp. 356–383.

ABSTRACT: The effects of testing procedures and material characteristics on the cyclic triaxial strength of cohesionless soils were reviewed with the intent of categorizing the significance of these factors for cognizance in future testing standards. It was found that specimen preparation methods, differences between intact and reconstituted specimens, density, and prestraining have major effects on cyclic strength. Intermediate but significant effects influencing cyclic strength are confining stress, loading wave form, material grain size (D_{50}) and gradation, overconsolidation ratio (OCR), and consolidation stress ratio (K_c). Other factors having minor effects are freezing intact specimens, loading frequency, specimen size, and frictionless caps and bases.

Future testing programs or standards should consider these factors and their effects on test results.

KEY WORDS: cyclic triaxial, liquefaction, test procedures, cohesionless soils, soils

Application of the cyclic triaxial test to liquefaction and dynamic strength of soils under earthquake loadings had its conception in 1966 when Seed and Lee [*1*][2] produced, in the laboratory, liquefaction of sand by cyclic loading. During the past decade the test has steadily increased in usage as the predominant laboratory test for evaluating earthquake response of soils. The test has even broadened its utility to where foundation problems of offshore structures under storm wave action have been evaluated by cyclic triaxial tests [*2,3*]. Nevertheless, despite this broad usage, several limitations of the test have been recognized. Even Seed and Lee [*1*] realized that shear stress induced in horizontal ground surfaces could best be modeled in the laboratory by cyclic simple shear tests, and that the triaxial test was only an approximate reproduction of these conditions. Later in 1968 [*4*] and 1971 [*5*] Seed and Peacock, realizing that cyclic simple shear strengths

[1] Research civil engineer, Soil Mechanics Division, Soils and Pavements Laboratory, U.S. Army Engineer Waterways Experiment Station, Vicksburg, Miss. 39180.

[2] The italic numbers in brackets refer to the list of references appended to this paper.

were about 35 to 50 percent less than comparable cyclic triaxial strengths, provided "correction factors" to more closely align cyclic triaxial strengths with estimated field response. Another controversy which has arisen in the literature concerns the definition as to whether "liquefaction" as defined by Casagrande actually occurs in the cyclic triaxial test or whether a phenomenon entitled "cyclic mobility" [*6*] occurs, which for dilative soils is merely a redistribution of void ratios within the specimen during cyclic loading.

The purpose of this paper is not to discuss the applicability of the cyclic triaxial test, despite the aforementioned limitations; rather, its intent is to review the literature, including appropriate papers in this volume, and categorize various factors influencing cyclic triaxial test results and their significance for cognizance in future testing standards.

Testing Equipment and Procedures

A recent cooperative testing program by eight laboratories [*7*], using both closed-loop electro-servohydraulic and pneumatic loaders to evaluate the cyclic strength of a "standard" sand, showed that good agreement could be obtained when proper attention was given to what normally would be considered as minor details in specimen preparation and testing (see Fig. 1). These experiences provided a nucleus for performance specifications [*8,9*] which contain specific guidance concerning loading equipment, instrumentation, triaxial chambers, specimen preparation, and data reduction. In addition, required standards regarding loading wave form and amount of acceptable "fall-off upon liquefaction," triaxial cell design, alignment criteria, load rod connections, pressure control systems, instrumentation requirements and specifications, physical measurement of specimens, degree of saturation, and data reduction and presentation are discussed; see Refs *8* and *9* for this information.

Testing Procedures Affecting Cyclic Triaxial Strength

Specimen Preparation

In 1974, Ladd [*10*] focused attention on the effects that specimen preparation procedures have on the cyclic triaxial strength of sands. He conducted cyclic triaxial tests on saturated specimens of three different sands using two methods of specimen preparation, (1) dry vibration and (2) wet tamping. His results showed that for specimens compacted to the same density, differences in liquefaction potential up to 100 percent could occur, with the wet-tamped specimens always being stronger.

The most comprehensive study regarding specimen preparation effects on cyclic triaxial strength of sands was conducted by Mulilis et al [*11*], who

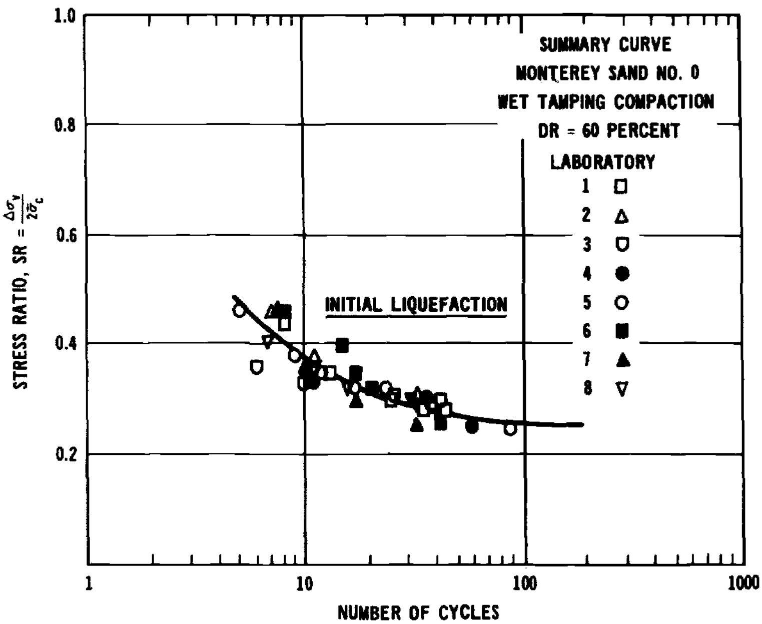

FIG. 1—*Summary curve showing stress ratio versus number of cycles to initial liquefaction for all test results (from Ref 7).*

evaluated 11 different specimen preparation procedures. These results on isotropically consolidated specimens of Monterey No. 0 sand prepared at D_r = 50 percent are presented in Fig. 2. The weakest specimens were formed by pluviating sand through air, while the strongest were those formed by vibrating the soil in a moist condition. The maximum difference in stress ratio causing initial liquefaction was about 110 percent at 10 cycles. It was also indicated that effects due to specimen preparation method may be different for different sands.

Elsewhere in this volume, Mulilis et al [12] present data reproduced here as Fig. 3 which show that specimens of Monterey No. 0 sand prepared to a relative density of 60 percent by "moist tamping" were approximately 58 percent stronger than comparable specimens prepared by dry rodding.

Mulilis et al [12] also presented results concerning effects using a procedure of undercompaction during specimen preparation. The concept of undercompaction recognizes that when compacting a loose specimen in layers, each successive layer densifies the material beneath it. Hence undercompaction consists of preparing the initial layers looser than the final desired density by a certain percentage, with succeeding layers being placed

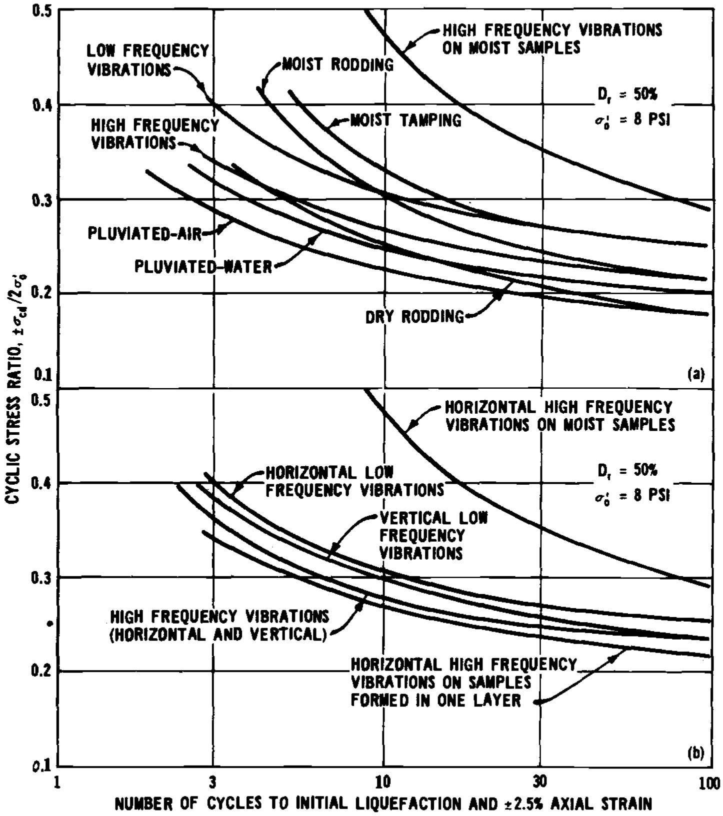

FIG. 2—*Cyclic stress ratio versus number of cycles for different* (a) *vibratory compaction procedures*; (b) *compaction procedures* (*from Ref* 11).

denser, or at a lower percent undercompaction; the result hopefully will be a uniform specimen with respect to density. The percent undercompaction used for these tests was 10 percent. It was found that undercompacted specimens were about 10 percent stronger than specimens which received no variable compaction. These authors [*12*] also showed that changing the diameter of the compaction foot from 0.95 cm (3/8 in.) that is, rodding) to 3.56 cm (1.4 in.) or half the specimen diameter (that is, tamping) or that varying the molding water content from 12.8 percent to 8 percent produced practically no significant effect on cyclic strength.

These results concerning specimen preparation effects on cyclic strength of sands obviously indicate that method of preparation imparts to specimens a different structure (fabric) [*13*] or K_0 values or both.

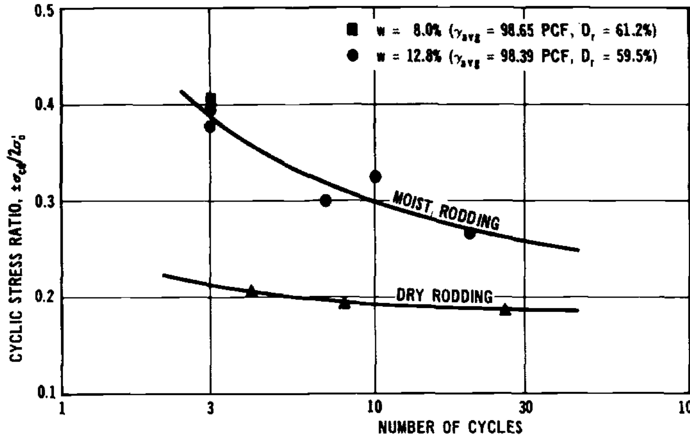

FIG. 3—*Effect of specimen preparation method and molding water content on number of loading cycles to cause initial liquefaction (rectangular wave) (from Ref* 12).

Effects of Reconstitution Versus Intact Specimens

Because of the aforementioned large effects of specimen preparation, a dilemma exists as what error is introduced in results due to reconstituting specimens. Obviously, testing undisturbed specimens would circumvent these specimen preparation effects, inasmuch as structure, K_0 stresses, density, and stress history would represent field conditions. Unfortunately, it is impossible to obtain a truly "undisturbed" specimen as sampling and specimen preparation procedures reduce the *in situ* total stresses to an isotropic state with possible specimen disturbance. Nevertheless, for laboratory tests a specimen could be considered undisturbed for practical purposes, provided sampling and specimen preparation did not alter the soil structure, void ratio, or water content [*14*]. In this context, comparisons between intact, relatively undisturbed and reconstituted specimens should provide some estimate (correction factor) for evaluating field strengths.

In 1976, Marcuson and Townsend [*15*] reported that isotropically consolidated undisturbed specimens from Fort Peck Dam were approximately 70 to 80 percent more stable than specimens of the same material reconstituted to the same density using a "dry rodding" specimen preparation procedure. They also reported that five other laboratories observed that reconstituted specimens generally gave lower strengths than undisturbed specimens.

In 1977, Mulilis et al [*11*] tabulated for various soils the effects of reconstitution, which are reproduced as Table 1. This table shows that the ratio of undisturbed to reconstituted strengths varies from 1.0 to 2.0, that is, no effect due to reconstitution to a 100 percent strength loss depending upon

TABLE 1—*Comparison of undisturbed and remolded strength* (*from Ref* 11, 15, 37).

Firm	Project	Ratio of Undisturbed to Remolded Strength	Soil Type	Method of Remolding
Woodward-Clyde (Oakland, Calif.)	South Texas	1.00	silty fine sand, D_{50} = 0.07 to 0.27 mm[a]	moist tamping, 3/4-in.[b]-dia tamping foot
Woodward-Clyde (Orange, Calif.)	San Onofre	1.15	well-graded coarse to fine sand, 15%—#200 sieve	moist tamping, 3/4-in.-dia tamping foot
University of California, Berkeley	Blue Hills, Texas	1.15	uniform fine silty sand, D_{50} = 0.4 mm, 8 to 15%—#200 sieve	moist tamping, 1/4-in.dia tamping foot
Dames & Moore (San Francisco, Calif.)	Allens Creek (heat sink area)	1.20	fine silty, clayey sand, D_{50} = 0.03 to 1.6 mm, 0 to 40%—#200 sieve	moist tamping, 1-in.-dia tamping foot
Dames & Moore (San Francisco, Calif.)	Allens Creek (plant area)	1.27	fine silty, clayey sand, D_{50} = 0.03 to 1.6 mm, 0 to 40%—#200 sieve	moist tamping, 1-in.-dia tamping foot
Converse-Davis	Perris Dam	1.45	clayey sand, LL[c] = 26, PI[d] = 11, 44%—#200 sieve	moist tamping, 1/2-in.-dia tamping foot
Law Engineering and Testing	Florida sand	1.30	silty sand with shells	dry vertical vibrations, frequency = 120 Hz
U.S. Army Engineer Waterways Experiment Station	Ft. Peck Dam (foundation)	1.65 to 1.80	uniform fine silty sand	dry rodding (3/8-in.-dia foot), followed by static compaction
U.S. Army Engineer Waterways Experiment Station	Ft. Peck Dam (shell)	1.70 to 2.00	uniform fine to medium sand	dry rodding (3/8-in.-dia foot), followed by static compaction

[a] 1 mm = 0.04 in.
[b] 1 in. = 25.4 mm.
[c] LL = Liquid Limit.
[d] PI = Plasticity Index.

the method of reconstitution and site. By comparing these results with those in Fig. 2, they noted that the moist-tamping specimen preparation gave the highest cyclic strength, and hence would require the least amount of correction for estimating undisturbed strengths.

Silver and Ishihara [*16*] recently compared the cyclic strength of reconstituted specimens of Niigata sand prepared by pluviation through water followed by light tapping to achieve comparable densities of undisturbed specimens that, after drainage, had been frozen at the site in their sampling tube and transported to the laboratory. These test results showed that the ratio of undisturbed to reconstituted strengths ranged from 1.14 to 1.22. Since Mulilis et al [*11*] had shown that other specimen preparation techniques could provide higher strengths, Silver and Ishihara compared cyclic strengths by various preparation procedures with that by pluviation through water, and concluded that moist rodding should have closely approximated undisturbed strengths. Examination of Table 1, however, shows that in most cases undisturbed strengths are higher than those reconstituted by moist tamping. This fact, plus data in Fig. 2 showing that moist tamping gave the highest strength for different methods of preparation, would indicate that for some sites current specimen reconstitution procedures cannot duplicate field strengths.

In their paper elsewhere in this volume, Ishihara et al [*17*] compared the undisturbed cyclic strengths of alluvial deposits in Toyoko with reconstituted specimens prepared by pluviation through water. These comparisons, presented in Fig. 4, show that undisturbed specimens on an average were 15 percent stronger than comparable density-reconstituted specimens.

Effects of Freezing Intact Specimens

One method of preserving the fabric of clean sands during transportation and storage is freezing. The method of course is restricted to free-draining clean sands where pockets of water could not occur and form ice lenses during freezing, and assumes a priori that freezing does not affect cyclic strength. Walberg [*18*] recently examined freezing effects on cyclic strength of undisturbed and reconstituted sand specimens. In his investigations, 2.8-in.-diameter (71 mm) pairs of undisturbed specimens were prepared by hand trimming at a dewatered site; one specimen was frozen using dry ice, while the other was carefully protected during transportation to the laboratory. Measurements indicated that no change in length of specimens occurred during freezing or transportation. Although some differences in relative density values existed between frozen and nonfrozen specimens (possibly due to nonuniformities of the deposit or problems in determining relative density), Walberg's results indicated that freezing had practically no effect on cyclic strength.

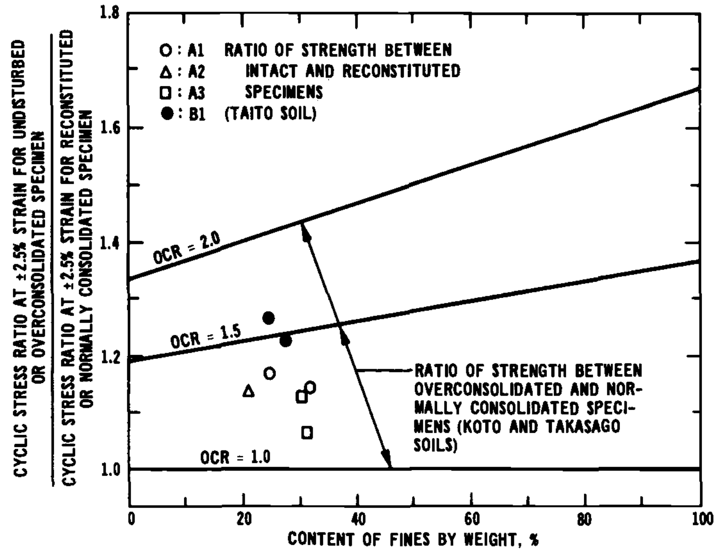

FIG. 4—*Comparison of cyclic strength of intact specimens with that of overconsolidated specimens* (*from Ref* 17).

In another more closely controlled test series, specimens of Monterey No. 0 sand were prepared to 50 and 60 percent relative density by moist tamping, frozen, and the cyclic strengths compared with those of Mulilis et al [*11*] and Silver et al [*7*], respectively. Figure 5 presents these results and indicates that freezing has insignificant effects on the cyclic strength of clean, drained sands.

Effect of Confining Stress (σ_3)

In their initial publication, Seed and Lee [*1*] reported that the number of cycles required for liquefaction increased as confining pressure also increased for specimens prepared such that they had the same void ratio after consolidation. This result was of special interest as it is completely the reverse of that which might be anticipated from static test results. Since critical void ratio is not a constant but decreases as confining pressure increases, it could be assumed that under a higher confining pressure a saturated sand would exhibit compressional characteristics and would be less stable than under low confining pressures, which produce dilatant responses.

Finn et al [*19*] examined data from previous triaxial tests by Lee and Seed [*20*] and observed that the relationship between cyclic shear stress required to cause initial liquefaction in a specific number of cycles and effective confining pressure was linear for any given void ratio. Hence,

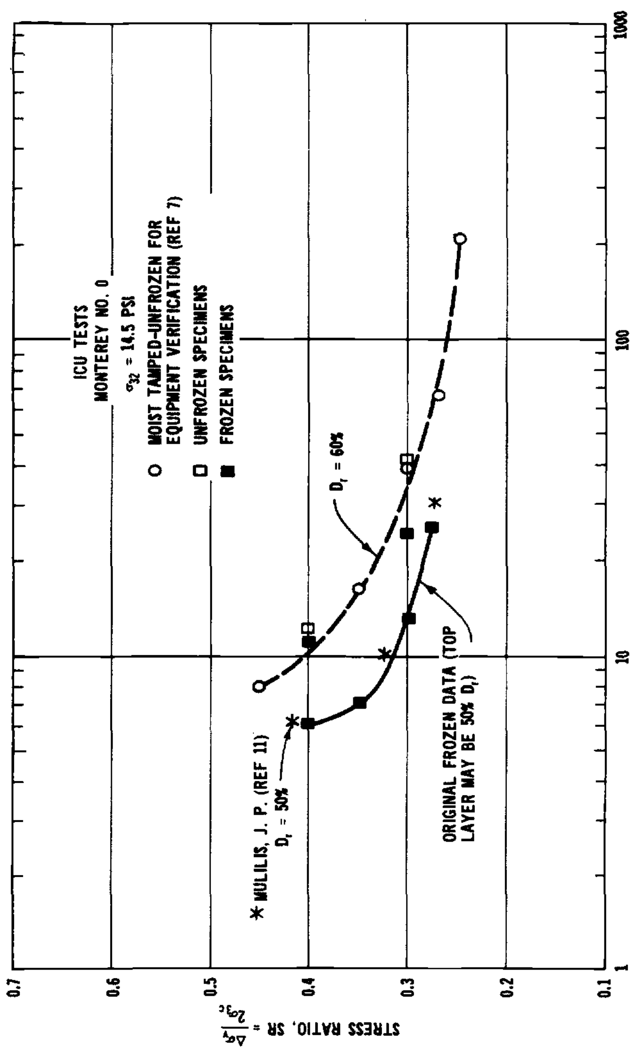

FIG. 5—*Effects of freezing on moist-tamped specimens of Monterey No. 0 sand (from Ref 18).*

initial liquefaction will always be achieved in the same number of cycles for a given void ratio if the tests are conducted at the same initial effective stress ratio, $R = \sigma_{dc}/2\sigma_c$. This finding led to the present data presentation of cyclic stress ratio, $\sigma_{dc}/2\sigma_c$ versus number of cycles.

Conversely, Mulilis [*21*] presents data, Fig. 6, which show that the stress ratio decreases with increasing confining pressure. The magnitude of stress ratio decrease ranged from 0.004 to 0.0007 per psi increase in confining pressure, depending upon the method of specimen preparation. Similar data [22] shown in Fig. 7 show that, based upon relative density, the magnitude of stress ratio decrease for initial liquefaction in 10 cycles is 0.0035 and 0.0012 per psi increase in confining pressure for 60 and 40 percent relative density, respectively.

Castro and Poulos [*6*] also show that stress ratio decreases with increasing confining pressure for various relative densities and soil types.

These data demonstrate that cyclic stress ratio decreases with increasing confining pressure and that the magnitude of this decrease is dependent upon relative density, soil type, and specimen preparation procedure [*23*]. Nevertheless, as pointed out by Lee and Focht [*2*], for practical purposes within small ranges of pressure, cyclic strength is directly proportional to effective confining pressure.

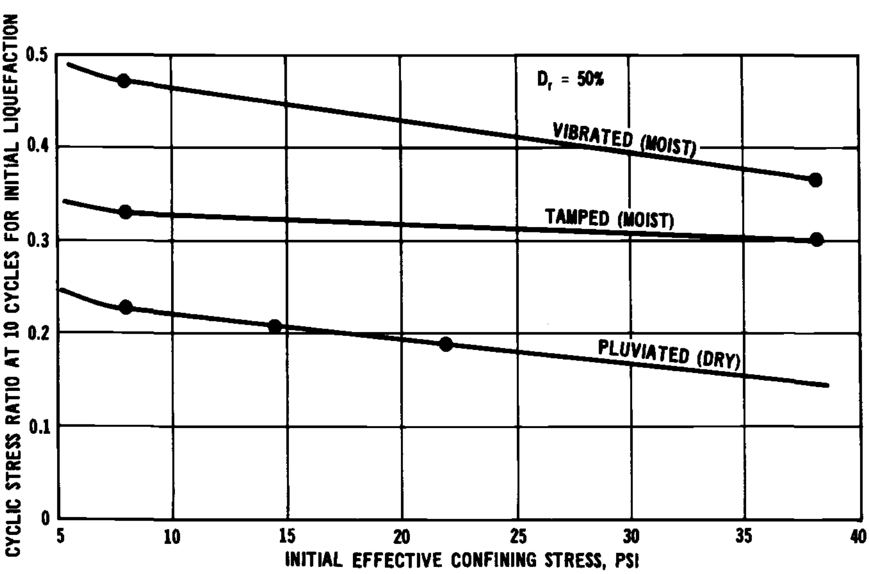

FIG. 6—*Cyclic stress ratio at 10 Hz for initial liquefaction versus initial effective confining stress* (*from Ref* 21).

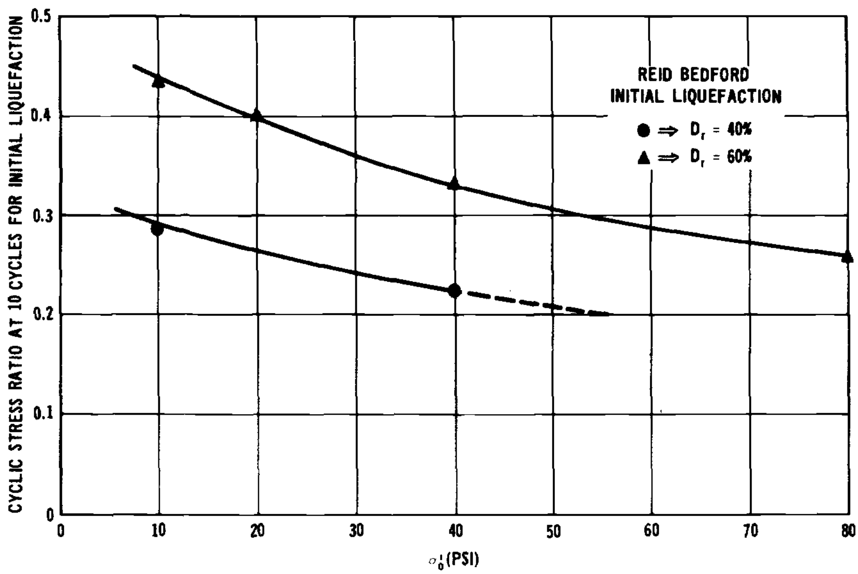

FIG. 7—*Cyclic stress ratio at 10 Hz for initial liquefaction versus confining pressure (from Ref 22).*

Effect of Loading Wave Form

In 1968, Lee and Fitton [*24*] found that peaked (triangular) loading wave forms gave somewhat higher strengths than rectangular loading wave forms. For sands, this effect was approximately 10 percent, while for silts a 5 percent effect was noted. Seed and Chan [*25*] and Thiers [*26*], in investigations on loading wave effects on undisturbed sensitive clays, found that peaked (triangular) loading wave shapes gave 5 to 20 percent higher strengths than would be obtained under rectangular loading. Similarly, Silver et al [*7*] showed that rectangular loadings with fast rise times caused stress waves in the specimen and corresponding "ringing" in the pore pressure traces, resulting in cyclic strengths 15 percent lower than those tested using sine wave or degraded rectangular loadings. They concluded that rectangular loading wave forms with fast rise times should not be used for cyclic triaxial testing.

In their accompanying paper in this volume, Mulilis et al [*12*] compared the effects of rectangular, triangular, and sine wave loadings. These results, Fig. 8, show that the order of increasing strength was rectangular, triangular, and sine, with triangular and sine wave loading strengths being 13 and 30 percent stronger than rectangular loadings, respectively.

These results consistently demonstrate that rectangular loading wave forms produce cyclic strengths lower than smooth sine wave loading, with

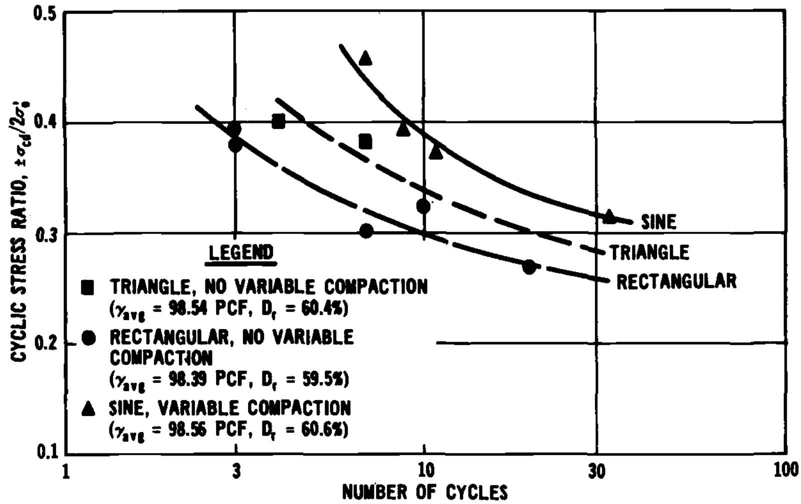

FIG. 8—*Effect of loading wave form on cycles to initial liquefaction for moist-tamped specimens* (*from Ref* 12).

degraded rectangular or triangular loading wave forms or both having intermediate strengths.

Common methods of analyses, where stresses induced in the ground by earthquakes are compared directly with those that cause liquefaction or excessive deformation in laboratory specimens, require conversion of the erratic and irregular earthquake stress history into an equivalent uniform cyclic stress series as imposed on laboratory specimens. This conversion is required inasmuch as laboratory tests are generally performed using uniform loading wave forms. Ishihara and Yasuda [*27*] and Annaki and Lee [*28*] have confirmed the validity of the equivalent uniform cycle concept by performing cyclic triaxial tests with irregular loading wave forms. Ishihara and Yasuda found that when the maximum stress of the irregular loading trace was applied in extension, liquefaction occurred at a lower stress ratio, $\sigma_{max}/2\sigma_c$, than for loadings with the maximum stress applied in compression. Similarly, Annaki and Lee [*28*] observed that when converting from irregular to uniform cycles, extension peaks produced about 90 percent of the total damage, because the undrained strength of sand is less in extension than compression. Because of this asymmetric effect existing in triaxial tests, good agreement in converting from irregular to uniform cycles was obtained only when the damaging effects of compression and extension cycles were considered separately. The authors of both papers [*27,28*] indicate that cyclic triaxial tests are limited by asymmetric effects not found in simple shear or torsional shear equipment.

Effects of Frequency on Cyclic Strength

Lee and Fitton [*24*], Wong et al [*29*], Mulilis [*21*], Wang [*30*], and Lee and Focht [*2*] have evaluated frequency effects over a range of 1 to 60 cpm. Wang's experiments were over a range of 60 to 1680 cpm but the load wave form transitioned from rectangular to rounded triangular at the higher frequencies. Lee and Fitton and I ee and Focht found that slower loading frequencies produced slightly (<10 percent) lower strengths. Wong et al [*29*], Mulilis [*21*], and Wang [*30*] found that slower frequencies gave slightly higher strengths (approximately 10 percent). Although this is conflicting, it can be safely concluded that frequency effects have only a minor (<10 percent) effect on cyclic strength of cohesionless soils.

An interesting sidelight of Wang's experiment was the effect of confining medium on frequency effects. When water was used as a confining medium, both loose and dense specimens failed prematurely at a cyclic loading frequency of 300 cpm due to a secondary resonant effect, but this effect disappeared when air was substituted as the confining medium.

Effect of Specimen Size

Lee and Fitton [*24*] and Wang [*30*] compared the effects of size on 35.6- and 71.1-mm (1.4 and 2.8 in.) diameter specimens and found that it has very little effect. Wong et al compared the effects of size on 70- and 300-mm (2.8 and 12 in.) diameter specimens with similar height-to-diameter ratios. Their results, Fig. 9, show that the 300-mm (12 in.) diameter specimen is approximately 10 percent weaker than the 71-mm (2.8 in.) diameter specimen.

Wang [*30*] compared the effects of height-to-diameter ratios of 1.0 to 2.3; however, these tests were conducted using full-friction stones. As might be anticipated, the specimens with a height-to-diameter ratio of 1.0 were approximately 20 to 50 percent stronger than the standard specimens.

Effect of Frictionless Caps and Bases

When using frictionless end platens, a slower rate of load application will be required in cyclic tests in order to allow the grease used to reduce friction to function. In this context, Mulilis [*21*] conducted cyclic triaxial tests at 1 cpm on Monterey No. 0 sand. His results, Fig. 10, show that frictionless end platens had about the same strength as full-friction end caps. Wang [*30*] conducted tests at a frequency of 2 Hz comparing "very rough" and "smooth" end platens. Since testing was at 2 Hz, no grease was used, rather trends were examined. His data showed that cyclic strength was insensitive to cap and base roughness, with smooth-end platens being approximately 5 percent stronger.

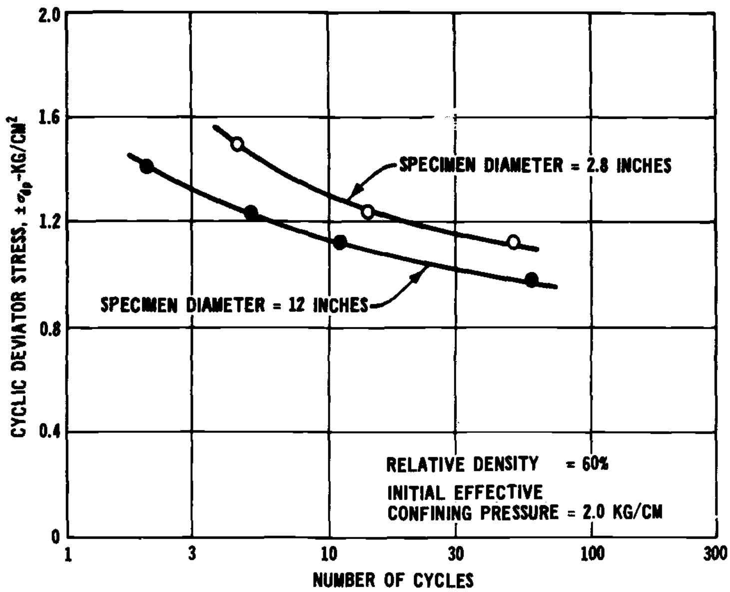

FIG. 9—*Effect of specimen size on cyclic stresses causing initial liquefaction of Monterey sand (from Ref 29).*

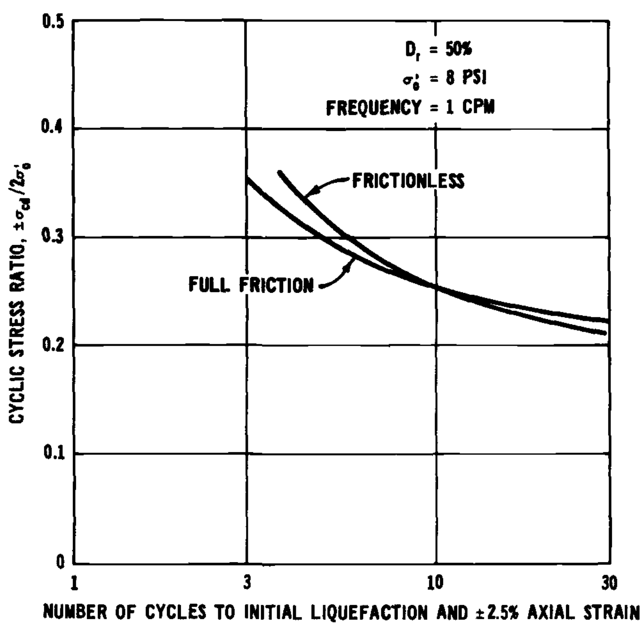

FIG. 10—*Comparison of full-friction and frictionless end platens (from Ref 21).*

Lee [31] compared cyclic strengths of loose and dense specimens with full-friction caps and bases tested at 2 Hz with loose and dense specimens with frictionless caps and bases tested at 1 and 0.05 Hz. The loading wave form for tests at 2 Hz was rectangular, while those for 1 and 0.05 Hz were rounded rectangular and triangular, respectively. Disregarding frequency and wave-form differences which may have made significant contributions, these results showed that frictionless caps and bases were 25 and 58 percent stronger, respectively, for loose and dense specimens tested using full-friction end platens.

Factors Affecting Cyclic Triaxial Strength

Effects of Relative Density

The effect of relative density on cyclic strength was recognized early in the history of cyclic tests. In 1967, Lee and Seed [20] reported that cyclic stress required to cause initial liquefaction increased linearly to approximately 60 percent relative density. At relative densities below 50 percent, complete liquefaction occurred almost simultaneously, and relative densities above 70 percent were required for safety against large strains. Seed and Idriss [32] used this linear relationship to correct densities to 50 percent relative density, whereby

$$\frac{\sigma_{dc}}{2\sigma_c}(D_r) = \frac{\Delta\sigma_{dc}}{2\sigma_c}(D_r = 50\%)\frac{D_r}{D_{r\,50\%}}$$

Mulilis [21] also shows that stress ratio to cause liquefaction in 10 cycles is linear with relative density to approximately 70 percent D_r. The data [22] presented in Fig. 11 show that the slope of this linear relationship is a function of confining pressure. Additional data [23] suggest that this linear relationship is also a function of failure criteria, and at 20 percent double-amplitude strain the relationship is linear only to approximately 40 percent D_r.

Effects of Particle Size and Gradation

Early research by Lee and Fitton [24] compared the effects of particle size based upon mean grain diameter D_{50} and found that as grain size increases, the cyclic strength also increases, with very fine sands having about half the cyclic strength of gravels. Likewise, data by Wong et al [29], Fig. 12, summarize the effects of particle size on cyclic strength, and show a 30 to 60 percent increase in cyclic strength to cause ±2.5 percent and ±10 percent strain, respectively, as the mean grain size, D_{50}, increases from 0.1 to 30 mm. At the opposite end of the grain size distribution, as

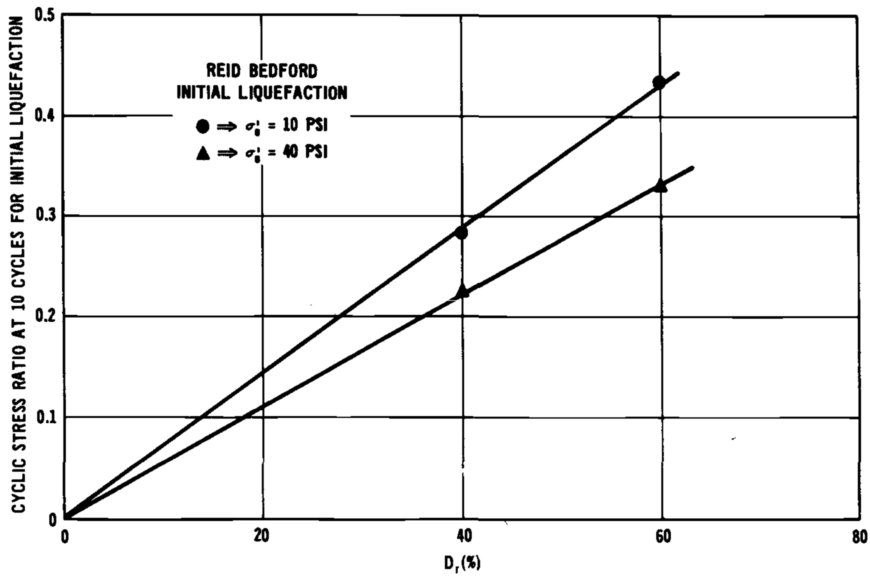

FIG. 11—*Cyclic stress ratio at 10 Hz for initial liquefaction versus relative density (from Ref 22).*

the mean grain diameter, D_{50}, continues to decrease to silt and clay sizes, the cyclic strength rapidly increases. In the Ishihara et al paper elsewhere in this volume [*17*], data showing a 28 percent cyclic strength increase as D_{50} decreases from 0.1 to 0.01 mm are presented. Hence, materials having a D_{50} of approximately 0.1 mm possess the least resistance to cyclic stresses.

Because testing large particle sizes requires large specimens, modeling large particle sizes to use smaller test specimens is popular. In Fig. 12, the 12-in.-diameter (304.8 mm) data are for essentially parallel gradations. However, the results show that the Oroville Dam material [D_{50} = 28.6 mm (1.1 in.)] is 30 percent stronger than the Monterey sand [D_{50} = 3.3 mm (0.1 in.)]. Hence this technique of modeling cohesionless materials by parallel gradation, which has been successful for modeling static strengths [*33*], is not appropriate for cyclic testing.

Contrary to their expectations, Wong et al [*29*] found as shown in Fig. 13 that well-graded material was somewhat weaker than uniformly graded material. This finding was attributed to a greater densification tendency in well-graded soils, as finer particles move into voids between larger particles, than occurs in uniformly graded soils. This densification tendency would be reflected as increased pore pressure rise. In addition, the degree of membrane compliance for uniform soils would tend to cause higher strengths than for well-graded soils.

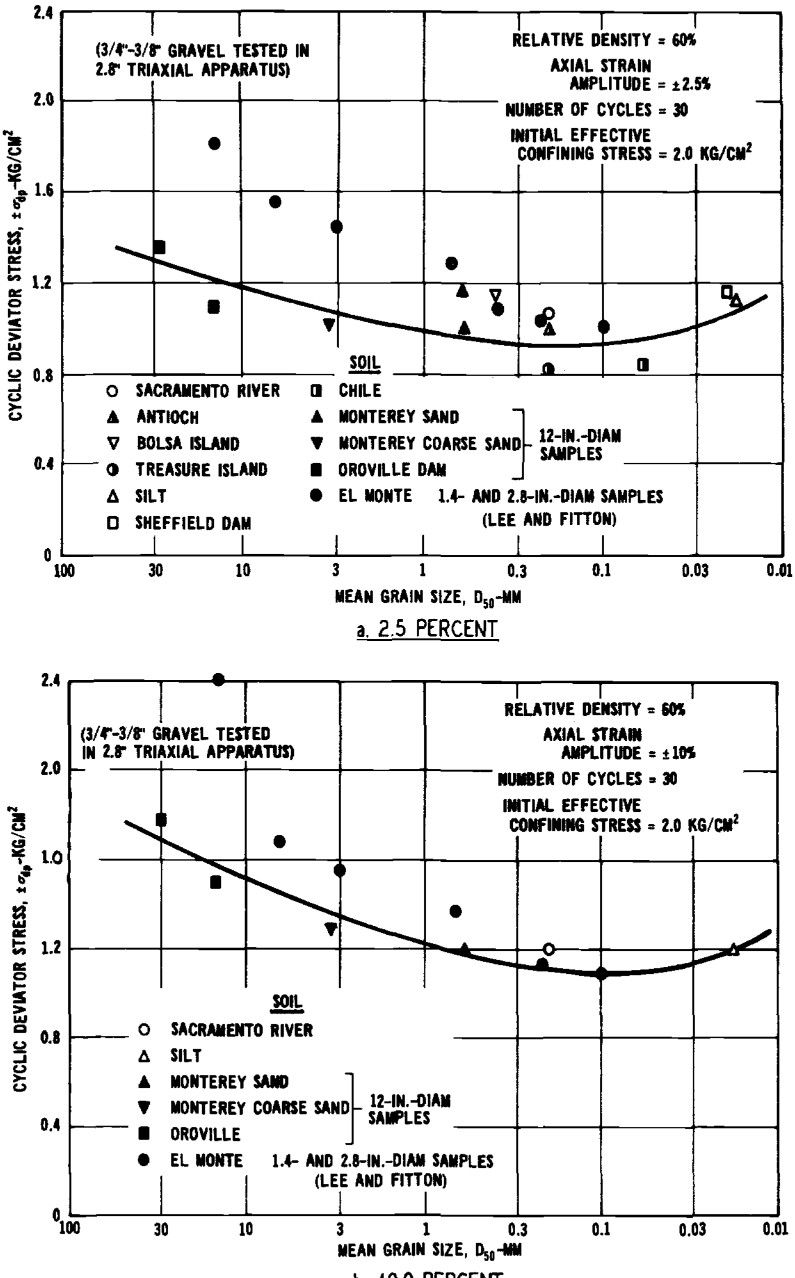

FIG. 12—*Cyclic deviator stresses causing axial strain amplitude for different grain sizes (from Ref* 29).

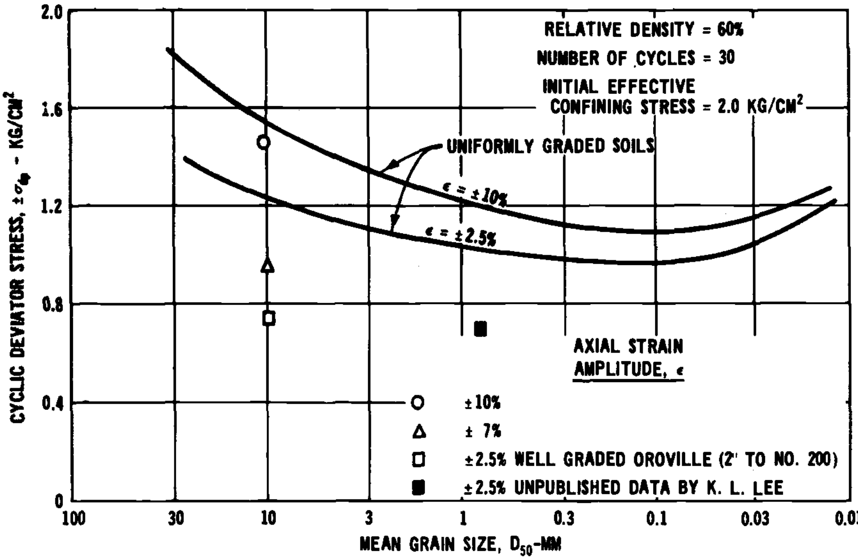

FIG. 13—*Comparison of cyclic loading strengths of uniformly graded and well-graded soils (from Ref 29).*

Effects of Prestraining

Finn et al [*34*], evaluating the effects of reliquefaction in cyclic triaxial tests, found that once a specimen has liquefied and reconsolidated to a denser structure, despite this densification, the specimen is much weaker to reliquefaction. For example, a specimen liquefied in 26 cycles at a void ratio of 0.660 was consolidated at a void ratio of 0.626, yet when resubjected to the same cyclic stress failed in 1.5 cycles. Conversely, when a specimen is subjected to small strains during undrained cyclic loading and stopped prior to liquefaction, consolidated, and undrained cyclic stresses reapplied, the specimen is considerably more resistant to liquefaction than can be attributed to the slight densification occurring during consolidation. This increased resistance to liquefaction due to small shear strains (<0.5 percent for 15 cycles was attributed to structural rearrangement within the specimen and increased interlocking of particles.

Similar experiences have been reported by Wang [*30*] and Lee and Focht [*2*], where cyclic loading specimens to preliquefaction pore pressures, reconsolidating, and recyclically loading caused substantially stronger specimens, despite no significant densification occurring during reconsolidation. The consequences of this strengthening phenomenon due to small shear strains have been shown [*22*] to preclude using the same specimen for small strain properties tests and then using the same specimen to evaluate its liquefaction potential. Likewise, a technique of increasing the applied stress ratio during a test where more cycles than of interest have been applied to a specimen cannot help to produce meaningful results.

Mori et al [35] investigated the effects of sampling on strain history. Their tests, Fig. 14, compare the results of (1) specimens with no seismic history (that is, no prestraining), (2) specimens with some seismic history (prestraining) caused by applying several loading cycles, releasing the small pore pressure resulting from these loading cycles, thus allowing consolidation, and (3) specimens with the same seismic history as (2) applied, but with the confining pressure then reduced to 3.45 kPa (0.5 psi) to simulate "perfect sampling" and the initial confining pressure reapplied as shown. Although the strain history increased the liquefaction resistance, about 35 percent of this resistance was lost as a result of reducing and reapplying

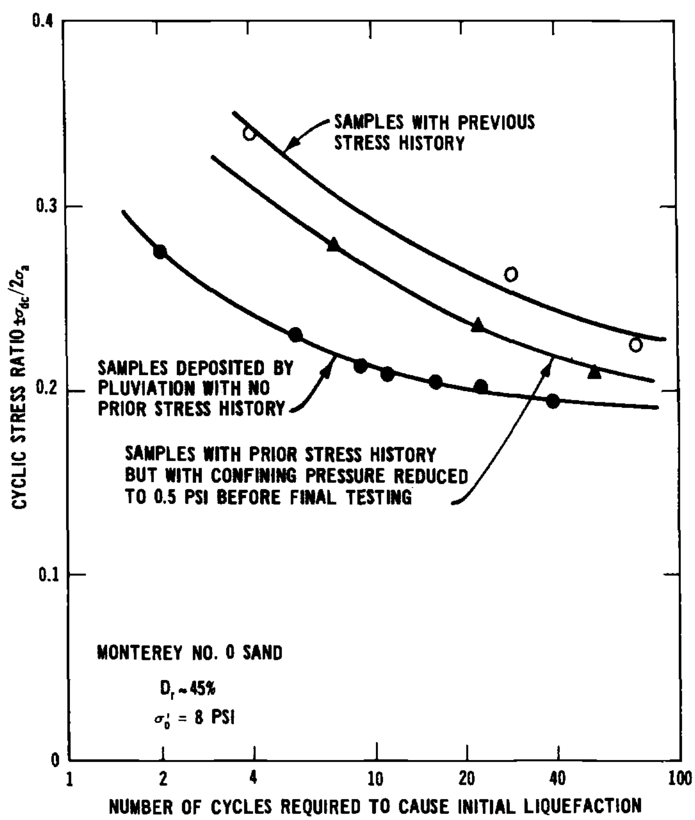

FIG. 14—*Effect of stress reduction on liquefaction characteristics of sand with prior stress history (from Ref 35).*

the chamber pressure, thereby suggesting that *in situ* strengths will also be reduced by sampling procedures.

Effects of Overconsolidation Ratio and K_o

Seed and Peacock [*5*] presented results of simple shear tests illustrating that as the overconsolidation ratio (OCR) increased from 1 to 4 and 1 to 8, the stress ratio, τ/σ_o, required to cause initial liquefaction in 30 cycles was 75 and 150 percent higher, respectively. Confirmation of these findings was observed by Lee and Focht [*2*], who indicated an increase in cyclic stress ratio of about 30 percent for an OCR of 3 for very dense sand. Likewise, Ladd [*23*] observed an increase in cyclic strength of about 20 percent for an OCR of 2.0. In addition, this increase in cyclic strength with OCR is a function of the fines content.

In their paper in this volume, Ishihara et al [*17*] present results, Fig. 15, which show that cyclic strength increases as OCR and fines content increase. For specimens with no fines, a strength increase of 30 percent was observed for an increase in OCR from 1.0 to 2.0, while for the same OCR increase an 80 percent increase in cyclic strength was observed for a specimen with 100 percent fines. By comparing the results of reconstituted specimens formed by pluviation through water and consolided to an OCR of 2.0 with undisturbed specimens, it was found that the higher strengths

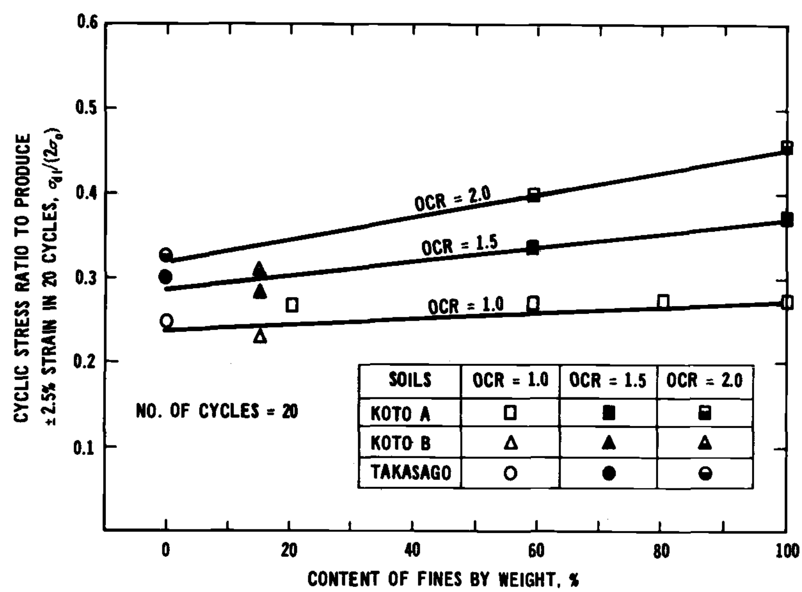

FIG. 15—*Relationship between cyclic strength and fines content in soils* (*from Ref* 17).

associated with undisturbed specimens could be attributed to a slight over-consolidation of 2.0

Effects of Consolidation Ratio, K_c

Since many soil deposits or soil structures (embankments) do not have horizontal surfaces, consolidation under anisotropic stress conditions are required for analyses [*36,37*]. Typical data from anisotropically consolidated tests presented in Fig. 16 shows that, for a given confining pressure, the maximum deviator stress required to cause a critical strain for a specified number of cycles increases with the K_c ratio. In their early investi-

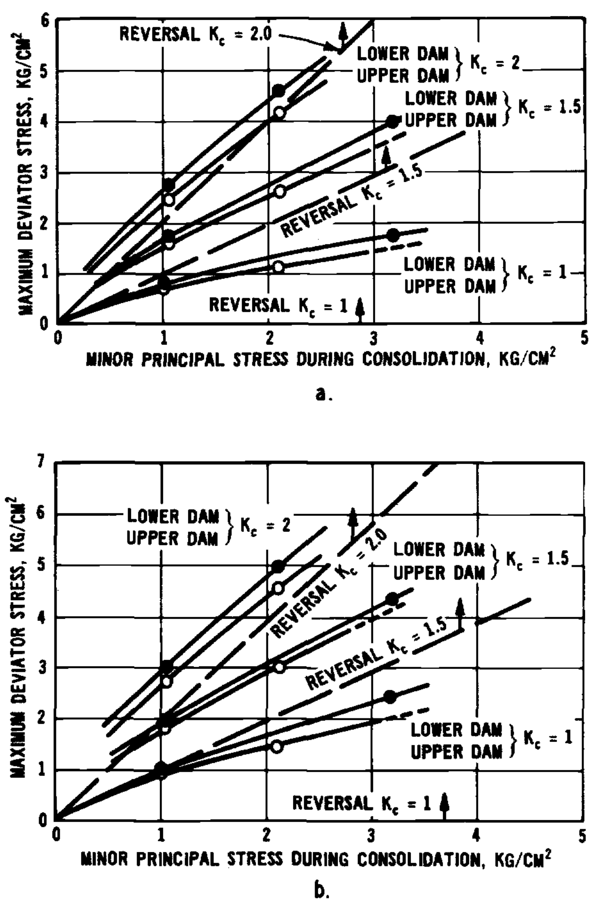

FIG. 16—*Cyclic stresses causing liquefaction and 5 percent strain in* (a) *2 cycles and* (b) *5 cycles for hydraulic sand fill* (*from Ref* 36).

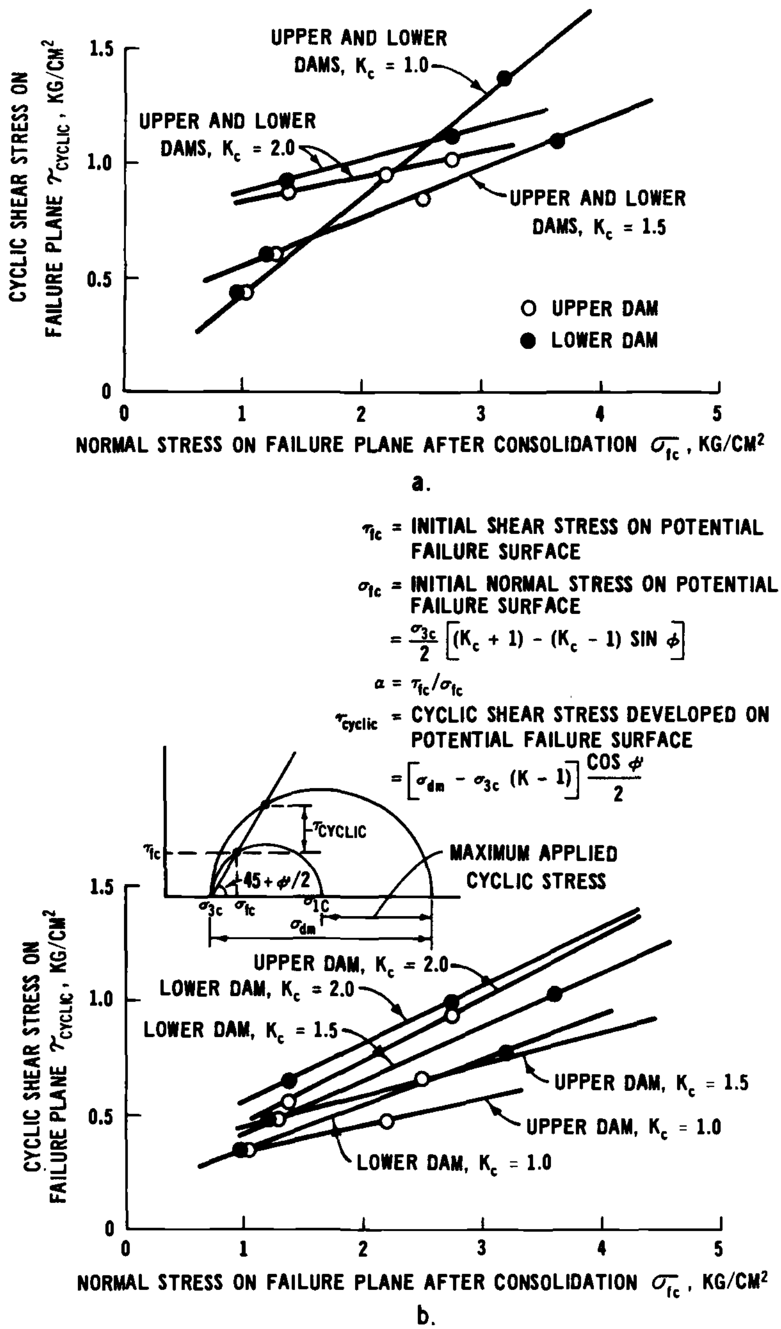

FIG. 17—*Cyclic shear stresses on 60-deg failure plane causing liquefaction and 5 percent strain in* (a) *2 cycles,* (b) *5 cycles for hydraulic sand fill from San Fernando Dams* (*data from Ref* 36).

TABLE 2—*Summary of factors affecting cyclic triaxial strength of cohesionless soils.*

Variable Effect of	Testing Conditions and Materials	Effect (Result)	Source
Testing laboratory and equipment	"standard sand" tested by eight different laboratories following specified testing procedures and conditions. Monterey No. 0 sand	excellent agreement between laboratories provided strict adherence to testing procedures followed	[7, 8]
Specimen preparation	specimens formed by pluviation through air or water, vibration, or tamping in dry or moist condition. Monterey No. 0 sand, 50% D_r and other soils.	weakest specimens formed by pluviation through air, while strongest formed by vibrating in moist condition. Difference in stress ratio for failure can be 110%	[10-12]
Reconstituted versus intact	"intact" (relatively undisturbed) specimens tested, then remolded and reconstituted to same density and retested under same conditions as intact. A variety of sands and specimen preparation techniques for reconstitution used	intact specimens stronger than reconstituted. Strength decreases range from 0 to 100% depending upon material and reconstitution method	[15, 11, 16, 17]
Freezing intact specimens	intact specimens transported to laboratory in frozen and unfrozen condition, reconstituted specimens frozen in laboratory and compared with unfrozen specimens	no effect, with testing variation, due to freezing	[18]
Confining stress, σ_3	tests conducted at a variety of confining stresses on variety of sands	within small range of pressures, cyclic strength is directly proportional to confining stress	[1, 19, 2]
		cyclic stress ratio decreases with increasing confining pressure 0.0007 to 0.004 per psi increase in σ_3	[21, 22, 6]
Loading wave form	tests conducted using rectangular, rounded rectangular, triangular, and sine wave loading shapes	order of increasing strengths: rectangular, degraded rectangular or triangular, sine. Sine wave approximately 30% stronger than rectangular	[24-26, 7, 12]
	irregular wave forms simulating earthquake stress histories evaluating equivalent cycle concept	equivalent cycle approach valid. Cyclic triaxial affected by extension more than compression	[27, 28]
Frequency	frequencies with combined range of 1 to 1680 cpm for various sands. Typical ranges, 1 to 20 or 5 to 60 cpm evaluated for one sand	slower loading frequencies have slightly higher strengths. For range of 1 to 60 cpm, effect is 10%	[24, 29, 2, 21, 30]
	water and air used as confining media while evaluating frequency effects	water may affect results at 5 Hz	[30]
Specimen size	strengths of 35.6- and 70-mm [a]-dia specimens compared with strengths of 70- and 300-mm-dia specimens	no effect for this range 300 mm dia approximately 10% weaker	[24, 30, 29]

Frictionless caps and bases	specimens tested with friction and frictionless caps and bases at frequencies slow enough to allow grease to function	no effect between full friction and frictionless caps and bases	[21, 30, 31]
Relative density	tests conducted on variety of cohesionless soils over wide range of stress and testing conditions	cyclic strength increases dramatically with increasing density. Linear relationship between cyclic stress ratio and relative density to approximately 60% D_r, but slope is dependent on soil type, fabric, confining pressure, and failure strain	[20, 32, 21, 23]
Particle size and gradation	cyclic strengths of different soils at comparable testing conditions compared on basis of mean grain diameter, D_{50}	sands have $D_{50} \approx 0.1$ mm have least resistance to cyclic loading. As D_{50} increases from 0.1 to 30 mm, a 60% strength increase observed; as D_{50} decreases from 0.1 mm to silt and clay sizes, rapid increase in strength observed	[24, 29, 17, 23]
	well-graded material compared with uniformly graded material both having same D_{50} size	well-graded somewhat weaker than uniformly graded material	[29]
Prestraining	specimens liquefied by cyclic loading, reconsolidated and reliquefied by applying same original cyclic load	despite increase in density due to consolidation, liquefaction causes considerably weaker specimen	[34]
	specimens prestrained to 50 to 80% pore pressure response, reconsolidated, and reloaded cyclicly	precycling greatly strengthens cyclic strength	[34, 2, 30, 22, 35]
Overconsolidation ratio (OCR)	specimens overconsolidated by consolidating to higher stresses and rebounded to lower testing stresses	OCR's of 1 to 4 and 1 to 8 increased cyclic simple shear stress ratios 75 and 150%, respectively	[5]
		OCR of 1 to 2 increased cyclic strengths 30 to 80% depending upon amount of fines. Amount of fines affect OCR	
Consolidation ratio K_c	specimens consolidated anisotropically for variety of confining stresses and subjected to reversing and nonreversing cyclic stresses	maximum deviator stress required for failure increases with K_c ratio for given $\bar{\sigma}_{3c}$	[36]
		method of presenting data influences conclusions; τ_{cf} versus σ_{fc} recommended	
		isotropic consolidation may not always provide conservative results	

[a] 1 mm = 0.04 in.

gations, Lee and Seed [38] found that this increase was a function of initial confining pressure, and density.

Castro and Poulos [6], however, point out that intuitively the opposite effect, that is, cyclic strength for a critical strain in a specified number of cycles, should decrease with increasing K_c, as at higher K_c ratios the specimen is initially nearer failure. Furthermore, the data indicating that cyclic strength increases with K_c ratio suggest an unreasonable conclusion that steeper slopes are safer against earthquake loadings.

Lee and Seed [38] also observed in anisotropically consolidated tests that in cases where $\sigma_{dc}/2\sigma_{3c} < (K_c - 1)/2$, that is, where no stress reversal occurs and the net axial stress is always the major principal stress, initial liquefaction did not occur; rather, only progressive deformation occurred with increasing cycles to a limiting strain. Conversely, in comparable tests where stress reversal did occur, that is, where $\sigma_{dc}/2\sigma_{3c} > (K - 1)/2$, initial liquefaction and associated strains were observed. For the data presented in Fig. 16, all points were for stress reversal conditions, but for 5 percent strain in 5 cycles the distance between reversal and nonreversal is less. From these considerations, it is obvious that, as the K_c ratio increases, so must the cyclic deviator stress, σ_{dc}, and the maximum deviator stress in order to achieve stress reversal for a given σ_{3c}.

In his paper in this volume, Haimson [39] conducted cyclic triaxial tests to determine the fatigue strength of rocks. In comparing cyclic uniaxial tension or cyclic uniaxial compression with cyclic tension-compression loadings, that is, stress reversal loadings, he found that the most damaging cyclic loading was also that of stress reversal.

Considering that analyses involving anisotropic consolidation compare laboratory strengths on potential failure planes, $45 + \emptyset/2$, and that anisotropic consolidation increases the normal stress on the failure plane (which also increases the cyclic shear stress), a more appropriate presentation of the data is made in Fig. 17. In this case, τ-cyclic is the cyclic shear stress on the potential failure plane while σ_{fc} is the normal stress on this plane during consolidation. These results replotted in this fashion show that in some cases isotropic consolidation will provide conservative estimates, while in other cases anisotropic consolidation will provide a lower shear strength; that is, τ-cyclic required for 5 percent strain is greater for anisotropically consolidated specimens than for isotropically consolidated specimens, and vice versa.

Summary and Conclusions

The effects of these various testing and material factors on the cyclic triaxial strength of cohesionless soils and their relative magnitudes are summarized in Table 2.

Specimen preparation methods, differences between intact and reconstituted specimens, density, and prestraining have the greatest relative effect on cyclic strength. In addition, confining stress, loading wave form, material grain size (D_{50}) and gradation, OCR, and consolidation stress ratio (K_c) have noticeable but less significant effects. Apparently, various testing equipment and laboratories can repeat results, provided careful attention is given minor details. The effects of freezing, loading frequency, specimen size, and frictionless caps and bases have relatively minor effects on cyclic triaxial strengths.

Based upon these considerations, it is obvious that any ASTM testing procedures or test programs should include these factors and their effects on test results.

Acknowledgments

The information contained herein was collected during research conducted at the U.S. Army Engineer Waterways Experiment Station (WES) under sponsorship of the Office, Chief of Engineers. The author wishes to express his appreciation to his colleagues at WES who provided data and reviewed the manuscript.

References

[1] Seed, H. B. and Lee, K. L., *Journal of Soil Mechanics and Foundations Division*, American Society of Civil Engineers, Vol. 92, No. SM6, Nov. 1966, pp. 105–134.

[2] Lee, K. L. and Focht, J. A., Jr., *Journal, Geotechnical Engineering*, American Society of Civil Engineers, Vol. 100, No. GT1, Jan. 1975, pp. 1–18.

[3] Bjerrum, L., *Geotechnique*, Vol. 23, No. 3, 1973, pp. 319–358.

[4] Peacock, W. H. and Seed, H. B., *Journal of Soil Mechanics and Foundations Division*, American Society of Civil Engineers, Vol. 94, No. SM3, May 1968, pp. 689–708.

[5] Seed, H. B. and Peacock, W. H., *Journal of Soil Mechanics and Foundations Division*, American Society of Civil Engineers, Vol. 97, No. SM8, Aug. 1971, pp. 1099–1119.

[6] Castro, G. and Poulos, S. J., "Factors Affecting Liquefaction and Cyclic Mobility," American Society of Civil Engineers, Preprint 2752, Liquefaction Problems in Geotechnical Engineering, Philadelphia, Pa., Sept. 1976.

[7] Silver, M. L. et al, *Journal of Geotechnical Engineering Division*, American Society of Civil Engineers, Vol. 102, No. GT5, May 1976, pp. 511–524.

[8] Silver, M. L., "Laboratory Triaxial Testing Procedures to Determine the Cyclic Strength of Soils," Report No. NUREG-31, U. S. Nuclear Regulatory Commission, Washington, D. C., 1976.

[9] EM 1110-2-1906, Laboratory Soils Testing, Appendix XA, Cyclic Triaxial Test (in preparation), 1977.

[10] Ladd, R. S., *Journal of Geotechnical Engineering Division*, American Society of Civil Engineers, Vol. 100, No. GT10, Oct. 1974, pp. 1180–1184.

[11] Mulilis, J. P., Seed, H. B., Chan, C. K., Mitchell, J. K., and Arulanandan, K., *Journal of Geotechnical Engineering Division*, American Society of Civil Engineers, Vol. 103, No. GT2, Feb. 1977, pp. 91–108.

[12] Mulilis, J. P., Townsend, F. C., and Horz, R. C., this publication, pp. 265–279.

[13] Mitchell, J. K., Chatoian, J. M., and Carpenter, G. C., "The Influences of Sand Fabric on Liquefaction Behavior," WES CR S-76-5, U.S. Army Engineer Waterways Experiment Station, Corps of Engineers, Vicksburg, Miss., June 1976.

[14] Hvorslev, M. J., "Subsurface Exploration and Sampling of Soils for Civil Engineering

Purposes," Report on a Research Project of the American Society of Civil Engineers, U. S. Army Engineer Waterways Experiment Station, Corps of Engineers, Vicksburg, Miss., Nov. 1949.
[*15*] Marcuson, W. F., III, and Townsend, F. C., "Effects of Specimen Reconstitution on Cyclic Triaxial Results," WES Miscellaneous Paper S-76-5, U.S. Army Engineer Waterways Experiment Station, Corps of Engineers, Vicksburg, Miss., April 1976.
[*16*] Silver, M. L. and Ishihara, K., "Comparison Between the Strength of Undisturbed and Reconstituted Sands from Niigata, Japan," Contract Report, U.S. Army Engineer Waterways Experiment Station, Corps of Engineers, Vicksburg, Miss., (in preparation), April 1977.
[*17*] Ishihara, K., Sodekawa, M., and Tanaka, Y., this publication, pp. 246-264.
[*18*] Walberg, F. C., "Soils—Investigation of Effects of Freezing Sand Samples," Presentation 12, Division Laboratory Conference, Corps of Engineers, Dallas, April 1977.
[*19*] Finn, W. D. L., Pickering, D. J., and Bransby, P. L., *Journal of Soil Mechanics and Foundations Division*, American Society of Civil Engineers, Vol. 97, No. SM4, April 1971, pp. 639-660.
[*20*] Lee, K. L. and Seed, H. B., *Journal of Soil Mechanics and Foundations Division*, American Society of Civil Engineers, Vol. 93, No. SM1, Jan. 1967, pp. 47-70.
[*21*] Mulilis, J. P., "The Effects of Method of Sample Preparation on the Cyclic Stress-Strain Behavior of Sands," EERC Report 75-18, College of Engineering, University of California, Berkeley, July 1975.
[*22*] Townsend, F. C. and Mulilis, J. P., "Liquefaction Potential of Sands Under Static and Cyclic Loadings," U.S. Army Engineer Waterways Experiment Station, Corps of Engineers, Vicksburg, Miss. Report, (to be published), 1978.
[*23*] Ladd, R. S., Lecture Notes—Short Course, "Quality Geotechnical Lab. Testing—Cyclic Behavior of Sands as Determined in the Laboratory for Earthquake Analysis," University of Missouri, Rolla, May 1976.
[*24*] Lee, K. L. and Fitton, J. A. in *Vibration Effects of Earthquakes on Soils and Foundations, ASTM STP 450*, American Society for Testing and Materials, 1969.
[*25*] Seed, H. B. and Chan, C. K., "Pulsating Load Tests on Samples of Clay and Silt from Anchorage, Alaska," Appendix C, Report on Anchorage Area Soil Studies to U. S. Army Engineer District, Anchorage, Alaska, Shannon & Wilson, Inc., Seattle, Wash., Aug. 1964.
[*26*] Thiers, G. R., "The Behavior of Saturated Clay under Seismic Loading Conditions," Ph.D. Thesis, Department of Civil Engineers, University of California, Berkeley, 1965.
[*27*] Ishihara, K. and Yasuda, S. "Sand Liquefaction Due to Irregular Excitation," *Soils and Foundations*, Vol. 12, No. 4, Dec. 1972.
[*28*] Annaki, M. and Lee, K. L., "Equivalent Uniform Cycle Concept for Soil Dynamics Liquefaction Problems in Geotechnical Engineering," American Society of Civil Engineers, Preprint 2752, Philadelphia, Pa., Sept. 1976.
[*29*] Wong, R. T., Seed, H. B., and Chan, C. K., *Journal of Geotechnical Engineering Division*, American Society of Civil Engineers, Vol. 101, No. GT6, June 1975, pp. 571-583.
[*30*] Wang, M-S., "Liquefaction of Triaxial Sand Samples Under Different Frequencies of Cyclic Loading," ME Thesis, University of Western Ontario, May 1972.
[*31*] Lee, K. L., "Influence of End Restraint in Cyclic Triaxial Tests," WES CR S-76-1, U.S. Army Engineer Waterways Experiment Station, Corps of Engineers, Vicksburg, Miss., March 1976.
[*32*] Seed, H. B. and Idriss, I. M., "A Simplified Procedure for Evaluating Soil Liquefaction Potential," EERC Report No. 70-9, College of Engineering, University of California, Berkeley, Nov. 1970.
[*33*] Marachi, N. D., Chan, C. K., Seed, H. B., and Duncan, J. M., "Strength and Deformation Characteristics of Rockfill Materials," Report No. TE 69-5, Geotechnical Engineering, University of California, Berkeley, Sept. 1969.
[*34*] Finn, W. D. L., Bransby, P. L., and Pickering, D. J., *Journal of Soil Mechanics and Foundations Division*, American Society of Civil Engineers, Vol. 96, No. SM6, Nov. 1970, pp. 1917-1934.

[35] Mori, K., Seed, H. B., and Chan, C. K., "Influence of Sample Disturbance on Sand Response to Cyclic Loading," UCB/EERC 77/03, College of Engineering, University of California, Berkeley, Jan. 1977.
[36] Seed, H. B., Idriss, I. M., Lee, K. L., and Makdisi, F. I., *Journal of Geotechnical Engineering Division*, American Society of Civil Engineers, Vol. 101, No. GT9, Sept. 1975, pp. 889–911.
[37] Marcuson, W. F., III, and Krinitzsky, E. L., "Dynamic Analysis of Ft. Peck Dam," WES TR S-76-1, U.S. Army Engineer Waterways Experiment Station, Corps of Engineers, Vicksburg, Miss., April 1976.
[38] Lee, K. L. and Seed, H. B., "Strength of Anisotropically Consolidated Samples of Saturated Sand Under Pulsating Loading Conditions," Report No. TE-66-3, Department of Civil Engineering, University of California, Berkeley, July 1966.
[39] Haimson, B. C., this publication, pp. 228–245.

V. P. Drnevich[1]

Resonant-Column Testing—Problems and Solutions

REFERENCE: Drnevich, V. P., "**Resonant Column Testing—Problems and Solutions,**" *Dynamic Geotechnical Testing, ASTM STP 654,* American Society for Testing and Materials, 1978, pp. 384–398.

ABSTRACT: The resonant-column test is a relatively nondestructive test employing wave propagation in cylindrical specimens of soil and rock. Test results are usually quite accurate, but in some cases insufficient coupling exists between specimen and apparatus or specimens are too stiff for a given apparatus, or both. A criterion is given to evaluate whether a coupling problem exists and solutions are suggested. Procedures for evaluating limiting specimen stiffness and maximum strain amplitude capabilities are given. Solutions for reducing air migration problems during long-term tests are presented. Finally, a simple method for estimating strain amplitudes during a test is demonstrated for both shear and axial compression.

KEY WORDS: air migration, confining media, coupling, data reduction, laboratory testing, limits of apparatus, resonant column, rock, shear stress, shear tests, soils, soil dynamics, specimen stiffness, strain, test apparatus, testing techniques, triaxial test

The resonant-column test method determines modulus and damping in soils by means of propagating waves in a cylindrical soil specimen (column). If a sinusoidal torque is applied to the specimen, shear waves are propagated, and if a sinusoidal axial compression is applied, compressional waves are propagated. (Compressional waves in the cylindrical soil specimen are different from compressional waves *in situ* and hence the term rod wave is sometimes used to distinguish between the two.) In the test, the frequency of the applied torque (or force) is adjusted until resonance occurs. This frequency plus the magnitude of applied torque (or force) and the magnitude of the resulting motion are used to calculate the modulus, damping, and strain amplitude. Details of these procedures are provided by Drnevich et al [*1*].[2] When torsion is applied, shear modulus and shear damping are obtained as functions of shear strain amplitudes. When axial

[1] Professor of civil engineering, University of Kentucky, Lexington, Ky. 40502.
[2] The italic numbers in brackets refer to the list of references appended in this paper.

compression is applied, Young's modulus and damping due to rod compression are obtained as functions of axial strain amplitudes.

Resonant-column tests can give very accurate test results for strain amplitudes as low as 0.0001 percent. The upper limit of strain amplitude can be as high as 0.1 percent or even 1.0 percent.

As with most tests, inaccurate results can be obtained when (1) improperly calibrated equipment is used, (2) the limits of the equipment are exceeded, (3) poor test procedures are used, (4) samples are poor, or (5) the imposed confining stresses are not appropriate. Most of the aforementioned items are addressed by Drnevich et al [1]. However, another source of inaccuracy, dealing with coupling between the specimen and end platens for torsion, is discussed and specific recommendations are presented for solving this problem. Another topic, concerned with the maximum stiffness of specimens to be tested in a given apparatus, has not been previously covered and is done so herein.

In recent years, attention has been drawn to the fact that "time effects" can help account for the difference between moduli obtained in the laboratory and results obtained in the field. In order to determine the magnitude of time effects, longer-term laboratory tests (on the order of several days or more) must be performed, and associated with the longer time is the problem of air migration through the confining medium and membrane into the specimen pore space. Means of reducing air migration problems are also presented herein.

Finally, two other "problems" are discussed. They relate to improving test procedures. The first is a method to estimate the maximum strain amplitude capability of a given device considering specimen characteristics, and the second is a systematic and simplified procedure for quickly determining the strain amplitude from transducer output readings and system frequencies.

Coupling Between Platens and Specimen for Torsional Motion

For stiff soil specimens, frozen soils, weathered rock, and rock cores, the possibility exists that complete coupling will not exist between the specimen and end platens. Since coupling is a function of the coefficient of friction and the applied shear stress, it is most likely that complete coupling will exist at ultralow shear-strain amplitudes. However, as shear-strain amplitudes increase, shear stresses increase and incomplete coupling can possibly occur. During the operation of a test, it is nearly impossible to tell that the slipping between platens and specimens is occurring. The effect of slipping is to give lower shear modulus and higher damping than actually exists at a given shear-strain amplitude.

The problem can be handled quite simply. First of all, complete coupling can be assumed to exist if the generated shear stress is less than the coefficient of friction multiplied by the effective normal contact stress. From the Naval Facilities Engineering Command manual, (NAVFAC) [2], the minimum coefficient of friction given between soils (including rock) and other materials is 0.2. Consequently, in a given test where no special precautions are taken, if the mobilized shear stress is less than 0.2 times the effective normal contact stress, complete coupling can be assumed to exist. For convenience, the following equation may be used to establish that complete coupling exists

$$\gamma G / \sigma_a' < 0.2 \tag{1}$$

where

γ = shear strain amplitude,
G = shear modulus, and
σ_a' = effective axial stress applied by platen to the specimen.

For cases where Eq 1 is not satisfied, special top and bottom platens are required. When testing soils, the use of porous disks (stones, bronze, or stainless steel) with embedded razorblade vanes protruding approximately 1.5 mm (0.06 in.) is usually sufficient to ensure complete coupling (see Fig. 1). By use of these vanes, the maximum shear stress is increased to the shear strength of the soil. They may also cause some very minor disturbances to the soil in the immediate vicinity of the platens. However, no corrections are recommended to account for this. (When the porous disks are used, the disks themselves must be securely fastened to the platens by means of epoxies, machine screws, or both.)

When very stiff specimens are to be tested (so stiff that the razorblade vanes cannot easily penetrate the specimen), adhesives or cements must be used to bond the platens to the specimen. A variety of quick-setting compounds can be used which range from epoxy to patching or capping compounds, or both. It is important that these compounds do not physically affect the specimen or the membranes enclosing the specimen. For example, dry specimens or those with low degrees of saturation may absorb moisture from compounds that are mixed with water. This is a problem if the specimen is not going to be saturated prior to testing. On the other hand, compounds and epoxies that make use of solvents may attack membranes, causing leaks to occur. Some experimentation with a given compound may be necessary before it is put into general use.

Upper Limit of Specimen Stiffness for a Given Apparatus

Two criteria are used to establish the upper limit of specimen stiffness that can be allowed in a given apparatus. The first is that the specimen modulus should be less than ten percent of the modulus of the material

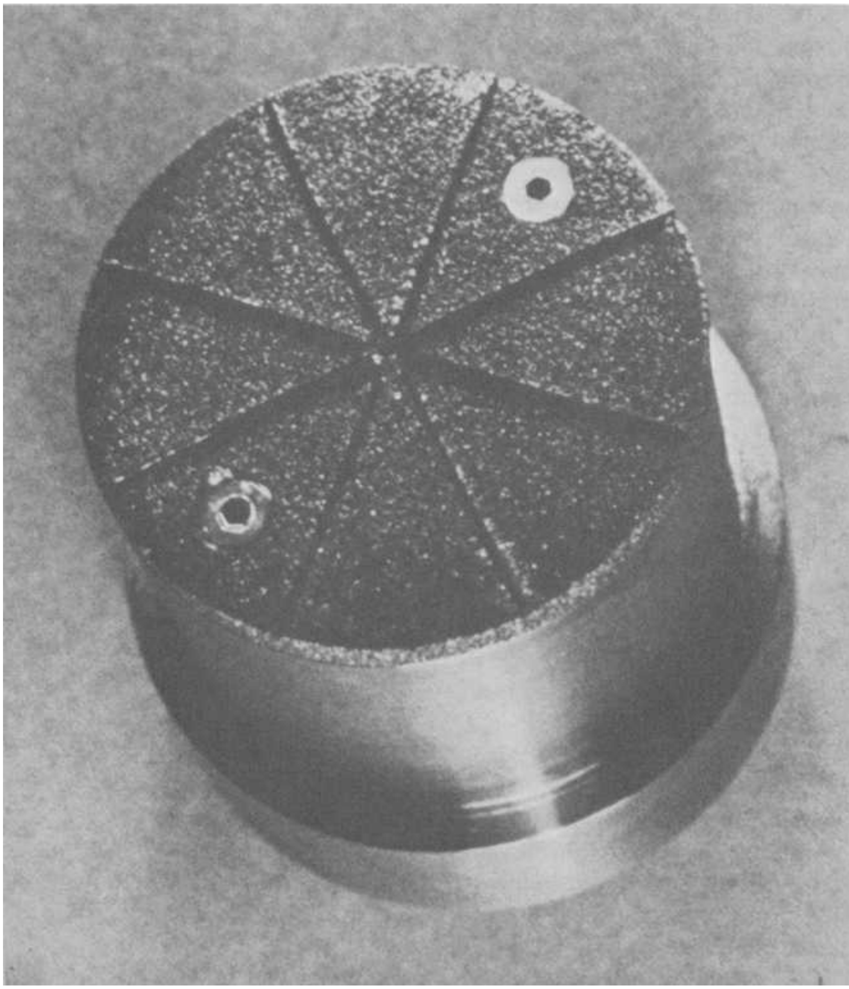

FIG. 1—*End platen with razorblade vanes.*

from which the apparatus is constructed. The second is that the assumed boundary conditions must hold. The rationale for the first criterion is that if both the apparatus and the specimen had nearly the same moduli, then the platens and other portions of the apparatus would deform during testing and measurements made would not accurately represent soil properties. It can be shown that the error in modulus is proportional to the ratio of moduli. For example, if the combined length of both end platens were equal to the length of the specimen and if the modulus of the specimen were 10 percent of the modulus of the platen material, the measured modulus would be approximately ten percent low.

The second criterion is particularly applicable to those apparatuses that assume that one end of the specimen is rigidly fixed such as the popular Hardin and Drnevich devices. If, in reality, the "fixed" end deforms during a test, the modulus results will be lower than actually exist in the specimen because the effective length is longer. To prevent this, the overall stiffness of the fixed end should be ten times greater than the stiffness of the stiffest specimen to be tested. In order to achieve this stiffness, it is important that the fixed-end platen be attached to a relatively stiff and massive portion of the apparatus and that the apparatus be firmly anchored to a large mass.

If the stiffness of the specimen exceeds the limiting criterion, the size of the specimen can be modified to give a lower stiffness. Specimen stiffness in torsion is given bv

$$K_{\text{torsion}} = \pi d^4 G/(32L) \tag{2}$$

where

d = specimen diameter,
G = shear modulus, and
L = specimen length.

For axial compression, the specimen stiffness is given by

$$K_{\text{axial compression}} = \pi d^2 E/(4L) \tag{3}$$

where E is Young's modulus.

Note that for both cases the stiffness is strongly influenced by the specimen diameter and length. Thus, to reduce specimen stiffness for a given soil or rock, the ratio of d/L must be decreased by either decreasing the diameter or increasing the length, or doing both.

The recommended upper limit of specimen stiffness for the Drnevich fixed-free apparatus for the case of torsion is 12 000 $N \cdot$ m/rad (100 000 lb·in./rad). Since resonant frequency and stiffness of specimen are directly related, the specimen stiffness will be less than the foregoing recommended value when the operating, first-mode resonant frequency of the system is given by

$$f_n < 1/(2\pi)\sqrt{K_L/J_o} \tag{4}$$

where

K_L = recommended upper limit of specimen torsional stiffness, and
J_o = polar mass moment of inertia of portion of apparatus connected to free end of specimen.

For the case of longitudinal motion (rod compression wave propagation) in the Drnevich device, the recommended upper limit of specimen stiffness is 4.5 MN/m (25 000 lb/in.). Likewise, the specimen stiffness is less than the recommended upper limit when the first-mode system resonant frequency is given by

$$f_n < 1/(2\pi)\sqrt{K_L/M_o} \tag{5}$$

where

K_L = recommended upper limit of specimen axial stiffness, and
M_o = mass of equipment attached to the free end of specimen.

For the Hardin apparatus [3], where the specimen boundary conditions are commonly referred to as fixed base-spring top, the recommended upper limit of specimen shear stiffness, K_L, is 3000 N · m/rad (27 000 lb · in./rad). Because this type of apparatus has a spring connected to the top platen, the spring gives the value of the apparatus spring constant, K_{app}, and it, combined with the polar mass moment of inertia of the portion of the apparatus connected to the top of the specimen, gives the apparatus frequency, f_{app}. For this apparatus, the recommended upper limit of specimen stiffness is not exceeded when the system resonant frequency is given by

$$f_n < f_{app}\sqrt{1 + K_L/K_{app}} \tag{6}$$

A third type of apparatus, where one platen is restrained by a spring and the other is free of restraints, is also commonly used. The driving force (or torque) is applied to the end of the specimen that is restrained by the spring. For the apparatus developed at the University of Kentucky, the recommended maximum specimen torsional stiffness, K_L, is 2 MN · m/rad (2×10^7 lb · in./rad). This recommended limit is not exceeded when the system resonant frequency is given by

$$f_n < 1/(2\pi)\sqrt{K_L/J_p} \tag{7}$$

where J_p is the polar mass moment of inertia of the portion of the apparatus attached to the free end of the specimen (nondriven end).

Equations 4 and 6 are based on the assumption that the system behavior can be approximated by a single-degree-of-freedom system. This approximation is relatively good when the ratio of apparatus inertia (of the platen where force or torque input occurs) to specimen inertia is greater than ten. For apparatus listed in the foregoing, this is practically always the case unless larger than usual [36 or 50 mm (1.4 or 2.0 in.) diameter] specimens are being tested.

The upper limit values of specimen stiffnesses given herein are the best-estimate values given by the author in 1977 for (and only for) the apparatus listed. They are based on results of tests with metal calibrating rods of various stiffnesses and on experience from testing a wide variety of soil types and specimen sizes. Modifications in the design of an apparatus could significantly change these values.

Air Migration Through Membrane

It has been shown that wave propagation velocities in soils continue to increase after primary compression is complete, and further that this increase is proportional to the log-of-time in secondary compression [*4–8*]. In order to adjust laboratory-obtained velocity data to field conditions, it is important to determine this increase of velocity for at least one log-of-time cycle in secondary compression after the end of primary consolidation. This means that tests must last several days or more, and in the case of staged pressure testing where the specimen is reconsolidated to different confining stresses, the test duration could last a week or more.

In practically all approaches, the confining stress is applied by regulated compressed air, and an air-water interface exists either within or outside the pressure chamber. Consequently, with long durations of time, air migrates through the water and through the membrane(s) into the specimen pore space, causing a reduced degree of saturation. The reduced degree of saturation may affect modulus and damping values, particularly in clays.

Several techniques are useful in reducing this migration. The use of a coating of vacuum grease on the exterior of the membrane is helpful. A second membrane, also coated with vacuum grease and placed over the first, is even more beneficial. The confining medium, if it is water, should be de-aired by boiling or vacuuming or both. Other confining media such as mineral oil and silicone oil, which are less permeable to air, may also be effectively used. Glycerin is more permeable than water and should not be used. Marcuson and Wahls [*9*] report that mercury can be very effective and that it does not significantly affect test results. When mercury is used, a special low-volume container adjacent to the specimen is used so that large quantities of mercury are not needed. It should be pointed out that mercury vapors are *deadly poisonous* and that special safety precautions are necessary when using it. The special low-volume container adjacent to the specimen would also be beneficial for use with the other suggested confining media since it would significantly reduce the area of the air-confining medium interface.

The problem of air migration can also be reduced by speeding up the primary consolidation process so that the total testing time is reduced. Primary consolidation is speeded up by decreasing the drainage path length. The most effective way of doing this is to utilize filter paper strips around the perimeter of the specimen and to have porous disks at each end of the specimen. Filter paper strips made from conventional laboratory filter paper have a negligible effect on test results for all but the softest of specimens.

Estimating the Maximum Strain Amplitude Capability of an Apparatus

The single-degree-of-freedom analogy may be used to estimate the maximum strain amplitude capabilities of a given apparatus as long as two conditions are met.

1. Specimen boundary conditions are such that one end of the specimen is rigidly fixed.
2. The inertia of the portion of the apparatus attached to the free end of the specimen is large (greater than a factor of ten) compared with the inertia of the specimen.

In general, the analogy applies to most apparatuses where one end of the specimen is rigidly fixed such as the Drnevich and Hardin apparatuses. By assuming the specimen to be a massless, Kelvin-Voigt material, the maximum shear-strain amplitude capability, in percent, is given by

$$\gamma(\%) = 1.7 \times 10^4 (ATC)/[D(\%)(SAFT)] \tag{8}$$

where

ATC = torque capability of apparatus,
$D(\%)$ = expected shear damping ratio, in percent, of specimen at maximum shear strain, and
$SAFT$ = specimen-apparatus factor for torsion, which is given by

$$SAFT = Gd^3 + K_{app}L/(\pi d) \tag{9}$$

where

G = shear modulus at maximum shear strain,
d = specimen diameter,
K_{app} = apparatus torsional spring constant, and
L = specimen length.

For convenience, Eqs 8 and 9 are incorporated into Fig. 2.

For the case where axial compression waves are generated, the maximum axial strain, in percent, is given by

$$\epsilon(\%) = 2 \times 10^4 (AFC)/[D(\%)(SAFL)] \tag{10}$$

where

AFC = force capability of apparatus,

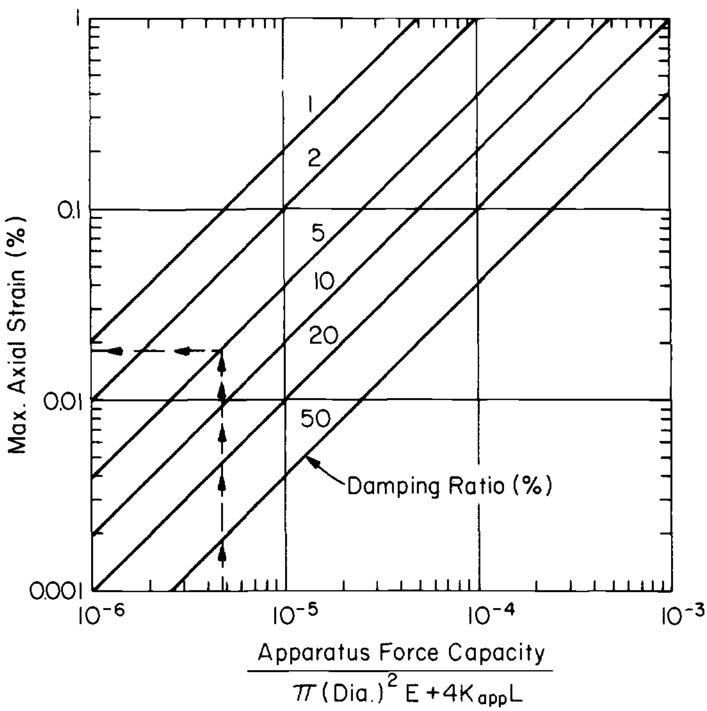

FIG. 2—*Maximum axial strain capability of resonant-column apparatus.*

$D(\%)$ = expected axial compression damping ratio, in percent, of specimen at maximum axial strain, and

$SAFL$ = specimen-apparatus factor for axial compression given by

$$SAFL = \pi d^2 E + 4K_{app} L \tag{11}$$

where

E = Young's modulus at maximum axial strain, and

K_{app} = apparatus longitudinal spring constant.

For convenience, Eqs 10 and 11 are incorporated into Fig. 3.

The use of Eqs 8 and 9, Eqs 10 and 11, or Figs. 2 or 3 requires that specimen modulus and damping at maximum strain be known. For practical purposes, an estimate of the maximum strain capability can be made by assuming reasonable values for these parameters. For the case of torsion, values for these parameters may be obtained by use of the equations and curves presented by Hardin and Drnevich [*10,11*].

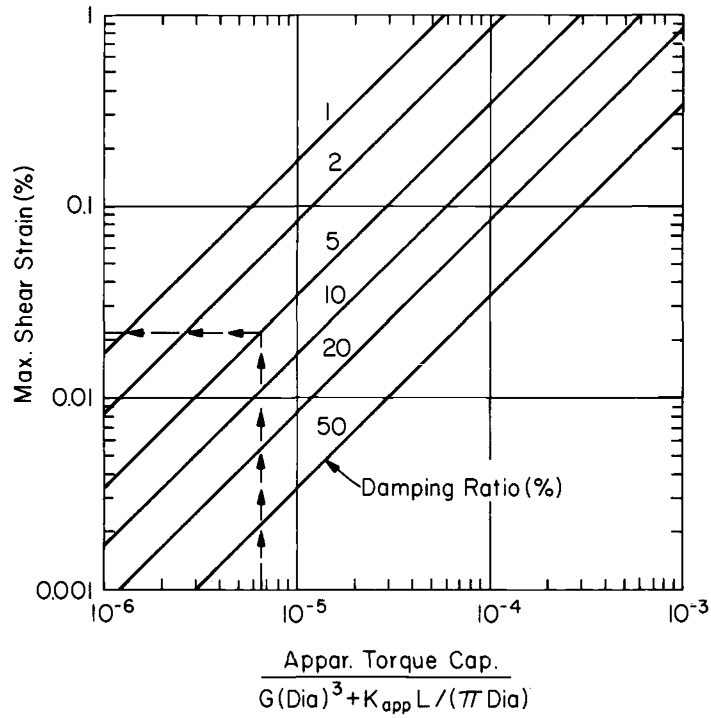

FIG. 3—*Maximum shear-strain capability of resonant-column apparatus.*

Estimating Strain Amplitude During a Test

During the operation of a resonant-column test, the ability to quickly determine vibration strain amplitudes is quite helpful in planning subsequent stages of testing and checking reduced data. Since most apparatuses employ accelerometers or velocity transducers to measure dynamic motion, determination of strain amplitude from the output of these transducers can be tedious. The problem can be greatly simplified by constructing simple-to-use graphs that incorporate the characteristics of a given apparatus. The procedure for constructing such a graph is outlined in the following and several examples are given.

Piezoelectric accelerometers are the most commonly used accelerometers in resonant-column equipment. These produce an electrical charge which is proportional to acceleration. Either a charge amplifier or a cathode follower must be used to convert the electrical charge to a voltage. The accelerometer in combination with a charge amplifier or cathode follower produces a calibration factor which is commonly given in terms of peak millivolts per peak-g (pk-mV/pk-g) where g is the acceleration of gravity.

The output from the charge amplifier or cathode follower is usually read on a digital or analog a-c voltmeter calibrated to give root-mean-square (rms) values of voltage. Acceleration in terms of meters per second or inches per second can be obtained by

$$a = \sqrt{2}(GF)\,(ATO)/(ACF) \tag{12}$$

where

GF = 9.80 (m/s/g) or 386 (in./s/g), depending on system of units desired,
ATO = acceleration transducer output in rms millivolts, and
AFC = accelerometer-charge amplifier (or cathode follower) calibration factor in terms of peak-millivolts/peak-g.

Since sinusoidal motion exists, displacement is related to acceleration by

$$\Delta = a/(2\pi f)^2 \tag{13}$$

where f is the frequency of motion in Hertz.

If a velocity transducer is used, the calibration factor is usually in terms of millivolts per meter per second or millivolts per inch per second. Likewise, output is commonly read with an a-c voltmeter calibrated to give rms values of voltage. Velocity in meters per second or inches per second can be obtained from

$$v = \sqrt{2}\,(VTO)/(VCF) \tag{14}$$

where

VTO = velocity transducer output in rms millivolts, and
VCF = velocity transducer calibration factor in meters per second o. inches per second, depending on system of units desired.

For sinusoidal motion, displacement is related to velocity by

$$\Delta = v/(2\pi f) \tag{15}$$

Now in the resonant-column apparatus where axial compression waves are propagated, axial strain is related to axial displacement by

$$\epsilon(\%) = \Delta\, 100\%\, SF/L \tag{16}$$

where

SF = strain factor to account for mode shapes within specimen, and
L = specimen length.

The strain factor is discussed in Drnevich et al [1] and for most common apparatuses can be assumed equal to unity (at least for estimating strain amplitudes).

When an accelerometer is used, axial strain amplitude can be calculated from an equation obtained by substituting Eq 12 into Eq 13 and then substituting the result into Eq 16

$$\epsilon(\%) = 3.58\,(GF)\,(ATO)\,(SF)/[(ACF)\,(f)^2\,L] \tag{17}$$

For a given apparatus, ACF is known, and for a given specimen, L is known. The term GF is defined by the system of units (see Eq 12) and the value of SF may be assumed to equal unity. Thus, the axial strain is a function of accelerometer output, ATO, and frequency, f. For example, let the value of ACF be 2500 pk-mV/pk-g, L be 0.0800 m, and GF in International System of Units (SI) be 9.80 m/s. Equation 17 reduces to

$$\epsilon(\%) = 0.175\,(ATO)/f^2 \tag{17a}$$

which is plotted in Fig. 4. To use Fig. 4, enter the abscissa with the reading from the a-c voltmeter and the ordinate with the system resonant frequency. Interpolate the axial strain amplitude from the values given on the diagonal lines.

If a velocity transducer is used, substitute Eq 14 into Eq 15 and then substitute the result into Eq 16, which gives

$$\epsilon(\%) = 22.5\,(VTO)\,(SF)/[(VCF)\,fL] \tag{18}$$

This equation, like Eq 17, is only a function of voltage reading and frequency for a given apparatus and it may be plotted in a graph similar to Fig. 4 except that the diagonal lines will be on a one-to-one slope.

For torsional motion and shear strain amplitudes, the approach is quite similar. In this situation, the transducer (either acceleration or velocity) is placed some distance from the axis of rotation. This is commonly called the transducer lever arm, TLA. Thus rotation, θ, is given by

$$\theta = \Delta/TLA \tag{19}$$

Shear strain amplitude is defined by

$$\gamma(\%) = \theta\,dSF\,100\%/(3L) \tag{20}$$

This equation gives the average shear strain, which is two-thirds of the peak shear strain at the edge of a solid cylindrical specimen. If an accelero-

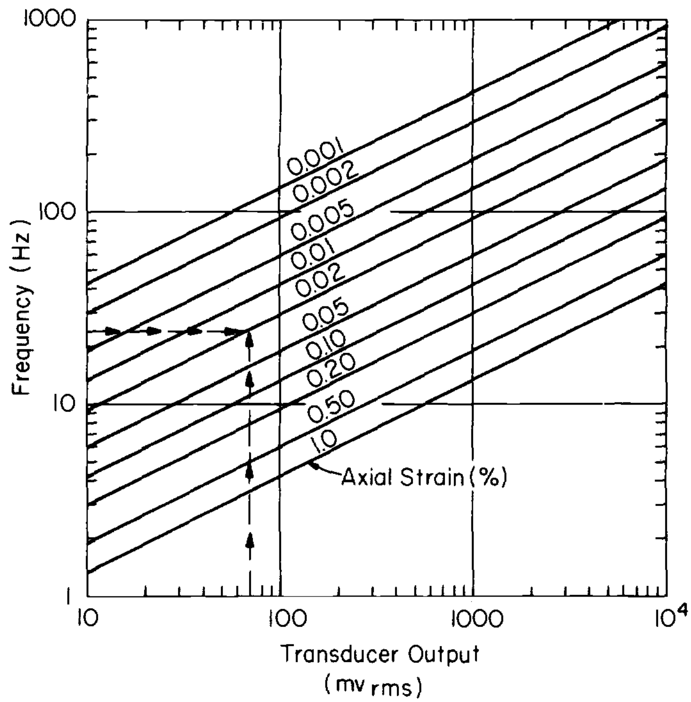

FIG. 4—*Example of graph for quick determination of axial strain amplitude.*

meter is used, the equation defining shear-strain amplitude can be obtained by use of Eqs 12, 13, 19, and 20 to give

$$\gamma(\%) = 1.19\,(GF)\,(ATO)\,d\,(SF)/[(ACF)\,(TLA)\,(f)^2\,L] \tag{21}$$

For a given apparatus, specimen length-to-diameter ratio, and system of units, this equation is a function only of the a-c voltmeter reading and the system frequency. For example, consider the same accelerometer characteristics as in the axial compression example plus a *TLA* of 0.0346 m and a specimen length-to-diameter ratio of 2.24. Equation 21 becomes

$$\gamma(\%) = 6.04\,(ATO)/f^2 \tag{21a}$$

and this is plotted in Fig. 5. Use of Fig. 5 is identical to use of Fig. 4, which was described earlier.

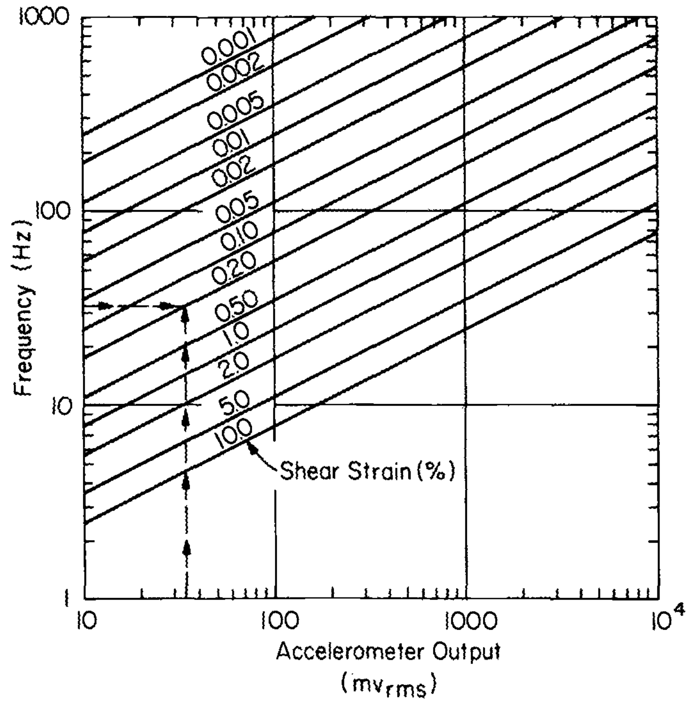

FIG. 5—*Example of graph for quick determination of strain amplitude.*

If a velocity transducer is used, Eqs 14, 15, 19, and 20 may be used to give

$$\gamma(\%) = 7.50\,(VTO)\,d\,(SF)/[(VCF)\,(TLA)fL] \tag{22}$$

This equation, like Eq 21, is a function only of a-c voltage reading and frequency for a given apparatus and specimen length-to-diameter ratio and may be plotted in a graph similar to Fig. 5 except that the diagonal lines will be on a one-to-one slope.

Summary and Conclusions

Five aspects of resonant-column testing were addressed. The first dealt with coupling between the platens and the specimen for torsional motion. It was proposed that the mobilized friction between the specimen and platens be compared with the maximum possible, which was calculated based on a conservative assumption of 0.2 for the coefficient of friction.

Criteria for the upper limit of specimen stiffness were considered. Means of calculating this upper limit of specimen stiffness for various apparatus boundary conditions were established and quantitative values were given for specific apparatus. These upper limit stiffnesses were then translated to convenient upper-limit system resonant frequencies.

Air migration through confining media and membranes was discussed. Several suggestions were made to reduce air migration. They include methods of speeding up the primary consolidation process as well as use of multiple membranes and various liquids for the confining media.

Two items associated with strain amplitude were presented. The first was concerned with estimating the maximum strain amplitude capability of a given apparatus. It was shown that apparatus force (or torque) capabilities, specimen modulus, damping, length, and diameter all are important in determining maximum strain amplitude.

It was shown that the strain amplitude developed during testing can be quickly determined by use of a simple equation or graph. Procedures as well as examples were given for developing this equation and graph for a specific apparatus and specimen configuration.

The work presented herein can be used to establish the limitations of resonant-column apparatus, to improve the test techniques and, consequently, to improve the quality of test results.

References

[*1*] Drnevich, V. P., Hardin, B. O., and Shippy, D. J., this publication, pp. 91-125.

[*2*] *Design Manual—Soil Mechanics, Foundations, and Earth Structures,* Department of the Navy, Naval Facilities Engineering Command, NAVFAC DM-7, March 1971, Table 10-1, p. 7-10-7.

[*3*] Hardin, B. O. in *Special Procedures for Testing Soil and Rock for Engineering Purposes, ASTM STP 479,* American Society for Testing and Materials, 1970, pp. 516-529.

[*4*] Afifi, S. A. and Woods, R. D., *Journal of the Soil Mechanics and Foundations Division,* American Society of Civil Engineers, Vol. 97, No. SM10, Oct. 1971, pp. 1445-1460.

[*5*] Afifi, S. A. and Richart, F. E., Jr., *Soils and Foundations* (Japan), Vol. 13, No. 1, March 1973, pp. 77-95.

[*6*] Stokoe, K. H. and Richart, F. E., Jr. in *Proceedings,* Eighth International Conference on Soil Mechanics and Foundation Engineering, Moscow, Vol. 1, Part 2, 1973, pp. 403-409.

[*7*] Anderson, D. G. and Woods, R. D. in *Proceedings,* Geotechnical Engineering Division, American Society of Civil Engineers, Specialty Conference on Insitu Measurement of Soil Properties, Raleigh, N.C., Vol. 1, June 1975, pp. 69-92.

[*8*] Anderson, D. G. and Stokoe, K. H., II, this publication, pp. 66-90.

[*9*] Marcuson, W. F., III, and Wahls, H. E., this publication, pp. 125-147.

[*10*] Hardin, B. O. and Drnevich, V. P., *Journal of the Soil Mechanics and Foundations Division.* American Society of Civil Engineers, Vol. 98, No. SM6, June 1972, pp. 603-624.

[*11*] Hardin, B. O., and Drnevich, V. P., *Journal of the Soil Mechanics and Foundations Division,* American Society of Civil Engineers, Vol. 98, No. SM7, July 1972, pp. 667-692.